

2.5 GEOLOGY, SEISMOLOGY, AND GEOTECHNICAL ENGINEERING

{This section of the U.S. EPR FSAR is incorporated by reference with the following supplements.

The summary includes a synopsis of FSAR Section 2.5.1 through Section 2.5.5, including a brief description of the site, investigations performed, results of investigations, conclusions, and identification of the organization that performed the work.

This section is intended to demonstrate compliance with the requirements of paragraph (c) of 10 CFR 100.23, "Geologic and Seismic Siting Criteria" (CFR, 2007a). Regulatory Guide (RG) 1.208, "A Performance-Based Approach to Define the Site-Specific Earthquake Ground Motion", (NRC, 2007a) is the primary guidance document for the development of the site Probabilistic Seismic Hazard Analysis (PSHA) and Ground Motion Response Spectrum (GMRS).

The terms site region, site vicinity, site area, and site are used in this section to describe the specific areas of investigation. These terms correspond to the following areas:

1. The site region is that area within 200 miles (322 km) of the site location.
2. The site vicinity is that area within 25 miles (40 km) of the site location.
3. The site area is that area within 5 miles (8 km) of the site location.
4. The site is that area within 0.6 mile (1 km) of the site location.

SUMMARY

The proposed Bell Bend Nuclear Power Plant (BBNPP) site is located south and west of the existing Susquehanna Steam Electric Station (SSES) in Salem Township, Luzerne County, Pennsylvania. The BBNPP site is found approximately 5 mi (8 km) northeast of the Borough of Berwick, Pennsylvania, and 1.5 mi (2.4 km) to the north and west of the north branch of the Susquehanna River. The major metropolitan centers closest to the site include: Wilkes-Barre, located 19 mi (31 km) to the northeast; Allentown, PA, approximately 50 mi (80 km) to the southeast; and Harrisburg, PA, which is approximately 70 mi (100 km) to the southwest.

The BBNPP Owner Controlled Area (OCA) is 882 ac (357 ha). The BBNPP site occupies an area of 424 acres (172 hectares) within the OCA. The BBNPP is not within the Exclusion Area Boundary for SSES Units 1 and 2.

For the establishment of the horizontal datum, Pennsylvania State Plane Coordinate System (North Zone), North American Datum of 1983 (NAD 1983) is utilized. For the establishment of the vertical datum, North American Vertical Datum of 1988 (NAVD 88) is utilized, unless stated otherwise.

FSAR Section 2.5 provides information on the seismic, geologic, and geotechnical characteristics of the site and the region surrounding the site. The purpose of this information is to permit an adequate evaluation of the proposed site, to support evaluations performed to estimate the site-specific ground motion response spectrum (GMRS), and to permit adequate engineering solutions to actual or potential geologic and seismic hazards at the proposed site. Details of the studies and investigations performed as well as the findings and conclusions are presented in Section 2.5.1 through Section 2.5.5.

The primary conclusions of Section 2.5 are as follows:

1. **Section 2.5.1 Basic Geologic & Seismic Information** - The site lies in a stable geologic region, and no geologic or man-made hazards are identified within the site area. The site is located in a region that has experienced only infrequent minor earthquake activity, with only 5 seismic events detected within a 50-mile (80-km) radius of the site."
2. **Section 2.5.2 Vibratory Ground Motion** - A PSHA was developed in accordance with Regulatory Guide (RG) 1.208 (NRC, 2007a), using: (1) the EPRI/DOE/NRC (2012) Central and Eastern United States (CEUS) Seismic Source Characterization (SSC) model and (2) the EPRI (2004, 2006a) ground motion model. Based on the PSHA, deaggregation was carried out to identify controlling earthquakes and associated response spectra. The controlling earthquakes were used along with a site geotechnical model to perform site response analysis. The site response was combined with the uniform hazard response spectra (UHRS) from the PSHA according to Approach 2B of NUREG/CR-6728 (McGuire, 2001) to obtain hazard-consistent UHRS at the surface. The surface UHRS were then used to develop a performance based Ground Motion Response Spectra (GMRS) following RG 1.208.
3. **Section 2.5.3 Surface Faulting** - The site vicinity exhibits little evidence of faulting and all of it is non-capable. In addition, a targeted field investigation for the site vicinity discovered no evidence of paleoliquefaction features.
4. **Section 2.5.4 Stability of Subsurface Materials and Foundations** - Subsurface investigations concluded that the site analysis was bounded by the U.S. EPR FSAR for settlement, bearing capacity, hydraulic gradient and that the subsurface bedrock materials are stable with no potential for soil liquefaction. The Nuclear Island will be founded on either the Mahantango Formation or concrete fill.
5. **Section 2.5.5 Stability of Slopes** - The site exhibits limited natural slopes and the only permanent slopes are those for the Essential Service Water Emergency Makeup System (ESWEMS) Retention Pond. All permanent and temporary slopes are shown to have adequate stability safety factors.

Additional details are summarized below.

Basic Geologic and Seismic Information

Regional Geology

The BBNPP site lies within the Appalachian Mountain Section of the Ridge and Valley Province that consists of long, narrow ridges and broad to narrow valleys exhibiting moderate to very high relief. These ridges and valleys are a direct result of lithologic disparities in erosional resistance and the folded and faulted structures developed in the geologic past, when the mountains were built, during the Alleghanian Orogeny.

This Province is primarily a zone containing Cambrian to Pennsylvanian rocks that were folded and faulted during the Alleghanian Orogeny that occurred during late Pennsylvanian through Permian times, nearly 300 million years ago. In addition to the geologic events that affected the entire Ridge and Valley Physiographic Province, three glacial advances affected the site vicinity during the Pleistocene Epoch.

The BBNPP site region is located in a stable continental region (SCR) characterized by low rates of crustal deformation with no active plate boundary conditions. Beyond the site region, features or areas with repeated large magnitude (moment magnitude, M , equal to or greater than 6.5) earthquakes (RLMEs) are documented. Those with a potential impact on seismic hazard at the site are included in the PSHA.

Site Geology

Significant surface and subsurface investigations were conducted for the BBNPP site area foundation investigation, including field surveys, drilling, and geophysical exploration. Additional information was obtained from the SSES FSAR (SSES FSAR, 2003).

The site is adjacent to the Susquehanna River near the southern edge of glaciation in Pennsylvania. The BBNPP site area is located within the Susquehanna Lowland Section of the Ridge and Valley Physiographic Province which is bordered by the Anthracite Valley Section to the west and north, the New England Province to the east, and the Piedmont and Blue Ridge Provinces to the south. The site area is underlain by folded Late Silurian, Devonian, and Early Mississippian formations. More specifically, the site bedrock is Upper Devonian Mahantango Formation. The most recent geologic influence on the site is the Wisconsinan glaciation that deposited glacial materials (including kame terrace, moraines and outwash) on the bedrock surface in a layer approximately 40 feet thick.

The topography within 5 mi (8 km) of the site consists of low to moderately high, linear ridges and valleys that primarily follow structural trends. Local elevations range from about 260 ft (79 m) to nearly 2,368 ft (722 m). The BBNPP is constructed at a final grade elevation of 719 ft (219 m) and is set back approximately 8,000 ft to 10,000 ft (2,438 m to 3,048 m) from the River bank.

The local geologic formations were subjected to a series of mountain-building episodes, including the Grenville, Taconic and Alleghanian orogenies. The local structure of the Ridge and Valley Province was imparted to the area during the Alleghanian Orogeny at the end of the Permian Period, nearly 250 million years ago. The site geologic history has been quiet since the end of the Permian. At that time the local portion of the crust became more stable and tensional stresses predominated through the Cretaceous Period. The only disturbance of this quiet state was the advance of several ice sheets in the Pleistocene. However, because the site is located at the extreme southern limit of the glaciated area, the ice sheets were at their thinnest and any crustal depression or subsequent rebound from the ice load has been minimal.

Geologic studies to determine the site structural characteristics were performed utilizing data obtained from site borings and geophysical surveys. In addition, bedrock exposures were mapped throughout the site area. A thorough search for faulting and detailed mapping of excavations was also performed. The site occupies a position on the northern limb of the northeast end of the Berwick Anticline. A pair of faults has been mapped near the axis of the anticline, but they are related to the Alleghanian Orogeny, and are not active today. No geologic hazards were identified during either investigation.

The site is located in a region that has experienced only infrequent minor earthquake activity, with only 5 seismic events detected within a 50-mile (80 km) radius of the site.

Investigations at the site have not revealed any adverse geologic conditions that can be attributed to human activity. The addition or withdrawal of subsurface fluids, including ground water, at the site has not been significant. Material extraction in the site vicinity has

consisted of minor amounts of sand and gravel for road building. At present, there are no active mining operations within 11 miles (18 km) of the site. There was no mining or petroleum production in the site area that would cause surface or subsurface subsidence.

Vibratory Ground Motion

Section 2.5.2 provides a detailed description of the vibratory ground motion assessment that was carried out to develop the BBNPP GMRS. Development of the GMRS is the first step in defining the site Safe Shutdown Earthquake (SSE) response spectra. The site SSE for the BBNPP is discussed in Section 3.7.1.1.1 and forms the basis for reconciliation with the Certified Seismic Design Response Spectra (CSDRS). The vibratory ground motion assessment was performed using a Probabilistic Seismic Hazard Analysis (PSHA). The PSHA was conducted in accordance with RG 1.208 (NRC, 2007a).

The PSHA was carried out using the EPRI/DOE/NRC (2012) CEUS SSC model and the EPRI (2004, 2006a) ground motion model. Distributed seismicity source zones lying wholly or partially within the 200-mi (322-km) site region were included, along with selected, more distant RLME sources. Investigations of the site vicinity identified no local seismic sources that would need to be added to the EPRI/DOE/NRC (2012) model. The PSHA provides the annual frequency of ground motion exceedance for a generic CEUS hard rock site condition. In addition to mean and fractile hazard curves, UHRS are also developed for 10^{-4} , 10^{-5} , and 10^{-6} mean annual frequencies of exceedance.

The PSHA results for 10^{-4} , 10^{-5} , and 10^{-6} mean annual frequencies of exceedance are deaggregated to identify the fractional hazard contribution associated with various magnitude-distance bins. To support site response analyses, deaggregation is carried out for low frequency (LF) (average of 1-Hz and 2.5-Hz) spectral acceleration (SA) hazard and for high frequency (HF) (average of 5-Hz and 10-Hz) SA hazard. In addition, deaggregation is carried out for 0.5-Hz and 25-Hz SA hazard to facilitate development of smoothed UHRS.

Following RG 1.208 (NRC, 2007a), the deaggregated hazard forms the basis for identifying controlling earthquakes. Controlling earthquakes are determined for LF and HF oscillator frequencies and for 10^{-4} and 10^{-5} mean annual frequencies of exceedance. For each combination of frequency range and frequency of exceedance, three controlling earthquakes are developed to take into account the range in magnitude contributing the hazard.

For each controlling earthquake, a spectral shape is determined from NUREG/CR 6728 (McGuire, 2001). Then the spectral shape is scaled to match the rock UHRS at the appropriate oscillator frequency (1.75 Hz and 7.5 Hz for the LF and HF controlling earthquakes, respectively) to give the controlling earthquake response spectra. Next, time histories that spectrally match the controlling earthquake response spectra are developed.

Site response analysis takes into account the effect on ground motion of the material underlying the site. Inputs to the site response analysis consist of hard rock ground motion based on the PSHA and a geotechnical model of the site materials. Ground motion is represented by the time histories that are spectrally matched to the scaled controlling earthquake response spectra. The geotechnical model is determined from results of the site-specific BBNPP subsurface geophysical and geotechnical investigations. Variability in site material properties is accommodated in the analysis through the use of randomized shear-wave velocity profiles and dynamic property curves that are based on the best-estimate profile and curves.

The site response analysis is expressed as site amplification factors corresponding to each combination of response frequency and frequency of exceedance. These factors are applied to the rock UHRS following RG 1.208 (NRC, 2007a) to give mean UHRS at the surface. The GMRS is then determined from the surface UHRS with 10^{-4} and 10^{-5} mean annual frequencies of exceedance, following the performance-based approach described in RG 1.208 (NRC, 2007a). A vertical-to-horizontal spectral ratio function is subsequently used to calculate the vertical GMRS.

Surface Faulting

To assess the potential or lack of potential for surface rupture in the site region, a variety of detailed subsurface and surface investigation tools were employed. A detailed review of existing information was performed, including geologic maps, seismologic survey data, the USGS earthquake catalog, aerial and satellite imagery, local knowledge from local researchers, and published references. Review of the geotechnical drilling information from the adjacent SSES site was undertaken to verify the lateral continuity of strata across the BBNPP site. In 2007 and 2010 a surface outcrop survey was carried out within the site area. In addition, in the fall of 2008 and spring of 2009, additional field investigations were performed by geologists and engineers to assess the presence of paleoliquefaction features along waterways within the site vicinity, and also to obtain ground truth regarding the presence and surface expression of nearby Paleozoic-age faults.

Seismic refraction studies in 2008 and 2010 show no indication of offset of the top of the Mahantango Shale, which is the local bearing stratum in the site area.

There are no documented zones of Quaternary deformation within the BBNPP site vicinity. No evidence of seismic-related disturbance was found within the Mahantango Shale or the overlying glacial and post-glacial deposits.

It has been determined that there is no potential for tectonic rupture within the site area, and there are no capable tectonic sources within the site vicinity.

Stability of Subsurface Materials and Foundations

The natural topography at the BBNPP site, at the time of the subsurface exploration, was a downward gentle slope towards the west and south of the Power Block, and gently sloping within the vicinity of the ESWEMS Retention Pond. The maximum variation in relief was about 135 ft (41 m) across the site.

The upper 420 ft (128 m) of the subsurface structure were the subject of subsurface investigation. The site geology is comprised of an overburden soil deposit underlain by bedrock. In general, the subsurface is divided into the following stratigraphic units:

- ◆ Overburden Soil – Glacial Till
- ◆ Mahantango Formation – this unit was further divided into three horizons for the BBNPP site as follows
- ◆ Weathered Rock – intensely weathered yellowish gray shale
- ◆ Transition Zone – moderately weathered, moderately fractured, medium to dark gray shale

- ◆ Sound (Competent) Rock – massive medium to dark gray shale

The field investigation for the site was performed in accordance with NRC RG 1.132, "Site Investigations for Foundations of Nuclear Power Plants" (NRC, 2003a). A thorough field investigation program was planned and implemented, and included the following:

- ◆ Boring Program
 - ◆ Wash Rotary Drilling and Standard Penetration Test
 - ◆ Rock Coring (NQ Wireline)
- ◆ In-Situ Pressure meter Testing
- ◆ Geophysical Exploration
 - ◆ Downhole Tests
 - ◆ PS Suspension Logging Tests
 - ◆ Deviation Surveys
 - ◆ Seismic Refraction Surveys

In total, 44 boreholes were completed for the BBNPP site, of which 27 boreholes were located in the vicinity of the proposed Category 1 structures. One boring was extended to 420 feet (128 m) for detailed core logging and geophysical testing at the location of the reactor building. Geophysical testing was also performed in two additional borings in the Power Block area.

A Hydrogeologic Field Investigation collected site-specific data to support a comprehensive hydrogeological evaluation of the plant site and surrounding areas. The data collected were utilized to support the surface hydrology analysis, hydrogeological characterization, and the development of a groundwater flow model.

A comprehensive laboratory testing program was performed on disturbed and undisturbed soil and rock samples, including the following:

1. Index and engineering classification
2. Strength
3. Consolidation
4. Permeability
5. Chemical Tests
6. Resonant Column-Torsional Shear
7. Free-Free Resonant Column

The number and type of tests performed are consistent with the field investigation findings and the overall uniform conditions found at the site, and were performed in accordance with

the guidance of the NRC RG 1.138 , "Laboratory Investigations of Soils and Rocks for Engineering Analysis and Design of Nuclear Power Plants" (NRC, 2003b).

Category 1 Granular Structural Fill and Backfill for the eventual construction of the plant was identified from local sources and tested to determine the relevant engineering properties to be used in design analyses.

Recommendations of Soil, Fill and Rock properties were developed for all materials based on a combination of field measurements, laboratory testing, engineering analysis and judgment, and reference materials. Recommended properties are summarized in Section 2.5.4.2.5.

Foundation interfaces between the planned structures and site foundation materials were evaluated, and design parameters selected, in accordance with the requirements for Combined License (COL) applicants referencing the U.S. EPR FSAR.

Stability of Slopes

The natural topography at the BBNPP site, at the time of subsurface exploration, was a downward gentle slope towards the west and south of the Power Block, and gently sloping within the vicinity of the ESWEMS Retention Pond.

The site is graded to establish the final grade for the project, resulting in minor cuts and fills, as well as slopes.

The stability of temporary and permanent slopes was evaluated using limit equilibrium methods, resulting in a Factor of Safety for the slope section analyzed.

The ESWEMS Retention Pond slopes are the only permanent slopes for the BBNPP. Slope stability analysis results indicate that the pond side slopes have Factor of Safety values in excess of 1.2, indicating that the proposed slope design and configuration is stable under all considered loading conditions.

Temporary cut and fill slopes exist in dry conditions during construction. Slope stability analysis results indicate the temporary slopes have Factor of Safety values in excess of 1.3, indicating that the proposed slope design is stable under all considered loading conditions.}

2.5.1 Basic Geologic and Seismic Information

The U.S EPR FSAR includes the following COL Item in Section 2.5.1:

A COL applicant that references the U.S. EPR design certification will use site-specific information to investigate and provide data concerning geological, seismic, geophysical, and geotechnical information.

This COL Item is addressed as follows:

{This section presents information on the geological and seismological characteristics of the site region (200 mi (322 km) radius), site vicinity (25 mi (40 km) radius), site area (5 mi (8 km) radius) and site (0.6 mi (1 km) radius). Section 2.5.1.1 describes the geologic and tectonic characteristics of the site region. Section 2.5.1.2 describes the geologic and tectonic characteristics of the site vicinity, site area, and site. The geological and seismological information was developed in accordance with the following NRC guidance documents:

- ◆ Regulatory Guide 1.70, Section 2.5.1, "Basic Geologic and Seismic Information," (NRC, 1978)
- ◆ Regulatory Guide 1.206, Section 2.5.1, "Basic Geologic and Seismic Information," (NRC, 2007a) and
- ◆ Regulatory Guide 1.208, "A Performance-based Approach to Define the Site-specific Earthquake Ground Motion," (NRC, 2007b).

The geologic and seismic information compiled and integrated in this section indicates that the site is suitable from a geologic and seismic perspective. The information provides the basis for characterization of seismic sources to be included in a PSHA, the results of which support development of the surface ground motion response spectra (GMRS) used in defining the safe shutdown earthquake (SSE). Seismic source inputs to the BBNPP site PSHA are taken from "Central and Eastern United States Seismic Source Characterization for Nuclear Facilities" (EPRI/DOE/NRC, 2012). This model was developed to replace "Seismic Hazard Methodology for the Central and Eastern United States" (EPRI, 1986) and "Seismic Hazard Characterization of 69 Nuclear Plant Sites East of the Rocky Mountains" (Bernreuter, 1989), and represents the most up-to-date characterization of seismic sources for the CEUS. It systematically considered and documented the evaluation of geologic, geophysical, tectonic, and seismic information relevant to seismic source characterization for the CEUS. The information described in this section does not support or require that any seismic sources in the EPRI/DOE/NRC (2012) CEUS SSC model be updated, nor that any new seismic sources be added to the existing model.

2.5.1.1 Regional Geology (200 mi (322 km) radius)

This section discusses the physiography, geologic history, stratigraphy, and tectonic setting within a 200 mi (322 km) radius of the site. The regional geologic map and regional physiographic map, as shown in Figure 2.5-124 and Figure 2.5-5 (USGS, 2002b), respectively contain information on the geology, stratigraphy, and tectonic setting of the region surrounding the BBNPP site. Summaries of these aspects of regional geology are presented to provide the framework for evaluation of the geologic and seismologic hazards presented in the succeeding sections.

2.5.1.1.1 Regional Physiography and Geomorphology

The BBNPP site lies within the Ridge and Valley Physiographic Province, and the region within a 200 mi (322 km) radius of the site encompasses parts of seven other physiographic provinces. As shown in Figure 2.5-5, these are the Appalachian Plateaus Province, the Piedmont Province, the New England Province, the Atlantic Coastal Plain Province, the Blue Ridge Province, the Central Lowlands Province, and the Adirondack Province (USGS, 2002b). Each of these physiographic provinces is briefly described in the following sections. A map showing the different sections and subsections within the physiographic provinces of Pennsylvania, as depicted by the Pennsylvania Geological Survey (PGS) (Sevon, 2000b), is shown on Figure 2.5-126.

2.5.1.1.1.1 Physiography and Geomorphology of the Ridge and Valley Physiographic Province

The Ridge and Valley Physiographic Province occupies most of central Pennsylvania, extending from the West Virginia and Maryland borders to northeastern Pennsylvania including most of the site vicinity. The Ridge and Valley Province is bordered to the west and north by the Appalachian Plateaus Province and to the southeast by the Piedmont Province as shown in Figure 2.5-125 (Barnes, 2002), Figure 2.5-5 (USGS, 2002b), and Figure 2.5-126 (Sevon,

2000b). On a regional scale, the Ridge and Valley Province extends in a northeast striking zone of varying width from Alabama to New Jersey. The Ridge and Valley Province is primarily a zone containing Cambrian to Pennsylvanian rocks folded and faulted during Alleghenian orogenic events that affected eastern North America during Late Mississippian through Permian times (Hatcher, 1987). Folding resulted in complex geologic structure including synclinal, anticlinal, and nappe structures, while faulting resulted in thrust faults and lateral ramp thrusts. In addition, significant strike slip components are recognized in many Ridge and Valley Faults (Faill, 1999a).

The complex geologic structure and varying lithologies, including repetition of some parts of the stratigraphic section, directly affect the geomorphology of the region and site vicinity. The Susquehanna Lowland Section of the Ridge and Valley Province consists of long, narrow ridges and broad to narrow valleys exhibiting moderate to very high relief that exist as a direct result of lithologic disparities in resistance to erosion and location of these resistant lithologies directly related to structure. These ridges typically are the remnant flanks of breached anticlines, typically capped by Cambrian sandstone and quartzite, and synclines underlain by resistant cherty limestones and sandstones of the Upper Silurian and Lower Devonian Keyser and Oriskany formations (DCNR, 2008a).

In addition to the importance of lithology in defining resistance to erosion and the formation of ridges versus valleys, the susceptibility of limestone and dolomite within the Ridge and Valley Province has resulted in significant formation of karst features such as caverns, surface subsidence and collapse, springs, and disappearing streams. Limestone and/or dolomite formations occur in various thicknesses in Cambrian through Pennsylvanian rocks in the Ridge and Valley Province. While not as prevalent as in the Appalachian Plateaus Province, karst features are significant in the Ridge and Valley Province. In addition, the abundant fractures, folds, and faults of the Ridge and Valley Province serve as zones where dissolution can initiate and concentrate. However significant the presence of karst features throughout some of the Ridge and Valley Province, there is only a small area of potential karst feature development in the extreme western extent of the site area (5 mi (8 km) radius). Based on the lithology of the Mahantango shale and of the Timmers Rock Sandstone, bedrock at the site exhibits no potential for karst development within the site location (0.6 mi (1 km) radius).

The Ridge and Valley Province has a sub-section known as the Great Valley Section, as depicted on Figure 2.5-125. The Great Valley Section of the Ridge and Valley Province consists of a very broad lowland that lies south of the Blue Mountain Section as depicted in Figure 2.5-126 in southeastern Pennsylvania. The lowland has gently undulating hills eroded into shales and siltstones on the north side of the valley and a lower elevation, flatter landscape developed on limestones and dolomites on the south side (DCNR, 2008b). In the Appalachian Mountain Section to the west of the southern portion of the Great Valley Section, elevations range from 440-2,775 ft (134-846 m) (DCNR, 2008e) while elevations in the Great Valley Section range from 140 -1,100 feet (43 -335 m) (DCNR, 2008b). In addition to the geologic events that affected the entire Ridge and Valley Physiographic Province, four glacial events affected the site region (200 mi (322 km) radius).

Three of four main periods of continental glaciation occurring in Pennsylvania directly affected the site vicinity (25 mi (40 km) radius) as shown on Figure 2.5-127 (Sevon, 2000c). The four glacial events occurred in the following order from oldest to youngest; Early Pleistocene, Early Middle Pleistocene, Middle Pleistocene, and Late Pleistocene (Braun, 2004). The oldest glaciation extended the farthest south, with each subsequent glacial event not advancing past

the previous one, as shown in Figure 2.5-127. These older glacial advances are more difficult to identify due to the eroding attributes of more recent glaciers.

The area south of the Late Pleistocene glacial limit is characterized by extensive colluvial deposits and other features of periglacial origin (Braun, 2004) including frost riving and congelifluction (Sevon, 1999a). The limit of the Late Pleistocene glacial event, also known as the Late Wisconsinan (17,000-22,000 yrs), is marked by heads-of-outwash in the valleys with an indistinct moraine on adjacent hillsides (Braun, 2004) and is labeled as Olean Till as shown in Figure 2.5-127.

The overall trend of the Late Wisconsinan margin across northeastern Pennsylvania is approximately west-northwest, and hilltop striae on the Appalachian and Pocono plateaus within 30 mi (48 km) of the margin indicate a regional ice flow direction of north-south to south-southwest (Braun, 1988). The Late Illinoian (132,000-198,000 yrs) glacial event advanced only a few miles from the more recent Late Wisconsinan event, as shown in Figure 2.5-127, and is identified by heads-of-outwash in the valleys and discontinuous patches of till or colluvium derived from till (Braun, 1988). Pre-Illinoian glaciations advanced approximately 20-40 mi (32-64 km) beyond the Late Illinoian limit, as shown in Figure 2.5-127. Glacial lake sediments and two belts of "markedly thicker glacial deposits" suggest that Pre-Illinoian stage (>770,000 yrs) northeastern Pennsylvania was subjected to two glacial events (Braun, 2004). The first extended to the maximum glacial limit as shown in Figure 2.5-127, and the second extended only several miles northeast of the maximum glacial limit (Braun, 2004). In addition to the deposition of glacial sediments, surface hydrology has been affected by glacial melt and outwash. During glacial retreats, large volumes of glacial melt-waters formed broad, high energy streams including the Susquehanna, and other neighboring rivers such as the Delaware and Potomac Rivers.

The geologic structure, lithologic makeup, and glacial history of the Ridge and Valley Province define the physiography and geomorphology of the majority of the site vicinity (25 mi (40 km) radius and the site area (5 mi (8 km) radius) (Figure 2.5-125). The site area (5 mi (8 km) radius) physiography is discussed in further detail in Section 2.5.1.2.1.

2.5.1.1.1.2 Physiography and Geomorphology of the Appalachian Plateaus Physiographic Province

Located west of the Ridge and Valley Province, the Appalachian Plateaus Physiographic Province includes the western part of the Appalachian Mountains, and stretches from New York to Alabama. The mountains within the Appalachian Plateaus Province are generally long, narrow, and even crested, while the valleys are highly variable in width and elevation (Way, 1999). Much of the current day landscape of this Province in Pennsylvania developed during multiple periods of glaciation within the Pleistocene Epoch (Way, 1999).

The Allegheny Front is the topographic and structural boundary between the Appalachian Plateaus and the Ridge and Valley Province (Clark, 1992). It is a bold, high escarpment, underlain primarily by clastic sedimentary rocks capped by sandstone. In eastern West Virginia, elevations along this escarpment reach 4,790 ft (1,460 m) (Hack, 1989), while in Pennsylvania, its highest point is 3,213 ft (979 m) (DCNR, 2007f). West of the Allegheny Front, the Appalachian Plateaus topographic surface slopes gently down to the northwest.

A large portion of the Appalachian Plateaus Province lies within 200 mi (322 km) of the BBNPP site as shown in Figure 2.5-5; the Province makes up the northern portion of the site vicinity (25 mi (40 km) radius) as depicted on Figure 2.5-125.

2.5.1.1.1.3 Physiography and Geomorphology of the Piedmont Physiographic Province

The Piedmont Physiographic Province extends southwest from New York, through southeast Pennsylvania, to Alabama and lies southeast of and adjacent to, the Ridge and Valley Physiographic Province as shown in Figure 2.5-5. The Piedmont Province is about 60 mi (97 km) wide in southeastern Pennsylvania and narrows northward to about 10 mi (16 km) wide in southeastern New York (Figure 2.5-5). Elevation in the Piedmont Province ranges from 20-1,355 feet (6-413 m) (DCNR, 2007b; DCNR, 2007c; and DCNR, 2007d).

In Pennsylvania, the Piedmont Province is divided into the Piedmont Lowland Section, the Gettysburg-Newark Lowland Section, and the Piedmont Upland Section. With the exception of the Piedmont Lowland Section, the majority of the Piedmont Province consists mainly of rolling low hills and valleys (DCNR, 2007a). The Piedmont Lowland Section consists of broad, moderately dissected valleys separated by broad low hills and is developed primarily on limestone and dolomite rock highly susceptible to karst topography (DCNR, 2007b). The Gettysburg-Newark Lowland Section runs adjacent to the Great Valley Section of the Ridge and Valley Province as shown in Figure 2.5-126. The Gettysburg-Newark Section consists of rolling low hills and valleys developed on sedimentary fluvial and lacustrine clastic rock deposits that represent a series of exposed faulted rift basins (Root, 1999). Metamorphic rocks of varying affinity comprise the surface rock outside of the rift basins within the Gettysburg-Newark Lowland Section. The Piedmont Upland Section exhibits gently rolling hills and valleys. Drainage in the Piedmont Upland Section is often controlled by a well developed foliation in predominant schists with drainage developing along foliation or normal to foliation (DCNR, 2007d).

Geologically, the Piedmont Province consists of a variety of sharply folded and faulted supracrustal metasedimentary and plutonic intrusive rocks that are generally younger than the 880-1,000 million year old rocks of the Blue Ridge Province to the west (Milici, 2009). In addition, thick sections of Early Mesozoic sedimentary rocks containing intruded and extruded mafic igneous rocks fill rift basins that are widely distributed in the Piedmont and beneath the Atlantic Coastal Plain. The metasediments within the Piedmont Province may be as young as Ordovician. These Precambrian through Lower Paleozoic crystalline rocks extend to the east under the Upper Jurassic through Cenozoic sediments of the Atlantic Coastal Plain Province.

2.5.1.1.1.4 Physiography and Geomorphology of the New England Physiographic Province

The New England Physiographic Province is bounded on the north by the Ridge and Valley Province and on the south by the Piedmont Province as shown in Figure 2.5-5. The New England Province, aligned in a northeast-southwest direction, extends from the eastern border of Pennsylvania to mid-southeastern Pennsylvania occupying only a small amount of the site region as compared to the surrounding provinces. The province has an average width of about 5 mi (8 km) within Pennsylvania (Figure 2.5-125), and consists of circular to linear, rounded low hills or ridges that project upward in significant contrast to surrounding lowlands (DCNR, 2007e). The hills and ridges are made up of granitic gneiss, granodiorite, and quartzite thus making them very resistant to erosion (DCNR, 2007e). This province has a local relief ranging from 300-600 ft (91-183 m) with elevations ranging from 140-1,364 ft (43-416 m) (DCNR, 2007e).

2.5.1.1.1.5 Physiography and Geomorphology of the Atlantic Coastal Plain Physiographic Province

The Atlantic Coastal Plain Physiographic Province lies east of, and adjacent to, the Piedmont Province and occupies much of the eastern seaboard, as shown in Figure 2.5-5. In Pennsylvania, this area is designated as the Lowland and Intermediate Upland Section of the Atlantic Coastal Plain Province as shown in Figure 2.5-125. This section consists of a flat upper terrace surface that is cut by numerous short streams, which are typically narrow and steep sided (DCNR, 2008c). The province is aligned in a northeast-southwest direction and is, on average, 6 mi (10 km) wide in Pennsylvania but attains a width of up to 50 mi (80 km) in New Jersey (Figure 2.5-5). The unconsolidated to poorly consolidated sand and gravel deposits of the Coastal Plain, dip gently to the southeast (NJGS, 2003). These sediments rest on various metamorphic rocks (DCNR, 2008c). Local relief is very low in the Lowland and Intermediate Upland Section in Pennsylvania, and elevations range from sea level to 200 ft (61 m) (DCNR, 2008c). The highest elevation of the Atlantic Coastal Plain Province in New Jersey is 391 ft (119 m) (NJGS, 2003).

2.5.1.1.1.6 Physiography and Geomorphology of the Blue Ridge Physiographic Province

The Blue Ridge Province extends less than 50 miles (80 km) into Pennsylvania from the south and is approximately 70 miles (113 km) from the BBNPP site (Figure 2.5-5). The Blue Ridge Physiographic Province is bounded on the east by the Piedmont Province and on the west by the Valley and Ridge Province as shown in Figure 2.5-5 (USGS, 2002b). However, the State of Pennsylvania does not include the Blue Ridge in the statewide designation of physiographic provinces. Instead, this region of Pennsylvania is considered the South Mountain Section of the Ridge and Valley Province as shown in Figure 2.5-125 (Sevon, 2000b).

The Blue Ridge Province, also known as the Blue Ridge Thrust Belt Province (Milici, 2009), underlies parts of eight States from central Alabama to southern Pennsylvania in a northeast-southwest direction and is underlain primarily by metamorphosed Precambrian and Early Paleozoic igneous and sedimentary rock (VADOT, 2008). The Blue Ridge Province is recognized as the core of the Appalachian Mountains, emplaced during Alleghanian tectonism along a regional detachment structure (Hatcher, 1987).

Along its western margin, the Blue Ridge is thrust over the folded and faulted margin of the Appalachian basin, so that a broad segment of Paleozoic strata extends eastward for tens of miles, buried beneath these subhorizontal crystalline thrust sheets. At the surface, the Blue Ridge consists of a mountainous to hilly region, the main component of which is the Blue Ridge Mountains that extend from Georgia to Pennsylvania. Surface rocks consist mainly of a core of moderate- to high-rank crystalline metamorphic or igneous rocks, which, because of their superior resistance to weathering and erosion, commonly rise above the adjacent areas of low-grade metamorphic and sedimentary rock (Milici, 2009). The province is bounded on the north and west by the Paleozoic strata of the Appalachian Basin Province and on the south by Cretaceous and younger sedimentary rocks of the Gulf Coastal Plain. It is bounded on the east by metamorphic and sedimentary rocks of the Piedmont Province.

Soils of the Blue Ridge are predominantly colluvium with small amounts of alluvium along the rivers and streams (VADOT, 2008). Residuum occurs locally but is limited in thickness and lateral extent due to aggressive erosive forces caused by steep topography. The Blue Ridge is a long, linear province which ranges in width from about 5 mi (8 km) in Maryland to over 50 mi (80 km) in North Carolina. Elevations in the Blue Ridge Province exceed 6,600 (2,012m) feet in North Carolina and Tennessee.

Reconstructions for the central Appalachians disagree about the boundary between North American native terranes and accreted exotic terranes. Horton (1991) in Kline, 1991, interpreted part of the Virginia Blue Ridge province as an exotic terrane, called the Jefferson terrane, accreted to North America in the Ordovician. Kline (Kline, 1991) implies a common provenance for all the sediments and casts doubt on the exoticism of the Jefferson terrane based on the presence of a common suite of distinctive detrital grains in Jefferson terrane units and in proven native North American metasedimentary rocks and basement.

2.5.1.1.1.7 Physiography and Geomorphology of the Central Lowlands Physiographic Province

The Central Lowlands Physiographic Province, also known as the Ontario Lowlands, has relatively low relief (Komor, 1998) and is located between the Appalachian Plateaus Province to the south and Lake Ontario to the north as seen on Figure 2.5-5. The Central Lowlands were subjected to glaciation and as a result, consist mainly of unconsolidated surficial materials including mostly sands and gravels (DCNR, 2008d). Elevation within the province ranges from 570 ft (174 m) to approximately 1,000 ft (305 m) as erosion processes along the shores of Lake Erie have created a steep lake-land interface along much of the shoreline (DCNR, 2008d).

2.5.1.1.1.8 Physiography and Geomorphology of the Adirondack Physiographic Province

The Adirondack Physiographic Province has moderate to high relief throughout and its circular shape attains a diameter of over 150 mi (241 km). Elevations within the Adirondack Province range from 1,500 ft. (457 m) to 5,344 ft.(1,629 m) The Adirondack Physiographic Province is located in northern New York and is surrounded by the Ridge and Valley Province to the southeast, the Appalachian Plateaus to the south, the Central Lowlands Province to the west, and the St. Lawrence Valley Province to the north and east as seen in Figure 2.5-5. The Adirondacks are primarily Precambrian to Early Paleozoic, metamorphic rocks and are part of the great Canadian Shield that has been uplifted to its present day geography (McDonnell, 2008). The bedrock generally forms long, straight valleys, gently curved ridges, and a radial drainage pattern (Komor, 1998) throughout the province.

2.5.1.1.2 Regional Geologic History

The BBNPP site is located within the Appalachian orogenic belt, a geologic region marked by a complex history of orogenic events, rift sequences, subsequent depositional sequences, eustatic and local sea level changes, and glacial events. The region's position along an active continental margin at intervals in the Proterozoic and Paleozoic Era has developed the structural and stratigraphic characteristics that define the seismotectonic setting. Episodes of continental collisions, depicted on Figure 2.5-6, have produced a series of terranes separated, in part, by low angle detachment faults (Pohn, 2000). Sources of seismicity may occur in the stratigraphy along structures within the North American basement, along the terranes, and over-thrust plates. Tectonic episodes of continental rifting (Figure 2.5-6) have produced high angle normal and boundary faults that extend to the aforementioned detachment faults and in some cases through the upper crust. Direct evidence of these deformational events is visible in the Ridge and Valley province, as described in Section 2.5.1.1.4.3, and borehole data as described in Section 2.5.1.1.3 which identifies the Precambrian rock as Grenvillian.

The site region is located currently on the passive margin of the North American plate following latest Permian and Early to Middle Mesozoic Era continental extension and rifting. The events that have affected the site region (200 mi (322 km)) are discussed in terms of

orogenesis, depositional basins and environments, and their effects on site region (200 mi (322 km)) to site vicinity (25 mi (40 km) radius) geology.

2.5.1.1.2.1 Grenville Orogeny

The Grenville Orogeny occurred as a result of the Mesoproterozoic collision of North and South America (Eriksson, 2003) during the construction of the supercontinent Rodinia (Millot, 2001) between 1.0 and 1.20 Ga (Murphy, 2000). The Grenville Orogeny occurred along the southern and eastern margin of the North American craton and resulted in the accretion and crustal evolution of the eastern and southern margins of the North American Craton during the Proterozoic. Crustal evolution along the edge of the craton during the Grenville orogeny has been studied to determine its role in evolution of the Appalachian Orogen (Mueller, 2008). This Proterozoic orogenic province (the Grenville Province) is comprised of a "laterally continuous region of high grade, polymetamorphic terranes and is also recognized as a multiphase orogenic event with distinct zones connected by ductile shear zones" (Streepey, 2001). The Grenville Province is also described as primarily orthogneisses (Mueller, 2008). Grenville basement rocks outcrop in numerous locations along the Appalachian Mountains from Alabama through Nova Scotia and in Texas (Reese, 2004) and form the basement upon which Paleozoic orogenic and depositional events and sequences occurred. The most significant outcrop of the Grenville Province within the site region is the Adirondack Mountains. The location of the Adirondack physiographic province, comprised of the Grenville age Adirondack Mountains, is depicted on Figure 2.5-5. The site region (200 mi (322 km) radius), site vicinity (25 mi (40 km) radius), site area (5 mi (8 km)) and site location (0.6 mi (1 km) radius) all have Grenville rocks as the Precambrian basement. The depth to Grenville basement at the BBNPP site is approximately 33,000 ft (10,058 m) as shown on Figure 2.5-132.

2.5.1.1.2.2 Late Precambrian to Late Cambrian Rifting and Late Precambrian to Late Ordovician Deposition

Following the Grenville orogeny, Late Neoproterozoic to Early Cambrian rifting initiated the breakup of the supercontinent, Rodinia, and led to the formation of basins in which Late Precambrian sediments accumulated. Rift-related structures such as the Central Pennsylvania trough, a northeast trending rift graben that exists to the south approximately 50 miles (80 km) from the BBNPP site, are analogous to a series of basement troughs that formed during the opening of the Iapetus Ocean (Gao, 2000).

Age analysis of a group of intrusive to hypabyssal rocks associated with rift-related normal faulting in the North Carolina and Virginia Blue Ridge reveal age ranges from 760 to 700 Ma (Bailey, 1998) and ages of initial Rodinian breakup have been determined at 780 Ma (Harlan, 2003), indicating a time range for initial rifting. Rifting continued into Earliest Cambrian until the completion of the opening of the Iapetus Ocean and change to a passive continental margin approximately at the Late Cambrian (Gao, 2000).

The initiation of rifting was also the onset of the deposition of a thick sequence of terrigenous and volcanic detritus, carbonate rocks, and distal more argillaceous sediment in the Appalachian foreland basin that indicates a predominantly transgressive sea with minor local and temporal exceptions (Kauffman, 1999 and Hasson, 1988). Contribution of detritus to the basin from the Grenville Province is established by a predominance of detrital zircons in Cambrian sandstones (Eriksson, 2003). Sediment load enhanced basin subsidence and faulting, which resulted in localized zones of sequence thickening (Hasson, 1998) during the Middle Cambrian through the termination of rifting. The Waynesboro, Pleasant Hill, and Warrior Formations represent the site area (5 mi (8 km) radius) stratigraphy that is part of this sequence (Figure 2.5-13).

Deposition of terrigenous and carbonate sequences continued along the passive margin of the North American craton from the Late Cambrian through the Late Ordovician. Fluctuations in sea level shifted the shoreline and depositional environment throughout this time as indicated by stratigraphic variations from sandstones to shales.

The west-northwest extent of lapetan rifting is significant to the current seismic regime. Faults related to lapetan rifting and the lapetan passive margin have been postulated as the source of seismic activity in Tennessee, Virginia, and Quebec (Wheeler, 1996). Specific seismogenic sources are discussed in detail in Section 2.5.2.

2.5.1.1.2.3 Taconic Orogeny and Clastic Wedge Deposition

The North American craton became a convergent margin with the onset of the Taconic Orogeny at the end of the Middle Ordovician and continuing through the Middle Silurian (Gao, 2000). The Taconic Highlands, an island arc terrane (Trembley, 1997) converged to the east of the North American craton and became the dominant source of detritus to the Appalachian basin. Along the margin of the craton, especially in New England and Canada, suites of ocean floor and island arc material were accreted to the continent along with what is regionally called the Taconic Thrust Belt (Hayman, 2002).

Deformation from the Taconic orogeny was imparted throughout the continental margin, as metamorphic events of Taconian (457 Ma) time are recorded in the Blue Ridge of western North Carolina (Moecher, 2004). An example of Taconic deformation within the site region (200 mi (322 km) radius) is the development of the Hamburg Nappe, an overthrust fold derived from folding of basinal sediment due to thrusting of the Taconic front onto the continent (Faill, 1999b). Behind the Hamburg Nappe were a series of other nappes composed mostly of carbonate cover overlying or wrapping around Grenville crystalline core rocks. Converging from different parts of the continental shelf, they were tectonically superimposed partially overlapping along the Appalachian trend (Faill, 1999b). These nappes are the Lebanon Valley, the Irish Mountain, the Applebutter, the Musconetcong, and the Lyon Station-Paulins Kill which together, compose the Musconetcong nappe megasystem (Faill, 1999b).

Comprised of slabs of the Brandywine Microcontinent during the Taconic Orogeny, the West Chester, Avondale and Woodville Massifs were thrust northwestward upon the continental shelf onto previously emplaced Octoraro Sea deposits (Faill, 1999b). A location map for the West Chester and Avondale massifs is shown in Figure 2.5-152 (Low, 2002). The Street Road Fault separates the Avondale Massif to the southeast from the West Chester Massif to the northwest (Bosbyshell, 2009). The Rosemont Fault to the east of the Avondale Massif separates the massif complex from the Wissahickon (Philadelphia Terrane) and the James Run and Wilmington Complex magmatic arcs (Faill, 1999b). Included and exposed in both the West Chester and Avondale Massifs are basement rocks of the Baltimore Gneiss, including a variety of compositions at amphibolite and granulite grade metamorphism. Granulite facies metamorphism is found in the eastern Avondale, but comprises most of the West Chester Massif, composed of heterogeneous felsic, intermediate and mafic compositions of gneiss (Blackmer, 2005). The idealized cross section in Figure 2.5-154 shows the close relation of these two massifs with the Philadelphia terrane to the SE, as well as the Reading meganappe to the NW.

During this time the site region (200 mi (322 km) radius) existed within the Appalachian basin and received significant amounts of detritus derived from the Taconic Highlands to the east and significantly less detritus from the continent. This led to a clastic wedge thickening to the

east toward the Taconic sediment source (Thompson, 1999 and Castle, 2005) and thinning toward the continental margin. The timing of the Taconic Orogeny ranges from the Middle Ordovician into the Middle Silurian. The site vicinity (25 mi (40 km) radius) was positioned on the western side of the Appalachian basin during the Taconic Orogeny. The effect of the Taconic Orogeny and Clastic Wedge deposition on the site vicinity (25 mi (40 km) radius) and site area (5 mi (8km) radius) is primarily the deposition of the Middle Ordovician to Lower Silurian strata as noted on Figure 2.5-13. The Martinsburg, Bald Eagle and Juniata Formations were derived from the erosion of the tectonic highland. The composition of the aforementioned Formations is provided in Section 2.5.1.1.3.

2.5.1.1.2.4 Middle Silurian through Early Devonian

During the Middle Silurian through Early Devonian Time the site region (200 mi (322 km) radius) existed as part of an extensive basin of deltaic, reef, alluvial and shallow marine environments (Ver Straeten, 2000, and Diedrich, 1999). The Keefer, Bloomsberg, and Mifflintown Formations are the representative strata for this time. The eastern margin of the North American craton was passive while the eroding Taconic Highlands continued to load sediment into the Appalachian Basin.

2.5.1.1.2.5 Acadian Orogeny

The Acadian Orogeny began at the onset of the Middle Devonian within the site region (200 mi (322 km) radius), the result of the Avalon Terrane and Baltica (Eusden, 2000) converging with the North American craton. The Acadian Orogeny affected the northern Appalachians of New England in the Late Silurian (Bradley, 2002). The site vicinity (25 mi (40 km) radius) remained within the Appalachian basin area while the Acadian mountain range, to the east of the site area, was subjected to erosional processes. These eroded sediments were deposited in the site area and are represented by the modern day black and gray shales of the Marcellus formation that underlie the site (Ver Straeten, 2000).

The effect of the Acadian Orogeny is more pronounced in terms of metamorphism and magmatism in the northeastern United States (Maine, New Hampshire, Vermont), but is significant to the site area in that the source material for the formation of the Devonian rocks, notably the Marcellus and Mahantango Formations, that outcrop in the site area was primarily derived from the Acadian Highlands. Ver Straeten (Ver Straeten, 2000) identifies the progression of a terrigenous clastic wedge from the orogenic belt to the west during multiple phases of orogenic uplift during the Devonian that was the source of Devonian deposition. Basin flexure and bulging produced local sea level and depositional environment changes that resulted in reef structures that are noted in the Onondaga Formation which outcrops within the site area (5 mi (8 km) radius).

The Acadian Orogeny and syn-orogenic deposition within the BBNPP site region (200 mi (322 km) radius) came to a close at the Middle Mississippian period. Upper Devonian and Lower Mississippian strata were deposited in the site vicinity (25 mi. (40 km) radius) but have been eroded by subsequent uplift during the Alleghanian Orogeny. The Middle Mississippian through Middle Pennsylvanian, approximately 350-300 Ma (Hatcher, 1987) was an orogenic hiatus in which the Mauch Chunk and Pottsville Formations were deposited within the site region and site area. The composition of the aforementioned Formations is provided in Section 2.5.1.1.3.

2.5.1.1.2.6 Alleghanian Orogeny

Convergence of Peri Gondwana with Laurentia at margins identified in modern geographic terms as northwest Africa and eastern North America led to the formation of the

supercontinent of Pangaea. The continental collision caused the eastern and southern margins of North America to undergo uplift and deformation in what is referred to as the Alleghanian Orogeny. Late Pennsylvanian dextral transpression (a combination of convergent and transform plate boundaries) was the initial interaction of the aforementioned continents (Engelder and Whitaker, 2006). As the convergent margin evolved in the Early Permian, intense brittle and ductile deformation in the form of thrusting, folding, and varying degrees of metamorphism took place (Steltenpohl, 1988 and Shumaker, 2002). This kinematic change from dominant dextral transpression in the Pennsylvanian to northwestward compressional (shortening) deformation in the Permian was likely due to the oblique nature of the collisional orogen or a plate rotation (Becker, 2006). This inference is supported by detrital zircon age populations of Pennsylvanian and Permian rocks that formed from erosion of the Alleghanian highlands and deposited to the west in the Appalachian basin (Becker, 2006).

The current geologic setting along the eastern, southeastern, and south-central (although much is now buried under Gulf Coast Basin sediment) United States is strongly defined by Alleghanian deformation. In many cases, pre-existing faults related to Grenville, Taconic, or Acadian deformation were reactivated to develop regional detachment structures or decollements along which the Piedmont, Blue Ridge, and Ridge and Valley were transported as much as 180 mi (300 km) to the northwest in the Middle to Late Permian (Engelder, 2006). This crustal shortening and overthrusting developed the structural setting of deep seated regional thrust faults, intense folding, and varying degrees of metamorphism that is prevalent in the Ridge and Valley, Blue Ridge, and Piedmont Physiographic provinces.

The southern Appalachians seem to have a slightly different kinematic history than the northern salient. Based on calcite twinning patterns, it is thought that left-lateral transpression occurred in the southern segment of the Appalachian salient while dextral transpression occurred in the northern segment of the salient in Pennsylvanian times (Ong, 2007). However, evidence of dextral shear sense on faults in Alabama indicates that the dominant dextral shear became active in the southern Appalachians during the Late Paleozoic (Steltenpohl, 1988). This predominant dextral transpression is at least partially responsible for the oroclinal structures in the Ridge and Valley and Blue Ridge Provinces. A large oroclinal component of the Ridge and Valley exists within the site region (200 mi (322 km) radius) that can be seen on Figure 2.5-124 as the change in regional structural fabric from a north east strike to an east-northeast strike. Change of structural orientation of 19 degrees to the east of dominant strike is measured in northeast Pennsylvania (Harrison, 2004).

Examples of Alleghanian deformation within the site vicinity (25 mi (40 km) radius) and site area (5 mi (8 km) radius) include the Berwick and Light Street Faults, depicted on Figure 2.5-139 and discussed in Section 2.5.1.2.4.1 and Section 2.5.1.2.6.4. These faults are recognized as exhibiting reverse, to the northwest vergence and are classified as Alleghanian thrust faults (Inners, 1978). Field studies did not identify offset in terrace gravels overlying the Light Street and Berwick Faults (Inners, 1978). In addition, the Berwick Anticlinorium, an east-northeast striking, gently northeast plunging anticline trends directly through the site area (5 mi (8 km) radius). The Berwick Anticlinorium is a symmetrical structure in the site area (5 mi (8 km) radius) with both the north-northwest and south-southwest limbs dipping with an averaged 35 degree NNW and SSW respectively (Inners, 1978). The orientation of this structure is consistent with classic Ridge and Valley Alleghanian deformation as presented by Hatcher (Hatcher, 1987).

In addition to crustal deformation, the Alleghanian Orogeny had an important effect on the depositional regime in the Appalachian Basin and essentially closed the basin at the end of the

Permian. Marked changes in Pennsylvanian rocks are a result of syn-orogenic flysch deposits derived from the uplifted continental margin (Thomas, 2004). The Pottsville, Conemaugh, Allegheny, and Monongahela Formations that lie within the site region (200 mi (322 km) radius) and exhibit lithologies that were influenced by Alleghanian derived detritus exemplify this relationship. Within the site area (5 mi (8 km) radius) the Pottsville and Llewellyn Formations, as shown on Figure 2.5-139 exhibit the Alleghanian sedimentary source.

The Ridge and Valley Province, within which the site area (5 mi (8km) radius) mostly lies, is bounded to the northwest by the Allegheny structural front that separates the Appalachian Plateaus Province from the Ridge and Valley Province. Surface expression of Alleghanian deformation within the Appalachian Plateaus Province is less intense than in the Ridge and Valley. Alleghanian stress was accommodated differently in different lithologies, resulting in less pronounced deformation (more gentle folding and fewer thrust faults) within the surface strata (Schumaker, 2002). Deformation during the Alleghanian is most notable as uplift of the Appalachian Plateaus Province and brittle deformation. The current structural setting on cross section view of the site region (200 mi (322 km) radius) is depicted on Figure 2.5-7. The structural and physiographic position of the site area at the end of Pennsylvanian time placed it at elevations above depositional levels, and sub-aerial exposure and erosion ensued.

A recent re-interpretation of the depositional setting of the Spechty Kopf and Rockwell Formations in the central Appalachian basin of Pennsylvania and Maryland indicates that there was a global cooling causing a glacial period during Late Devonian time (Brezinski, 2010). These deposits are representative of continental glaciers that formed from coalescing valley glaciers from the Alleghanian highlands to the east. This succession constitutes a rarely preserved advance and retreat of a terrestrial glacier that was much more intense than previously inferred. Rapid subsidence of the Appalachian Basin allowed clastic wedge deposits to cover and preserve this thin sequence of glacial and glaciofluvial deposits in a continuous 25 mi by 250 mi (40 km by 400 km) belt (Brezinski, 2010).

2.5.1.1.2.7 Early Mesozoic Extensional Episode (Triassic Rifting)

During the Late Triassic, at the onset of the breakup of Pangaea, the eastern North American plate and African plate began to separate to create the Atlantic Ocean. A series of rift basins developed, such as the Gettysburg-Newark basin in southeastern Pennsylvania, in what is referred to as the North American Rift System (Schlische, 2002). The rift basins are arranged primarily in northeast-southwest asymmetric trend and are located from Florida to the Grand Banks of Canada (Withjack, 1998). Normal faulting under the northwest-southeast extensional stress regime often occurred along pre-existing Paleozoic structures (Olsen, 1990).

Subsequently, the basins were filled with sediments such as conglomerates, sandstones and shales and exhibit evidence of syn-rift deposition (lessening of offset upward in the basin deposits) (Schlische, 2002). The Culpepper, Gettysburg, Newark, Hartford, Taylorsville, and Norfolk Basins lie within or near the site region (200 mi (322 km) radius), and some are shown on Figure 2.5-159.

Figure 2.5-7 shows the Newark Basin in a cross section of the Middle U.S. Atlantic Passive Margin. Schlische and Withjack (Schlische, 2003; Withjack, 2005) include the Taylorsville and Norfolk Basins as part of these Mesozoic Basins. They also consider the Hartford Basin as a sub-basin of the Connecticut Valley Basins, which also includes the small Deerfield sub-basin further north. Figure 2.5-153 (Schlische, 2003) depicts a geologic map and cross sections of an idealized, dip-slip dominated Mesozoic rift basin in eastern North America (a) with syn-rift units thickening toward the border fault in transverse section and thickening toward the

center of the basin in longitudinal section. Figure 2.5-153 also shows a geologic map of an idealized rift basin containing multiple sub-basins related to large-scale segmentation of a border-fault system (b). A geologic map of a basin with both dip-slip and strike slip dominated margins is shown in (c). The idealized basin geometry shown in Figure 2.5-153 does not include the effects of basin inversion.

As basin subsidence continued through the Triassic, the depositional environment within the basin became increasingly sub-aqueous. Outboard of the basins, carbonate platform deposition along the nascent continental margin occurred. Mantle derived basaltic intrusions occurred within the faulted crust which are evident in diabase dikes and sheets of the Piedmont Province of the eastern United States (Philpotts, 1985). During the Early Jurassic period, the process of seafloor spreading caused deep-seated magma to approach the surface. Volcanic deposits ranging from 6-9.3 mile (10-15 km) thickness formed along the entire U.S Atlantic margin in the Middle Jurassic (Sheridan, 1993). The magma created the basalt located in the Gettysburg-Newark basin of the Piedmont province (Schlische, 2003). Northwest-southeast-directed post rift activities in the Mesozoic basin caused inversion to many structures developed during this time (Withjack, 1998). Following rifting, subsidence, and volcanism, the Atlantic Margin became a passive margin.

The effects of Mesozoic rifting affect the site region (200 mi (322 km) radius) with structures possible impact on seismic potential. Specific faults that have been postulated to have seismogenic potential (e.g., Ratcliffe, 1971) are discussed in later sections: e.g., the Ramapo Fault (Section 2.5.1.1.4.4.1.2), the Martic Fault (Section 2.5.1.1.4.4.3.14), the East Border Fault (Section 2.5.1.1.4.4.3.15), and the Yellow Breeches Fault (Section 2.5.1.1.4.4.3.5). In the EPRI/DOE/NRC (2012) CEUS SSC model, a history of Mesozoic or younger extension is used as a basis to discriminate source zones with different potential for maximum magnitude and future earthquake rupture characteristics.

2.5.1.1.2.8 Late Mesozoic and Cenozoic History

During the Cretaceous Period of the Mesozoic Era, the site vicinity (25 mi (40 km) radius) and the majority of the site region (200 mi (322 km) radius) experienced sub-aerial exposure. The notable exception is the Atlantic Coastal Plain Physiographic Region (Figure 2.5-5) that was inundated by the transgressive Cretaceous sea within which significant deposition took place (Southworth, 2006). The extent of the Cretaceous transgressive sea was well inland of the current Atlantic Coastal Plain limit, but erosion during the Cenozoic Era moved the limit of the sedimentary Atlantic Coastal Plain to the east and southeast (Jordan, 1982; Braun, 2003; Ator, 2005). The Atlantic Coastal Plain remained inundated during much of the Cenozoic Era as exemplified by Paleocene through Pleistocene deposits as shown on Figure 2.5-124. Inland of the shoreline from the Cretaceous Period to Early Cenozoic Era, the majority of the site region (200 mi (322 km) radius) was subjected to chemical and physical weathering and erosion at varying degrees of intensity based on climatic conditions (Sevon, 1999b). The depositional setting that has existed throughout the Cenozoic within the site vicinity (25 mi (40 km) radius) and site area (5 mi (8 km) radius) is topographic lows upon which alluvial and lacustrine deposits accumulated. The one exception to this setting was the advance of glacial ice sheets that had significant effects in terms of exhuming and re-depositing surficial material on a regional scale. These effects changed the surface loading and unloading conditions (which can initiate deformation in the rock mass) on the site vicinity (25 mi (40 km) radius) and site area (5 mi (8 km) radius) (Sevon, 1999b).

From Pre-Illinoian to Late Wisconsinian time, three major glacial advances occurred into the BBNPP site area. The glaciers extended into the northern portion of Pennsylvania and covered

most of the Appalachian Plateaus Province. The Pre-Illinoian glaciers migrated south more than 770,000 years ago while the most recent (Wisconsinan) occurred about 17,000-22,000 years ago (Barnes, 2002; Braun, 2007). Figure 2.5-127 shows the limit of glacial advance in Pennsylvania with the site vicinity (25 mi (40 km) radius) superimposed. A map showing surficial glacial deposits within the BBNPP site (0.6 mi (1 km) radius) is presented on Figure 2.5-136.

The glacial advances scoured valleys and deposited till, sand and gravel outwash material throughout BBNPP site area while the nearby Susquehanna River deposited sand and gravel outwash, filling the bottoms of valleys. During the period of elevated physical weathering, freezing and thawing at the surface caused the breakup of large quantities of rock at the crests of ridges in the Ridge and Valley Province (Sevon, 1999a). As a result, the crests of these ridges were lowered by several feet. In addition, loose talus rock accumulated on the slopes of many ridges within central Pennsylvania (Sevon, 1999a).

The current geologic processes affecting the site are limited to weathering and erosion of existing material, and to the regional stress field that affects the passive Atlantic margin. Figure 2.5-8 shows the current stress fields in the eastern portion of North America. Isostatic uplift has been minimal and has remained relatively constant throughout the Cenozoic (Matmon, 2003). With respect to seismic and geologic hazards, the site vicinity (25 mi (40 km) radius) the site area (5 mi (8 km) radius), and the site location (0.6 mi (1 km radius) are positioned in a stable geologic setting.

2.5.1.1.3 Regional Stratigraphy

This section contains information on the regional stratigraphy within the major physiographic provinces in the northeastern United States that are located within the BBNPP site region. The regional geology and generalized stratigraphy within a 200 mi (322 km) radius of the BBNPP site is presented schematically in Figure 2.5-124.

Reports and scientific journal articles, published primarily by staff of the U.S. Geological Survey (USGS) and the Pennsylvania Geological Survey, have been used to develop the following descriptions of regional and local geology. After a thorough search and evaluation of literature ranging from the 1930s to 2008, the references cited in this document are considered to be the leading and most authoritative references relative to BBNPP regional geology, stratigraphic nomenclature, and stratigraphic relationships. In some cases, the best sources of information (most complete and most detailed) for local geology were published in the 1970s and 1980s. In all cases, when more recent publications provide new information, new data, or reinterpretations of old concepts, the newer information has been used and has been cited.

2.5.1.1.3.1 Stratigraphy of the Ridge and Valley Physiographic Province

2.5.1.1.3.1.1 Pre-Cretaceous Basement Rock

2.5.1.1.3.1.1.1 Precambrian

The crystalline basement rock underlying Pennsylvania is of Precambrian age (Saylor, 1999) and rarely exposed, except in the Piedmont Province of southeastern Pennsylvania (Figure 2.5-125). Estimated depth of this basement rock at the BBNPP site is approximately 33,000 ft (10,058 m) below ground surface (bgs), as shown in Figure 2.5-132. Due to the lack of exposure and the relatively great depth to Precambrian rocks in the Ridge and Valley Province, information on Precambrian basement rock is extrapolated from several exploratory wells in western Pennsylvania (Saylor, 1999; Gold, 2008). It is inferred from these deep wells that the Precambrian basement is approximately 1 billion years (Ga) old (Gold, 2008) and it is

composed of metamorphosed greenschist or amphibolite. It is also inferred that this Precambrian basement is a regular, gently sloping surface, dipping eastward and forming the western margin of the Appalachian miogeosyncline (Saylor, 1999). Earliest deformation of this basement rock appears to have occurred during the Grenville Orogeny (Saylor, 1999), resulting in multiple folding events and faulting. Due to the heavily metamorphosed state of this Precambrian basement, little is known about the depositional environment of the original sedimentary deposits.

The closest boreholes to the BBNPP site that penetrate the Precambrian basement rock are located in Erie and Crawford counties, Pennsylvania, about 200 mi (322 km) northwest of the BBNPP site (Figure 2.5-124). The borings that penetrate the underlying Precambrian basement in northwestern Pennsylvania, eastern Ohio, and northern West Virginia have encountered metamorphic or igneous rocks (Saylor, 1999). For example, a well labeled Temple No. 1 in Mercer County, PA, located approximately 208 mi (335 km) west of the BBNPP site, was drilled into a biotite granite/quartz-biotite gneissic basement rock at 9,810 ft (2,990 m) depth (Saylor, 1999). Another well, labeled Fleck in Mercer County PA, located 205 mi (330 km) west of the BBNPP site, was drilled into basement rock at a depth of 9,136 ft (2,785 m) with rock composition including weathered chloritic schist and granite grading into gneiss (Saylor, 1999). The Precambrian basement rock was only sampled in the drill cuttings and suggests a gneiss/schist from the mineralogy present (i.e., biotite, chlorite, and clear quartz).

2.5.1.1.3.1.1.2 Cambrian Period

Overlying the Precambrian metamorphic and igneous basement of the Ridge and Valley Province are the clastic sedimentary deposits of the Early Cambrian with a transition to the carbonate rich sediments of the Early Ordovician. Early Cambrian deposits created a wedge of terrigenous sediments, best described today as the Chilhowee Group, which were deposited along the continental margin as the marine waters of the Iapetus (Proto-Atlantic) Ocean slowly transgressed across the continent shortly after the Grenville Orogeny (Kauffman, 1999). Above the clastic sediments of the Chilhowee Group is the brown sandstone interbedded with red and green shale beds of the Waynesboro Group (Kauffman, 1999). The Waynesboro Group, according to Kauffman (Kauffman, 1999) is the oldest exposed outcrop in Central Pennsylvania with an Early to Middle Cambrian age.

As the Early Cambrian seas transgressed in a generally northwesterly direction sandy coastal deposits in Pennsylvania are represented by the Eocambrian Chickies, Weverton and Harpers formations and the Late Middle Cambrian Potsdam Sandstone (Kauffman, 1999) (Figure 2.5-128 and Figure 2.5-52). Deposition of these sediments was followed by deposition of a carbonate platform (Bradley, 1989; Kauffman, 1999) that shows signs of uplift and erosion during the Taconic Orogeny during the Ordovician (Bradley, 1989). Overlying the Potsdam sandstone and Waynesboro Group is a limestone formation identified as the Warrior Formation (Ryder, 1992) of Middle to Late Cambrian age. The lithology of the Warrior Formation is further defined by Kauffman (Kauffman, 1999) as a dark, fossiliferous, fine grained limestone interbedded with silty dolomite and has a thickness of up to 1,340 ft (408 m) in the Ridge and Valley Province. Bordering the Cambrian-Ordovician contact and overlying the Warrior Formation is the Gatesburg Formation Figure 2.5-13. The Gatesburg Formation consists of a series of sequential sandstone and dolomite units and can be labeled as Late Cambrian age through the identification of gastropod fossils in the uppermost member (Ryder, 1992).

2.5.1.1.3.1.1.3 Ordovician Period

Significant deposition of sediment occurred in the Appalachian Basin during the Ordovician Period, and these sediments are present throughout the Ridge and Valley Province from West Virginia up through Maryland eastward to northeastern Pennsylvania and New York (Figure 2.5-124). The Ridge and Valley rocks of Ordovician age are primarily sedimentary in nature, with evidence of uplifting during the Taconic Orogeny. According to Thompson (Thompson, 1999), the Ordovician sedimentation can be broken down into three major phases with Early Ordovician being a depositional environment of a stable carbonate-platform. During Middle Ordovician, there was a submergence of the carbonate-platform, due to the Taconic Orogeny, with marine limestone and siliciclastic sedimentation during the submergence (Thompson, 1999). This submergence resulted in the creation of a basin which was infilled with additional marine limestone and siliciclastic sediments (Thompson, 1999). Stratigraphically, Early Ordovician rocks are generally referred to as part of the Beekmantown Group (Harper, 2003), are composed primarily of dolomite-limestone, and reach a thickness of up to 4,200 ft (1280 m) (Thompson, 1999) (Figure 2.5-129 and Figure 2.5-13). The Middle Ordovician shows a transition zone from the dolomite-limestone to rocks of primarily limestone composition deposited in both shallow and deep-water environments (Thompson, 1999). In central-Pennsylvania, the Loysburg Formation best represents this transition from a tidal-zone to a shallow marine zone with a dolomitic and stromatalite rich limestone underlying a coarse grained, fossiliferous limestone (Thompson, 1999). It is also during the Middle Ordovician that the Iapetus Ocean stopped widening and began to close; meaning this formerly passive area of sedimentation became tectonically active, thus giving birth to the Taconic Orogeny (Cotter, 2008). This active margin setting became the depositional environment of the sandstone and greywacke-shales that comprise almost 3,500 ft (1,067 m) of Late Ordovician formations including the Juniata, Bald Eagle, and Reedsville Formations of central Pennsylvania (Figure 2.5-129 and Figure 2.5-13).

2.5.1.1.3.1.1.4 Silurian Period

During the Early Silurian Period, shallow marine conditions returned to central Pennsylvania (Cotter, 2008) as it became a depositional environment for sediments being eroded and transported from the Taconic highlands to the east. The Silurian basement rocks throughout Pennsylvania have a thickness ranging from 3,000 ft (914 m) in central Pennsylvania to 4,000 ft (1,219 m) in northeastern Pennsylvania (Laughrey, 1999). The Silurian represents a transition from a coastal plain in the east to a delta in the west, through the alluvial clastic deposits of the Shawangunk and Tuscarora formations (eastern and central Pennsylvania respectively) to the offshore facies of the Medina Formation of western Pennsylvania (Laughrey, 1999). The Tuscarora Formation, prevalent throughout the Ridge and Valley Province in central Pennsylvania, is composed primarily of quartzose, sublithic, and argillaceous sandstones and shales (Laughrey, 1999) and ranges in thickness from 492 ft (150 m) to 656 ft (200 m). The Rose Hill, Keefer, and Mifflintown formations (in ascending order) are the stratigraphic members overlying the Tuscarora Formation (Figure 2.5-13). The Rose Hill Formation is defined as predominantly an olive shale with interbedded layers of hematitic sandstone, purplish shale, and fossiliferous limestone (Laughrey, 1999). The Keefer Formation is described mainly as a quartzose and hematitic sandstone with some mudstone and the overlying Mifflintown Formation is composed of shallow marine mudrocks and limestones (Laughrey, 1999). Above the Mifflintown Formation the Bloomsburg Formation, a grayish-red clay-siltstone with some interbedded sandstone, transitions to the limestone and thin shale beds of the Tonoloway Formation (Laughrey, 1999).

2.5.1.1.3.1.1.5 Devonian Period

In Pennsylvania, Devonian-age rocks represent a "westward-thinning wedge of sediments" that range in thickness from 2,400 ft (732 m) in the western portion of the state, to over 12,000 ft (3,658 m) in the east (Harper, 1999). These Devonian sediments are generally broken down into two basic groups: the Pre-Acadian Orogeny comprised of stable shelf sedimentary deposits and Post-Acadian Orogeny strata that emphasize the presence of "tectonism, subsidence, and filling of a foreland basin" (Milici, 2006). The Keyser Formation forms the base for the Devonian-age rocks of the Ridge and Valley Province in Pennsylvania. This formation is primarily composed of gray, fossiliferous limestone (Laughrey, 1999). Above the Keyser Formation lie other stages of the Lower Devonian, including (in ascending order) the cherty limestone of the Helderberg Stage, the quartz rich sandstones, shales and siltstones of the Deerpark Stage, and the detrital sediments of the Onesquethawan Stage (Harper, 1999). The Onesquethawan Stage carries into and becomes the basement for the Middle Devonian timeframe which consists of basinal marine shales to nonmarine sandstone. Other stages within the Middle Devonian Ridge and Valley Province include the fossiliferous shale of the Needmore Formation, the argillaceous and silty Selinsgrove Limestone, the volcanic Tioga ash and shales, and the Marcellus and Mahantango shales of the Hamilton Group (Harper, 1999). The Marcellus shale is a carbonaceous black shale that has recently become the target of much natural gas exploration in Pennsylvania. The Mahantango Formation, which comprises the bedrock of the BBNPP site, is described by Harper (Harper, 1999) as "a complex series of interbedded shales, siltstones, and sandstones ranging from 1,200 ft (366 m) to 2,200 ft (671 m) thick." Milici (Milici, 2006) also refers to the Mahantango Formation as silty shale. The fossiliferous shaley limestone of the Tully Limestone Formation forms the uppermost portion of the Mahantango Formation (Harper, 1999).

The marine and non-marine rocks of the Late Devonian Period represent sediment deposition during the progradation of the Catskill deltaic system (Harper, 1999). This system, as it relates to the Ridge and Valley Province in central Pennsylvania, can be "broadly defined" by four main depositional episodes including (in ascending order) the rarely fossiliferous basinal shales of the Harrell Formation, the interbedded shales, siltstones, and sandstones of the Brallier Formation (equivalent to the Trimmers Rock Formation), the shales, thin siltstone, sandstones, and conglomerates of the Scherr and Lock Haven Formations, and the nonmarine sandstones and mudrock that overlap the Devonian-Mississippian boundary (Harper, 1999).

2.5.1.1.3.1.1.6 Mississippian Period

The Mississippian Period of the Ridge and Valley Province is a topic of on-going research but the most commonly accepted 'boundary' between the Mississippian and Late Devonian is the Spechty Kopf Formation (Berg, 1999). The Spechty Kopf Formation, which ranges up to 1,280 ft (390 m) in thickness, is typically associated with the unconformity lying between the Catskill Formation and the fluvial sandstones of the Pocono Formation (Berg, 1999). The Spechty Kopf Formation is predominantly sandstone with some interbedded shale and siltstone. Above it lies the Pocono Formation, which, in northeastern Pennsylvania, consists mainly of medium- to coarse-grained sandstones and conglomerates (Brezinski, 1999). In central Pennsylvania, the Pocono Formation is better represented by the Huntley Mountain and Rockwell Formations which are characterized by greenish-gray to tan sandy siltstone and silty shale with some sandstone (Brezinski, 1999). However, more recent studies (Brezinski, 2010) have concluded that the Spechty Kopf formation and the Rockwell Formation are glacial and glaciofluvial deposits. These deposits are restricted to a continuous package within a 25 mi by 250 mi (40 km by 400 km) outcrop that indicates that the Devonian-Mississippian boundary was a time of global cooling with continental glaciers present in Pennsylvania (Brezinski, 2010). The red shales, sandstones, and conglomerates of the Mauch Chunk Formation (Van

Diver, 1993) mark the original uplifting of the Alleghanian Orogeny, as well as the uppermost boundary of the Mississippian strata in the Ridge and Valley Province. The Mauch Chunk Formation varies in thickness throughout the state, but is generally between 3,000 ft (914 m) and 4,000 ft (1,219 m) thick (Brezinski, 1999).

2.5.1.1.3.1.1.7 Pennsylvanian Period

Above the Mauch Chunk Formation in northeastern and central Pennsylvania lies the Lower Pennsylvanian Pottsville Formation, which ranges in thickness from 100 ft (30 m) to 1,600 ft (488 m) and is composed mainly of conglomerate and conglomeratic sandstone, with some sandstone and coal (Edmunds, 1999). Overlying the Pottsville Formation and marking the boundary between the Pennsylvanian and Permian Periods is the Llewellyn Formation. The Llewellyn Formation has a thickness of up to 3,500 ft (1,067 m) and consists mainly of conglomerates and sandstones with numerous coal beds and some clayey shale (Edmunds, 1999).

As shown in Figure 2.5-124 and Figure 2.5-125, there are no post-Pennsylvanian age rock units present in the Ridge and Valley Province of Central and Northeastern Pennsylvania. Subsidence and deposition in the northern end of the Appalachian Basin ended in the Pennsylvanian Period with the beginning of the Alleghanian Orogeny (Fail, 1998). Although thrust sheets and alluvial fans may have caused an overburden of 4-5 mi (6-8 km) thick in the region during the Alleghanian Orogeny (Fail, 1998), there is no preserved geologic materials in the Ridge and Valley Province from between the Pennsylvanian period and the Pleistocene glacial epochs. During this long time period, the Paleozoic rocks were subjected to weathering and erosion processes.

2.5.1.1.3.1.2 Tertiary and Quaternary Deposits

No Tertiary or pre-Pleistocene Quaternary deposits are identified in the Ridge and Valley Province.

Pleistocene glaciers advanced over the northeastern end of the Ridge and Valley Province and covered the bedrock with variable thicknesses of glacial deposits, including tills, kame terraces, eskers, and outwash (Sevon, 2000c). The thickest glacial deposits include kame terraces and outwash, which was deposited along major valleys leading away from retreating glaciers (Sevon, 1999a). These deposits can be more than 200 feet (60 m) thick and contain boulders, gravel, and coarse sand (Sevon, 1999a).

2.5.1.1.3.2 Stratigraphy of the Piedmont Physiographic Province

There are three distinct sections that comprise the Piedmont Physiographic Province. The first is the Gettysburg-Newark Lowland, the second is the Piedmont Lowland, and the third is the Piedmont Upland (Figure 2.5-126 shows the locations of these sections).

2.5.1.1.3.2.1 Gettysburg-Newark Lowland Section

The Gettysburg-Newark Lowland Section forms a 140-mile (225-km) arc across southeastern Pennsylvania with a series of exposed rift basins of Late Triassic to Early Jurassic age that are filled with fluvial and clastic sediments. Sediments filling the basins include conglomerates, shales, siltstones, and sandstones. These basins are underlain by nonmetamorphic Cambrian and Ordovician basement rocks and are bordered "by a continuous, complex system of normal faults" (Root, 1999).

2.5.1.1.3.2.2 Piedmont Lowland Section

Mesozoic sedimentary rocks of the Piedmont Province occur primarily within the highly folded and faulted region of the Piedmont Lowland section (Figure 2.5-126). The sediments were deposited in a series of northeast-trending basins. Sediments filling the basins include conglomerates, shales, siltstones and sandstones, and basic igneous intrusive dikes, diabase, and lava flows (VADOT, 2008). The Lower Mesozoic sediments deposited in these basins usually are referred to as Triassic basin deposits, although the basins are now known to also contain Lower Jurassic rocks. The folding and faulting of this section, as well as lithologies, are very similar to those found in the Great Valley Section of the Ridge and Valley Province, where Cambrian quartzite and Precambrian gneiss are brought into contact with rocks as young as the Early Ordovician (Gray, 1999).

2.5.1.1.3.2.3 Piedmont Upland Section

Crystalline rocks primarily occur within the Piedmont Upland section of the Piedmont Province. The crystalline rocks consist of deformed and metamorphosed meta-sedimentary and meta-igneous rocks, with overlying saprolite (VDEQ, 2008). The rocks belong to a number of northeast-trending belts that are defined on the basis of rock type, structure and metamorphic grade and are interpreted to have formed along and offshore of ancestral North America (Pavlides, 1994).

Surficial sediments in the Piedmont Province consist of residual and transported material. The residual soils have developed in place from weathering of the underlying rocks, while the transported material - alluvium and colluvium - has been moved by water or gravity and deposited as unconsolidated deposits of clay, silt, sand, and gravel. Surficial sediments in the Piedmont Upland section are interpreted to be the product of Cenozoic weathering, Quaternary periglacial erosion and deposition, and recent anthropogenic activity (Sevon, 2000a).

Residual soil in the Piedmont Province consists of completely decomposed rock and saprolite. Residual soils occur almost everywhere, except where erosion has exposed the bedrock on ridges and in valley bottoms. Saprolite comprises the bulk of residual soil in the Piedmont Province and is defined as an earthy material in which the major rock-forming minerals (other than quartz) have been altered to clay but the material retains most of the textural and structural characteristics of the parent rock. The saprolite forms by chemical weathering, its thickness and mineralogy being dependent on topography, parent rock lithology, and the presence of surface and/or groundwater (Cleaves, 1992).

Colluvium in the Piedmont Province occurs discontinuously on hilltops and side slopes, while thicker colluvium occurs in small valleys lacking perennial streams. Alluvium is present in all valleys with perennial streams (Sevon, 2000a).

2.5.1.1.3.3 Stratigraphy of New England Physiographic Province

The basement rocks of the Reading Prong Section of the New England Physiographic Province are believed to have formed during the Grenville Orogeny and are composed of metamorphosed sedimentary rocks. These rocks were then subjected to the intense thrust faulting and continual folding associated with the Taconic Orogeny, thus creating a complex nappe megasystem (Drake, 1999). Continued folding and faulting during the Alleghanian Orogeny has led to "extremely complicated geologic relations" (Drake, 1999) within the Reading Prong. The Middle Proterozoic carbonate and crystalline rocks that were transported otop of the basement rocks (Drake, 1999), were also subjected to folding and faulting and range in sequence depending upon the area of the Reading Prong being studied.

Seismic-reflection studies have suggested that the basement of the Reading Prong ranges in thickness from 15,000 ft (4,572 m) in the easternmost part of the Pennsylvania, to 45,000 ft (13,716 m) in Lebanon and Lancaster Counties (Drake, 1999).

2.5.1.1.3.4 Stratigraphy of Atlantic Coastal Plain Physiographic Province

The Atlantic Coastal Plain Physiographic Province covers more than 3,200 mi (5,150 km) from Cape Cod to the Yucatan Peninsula, and forms the continental shelf along the Atlantic Ocean (Komor, 1998). The province represents repeated cycles of transgression and regression of the ocean resulting in over 100 million years of sediment accumulation (Komor, 1998). Underlying most of the Atlantic Coastal Plain Physiographic Province are sediments of Cretaceous and Tertiary age with Pleistocene fluvial sediments overlying areas in and around the part of the province within the state of New Jersey. A record of Cretaceous to Quaternary exhumation of the Appalachians is preserved in the Coastal Plain sediments (Pazzaglia, 2006). These Cretaceous sediments, in addition to glacial outwash deposits from the Pleistocene continental glaciers, comprise the underlying geology of Long Island and the eastern shores of Staten Island (Komor, 1998). The total sediment accumulation in the Atlantic Coastal Plain Province is nearly 30,000 ft (9,144 m) thick (Komor, 1998).

2.5.1.1.3.5 Stratigraphy of Appalachian Plateaus Physiographic Province

The Appalachian Plateaus Physiographic Province is underlain by rocks that are continuous with those of the Ridge and Valley Province but, in the Appalachian Plateaus, the layered rocks are nearly flat-lying or gently tilted and warped, rather than being intensely folded and faulted. Rocks of the Allegheny Front along the eastern margin of the province consist of thick sequences of sandstone and conglomerate, interbedded with shale, ranging in age from Devonian to Pennsylvanian. The stratigraphic formations in the Appalachian Plateaus are nearly identical to the strata in the Ridge and Valley Province. Changing paleoclimate particularly influenced depositional patterns during the Upper Middle and Late Pennsylvanian, resulting in cyclothems with altered red beds, thick paleosols, and lacustrine carbonates, rather than the typical coal-clastic cyclothems of the Early and Middle Pennsylvanian to the south (Greb, 2008). In southwest Pennsylvania (Figure 2.5-125) and West Virginia, however, the Appalachian Plateaus Province includes sedimentary rocks of Permian age (sandstones, shales, and coal seams) (Hack, 1989).

The Appalachian Plateaus Province is the only one of the provinces described above that has rock strata and glacial deposits that are similar to the geologic formations found at the BBNPP site. The rocks of these two provinces (Appalachian Plateaus and the Ridge and Valley) were deposited in the same general Appalachian structural basin (miogeosyncline) and the sedimentary formations are continuous across the two provinces. There are, however, great differences in geologic age, in structural and tectonic features, and sediment provenance between the Ridge and Valley geologic formations and the geologic materials found in the adjacent physiographic provinces to the east and south.

2.5.1.1.4 Regional Tectonic Setting

This section provides an overview of the tectonic setting of the BBNPP site region. The overview addresses the plate tectonic framework of the region and summarizes information on tectonic features identified from geophysical and geological data. The seismotectonic framework forms the foundation for assessment of seismic sources.

Seismic sources used in the evaluation of vibratory ground motion for the BBNPP site are taken from the EPRI/DOE/NRC (2012) CEUS SSC model. This model was developed following a formal process to provide confidence that it represents the center, body, and range of

technically defensible interpretations regarding seismic sources in the CEUS. The process followed guidance described in NUREG/CR-6372 (SSHAC, 1997) and NUREG-2117 (NRC, 2012). In the context of these documents, a Level 3 study was carried out.

In a SSHAC Level 3 Study for SSC, a Technical Integration (TI) Team evaluates data and interpretations compiled from the scientific community. Workshops are held to facilitate identification of key issues and the data available to address them and also to discuss interpretations, models, and approaches for SSC. During the workshops, resource experts and proponent experts present information to the TI Team. The workshop format allows the TI Team to question the experts on the basis and limitations of their data and models. Interaction among the experts is also encouraged to clarify the strengths and weaknesses of interpretations and approaches. Consideration and evaluation of information for the EPRI/DOE/NRC (2012) CEUS SSC was documented by the TI Team on Data Summary Sheets and Data Evaluation Sheets.

Following their evaluation of the data and models, the TI Team integrates the information to develop a SSC model that represents the center, body, and range of technically defensible interpretations. The Data Evaluation Sheets document how each piece of information was used to develop the integrated model. Using a preliminary version of the SSC model, seismic hazard and sensitivity calculations are carried out and used to provide feedback to the TI Team in a third workshop. Feedback is also provided by a participatory peer review panel to assure that the technical basis and justification for the model choices are well founded and documented.

Because of the high level of documentation provided in the EPRI/DOE/NRC (2012) CEUS SSC report, detailed descriptions of the tectonic basis for seismic source zone characteristics are not provided here. Rather, an overview of the tectonic setting is provided along with more focused discussions of some tectonic features that are relevant to the evaluation of seismic sources for the BBNPP site for either technical or historical reasons. All of the information summarized below was considered by the SSC TI Team in developing the EPRI/DOE/NRC (2012) CEUS SSC model.

The seismic sources from the EPRI/DOE/NRC (2012) CEUS SSC model that are used in the PSHA for the BBNPP site are described in Section 2.5.2.

2.5.1.1.4.1 Contemporary Plate Tectonic Setting of the Atlantic Margin

The Late Precambrian to recent geologic history and plate tectonic evolution of the site region is summarized in Section 2.5.1.1.2 and Figure 2.5-6. Several studies address the relationship between the stratigraphy and structure during the Paleozoic era as it relates to orogenies and plate tectonics (Pazzaglia, 1994) (Pohn, 2000 and 2001) (Hibbard, 2006) (Cotter, 2008). The three main orogenic phases during the Paleozoic - Taconic, Acadian, and Alleghanian Orogenies - begin with accumulation of marine sediments and volcanic deposits, followed by structural folding and faulting, and end with tectonic uplift of mountains, and erosion of uplifted land. A particular consequence of orogeny is the production of sediment as uplifted mountains erode. Thus, each phase created a delta, filling shallow seas on the continental side of the orogeny. Clastic fans were deposited in terrestrial, coastal, near-shore, and off-shore settings (Aber, 2001).

During the break up of Pangaea in the Triassic, rift basins developed in eastern North America that were typically asymmetrical and trended northeast to southwest. The current Atlantic passive margin has evolved since this rifting initiated in the Late Triassic. The progression from

active continental rifting to sea-floor spreading and a passive continental margin included: (1) initial rifting and hot-spot plume development, (2) thinning of warm, buoyant crust with northwest-southeast extension, normal faulting and deposition of syn-rift sedimentary and volcanic rocks, and (3) cooling and subsidence of thinned crust and deposition of post-rift sediments on the coastal plain and continental shelf, slope, and rise (Klitgord, 1988) (Klitgord, 1995). The transition between the second (rifting) and third (drifting) phases during the Early Jurassic marked the initiation of a passive margin setting for the site region, in which active spreading migrated east, away from the margin.

The continental margin moved away from the spreading center of the mid-Atlantic and horizontal northwest-southeast tension changed to horizontal compression as gravitational potential energy from the spreading ridge exerted a lateral "ridge push" force on the oceanic crust. Contractual post-rift deformation is interpreted to record the change in stress regime from horizontal maximum extension during rifting to horizontal maximum compression during passive margin drifting (e.g., (Sanders, 1963) (Swanson, 1982) (Wentworth, 1983) (Withjack, 1998) (Schlische, 2003)). Northwest-southeast directed post-rift activities in the Mesozoic basin caused inversion to many structures present during this time (Withjack, 1998). The transition from a rift to a drift margin through the remainder of the Mesozoic and into the Cenozoic along with the westward push of the continental divide, dominated the tectonic and geomorphic development of the eastern United States up to the modern time period (Schlische, 2003).

Latest tectonic processes in the Cenozoic Era include vertical tectonics associated with lithospheric flexure (Pazzaglia, 1993). Vertical tectonics are dominated by cooling of the extended continental, transitional, and oceanic crust as the spreading center migrated eastward, and the erosion of the Appalachian Mountains to the Coastal Plain and extension of the Continental Shelf and Slope.

Based on models of the Cenozoic flexural deformation, surface material from the Appalachian Mountains eroded and was deposited on the Coastal Plain and Continental Shelf (Pazzaglia, 1993). The sediment is mainly deposited in the Salisbury Embayment and Baltimore Canyon Trough (Figure 2.5-7). The flexural hinge that is the axis between deposition and downward pressure to the east and uplift due to erosion to the west is known as the Fall Zone (Pazzaglia, 2006). An elastic model predicts the uplift in the Piedmont Province to be as much as 33 ft (10 m) per million years (Pazzaglia, 1994). Figure 2.5-7 illustrates present conditions with a location map and composite cross section of the middle U.S. Atlantic passive margin (Pazzaglia, 2004). The Susquehanna River terrace profiles, the Coastal Plain stratigraphic sections, geodynamic model cross-sections, and offshore load volumes are defined along cross section A-A', in the lower part of Figure 2.5-7.

2.5.1.1.4.2 Origin and Orientation of Contemporary Tectonic Stress

The World Stress Map (WSM) is the global repository for contemporary tectonic stress data from the Earth's crust (e.g., Heidbach, 2008). It was originally compiled by a research group headed by Mary Lou Zoback as part of the International Lithosphere Program (ILP). Since 1995 the WSM is a research project of the Heidelberg Academy of Sciences and Humanities. The WSM research team is integrated into the Tectonic Stress Group of the Geophysical Institute at the Karlsruhe University. The WSM is a task group of the International Association of Seismology and Physics of the Earth's Interior (IASPEI) (Heidbach, 2008).

As observed in Figure 2.5-8 (Heidbach, 2008) throughout the BBNPP site region, the P axes of the stress indicators are oriented NE-SW and are aligned with the direction of the current plate

driving stress that in the BBNPP region is characterized by northeast-southwest-directed horizontal compression.

Studies of the state of stress in the CEUS have included those addressing stress magnitudes in the crust, deformation of intraplate lithosphere, joints and veins in regional tectonic perspective, and contemporary stress variations (Herman, 2005) (Zoback, 2002 and 1991) (Engelder, 2001) (Hancock, 1989) (Evans, 1989) (Hickman, 1985). As indicated in these studies, the tectonic stress created by the Mid Atlantic ridge produces a stress orientation aligned northeast to southwest on the North American plate. They also indicated that the lithosphere cannot be deformed more rapidly because of the limited amount of tectonic force available to drive that deformation in the current stress field (Zoback, 2002) and that the stress field for the site region is considered stable. Other potential forces acting on the North American plate are considered minor.

Study of neotectonic joint attributes by Hancock (Hancock, 1989) and Engelder (Engelder, 1980) that included the Appalachian Plateau and other places in England, France, the Arabian Platform and the Ebro basin in Spain, showed that late-formed joints have potential value for tracking the contemporary stress field in regions where in-situ measurements are not available. Their conclusion showed that these late-formed joints have the characteristics of neotectonic joints and are approximately parallel to directions of contemporary horizontal maximum stress (SH) known from in-situ stress measurements. The latter shows that although there may be a slight misalignment between joint strike and the direction of the greatest horizontal stress, these joints reflect the contemporary stress field.

Despite the most common orientation of joints in the Appalachian Mountains being northeast-southwest to east northeast-west southwest, the vast majority are not neotectonic joints related to the current northeast-southwest maximum horizontal compressive stress regime as originally thought (Engelder, 2009). Through study of jointing in the Appalachian foreland of Virginia, Pennsylvania and New York, particularly in the pervasively jointed organic black shales, it was shown that there are three common joint sets (Engelder, 2009). While there are neotectonic east northeast-west southwest joints (J_3), the vast majority of joints in this orientation are early joints (J_1) related to propagation in the pre- or early Alleghenian orogeny times. This became clear when it was observed that the J_1 joints were folded along with bedding (Engelder, 2009).

There is also an early east-northeast face cleat development in coal beds throughout the central and southern Appalachians that was initiated during burial that is correlative with the dominant J_1 joint formation (Engelder, 2006). Vertical joints cross-cutting a folded succession are interpreted as J_3 joints related to the contemporary stress regime. The similarity of the J_1 and J_3 orientations is merely a geologic coincidence (Engelder, 2009).

The second northwest-southeast oriented joint set (J_2) typically cross cuts J_1 orthogonally when they are observed in the same bed (Engelder, 2009). The J_2 joints, or cross-fold joints, clearly formed later because they commonly end at J_1 joints as well as strike across fold axes (Lash, 2009), thereby forming a radial pattern along the oroclinal bend of the central Appalachian Mountains (Engelder, 2009). However, J_1 joints are commonly observed abutting and curving into J_2 joints. This is due to reactivation of short J_1 during Miocene exhumation under the east northeast-west southwest contemporary stress regime (Lash, 2009). The reactivated J_1 joints were driven along curving paths into abutting contacts with the J_2 , which is a manifestation of slip on J_2 joints under relatively low contact stress following reactivation of J_1 joints (Lash, 2009).

In developing the EPRI/DOE/NRC (2012) CEUS SSC model, the TI Team considered and used data from the World Stress Map and other stress data as documented on Data Evaluation Sheets (EPRI/DOE/NRC, 2012).

2.5.1.1.4.3 Gravity and Magnetic Data and Features of the Site Region and Site Vicinity

Regional maps of the gravity and magnetic fields are presented for North America by the Geological Society of America (GSA), as part of the Society's Decade of North America Geology (DNAG) project (Tanner, 1987) (Hinze, 1987) as shown in Figure 2.5-9 and Figure 2.5-10 (Kucks, 1999) and Figure 2.5-11 and Figure 2.5-12 (Bankey, 2002).

These maps present the potential field data at 1:5,000,000-scale, and show gravity and magnetic anomalies. Regional gravity anomaly maps are based on Bouguer gravity anomalies onshore and free-air gravity anomalies offshore. The primary sources of magnetic data reviewed for this BBNPP study are from aeromagnetic surveys onshore and offshore (Kucks, 1999). Large-scale compilations (1:2,500,000-scale) of the free-air anomalies offshore and Bouguer anomalies onshore were published in 1982 by the Society of Exploration Geophysicists (Lyons, 1982) (Sheridan, 1988). The DNAG magnetic anomaly maps were based on a prior analog map of magnetic anomalies of the U.S. published in the early 1980's (Zietz, 1982) (Behrendt, 1983) (Sheridan, 1988).

In addition, the DNAG Continent-Ocean transect program published a synthesis of gravity and magnetic data with seismic and geologic data (Klitgord, 1995). The following sections discuss the gravity and magnetic anomalies.

2.5.1.1.4.3.1 Gravity Data and Features

Gravity data compiled at 1:5,000,000-scale for the DNAG project provide documentation of previous observations that the Regional Bouguer anomaly gravity field in the site region is characterized by a long-wavelength, east-to-west gradient over the continental margin (Kucks, 1999) (Figure 2.5-9, Figure 2.5-156 and Figure 2.5-157). Bouguer gravity anomaly values increase eastward from about -80 milligals (mgal) in the Ridge and Valley Province of western Virginia to about +10 mgal in the Coastal Plain Province (Figure 2.5-9, Figure 2.5-156 and Figure 2.5-157). Gravity highs, or positive anomalies, are created by accumulations of dense rock units while gravity lows are from mass deficiencies. The folded and faulted structures, basins, igneous intrusions, lithologic variations, and basement uplifts create variations in mass. Gravity anomalies occur from density contrast in size, depth, and structural depth. Long wavelengths show shallow structures or highly concentrated deep structures. Shorter wavelengths are created by shallower structures (Lavin, 1999). As shown on (Figure 2.5-9, Figure 2.5-156 and Figure 2.5-157), a gravity anomaly gradient extends from Canada to Alabama and parallels the Appalachian Mountains. The Mesozoic rift basins show gravity lows and northeast-trending border faults (Figure 2.5-157).

The gravity anomaly map also shows northeast--trending, long wavelength gravity highs and lows. The alignments are variations of thickness of the sedimentary rocks and crustal structures (Lavin, 1999). Low gravity dominates the western part of Pennsylvania and eastern Ohio, including areas such as the Beaver Falls gravity low. The Chambersburg anomaly is another low, broad, northeast--trending gravity low, which extends the length of the Appalachian Mountain system. The Somerset gravity high in southwestern Pennsylvania is thought to coincide with a regional basement high that is about 3.5 to 4 mi (6 km) below the surface, although a deeper source has also been suggested for this anomaly. In the northwest of Pennsylvania, the Kane gravity high marks a paleo-topographic high that was uplifted from Early Devonian through Early Pennsylvanian time and controlled the sedimentation patterns

and composition in the Pennsylvanian Epoch (Figure 2.5-9) (Lavin, 1999). In the northeast, the Scranton gravity high (Feature 34 on Figure 2.5-157 and Figure 2.5-9) is surrounded by the Williamsport and Reading lows. The lows are deep Paleozoic sedimentary basins and/or increased crustal thickness. The Scranton gravity high is related to mafic material during Late Precambrian rifting (Lavin, 1999). The Newport gravity high, directly southwest of the Scranton gravity high, is believed to be a separate, but related feature that might represent the site of a triple junction.

As part of the EPRI/DOE/NRC (2012) CEUS SSC project, gravity anomaly data were compiled and evaluated (EPRI/DOE/NRC, 2012). To support development of the SSC model, Bouguer, free-air, and isostatic anomaly and various derivative datasets were developed. Any use of these datasets in characterizing specific seismic sources is documented in Data Evaluation Sheets (EPRI/DOE/NRC, 2012, Appendix C) and in the description of each source in the report.

2.5.1.1.4.3.2 Magnetic Data and Features

Magnetic data compiled for the 2002 Magnetic Anomaly Map of North America reveal numerous northeast-southwest-trending magnetic anomalies, generally parallel to the structural features of the Appalachian orogenic belt (Bankey, 2002) (Figure 2.5-11). The magnetic map allows a visualization of the geological structure of the upper crust in the subsurface showing the spatial geometry of bodies of rock and the presence of faults and folds. Prominent north- to northeast-trending magnetic anomalies in the BBNPP site region (Figure 2.5-158 and Figure 2.5-159) include the interior New York-Alabama Lineament, the New Bloomfield high, subsurface nappes near Scranton and Allentown, anomalies over largely subsurface Proterozoic rocks at the Reading Prong, Philadelphia and Lancaster, and an inferred basement fault located south of Pittsburgh, the Pittsburgh-Washington Lineament (King, 1999).

The 1,000 mi (1,600 km) long lineament in aeromagnetic anomaly maps of the eastern U.S. is referred to as the "New York--Alabama Lineament" (NY-AL) (King, 1978) (Figure 2.5-158). The NY-AL primarily is defined by a series of northeast--southwest trending linear magnetic anomalies in the Ridge and Valley province of the Appalachian fold belt. At its closest approach, the NY-AL is located about 50 mi (80 km) northwest of the BBNPP site. Based on studies by King (King, 1999), the NY-AL divides the basement into two magnetically distinct areas (Figure 2.5-11 and Figure 2.5-158). To the southeast, the few anomalies present are very broad and have gentle gradients consistent with the profound basement depths of the region. To the northwest, numerous anomalies indicate a basement composed of large units of rock with strongly contrasting magnetic properties. King (King, 1999) has interpreted the NY-AL to be a major strike-slip fault in the Precambrian basement beneath the thin-skinned, fold-and-thrust structures of the Ridge and Valley.

The Clingman-Ocoee lineament is an approximately 750 mi (1,207 km) long, northeast-trending aeromagnetic lineament that passes through parts of the Blue Ridge and eastern Ridge and Valley provinces from Alabama to Pennsylvania (King, 1999). The Clingman-Ocoee lineament is sub-parallel to and located about 30 to 60 mi (48 to 97 km) east of the NY-AL, and, at its closest approach, about 30 mi (48 km) southeast of the BBNPP site (Figure 2.5-11). The Clingman-Ocoee lineament is interpreted to represent a source or sources in the Precambrian basement beneath the accreted and transported Appalachian terrains (Nelson, 1983). The Clingman-Ocoee block is a Precambrian basement block bounded by the NY-AL and Clingman-Ocoee lineament (Johnston, 1985b).

The Newark and Gettysburg rift basins consist of Mesozoic clastic rocks (Featured on Figure 2.5-159) that have been downfaulted against Proterozoic and Paleozoic rocks (King, 1999). Magnetic anomalies related to elongated shaped bodies of diabase are present within these basins.

The Buckingham Mountain anomaly is produced by a fault-bound sliver of Paleozoic and Proterozoic rock creating a northeast trending ridge, and dividing the Newark basin. The faults cut the Mesozoic rocks and are bound to the south by small diabase sheets and bound larger sheets to the north of the anomaly. The Buckingham magnetic high indicates a large subsurface ridge of magnetic Proterozoic rocks extending 15 mi (24 km) southwest from the state line (King, 1999).

The magnetic anomalies over the Reading Prong (Feature 51 on Figure 2.5-158) are produced by a complex of magnetite-rich, gneissic Proterozoic rocks at the surface (King, 1999). These rocks are related to the center of a nappe system that is over thrust from the southeast. Small anomalies occur east of Lancaster and are related to gneisses exposed in the Minde Ridge anticline and related structures. The magnetic data indicate similar rocks at shallow depths to the west toward Lancaster and to the east of the Honey Brook Upland, under the Triassic Basin (King, 1999).

As part of the EPRI/DOE/NRC (2012) CEUS SSC project, magnetic anomaly data were compiled and evaluated (EPRI/DOE/NRC, 2012). To support development of the SSC model, various anomaly and derivative datasets were developed. Any use of these datasets in characterizing specific seismic sources is documented in Data Evaluation Sheets (EPRI/DOE/NRC, 2012) and in the description of each source in the report.

2.5.1.1.4.4 Regional Tectonic Structures

The EPRI-SOG SSC project characterized tectonic features with possible seismic potential. Following a comprehensive approach, the features were systematically evaluated with respect to a set of criteria to assess their probability of activity. While comprehensive, the approach resulted in SSC models that included a large number of seismic sources that had a low probability of activity. Most seismic sources were feature-based. A map of tectonic features from the EPRI-SOG that are located in the BBNPP site region and environs is shown in Figure 2.5-131.

In developing the EPRI/DOE/NRC (2012) CEUS SSC model, tectonic features were evaluated and, if appropriate, integrated into the SSC. For the EPRI/DOE/NRC (2012) study, however, tectonic features were generally not the primary basis for defining sources. They were one of many different datasets that were considered. While some sources are based on specific features (e.g., New Madrid Fault System, Meers Fault), most incorporate tectonic features in a more general sense (e.g., a broad area of continental crust that underwent extension since the beginning of the Mesozoic Era).

Tectonic features that were compiled and considered in developing the EPRI/DOE/NRC (2012) CEUS SSC model are incorporated in the project's GIS database (EPRI/DOE/NRC, 2012). Evaluation and use of the data is documented on Data Evaluation Sheets (EPRI/DOE/NRC, 2012) and in the report.

Tectonic features within or partially within the 200 mi (322 km) BBNPP site region are described in this section, based on the following breakdown:

- ◆ Quaternary Tectonic Features (Section 2.5.1.1.4.4.1)
- ◆ Relevant Tectonic Features with Associated Seismicity (Section 2.5.1.1.4.4.3)
- ◆ Relevant Tectonic Features with No Associated Seismicity (Section 2.5.1.1.4.4.3)

Relevant tectonic features with associated seismicity located outside of the BBNPP site region (e.g., the Central Virginia, New Madrid, Charleston, and Charlevoix-La Malbaie seismic zones) are discussed in Sections 2.5.2.1.2 and 2.5.2.2.1.

2.5.1.1.4.4.1 Quaternary Tectonic Features

The U.S. Geological Survey maintains a nationwide database on features that have known or suggested Quaternary tectonic faulting. Geologic information on the Quaternary faults, folds, and earthquake-induced liquefaction in the eastern United States was compiled by Crone (Crone, 2000). An update containing new assessments was published by Wheeler (Wheeler, 2005). Tectonic features described by Crone and Wheeler (Crone, 2000), and Wheeler (Wheeler, 2005) (Wheeler, 2006) are included on Figure 2.5-131.

The features are categorized into one of four Classes, as follows (Crone, 2000).

Category	Number of Features in BBNPP Site Region	Description
Class A	1	Geologic evidence demonstrates the existence of a Quaternary fault of tectonic origin, whether the fault is exposed by mapping or inferred from liquefaction or other deformational features.
Class B	0	Geologic evidence demonstrates the existence of Quaternary deformation, but either (1) the fault might not extend deeply enough to be a potential source of significant earthquakes, or (2) the currently available geologic evidence is too strong to confidently assign the feature to Class C but not strong enough to assign it to Class A.
Class C	16	Geologic evidence is insufficient to demonstrate (1) the existence of tectonic faulting, or (2) Quaternary slip or deformation associated with the feature.
Class D	0	Geologic evidence demonstrates that the feature is not a tectonic fault or feature. This category includes features such as joints, landslides, erosional or fluvial scarps, or other landforms resembling fault scarps but of demonstrable nontectonic origin.

Note that only one (1) feature identified in Figure 2.5-131 was categorized as Class A - demonstrating convincing evidence of Quaternary activity. This is the Newbury Liquefaction Feature. This feature is outside the BBNPP site region (200 mi (322 km) radius). No features in the site region were designated as Class B (i.e., evidence of Quaternary deformation, but either do not extend deeply enough to generate significant earthquakes or the evidence is not sufficiently convincing for a Class A designation).

Sixteen (16) Class C features are identified in (or as extending into) the site region and are shown in Figure 2.5-131.

The seventeen Class A and Class C features with known or possible Quaternary deformation are listed below and then described.

1. Newbury Liquefaction Feature (Class A)

2. Ramapo Fault System (Class C)
3. Furlong-Flemington Fault System (Class C)
4. Kingston Fault (Class C)
5. New York Bight Fault (Class C)
6. Mosholu Fault (Class C)
7. New Castle County Faults (Class C)
8. Upper Marlboro Faults (Class C)
9. Dobbs Ferry Fault Zone (Class C)
10. Lancaster Seismic Zone (Class C)
11. Cacoosing Valley Earthquake Sequence (Class C)
12. Moodus Seismic Zone (Class C)
13. Clarendon-Linden Fault Zone (Class C)
14. Offset Glaciated Surfaces (Class C)
15. Fall Lines of Weems (Class C)
16. Everona Fault-Mountain Run Fault Zone (Class C)
17. Stafford Fault System (Class C)

2.5.1.1.4.4.1.1 Newbury Liquefaction Features (Class A)

The Newbury area lies in northeastern Massachusetts 300 miles (480 km) to the northeast of the BBNPP site. Crone and Wheeler (Crone, 2000), in their compilation of faults and tectonic features of the CEUS, identify a Class A feature near Newbury (Essex County, MA) based on eyewitness reports of liquefaction during an earthquake in 1727 (MMI VII, Magnitude = 4.8) and sand dikes that were attributed to the 1727 earthquake. Tuttle (Tuttle, 1991) concluded that the liquefaction was caused by strong ground motion but the causative fault responsible for the ground motion and liquefaction remains unidentified. The zone of liquefaction is about 260 mi (420 km) northeast of the BBNPP site (Feature 21 in Figure 2.5-131).

In developing the EPRI/DOE/NRC (2012) CEUS SSC model, information on the Newbury Liquefaction Features was considered and evaluated. Based on the evaluation and integration of available data, the TI Team did not identify the Newbury Liquefaction Features as a specific seismic source. Because the liquefaction data are sparse and do not provide a basis for recurring earthquakes of moment magnitude (**M**) 6.5 or greater, they do not meet the criteria for a separate Repeated Large Magnitude Earthquake (RLME) source. Rather, recurrence of earthquakes in the Newbury area is represented by distributed seismicity source zones.

2.5.1.1.4.4.1.2 Ramapo Fault System (Class C)

The Ramapo Fault System is located in northern New Jersey and southern New York State, approximately 124 mi (200 km) north-northeast from the BBNPP site (Feature 15 in Figure 2.5-131). This fault system consists of northeast-striking, southeast-dipping, normal

faults along the border of the Mesozoic Newark Basin (Jacob, 2004). While the faults were most recently active during Mesozoic rifting, Ratcliffe interprets geologic data to demonstrate previous activity during Proterozoic.

Historical seismicity is spatially associated with the Reading Prong and Newark Basin to the northwest and southeast of the Ramapo Fault System, respectively. Sykes (Sykes, 2008) uses the term "Ramapo Seismic Zone" (RSZ) to describe the 7.5 mi (12 km) wide eastern area of Reading Prong.

With the advent of increased seismic monitoring in the 1970's, microearthquakes were detected and located in the Ramapo Seismic Zone. Aggarwal (Aggarwal, 1978) interpreted earthquake locations and focal mechanisms to indicate reverse slip on a surface dipping 60°-65° southeast, consistent with the trace of the Ramapo Fault. Based on the history of repeated slip during the Proterozoic and the spatial correlation of epicenters with the fault trend, Aggarwal (Aggarwal, 1978) concluded that the Ramapo Fault System is active. Similarly, Yang (Yang, 1981) concluded that the Ramapo Fault System is probably the most active fault system in the greater New York City area.

However, as additional microearthquakes occurred and were studied, and earlier focal mechanisms were re-evaluated the evidence showed that, while spatially associated with the trend of the Ramapo fault, the sense of faulting was inconsistent with its reactivation. For example, Seborowski (Seborowski, 1982) determined a composite focal mechanism solution from a sequence of microearthquakes near the fault that indicated reverse motion on a north-northwest striking fault plane in response to east-northeast compression. This observation is consistent with east-northeast trend of the maximum horizontal compressive stress direction throughout most of the eastern United States (Crone, 2000).

An improved 3-D velocity model (Thurber, 1985), which shows 10-15 percent velocity difference across the Ramapo Fault, allowed the hypocenters of the earthquakes studied by Aggarwal (Aggarwal, 1978) to be relocated. Kafka (Kafka, 1985) used earthquake data of the greater New York City area and refined the catalog to eliminate station and detection bias from the network seismicity. This allowed for uniform measurement of magnitudes and earthquake locations. The results showed half of the earthquakes occurred about 6 mi (10 km) from the Ramapo Fault and about half were located about 31 mi (50 km) from this fault -- around the northern part of Newark Basin. Kafka (Kafka, 1985) concludes that "while the Ramapo Fault can by no means be ruled out as a possible source zone for earthquakes in the greater New York City area, the cause of earthquakes in this region is, in the final analysis, still unknown." In general, even though the epicenters align along the Ramapo Fault, the association is less significant than the one suggested by Aggarwal (Aggarwal, 1978) in which the Ramapo Fault system seems to dominate the seismicity (Crone, 2000).

Results of core analyses from boreholes in the vicinity of the Ramapo Fault in New York and New Jersey are inconsistent with reactivation of Ramapo Fault and related faults in the present-day stress field (Ratcliffe, 1984). Results of further core analyses from six localities near the Ramapo and other basin-border faults showed that the most recent slip was extensional at each locality and deformation did not extend beyond the Mesozoic (Sykes, 2008).

Crone and Wheeler (Crone, 2000) summarized a few reports that indicate some forms of Quaternary deformation occurred near the Ramapo Fault, but argue that none of the reports provide convincing evidence for Quaternary faulting or sudden offset which can be used to distinguish prehistoric seismic slip from aseismic creep. The Ramapo Fault has been assigned

as a Class C feature because evidence for Quaternary faulting has not been identified (Crone, 2000).

In developing the EPRI/DOE/NRC (2012) CEUS SSC model, information on the Ramapo Fault System and Ramapo Seismic Zone was considered and evaluated. Based on the evaluation and integration of available data, the TI Team did not identify the Ramapo Fault as a specific seismic source. Future seismicity in the vicinity of the Ramapo Fault System is represented by various distributed seismicity seismic sources.

2.5.1.1.4.4.1.3 Furlong-Flemington Fault System (Class C)

The Furlong Fault is located in the western portion of the Newark Basin, near New Hope in eastern Pennsylvania. This major intrabasinal Mesozoic fault connects to the north, with the Flemington fault in New Jersey (Ratcliffe, 1988). It is located about 75 mi (121 km) southeast of the BBNPP (Feature 24 in Figure 2.5-131). The Furlong and Flemington faults have been considered as one fault system (Root, 1999). Ratcliffe (Ratcliffe, 1988), using data from coring and surface observations, determined that the Furlong-Flemington fault zone consists of two closely parallel faults that dip at 47° to 50° to the southeast. Structural analysis also indicated a normal fault with some component of strike slip for the Furlong fault. Many of the Mesozoic border faults, such as the Ramapo and Flemington faults, coincide with Paleozoic thrust faults. It seems that the reactivation of the Paleozoic thrusts by Mesozoic border faults controlled the overall structure of the basin (Ratcliffe, 1985). However, there is no indication or evidence of later activity for the fault system. Seismicity has not been associated with either the Flemington or Furlong faults or with larger Chalfont Fault, which is intersected by the Furlong Fault. Based on the lack of evidence of Recent or Quaternary activity, the Furlong-Flemington Fault System has been assigned as a Class C feature (Crone, 2000).

In developing the EPRI/DOE/NRC (2012) CEUS SSC model, information on the Furlong-Flemington Fault System was considered and evaluated. Based on the evaluation and integration of available data, the TI Team did not identify the Furlong-Flemington Fault System as a specific seismic source. Future seismicity in the vicinity of the Furlong-Flemington Fault System is represented by various distributed seismicity seismic sources.

2.5.1.1.4.4.1.4 Kingston Fault (Class C)

The Kingston Fault is located in central New Jersey, approximately 87 mi (140 km) east-southeast of the BBNPP (Feature 6 in Figure 2.5-131). The Kingston Fault is 8 mi (13 km) long, north-to-northeast striking with a nearly vertical dip (Owens, 1995). The fault is located in the Mesozoic formation of the Newark Basin (Crone, 2000). Parker (Parker, 1990) showed the northern part of the fault trace on his map and reported a dip of 85° SE with extensional slip during the formation of the Basin in the Mesozoic (Stanford, 1995). Results of well, boring, and geophysical data showed movement of the southeast side of the fault based on the thickened Pliocene gravel across the fault, which is overlain by Late Pleistocene gravel, which is not offset by the fault, indicating the fault probably moved during Pliocene or Early to Middle Pleistocene (Stanford, 1995). Quaternary activity for the fault can not be demonstrated and the fault slip rate is unknown. Additionally, no paleoseismological study has been performed on the thickness of the Pliocene gravel to determine seismic creep, or different episodes of seismic faulting (Crone, 2000). According to Wheeler (Wheeler, 2005), the Kingston Fault was assigned as a Class C feature. No seismicity has been associated with the fault.

In developing the EPRI/DOE/NRC (2012) CEUS SSC model, information on the Kingston Fault was considered and evaluated. Based on the evaluation and integration of available data, the

TI Team did not identify the Kingston Fault as a specific seismic source. Future seismicity in the vicinity of the Kingston Fault is represented by various distributed seismicity seismic sources.

2.5.1.1.4.4.1.5 New York Bight Fault (Class C)

On the basis of seismic surveys, the New York Bight Fault is characterized as an approximately 31 mile (50 km) long, north-northeast-striking fault, located offshore of Long Island, New York (Schwab, 1997) (Hutchinson, 1985) (Feature 5 in Figure 2.5-131). It is 115 mi (185 km) east of the BBNPP site, and parallel to the New Jersey coast (Hutchinson, 1985). The fault offsets Upper Cretaceous rocks and Lower Tertiary and Quaternary deposits, therefore it may be as young as the Quaternary (Hutchinson, 1985).

The fault was mapped (Crone, 2000) along 24 mi (39 km) of its northern extension and dips almost vertically and was traced to within 6 mi (10 km) of the Long Island Coast (Lotto, 1997). Cretaceous to Eocene strata have been offset by the fault, but an unconformity that separates the Eocene and Miocene strata (and Miocene strata overlying it) are not offset sufficiently within the resolution of the available seismic profiles (Hutchinson, 1985), indicating that the fault is Oligocene at youngest. Later seismic reflection work indicated that middle to Late Quaternary sediments overlay Cretaceous and Tertiary strata at the fault (Lotto, 1997). These Quaternary sediments are not offset within the resolution of the measurement (3 ft (0.9 m)) (Crone, 2000).

Seismicity with small magnitudes (less than 3.00) has been located within 13 mi (21 km) from the fault. The location error for the offshore earthquakes exceeds 6 mi (10 km) (Yang, 1981) because of the seismic station distribution; therefore the location of these events is not reliable. Crone (Crone, 2000) and Wheeler (Wheeler, 2006) classify the New York Bight Fault Zone as a Class C feature, based on the lack of Quaternary activity evidence.

In developing the EPRI/DOE/NRC (2012) CEUS SSC model, information on the New York Bight Fault was considered and evaluated. Based on the evaluation and integration of available data, the TI Team did not identify the New York Bight Fault as a specific seismic source. Future seismicity in the vicinity of the New York Bight Fault is represented by various distributed seismicity seismic sources.

2.5.1.1.4.4.1.6 Mosholu Fault (Class C)

The Mosholu Fault is located in Bronx County, New York City, New York (Wheeler, 2006). The fault is approximately 135 mi (217 km) east of the BBNPP (Feature 4 in Figure 2.5-131). The Mosholu Fault was originally mapped and renamed by Baskerville (in Crone, 2000) and has been located by geological mapping and subsurface data (Crone, 2000). The fault is a 5.7 mi (9.2 km) long northwest trending right-lateral oblique-slip fault with a steep dip that crosses the Bronx River channel (Crone, 2000).

Merguerian (Merguerian, 1996) suggested that the fault showed postglacial age (since last glacial advance ~12,000 years ago) uplift forming a northwest-trending bedrock high approximately 0.3 mi (0.5 km) northeast of the Mosholu fault trace (Crone, 2000). This bedrock high, or "bulge", is a feature shown by depth-to-bedrock profiles, topographic maps, and surface exposures. The formation of the bulge is thought to have blocked the Bronx River which caused the creation of a lake behind the uplift where clay deposits settled overlying the older glacial deposits. Evidence for this is surface deformation is that the Bronx River changes course to the southeast at the bulge, the existence of the Webster Avenue lowland just south of the bulge and the clay overlying the glacial deposits north of the bulge, (Merguerian, 1997). The river would then have diverted southward across the upland, cutting the Snuff Mill gorge,

through which the Bronx River currently flows, and eventually draining the lake through the gorge (Crone, 2000). This evidence indicates that the change in river course resulted from neotectonic uplift of a block of bedrock along the northeast side of Mosholu fault in the Quaternary Period.

Crone (Crone, 2000) suggests that the bulge formed in a compressional bend during post-glacial sinistral slip on the Mosholu fault, and that once formed, the topographic expression of the bulge might have been accentuated by post-glacial fluvial erosion. However, Merguerian (Merguerian, 1997) could not conclusively prove that the uplift occurred seismically and mentioned that none of the previous New York City's magnitude approximately 5.0 earthquakes of 1737, 1783, and 1884 have been connected with surface blockage of crustal rocks and that it has not been possible to associate historic earthquakes with the faults in the New York City area. Furthermore, earthquakes have not been associated with the Mosholu Fault, but the fault has not been studied in detail for paleoseismological evidence of possible Quaternary activity. There is also no evidence with which to determine whether the uplift, if seismic, occurred in one large earthquake or many smaller ones (Crone, 2000). However, based on the circumstantial evidence from the Bronx River, Merguerian (1997) suggests that NW-trending faults in New York City area, such as the Mosholu Fault and the Dobbs Ferry Fault, are seismically capable. Overall, the attribution of the uplift to post-glacial slip on the Mosholu fault is a reasonable inference, but is not demonstrated (Crone, 2000). The Mosholu Fault has been assigned to Class C by Crone (Crone, 2000).

In developing the EPRI/DOE/NRC (2012) CEUS SSC model, information on the Mosholu Fault was considered and evaluated. Based on the evaluation and integration of available data, the TI Team did not identify the Mosholu Fault as a specific seismic source. Future seismicity in the vicinity of the Mosholu Fault is represented by various distributed seismicity seismic sources.

2.5.1.1.4.4.1.7 New Castle County Faults (Class C)

The New Castle County faults are characterized as 146 mi (235 km) long buried north and northeast-striking faults that displace an unconformable contact between Precambrian to Paleozoic bedrock and overlying Cretaceous deposits. The faults are located in northern Delaware, near New Castle, about 150 mi (242 km) southeast of the BBNPP site (Feature 9 in Figure 2.5-131).

Based on research (Spoljaric, 1973), a graben is present in New Castle County with a northeastern strike near Delaware City. The graben is bounded by faults that are part of the basement fault that underlies the Coastal Plain of Northern Delaware. The bounding faults have shown displacements ranging from 32 to 98 ft (10 to 30 m) across the basement-Cretaceous boundary (Spoljaric, 1972). Along this fault zone, earthquakes have occurred with magnitudes as high as 3.8.

According to studies completed by the Delaware Geological Survey (DGS) (McLaughlin, 2002), a subsurface investigation utilizing seismic reflection and seismic refraction, subsurface drilling, geophysical logging and trench excavation was performed to potentially locate displacement from faults near New Castle, Delaware. No shallow faults were detected during the subsurface drilling program and trench excavation. The seismic section exhibited extensive faulting at the investigation site where the New Castle fault is projected. DGS concluded that minimal, if any, modern fault activity occurred in the area of New Castle County. Wheeler (Wheeler, 2005) characterizes the New Castle County faults as a Class C features.

In developing the EPRI/DOE/NRC (2012) CEUS SSC model, information on the New Castle County Faults was considered and evaluated. Based on the evaluation and integration of available data, the TI Team did not identify the New Castle County Faults as a specific seismic source. Future seismicity in the vicinity of the New Castle County Faults is represented by various distributed seismicity seismic sources.

2.5.1.1.4.4.1.8 Upper Marlboro Faults (Class C)

The Upper Marlboro Faults are located in Prince Georges County, Maryland, approximately 150 mi (241 km) southeast of the BBNPP site (Feature 25 in Figure 2.5-131). The faults are a series of features, which cut the Coastal Plain sediments (Crone, 2000). The faults have a low angle dip, which is more consistent with a surficial origin, and extend to hypocentral depths (Crone, 2000). Wheeler (Wheeler, 2006) related the faults to surficial land slides based on low angle dips. The faults are designated as a Class C feature by Crone (Crone, 2000) and Wheeler (Wheeler, 2006) because the faults exhibit no evidence of Quaternary activity. Seismicity has not been spatially associated with the fault.

In developing the EPRI/DOE/NRC (2012) CEUS SSC model, information on the Upper Marlboro Faults was considered and evaluated. Based on the evaluation and integration of available data, the TI Team did not identify the Upper Marlboro Faults as a specific seismic source. Future seismicity in the vicinity of the Upper Marlboro Faults is represented by various distributed seismicity seismic sources.

2.5.1.1.4.4.1.9 Dobbs Ferry Fault (Class C)

The Dobbs Ferry Fault is located in Westchester County, New York about 6 mi (10 km) north-northeast of New York City (Wheeler, 2006). The fault is approximately 155 mi (249 km) east of the BBNPP (Feature 3 in Figure 2.5-131). The Dobbs Ferry Fault is a zone of abundant fractures and joints that extends southeastward from the east bank of the Hudson River and crosses the Bronx River.

The fault had dextral slip during the Mesozoic as part of the Pangaea separation (Crone, 2000). Different orientations of superimposed slickensides show more than one episode of slip on the fault. Sinistral slip can be inferred from the majority of slip sense indicators, which is consistent with the present day, east-northeast, regional orientation of the maximum horizontal compressive stress. Some indicators are dextral and older, and perhaps date from Mesozoic extension (Crone, 2000).

The October 19, 1985, Ardsley earthquake, with a magnitude of 4.1 along with six aftershocks ranging from 4 to 4.5 in magnitude, occurred in southern Westchester County, New York, approximately 19 mi (30 km) north of central Manhattan, approximately 125 mi (201 km) east of the BBNPP site. The location of the first six aftershocks (within a week of the main shock) defined a vertical northwest trending rupture zone with an approximate diameter of 2300 ft (700 m) and a depth ranging from 2.8 to 3.4 mi (4.5 to 5.5 km). The rupture zone corresponds directly to a 0.6 mi (1 km) segment of the Dobbs Ferry Fault (Hough, 1991). First motion data of the main shock and this group of aftershocks yielded well constrained focal mechanism solutions indicating sinistral slip on a northwest striking plane (Hough, 1991) (Crone, 2000). Later aftershocks defined a northeast striking plane. These results led Seeber (Seeber, 1998) to conclude that the earthquakes probably occurred on the fault zone without surface rupture along its trace.

Crone (Crone, 2000) designates the Dobbs Ferry Fault as a Class C feature because there is no paleoseismological evidence for prehistoric Quaternary seismic faulting along the Dobbs Ferry Fault.

In developing the EPRI/DOE/NRC (2012) CEUS SSC model, information on the Dobbs Ferry Fault was considered and evaluated. Based on the evaluation and integration of available data, the TI Team did not identify the Dobbs Ferry Fault as a specific seismic source. Future seismicity in the vicinity of the Dobbs Ferry Fault is represented by various distributed seismicity seismic sources.

2.5.1.1.4.4.1.10 Lancaster Seismic Zone (Class C)

The Lancaster Seismic Zone (LSZ) is located in southeast Pennsylvania and approximately coincides with Lancaster County (Armbruster, 1987). The seismic zone is of circular shape with a diameter of about 30 mi to 40 mi (50 km to 60 km) and is 55 mi (88 km) south of the BBNPP site (Crone, 2000) (Feature 8 in Figure 2.5-131). The area has been a source of seismicity for more than 2 centuries.

The LSZ consists of short discontinuous north striking faults that transect Triassic and Paleozoic rocks (Armbruster, 1987). Many studies provide evidence for a high density of northstriking, near surface structures and fractures in the LSZ (Crone, 2000). Some of the previous work, summarized by Crone (Crone, 2000), was interpreted to indicate a seismically active fault, or fault zone, in the LSZ.

Faults within the LSZ developed during the Early Mesozoic extension related to opening of the Atlantic Ocean. The LSZ crosses the Newark-Gettysburg Triassic rift basin which consists of extensional faults associated with Mesozoic rifting. The basin itself and the pre-Mesozoic basement below it appear to be aseismic. The epicenters forming the LSZ reflect this pattern; most well-located epicenters lie directly outside the Gettysburg-Newark Basin (Scharnberger, 2006) occurring on both sides of the basin where the basin is at its narrowest, between the Newark and the Gettysburg portions (Armbruster, 1987).

The LSZ marks the southwestern edge of the Newark Basin Seismic Zone (NBSZ) (Crone, 2000). Thrust faults and folds (formed during the Paleozoic Appalachian orogeny) and extensional faults (associated with Mesozoic rifting) are among the main structures along the NBSZ and LSZ (Crone, 2000). This seismicity is part of a belt that correlates with the crystalline slab emplaced on the craton by the Paleozoic detachment (Armbruster, 1987). Regional Jurassic dikes, striking north-northeast, traverse the LSZ. Coinciding with brittle faults, many of these dikes are perhaps among the youngest structures in the region and may persist as large planar zones of weakness and cut through the crust (Seeber, 1998).

In the western part of the Lancaster Seismic Zone, the epicenters of 11 events from 1889 through 1994 (with magnitudes of about 3.0 to 4.6) define a north-south trend that intersects the juncture between the Gettysburg and Newark sub-basins (Armbruster, 1987). The highest magnitude earthquakes were at Marticville in 1984 at a magnitude of 3.7 and Cacoosing Valley in 1994 at a magnitude of 4.6. The earthquakes occurred 31 mi (50 km) apart and were interpreted by Armbruster (Armbruster, 1987) to be related to tectonic fault lines.

The 1984 Marticville earthquake was the second-largest recorded event of the LSZ. Armbruster (Armbruster, 1987) suggested a shallow fault (centered at 2.5 mi (4.0 km) depth) based on the hypocentral distribution and first motion data from several recorded earthquakes of the 1984 sequence. While not spatially correlated with the trend of Paleozoic

structures in the epicenter area, the 1984 rupture geometry conforms to the strike of the Jurassic dikes and their associated faults. Earthquakes in the zone may be related with the Rockhill dike in particular (which bisects the LSZ and is close to the 1984 rupture area) and its related faults (Armbruster, 1987).

The January 16, 1994 Cacoosing Valley earthquake which struck the northeastern edge of the zone, is known to be the largest earthquake of the LSZ (Seeber, 1998). The Cacoosing Valley earthquake was of magnitude 4.6 and Modified Mercalli Intensity (MMI) VI-VII. The associated earthquake sequence, from 1994 to 1997, is discussed in more detail in Section 2.5.1.1.4.4.1.11. As is the case of 1984 Marticville earthquake, the 1994 Cacoosing Valley earthquake, and its aftershocks, provided seismological evidence for an active fault in the LSZ. The suggested faults, for both the 1984 and 1994 earthquakes, were based merely on seismological evidence. Geological evidence, such as surface rupture or liquefaction, has not been found in either case (Crone, 2000).

No other evidence of Quaternary faulting (e.g., paleoliquefaction) in the LSZ has been reported and, thus, it is designated a Class C feature (Crone, 2000). Crone (Crone, 2000) notes that even short and shallow faults can host earthquakes as demonstrated by the unusually shallow seismicity of the LSZ. There might be other deeper geologic controls on seismicity which are reflected by the shallow faults of the LSZ (Wise, 1998).

In developing the EPRI/DOE/NRC (2012) CEUS SSC model, information on the LSZ was considered and evaluated. Based on the evaluation and integration of available data, the TI Team did not identify the LSZ as a specific seismic source. Future seismicity in the vicinity of the LSZ is represented by various distributed seismicity seismic sources.

2.5.1.1.4.4.1.11 Cacoosing Valley Earthquake Sequence (Class C)

The 1993 to 1997 Cacoosing Valley earthquake sequence occurred along the eastern margin of the Lancaster Seismic Zone with the main shock occurring on January 16, 1994, near Reading, Pennsylvania about 52 mi (84 km) south of the BBNPP site (Crone, 2000) (Feature 7 in Figure 2.5-131). The environment of the Cacoosing Valley consists of many preexisting structures; the Paleozoic thrust and fold belts, Mesozoic rifting which created the Atlantic Ocean, and Jurassic igneous dikes. The largest earthquake associated with this sequence is an event of magnitude 4.6 (Crone, 2000). Forty one (41) aftershock hypocenters occurred within a cylindrical area defined by a 1 mi (1.6 km) diameter and a depth ranging from 0 to 2 mi (0 to 3.2 km). The sequence was orientated N43° W, dipping 54° SW. The main shock occurred at a depth of 1 mi (1.6 km) and aftershocks occurred from that depth to the surface (Seeber, 1998). The earthquake triggered nontectonic deformation such as sinkholes, which are common in the karst environment (Seeber, 1998).

The main shock occurred under an abandoned quarry. In December 1992, the quarry was allowed to flood with water rapidly. The unloading of the quarry, which then was abandoned and flooded with water, created enough strain to cause the rupture, most likely along preexisting structures (Seeber, 1998). The rupture zone, inferred from the aftershock locations, matched a nodal plane with reverse and left-lateral slip (strike 135°, dip 54° SW) of a focal mechanism obtained from aftershock first motions and main shock waveforms. However, the rupture did not correlate with any of the mapped faults in the area (Seeber, 1998), and the earthquake did not rupture the ground surface.

Wheeler (Wheeler, 2006) defines the seismic event as a feature where there is not sufficient evidence to demonstrate that other faulting occurred in the Quaternary and assigns the

Cacoosing Valley earthquake sequence as a Class C feature. Additional information relative to the earthquake is in Section 2.5.1.1.4.4.2.1.

In developing the EPRI/DOE/NRC (2012) CEUS SSC model, information on the Cacoosing Valley earthquake sequence was considered and evaluated. Based on the evaluation and integration of available data, the TI Team did not identify the Cacoosing Valley earthquake sequence as a specific seismic source. Future seismicity in the vicinity of the Cacoosing valley earthquake sequence is represented by various distributed seismicity seismic sources.

2.5.1.1.4.4.1.12 Moodus Seismic Zone (Class C)

The Moodus Seismic Zone is located in Middlesex and New London County, Connecticut (Wheeler, 2005). The seismic zone is approximately 190 mi (306 km) northeast of the BBNPP (Feature 1 in Figure 2.5-131). The town of Moodus is located about 20 mi (32 km) southeast of Hartford, Connecticut.

The area around the towns of Moodus and Haddam has been the most seismically active region in Connecticut, and the earliest records of earthquake activity in the area date back to the second half of the 16th century (Ebel, 1982). The largest historical earthquake occurred in 1791 and had an estimated MMI in the range of VI-VIII (Ebel, 1982) (Crone, 2000). Four shallow microearthquakes occurred in the Moodus Seismic Zone in 1980's (Ebel, 1982) (Ebel, 1989). The seismic sources of the earthquakes were reviewed utilizing geological and geophysical methods (Koch, 1978) (Crone, 2000), but no causative fault has been identified (Crone, 2000). No evidence of liquefaction or paleoliquefaction has been found in the reconnaissance efforts in the Moodus area (Gelinias, 1993). Accordingly, Crone (Crone, 2000) assigns the seismic zone as a Class C feature.

In developing the EPRI/DOE/NRC (2012) CEUS SSC model, information on the Moodus Seismic Zone was considered and evaluated. Based on the evaluation and integration of available data, the TI Team did not identify the Moodus Seismic Zone as a specific seismic source. Future seismicity in the vicinity of the Moodus Seismic Zone is represented by various distributed seismicity seismic sources.

2.5.1.1.4.4.1.13 Clarendon-Linden Fault Zone (Class C)

A major north-south trending system of thrust faults forms the Clarendon-Linden Fault Zone. The fault zone is approximately 150 mi (241 km) from the BBNPP site (Feature 20 in Figure 2.5-131). The fault zone extends over 60 mi (97 km) from near Lake Ontario in western New York State to northern Allegany County, New York (Fletcher, 1977). According to recent work, it further extends into central Allegany County, near the Pennsylvania border (Crone, 2000). The presence of a north-south striking fault was inferred from the surface geology of the area (Herrmann, 1978). Since then, the fault zone has been mapped geologically at the surface and characterized by geophysical methods such as seismic reflection within the subsurface (Crone, 2000).

The August 12, 1929 Attica earthquake, with an estimated magnitude of 5.2 (Street, 1977) and epicentral intensity of VIII, was located near the Clarendon-Linden Fault Zone. Herrmann (Herrmann, 1978) studied two other events (both with epicentral intensities VI) that occurred on January 1, 1966 and June 12, 1967 in the Attica region, and found shallow depth 1 mi to 2 mi (1.6 km to 3.2 km) for both events. The historical seismicity also shows a diffuse east-west trend that does not correlate with the north-south trend of the structure around Attica. Fault plane solutions for 1966 and 1967 events showed similar nodal planes for both events striking

about 120° and 20°. The NNE nodal plane is parallel to the Clarendon-Linden structure (Herrmann, 1978).

There is no paleoseismological evidence of Quaternary slip on the fault zone so the zone has been assigned as a Class C feature by Crone (Crone, 2000). Tuttle (Tuttle, 2002) concluded that the Clarendon-Linden Fault Zone has not generated large events (moment magnitude > 6) during the past 12,000 years based on the lack of earthquake-induced liquefaction features along the fault zone, including the area of the 1929 Attica earthquake. Tuttle (Tuttle, 2002) concluded, however, that the Clarendon-Linden Fault Zone is capable of producing future M 5 events.

In developing the EPRI/DOE/NRC (2012) CEUS SSC model, information on the Clarendon-Linden Fault Zone was considered and evaluated. Based on the evaluation and integration of available data, the TI Team did not identify the Clarendon-Linden Fault Zone as a specific seismic source. Future seismicity in the vicinity of the Clarendon-Linden Fault Zone is represented by various distributed seismicity seismic sources.

2.5.1.1.4.4.1.14 Offset Glaciated Surfaces (Class C)

Small steeply dipping faults offset glacially smoothed rock surfaces at different locations in the northeastern U.S. including Maine, Massachusetts, New Hampshire, New York, and Vermont (Crone, 2000). The closest offset glaciated surfaces are located 75 mi (121 km) northeast of the BBNPP site (Feature 23 in Figure 2.5-131). The dominantly dip slip offsets are typically small in the range of millimeter to decimeter, with some exceptions of larger displacements up to one (1) meter. Crone (Crone, 2000) summarizes a few studies of such features, but indicates that no systematic and comprehensive field or literature search has been done for such localities in the Northeast.

Although some studies favor a tectonic origin over other processes (Oliver, 1970), frost heaving is the likely origin for the offset glaciated surfaces (Crone, 2000). In the Hudson River Valley of eastern New York, Quebec, and New Brunswick, the small faults show offsets that are uniform in size over distance and are parallel to the strike of cleavage in heaved irregular sized blocks. According to Crone (Crone, 2000), tectonic origin of the small faults in the present-day stress field is unlikely because these small faults have been found in all orientations (Crone, 2000). Ratcliffe (Ratcliffe, 1982), who studied Paleozoic slates, also favors frost heaving over recent tectonic activity as the origin of the examined small faults.

Crone (Crone, 2000) concludes that evidence supports frost-wedging more than any other process as the likely origin of the small faults offsetting glaciated surfaces. Even if of tectonic origin, these small faults do not penetrate downward to significant depths and therefore are not capable of generating large earthquakes. Crone (Crone, 2000) mentions that offset glaciated surfaces are Quaternary in age but classify them as Class C features based on the conclusion that the small faults with limited length and depth extent do not affect seismic hazard significantly. These small faults have been observed over a large area in 5 states and there has been no seismicity associated with them.

In developing the EPRI/DOE/NRC (2012) CEUS SSC model, information on the offset glaciated surfaces was considered and evaluated. Based on the evaluation and integration of available data, the TI Team did not identify offset glaciated surfaces as a specific seismic source. Future seismicity in the vicinity of offset glaciated surfaces is represented by various distributed seismicity seismic sources.

2.5.1.1.4.4.1.15 Fall Lines of Weems (Class C)

Weems (Weems, 1998) identified numerous short stream segments or fall zones with steep gradients while examining longitudinal profiles of major rivers that flow southeastward or northwestward across the Piedmont and Blue Ridge provinces of North Carolina and Virginia. The northeastern tip of the Blue Ridge fall line is located about 140 mi (225 km) southwest of the BBNPP site (Feature 26 in Figure 2.5-131).

Weems (Weems, 1998) noticed the alignment of fall zones of different streams and used the term "fall lines" for the curvilinear trend of the alignments. He defined seven fall lines that trend northeastward, paralleling the regional tectonic fabric and gravitational gradient of the Appalachian Orogeny. The fall lines tend to merge northeastward. Weems (Weems, 1998) states that "limited available evidence favors a neotectonic origin" for the fall lines and rules out climate control.

Wheeler (Wheeler, 2005) argues that the identification of fall zones is subjective; therefore Weems' (Weems, 1998) arguments and conclusions depend on the choice of the fall zones. Wheeler (Wheeler, 2005) concludes that tectonic faulting is not yet demonstrated for the fall lines and assigns the fall lines as a Class C feature. The fall lines of Weems have not been associated with seismicity.

In developing the EPRI/DOE/NRC (2012) CEUS SSC model, information on the fall lines of Weems (Weems, 1998) was considered and evaluated. Based on the evaluation and integration of available data, the TI Team did not identify the fall lines as a specific seismic source. Future seismicity in the vicinity of the fall lines is represented by various distributed seismicity seismic sources.

2.5.1.1.4.4.1.16 Everona Fault-Mountain Run Fault Zone (Class C)

The Mountain Run Fault Zone is a regional geologic and tectonic feature of central Virginia, which extends from the eastern margin of the Mesozoic Culpeper Basin near the Rappahannock River southwestward, to near Charlottesville, VA (Pavlides, 1986) (Pavlides, 1994). The 60 to 95 mi (97 to 153 km) long, northeast trending fault zone is located about 180 mi (290 km) southwest of the BBNPP site (Wheeler, 2006) (see Feature 16 in Figure 2.5-131). The fault zone forms part of the southeast boundary of Early Mesozoic Culpeper Basin.

The Everona Fault occurs in close proximity to the Mountain Run Fault Zone (about 0.6 mi (1.0 km)) and has an estimated age of Late Cenozoic (Crone, 2000) (Bobyarchick, 2007). The fault exhibits reverse movement and dips about 20° NW, truncating layers of rock in the footwall of the Mountain Run fault zone (Bobyarchick, 2007). This small fault displaces the base of Late Tertiary or Pleistocene gravel located about 0.6 mi (1.0 km) west of the Mountain Run Fault Zone (Wheeler, 2006).

Thrust faulting along the Mountain Run Fault Zone started at the end of Ordovician, as represented by mylonite. Subsequent strike-slip movement in the fault zone, related to extension and formation of the Culpeper Basin, occurred prior to Middle Mesozoic, as concluded from undeformed basaltic dikes of Jurassic age that cut the Mountain Run Fault Zone rocks (Pavlides, 1994). To the northeast, two scarps occur along the fault zone: (1) Mountain Run scarp, located on the southeast side of the Mountain Run Fault Zone, extends for 8 mi (13 km), and (2) Kellys Ford scarp, located on the northeast part of Mountain Run Fault Zone, is 1.2 mi (2 km) long and is the southeastern bounding fault of the Mesozoic Culpeper Basin (Pavlides, 1994). Pavlides (Pavlides, 1994) argued that the rugged topography of both scarps implies Cenozoic or possibly Pleistocene age. Based on the displaced sub-unconformity

saprolites overlaying a basal gravel cover layer in the area, the Everona Fault is a structure of tectonic origin involving the basement, and is not confined to the overlying surficial deposits (Bobyarchick, 2007).

Crone (Crone, 2000) and Wheeler (Wheeler, 2006) conclude that, while the faulting at Everona is likely to be of Quaternary age, no Quaternary activity has been demonstrated for the feature. They classify the feature as Class C, but mention that this feature did not have a detailed paleoseismological study to determine whether it has been a site of Quaternary earthquake. Additional investigation has been done for the North Anna Early Site Permit which shows that Mountain Run Fault Zone has not been active during the Quaternary (Bobyarchick, 2007).

In developing the EPRI/DOE/NRC (2012) CEUS SSC model, information on the Everona Fault-Mountain Run Fault Zone was considered and evaluated. Based on the evaluation and integration of available data, the TI Team did not identify the Everona Fault-Mountain Run Fault Zone as a specific seismic source. Future seismicity in the vicinity of the Everona Fault-Mountain Run Fault Zone is represented by various distributed seismicity seismic sources.

2.5.1.1.4.4.1.17 Stafford Fault System (Class C)

The Stafford fault system approaches within 180 mi (290 km) south of the site (Feature 18 on Figure 2.5-131). The 42 mi (68 km) long fault system strikes approximately N35°E for a distance of 45 mi (72 km) along the west bank of the Potomac River in northeastern Virginia (Mixon, 1977). The Stafford Fault System consists of five northwest dipping, high-angle reverse faults and follows the inner margin of the Coastal Plain province. Four faults, the Dumfries Fault Zone, Fall Hill Fault, Hazel Run Fault, and an unnamed fault, strike northeast. The fifth fault is the Brooke Fault Zone, northeast of the unnamed fault. Toward its northernmost end, the Brooke Fault Zone is named the Tank Creek Fault (Wheeler, 2005). The Stafford Fault System was originally activated in the Early Cretaceous time. The Fall Hill Fault shows additional displacement of Pliocene-Pleistocene-age sandy gravel, and Cretaceous strata (Mixon, 2000).

Recurrent movement has been demonstrated on the Stafford Fault System by displacements that decrease upward in the Coastal Plain (Mixon, 1977). None of the reports and maps used by Wheeler (Wheeler, 2005) documented Quaternary activity on any faults of the Stafford Fault System. The youngest movement, demonstrating Late Tertiary activity, has been documented on the Fall Hill Fault, of the Stafford Fault System, which offsets Pliocene-Pleistocene sandy gravel (Wheeler, 2005). The Stafford Fault System was assigned to Class C based on lack of evidence of Quaternary slip.

Marple (Marple, 2004) suggested a significantly longer Stafford Fault System that extends from Fredericksburg, Virginia to New York City (Marple, 2004). It was proposed as part of a northeastern extension of the East Coast Fault System, previously postulated by Marple (Marple, 2000). Despite the suggested correlation of some historical earthquakes with the northern extension of the fault system by Marple (Marple, 2000), seismicity data show a poor association between earthquake epicenters and the extended segment of the Stafford Fault System.

In developing the EPRI/DOE/NRC (2012) CEUS SSC model, information on the Stafford Fault System was considered and evaluated. Based on the evaluation and integration of available data, the TI Team did not identify the Stafford Fault System as a specific seismic source. Future

seismicity in the vicinity of the Stafford Fault System is represented by various distributed seismicity seismic sources.

2.5.1.1.4.4.2 Relevant Tectonic Features with Associated Seismicity

Within a 200 mi (322 km) radius of the BBNPP site, eight (8) Relevant Tectonic Features with Associated Seismicity (Shown on Figure 2.5-131) were identified. Descriptions follow for the eight (8) features that were evaluated as possible contributors to the seismic hazard at the BBNPP site.

These features are labeled below with the reference numbers utilized on Figure 2.5-131 in parentheses:

1. New York-Alabama Lineament (28)
2. Hudson River Valley Trend (27)
3. Pittsburgh-Washington Lineament (30)
4. Tyrone-Mt. Union Lineament (29)
5. Bristol Block Geopotential Trends (31)
6. Reading Prong (51)
7. Peekskill-Stamford Seismic Boundary (52)
8. Dillsburg microearthquake swarm (53)

2.5.1.1.4.4.2.1 New York-Alabama Lineament

The northeast trending New York-Alabama Lineament (NY-AL) is characterized by aeromagnetic mapping and regional gravity data which extends more than 1,000 mi (1,609 km) from Alabama to New York (King, 1978). The closest approach of the NY-AL is approximately 30 mi (48 km) west of the BBNPP site (Feature 28 in Figure 2.5-131, Figure 2.5-156 and Figure 2.5-158). The NY-AL in Pennsylvania has been disrupted or offset between two major features called the Tyrone-Mt. Union (TMU) lineament and the Pittsburgh-Washington (PW) lineament (Lavin, 1982). The TMU and PW crustal features define the boundaries of a northwest trending feature called the Lake Erie-Maryland crustal block. A right-lateral offset of 38 mi (61 km) along the TMU is indicated by disruption of the NY-AL in southwestern Pennsylvania (Lavin, 1982). Earthquakes have occurred at different locations along the feature, however, their association with the feature cannot be established (EPRI, 1986). Johnston (Johnston, 1985a) concluded that between 80% and 90% of southern Appalachian earthquakes recorded from 1981 to 1983 lie between the NY-AL and a parallel structure to the southeast called Clingman-Ocoee lineament. Johnston (Johnston, 1985a) further concludes that the NY-AL and the Clingman-Ocoee lineament do not appear to be seismogenic but rather bound the crustal block that generates the earthquakes. Appalachian seismicity occurs beneath the decollement which separates thrust and folded Paleozoic rocks from Precambrian basement rocks, indicating that Appalachian seismicity is not related to tectonic and geological features at the surface (Johnston, 1985b).

Kauffman (Kauffman, 1999) inverted travel time residuals from relocated earthquakes in southeastern Tennessee to obtain the velocity structure of the local upper crust. They stated that the results do not agree with the NY-AL as a linear feature extending through southeastern Tennessee parallel to contours in gravity anomalies. The southeastern Tennessee

seismicity is not constrained by major crustal features but is rather associated with low velocity regions at midcrustal depths. Joint hypocenter-velocity inverted on the eastern Tennessee seismic zone suggests a strong low-velocity zone parallel to the seismicity with a northeast trend. The southern margin of this trend coincides with the NY-AL. According to Vlahoic (Vlahoic, 1998), research utilizing 3-D velocity earthquake data showed that most earthquakes were located in regions of average velocity or small velocity anomalies, rejecting the association of eastern Tennessee seismicity with low velocity regions in the crust (Vlahoic, 1998).

In developing the EPRI/DOE/NRC (2012) CEUS SSC model, information on the NY-AL was considered and evaluated. Based on the evaluation and integration of available data, the TI Team did not identify the NY-AL as a specific seismic source. Future seismicity in the vicinity of the NY-AL is represented by various distributed seismicity seismic sources.

2.5.1.1.4.4.2 Hudson River Valley Trend

Also known as the Hudson River Line (HRL), this feature trends north-south for about 156 mi (251 km) along the Hudson River Valley in New York, coming as close as 120 mi (193 km) NE of the BBNPP site (Feature 27 in Figure 2.5-131, Figure 2.5-156 and Figure 2.5-158). The feature is weakly associated with the western part of an isostatic gravity low that extends from the New Jersey border to the southeastern edge of Adirondack gravity high. Due to large uncertainty in subsurface geometry, the actual structure of the gravity feature is not determined (EPRI, 1986).

Based on early instrumentally recorded microseismicity (Yang, 1981), the feature was seismically limited. Subsequent observations of seismicity indicate that few earthquakes are located along some parts of the trend. Moderate-sized earthquakes occur only near the edges of the feature. The overall spatial distribution of seismicity does not indicate the localization of activity along the trend. Recent earthquakes west of the Hudson River range in estimated depth from 9 to 12 mi (14 to 19 km), indicating the possibility of a deep structure, but this is not supported by the isostatic gravity data (Yang, 1981). No evidence of the recent tectonic activity has been demonstrated and, based on the foregoing discussion, seismicity is only poorly associated with the feature.

In developing the EPRI/DOE/NRC (2012) CEUS SSC model, the Hudson River Valley Trend was not explicitly evaluated. However, seismicity and geophysical data underlying the interpreted trend were considered and evaluated in developing the model. Based on the evaluation and integration of available data, the TI Team did not identify the Hudson Valley River Trend as a specific seismic source. Future seismicity in the vicinity of the Hudson Valley River Trend is represented by various distributed seismicity seismic sources.

2.5.1.1.4.4.3 Pittsburgh-Washington and Tyrone-Mt Union Lineament

These two lineaments have been identified from analysis of regional gravity and magnetic patterns, LANDSAT images and geological data (Lavin, 1982). Trending NW-SE, they cross the Appalachian orogen to the vicinity of Lake Erie (EPRI, 1986). The Pittsburgh-Washington (PW) and Tyrone-Mt. Union (TMU) lineaments are interpreted as expressions of deep crustal fracture zones that extend over a distance of 375 mi (600 km) across western Pennsylvania and parts of surrounding states. The PW and TMU lineaments are located approximately 115 mi (185 km) southwest of BBNPP site (Features 29 and 30 in Figure 2.5-131, Figure 2.5-156 and Figure 2.5-158) (Rodgers, 1984).

The TMU and PW lineaments are parallel and form the NE and SW boundaries, respectively, of the Lake Erie-Maryland crustal block (Lavin, 1982). Major crustal displacements occurred along

the TMU lineament during Late Cambrian to Early Ordovician time. There is no concentration of seismicity along the TMU lineament.

Evidence for displacement along PW lineament is not as strong as for the TMU lineament. A concentration of seismicity is observed near the northern end of PW lineament in northeastern Ohio, but earthquake activity is not localized along the feature in general (EPRI, 1986).

In developing the EPRI/DOE/NRC (2012) CEUS SSC model, the PW and TMU lineaments were not explicitly evaluated. However, seismicity and geophysical data underlying the interpreted lineaments were considered and evaluated in developing the model. Based on the evaluation and integration of available data, the TI Team did not identify the PW and TMU lineaments as a specific seismic source. Future seismicity in the vicinity of the PW and TMU lineaments is represented by various distributed seismicity seismic sources.

2.5.1.1.4.4.2.4 Bristol Block Geopotential Trends

The Bristol Block is an area of magnetic and gravity lows and extends from Tennessee to Pennsylvania. It is bordered by the NY-AL on the west, and by the Clingman-Ocoee lineament on the east (Feature 31 on Figure 2.5-131, Figure 2.5-156 and Figure 2.5-158). The northern portion of the Block is located about 80 mi (130 km) southwest of the site (EPRI, 1986).

The Bristol Block includes a series of low gravity and magnetic anomalies. Some seismicity is associated with the block and, because of the large area of the geophysical anomalies, some earthquakes are spatially associated with them. In particular, the Giles County, Virginia seismic zone is located within the Bristol Block. However, not all inferred tectonic features (i.e., geophysical anomalies) are associated with seismicity.

In developing the EPRI/DOE/NRC (2012) CEUS SSC model, the Bristol Block was not explicitly evaluated. However, seismicity and geophysical data underlying the hypothesized block were considered and evaluated in developing the model. Based on the evaluation and integration of available data, the TI Team did not identify the Bristol Block as a specific seismic source. Future seismicity in the vicinity of the Bristol Block is represented by various distributed seismicity seismic sources.

2.5.1.1.4.4.2.5 Reading Prong

The Reading Prong massif is a major Precambrian complex, one of several outcropping between the sedimentary rocks of the Appalachian basin and the Paleozoic metamorphic terrains of New England and the southeastern Piedmont (Wolf, 2003). At its closest approach, it is approximately 50 mi (80 km) east of the BBNPP site (Feature 51 in Figure 2.5-131).

Metamorphism of the Reading Prong rocks occurred during the Grenville Orogeny, approximately 1.2 billion years ago, and the area was also extensively intruded by synorogenic granites during the same Grenville event. Subsequently, between the Late Proterozoic and the Mesozoic, the rocks throughout the region suffered periodic episodes of deformation. An especially intense episode occurred during the Late Permian Alleghanian Orogeny when the region was pervasively fractured during the development of imbricated thrust sheets (Wolf, 2003).

The rocks of the Reading Prong are allochthonous and represent an overlapping stack of thrust sheets that have been thrust over the Paleozoic Rocks of the Great Valley to the north

(Senior, 2006). The thrusting juxtaposed the Precambrian rocks in a structurally high position relative to the thick section of Lower Paleozoic rocks immediately to the west.

A schematic representation of the development of the Reading Prong nappe megasystem is depicted in Figure 2.5-155 (Drake, 1999). In Figure 2.5-155 (Item A), extensional faults related to the opening of a small ocean basin or the Iapetus Ocean formed on the margin of the Laurentian craton during the Late Proterozoic or earliest Cambrian. Continuing in Figure 2.5-155 (Item B), the shelf collapse related to the attempted subduction of Laurentia beneath the Microcontinent at the beginning of the Taconic orogeny allowed the formation of the Martinsburg foreland basin during the Middle Ordovician. Finally in Figure 2.5-155 (Item C) the closing of the small ocean basin or the Iapetus Ocean during the early Late Ordovician Taconic orogeny reactivated the extensional faults as thrust faults, forming the nappe megasystem.

Subsequent thrust faulting during the Alleghanian Orogeny greatly complicated the nappe megasystem. Rifting related to the opening of the Atlantic Ocean during the Late Triassic reactivated the thrust faults on the southeast as listric extensional faults. The amount, if any, of extensional movement of the other thrust faults is currently not known. This model presented by Drake (Drake, 1999) suggests three periods of movement on the same faults: extensional, contractional, and extensional. Figure 2.5-154, in a non-eroded idealized cross section, shows the close relation between the Reading Prong Province and the nappes that contain the West Chester and Avondale Massifs, as well as the Philadelphia Terrane to the SE. Continental shelf that constitutes the ramp, in which the Reading megasystem and the York terrane are thrust, is shown to the NW.

Sykes (Sykes, 2008), as a result of the observations on a catalog of 383 earthquakes in the Greater New York City - Philadelphia Area, observes that most hypocenters are concentrated in older terranes bordering the Mesozoic Newark basin (Reading, Manhattan, and Trenton prongs) and in similar rocks found at a shallow depth beneath the coastal plain from south of New York City across central New Jersey.

This seismicity includes a belt of activity of about 30 km (18.6 mi) located to the northwest of the Newark basin. This belt contains earthquakes that occurred in 1881, 1951, 1957, and 2003 plus numerous smaller earthquakes. Most of these earthquakes, especially those located instrumentally, are concentrated in the eastern Reading Prong between the Green Pond syncline and the Mesozoic Ramapo Fault.

Other activity in the Reading Prong extends as far northwest as the westernmost outcrops of Precambrian rock. A band of high activity strikes about N 100 W and extends from the Ramapo Fault across the entire Reading prong (Sykes, 2008). The lower boundary of activity beneath the Reading Prong appears to dip southeasterly and may be controlled by one or more Paleozoic imbricate thrust faults that sole into a master sub-horizontal detachment fault whose depth is as great as the 12-15 km (7-9 mi) (Sykes, 2008).

In developing the EPRI/DOE/NRC (2012) CEUS SSC model, information on the Reading Prong was considered and evaluated. Based on the evaluation and integration of available data, the TI Team did not identify the Reading Prong as a specific seismic source. Future seismicity in the vicinity of the Reading Prong is represented by various distributed seismicity seismic sources.

2.5.1.1.4.4.2.6 Peekskill-Stamford Seismic Boundary

Instrumental data recorded since 1971 shows that activity in the Manhattan Prong cuts off abruptly along a nearly vertical, northwest-striking boundary that extends from Stamford, Connecticut, to Peekskill, New York (Feature 52 on Figure 2.5-131). The boundary is named the Peekskill-Stamford boundary by Sykes and others (Sykes, 2008). Identification of the boundary became possible after accurate locations and depths of earthquakes, especially those east of the Hudson River, became available with the installation of a seismic station near the New York-Connecticut border in 1971. The Peekskill-Stamford boundary coincides near its western end with the boundary between the Manhattan Prong and the Hudson Highlands, and it may be considered as a ramification of the Ramapo Fault Zone. There are no large magnitude earthquakes associated with this feature, although micro seismicity is present.

In developing the EPRI/DOE/NRC (2012) CEUS SSC model, information on the Peekskill-Stamford Seismic Boundary was considered and evaluated. Based on the evaluation and integration of available data, the TI Team did not identify the Peekskill-Stamford Seismic Boundary as a specific seismic source. Future seismicity in the vicinity of the Peekskill-Stamford Seismic Boundary is represented by various distributed seismicity seismic sources.

2.5.1.1.4.4.2.7 Dillsburg Microearthquake Swarm

From October 2008 (or earlier) through August 2009, an intense microearthquake swarm of over 600 felt events occurred near Dillsburg, York County, Pennsylvania (Kim, 2009). The area is located near the northern margin of the Gettysburg Mesozoic basin, approximately 80 miles (129 km) southwest of the BBNPP site. This swarm of activity was studied by Kim (2009) in 2008.

Seismograph stations in the mid-Atlantic region detected and located the activity which included 23 shocks with magnitudes ranging from 0.8 to 2.9. Based on reports from residents, the apparent center of the seismic activity was around Old York Road and Mandy Lane in York County (Kim, 2009). To better characterize and understand the seismic activity, a portable seismograph network was installed around the center of activity from October 24 through December 11, 2008. This network detected 49 microearthquakes distributed along an approximately 1 mile (1.5 km) long northwest-southeast linear trend along Old York Road, but only one (M 1.4) was large enough to be detected by regional permanent networks (Kim, 2009). The hypocenters for these shocks were less than 0.6 mi (1 km), with an average depth of about 1600 ft (0.5 km) (Kim, 2009). Despite their small magnitudes, the earthquakes caused booming sounds and noticeable shaking but no significant damage was reported. The shallow depth corresponds roughly to the base of a thick sheet of diabase rather than a well-defined fault (Kim, 2009).

The diabase was mined in the past for iron, but the focal depths are deeper than would be expected if the old mines had a direct role in the origin of the earthquakes. Instead, it is theorized that the activity is due to a concentration of stress along the contact between the diabase and underlying sedimentary rocks due to a contrast in strength between the two different rock types under the current east northeast-west southwest horizontal compressional stress regime in the eastern U.S. (Kim, 2009). The seismic activity may be localized along this contact by the presence of a preexisting zone of weakness (fractures) in the rock. Another contributing factor could be if there was a recent change in the level of the groundwater table in the area. The exact cause and timing of the earthquake swarm at this point is still unknown.

In developing the EPRI/DOE/NRC (2012) CEUS SSC model, information on the Dillsburg Earthquake Swarm was not explicitly evaluated. However, earthquakes from the swarm through 2008 with magnitude greater than 2 are included in the CEUS SSC earthquake catalog and thus form part of the database used to evaluate and integrate available information to characterize seismic sources. Future seismicity in the vicinity of the Dillsburg Earthquake Swarm is represented by various distributed seismicity seismic sources that are included in the BBNPP site PSHA.

2.5.1.1.4.4.3 Relevant Tectonic Features with No Associated Seismicity

A total of 24 tectonic features have been identified with no associated seismicity.

Of these 24, six are located within the site vicinity (25 mi (40 km) radius). Tectonic structures and features closest to the BBNPP site are relatively more important because of their proximity and are discussed first. These six features and other structures listed in this subsection are shown on Figure 2.5-140 (site vicinity), Figure 2.5-131, and Figure 2.5-139 (site area). Based on review of published literature and historical seismicity, there is no reported geomorphic expression, historical seismicity, or Quaternary deformation along any of the twenty four features identified below. Thus they are not considered to be a capable tectonic source for calculating the seismic hazard for BBNPP.

- ◆ Berwick Anticlinorium (Section 2.5.1.1.4.4.3.1)
 - ◆ Light Street Thrust Fault (Section 2.5.1.1.4.4.3.1.1)
 - ◆ Berwick Fault (Section 2.5.1.1.4.4.3.1.2)
- ◆ Lackawanna Synclinorium (Section 2.5.1.1.4.4.3.2)
- ◆ Anthracite Region (Section 2.5.1.1.4.4.3.3)
- ◆ Catawissa-McCauley Mountain Synclinorium (Section 2.5.1.1.4.4.3.4)
- ◆ Scranton Gravity High (Section 2.5.1.1.4.4.3.5)
- ◆ Yellow Breeches Fault Zone (Section 2.5.1.1.4.4.3.6)
- ◆ Rome Trough (Section 2.5.1.1.4.4.3.7)
- ◆ Pleasant Valley-Huntingdon Valley Fault (Section 2.5.1.1.4.4.3.8)
- ◆ Transylvania Fault Zone (Section 2.5.1.1.4.4.3.9)
- ◆ Plummers Island and Pleasant Grove Shear Zones (Section 2.5.1.1.4.4.3.10)
- ◆ Newark-Gettysburg Basin (Section 2.5.1.1.4.4.3.11)
- ◆ Hartford Basin (Section 2.5.1.1.4.4.3.12)
- ◆ Connecticut Basin (Section 2.5.1.1.4.4.3.13)
- ◆ Brandywine Fault System (Section 2.5.1.1.4.4.3.14)
- ◆ Martic Fault (Section 2.5.1.1.4.4.3.15)
- ◆ East Border Fault (Section 2.5.1.1.4.4.3.16)

- ◆ Broadtop Synclinorium (Section 2.5.1.1.4.4.3.17) |
- ◆ Sweet Arrow Fault (Section 2.5.1.1.4.4.3.18) |
- ◆ Chestnut Ridge Anticline (Section 2.5.1.1.4.4.3.19) |
- ◆ Philadelphia Structural Block (Section 2.5.1.1.4.4.3.20) |
- ◆ Potomac and Westminster Terranes including the Pleasant Grove Shear Zone (Section 2.5.1.1.4.4.3.21) |
- ◆ Baltimore Gneiss Terrane (Section 2.5.1.1.4.4.3.22) |

2.5.1.1.4.4.3.1 Berwick Anticlinorium

The principal bedrock structure within the site area is the Berwick Anticlinorium (also referred to as the Montour Anticline (Pohn, 2000)), which has been described (Inners, 1978) as "a moderately complex, first order fold which trends in a northeast-southwest direction". The bedrock map and section of the Berwick Quadrangle (Inners, 1978) shows the formations at the BBNPP site area to consist of Silurian, Devonian, and Carboniferous rocks that have been gently folded, with limited faulting (Figure 2.5-134 and 137). The BBNPP site is situated on the northern limb of the fold, with beds that are dipping between 10 and 20 degrees to the north-northwest. Two faults have been mapped in the vicinity: the Light Street fault located on the northern limb of the fold, and the Berwick fault, inferred to be on the southern limb of the fold. The northeast ends of both faults lie within the site area, but do not directly underlie the Site. Both faults are considered folded faults, therefore there is limited chance for these to be reactivated in the contemporary stress regime. |

Inners (1978) prepared a lithostratigraphic column along an almost 9 mi (14.5 km) long stretch of the Berwick Quadrangle that intersects much of the BBNPP site area. When these stratigraphic columns are compiled into a cross section (Figure 2.5-137), they collectively provide an almost 9 mi (14.5 km) long, nearly continuous exposure of Silurian, Devonian, and Mississippian formations. Inners (1978) stratigraphic analysis indicates that these Paleozoic formations dip to the north on the north side of the Susquehanna River and dip to the south on the south side. Erosional processes of the Berwick Anticlinorium have produced two mountain ridges, Lee Mountain to the north of the site and Nescopeck Mountain to the south, and have produced similar topography on each mountain (Inners, 1978). The Light Street and Berwick faults are also mapped on this cross section, as seen in Figure 2.5-137. The apparent structural relief of the Berwick Anticlinorium is approximately 12,000 ft (3,658 m) with a wavelength of about 8.2 mi (13.2 km) (Inners, 1978). Quaternary deposits overlying the site show no signs of faulting or folding. |

2.5.1.1.4.4.3.1.1 Light Street Thrust Fault

The Light Street Thrust Fault is the wedge fault located approximately 2 mi (3.2 km) west of the BBNPP site and is the closest tectonic feature to the BBNPP site. The fault dips to the south, at a small angle of 10 to 30 degrees to stratigraphic bedding, and has a northeast-southwest orientation (Inners, 1978). The fault is located in the north side of the Berwick anticlinorium and extends for about 20 mi (32 km) west of Berwick. The fault overlaps the Old Port and Keyser formations. Based on review of published literature and historical seismicity, there is no reported geomorphic expression, historical seismicity, or Quaternary deformation along the Light Street Thrust Fault. Thus, this feature is not considered to be a capable tectonic source. |

2.5.1.1.4.4.3.1.2 Berwick Fault

In conjunction with the Light Street Fault as discussed above, the Berwick Fault is mapped as inferred and is based on limited surface data and a water well log drilled at the Berwick Lumber and Supply Company at 329 West Second Street in Berwick, PA (Inners, 1978). The BBNPP site investigators were unable to locate this well and it was possibly abandoned prior to the site investigation. The inferred Berwick Fault lies within the site area and comes to within approximately 3.5 mi (5.6 km) of the BBNPP site. The exact length of the Berwick Fault is not completely mapped and is believed to be a south-dipping reverse fault on the south flank of the BBNPP (Inners, 1978).

Inners (Inners, 1978) also states that the Berwick fault extends east-northeastward into an exposed third order anticline in the Marcellus-Mahantango interval. Inners (Inners, 1978) attributes the presence of the Berwick Fault to the folding and faulting actions that occurred at the site area during the Alleghanian Orogeny. There is no seismicity associated with this feature, nor is there any geomorphic evidence of Quaternary deformation. The Berwick fault is not considered to be a capable tectonic source.

A review and interpretation of aerial photography and digital elevation models of the BBNPP site area identified few discontinuous north to northeast-striking lineaments. None of these lineaments were interpreted as fault-related, nor coincident with the Light Street Fault, Berwick Fault, or the other previously inferred Paleozoic structures mapped by Inners (Inners, 1978) and Berg (Berg, 1980). A review of regional geologic sections suggest that the features postulated by Inners (Inners, 1978), if present, are not moderate or prominent structures, and do not deform Quaternary strata. In summary, on the basis of regional and site geologic and geomorphic data, there are no known faults within the site area that pose a structural hazard to the site, including the poorly constrained Light Street and Berwick faults that lie within the southwestern section of the 5 mi (8 km) radius of the site.

2.5.1.1.4.4.3.2 Lackawanna Synclinorium

The Lackawanna Synclinorium is a first order fold syncline that trends southwest-northeast. Its western extent is mapped north-northeast of the BBNPP site area just outside of the 5 mi (8 km) radius (Feature 2 on Figure 2.5-131 and Figure 2.5-139) (Inners, 1978). The Lackawanna Synclinorium is a 68 mi (110 km) long structural trough in the Appalachian foreland of northeastern Pennsylvania with a maximum width of 9 mi (15 km) (Harrison, 2006).

There are numerous unnamed faults within the Lackawanna Synclinorium. These are folded faults and as result there is limited chance for these to be reactivated in the contemporary stress regime.

In map view (Figure 2.5-140), its hinge displays a concave-to-the-foreland (concave towards the west) curve. Explanation of its map-view curvature with respect to the regional structural grain has led to multiple tectonic models for the synclinorium and the Pennsylvania salient (Harrison, 2006). The entire synclinorium was thought to be an Alleghanian thin-skinned contractional structure that formed similarly to the fold trains of the central Appalachian Valley and Ridge province (Harrison, 2004). Interpretation of seismic reflection data across the structure, however, suggests that the synclinorium formed primarily by the removal of salt. The trend of the central and northern synclinorium reflects the location of the collapse of the Upper Silurian Salina salt and the north-northwest trend does not represent a significant east-west shortening event (Harrison, 2006; Frey, 1973). In the southern synclinorium, the structure translated northwestward over a thrust ramp joining detachments in the Cambrian Waynesboro Formation and the Salina Group (Harrison, 2004).

Thus, only the southern part of the basin was affected by significant layer parallel shortening (LPS) and folding. The dominant approximately 75-degree LPS fabrics (folds, faults, cleavage) in the synclinorium that parallel the regional folds of the Valley and Ridge, formed in the hanging-wall strata above the Pottchunk fault, a basin-wide Alleghanian detachment (Harrison, 2006). Crosscutting relationships of LPS structures from within the synclinorium indicate that the horizontal component of shortening rotated approximately 45 degrees clockwise through time suggesting that movement along the Salina Group detachment followed movement along the Pottchunk fault (Harrison, 2006). After movement along the Pottchunk fault, collapse of the post-Salina overburden formed much the synclinorium. Thus, the Lackawanna synclinorium is a structure affected by pulses of deformation and overburden collapse (Harrison, 2006).

In addition to the flexural-slip mechanisms responsible for many of the folds in the mapped area of Figure 2.5-140, flexural-flow folding was likely another strong component to their formation (Inners, 1978). Inners (Inners, 1978) identifies several features of flexural-slip folds evident in the Berwick Quadrangle including the common occurrence of slickenlines on bedding surfaces and maintenance of approximately the same bedding thickness across the folds. Flexural-flow folding characteristics, within any structure, include prominent cleavage in argillaceous rocks and thickening of beds within the hinges.

There is no seismicity associated with the features (Inners, 1978); the hypothetical features are not aligned or associated with gravity and magnetic anomalies, nor are there data to indicate that the features proposed by Inners (Inners, 1978) are capable tectonic sources.

2.5.1.1.4.4.3 Anthracite Region

The Anthracite region (Feature 35 on Figure 2.5-131), located on the diminishing, east-plunging, first-order folds in eastern Pennsylvania, is the most faulted area of the Appalachian Ridge and Valley province (Faill, 1999a). It is composed of four main fields, the Northern, Eastern Middle, Western Middle and Southern Anthracite Fields (Hornberger, 2004). The Northern Field is situated in the Lackawanna Synclinorium described above, and the other three fields make up the Anthracite Upland Section south of the BBNPP site. According to Wood (1986 in Hornberger, 2004): "Each coal field of the Anthracite Region is a complexly folded and faulted synclinorium, with structural trends between N55°E and N85°E. The Southern field is the most highly deformed, with several highly faulted, closely spaced synclinal basins. Deformation is most complex toward the southeast, where it is characterized by hundreds of thrust, reverse, tear and bedding plane faults and tightly compressed, commonly overturned folds." The Southern field is structurally complex with large structural features such as the Minersville Synclinorium, the New Bloomfield Anticlinorium and the Broad Mountain Anticlinorium, as well as individual anticlines, synclines and fault complexes within these three major structural features (Hornberger, 2004). The dominant faults consist of thrust faults, as part of the base décollement. The thrust faults are dominantly located in the cores of the anticlines. These faults tend to be low angle dipping and transect the bedding planes along the northwest limbs of the folds (Faill 1999a). Other faults associated with these structures are steeply dipping and are parallel to the stratigraphic beds located in the southeast limbs of the anticlines. The highly faulted zone of the Western Middle and Southern fields are as close as 15 mi (24 km) south of the site. However, these fault systems were last active during the post-Carboniferous period (Allegheny Orogeny) and are no longer a seismic hazard. Based on a review of published literature and historical seismicity, there is no reported geomorphic expression, historical seismicity, or Quaternary deformation along the Anthracite region. Although this feature is not considered to be a capable seismic source, there have been reported earthquake epicenters associated with mining activities (collapse, blasting).

2.5.1.1.4.4.3.4 Catawissa-McCauley Mountain Synclinorium

The only mention to this structure is in Inners (Inners, 1978) when he refers to the two first order Alleghanian Orogeny related folds structures (Lackawanna Synclinorium and Catawissa-McCauley Mountain Synclinorium) shown Figure 2.5-139 and Figure 2.5-140. The mapped axes of both first-order folds are conjectural when the exact location cannot be determined due to the lack of outcrop in the glaciated valleys (Inners, 1978).

Inners (Inners, 1978) identified in the extreme southeast corner of the Berwick Quadrangle, a synclinal axis that can be mapped in the Mauch Chunk Formation along Nescopeck Creek that may represent the main axis of the Catawissa-McCauley Mountain Synclinorium. Alternatively, Inners (Inners, 1978) also considers that this axis may define only one of several en echelon second-order synclines that form the synclinorium in this area. There is no historic or recorded earthquake epicenters associated with this structure. The Catawissa-McCauley Mountain Synclinorium is not considered to be a capable tectonic source.

2.5.1.1.4.4.3.5 Scranton Gravity High

The Scranton Gravity High (SGH) is located underneath the BBNPP site (Feature 34 in Figure 2.5-157, and in Figure 2.5-159). The SGH extends about 250 mi (402 km) from Albany, New York, to Harrisburg, Pennsylvania. The large gravity anomaly covers portions of the Appalachian Plateaus and Ridge and Valley Provinces (Hawman, 1992). There is no apparent relationship to the seismicity in the area of the SGH, which is sparse. Earthquakes occur southeast of SGH in southeastern Pennsylvania and Western New Jersey, but there is no localization of events along the feature (EPRI, 1986). Therefore, the SGH is not considered to be a capable tectonic source.

2.5.1.1.4.4.3.6 Yellow Breeches Fault Zone

The northeast-striking, southeast-dipping Yellow Breeches Fault is located within the northeastern portion of the Ridge and Valley Physiographic Province in southeastern Pennsylvania (Feature 10 on Figure 2.5-131). The fault is a very low angle (sub-horizontal) thrust that divides the Martinsburg/Hamburg foreland segment, separating the Cumberland Valley stratigraphic sequence to the north from the Lebanon Valley stratigraphic sequence to the south of the décollement (Root, 1977b). However, a lithologic comparison can be made between greenschist grade Hamburg succession rocks carried on the Yellow Breeches fault and allochthonous units of lower grade north of that fault emplaced within the main outcrop belt of the Martinsburg foreland basin (Ganis, 2005).

This décollement represents an upper-level detachment above a deeper décollement about 5 mi (8 km) deep (Faill, 1999a). Rock slices of the Lebanon Valley sequence make up the Yellow Breeches thrust plate that is part of the inverted limb of a regional nappe (the southernmost extension of the Reading Prong nappe megasystem) emplaced upon the South Mountain anticlinorium (Root, 1977b). However, Yellow Breeches thrusting is much younger than nappe development and only slightly younger than the South Mountain deformation having formed during the Late Alleghanian orogeny (Root, 1977b). Based on published literature, no seismicity is attributed to the Yellow Breeches fault zone and published literature does not indicate that it offsets Late Cenozoic deposits or exhibits geomorphic expression indicative of Quaternary deformation. Therefore, this Paleozoic fault is not considered to be a capable tectonic source (Wheeler, 2006).

2.5.1.1.4.4.3.7 Rome Trough

The Rome Trough is a Cambrian extensional graben system that extends from northern Tennessee, northeastward through Kentucky, West Virginia, and into western Pennsylvania

(Figure 2.5-157 and Figure 2.5-159). This northeast-trending graben, which underlies the Appalachian Plateaus Province, is mainly characterized by normal faults of Early Paleozoic age. Conversely, complex folds and thrust faults of Late Paleozoic age characterize the eastern Appalachian Plateau (Kulander, 2005). Kulander (Kulander, 2005) studied data from seismic lines across the Rome trough in West Virginia, western Maryland, and southwestern Pennsylvania. Basement-involved thrust faults have been reported in some parts of the Rome trough and attributed it to regional compression dating 0.8-1.0 billion years ago. Major normal movements along the Rome trough boundary faults occurred in the Early to Middle Ordovician, and no other movement seems to have occurred since then (Kulander, 2005). However, the details of basement structure in western Pennsylvania and interpretations of the faults accompanying the Rome trough are based on limited data (Ryder, 1992). The association of this feature with seismicity is also limited. Therefore, the Rome trough is not considered to be a capable tectonic source.

2.5.1.1.4.4.3.8 Pleasant Valley-Huntingdon Valley Fault

Pleasant Valley-Huntingdon Valley Fault is the eastward continuation of the Cream Valley fault (Feature 12 in Figure 2.5-131). The fault separates the Baltimore Gneiss, overlain by the Chickies and Ledger Formation on the north, from Wissahickon Formation schist on the south. The fault was active during the post Ordovician period and is located 120 mi (193 km) south of the site (Crawford, 1999). Major subvertical northeast striking faults, including the Brandywine Manor fault, the Cream Valley fault, the Pleasant Valley-Huntingdon Valley Fault, and the Rosemont fault, intersect through the blocks containing Grenville-age gneisses and juxtaposed them against younger rocks. The Pleasant Valley-Huntingdon Valley Fault borders the Piedmont Upland Section, Piedmont Lowland Section, and Gettysburg-Newark Lowland Section. Based on review of published literature and historical seismicity, there is no reported geomorphic expression, historical seismicity, or Quaternary deformation along the Huntingdon Valley Fault. Therefore, this feature is not considered to be a capable tectonic source.

2.5.1.1.4.4.3.9 Transylvania Fault Zone

The Transylvania Fault Zone, near the latitude 40° N, extends from the Early Mesozoic Gettysburg Basin (Feature 17 in Figure 2.5-131), in Pennsylvania, westward into Ohio and striking at roughly 270 degrees (Dodson, 2008). The fault system is located approximately 170 mi (274 km) west of the BBNPP site (Berg, 1980). The fault zone is mapped as large sub-vertical east-west trending faults extending through the Blue Ridge, Great Valley and Ridge and Valley provinces. Through the Appalachian Plateau, the fault zones are detected through subsurface records and geophysical studies. Root (Root, 1977a) proposed a zone of east-west trending faults that extend from the eastern margin of the Blue Ridge to the Allegheny front near latitude 40° N, for about 75 mi (121 km). The fault zone transects strata nearly across the entire length of Pennsylvania. In the eastern part of the region two faults, 9 mi (14 km) apart, have been previously mapped for about 23 mi (37 km). These are Shippensburg and Carbaugh-Marsh Creek faults which extend east-west in parallel. Root (Root, 1977a) describes the following faults in the zone: Sideling Hill, Breezewood, Everett gap, and Wills Mountain faults. Root (Root, 1977a) does not consider the fault zone as a major transcurrent fault because the apparent strike-slip movement associated with the fault is no more than 2.5 mi (4 km). Root (Root, 1977a) concludes that the Transylvania fault zone is a fundamental fracture, which possibly extends through the continental plate. The fault system originated in the Precambrian, and was reactivated during the Taconic Orogeny in the Middle Ordovician and again in the Carboniferous Period during the Alleghanian Orogeny. The Transylvania fault also reactivated in the Early Jurassic (Root, 1977a). This fault zone has not been associated with seismicity. Based on review of published literature and historical seismicity, there is no

reported geomorphic expression, historical seismicity, or Quaternary deformation along the Transylvania fault zone. Therefore, this feature is not considered to be a capable tectonic source.

2.5.1.1.4.4.3.10 Plummers Island and Pleasant Grove Shear Zones

The Plummers Island Shear Zone and Pleasant Grove Shear Zone are thrust faults that include the Plummers Island fault, Pleasant Grove fault, Hyattstown fault and Martic fault (Kunk, 2004). The faults strike in a northeast-southwest trend with a high angle westerly dipping orientation and are located in the south central Appalachians (Feature 13 in Figure 2.5-131). The fault zones are located 175 mi (282 km) south of the BBNPP site (Kunk, 2004). The faults were active during the Acadian Orogeny in the Early Devonian period and reactivated in the Carboniferous period during the Alleghanian Orogeny, and are part of the south central Appalachians. Based on review of published literature and historical seismicity, there is no reported geomorphic expression, historical seismicity, or Quaternary deformation along the Plummers Island shear zone or the Pleasant Grove shear zone. Therefore, these features are not considered to be capable tectonic sources (Wheeler, 2006).

2.5.1.1.4.4.3.11 Newark-Gettysburg Basin

The Newark-Gettysburg (NG) Basin extends from southeast New York through New Jersey to southern Pennsylvania (Faill, 1973), and is located south approximately 60 mi (97 km) of the BBNPP site (Figure 2.5-157). The NG Basin, one of the several Triassic basins in eastern North America, was developed either by downthrown blocks and subsequent sediment deposition from the northwest and southeast direction or as fault-troughs or grabens with faulting and sedimentation occurring at the same time. The Newark and Gettysburg basins are two separate basins that formed the NG Basin. These two basins along with Culpeper Basin and Barbourville Basin (both in Virginia) are the remnants of a larger Triassic feature called the Birdsboro Basin (Faill, 2004). Faults and folds have subsequently tilted and deformed the Birdsboro Basin in the Early Jurassic with a dominant northeast striking structural trend within the basin (Faill, 2004). Border faults, normal faulting and wrench faulting are associated with the NG basin. Significant examples are the Ramapo Fault system in northern New Jersey which bounds the northwest portion of the Newark Basin, and the Furlong Fault, Hopewell Fault and Chalfont Fault which were generated by wrench faulting within the NG basin (Root, 1999).

Seismicity occurs near the edges of the basin with two notable concentrations of earthquakes. One concentration is near the transition from the Newark Basin into the Gettysburg Basin, which corresponds to the Lancaster Seismic Zone (LSZ) south of the narrowest section of the NG Basin (Armbruster, 1987). The other concentration occurs near the Maryland-West Virginia border, outside the southern edge of the basin. Most well-located epicenters in the LSZ are located just outside the NG Basin (Scharnberger, 2006; EPRI, 1986). A detailed description for the LSZ is provided in Section 2.5.1.1.4.4.1.10.

2.5.1.1.4.4.3.12 Hartford Basin

The Hartford Basin of Connecticut and southern Massachusetts (Figure 2.5-157), along with the much smaller Deerfield and Northfield Basins, are Sub-basins of the larger Connecticut Valley Basin (Resor, 2005; Schliche, 2003). The Hartford Basin's gross structure is a half graben with a master west dipping normal fault on the eastern border and a smaller east-dipping fault on the western border (Resor, 2005). The East Border fault therefore has the larger net vertical slip (Rodgers, 1985) and is located approximately 180 mi (290 km) east of the BBNPP site (Figure 2.5-158) and extends about 130 mi (209 km) from near Bellow Falls, New Hampshire to New Haven, Connecticut (Hibbard, 2006) and further to Long Island Sound. The West Border Fault has much less net slip and is therefore not as significant as the East Border Fault. The East

Border Fault strikes generally north and dips west with a listric geometry, and changes in strike to north-northeast from central Connecticut towards the south (Wheeler, 2005). Sedimentation continued until the Early Jurassic period during which the basin also experienced intrusive volcanic activity (Bennington, 2006). Core data from Thompson (1999 in Wheeler, 2005) indicated that stratigraphy at Farm River marsh, nearly 1 mi (1.6 km) inland from the Long Island Sound, showed the downthrown block of the southeastern portion of the marsh with respect to the northwestern portion coincided spatially with the buried trace of the fault. This led to the conclusion that the fault has been active since 2000 years ago, having been reactivated as a reverse fault in the present day compressional field (Wheeler, 2005).

Wheeler (Wheeler, 2005) argues that no fault surface has been reported within the overlying marsh deposits. In addition, the downthrown block shows the displacement across a wide slope as opposed to a sharp offset on a fault plane. The area also lacks evidence for sudden movements that would imply tectonic faulting. Wheeler (Wheeler, 2005) concludes that evidence of faulting has not been reported in Quaternary sediments of the Farm River marsh and accordingly classifies the East Border fault as Class C. Seismicity has not been associated with the East Border fault. Therefore, it is concluded that the Hartford Basin is not a capable tectonic source.

2.5.1.1.4.4.3.13 Connecticut Basin

The Connecticut Basin also known as the Connecticut Valley Basin is the largest onshore Mesozoic-age graben in New England (Wheeler, 2005). From Long Island Sound in the south, the basin crosses through central Connecticut and Massachusetts. The basin is located approximately 175 mi (282 km) northeast of the site (Figure 2.5-157 and Figure 2.5-159). This larger basin has sometimes been confused with the smaller Hartford Basin (Wheeler, 2005), which along with the Deerfield and Northfield Sub-basins, comprise the whole of what is known as the Connecticut Valley Basin (Resor and deBoer, 2005). This confusion likely comes from the fact that the Hartford Basin makes up the vast majority of the Connecticut Valley Basin and that both basins were formed by normal movement on the East Border Fault (Section 2.5.1.1.4.4.3.16). Rocks deposited in the basin are of the Newark Super Group sedimentary series (Schlische, 2003) and sedimentation continued until the Early Jurassic period during which the basin also experienced intrusive volcanic activity (Bennington, 2006).

Even though seismicity has been associated with the Connecticut Basin, Quaternary activity has not been demonstrated for the structures within the basin or for its boundary faults. Therefore it is concluded that the Connecticut Basin is not a capable tectonic source.

2.5.1.1.4.4.3.14 Brandywine Fault System

The Brandywine Fault System is located approximately 180 mi (290 km) south of the site and north of the Potomac River (Feature 19 in Figure 2.5-131). The 12 to 30 mi (19 to 48 km) long Brandywine fault system consists of a series of en echelon high angle reverse fault segments with associated flexing of the overlying Coastal Plain sedimentary strata (Cumbest, 2000). The fault system trends north-northeast with displacements ranging from a few feet to 250 ft (76 m). The Brandywine Fault System consists of the Cheltenham Fault and Danville Fault (Cumbest, 2000). The Brandywine Fault System was active in the Cretaceous and Middle Eocene and Middle Miocene (Mixon, 1977).

The Brandywine Fault System is located 6 mi to 12 mi (10 km to 19 km) east of the Stafford Fault Zone and strikes roughly parallel to it. Wheeler (Wheeler, 2005) considers Skinkers Neck and Brandywine as a single fault zone, southeast of Stafford Fault System. Compared to

Stafford Fault System, the Skinkers Neck-Brandywine Fault Zone is less known and its boundary is shown by dashed line (inferred) in the map of Mixon (2000). The last activity of the fault was during the Miocene. There is no seismicity associated with the fault system and no evidence of Quaternary activity has been demonstrated. Therefore, the Brandywine Fault System is not considered as a capable tectonic source (Wheeler 2005).

2.5.1.1.4.4.3.15 Martic Fault

The Frederick Valley lies near the western edge of the Piedmont physiographic province of Maryland, with the Martic fault being the eastern boundary of this valley (Southworth, 2002). This fault is located 95 mi (153 km) SSW of the BBNPP site (Feature 11 in Figure 2.5-131).

This fault juxtaposes low-grade metamorphic phyllites against Early Paleozoic carbonates. Little difference on topographic relief exists between the Early Paleozoic carbonates of the Frederick Valley and the rocks of the Triassic basins because much of the Triassic bedrock is composed of detrital limestone and dolomite whose clasts are Early Paleozoic in age (Southworth, 2002).

The Martic fault is the structurally lowest fault in a stack of imbricate thrust sheets of the Westminster terrane that were probably active in all orogenies of the Paleozoic era (Southworth, 2002). The other two structurally higher thrusts to the east are the Barnesville-Monrovia, and the Hyattstown thrust faults.

The Martic thrust fault cuts up section westward, placing Ijamsville Phyllite on rocks of the Urbana, Araby, and Frederick Formations; the fault is folded with the footwall rocks. Within the thrust sheet there are early (now folded) and late (cut existing faults) thrust faults, reactivated thrust faults, and numerous small intraformational faults of limited displacement (Southworth, 2002). Rocks of the Ijamsville Phyllite of the Martic thrust sheet have a composite foliation that consists of a transposition foliation that is overprinted with phyllonitic foliation, and several generations of cleavage. Vein quartz that impregnates the rock has been sheared, transposed, and folded into steep isoclinal folds. These steep F1 folds were deformed by westward-verging, inclined F2 folds that plunge steep to gentle in all directions.

There is no seismicity associated with this fault, and it is not considered to be a capable tectonic source under the present stress regime.

2.5.1.1.4.4.3.16 East Border Fault

The East Border Fault is the eastern limit of the Hartford Basin 180 mi (290 km) east of the BBNPP site (Feature 22 in Figure 2.5-131). The East Border Fault is generally north striking, western dipping normal fault with a listric subsurface geometry (Wheeler, 2005). The East Border Fault of the Connecticut Valley Basin, along with the Deep River Basin in South Carolina, are the only exposed Mesozoic rift basins (half-grabens) that do not have easterly dipping western border faults (Benson, 1992). Southward from central Connecticut the fault curves to strike north-northeast and, farther south, northeast. As the fault crosses the shore of Long Island Sound, it curves more to strike east-northeast before returning to a northeast strike under the Sound (Rodgers, 1985).

Where the fault traces across Long Island, Thompson (2000 and 2001 in Wheeler, 2005) reconstructed the past geographic distributions of high marsh (salt marsh; infrequently flooded by salt water) and low marsh (flooded by tides), relative sea-level rise curves, and paleohistories of vertical offsets of dated, originally horizontal peats at the Farm River Marsh on Long Island. The stratigraphy of the southeastern part of the marsh, which coincides

spatially with the buried trace of the East Border fault, is dominated by low marsh and mudflat deposits, while the stratigraphy of the northwestern marsh is predominantly high marsh deposits. The authors indicate that this means that the sea level rose in the southern part of the Farm River marsh more rapidly than in the northwestern part of the marsh implying that the southeastern part of the marsh was downthrown on the East Border Fault with respect to the northwestern marsh.

Several questions remain to be answered with respect to the Quaternary activity of this fault (Wheeler, 2005): Why is there no reported surface faulting within the till or the overlying marsh deposits?, Could an erosive event provide a possible alternative explanation for parts of the transition?, and Why is there a lack of evidence that individual increments of the downthrowing occurred suddenly, within the seconds to minutes that an earthquake rupture lasts, or at least more suddenly than could be produced by any alternative, non faulting mechanism (Obermeier, 2009) (Wheeler, 2005)?

These questions and possible alternative explanations mean that faulting has not been demonstrated in the Quaternary sediments of the Farm River marsh. Wheeler (Wheeler, 2005) designates the East Border fault as a Class C feature. It is not considered to be a capable tectonic source.

2.5.1.1.4.4.3.17 Broad Top Synclinorium

The Broad Top synclinorium is a large regional synclinorium which extends from central Pennsylvania to western Virginia. It is the most western of the synclinoria in the Valley and Ridge province (Jacobein, 1974) and is located 100 mi (161 km) WSW of the BBNPP site on its closest position (Feature 48 in Figure 2.5-131). The Broad Top Synclinorium is northeast-southwest trending first order fold with a southwest plunge (McElroy, 2007). Although the synclinorium is broken into a series of folded and faulted structures, its basic structural style reflects both basement movement and thin-skinned tectonics.

More than 125 mi of seismic surveys, 22 wells, and surface maps were analyzed by Jacobeen (Jacobein, 1974) to determine the precise relation of basement to thin-skinned tectonics. This relation, as interpreted, indicates that Taconic and older, tension-induced features have a pronounced effect on the localization and genesis of the ramping of décollements. This ramping, in turn, produces many of the large, prominent, first-order structural features in both the Valley and Ridge, and the Plateau provinces of the Appalachian basin, such as the Allegheny Front. The décollement ramping also induces formation of smaller, second-order features and other flexures and faults within the Broad Top synclinorium.

Folds in the Broad Top synclinorium strike in an average N30°E direction and have been mapped as long, continuous features, extending over 100 mi (161 km) (Jacobein, 1974). Along the strike of the structures, outcrops indicate an en echelon structural trend of anticlinal and synclinal axes that are roughly parallel and doubly plunging as their axes rise and fall in a series of domes and saddles (Jacobein, 1974). The southwest plunge of the Broad Top Synclinorium results in exposure of the Late Devonian Brallier Formation along its axis. Dips are steeper on its southeast flank and there are smaller folds contained within it while overturning of fold limbs occurs north and west of Garret Knob (McElroy, 2007).

The structure of the Broad Top synclinorium as seen today represents the interaction between Taconic block faulting and Late Paleozoic thrusting. Such Late Paleozoic thrusting, which dominates the structure in the Appalachians, is believed to be modified and localized by older structures in other areas.

There is no seismicity associated with this fault, and it is not considered to be a capable tectonic source under the present stress regime.

2.5.1.1.4.4.3.18 Sweet Arrow Fault

The Sweet Arrow fault, located between Swatara Gap and New Ringgold, in east-central Pennsylvania, is located 50 miles (80 km) to the southeast of the site (Feature 49 on Figure 2.5-131). It is a thrust fault separating the overturned rocks to the north from the upright rocks to the south (Wood, 1961), and has a dip of 40° to 70° to the south and a throw that can reach several thousand feet. It was recognized by Wood (Wood, 1961) from the thinning and offsetting of stratigraphic units and the truncation of structural features in the area. The fault cuts through rocks of Silurian and Devonian ages, and is buried in many places beneath heavy talus slopes. Wood (Wood, 1961) never mentioned the cross-cutting of younger rocks, including rocks of Quaternary age, but the sense of the motion on the fault (thrust from the southeast) is consistent with the stress regime that existed during the Alleghanian Orogeny, when other similar faults were active. There is no seismicity associated with this fault, and it is not considered to be a capable tectonic source under the present stress regime.

2.5.1.1.4.4.3.19 Chestnut Ridge Anticline

The Chestnut Ridge anticline is a major regional feature of the Appalachian fold belt (Feature 50 on Figure 2.5-131). Its western limb forms a 100 mi-long (185 km) segment of a physiographic break called the Intra-Plateau Front (Gwinn, 1964). The Front separates the Allegheny Mountains (Figure 2.5-126), with their high-relief open folds (1000 ft [305 m] of relief), from the lowlands and low folds of the Pittsburgh Plateau to the west (Shumaker, 2002).

The original widely accepted structural model for formation of folds in the outer central Appalachian foreland during the Alleghanian Orogeny was partially based on the geologic structure of the North Summit field, a natural gas field on the structural culmination of the long and narrow Chestnut Ridge anticline. The model includes a simple surface anticline that is detached in Silurian Salina Group salts and cored by imbricated Devonian rocks thrust inward toward a depressed axial low (Shumaker, 2002).

More recent reinterpretations of cross-sections across the Chestnut Ridge anticline interpreted from well data indicate a different structural formation (Shumaker, 2002). The old model involves space problems within collapsing synclines above competent reservoir rocks such as the Huntersville-Helderberg lithostructural unit. These problems can be resolved by distortion and evacuation of overlying, incompetent Hamilton Group rocks. Therefore, Huntersville-Helderberg rocks within the Chestnut Anticline deformed into a variety of structural shapes, not solely the imbricated model that traditionally has been applied to Plateau folds of the central Appalachian foreland. There is no seismicity associated with this structure, and it is not considered to be a capable tectonic source under the present stress regime.

2.5.1.1.4.4.3.20 Philadelphia Structural Block

The Philadelphia Structural Block is located in the Piedmont physiographic province of Pennsylvania and New York (Figure 2.5-154 and Figure 2.5-169). This block is currently comprised of three stratigraphic units; the Wissahickon Formation, the Wilmington Complex, and the Springfield Pluton. Originally the Block was comprised of only the Wissahickon Formation which is thought to have originated as part of a peri-Gondwanan back-arc basin during the Late Cambrian or Early Ordovician (Bosbyshell, 2009). Metamorphism of the Wissahickon Formation began during the Taconic Orogeny with the collapse of the

Cambrian-Ordovician Laurentian passive margin beneath the Wilmington Complex, the root of the Taconic volcanic arc. This collapse created the Llanerch Thrust Zone. The Wilmington Complex was then thrust over the Wissahickon Formation, concurrent with the intrusion of the Springfield granodiorite pluton into the Wissahickon (Valentino, 1999).

Significant transcurrent displacements along ductile shear zones indicate a tectonic history of oblique convergence and orogen-parallel displacement (Hill, 2006). These strike-slip shear zones bound and cross-cut the Philadelphia Structural Block. To the northwest the block is bound by the Rosemont Shear Zone, and to the north, the Pleasant Grove-Huntingdon Valley Shear Zone. These shear zones separate the Philadelphia Structural Block from the West Chester and Avondale Grenvillian basement massifs. Another shear zone, the Crum Creek, cross cuts the metamorphic zones of the Wissahickon formation and is thought to be the conjugate pair of the Rosemont shear zone (Valentino, 1995). The most pervasive period of metamorphism in the Wissahickon Formation and the right-lateral transpressive deformation in the Rosemont Shear Zone, and corresponding sinistral movement along the Crum Creek Shear Zone, are Devonian in age (Bobsyshell, 2009). This timing correlates with the Acadian Orogeny in the Central Appalachians.

There is no seismicity associated with this structure, and it is not considered to be a capable tectonic source under the present stress regime.

2.5.1.1.4.4.3.21 Potomac and Westminster Terranes including the Pleasant Grove Shear Zone

The Westminster and Potomac Terranes are exposed in Maryland, Virginia and Washington DC (Figure 2.5-169). It is proposed that the Potomac was thrust onto the Westminster along the Pleasant Grove Fault during the Devonian Acadian Orogeny (Figure 2.5-167). The Westminster was thrust westward along the Martic Thrust onto the Cambrian/Ordovician continental margin during the Ordovician Taconic Orogeny (Kunk, 2004).

The rocks of the Westminster Terrane are dominated by phyllites and are proposed to represent offshore, deepwater, post rift deposits (Kunk, 2004). Rocks of the Potomac Terrane are proposed to be turbidites deposited in a deep ocean trench. Within the Piedmont Province, the Westminster and Potomac Terranes show foliation that mainly strikes northeasterly and dips steeply to the southeast (Southworth, 2006).

The Pleasant Grove Fault, also known as the Pleasant Grove Shear Zone is approximately 60-km long and the zone of deformation is as much as 3-km wide (Southworth, 2006). The shear zone contains dextral strike-slip indicators and similar deformational structures on both the east and west sides of the fault. Along the length of the shear zone, cooling ages range from 371 Ma in the Potomac Terrane to 364-308 Ma north of the Potomac River (Devonian to Carboniferous). The age of most recent dextral shearing is indicated by mica growth and has been dated at approximately 311 Ma (Southworth, 2006). Figure 2.5-167 shows part of Potomac River region depicting the Westminster and Potomac Terranes tectonostratigraphic location and relationships with bordering terranes and associated shear zones.

2.5.1.1.4.4.3.22 Baltimore Gneiss Terrane

The Baltimore Gneiss is defined as the basement gneisses observed at the lowest stratigraphic level in the Central Piedmont. Plank (Plank, 2000) reports that the gneiss has been observed in the cores of thirteen anticlines, domes and nappes from Baltimore, MD to Philadelphia, PA. It is a Proterozoic-age gneiss containing quartz, pink/white feldspar, biotite, garnet, hornblende, magnetite, titanite and zircon. The Glenarm and Wissahickon group rocks were deposited in

marine rift basins floored by Baltimore Gneiss (Blackmer, 2005). The gneiss is also exposed in the Avondale and West Chester Massifs and includes amphibolite and granulite grade metamorphic compositions. The Setters Formation and Cockeysville Marble also unconformably overlie the Baltimore Gneiss (Blackmer, 2005). The northeast-southwest belt of metamorphic rocks northwest of Baltimore, which commonly includes exposures of Baltimore Gneiss, is known as the Baltimore Gneiss Terrane. The Grenville-age gneiss and sediments were thrust northwestward into a nappe structure and deformed during the Ordovician Taconic Orogeny (Lang, 1996). Figure 2.5-168 shows the Baltimore Gneiss tectonostratigraphic location within the Eastern Maryland Piedmont depicting the relationships with bordering terranes.

2.5.1.2 Site Geology

The U.S. EPR FSAR includes the following COL Item in Section 2.5.1.2:

Site-specific geology information will be addressed by the COL applicant.

This COL Item is addressed as follows:

Sections 2.5.1.2.1 through 2.5.1.2.6 are added as a supplement to the U.S. EPR FSAR.

The following subsections provide a summary of geologic conditions in the BBNPP site area (5 mi (8 km) radius) and site location (0.6 mi (1 km) radius). These subsections present information concerning the physiography, geomorphology, geologic history, stratigraphy, structural geology, geologic hazard evaluation, and engineering geology evaluation related to the BBNPP site. The information presented is based on a review of previous reports and documents, a review of geologic literature, communications with geologists and other researchers who are familiar with previous studies in the site area, and geotechnical and geologic field investigations conducted at and in the vicinity of the BBNPP site. A geologic map of site area (5 mi (8 km) radius) is shown on Figure 2.5-139, and a geologic map of the site location (0.6 mi (1 km) radius) is shown on Figure 2.5-138.

2.5.1.2.1 Site Area Physiography and Geomorphology

The BBNPP site area is located within the Susquehanna Lowland Section of the Ridge and Valley Physiographic Province, which is bordered by the Appalachian Plateaus Province to the west and north, the New England Province to the east, and the Piedmont and Blue Ridge Provinces to the south (Figure 2.5-5 and Figure 2.5-126). Additionally, within the Ridge and Valley Physiographic Province, the Anthracite Valley Section of the Ridge and Valley Province borders the Susquehanna Lowland Section to the north of the site and the Anthracite Upland Section borders on the south (Figure 2.5-126).

The topography within 5 mi (8 km) of the site consists of low to moderately high, linear ridges and valleys that primarily follow structural trends with elevations ranging from about 463 ft (141 m) msl to 1,778 ft (542 m) (Figure 2.5-3). To the north of the site, elevation increases to greater than 1,500 ft (457 m) msl at the peak of Lee Mountain. With the increase in elevation, the steepness in the slope, from the top of the mountain to the banks of the Susquehanna River, also increases to near vertical northeast of the site. Approximately 10,000 ft (3,048 m) south of the site, on the south side of the Susquehanna River is a steep embankment, which reaches an elevation of approximately 900 ft (275 m). Further to the south of the site, approximately 4.8 miles (7.6 km), is the ridge of Nescopeck Mountain which reaches over 1,700 feet (520 m) at the edge of the site area (5 mi (8 km) radius) (Figure 2.5-3).

The site is well-drained principally by Walker Run, which flows from north to south along the west border of the site then to the south and southwest until it reaches the Susquehanna River. There is also an unnamed, unmapped tributary that flows from east to west just to the south of the site, feeds the mapped wetlands area to the southwest of the site, and ultimately drains into Walker Run. Drainage within 5 miles of the site is primarily a moderately developed trellis pattern with ridges and valleys forming sub-parallel drainage systems. These connect at abrupt incisions nearly normal to a ridge, or at the termination of a ridge, and drain down gradient toward the Susquehanna River. Streams that incise into the glacial deposits establish a dendritic pattern that is not subject to the effect of geologic structure. The longest stream near the site is the previously mentioned Walker Run which is approximately 2 mi (3.2 km) long and ultimately drains into the Susquehanna River. Ephemeral stream channels in the vicinity of the BBNPP site flow directly into the Susquehanna River. These limited stream channels maintain dendritic patterns that are observed to be minimally affected by the geologic structure as they incise into the underlying Trimmers Rock and Mahantango formations and glacial sediments.

The site area bedrock geologic map (Figure 2.5-139), compiled by (Berg, 1980) and (King, 1974) indicates that most of the site area (5 mi (8 km) radius) surrounding, and including, the BBNPP site is underlain by Late Silurian, Devonian, and Early Mississippian bedrock. More specifically, the site bedrock is Upper Devonian Mahantango Formation. The most recent geologic influence on the site, not including sub-aerial exposure and erosion, is the Wisconsin glacialiation that is discussed in Section 2.5.1.1.1. The relevance of this event to the physiography of the site is the deposition of glacial materials. Remnants of kame terrace and outwash labeled as stratified drift deposits of sand and gravel outwash depicted in Figure 2.5-137 are mapped as overlying site area bedrock at approximate elevation 660 ft (210m). This relationship is shown on the geologic cross section of the Berwick Quadrangle (Figure 2.5-135).

The BBNPP site is west of and adjacent to the SSES site. The SSES is located approximately 200 ft (61 m) above the Susquehanna River with a long, gradual slope leading from the SSES to the banks of the river. Private property borders the BBNPP property to the immediate south and west. The BBNPP will be constructed at a plant grade elevation of 719 ft (219 m) and will be set back 8,000-10,000 ft (2,438-3,048 m) from the Susquehanna River bank (Figure 2.5-3).

An additional significant geomorphological/physiographic aspect within the site area is the formation of moderate karst geomorphology approximately five miles to the south and west within the Tonoloway and Keyser Formations. The location of these strata is shown to the west of the site in Figure 2.5-139. The Tonoloway Formation is a thinly-bedded limestone up to 100 ft. (30 m) thick in the site area (5 mi (8 km) radius) and the Keyser Formation is a fossiliferous limestone up to 125 ft. (38 m) thick (Berg, 1980). Both lithologies are susceptible to the development of karst features due to dissolution of calcium carbonate within the rock. However, the formation of karst geomorphology is not applicable to the site location (0.6 mi (1 km) radius), as carbonate rocks are not at or near the surface of the site. Figure 2.5-13 establishes the depth to carbonate rocks at more than 1,500 ft. (457 m) beneath the surface at the site location (0.6 mi (1 km) radius), within the limestones of the Onondaga Formation (Middle Devonian). Core holes from field studies for the BBNPP site extend to depths as great as 420 ft. (128 m) and do not encounter the stratigraphic position of these formations beneath the site location (0.6 mi (1 km) radius).

Quaternary processes affecting the site are limited to weathering and erosion of existing material, and subjection to the regional stress field that affects the eastern half of the

continent. The site area (5.0 mile (8 km) radius) exhibits no physiographic characteristic that would detrimentally affect the BBNPP site.

2.5.1.2.2 Site Area Geologic History

This subsection presents an overview of the geologic history of the site area. The overall geologic history and tectonic framework of the region are outlined in Section 2.5.1.1.2 and Section 2.5.1.1.4 respectively. A detailed discussion of the surface faulting within 25 mi (40 km) of the BBNPP site area is provided in Section 2.5.3. The following geologic history of the area around the BBNPP site is summarized based on the recent detailed field studies, and literature review which includes compilations by the Pennsylvania Department of Conservation and Natural Resources and publications by Braun (Braun, 2007). Each has been integral in characterizing the site area (5.0 mile (8 km) radius).

The pre-Early Ordovician geologic history of the site area is inferred from scattered borehole data, geophysical surveys and a synthesis of published information. Limited geophysical and borehole data indicate that the basement rock beneath the site most likely consists of a crystalline metamorphosed greenschist or amphibolite (Gold, 2008). Although the basement has not been penetrated directly beneath the site with drill holes, regional geologic cross sections developed from geophysical, gravity and aeromagnetic, as well as limited deep borehole stratigraphic data beyond the site area suggest Precambrian (approximately +542 million years ago) rocks are most likely present at a depth of about 33,000 ft (10,058 m) beneath the site. Figure 2.5-130 shows the inferred depth of the Precambrian basement rocks beneath the BBNPP site.

Tectonic models discussed in Section 2.5.1.1.2 and Section 2.5.1.1.4 establish that the crystalline basement was accreted to the Proterozoic North American Craton during the Grenville Orogeny. The depositional environment for the Cambrian bedrock underlying the site is primarily a passive continental margin with a marine carbonate platform extending to a more distal setting upon which clays and silts were deposited (Gao, 2000). These sediments, deposited over a period of nearly 50 million years (approximately 542-488 million years ago), comprise the shales and limestones overlying the Grenville basement at the BBNPP site. The site area during the Ordovician (approximately 488-444 million years ago) represented an area of continued and increased deposition in an elongated basin along the continental margin. As discussed in Section 2.5.1.1.2.3, the Middle Ordovician to Late Ordovician with respect to the eastern margin of the North American craton, is affected by the Taconic Orogeny (Hurowitz, 2005). As the Taconic allochthon, a suite of oceanic and arc terranes, converged with the North American Craton, uplift of the area began and shifted the depositional environment from that of carbonate platform to a much shallower basin receiving coarser siliciclastic source material (Tremblay, 1997). Deposition of material from the Taconic Allochthon, as it approached from the east-southeast, yielded significant amounts of siliciclastic sediment to the basin. Shale and sandstone units that now outcrop in places throughout central Pennsylvania, but underlie the site area by thousands of feet (Thompson, 1999), were deposited at this time. As the Taconic front converged with the craton, portions of the ocean floor and island arc of the Taconic front were obducted onto the craton at the eastern portion of what is now defined as the site region (200 mi (322 km) radius), while some ocean floor subducted under the continent. At the close of the Ordovician, the site area (5 mi (8 km) radius) was located on the western portion of a depositional basin bounded on the west by the North American Craton and on the east by the Taconic Highlands (Thompson, 1999).

The continued erosion of the Taconic Mountains during the early part of the Silurian Period (444-416 million years ago) added to the sedimentation throughout the site area. This early

period of sedimentation differed from that of the Ordovician, in that the sand and gravels deposited during the Early Silurian were extremely quartz-rich in mineral composition (Barnes, 2002), thus creating a very erosion-resistant sandstone. After the Taconic Mountains were almost completely eroded away during the Late Silurian, carbonate sedimentation continued through the site area creating shale and limestone intervals (Laughrey, 1999).

The Devonian Period (approximately 416-359 million years ago) primarily marks the Acadian Orogeny (as discussed in Section 2.5.1.1.2.5), the result of the North American landmass colliding with the Avalon Terrane and Baltica (Eusden, 2000). The site area remained a basin area while the Acadian mountain range, to the east of the site area, was subjected to erosional processes. The effect of the Acadian Orogeny is more pronounced in terms of metamorphism and magmatism in the northeastern United States (Maine, New Hampshire, Vermont) (Eusden, 2000) but is significant to the site area in that the source material for the formation of the Devonian black and gray shales that outcrop, and underlie in the site area was primarily derived from the eroded Acadian Highlands (Ver Straeten, 2000). Ver Straeten (Ver Straeten, 2000) identifies the progression of a terrigenous clastic wedge from the orogenic belt to the west during multiple phases of orogenic uplift during the Devonian that was the source of Devonian deposition.

The Carboniferous Period (approximately 359-299 million years ago) is best described in two distinct categories including the older Mississippian and younger Pennsylvanian sub-periods of the Carboniferous Era. The Mississippian (approximately 359-318 million years ago) was a time of continued sedimentation from the Acadian mountains but a change of climate is represented in the lack of oxidation of rocks from this time frame (Barnes, 2002). Near the end of the Mississippian the site and surrounding area likely became poorly drained and was an area of thick forests and swamps. During the Early Pennsylvanian these forests deposited great amounts of organics which did not rot or oxidize due to the water rich environment of the swamps (Edmunds, 1999). These organics were then overlain by sediment deposits and compacted into the coal fields that occupy the Anthracite Valley Section to the north and the Anthracite Upland Section to the south of the site (Edmunds, 1999) (Figure 2.5-126). No Mississippian or Pennsylvanian rocks exist within the site location (0.6 mi (1 km) radius) due to uplift and erosion throughout geologic time. However, Mississippian and Pennsylvanian rocks are found within the site area (5.0 mi (8 km)) to the north and to the south of the site location as depicted on Figure 2.5-139.

The most significant geologic event to affect the structure of the site area is the Alleghanian Orogeny (discussed in detail in Section 2.5.1.1.2.5). Beginning in the Middle Pennsylvanian, continental convergence of North America and Africa began the multiple phases of the Alleghanian Orogeny which was the primary orogenic event to form the portion of the Appalachian Mountains that extend from northeast Alabama through Pennsylvania. The orogeny formed numerous thrust faults, fractures, anticlines and synclines throughout the Ridge and Valley, Piedmont, and Blue Ridge Physiographic Provinces from Alabama through Pennsylvania including the site area. Convergence from the southeast to the northwest created a structural fabric that strikes primarily northeast and dips to the northwest and southeast. Deformation was both ductile and brittle depending on pressure/temperature conditions. Offset along faults within the Ridge and Valley is primarily reverse dip slip but often has a strike slip component (Pohn, 2000).

The site area was subjected to brittle deformation in the form of folding and thrusting that developed the structural makeup of the Ridge and Valley Province within which the site area lies. The Berwick and Light Street Faults, depicted on Figure 2.5-139 and discussed in

Section 2.5.1.2.4.1 are examples of this Alleghanian deformation within the site area (5 mi (8 km) radius), and are not recognized as active. In addition, the Berwick Anticlinorium, an east-northeast striking, gently northeast plunging anticline trends directly through the site area (5 mi (8 km) radius). The Berwick Anticlinorium is a symmetrical structure with both the north-northwest and south-southeast limbs dipping with an averaged 35 degree NNW and SSE respectively (Inners, 1978). The structure imparted by the Alleghanian Orogeny is significant to the topography, drainage, and seismicity of the site area, defining the major landforms (elongated ridges and valleys), drainage patterns, and structural discontinuities within the Paleozoic strata.

By the end of the Permian Period, the Appalachian Mountains had been subjected to significant erosion providing source material for an alluvial plane across the site area (Edmunds, 1999). Publications (Pazzaglia, 2006,) describe the cycle of erosion and isostatic uplift as the dominant geologic process within the site area since the Late Permian, with the exception of discreet glacial periods that significantly altered and even reversed the erosion and uplift process.

The Triassic (approximately 251-199 million years ago), Jurassic (approximately 199-145 million years ago), and the Cretaceous (approximately 145-65 million years ago) Periods, all within the Mesozoic Era, were all times of slow erosional processes for many areas of Pennsylvania, including the site area (Barnes, 2002). During these periods of erosion, new drainage patterns and streams were formed. By the end of the Cretaceous Period, chemical alteration became the dominant erosional source of rocks that likely comprised the site area, changing them into clays and saprolite (MacLachlan, 1999). Rifting of Pangaea in the Late Permian and throughout much of the Triassic affected the site region (200 mi (322 km) radius) by changing the stress field to an extensional regime. Mesozoic rift basins and intrusive diabase dikes along rift structures mark the extensional effects on the North American Atlantic margin. The aforementioned extension related features do not occur within the site vicinity (25 mi (40 km) radius) nor the site area (5 mi (8 km) radius) (Figure 2.5-149).

Though there is little record as to what happened at or around the site area during the Cenozoic Period (approximately 65 million years to present), much can be inferred from the glacial deposits of the Quaternary Period (approximately 1.8 million years ago to present). It is theorized that during the Tertiary Period (approximately 65-1.8 million years ago) erosion at the site area continued with chemical alteration and erosion, primarily during the Early Tertiary, but transitioned to intense physical erosion during the Late Tertiary (Barnes, 2002). This physical erosion was the result of cooler and drier conditions. It is also believed that during this time many of the modern day rivers and streams, such as the Susquehanna, established themselves (Sevon, 1999b).

During the Quaternary, continental glaciers covered Canada and advanced into a small portion of Pennsylvania, including the site area (5 mi (8 km) radius), and site vicinity (25 mi (40 km) radius) as shown in Figure 2.5-127. The site area was subjected to three different periods of glaciation with the earliest occurring approximately 770,000 years ago and the most recent occurring approximately 17,000 to 22,000 yrs ago. These periods of glacial advance and retreat had both erosional and depositional effects on the site area, the degree of which is difficult to quantify. The main effect of glaciation on the site area was the effect of glacial outwash enhancing drainage patterns that were already in progress (Sevon, 1999a). During and after glacial retreat, the site has been an area of deposition for stratified drift which includes sand and gravel, kame terraces, and outwash. Hence, the surface at the site is comprised of glacial deposits from the Wisconsinan glaciation that is discussed in Section 2.5.1.1.2. Surficial

deposits are depicted on Figure 2.5-136 for the site location (0.6 mi (1 km) radius) and on Figure 2.5-137 for the Berwick Quadrangle.

Cenozoic faulting occurred in the Piedmont, especially along the contact of the Piedmont and Coastal plain, where a hinge line of erosional unloading and depositional loading roughly from northwest to southeast (Weems, 1998) is known to exist. Cenozoic faulting is also recognized in the Piedmont (Wentworth, 1983) approximately 50 miles from the site. In addition, Crone (2000) presents data for all Quaternary faults and possible tectonic features in the Eastern United States and report two sites in the Pennsylvania Ridge and Valley province. However, no seismic events or tectonic structures are reported within the site area (5 mi (8 km)) or the site vicinity (25 mi (40 km) radius). Capable seismic sources, their location, and affect on the site area (5 mi (8 km) radius) are addressed in Section 2.5.1.2.4.

The surface at the site is comprised of glacial deposits from the Wisconsinan glaciation that is discussed in Section 2.5.1.1.2. As briefly discussed in Section 2.5.1.2.1, with respect to physiography, the formation of karst features is also part of the geologic history of the site area (5 mi (8 km) radius). Approximately five miles to the west within the Tonoloway and Keyser Formations, as shown on Figure 2.5-139, karst feature development is exhibited. The Tonoloway Formation is a thinly-bedded limestone up to 100 ft. (30 m) thick in the site area (5 mi (8 km) radius) and the Keyser Formation is a fossiliferous limestone up to 125 ft. (38 m) thick. Both lithologies are susceptible to the development of karst features due to dissolution of calcium carbonate within the rock. However, the formation of karst geomorphology is not applicable to the site location (0.6 mi (1 km) radius), as carbonate rocks are not at or near the surface of the site (Inners, 1978). Figure 2.5-13 notes the stratigraphic position of these formations beneath the site location (0.6 mi (1 km) radius). The Tonoloway and Keyser Formations are at depths as great as 1,500 feet under the site location (0.6 mi (1 km) radius) due to the dip of the northern limb and plunge of the axis of the Berwick Anticlinorium.

The geologic history of the site is complex, but the current geologic processes affecting the site are limited to weathering and erosion of existing material, and subjection to the regional stress field that affects the passive Atlantic margin. Figure 2.5-8 (Heidbach, 2008) shows the current stress fields in the eastern portion of North America, and minimal isostatic uplift. With respect to seismic stability and geologic hazards due to the site area (5 mi (8 km) radius) geologic history, the site area (5 mi (8 km) radius) and site location (0.6 mi (1 km) radius) are positioned in a stable geologic setting.

2.5.1.2.3 Site Area Stratigraphy

As discussed in Section 2.5.1.1, the BBNPP site is located near the deepest portion of the Appalachian structural basin (see Figure 2.5-130). Approximately 33,000 ft (10,058 m) of Paleozoic rocks overlie the Pre-Cambrian basement at the BBNPP site. The regional source of sediments, the types of sediments, and the deformation of these sediments that fill the Basin are described in Section 2.5.1.1. This Section provides more detailed information related to the local stratigraphy, including the nomenclature of the formations, the lithologies, and the thickness of formations. In addition, any characteristics of the geologic media underlying the site that could impact the design or the safety of the BBNPP are presented in this section. Based on the drilling, geologic observations, and laboratory testing results, the rock formations below the BBNPP site are very competent and physically suitable to serve as a stable foundation for the BBNPP.

Site-specific information on the stratigraphy of geologic materials underlying and directly adjacent to the BBNPP site is based on the geologic/geotechnical investigations performed for

the BBNPP site and the historical investigations performed at the SSES site. The SSES site is located immediately adjacent to the BBNPP site and observations concerning its soil and rock formations are comparable with those from the BBNPP investigation borings. Given that the geologic conditions at the SSES and BBNPP sites are very similar, the available SSES data and information were used to supplement the BBNPP data and enhance the characterization of subsurface conditions at BBNPP.

A total of 44 boreholes and 51 monitoring wells were completed at BBNPP. Forty one of the monitoring wells were completed in late 2007 and early 2008, with the rest of the boreholes and monitoring wells having been completed in the spring of 2010 for sampling and standard penetration test (STP) purposes. In addition, 3 boreholes were performed for geophysical testing purposes. Of the 47 geotechnical and geophysical borings drilled during the BBNPP site investigation, 12 were 30 to 99 ft (9 to 30 m) deep, 18 were 100 to 199 ft (30 to 61 m) deep, 14 were advanced to a total depth between 200 and 299 ft (61 and 91 m) below ground surface (bgs), and 3 were drilled to a depth between 300 and 420 ft (91 and 128 m) bgs (Table 2.5-15). The deepest geotechnical boring advanced at the BBNPP site was boring G-401, which was drilled to a total depth of 420 ft (128 m) near the proposed centerpoint of the reactor building. All of the geotechnical and geophysical borings penetrated the full thickness of the residual soil deposits and at least 9.5ft (3 m) of the Middle Devonian Mahantango Formation. In addition, approximately 250 exploratory borings were drilled in soil and rock in late 1970, Spring 1971, and 1983 at or near the SSES site. Also, test pits were excavated at selected locations at or near the SSES site.

It is estimated that the full thickness of the Mahantango Formation at the BBNPP site is approximately 1,500 ft (457 m) (Inners, 1978). Thus, there are approximately 1,100 ft (335 m) or more of Mahantango Formation that lies beneath the deepest geotechnical boring at the BBNPP site. Geological information relative to the uppermost 420 ft. (128 m) of geologic strata at the site was derived from cores and drilling information obtained during the on-site BBNPP subsurface investigations. Stratigraphic information regarding the deeper geologic strata was obtained primarily from publications by the Pennsylvania Topographic and Geologic Survey which focus primarily on this area (e.g., Inners, 1978; Crawl, 1980; and Williams, 1987).

Characteristics of the basement rocks in Pennsylvania are extrapolated from the exposed metamorphic rock in the Piedmont Physiographic Province to the southeast and several exploratory wells in western Pennsylvania (Saylor, 1999). Based on available data (Saylor, 1999), it is likely that the basement rock beneath the site is similar to the schists and gneisses found in the Piedmont Physiographic Province, which is located approximately 50 mi (80 km) to the southeast of the BBNPP site as shown in Figure 2.5-126.

Paleozoic rocks of the Ridge and Valley Province are representative of formations deposited in a foreland basin that have undergone numerous cycles of marine regression/transgression. The Province extends from eastern New Jersey to Alabama and has been subjected to multiple orogenies. Stratigraphic formations, and their depositional environments, are also discussed in Section 2.5.1.1.2 and Section 2.5.1.1.3. A stratigraphic column created specifically for the BBNPP site and site area (5 mi (8 km) radius) is shown in Figure 2.5-13. The following Subsections describe each of the stratigraphic formations, in order of oldest to youngest.

2.5.1.2.3.1 Cambrian Formations

The oldest inferred Cambrian Formation underlying the site area is the Waynesboro Formation. The Waynesboro Formation consists of sandstone with interbedded red and green shales and has a thickness of approximately 1,000 ft (305 m) or more (Kauffman, 1999).

Overlying the Waynesboro Formation is the Pleasant Hill Formation, which is primarily a limestone formation with interbedded sandy and silty layers throughout (Kauffman, 1999). Overlying the Pleasant Hill Formation is the Warrior Formation. It is a dark, fossiliferous, fine grained limestone interbedded with silty dolomite, with a thickness up to 1,340 ft (408 m) (Kauffman, 1999). Overlying the Warrior Formation, and marking the Cambrian-Ordovician boundary, is the Gatesburg Formation. The Gatesburg Formation consists of a series of sequential sandstone and dolomite units that are fossiliferous (Ryder, 1992) and in excess of 1211 ft (369 m) thick (Gold, 2003). Both the Warrior and Gatesburg formations likely represent a shallow-water carbonate bank or shelf that was subjected to periodic episodes of near-drying conditions (Kauffman, 1999).

2.5.1.2.3.2 Ordovician Formations

Overlying the Upper Cambrian Gatesburg Formation are the Lower Ordovician formations that comprise the Beekmantown Group. These Lower Ordovician formations, from oldest to most recent, include the Stonehenge Formation, Nittany Dolomite, Axemann Limestone, and Bellefonte Dolomite. They are composed primarily of dolomites and limestones (Harper, 2003) and reach a combined thickness of up 4,200 ft (1,280 m) (Thompson, 1999).

The Middle Ordovician strata include the Loysburg Formation, the Black River Group, and the Trenton Group. The Loysburg Formation is typically a dolomitic and stromatalite rich limestone underlying a coarse grained, fossiliferous limestone (Thompson, 1999) with an average thickness of 263 to 475 ft (80 to 145 m). Overlying the Loysburg Formation is the Black River Group that consists of the Snyder and Linden Hall formations (Thompson, 1999) and attains a thickness of about 632 ft (193 m). These formations are composed primarily of siliciclastic clay and shale. Overlying the Black River Group are fine-grained, black, graded limestone and shales of the Solona and Coburn formations of the Trenton Group (Thompson, 1999).

Rocks of the Beekmantown Group, Loysburg Formation, Black River Group, Solona Formation, and Coburn Formation were deposited in marine to marginal-marine environments. Where a platform existed and the seas became progressively shallower, depositional environments became more intertidal (Thompson, 1999). The uppermost rocks within the Trenton Group belong to the Antes Formation, a fossiliferous, generally black, shale (Thompson, 1999) that was likely deposited in shallow water, above the wave base. The Antes, Coburn, and Salona formations collectively attain a thickness of approximately 842 ft (257 m).

Upper Ordovician strata include the Reedsville, Bald Eagle, and Juniata formations (in ascending order). The Reedsville Formation is approximately 600 to 1800 ft (183-549 m) thick and is composed primarily of interbedded shale and sandstone beds, with some limestone (Thompson, 1999; Gold, 2003). Like the Antes Formation underlying it, the Reedsville Formation was likely deposited in shallow water. The Bald Eagle Formation and the Juniata Formation are 700 to 1313 ft (213 to 400 m) and 600 to 1,125 ft (183 to 343 m) thick, respectively (Thompson, 1999; Gold, 2003). Both of these formations consist of nonfossiliferous sandstones, conglomerates, and mudstones, but differ in color with the Bald Eagle being gray and the Juniata red (Thompson, 1999). Unlike the Reedsville Formation, the Bald Eagle and Juniata formations are non-fossiliferous and non-marine. These formations were likely deposited near low-sinuosity streams on alluvial fans (Thompson, 1999).

2.5.1.2.3.3 Silurian Formations

The Tuscarora Formation typically marks the boundary between Late Ordovician and Silurian Periods. The Lower Silurian Tuscarora Formation is quartzose, sublithic, and argillaceous

sandstone with few shale beds throughout, and was deposited in a fluvial environment (Laughrey, 1999). The Tuscarora Formation ranges between 400 ft (122 m) and 700 ft (213 m) thick and is extremely resistant to erosion and weathering processes (Laughrey, 1999; Gold, 2003).

Overlying the Tuscarora Formation (in ascending order) are the Rose Hill, Keefer, Mifflintown, Bloomsburg, Wills Creek, Tonoloway, and Keyser formations, all of Silurian age (Figure 2.5-13). The Rose Hill Formation consists of olive shale with interbedded layers of hematitic sandstone, purplish shale, and fossiliferous limestone (Laughrey, 1999). Above the Rose Hill Formation lies the Keefer Formation, a quartzose and hematitic sandstone with some mudstone. The Rose Hill and Keefer formations combine for a thickness that ranges between 600 ft (183 m) and 1070 ft (326 m) (Gold, 2003). The Mifflintown Formation reaches a thickness of about 336 ft (102 m) (Gold, 2003) and is composed of sandy and silty shales, siltstone, and limestone of a shallow marine setting (Laughrey, 1999). The likely depositional environment for the Rose Hill, Keefer, and Mifflintown formations is that of a submarine ramp that deepened from the proximal basin margin (Laughrey, 1999) during the Taconic Orogeny, as discussed in Section 2.5.1.1.2.3 and Section 2.5.1.1.3.

Conformably overlying the Mifflintown Formation is the Bloomsburg Formation (Early Silurian), which consists primarily of grayish-red clay-siltstone with some interbedded fine- to coarse-grained sandstone beds. The Bloomsburg Formation ranges in thickness from 85 ft (26 m) to 464 ft (141 m). It is slightly fossiliferous and probably represents sediments deposited in deltaic waters with a high enough salinity to allow some fauna to exist (Laughrey, 1999).

Upper Silurian strata include the Wills Creek, Tonoloway, and Keyser formations. The Wills Creek Formation conformably overlies the Bloomsburg Formation, and consists primarily of claystone to silty claystone with some interbedded grayish-red sandstone and fine-grained argillaceous dolostone and dolomitic limestone. The Wills Creek Formation is approximately 750 ft (229 m) thick (Inners, 1978) and represents deposition in lagoonal, intertidal, and supratidal environments. The Tonoloway Formation is primarily a thinly-bedded limestone deposit with a few thin beds of calcareous shale (Laughrey, 1999); it is about 100 ft (30 m) thick (Inners, 1978). Both the Wills Creek and Tonoloway formations represent numerous shallowing-upward cycles that have been interpreted as repeated progradational events on very large tidal flats (Laughrey, 1999).

The Keyser Formation conformably overlies the Tonoloway Formation and consists mainly of medium to dark gray, fine-grained, fossiliferous limestone with minor interbeds of dark-gray calcareous clay shale. Some dark gray cherty nodules are present toward the upper part of the formation. The Keyser Formation straddles the boundary between the Late Silurian and Early Devonian as the formation represents continuous carbonate sedimentation from both periods and has a thickness of about 125 ft (38 m) (Inners, 1978).

2.5.1.2.3.4 Devonian Formations

The Devonian system of rocks is described as a westward-thinning wedge of sediments with a thickness of almost 11,000 ft (3,353 m) throughout much of Pennsylvania (Harper, 1999). The Upper Keyser Formation makes up the basal unit for the Devonian period formations.

Overlying the Keyser Formation is the Old Port Formation, which consists of (in ascending order) the Corriganville Limestone, the Mandata Shale, Shriver Chert, and Ridgeley Sandstone (Harper, 1999). The Corriganville Limestone consists of finely crystalline, thick to thinly-bedded limestone and ranges from 10 ft (3 m) to 30 ft (9 m) thick (Harper, 1999). The Mandata Shale is dark gray to black, thinly-bedded, siliceous shale, and ranges in thickness from 20 ft (6 m) to

100 ft (30 m) (Harper, 1999). Light colored cherty, mudstones and calcareous siltstones characterize the Shriver Chert (Harper, 1999), which ranges in thickness from 80 ft (24 m) to 170 ft (52 m). The Ridgeley Sandstone ranges in thickness from 8 ft (2 m) to 170 ft (52 m) and is generally white to light-gray, medium grained, quartzose sandstone (Harper, 1999). These units of the Old Port Formation represent the gradual deepening of the Appalachian basin and range in overall thickness from 100 ft (30 m) to 150 ft (46 m) in the site area (Inners, 1978).

The Silurian limestone formations (Wills Creek, Tonoloway, and Keyser) and the Devonian Old Port Formation contain minor dissolution features along bedding planes, fractures, and joints, which makes them relatively good aquifers at shallow depth (see Section 2.5.1.2). The total thickness of these formations is approximately 700 feet (213 m) and they are located at least 1,700 ft (518 m) below the BBNPP site. In general, due to their depth, dissolution features along bedding planes or fractures at this depth are very minor and will have no effect on the structural stability or strength of the overlying rock strata.

The Onondaga Formation (Middle Devonian) disconformably overlies the Old Port Formation and reaches a thickness of about 175 ft (53 m) in the site area (Inners, 1978). The Onondaga Formation consists of silty, shaley, and cherty limestones, and likely represents a shelf margin depositional environment (Harper, 1999). The upper part is a medium dark gray argillaceous, fine-grained, pyritic limestone with interbeds of medium dark gray calcareous clay shale (Selinsgrove Limestone Member) and the lower part is a medium to dark gray, calcareous, slightly silty, clay shale (Needmore Shale Member).

The Marcellus and Mahantango formations together form the Hamilton Group of Middle Devonian age (Figure 2.5-13). The Marcellus Formation, located below the Mahantango Formation, consists of approximately 350 ft (107 m) (Inners, 1978) of dark-gray to black shales that are carbonaceous, and contain pyrite and few fossils (Harper, 1999). The Marcellus Formation was likely deposited in a variety of shallow-water anoxic environments (Harper, 1999).

The Mahantango Formation overlies the Marcellus Shale and is the uppermost bedrock unit at the BBNPP site, as shown in Figure 2.5-13 and Figure 2.5-134. Harper (Harper, 1999) describes the Mahantango Formation as a complex series of interbedded shales, siltstones, and sandstones, ranging from 1,200 ft (366 m) to 2,200 ft (671 m) thick. Inners (Inners, 1978) reports the thickness of the Mahantango Formation is approximately 1,500 ft (457 m) in the site area. According to Inners (Inners, 1978), the Mahantango Formation consists primarily of

"medium dark to dark gray, silty to very silty claystone (95 percent), with some argillaceous, fine-grained limestone (5 percent) in the uppermost part. Claystone generally in poorly-defined beds 3 to 10 feet (1 to 3 m) thick; massive, often with profuse burrows; noncalcareous to very calcareous; medium-dark-gray, pyritic siderite and limestone nodules, 1 to 4 inches (2.5 to 10 cm) in diameter, are locally abundant and often form distinct bands; several calcareous, fossiliferous horizons 3 to 10 feet (1 to 3 m) thick and abounding in marine invertebrates, can be traced locally."

The Tully Member (or Tully Limestone Member) is found at the top of the Mahantango Formation and is medium dark gray (light gray where weathered), fossiliferous, argillaceous, fine-grained limestone and calcareous clay shale. It is approximately 50 to 75 feet (15 to 23 m) thick, but has been eroded from the crest of the Berwick Anticline at the site (Inners, 1978). The Mahantango Formation and the Tully Member represent marine sediments deposited on a

shallow subtidal shelf. Harper (1999) suggests that the Mahantango Formation was deposited as a prograding marine shoreline during the early stages of the Catskill Delta.

The shales and siltstones encountered during the BBNPP site investigation were typically dark gray, ranged in hardness from soft to moderately hard, increased progressively in the level of calcareous content with depth, and were slightly pyritic and fossiliferous throughout. The weathered shale that formed the uppermost bedrock surface typically ranges from 5 to 45 ft (1.5 to 13) thick, and is termed the Weathered Zone. Below the weathered shale, the rock becomes much harder and the rock quality designation (RQD) increases, ranging up to 100 percent with an average of 33 percent (see Figure 2.5-141 through Figure 2.5-146). The rock in this zone, termed the Transition Zone, is similar to the sound Mahantango Shale below it, but is highly fractured and can range from non-existent to 84 ft (0 to 25 m) thick. In 8 geotechnical borings, the Weathered Zone and the Transition Zone alternate back and forth. At the point where the highly fractured rock diminishes, the shale is termed the Sound Rock. The Sound Rock zone has an average RQD of 86 percent and in some cases, was so unfractured and competent that the shale cores were removed from the core barrels intact with no breaks at all (Figure 2.5-14). As discussed in Section 2.5.4.2, the Mahantango shale is a hard, competent bedrock unit. According to Inners (Inners, 1978), the Mahantango Formation has "high foundation support strength, suitable for heavy structures if excavated to sound bedrock." Physical properties of the shale bedrock are discussed in detail in Section 2.5.4.2.

The Mahantango Shale is the uppermost bedrock unit present throughout most of the BBNPP site, including all of the areas supporting safety-related structures. Another black shale (the Harrell Shale) is present between the Mahantango Shale and Trimmers Rock Formation in the northern portion of the site and is about 120 ft (37 m) thick (Inners, 1978). It conformably overlies the Mahantango Formation and marks the initial unit of the Upper Devonian strata. The Harrell Formation is typically represented by dark gray to grayish black, pyritic, organic-rich, clay shale and silty clay shales (Inners, 1978; Harper, 1999). The Harrell Shale was deposited in a poorly-oxygenated basinal marine environment. Where exposed today at the ground surface, the shale has moderately developed cleavage, is jointed, and forms splintery and platy fragments. The weathered surfaces can be covered by efflorescent secondary sulfate minerals. Because the shale has low resistance to weathering, it typically forms a swale at the foot of escarpments developed by the Trimmers Rock Formation (Inners, 1978). The swale that runs east to west along the northern edge of the SSES and the BBNPP sites (immediately south of Beach Grove Road) is shown as the outcrop area of Harrell Shale by Inners (Inners, 1978; Figure 2.5-134)

While the Mahantango and Harrell formations are the only two bedrock formations exposed at the BBNPP site, other younger Paleozoic Era formations that were deposited after the Harrell Formation exist within the site area (5 mi (8 km) radius), as shown in Figure 2.5-134, Figure 2.5-138, and Figure 2.5-139. These formations comprise the ridges and bedrock outcrops to the north and south of the site, such as Lee and Nescopeck Mountains, respectively.

The Upper Devonian Trimmers Rock Formation lies immediately above the Harrell Shale. It is composed primarily of medium to dark gray siltstone and shale (60 percent), medium to medium dark gray, thinly-bedded, very fine to fine grained sandstone (25 percent), and medium to dark gray silty clay shale (Inners, 1978; Harper, 1999). The Trimmers Rock Formation has a calculated thickness of approximately 3,000 ft (914 m) (Inners, 1978) and likely represents a delta-fed submarine slope of the Appalachian Basin. The Trimmers Rock Formation is resistant to erosion and forms steep escarpments on the north and south sides of

the Susquehanna River Valley. The east-west trending unnamed ridge that lies directly north of the BBNPP site is composed of Trimmers Rock Formation and the ground surface rises steeply going up the south flank of this ridge (Figure 2.5-4; Figure 2.5-151).

Above the Trimmers Rock Formation, within the site area, lie the members of the Upper Devonian Catskill Formation including (in ascending order) the Irish Valley, Sherman Creek, and Duncannon Members. Each member of the Catskill Formation ranges in thickness from 150 ft (46 m) to 3,700 ft (1,128 m) and generally consists of gray to red mudstones, claystones, siltstones, and conglomerates that were deposited in mixed continental, fluvial-deltaic, and marginal-marine environments (Inners, 1978; Harper, 1999).

The uppermost unit of Devonian age rocks in the site area is the Spechty Kopf Formation, which also spans into, and identifies the beginning of the Carboniferous Period. The Spechty Kopf Formation has a thickness of about 575 ft (175 m) near the crest of Nescopeck Mountain, but is absent north of the BBNPP site on Lee Mountain (Inners, 1978). It is composed mainly of medium gray to olive sandstone with other components including siltstone, shale, and conglomerates (Berg, 1999). The likely depositional environment of the Spechty Kopf Formation was that of ephemeral lakes formed on the surface of the Catskill alluvial plain (Berg, 1999).

2.5.1.2.3.5 Mississippian Formations

Mississippian rocks of the site area represent a transition from the prograding deltas of the Late Devonian Period (Brezinski, 1999) to Pennsylvanian rocks, which primarily represent sedimentary environments within an elongate basin aligned in a northeast to southwest direction (Edmunds, 1999).

The Devonian-Mississippian boundary is marked by the presence of the Upper Spechty Kopf Formation. Unconformably overlying the Spechty Kopf Formation is the Pocono Formation, which was likely deposited on a high-gradient alluvial plain or alluvial fan, is represented by beds of medium to coarse grained sandstone, siltstone, and conglomerates (Brezinski, 1999) with a thickness of about 600-650 ft (183-198 m) (Inners, 1978). Overlying the Pocono Formation within the 5 mile (8 km) site area radius, is the Mauch Chunk Formation, easily recognizable by its red to reddish-brown mudstone and siltstone with reddish-brown and greenish-gray sandstones and conglomerates (Brezinski, 1999). The Mauch Chunk ranges in thickness throughout the site area but has been estimated to be between 3,000 ft (914 m) to 4,000 ft (1,219 m) thick (Brezinski, 1999). The depositional environment of the Mauch Chunk Formation was likely that of a broad alluvial plain in which deposits came from two distinct sources. The first source was red clastics, likely derived from the Taconic highlands, and the second was quartz sand from the erosion of the previously deposited (Burgoon) sandstones (Brezinski, 1999).

2.5.1.2.3.6 Pennsylvanian Formations

The Mississippian-Pennsylvanian boundary in the site area is generally considered to be the top of the Mauch Chunk Formation and bottom of the Pottsville Formation. The Pennsylvanian Pottsville Formation overlies the Mauch Chunk Formation conformably and ranges in thickness from 100 ft (30 m) to 1,600 ft (488 m) (Edmunds, 1999). The Pottsville Formation consists mainly of a cobble and pebble conglomerate with some sandstones and finer clastics and coal (Edmunds, 1999).

The youngest rock formation within a 5 mi (8 km) radius of the site area, and overlying the Pottsville Formation, is the Llewellyn Formation. The Llewellyn Formation reaches a thickness

of approximately 3,500 ft (1,067 m) through other portions of Pennsylvania and generally consists of subgraywacke clastics, ranging from conglomerates to clay shale and containing numerous coal beds (Edmunds, 1999). The Llewellyn Formation is very resistant to erosion and forms the crest of Lee Mountain near the town of the Shickshinny, as seen in Figure 2.5-3.

2.5.1.2.3.7 Quaternary Deposits

The bedrock at the BBNPP site and the site area is mostly covered with a variable thickness of Pleistocene sediments including kame, kame terrace, outwash, ground moraine and end moraine deposits (Figure 2.5-136 and Figure 2.5-137). However, on the hill where the most of the BBNPP facilities are to be located, the surface is covered with residual soil with only thin localized patches of glacial till deposits. Inners (Inners, 1978) maps this hill as Woodfordian End Moraine deposits, but extensive site investigations do not find such deposits at the site. Inners (1978) did not have the benefit of such a detailed study of this particular location and his mapping therefore must be taken as inaccurate for this location. The hill likely was completely covered by some thickness of till after the glaciers retreated, but those deposits have been largely eroded away at this time.

Quaternary deposits of the site area are primarily the result of glacial deposition during at least three known glacial events that are believed to have impacted the site area. Of these three events, Quaternary deposits from two of them comprise the soil overburdens present within the site area. The earliest deposit is of Late Illinoian age (unnamed) and can be stratigraphically correlated to that of the Titusville Till in northwestern Pennsylvania, as shown in Figure 2.5-127. These Unnamed and Titusville Tills are described as a thin, gray to brown and grayish-red clay and sand (Sevon, 2000c). This was almost entirely eroded away during the next glacial advance through the site during the Wisconsinan Epoch (Crowl, 1999). The resulting glacial deposits from the Wisconsinan event is known as Olean Till, which is described as moderately thick, gray to grayish-red sandy till (Sevon, 2000c).

Lower elevations between ridges within the site area (e.g., Susquehanna River floodplain) are covered with thick deposits of stratified drift, as shown in Figure 2.5-137. The stratified drift, as defined by Sevon (2000c), is sand and gravel in eskers, kame terraces, and outwash. Stratified drift has been deposited the site area since the Late Illinoian (Sevon, 2000c), during periods of glacial melting and retreat.

2.5.1.2.4 Site Area Structural Geology

The structural geology of the BBNPP site described in this section has been developed using the following sources:

- ◆ the BBNPP site reconnaissance and subsurface explorations performed for this study,
- ◆ results of earlier investigations performed at the SSES site, and
- ◆ published geologic literature.

There have been no geologic structures identified during this investigation that pose a threat to the BBNPP site operations. The following discussions will support that conclusion by presenting the information on the geologic structures present within 25 miles (40 km) of the BBNPP site, and with increasing detail within the 5 mi (8 km) and 0.6 mi (1 km) distances from the site.

The following discussions present the current understanding of the geologic structures within the site vicinity, starting with the deep crystalline basement, followed by the overlying folded

and lithified sedimentary bedrock, and concluding with the on-site investigations conducted for this report. As reported in more detail in Section 2.5.1.1.4, there are faults and folds that occur within the 25 mi (40 km) BBNPP site vicinity (Figure 2.5-140 and Figure 2.5-134). These include the Light Street and Berwick faults within the Berwick Anticlinorium, the Lackawanna Synclinorium and the Catawissa-McCauley Mountain Synclinorium. Each will be discussed in turn in the following sections.

2.5.1.2.4.1 Structures in the Crystalline Basement

Available geophysical data in surrounding areas indicate that the basement likely consists of exotic crystalline magmatic arc material (Hansen, 1986; Glover, 1995). Regional geologic cross sections developed from geophysical, gravity, and aeromagnetic surveys, as well as limited deep borehole data from outside of the BBNPP site area, suggest that complexly deformed, metamorphosed crystalline igneous rocks of Precambrian and Paleozoic age are likely present at approximately -33,000 ft (-10,058 m) msl (Figure 2.5-130 and Figure 2.5-132) (Crawford, 1999; King, 1974; and Gold, 2005). The basement map in Figure 2.5-130 (Gold, 2005) confirms the depth to the basement rocks as well as the relative featureless nature of that surface beneath the site.

To supplement the discussion of basement structures, regional and site vicinity maps of the gravity and magnetic fields are presented in Figure 2.5-9 and Figure 2.5-10 (Kucks, 1999) and Figure 2.5-11 and Figure 2.5-12 respectively (Bankey, 2002). Regional Tectonic Features and Basins are depicted on potential base maps in Figure 2.5-156, Figure 2.5-157, Figure 2.5-158 and Figure 2.5-159. None of these data reveal new anomalies related to geologic structures. The following sections discuss the local gravity and magnetic anomalies, as presented in more detail in Section 2.5.1.1.4.3.

2.5.1.2.4.1.1 Gravity Data and Features

Anomalies in gravity data occur from density contrasts in size and depth of geologic structures. Gravity highs, or positive anomalies, are created by abundant thickness or shallow burial of dense features, while gravity lows are from mass deficiencies. Long wavelengths show deep structures or highly concentrated deep structures, and shorter wavelengths are created by shallower structures (Lavin, 1999).

As shown on Figure 2.5-10, the only feature relevant to the site vicinity is the Scranton gravity high, that has a northeast trend that is sub-parallel to the folds in the current mountains. The long wavelength of this high and the shallow gradients along its margins indicates its deep burial. The Scranton gravity high is related to dense mafic material that was emplaced during Late Precambrian rifting (Lavin, 1999).

2.5.1.2.4.1.2 Magnetic Data and Features

Magnetic data compiled for the 2002 Magnetic Anomaly Map of North America reveal numerous northeast-southwest trending magnetic anomalies, generally parallel to the structural features of the Appalachian orogenic belt (Bankey, 2002) (Figure 2.5-11). The magnetic map allows a visualization of the geological structure of the upper crust in the subsurface showing the spatial geometry of bodies of rock and the presence of faults and folds.

The BBNPP site is located in an area with few anomalies and with low gradients between anomalies (Figure 2.5-12). These conditions are consistent with the profound basement depths in the vicinity of the site. The BBNPP site is situated in the middle of a northeast-trending area of low magnetic relief related to a block of Precambrian basement

called the Clingman-Ocoee block that is bounded to the northwest by the New York-Alabama Lineament and to the southeast by the Clingman-Ocoee Lineament (Johnston, 1985b).

2.5.1.2.4.2 Berwick Anticlinorium

The principal bedrock structure within the site area is the Berwick Anticlinorium (also referred to as the Montour Anticline (Pohn, 2000)), which has been described (Inners, 1978) as "a moderately complex, first order fold which trends in a northeast-southwest direction". The bedrock map and section of the Berwick Quadrangle (Inners, 1978) shows the formations at the BBNPP site area to consist of Silurian, Devonian, and Carboniferous rocks that have been gently folded, with limited faulting (Figure 2.5-134 and Figure 2.5-135). The BBNPP site is situated on the northern limb of the fold. Two faults have been mapped in the vicinity: the Light Street fault located on the northern limb of the fold, and the Berwick fault, inferred to be on the southern limb of the fold. The northeast end of both faults lies within the site area, but do not directly underlie the site.

Unconformably overlying this Paleozoic bedrock is a thin covering of a few flat-lying post-Paleozoic formations composed primarily of glacial till and colluvium overburden, laid down by multiple Quaternary glacial events (Inners, 1978) (Figure 2.5-136 and Figure 2.5-137).

2.5.1.2.4.2.1 Light Street Fault

The 28 mile (46 km) (Klawon, 1995) long Light Street fault approaches to within 2 mi (3.2 km) of the BBNPP site (Figure 2.5-138 and Figure 2.5-140). The Light Street Fault brings into contact the Marcellus Formation with the Onondaga and Old Port formations. Based on published data (Inners, 1978; Gillmeister, 1993; Klawon, 1995) the nature of this fault is either (1) a thrust fault that dips in a southerly direction and eliminates a section of the stratigraphy between the Wills Creek and Marcellus formations; (2) the detachment of a major décollement that dips to the north; (3) a late stage left-lateral strike slip fault (Gillmeister, 1993); or (4) a combination of (1) and (2) (Inners, 1978). The simplest explanation for the fault occurrence in the area, as well as evidence gathered by Klawon (Klawon, 1995), indicates that it is a south-dipping reverse fault as mapped in Figure 2.5-134 and Figure 2.5-135.

The presence of the Light Street Fault is attributed to the folding and faulting actions that occurred at the site area during the Alleghanian Orogeny (Inners, 1978), approximately 340 to 250 million years ago. Figure 2.5-135 shows that the fault does not cut the Quaternary surface deposits overlying the area. This is confirmed by the surficial geologic map (Figure 2.5-137) that also shows no evidence of the fault penetrating those deposits.

There is no historical seismicity that is spatially related to this fault. A study of geologic features potentially resulting from Quaternary tectonic faulting in the Eastern United States (Wheeler, 2006), did not identify this fault as being active.

Because of the age of last motion on this fault, and its lack of historical seismicity, the Light Street Fault is not considered to be a capable tectonic source.

2.5.1.2.4.2.2 Berwick Fault

The Berwick Fault is identified by a repeating of the section of the Old Port and Keyser formations on the southern limb of the fold. The fault is inferred from limited surface data and from a water well log drilled at the Berwick Lumber and Supply Company at 329 West Second Street in Berwick, PA (Figure 2.5-134 and Figure 2.5-135) (Inners, 1978). The investigators were unable to locate this well and it appears to have been abandoned prior to the site investigation. The inferred Berwick Fault lies within the site area and its northeastern end

comes to within approximately 3.5 mi (5.6 km) of the BBNPP site. The length of the Berwick Fault is not completely mapped and is believed to be a south-dipping reverse fault on the south flank of the Berwick Anticlinorium (Figure 2.5-135) (Inners, 1978). The Berwick fault extends east-northeastward into an exposed third order anticline in the Marcellus-Mahantango interval (Inners, 1978).

This fault is like the Light Street fault, in respect to both its age and its lack of recent seismicity. Because the Berwick Fault is attributed to the folding and faulting actions that occurred during the Alleghanian Orogeny (Inners, 1978), and because there is no seismicity that is spatially related to this feature (Wheeler, 2006), the Berwick fault is not considered a capable tectonic source.

2.5.1.2.4.3 Lackawanna and Catawissa-McCauley Mountain Synclinoria

Sectional views of the site geology (Figure 2.5-132 and Figure 2.5-135) show these two folds to be synclines located beneath Lee and Huntington Mountains to the north (Lackawanna Synclinorium), and just beyond Nescopeck Mountain to the south (Catawissa-McCauley Mountain Synclinorium). The southern end of the Lackawanna Synclinorium (Inners, 1978) lies within the site area and a portion of it is shown in the northwest corner of Figure 2.5-134. The Lackawanna Synclinorium is a coal-bearing 68 mi (110 km) long structural trough in the Appalachian foreland of northeastern Pennsylvania (Harrison, 2004), that extends to the northeast of the site. The entire synclinorium was thought to be an Alleghanian thin-skinned contractional structure that formed similarly to the fold trains of the central Appalachian Ridge and Valley province (Harrison, 2004). However, interpretation of seismic reflection data from across the structure suggests that the synclinorium formed primarily by the removal of salt (Harrison, 2004).

The Catawissa-McCauley Mountain synclinorium is represented by the synclinal axis in the extreme lower right corner of Figure 2.5-134, just south of Nescopeck Mountain. The axes of this synclinorium follow the regional trends to the southwest-northeast, parallel with the axis of the Berwick Anticlinorium. This syncline has been delineated from numerous outcrop searches (Inners, 1978), geophysical data and a limited number of deep boreholes that penetrate the crust (Pohn, 2000). This fold is the northernmost part of the Anthracite Region located to the south of the site. The Anthracite region, located within a northeast plunging syncline, is the most faulted area of the Appalachian Ridge and Valley Province (Hornberger, 2004) (Figure 2.5-140). The dominant faults consist of thrust faults, as part of the base décollement which separates thrust and folded Paleozoic rocks from Precambrian basement rocks. The fault system has not been active since the post Carboniferous period and is located 20 mi (32 km) to the south of the site (Berg, 1980).

These folded features were formed at the same time as the Berwick Anticline (approximately 250 Ma), show limited faulting, and have no historical seismicity spatially related to them. Because of the age of the deformations and the lack of current seismicity related to them, these features are not considered to be capable tectonic sources.

2.5.1.2.4.4 Site Investigations

The investigations at the site include a subsurface investigation for the foundation study, a geophysical investigation, and a field reconnaissance to inspect surface features for evidence of deformation, including folding, faulting and liquefaction. A subsurface investigation was completed at the SSES site, adjacent to the BBNPP site to the east, as part of the FSAR process for that site. The conclusions of that investigation at the SSES location are relevant to the current study by reason of proximity and intended purpose.

2.5.1.2.4.4.1 Subsurface Investigations at the BBNPP Site

Geologic sections developed from geotechnical data collected from 44 boreholes as part of the BBNPP study (as discussed in Section 2.5.4) provide detailed information in the upper 420 ft (128 m) of strata for the presence of structures directly beneath the site. The investigation at the BBNPP site indicates that the site is underlain by unfaulted Middle Devonian shale of the Mahantango Formation. Bedding planes of the formation have been measured at and near the site with strike azimuth measurements ranging predominantly from 61 to 100 degrees and dip angles between 10 and 30 degrees to the north-northwest (Figure 2.5-138). The bedding plane observations within the Mahantango Formation are obscured by strong overprinting from a steeply dipping cleavage. Cleavage planes have been measured at and near the site with strike azimuth measurements ranging from 60 to 92 degrees and dip angles between 58 and 75 degrees to the south-southeast (Figure 2.5-138).

The top of the bedrock shale beneath the site is covered by a layer of residual soil that formed by weathering of the Mahantango Shale itself. Because of the location of the site on a topographic high, the vast majority of any younger sediment deposited during the retreat of the glaciers has been eroded away leaving only isolated locations of thin till. In the lower elevations of the site below the break in slope of the hill where the pond will be located, there is only glacial till and outwash deposits present overlying the bedrock as any residual soils at these elevations were removed by the advance of the glaciers (Figure 2.5-146). Figure 2.5-141 through Figure 2.5-145 show that the residual soils form a blanket that mimics the shape of the underlying bedrock surface. Since the time of glacial retreat, weathering and stress relief have left a pattern of weathered and fractured rock overlying the sound rock and underlying the residual soils. Cross sections prepared oblique to the previously mapped northeast-trending Light Street and Berwick faults (Figure 2.5-141 and Figure 2.5-142 show a slightly rolling bedrock surface below the BBNPP site, without offsets that would be characteristic of a faulted area.

Although the bedrock formations underlying the BBNPP site are dipping and have experienced folding during the Alleghanian Orogeny (Williams, 1987; Fail, 1999a), surficial sediments at the site display no signs of faulting or folding during the Pleistocene to Holocene time period, and rest unconformably on the eroded surface of the tilted beds of the local shale bedrock of the Mahantango Formation.

2.5.1.2.4.4.2 Geophysical Investigations

Because earth materials exhibit characteristic wave propagation velocities, they can be classified simply in terms of their seismic velocity. Hence, seismic refraction surveys were performed to support site characterization studies for the BBNPP (Section 2.5.4.2.2.3). The seismic refraction data were interpreted to assist in characterizing the local subsurface geologic materials regarding the thickness of the soil overburden, depths to weathered or fractured bedrock, and depths to competent bedrock. Seismic refraction surveys were operated along 9 profile lines totaling 7440 linear feet (2268 m) of coverage. The data for the surveys were collected from May 26 to June 5, 2010 using approved quality assurance procedures. The complete report of this survey (GeoVision, 2010) is included in the Appendices.

Figure 2.5-53 is a map depicting the layout of the 9 lines used during the survey (Lines A1 through A5, oriented east-west; and Lines B1 through B4, oriented north-south). Seismic refraction velocity profiles are presented on Figure 2.5-57 through Figure 2.5-65 with the vertical scale measuring elevation in feet. Tomographic inversion routines are the most appropriate data modeling technique for this site because velocity gradients are assumed to

be present within weathered bedrock at this site, and refraction tomography techniques are often able to resolve complex velocity structure (e.g. velocity gradients) that can be observed in bedrock weathering profiles. Layer based modeling techniques such as the Generalized Reciprocal Method (GRM) are not able to accurately model the velocity gradients that can be observed in weathered bedrock such as at the BBNPP. However, the GRM method was used to confirm velocity ranges in the tomographic models.

These interpreted velocity profiles indicate that the elevation of the competent rock is highest in the northern portion of the site, and forms an east-west to southeast-northwest trending depression in the central portion of the site with elevation increasing again to the south. Figure 2.5-66 is a representation of the surface of the competent bedrock. The top of this surface is based on an interpreted velocity in the 11,000 to 13,000 feet per second (ft/s) range (3,400 to 4,000 meters per second (mps)). The approximate locations of the top of the decomposed, weathered and competent shale identified in boreholes within 50 ft (15.2 m) of the seismic lines is included on the seismic models to aid with interpretation (Figure 2.5-57 through Figure 2.5-65).

Two possible weathered shale units are identified within the tomographic profiles; one based on geologic description (WS1) and the other based on the depth at which RQD exceeds 0% (WS2) (GeoVision, 2010). The locations of the 4,000, 6,000 and 12,000 ft/s (1,200, 1,800 and 3,700 mps) contours from intersecting lines are also shown on the seismic models for discussion. There is a distinct possibility at this site that velocity structure may be slightly different at intersecting lines because of the complex velocity structure of the weathered shale (GeoVision, 2010). Additionally, bedding and fracture attitudes relative to the seismic line orientation may have a significant impact on modeled seismic velocity structure. A review of the data in the figures shows no offsets or abrupt changes in the tops of the bedrock that could indicate recent deformation. See section 2.5.4 for a more detailed discussion of the geophysical analysis.

The map of the top of the competent Mahantango Shale from the boring log data (Figure 2.5-82) shows a surface similar to that shown in Figure 2.5-66 that was developed for the top of competent rock from the geophysical data. Both maps show that the interpreted elevation of the top of the competent rock, as mentioned above, is highest in the northern and southern portions of the site, with an east-west to southeast-northwest trending depression in the center of the site.

Because the interpreted upper surfaces of the decomposed shale and weathered shale (Figure 2.5-55 and Figure 2.5-56) generally parallel surface topography at the site, the depression in the top of the competent rock in the center of the site is related to a thickened weathered shale layer, as can be seen in the reflection profiles (Figure 2.5-57 through Figure 2.5-65) and cross-sections (Figure 2.5-141 through Figure 2.5-145). The reason for over-thickened weathered and fractured rock zone in the center of the site is presumably because this zone is located under a gully in the hill, which is oriented parallel to major structural orientations within the site area. Within this gully, precipitation is channeled off of the hill and leads to greater subsurface penetration of water within this zone, leading to deeper weathering and fracture propagation in the Mahantango Formation. However, because the top surfaces of the decomposed shale and weathered shale are parallel to the ground surface, with no obvious offset, it is clear that no Quaternary faulting has affected the site.

The close correlation between the seismic data and the boring log data, both in locating the top of rock elevation and in the lack of observed faulting in the rock mass, further confirms the interpretation by earlier researchers in the area (Inners, 1978, Williams, 1987) that there is no evidence of faulting in the Quaternary deposits underlying the site.

2.5.1.2.4.4.3 Interpretation of Aerial Photography and LIDAR Imagery

Aerial reconnaissance within a 25 mi (40 km) radius of the site was conducted by various personnel using aerial photographs from numerous publications. Figure 2.5-76 is a sample of the aerial imagery used, and it contains selected way points from the field reconnaissance. LIDAR imagery of the BBNPP site vicinity was also acquired for review and interpretation (Figure 2.5-160 through Figure 2.5-166). The LIDAR imagery contains elevation data with a 2 ft (0.6 m) contour interval (PAMAP, 2008). The aerial reconnaissance investigated geomorphology and targeted numerous previously mapped geologic features and potential seismic sources (e.g., Berwick fault, Light Street fault, and Berwick Anticlinorium).

Figure 2.5-147 and Figure 2.5-151 contain four topographic cross-sections (A, B, C on Figure 2.5-147, and D on Figure 2.5-151) based on the new LiDAR data set from Luzerne County. The intent of these figures is to review the LiDAR data set in both plan and section view to evaluate the detailed surface of the land as captured by the LiDAR process.

Figure 2.5-162 shows the BBNPP site geology on the LiDAR data base map. Figure 2.5-160 depicts the surficial sediment description including glacial derived features and deposit contacts overlaid on the LiDAR data base map. The same LiDAR data base map without the surficial sediment description is shown in Figure 2.5-161.

The site area geology is presented on the LiDAR data base map in Figure 2.5-162 and Figure 2.5-163 shows the same image without the site area geology coloration. Figure 2.5-164 is similar to Figure 2.5-163 but has the higher altitudes eliminated to show the detail for the lower elevations where the BBNPP site is located.

The site vicinity geology along with the LiDAR base map is presented in Figure 2.5-165. Figure 2.5-166 shows the LIDAR base map without the site vicinity geology coloration. Figure 2.5-165 and Figure 2.5-166 include not only the trace for the Lightstreet and Berwick faults, but also all of the described geologic features at this scale.

The interpretation of the plan-view LiDAR maps incorporates an evaluation of the fracture traces and lineaments visible on the images as linear valleys and swales and straight segments of streams. The features are especially visible for the site on Figure 2.5-161. The orientations of the fractures observed in the outcrop of the Mahantango Shale are within the reported envelope of orientations reported by Inners (Inners, 1978, Figure 3). There is a single dominant set striking just west of north, with a subordinate set at nearly right angles to the first. These appear to be nearly vertical. The right-angle bend in Walker Run to the southwest of the BBNPP center point, illustrates those trends, as the Run has eroded through the glacial cover to expose the underlying structures. Other orientations are present in the outcrop areas of formations to the north and south of the Mahantango, as is also reported by Inners (Inners, 1978, Figures 4 and 5).

The topographic cross sections presented in Figure 2.5-147 and Figure 2.5-151 display no offsets that are attributable to the actions of the Berwick or Light Street Faults. The current work confirms the work by Inners (Inners, 1978) who reports the faults to be locally buried beneath the glacial terrace gravels. In the excavations for the Susquehanna Units, Inners

(Inners, 1978) found several slickensided surfaces at low-angles to the bedding planes located less than 1 mile (1.6 km) to the east of the site (Figure 2.5-150). The displacement on these faults was generally less than 3 ft (1 m) (Inners, 1978). Inners (Inners, 1978) interpreted the surfaces as wedge faults that developed along small-scale drag folds associated with the Alleghanian Orogeny. The current investigation found similar slickensided surfaces, the closest at a distance of 0.45 miles (0.70 km) to the southwest of the site (Figure 2.5-150). The field team observed no offset of the glacial materials overlying these features.

As shown in the following section, field reconnaissance coupled with interpretation of remote imagery (review and inspection of features preserved on the images) shows that there are no geomorphic features indicative of potential Quaternary activity along trends of the postulated folds and faults interpreted by Inners and Williams (Inners, 1978; Williams, 1987). No features suggestive of tectonic deformation were observed in the Quaternary glaciofluvial deposits, and no potential liquefaction features were observed along the Susquehanna River.

2.5.1.2.4.4.4 Field Reconnaissance

Information developed from the literature and the imagery interpretation was supplemented by field reconnaissance within a 25 mi (40 km) radius of the site. These field-based studies were performed to verify, where possible, the existence of mapped bedrock faults in the BBNPP site area and to assess the presence or absence of geomorphic features suggestive of potential Quaternary fault activity along the mapped faults, or previously undetected faults. Features reviewed during the field reconnaissance and office-based analysis of aerial photography and LIDAR imagery were based on a compilation of existing regional geologic information in the vicinity of the BBNPP site.

Field reconnaissance was conducted by geologists in teams of two or more. Field reconnaissance visits in 2007, 2008, 2009, and 2010 focused on exposed portions of the Mahantango Formation, other formation exposures along the faces of Lee, Huntington and Nescopeck Mountains, and roads traversing the site vicinity. Key observations and discussion items were documented in field notebooks and photographs. Field locations were logged by hand on detailed topographic base maps and with hand-held Global Positioning System (GPS) receivers (Figure 2.5-148). There were no faults or other forms of deformation noted in the field. No surface expression of either the Berwick or Light Street faults was noted, consistent with the work of Inners (Inners, 1978). Figure 2.5-67 and Figure 2.5-68 (Waypoint 12 on Figure 2.5-148) show that there is no offset in the Quaternary deposits along Syber Creek, where the trace of Light Street Fault crosses it. Photos of the shale bedrock on the site show the steeply dipping nature of the strong persistent cleavage. Bedding dipping to the NNW is visible but highly obscured by this cleavage (Figure 2.5-73 and Waypoint WF3 on Figure 2.5-76). Outcrops in a nearby borrow area show an undeformed contact between the glacial overburden and the shale bedrock (Figure 2.5-74, and Figure 2.5-75 and Waypoint WF5 on Figure 2.5-76).

A supplemental reconnaissance was conducted during the fall of 2008, to investigate the occurrence of potential liquefaction features along the Susquehanna River. The field reconnaissance was carried out by a team of geologists and engineers from Paul C. Rizzo Associates, Inc, and John Sims & Associates from both the land and water approaches to the river banks. The investigation was conducted for the course of the river for a reach of 25 miles (40 km) upstream and downstream of the site (Figure 2.5-148). Because of the prevalent bedrock exposures in both the river banks and the river bottoms, few locations were found where liquefaction conditions were possible and no evidence that liquefaction had occurred. Figure 2.5-69 through Figure 2.5-72 show the rocky nature of the riverbed and its banks and

some of the typical exposures found during the investigation (for Waypoints WP1, WP10, WP20, and WP22 respectively).

A third reconnaissance was conducted during the Spring of 2009 to further investigate the occurrence of potential liquefaction features along the Susquehanna River. The study was conducted along approximately 10 miles of the Susquehanna River along the south and east bank in areas accessible by auto and on foot (Figure 2.5-148). The investigated areas lie south and east of the BBNPP site within the Berwick 7.5-minute topographic quadrangle.

Two tributaries of the Susquehanna River, the Wapwallopen and Little Wapwallopen creeks, were found to run on bedrock and are relatively small, but similar to other tributaries of the Susquehanna and this region. These two tributaries, like many other streams in the original study, have been disturbed by coal mining activities.

Following the additional reconnaissance, the conclusions about the low potential for liquefaction of the area remain unchanged. The rugged terrain of the Allegheny Mountains, narrow floodplains, and intense modification of the topography through anthracite coal mining confirm those conclusions. The Susquehanna River is a gently meandering river with numerous rock-core islands and boulder-cobble gravel bars. At nearly all sites that were visited, bedrock was present or nearby. The ubiquitous presence of bedrock at or near the surface militates against liquefaction and the presence of paleoliquefaction structures. The tributaries of the Susquehanna have narrow floodplains. Coal mining debris from mine waste dumps, carried by the tributary streams of the Susquehanna, form the visible floodplain deposits of the tributaries.

Fine-grained sediments, when present, are thin and lack the usual prerequisite for preservation of paleoliquefaction features, which is fine to medium sand overlain by 1-2 meters of fine upward silt with a clay cap. However, the banks are commonly vegetated, which significantly reduces accessibility to exposures in the river banks. Further modification of the banks by manmade stone walls, built to prevent erosion or the railroad right-of-way and sections of an early canal, exist through the studied section of the Susquehanna River.

In the spring of 2010, another reconnaissance was undertaken to investigate the portion of the site area (5 mile radius (8 km)) that was not investigated during the previous reconnaissance efforts due to the change in site location. Since the site location was relocated approximately 1,000 feet (305 m) north-northwest, the difference in the physical area between the two site areas forms a crescent shaped zone within the north-northwest edge of the new site area. At its thickest, the crescent is approximately 1,000 feet (305 m) wide and along the curvature it was about 15 miles (24 km) long.

As is typical with most of Pennsylvania and the site area, outcrop is limited. For this reason, targets for investigation and ground truthing were areas of known or suspected outcrop within and around the crescent zone. The main areas of investigation were therefore locations on Lee Mountain, Huntington Mountain, Shickshinny Mountain, Penobscot Mountain, and the Mocanaqua, Pond Hill and Berwick Heights areas, as well as a few locations outside of the site area where the Light Street Fault has been mapped.

In all outcrops investigated, orientation of bedding, joint surfaces and lineations were measured and rock lithology recorded. Due to prior detailed mapping in the area (Inners, 1978) all rock units had previously been identified. The other main objective of the reconnaissance was to look for any evidence of Quaternary faulting. The observations and

measurements made as part of this investigation did not reveal anything inconsistent with the findings of the previous BBNPP reconnaissance efforts or with prior geologic mapping in the areas (Inners, 1978). All measurements were consistent with the mapped structures, all rock lithologies were consistent with unit descriptions and no evidence of recent faulting was observed, including in the area of the mapped Light Street Fault.

2.5.1.2.4.4.5 Prior Work Completed at the SSES Units 1 and 2

A detailed subsurface exploration near the BBNPP site was performed earlier as part of the original SSES FSAR (SSES FSAR, 2003) for the SSES Units 1 and 2 foundation and supporting structures. That exploration covered an area that is located adjacent to the east side of the BBNPP site and addressed the same issues as the current BBNPP FSAR investigation. The high level of detail in that earlier study, and the close proximity to the BBNPP site make that study especially relevant to the current effort. The level of effort for that earlier FSAR study included drilling 250 geotechnical boreholes, collecting down-hole geophysical data, and acquiring seismic refraction data from across the site. Previous site investigations performed for the existing units are summarized in the SSES Final Safety Analysis Report (FSAR) (SSES FSAR, 2003). As cited in the SSES FSAR, these previous investigations provide the following results documenting the absence of Quaternary faults at and within the area of the BBNPP site:

- ◆ Interpretation of satellite photos and topographic maps. This interpretation revealed no evidence of surface rupture, surface warping, or offset of geomorphic features indicative of active faulting.
- ◆ Interviews with personnel from government agencies and private organizations. These interviews concluded that no known faults are present beneath the existing SSES Units 1 and 2 site area.
- ◆ Seismicity Analysis -This analysis showed that no microseismic activity has occurred in the site area; the site is located in a region that has experienced only infrequent minor earthquake activity approximately 35 mi (56 km) northeast of the BBNPP site, around the border of Lackawanna and Wyoming Counties; the closest fault-related epicentral location (the Anthracite Zone) is greater than 25 mi (40 km) away. No earthquake within 50 mi (80 km) of the SSES site has been large enough to cause significant damage in the time the region has been populated, approximately 270 years.
- ◆ Approximately 250 exploratory boreholes were drilled at the SSES Units 1 and 2 site area. Borehole data have provided evidence for the lateral continuity of strata across the existing SSES site area (SSES FSAR, 2003). The inspection of soil samples has revealed no adverse effects indicative of geologically recent or active faulting.
- ◆ Field reconnaissance of many surface outcrops at the site and within the 25 mi (40 km) radius of the site, coupled with geophysical surveys, provided no evidence for faulting at the SSES site.
- ◆ At the time of the original studies for the SSES FSAR in 1975 (SSES FSAR, 2003), published maps showing bedrock faults within a 5 mi (8 km) radius of the SSES site identified only the Light Street fault. The closest significant bedrock faults mapped prior to 1975 were faults located about 80 mi (129 km) southwest of the SSES site near Lewistown, PA (SSES FSAR, 2003).

2.5.1.2.5 Site Area Geologic Hazard Evaluation

This subsection identifies and discusses potential geologic hazards that could be present in the site area (within 5-mi (8-km) radius of the site). These potential geologic hazards include

rock dissolution features (caves and karst features), active deformation zones, landslides, abandoned underground mine cavities, and volcanism.

There are no caves or recognized karst features in the site area, and none were discovered during the investigations for BBNPP and SSES. Small- to medium-scale dissolution features occur in the site area where carbonate bedrock formations occur. Formations containing carbonate beds in the area include the Wills Creek, Tonoloway, Keyser, Old Port, and Onondaga formations of Silurian and Lower Devonian strata. These formations are at least 1,600 ft (488 m) below ground surface (bgs) at the BBNPP site and have not been penetrated by any borings at the site. These formations crop out or are located closer to the ground surface approximately 3 to 8 miles (5 to 13 km) southwest of the BBNPP site. Water wells in the Berwick area (southwest of the BBNPP site) are screened in the limestone formations and obtain ground water from dissolution features located along joints, fractures, and bedding planes (Inners, 1978). For example, the public water supply wells located in Berwick are screened in the Keyser Formation at depths of 87 to 160 ft (27 to 49 m) bgs and yield up to 500 gallons per minute (gpm) (1893 liters per minute (lpm)) (Williams, 1987). However, one well drilled to a depth of 515 feet (157 m) at the same location produced no water (Williams, 1987). This is an example supporting the general belief that fractures, dissolution features, and secondary permeability of the rock decreases with depth because the confining pressure within the rock increases with depth and causes the fractures to close. This is discussed in greater detail in Section 2.4.12.1.2.8. Because the carbonate formations are located at least 1,600 ft (488 m) bgs, the frequency and magnitude of fracturing and dissolution features should be minimal.

Inventories of caves and karst features in Pennsylvania show no caves or karst to be present in Luzerne or Columbia counties; all significant caves and karst features are located in southeast, central, and southwestern Pennsylvania. The nearest significant cave is Crystal Cave near Kutztown, Pennsylvania, which is located approximately 46 mi (74 km) from BBNPP. In summary, based on the absence of limestone dissolution features in the 0.6-mile (1 km) site radius and the depth of 1,600 ft (488 m) to limestone, karst is not a geologic hazard at the BBNPP site.

Major springs, defined as having flow rates of 100 gpm (379 lpm) or more, can be an indicator of carbonate formations and karst features. An inventory of major springs in the Ridge and Valley Province of Pennsylvania by the USGS (Saad, 1990) identified only one major spring in Luzerne or Columbia counties; this spring (Lu 8) discharges from the Mauch Chunk Formation, approximately 10 miles (16 km) southeast of the BBNPP site (Saad, 1990). The Mauch Chunk Formation consists of clastic sedimentary rocks ranging from claystone up to conglomeratic sandstones. There are no carbonate strata in this formation and this formation does not underlie the BBNPP site. Thus, there are no documented cases of springs in Luzerne or Columbia counties that infer the presence of karst or significant dissolution features in carbonate rocks.

The last major tectonic events that generated large-scale earthquakes, faults, and deformation along the eastern coast of the United States occurred in the Mesozoic Era (Triassic and Jurassic, approximately 250 Ma). Active deformation processes and seismic activity within the site vicinity have been minimal since the Mesozoic Era. The nearest sources of repeating large magnitude earthquakes are the Charlevoix Seismic Zone in Canada and the Charleston Seismic Zone in South Carolina. Thus, active deformation activities are not a source of significant geologic hazard in the BBNPP site vicinity (see also Section 2.5.1.1.4).

Because there are steep slopes and high topographic relief present in this portion of the Ridge and Valley Physiographic Province, landslides and other mass movements (e.g., soil slumping) can occur. Approximately 7.5 miles (12 km) north-northeast of the BBNPP site, is the location of one of the largest landslides in Pennsylvania. Approximately 4,000 years ago (ka), a rock block landslide on the south side of Schickshinny Mountain caused 20,260,000-27,450,000 yd³ (15,490,000-20,987,000 m³) of rock to move 1,250 ft (381 m) onto the Susquehanna River floodplain and partially diverted the Susquehanna River (Inners, 1988). Varnes (Varnes, 1978) defines a rock block slide as "a translational slide in which the moving mass consists of a single unit that is not greatly deformed". Another much smaller landslide located 2 miles (3.2 km) northeast of the first (9.5 miles (15.3 km) northeast of the BBNPP site), was witnessed in 1947. Rainfall of 6 inches within 2 hours likely caused approximately 122,000 yd³ (93,277 m³) to move downslope within a minute or two (Inners, 1988). Including the aforementioned landslides, thirteen rock block slides have been mapped between Nanticoke, PA and Schickshinny, PA (a distance of approximately 9 miles (14.5 km)) along the south side of Schickshinny Mountain, with a total volume of about 56,000,000 yd³ (42,815,000 m³) (Inners, 1988). All of these landslides, with the exception of the 1947 landslide, are prehistoric, having a maximum age of approximately 11 ka, and were the likely results of a combination of the dip-slope of Schickshinny Mountain being ultimately underlain by a weak mudstone, a relatively low dipping angle of the rock beds on the slope (approximately 20°), and the undercutting of the sandstone-mudstone bedding planes by the Susquehanna River (Inners, 1988). Inners (Inners, 1988) suggests that even though porewater pressure as a result of high-moisture conditions in the area was the most likely cause of many of these historic rock block landslides, the larger landslides probably required a longer 'wet' season and/or multiple year high-moisture conditions. All of these rockslides occurred at least 7.5 miles (12 km) upstream along the banks of the Susquehanna River. No landslides (historic or prehistoric) of this proportion have been recognized or mapped in the BBNPP site area.

Underground coal mining has occurred in the Pennsylvania anthracite fields since the early 1800s. Hundreds of miles of underground workings are located in four different anthracite basins. While underground mining is currently very limited, the abandoned workings still result in mine subsidence immediately over the mine workings. The nearest anthracite basin (the Northern Anthracite Basin) is located at least 4 mi (6 km) distance from the BBNPP site, and all coal-bearing formations within the site area have been eroded long ago, so coal mining and mine subsidence at this distance will have no potential effect on the construction or operations of the BBNPP.

Tectonic activities and volcanism have not occurred in the eastern United States since the Mesozoic Era. Volcanic activity during the past 2,000 years has only occurred in the Western United States. The area of greatest volcanic activity is associated with the Cascade Range in the states of Washington, Oregon and California. The last eruption was Mount St. Helens in 1980. This is over 2500 mi (4023 km) away from the BBNPP Site. Therefore, volcanism and related hazards are not a geologic hazard at the BBNPP site or vicinity.

Based on the discussion above, there are no geologic hazards that represent a risk to the construction or operation of the BBNPP.

2.5.1.2.6 Site Engineering Geology Evaluation

This section addresses the engineering significance of geologic and geotechnical characteristics of features and materials within the site area (5 mi (8 km) radius) and site location (0.6 mi (1 km) radius).

2.5.1.2.6.1 Engineering Soil Properties and Behavior of Foundation Materials

The overburden soil, based on engineering properties defined in Section 2.5.4., is not an adequate foundation substrate for safety related structures or facilities. The overburden soils are composed of mostly residual silty to clayey sand to poorly graded sand with gravel and poorly graded gravel or silty to clayey gravel with sand. This soil was formed from weathering and decomposition of the Mahantango Shale. Below the soil is a zone of soft weathered rock typically followed by a harder, competent shale that is very fractured. Due to the abundance of fracturing in this zone, these incompetent rock layers are also unsuitable for founding of safety related structures. As a result, the overburden soil and incompetent shale layers will be removed in order to found safety related structures or facilities on bedrock. Sound bedrock of the Mahantango Formation is encountered between 16 and 115.5 ft (5 - 35 m) below ground surface (bgs) at the BBNPP site location (0.6 mi (1 km) radius). Selected Category 1 structures will be founded on sound rock and the rock surface will be improved with removal of weathered and fractured rock, cleaning, and localized concrete fill as necessary. Engineering soil properties, including index properties, static and dynamic strength, and compressibility are discussed in Section 2.5.4. Variability and distribution of properties for the foundation bearing soils will be evaluated and mapped as the excavation is completed. Settlement monitoring will be based on analyses performed for the final design.

2.5.1.2.6.2 Unrelieved Residual Stresses in Bedrock

Due to the fact that bedrock within the site area (5 mi (8 km) radius) and the site location (0.6 mi (1 km) has been buried under a cover of glacial sediments since the Wisconsinan glacial event (17,000-22,000 my), it is expected that removal of the glacial overburden will cause unloading effects such as exfoliation jointing or opening of existing joints and subsequent slaking of the rock. Current investigation found that this glacial outwash and till glacial deposits are constricted to the location of the Essential Service Water Emergency Makeup System (ESWEMS), below the break in slope of the hill (Figure 2.5-146). Above the break in the slope, glacial deposits are sparse with the majority of the overburden described as residual soil that formed from weathering of the underlying shale bedrock (Figure 2.5-141, through Figure 2.5-145). The thickness of what could be associated with till deposits, is no more than 3 ft (0.9 m). Where fine grained sandstone layers were found deeper than this, it is interpreted as being part of the Mahantango Formation, as previously described. The superficial deposits in the site were disturbed for agricultural purposes and the surface was cleared of these very sparse erratics, which were plowed and then used to build the stone walls found in the site. The result of glacial erosion above the break in the slope is found to have only partially removed the top of the weathered bedrock, which is thicker in the top of the site location, and thins downhill towards the location of the Essential Service Water Emergency Makeup System (ESWEMS). The effects of isostatic rebound as a result of rapid erosion due to glacial melt and rapid reduction in normal stress due to glacial retreat is well established in the literature (Pelletier, 2004; Stern, 2005). In addition, geologic mapping in the site vicinity (5 mi (8 km) radius) revealed very continuous, low angle exfoliation fractures in the Mahantango Formation in outcrops which range up to ten feet in height. The presence of these fractures is a typical reaction to stress relief, and is an indication that unloading the rock by excavating overburden will result in the propagation of some low angle fractures that may necessitate further excavation or rock anchoring in some areas.

2.5.1.2.6.3 Zones of Alteration, Weathering, and Structural Weakness

Below the top of competent bedrock (as defined by weathering, fracture density and rock mass rating (RMR) scores), no unusual weathering profiles have been encountered during the site investigation. Calcareous zones, thin pyrite lenses and zones exhibiting increased fracture density at depth observed in isolated areas are the only other discrete zones that vary from

the preponderance of the competent rock. The site area bedrock geologic map and site location geologic map (Figure 2.5-139 and Figure 2.5-138, respectively), compiled by Berg (1980) and Schruben (1998) indicates that most of the site area (5 mi (8 km) radius) surrounding, and including, the BBNPP site are underlain by Late Silurian, Devonian, and Lower Mississippian bedrock. More specifically, the site location (0.6 mi (1 km) radius) bedrock is Upper Devonian Mahantango Formation (part of the Hamelton group) which serves as the foundation for SSES Units 1 and 2. (SSES FSAR, 2003). The most recent geologic influence on the site, not including sub-aerial exposure and erosion, is the Wisconsinan glaciation that is discussed in Section 2.5.1.1.1. The relevance of this glacial event with respect to alteration, weathering, and structural weakness is complex. Glacial scour removed weathered rock from the surface of the site area (5 mi (8 km) radius) and glacial deposits left behind after glacial retreat have altered the weathering rate at the bedrock interface; this effect is described in the location of the Essential Service Water Emergency Makeup System (ESWEMS), below the break in slope of the hill (Figure 2.5-146). However, due to the site location being on top of a local hill above the more glaciated valleys, very little of the glacial soils are present here. What remains below residual soil is a slightly to intensely weathered bedrock surface followed by a fractured zone. Based on the performance of the Mahantango Formation as the SSE Units 1 and 2 foundation, it is evident that, with proper excavation and foundation preparation, this rock is a suitable foundation bearing material for Category 1 structures. As noted previously, any zones of alteration, weathering, or increased joint or fracture density will be mapped during excavation and evaluated for removal, cleaning, and treatment to remediate any revealed unsafe conditions.

2.5.1.2.6.4 Deformational Zones

The Light Street fault and the Berwick Anticlinorium (Inners, 1978) have been mapped at or within the 5 mi (8 km) radius of the BBNPP site. The Berwick Anticlinorium is an east-northeast striking, gently northeast plunging anticlinal structure with an axial trace that trends directly through the site area (5 mi (8 km) radius) and site location (0.6 mi (1 km) radius). The Berwick Anticlinorium is a symmetrical structure in the site area (5 mi (8 km) radius) with the north-northwest and south-southeast dipping limbs with an averaged 35 degree NNW and SSE respectively. The relevance of the Berwick Anticlinorium is that the dips of the limbs have the potential to provide sliding planes within an excavation. In addition, axial plane cleavage may have the potential to result in toppling failure from an excavation slope. Any excavations into bedrock or bedrock slopes will be mapped and monitored during excavation and backfill.

Field mapping efforts did not successfully identify surface expression of the Light Street Fault. Deformation including fracturing and folding was mapped in outcrop and is discussed in Section 2.5.3.2. In addition, a thorough literature search was conducted to identify previous studies that have identified any form of deformation in the rock or identified in the stratified glacial deposits.

In addition, two other zones of deformation have been noted within the site area (5 mi (8 km) radius). These zones of deformation include the Lackawanna Synclinorium (Inners, 1978), which is located approximately 4 miles (6.4 km) northwest of the site, and the inferred Berwick fault (Inners, 1978), which is inferred to lie approximately 3 miles (4.8 km) southwest of the site (see Section 2.5.1). Neither of these features is considered a capable tectonic source, as defined in Appendix A of Regulatory Guide 1.165 (NRC, 1997).

Based on geologic mapping, interpretation of borehole data and interpretation of geophysical investigation, no deformation zones were encountered in the site investigation for the BBNPP that have a detrimental effect the engineering properties of the rock mass. In addition, no

deformational zones were encountered during the exploration or excavation for SSES Units 1 and 2. Detailed mapping of the excavation for the proposed excavation for the BBNPP Category 1 structures will document the presence, orientation, continuity, and classification of any deformational zone. Each deformational zone or structure will be evaluated as to its potential affect on the foundation.

2.5.1.2.6.5 Prior Earthquake Effects

One earthquake occurred within 25 miles (40 km) of the site (to the south) as shown on Figure 2.5-51. There are no reported earthquakes in the BBNPP site area (5 mi (8 km) radius). Studies of the SSES Unit 1 and 2 excavation, available outcrops within the BBNPP site area, and extensive exposures along the road cuts of Nescopeck and Lee Mountain, have not indicated any evidence for earthquake activity that affected the Paleozoic bedrock or Quaternary surficial deposits within the site area. Also, there are no historic accounts of earthquakes in the site area (5 mi (8 km) radius).

2.5.1.2.6.6 Effects of Human Activities

Previous investigations performed for the SSES Unit 1 and 2, and for this study identified no activities that would adversely affect the site. However, stones for construction material in the form of crushed rock have been quarried in the site vicinity. Sand and gravel also have been quarried, mostly along the Susquehanna River bank primarily for highway construction. Even though no mineral resources of economic significance and no mine workings are noted at the BBNPP site, there are deep anthracite coal mining operations located at 11 miles east of the BBNPP site near the town of Shickshinny. Additionally, oil and gas reserves have been explored near Harveys Lake, approximately 25 miles (40 km) north of the BBNPP site. There is limited withdrawal of groundwater or recharge through impoundments of water in the site area, and adverse effects related to pore pressure change from groundwater withdrawal or injection are not expected to occur at the BBNPP site.

2.5.1.2.6.6.1 Oil and Gas Production in the Site Region

The site region has had extensive oil and gas exploration and production throughout "recent" history with the vast majority having occurred in the Appalachian Basin, though much of it has not been systematically recorded (Ryder, 1995). Discovery of oil in the Drake well, Venango County, northwestern Pennsylvania in 1859 marked the beginning of the modern petroleum industry not just in the Appalachian Basin, but in the entire country (Milici, 2006). This discovery well, reported to have made at least ten barrels of oil per day for a year, and was the first oil produced commercially from a well drilled in the U. S., was produced from an Upper Devonian stray sandstone at a depth of about 70 ft (21 m) (Milici, 2006). It opened a prolific trend of oil and gas fields producing from Upper Devonian, Mississippian, and Pennsylvanian sandstone reservoirs that extends from southern New York, across western Pennsylvania, central West Virginia, and eastern Ohio, to eastern Kentucky (Ryder, 1995). From 1859 through 1993, approximately 2.3 billion barrels of oil (366 million cubic meters) and 31 trillion cubic feet of gas (TCFG) (878 billion cubic meters) have been produced from the trend (Ryder, 1995). Primary annual oil production in the trend peaked at about 36.3 million barrels of oil (MMBO) (5.7 million cubic meters) in 1900, whereas oil production from secondary recovery peaked at about 37.6 MMBO (6 million cubic meters) in 1937 (Ryder, 1995). More recently, exploration in the trend focused on gas in low-permeability sandstone reservoirs at depths between 4,500 and 6,000 ft (1370 and 1830 m) (Ryder, 1995).

A second major trend of oil and gas production in the Appalachian Basin began in 1885 continued into the early 1900's in Lower Silurian "Clinton" sandstone reservoirs in Ohio and Lower Silurian Medina Group sandstones in western New York (Ryder, 1995). Hydrofracing

techniques introduced in the early 1950's extended the Lower Silurian "Clinton" and Medina sandstone trend across most of central and eastern Ohio, northwestern Pennsylvania, western New York, and a small part of northeastern Kentucky. More recent exploration in the trend is for gas in low-permeability sandstone reservoirs at depths between 5,500 and 7,000 ft (1676 and 2134 m) (Ryder, 1995). Important gas discoveries from the Lower Devonian Oriskany Sandstone in Ohio, New York, and West Virginia, in the 1920-1930's opened a major gas-producing trend across parts of New York, Pennsylvania, Maryland, Ohio, West Virginia, Kentucky, and Virginia (Ryder, 1995). Overlying the Oriskany Sandstone is the fractured Middle Devonian Huntersville Chert, which is another important reservoir in the Oriskany trend in Pennsylvania, West Virginia, and Maryland. In the 1990's exploration was still active in this trend for gas trapped in faulted anticlines at depths between 6,000 and 9,000 ft (1830 and 2743 m) (Ryder, 1995).

Other locations underlain by Appalachian Basin strata have been relatively unsuccessful in production of oil and gas such as deep drilling in the late 1970's and early 1980's for gas in the Appalachian Fold and Thrust Belt east of the Allegheny structural front. Only two small oil fields discovered in southwestern most Virginia and five or six small gas fields elsewhere were productive in the folded and thrust rocks of this region (Ryder, 1995).

According to Ryder (1995), nineteen conventional plays and 16 unconventional plays are recognized in the Appalachian Basin Province. However, natural gas prices have steadily increased over the past few years and development of "unconventional" gas resources, such as gas shales have become of great interest (Sumi, 2008). Therefore, in the last ten years or so, Upper Devonian Black shales have become the most prolific and therefore explored play in the region. Upper Devonian Sandstones overlying the Black Shales have been tapped for over a century as they trap gas and oil sourced from the Shales (Ryder, 1995). However, the Devonian black shales themselves are actually the oldest gas play in the U.S. and include the Marcellus Shale, Rhinestreet Shale Member of the West Falls Formation, Pipe Creek Shale Member of the Java Formation, lower and upper parts of the Huron Member of the Ohio Shale, and Cleveland Member of the Ohio Shale (Ryder, 1995). The greatest thickness of combined black-shale units in the basin is in central Pennsylvania, where together, the units are about 1,400 ft (426 m) thick.

Oil and wet thermal gas are the expected hydrocarbon types in the play with production of the unit dependent upon the coincidence of several factors, including relatively abundant organic matter at suitable thermal maturity and a reservoir that is significantly enhanced by a naturally occurring fracture system (Ryder, 1995). Devonian source rocks in western New York and northwestern Pennsylvania are in the zone of oil generation, whereas Devonian source rocks in west-central Pennsylvania, southeastern Ohio, and northern and north-central West Virginia are in the zone of gas generation. The southeastern part of the play in southwestern Pennsylvania and adjoining West Virginia may be over mature with respect to the generation of oil and gas (Ryder, 1995).

Because of its large expanse, abundance of fractures, lower-density and high porosity, the Marcellus shale of the Hamilton Group (which underlies the Mahantango shale at the BBNPP site) has been the main target of exploration of all the Devonian Black Shales within the past ten to fifteen years in Pennsylvania and surrounding states (Milici, 2006; Sumi, 2008). The Marcellus shale spans a distance of approximately 600 miles (965 km), running from the southern tier of New York, through the western portion of Pennsylvania into the eastern half of Ohio and through West Virginia with an areal extent of about 54,000 square miles (140,000 square km) (Sumi, 2008) (Figure 2.5-170). The shale is extremely variable in thickness, ranging

from a few feet to more than 250 ft (76 m) in thickness, and generally becomes thicker to the east. The majority of the Marcellus shale is more than a mile deep, and in some areas it extends 9,000 ft (2743 m) below the surface (Sumi, 2008) (Figure 2.5-171).

Due to its great depth, the Marcellus Shale was not previously considered much of a resource, and is still a very expensive target with drilling costs approaching a million dollars for a traditional vertical well (Sumi, 2008). Because of the variability in geology and depth of the resource, the economic and technical feasibility of extracting the shale gas will vary from region to region, but with the current price of gas and conservative estimates of gas in place for the Marcellus shale at 168 TCFG (4.8 trillion cubic meters) and optimistic estimates up to 516 TCFG (14.6 trillion cubic meters) (Sumi, 2008), exploration is booming.

One of the main reasons that the Marcellus Shale has become such a valued target is because of its known abundance of natural fractures in the Appalachian Plateau as opposed to joint growth in gray shales and siltstones and particularly coarser grained rocks (Engelder, 2009). The most pervasive systematic joints observed in Devonian black shale of the Appalachian Plateau include sub-vertical east-northeast joints (J_1) and younger sub-vertical northwest-striking cross-fold joints (J_2) (Lash, 2009). Their formation was driven exclusively by fluid pressure generated as a consequence of hydrocarbon-related maturation supplemented by subsequent tectonic compaction during the Alleghanian tectonic cycle (Engelder, 2006; Lash, 2009).

Despite the presence of these joints, stimulation techniques to better link up the two crossing sets are taking place in abundance in Marcellus Shale production. This is done through hydraulic fracturing (fracking), which is the process of creating and expanding fractures around the wells by injecting a mixture of water, sand and chemicals under pressure. Such induced hydraulic fractures should propagate east-northeast to west-southwest because of the direction of the contemporary tectonic stress field (Engelder, 2009). This can be done in vertical wells, but because of the orientation of the natural joints, hydraulic fracture treatments in vertical wells are not capable of taking full advantage of the bulk permeability anisotropy of black shale, nor the normal stress-induced permeability anisotropy (Engelder, 2009). However, if a well is drilled horizontally through the Marcellus Shale in a north-northwest or south-southeast direction, the bulk permeability anisotropy can be best taken advantage of due to crossing the east-northeast oriented, more permeable J_1 joints (Engelder, 2009). The ability to economically stimulate the formation along the horizontal well bore has made many wells commercial successes and wells that were previously drilled vertically to access Marcellus Formation or other formations can be reused to drill horizontally through the Marcellus Shale (Sumi, 2008).

Overall, the areas of greatest Marcellus Shale gas development are north and northwest of the BBNPP site in the Appalachian Plateaus province, as shown on Figure 2.5-172. Records obtained from the Pennsylvania Department of Environmental Protection (PADEP, 2010), Bureau of Oil and Gas Management show that from January to August 2010 there have been four Marcellus Shale gas well permits issued in Columbia County with no wells drilled, and four permits issued in Luzerne County with one well drilled. These numbers are extremely low compared to the more northern and western counties in Pennsylvania that have over one thousand permits issued and five hundred wells drilled (Figure 2.5-172). The closest well to the BBNPP site is located 12.5 miles (20.1 km) to the west-northwest. Thus, the potential to find oil or gas deposits of economic value are very low for the area immediately surrounding the BBNPP site and therefore any associated hazards should be of very minimal concern.

2.5.1.2.6.7 Site Groundwater Conditions

A detailed discussion of groundwater conditions is provided in Section 2.4.12. Groundwater in the site area is founded in both the glacial overburden and bedrock formations. In the vicinity of the BBNPP site, the glacial overburden aquifer is the most capable aquifer for transmitting groundwater, and it is the source aquifer for many wells and springs in the county. Groundwater in the bedrock formations is present primarily in secondary openings, including fractures, joints, and bedding plane separations. As a result, the ability of the bedrock to store groundwater or yield to well is typically less than the overburden for formations. Because buildings will be founded on sound rock, both the glacial overburden and fractured bedrock aquifers will be affected by construction of the BBNPP. However, active dewatering methods within the sites are expected to limit the adverse effects in the aquifers during excavation and construction (see Section 2.4.12.5.1).

2.5.1.3 References

Aber, 2001. Appalachian Mountains, J. S. Aber, Website: http://academic.emporia.edu/aberjame/struc_geo/appalach/appalach.htm, Date accessed: January 23, 2008.

Aggarwal, 1978. Earthquakes, Faults, and Nuclear Power Plants in Southern New York and New Jersey, Science, Volume 200, p 425-429, Y. Aggarwal and L. Sykes, 1978.

Armbruster, 1987. The 23 April 1984 Martic Earthquake and The Lancaster Seismic Zone In Eastern Pennsylvania, Bulletin of the Seismological Society of America, Volume 77, Number 2, p 877-890, J. Armbruster and L. Seeber, 1987.

Ator, 2005. A Surficial Hydrogeologic Framework for The Mid-Atlantic Coastal Plain Professional Paper 1680, U.S. Geological Survey, U.S. Department Of The Interior, S.W., Denver, J.M., Krantz, D.E., Newell, W.L., Martucci, S.K., 2005.

Bailey, 1998. Late Neoproterozoic Extension-Related Magma Emplacement in the Central Appalachians: An Example from the Polly Wright Cove Pluton, The Journal of Geology, Volume 106, p 347-359, Christopher M. Bailey and Richard P. Tollo, 1998.

Bankey, 2002. Magnetic Anomaly Map of North America, U.S. Geological Survey Open File Report 02-414, scale 1:10,000,000, 1 sheet, V. Bankey, A. Cuevas, D. Daniels, C. Finn, I. Hernandez, P. Hill, R. Kucks, W. Miles, M. Pilkington, C. Roberts, W. Roest, V. Rystrom, S. Shearer, S. Snyder, R. Sweeney and J. Velez, 2002.

Barnes, 2002. The Geological Story of Pennsylvania (3rd ed.), Pennsylvania Geological Survey, 4th ser., Educational Series 4, p 1-44, J.H. Barnes and W.D. Sevon, 2002.

Becker, 2006. Linking Late Paleozoic sedimentary provenance in the Appalachian basin to the history of Alleghanian Deformation, American Journal of Science, vol. 306, p. 777-798, T.P. Becker, W.A. Thomas, and G.E. Gehrels, 2006.

Behrendt, 1983. Structural elements of the U.S. Atlantic margin delineated by the second vertical derivative of the aeromagnetic data, U.S. Geological Survey Geophysical Investigation Map GP-956, scale 1-2,500,000, J. Behrendt and M. Grim, 1983.

Bennington, 2006. Geology of New York and New Jersey, Hofstra University, 21 p, J. B. Bennington and C. Merguerian, 2006.

Benson, 1992. Map of the exposed and buried Early Mesozoic rift basins/synrift rocks of the U.S. Middle Atlantic Continental Margin, Miscellaneous Map Series No. 5, Delaware Geological Survey, University of Delaware, Newark, R. Benson, 1992.

Berg, 1980. Geologic map of Pennsylvania, Pennsylvania Geological Survey, 4th ser., Map1, scale 1:250,000, 3 sheets, T.M. Berg, 1980.

Berg, 1999. Part II, Stratigraphy and Sedimentary Tectonics, Chapter 8: Devonian-Mississippian Transition, in C.H. Shultz ed., *The Geology of Pennsylvania: Pennsylvania Bureau of Topographic and Geologic Survey Special Publication 1*, p 128-137, T.M. Berg, 1999.

Bernreuter, 1989. Seismic Hazard Characterization of 69 Nuclear Plant Sites East of the Rocky Mountains: Methodology, Input Data and Comparisons to Previous Results for Ten Test Sites., Technical Rept. Oct 86-Oct 88, Lawrence Livermore National Laboratory, CA, D. L. Bernreuter, J. B. Savy, J. C. Chen, R. W. Mensing, 1989.

Blackmer, 2005. Preliminary Bedrock Geologic Map of a Portion of The Wilmington 30- By 60-Minute Quadrangle, Southeastern Pennsylvania, Open-File Report OFBM-05-01.0, Pennsylvania Geological Survey, Fourth Series, Blackmer, G. C., Harrisburg, 2005.

Bobyarchick, 2007. Kinematics of the Everona Fault, Central Virginia, Bobyarchick Andy R., , Geological Society of America Abstracts with Programs, Session No. 33, Cenozoic Tectonics in the Southeastern United States, Vol. 39, No. 2, p. 89, March 2007.

Bosbyshell, 2009. Amphibolite Geochemistry in the Wissahickon Formation, Philadelphia, PA: New Results and Implications for Wilmington Complex- Laurentia Collision, Geological Society of America Abstracts with Programs, Vol. 41, No. 3, H. Bosbyshell.

Bradley, 2002. Emsian Synorogenic Paleogeography of the Maine Appalachians, *The Journal of Geology*, Volume 110, p 483-492, Dwight Bradley and Robert Tucker, 2002.

Bradley, 1989. Taconic Plate Kinematics as Revealed by Foredeep Stratigraphy, Appalachian Orogen, *Tectonics*, Volume 8, No. 5, p 1037-1049, D.C. Bradley, 1989.

Braun, 1988. Glacial Geology of the Anthracite and North Branch Susquehanna Lowland Regions, p 1-25, D. Braun, 1988.

Braun, 2003. Margin of Laurentide Ice to the Atlantic Coastal Plain: Miocene-Pleistocene landscape evolution in the Central Appalachians, in Easterbrook, D.J., ed., *Quaternary Geology of the United States*, INQUA 2003 Field Guide Volume, [Desert Research Institute], Braun, D.D., Pazzaglia, F.J., and Potter, N., Jr., 2003.

Braun, 2004. Late Wisconsin Deglaciation of the Great Bend-Tunkhannock Region of Northeastern Pennsylvania, Guidebook for the 67th Annual Reunion of the Friends of the Pleistocene, p 1-26, D. Braun, 2004.

Braun, 2007. Surficial Geology of the Red Rock 7.5-Minute Quadrangle, Luzerne, Sullivan, and Columbia Counties, Pennsylvania, Pennsylvania Geological Survey, Fourth series, Open-File Report OFSM 07-10.0, 19p, Portable Document Format (PDF), Duane D. Braun, 2007.

- Brezinski, 1999.** Part II, Stratigraphy and Sedimentary Tectonics, Chapter 9: Mississippian, in C.H. Shultz ed., *The Geology of Pennsylvania: Pennsylvania Bureau of Topographic and Geologic Survey Special Publication 1*, p 138-147, D.K. Brezinski, 1999.
- Brezinski, 2010.** Late Devonian glacial and associated facies from the central Appalachian Basin, eastern United States, *GSA Bulletin*, v. 122; no. 112, p. 265-281, David K. Brezinski, C. Blaine Cecil, and Viktoras W. Skema, 2010.
- Castle, 2005.** Petrophysics of Lower Silurian sandstones and integration with the tectonic-stratigraphic framework, Appalachian basin, United States, *AAPG Bulletin*, Volume 89, Number 1, p 41-60, James W. Castle and Alan P. Byrnes, January 2005.
- Clark, 1992.** Central Appalachian Periglacial Geomorphology, A Field Excursion Guidebook under the auspices of the 27th International Geographical Congress, Commission on Frost Action Environments, Agronomy Series Number 120, G. Clark, R. Behling, D. Braun, E. Ciolkosz, J. Kite and B. Marsh, August 1992.
- Cleaves, 1992.** Regoliths of the Middle-Atlantic Piedmont and Evolution of the Polymorphic Landscape, *Southeastern Geology*, Volume 39, Number 3 and 4, p 122-199, E. Cleaves, October, 1992.
- Cotter, 2008.** The Geologic History of Central Pennsylvania, Introduction, p 1-3, Plate Tectonics, p 1-4, Episode Two, p 1-7, End of Episode Two, p 1-2, Episode Three, p 1-2, Episode Four, p 1-4, E. Cotter, 2008.
- Crangle, 2002.** Stratigraphic Framework of Cambrian and Ordovician Rocks in the Central Appalachian Basin from Lake County, Ohio, to Juniata County, Pennsylvania, Revised and Digitized from Ryder 1992, *Stratigraphic Framework of Cambrian and Ordovician Rocks in the Central Appalachian Basin from Medina County, Ohio, through Southwestern and South-Central Pennsylvania to Hampshire County, West Virginia*, U.S. Geological Survey, Miscellaneous Investigation Series, Map I-2200. R.D. Crangle Jr., 2002.
- Crawford, 1999.** Part III, Structural Geology and Tectonics, Chapter 16: Piedmont Upland, in C.H. Shultz ed., *The Geology of Pennsylvania: Pennsylvania Bureau of Topographic and Geologic Survey Special Publication 1*, p 234-241, M.L. Crawford, W.A. Crawford, A.L. Hoersch, and M.E. Wagner, 1999.
- Crone, 2000.** Data for Quaternary Faults, Liquefaction Features, and Possible Tectonic Features in the Central and Eastern United States, East of the Rocky Mountain Front, U.S. Geological Survey, Open-File Report 00-260, p 1-332, A.J. Crone and R.L. Wheeler, 2000.
- Crowl, 1980.** Glacial Border Deposits of Late Wisconsinan Age in Northeastern Pennsylvania, Pennsylvania Bureau of Topographic and Geologic Survey, General Geology Report 71, G.H. Crowl and W.D. Sevon, 1980.
- Crowl, 1999.** Part II, Quaternary, Chapter 15, in C.H. Shultz ed., *The Geology of Pennsylvania: Pennsylvania Bureau of Topographic and Geologic Survey Special Publication 1*, p 224-232, G.H. Crowl and W.D. Sevon, 1999.
- Csontos, 2008.** New Madrid seismic zone fault geometry, *Geosphere*, Volume 4, No 5, p. 802-813, doi: 10.1130/GES00141.1; R. Csontos, and R.V. Arsdale, 2008.

Cumbest, 2000. Comparison of Cenozoic Faulting at the Savannah River Site to Fault Characteristics of the Atlantic Coast Fault Province: Implications for Fault Capability, U.S. Dept. of Energy Contract No. DE-AC09-96SR18500, 51 p, R. Cumbest, D. Wyatt, D. Stephenson, and M. Maryak, 2000.

DCNR, 2007a. Geologic Map of Pennsylvania, Pennsylvania Department of Conservation and Natural Resources, Website: <http://www.dcnr.state.pa.us/topogeo/maps/map7.pdf>, Date accessed: December 14, 2007.

DCNR, 2007b. Piedmont Lowland Section Piedmont Province, Pennsylvania Department of Conservation and Natural Resources, Website: <http://www.dcnr.state.pa.us/topogeo/map13/13pls.aspx>, Date accessed: December 14, 2007.

DCNR, 2007c. Gettysburg-Newark Lowland Section Piedmont Province, Pennsylvania Department of Conservation and Natural Resources, Website: <http://www.dcnr.state.pa.us/topogeo/map13/13gnls.aspx>, Date accessed: December 14, 2007.

DCNR, 2007d. Piedmont Upland Section Piedmont Province, Pennsylvania Department of Conservation and Natural Resources, Website: <http://www.dcnr.state.pa.us/topogeo/map13/13pus.aspx>, Date accessed: December 14, 2007.

DCNR, 2007e. Reading Prong Section, Pennsylvania Department of Conservation and Natural Resources, Website: <http://www.dcnr.state.pa.us/topogeo/map13/13rps.aspx>, Date accessed: December 14, 2007.

DCNR, 2007f. Allegheny Mountain Section Appalachian Plateaus Province, Pennsylvania Department of Conservation and Natural Resources, Website: <http://www.dcnr.state.pa.us/topogeo/map13/13alms.aspx>, Date accessed: August 9, 2010.

DCNR, 2008a. Trenton Black River Carbonates: Introduction, Pennsylvania Geological Survey, Pennsylvania Department of Conservation and Natural Resources, Website: <http://www.dcnr.state.pa.us/topogeo/tbr/tbrintro.aspx>, Date accessed: July 5, 2008.

DCNR, 2008b. Great Valley Section Ridge and Valley Province, Pennsylvania Department of Conservation and Natural Resources, Website: <http://www.dcnr.state.pa.us/topogeo/map13/13gvs.aspx>, Date accessed: January 22, 2008.

DCNR, 2008c. Lowland and Intermediate Upland Section Atlantic Coastal Plain Province, Pennsylvania Department of Conservation and Natural Resources, Website: <http://www.dcnr.state.pa.us/topogeo/map13/13lius.aspx>, Date accessed: January 22, 2008.

DCNR, 2008d. Eastern Lake Section Central and Lowland Provinces, Pennsylvania Department of Conservation and Natural Resources, Website: <http://www.dcnr.state.pa.us/topogeo/map13/13els.aspx>, Date accessed: April 10, 2008.

DCNR, 2008e. Appalachian Mountain Section Ridge and Valley Province, Pennsylvania Department of Conservation and Natural Resources, Website: <http://www.dcnr.state.pa.us/topogeo/map13/13ams.aspx>, Date accessed: August 9, 2010.

Diedrich, 1999. Depositional Cyclicity in the Lower Devonian Helderberg Group of New York State, The Journal of Geology, Volume 107, p 643-658, Nathaniel W. Diedrich and Bruce H. Wilkinson, 1999.

- Dodson, 2008.** Structural Geology of the Transylvania Fault Zone in the Appalachian Thrust Belt, Bedford County, Pennsylvania, Northeastern Section - 43rd Annual Meeting, E. Dodson, March, 2008.
- Drake, 1999.** Part III, Structural Geology and Tectonics, Chapter 17: South Mountain and Reading Prong, in C.H. Shultz ed., The Geology of Pennsylvania: Pennsylvania Bureau of Topographic and Geologic Survey Special Publication 1, p 242-255, A.A. Drake, Jr., 1999.
- Ebel, 1982.** The 1981 microearthquake swarm near Moodus, Connecticut, Geophysical Research Letters, Volume 9, Number 4. p 397-400, J. E. Ebel, V. Vudler, and M. Celata, 1982.
- Ebel, 1989.** A comparison of the 1981, 1982, and 1987-1988 microearthquake swarms at Moodus, Connecticut, Seismological Research Letters, Volume 60, p 177-188, J. E. Ebel, 1989.
- Edmunds, 1999.** Part II, Stratigraphy and Sedimentary Tectonics, Chapter 10: Pennsylvanian, in C.H. Shultz ed., The Geology of Pennsylvania: Pennsylvania Bureau of Topographic and Geologic Survey Special Publication 1, p 148-169, W.E. Edmunds, V.W. Skema, and N.K. Flint, 1999.
- Engelder, 1980.** On the Use of Regional Joint Sets as Trajectories of Paleostress Fields During the Development of the Appalachian Plateau, New York, Journal of Geophysical Research, Volume 85, Number B11, p 6319-6341, Terry Engelder and Peter Geiser, November 1980.
- Engelder, 2001.** Horizontal slip along Alleghanian joints of the Appalachian plateau: evidence showing that mild penetrative strain does little to change the pristine appearance of early joints, Tectonophysics 336, p 31-41, Terry Engelder, Benjamin F. Haith, Amgad Younes, 2001
- Engelder, 2006.** Early jointing in coal and black shale: Evidence for an Appalachian-wide stress field as a prelude to the Alleghanian orogeny, Geology, Volume 34, Number 7, p 581-584, Terry Engelder and Amy Whitaker, July 2006.
- Engelder, 2009.** Joint sets that enhance production from Middle and Upper Devonian gas shales of the Appalachian Basin, AAPG Bulletin, v.93, NO.7, p. 857-889, Terry Engelder, Gary C. Lash, and Redescal S. Uzcategui, 2009.
- EPRI, 1986.** Seismic Hazard Methodology for the Central and Eastern United States, EPRI Report NP-4726, Electric Power Research Institute, July 1986.
- EPRI, 1989.** Probabilistic Seismic Hazard Evaluations at Nuclear Power Plant Sites in the Central and Eastern United States: Resolution of the Charleston Earthquake Issue, NP-6395-D, Electric Power Research Institute, 1989.
- EPRI, 2004.** CEUS Ground Motion Project Final Report, EPRI Report 1009684, Electric Power Research institute, December, 2004.
- EPRI/DOE/NRC, 2012.** Technical Report: Central and Eastern United States Seismic Source Characterization for Nuclear Facilities, EPRI Report # 1021097, U.S. DOE Report # DOE/NE-0140, U.S. NRC NUREG-2115, Electric Power Research Institute, Palo Alto, CA, U.S. DOE, U.S. NRC, 2012.

Eriksson, 2003. Predominance of Grenvillian Magmatism Recorded in Detrital Zircons from Modern Appalachian Rivers, *The Journal of Geology*, Volume 111, p 707-717, Kenneth A. Eriksson, Ian H. Campbell, J. Michael Palin, and Charlotte M. Allen, 2003.

ESRI, 2007. Street Map Pro [CD-ROM], 2007 State Boundaries, Roads, Streams, County Boundaries, ESRI, 2007.

ESRI, 2008. World Shaded Relief Imagery, ESRI, Redlands, CA, USA, ESRI Website: <http://server.arcgisonline.com/ArcGIS/rest/services>, last accessed November 2008.

Eusden, 2000. Timing of the Acadian Orogeny in Northern New Hampshire, *The Journal of Geology*, Volume 108, p 219-232, J. Dykstra Eusden, Jr., Chris A. Guzowski, Alexander C. Robinson, and Robert D. Tucker, 2000.

Evans, 1989. Appalachian Stress Study, Analysis of Devonian Shale Core: Some Implications for the Nature of Contemporary Stress Variations and Alleghanian Deformation in Devonian Rocks, *Journal of Geophysical Research*, Volume 94, Number B6, p 7155-7170, Keith F. Evans, Gerhard Oertel, Terry Engelder, June 1989.

Fail, 1973. Tectonic development of the Triassic Newark-Gettysburg Basin in Pennsylvania, *Geological Society of America Bulletin*, Volume 84, p 725-740, R. T. Fail, 1973.

Fail, 1998. A Geologic History of The North-Central Appalachians, Part 3. The Alleghany Orogeny, *American Journal of Science*, Vol. 298, P. 131-179, Rodger T. Fail, 1998.

Fail, 1999a. Part III. Structural Geology and Tectonics, Chapter 19 Appalachian Mountain Section of the Ridge and Valley Province, in C.H. Schultz ed., *The Geology of Pennsylvania: Pennsylvania Bureau of Topographic and Geologic Survey Special Publication 1*, p 268-265, R. Fail and R. Nickelsen, 1999.

Fail, 1999b. Chapter 33 - Paleozoic in *The Geology of Pennsylvania, Commonwealth of Pennsylvania, Department of Conservation and Natural Resources, Bureau of Topographic and Geological Survey*, in C.H. Shultz ed., *The Geology of Pennsylvania: Pennsylvania Bureau of Topographic and Geologic Survey Special Publication 1*, Fail, R. T., 1999.

Fail, 2004. The Birdsboro Basin, *Pennsylvania Geology*, Volume 34, Number 4, p 2-11, R. T. Fail, 2004.

Fletcher, 1977. Earthquakes related to hydraulic mining and natural seismic activity in western New York State, *Journal of Geophysical Research*, Volume 82, p 3767-3780, J. B. Fletcher and L. R. Sykes, 1977.

Frey, 1973. Influence of Salina Salt on Structure in New York-Pennsylvania Part of Appalachian Plateau, *AAPG Bulletin*, Volume 57, Number 6, p 1027-1037, M. Gordon Frey, June 1973.

Ganis, 2005. Development Of The Martinsburg/ Hamburg Foreland Segment, *Geological Society of America Abstracts with Programs*, Vol. 37, No. 1, P. 17, G. Robert Ganis, 2005.

Gao, 2000. Along-Axis Segmentation and Growth History of the Rome Trough in the Central Appalachian Basin, *AAPG Bulletin*, Volume 84, Number 1, p 75-99, Dengliang Gao, Robert C. Shumaker, and Thomas H. Wilson, January 2000.

- Gelinas, 1993.** Evaluation of liquefaction-susceptible materials near moderate magnitude historical earthquakes in New England, [abs], *Seismological Research Letters*, Volume 64, p 259-260, R. L. Gelinas, H. M. A. Kempinen, and D. C. Amick, 1993.
- GeoVision, 2010.** Final Report - Seismic Refraction Investigation Bell Bend Nuclear Power Plant, Luzerne County, Pennsylvania Report 10171-03 Rev. 0, Report Prepared for RIZZO by GeoVision Geophysical Services, Corona, CA, August 2010.
- Gillmeister, 1993.** The Lightstreet Fault: Possible Alleghenian left-slip Deformation in Northeastern Pennsylvania, *Abstracts with Programs - Geological Society of America*, Vol. 25, Issue 6, p.165, Norman M. Gillmeister, 1993.
- Glover, 1995.** E-3 Southwestern Pennsylvania to Baltimore Canyon Trough, *Geological Society of America Centennial Continent/Ocean Transect #19*, L. Glover III and K. Klitgord, 1995.
- Gold, 2003.** Geological Report on the Skytop Road Cuts, Pennsylvania State University, Department of Geosciences, p 1-27, D.P. Gold and A.G. Doden, 2003.
- Gold, 2005.** Precambrian Basement Map of the Appalachian Basin and Piedmont Province of Pennsylvania, David P. Gold of the Department of Geosciences, Pennsylvania State University, in collaboration with S. S. Alexander (Pennsylvania State University), R. Cakir (Department of Geo-Environmental Engineering, Pennsylvania State University), A. G. Doden (GMRE Inc., State College, Pa.), and S.I. Root (Department of Geology, College of Wooster, Ohio), 2005.
- Gold, 2008.** Basement Depth and Related Geospatial Database for Pennsylvania, Pennsylvania Geological Survey, Open-File General Geology (OFGG) Report OFGG 05-01.0, p 1-6, D.P. Gold, 2008.
- Gray, 1999.** Chapter 18 Great Valley and Piedmont Lowland, Part III. Structural Geology and Tectonics, p 256-267, C. Gray and S.I. Root, 1999.
- Greb, 2008.** Appalachian sedimentary cycles during the Pennsylvanian: Changing influences of sea level, climate, and tectonics, *in* Fielding, C.R., Frank, T.D., and Isbell, J. L., eds., *Resolving the Late Paleozoic Ice Age in Time and Space: Geological Society of America Special Paper 441*, p. 235-248, S.P. Greb, J.C. Pashin, R.L. Martino, and C.P. Eble, 2008.
- Gwinn, 1964.** Thin Skinned Tectonics in the Plateau and Northwestern Valley and Ridge Provinces of the Central Appalachians: *Geological Society of America Bulletin*, v.75, p. 863-900, V.F. Gwinn, 1964.
- Hack, 1989.** Geomorphology of the Appalachian Highlands, R. Hatcher Jr., W. Thomas and G. Viele, eds., *The Geology of North America*, Volume F-2, *The Appalachian-Ouachita Orogen in the United States*, Geological Society of America, J. Hack, 1989.
- Hancock, 1989.** Neotectonic joints, *Geological Society of America Bulletin*, Volume 101, p 1197-1208, 11 figures, Paul L. Hancock and Terry Engelder, October 1989
- Hansen, 1986.** The Lithology and Distribution of Pre-Cretaceous basement rocks beneath the Maryland Coastal Plain, Department of Natural Resources Maryland Geological Survey Report of Investigations No. 44, 27 p, H. Hansen and J. Edwards Jr., 1986.

Harlan, 2003. Gunbarrel mafic magmatic event: A key 780 Ma time marker for Rodinia plate reconstructions, *Geology*, Volume 31, Number 12, p 1053-1056, Stephen S. Harlan, Larry Heaman, Anthony N. LeCheminant, and Wayne R. Premo, December 2003.

Harper, 1999. Part II. Stratigraphy and Sedimentary Tectonics, Chapter 7: Devonian, in C.H. Shultz ed., *The Geology of Pennsylvania: Pennsylvania Bureau of Topographic and Geologic Survey Special Publication 1*, p 108-127, J.A. Harper, 1999.

Harper, 2003. Ordovician Carbonates in Central Pennsylvania, Trenton and Black River Carbonates in the Union Furnace Area of Blair and Huntingdon Counties, Pennsylvania, *A Field Trip Guidebook for the Eastern Section AAPG Meeting*, J. Harper Ed., J. Harper, May 2003.

Harrison, 2004. The Lackawanna synclinorium, Pennsylvania: A salt-collapse structure, partially modified by thin-skinned folding, *Geological Society of America Bulletin*, Volume 116, Number 11/12, p 1499-1514, Michael J. Harrison, Stephen Marshak, John H. McBride, November/December 2004.

Harrison, 2006. Fold-Thrust Belt Structures Of The Lackawanna Synclinorium, Pennsylvania: Insight Into The Tectonic Evolution Of The Central Appalachians, *Northeastern Geology & Environmental Sciences*, v. 28, no. 4, p. 358-367, M.J. Harrison, 2006.

Hasson, 1988. Lithofacies and paleogeography of the Conasauga Group (Middle and Late Cambrian) in the Valley and Ridge province of east Tennessee, *Geological Society of America Bulletin*, Volume 100, p 234-246, Kenneth O. Hasson and C. Stephen Haase, February 1988.

Hatcher, 1987. Tectonics of the southern and central Appalachian internides, *Annual Reviews of Earth and Planetary Science*, Volume 15, p 337-362, R. Hatcher Jr., 1987.

Hawman, 1992. Structure of the crust and upper mantle beneath the great Valley and Allegheny Plateau of eastern Pennsylvania, II, Gravity modeling and migration of wide-angle reflection data, *Journal of Geophysical Research*, Volume 97, p 393-415, R. B. Howmann and R. A. Phinney, 1992.

Hayman, 2002. Reactivation of prethrusting, synconvergence normal faults as ramps within the Ordovician Champlain-Taconic thrust system, *GSA Bulletin*, Volume 114, Number 4, p 476-489, Nicholas W. Hayman and W. S. F. Kidd, April 2002.

Heidbach, 2008. The release 2008 of the World Stress Map (available online at www.world-stress-map.org), O. Heidbach, M. Tingay, A. Barth, J. Reinecker, D. Kurfess and B. Muller, 2008.

Herman, 2005. Joints and Veins in the Newark Basin, New Jersey in *Regional Tectonic Perspective, View from the 21st Century*, 22nd Annual Meeting of the Geological Association of New Jersey, College of New Jersey, Ewing, New Jersey, p 75-116, Gregory C. Herman, 2005.

Herrmann, 1978. A seismological study of two Attica, New York earthquakes, *Bulletin of the Seismological Society of America*, Volume 68, p 641-651, R. B. Herrmann, 1978.

Hibbard, 2006. Lithotectonic map of the Appalachian Orogen, Canada-United States of America, *Geological Survey of Canada Map 02096A*, 2 sheets, Scale 1: 1,500,000, J. Hibbard, C. Van Staal, D. Rankin and H. Williams, 2006.

Hickman, 1985. In Situ Stress, Natural Fracture Distribution, and Borehole Elongation in the Auburn Geothermal Well, Auburn, New York, *Journal of Geophysical Research*, Volume 90, Number B7, p 5497-5512, Stephen H. Hickman, John H. Healy, and Mark D. Zoback, June 1985.

Hill, 2006. The Role of Transcurrent Shear Zones in the History of the Wissahickon Formation, *Geological Society of America Abstracts with Programs*, Vol. 38, No. 7, pg. 301, M. Hill, October 2006.

Hinze, 1987. Magnetic Anomaly Map of North America, Decade of North American Geology (DNAG), Geological Society of America, W. Hinze and P. Hood, 1987.

Hornberger, 2004. Chapter 2. Geology of the Pennsylvania Coal Regions, Website: http://www.dep.state.pa.us/dep/deputate/minres/bmr/beneficial_use/10%20CHAPT%202/Chapter%202%20final.pdf, Date accessed: January 22, 2008.

Horton, 1991. Preliminary Tectonostratigraphic Terrain Map of the Central and Southern Appalachians, U.S. Geological Survey Miscellaneous Investigations Series Map I-2163, J. Horton, A. Drake and D. Rankin, 1991.

Hough, 1991. Seismological constraints on source properties of the $m_b=4.0$ 1985 Ardsley, New York Earthquake: A characteristic rupture?, *Journal of Geophysical Research*, Volume 96, Number B11, p 18,183-18,195, S. E. Hough and L. Seeber, 1991.

Hurowitz, 2005. Geochemistry of Cambro-Orodivician Sedimentary Rocks of the Northeastern United States: Changes in Sediment Sources at the Onset of Taconian Orogenesis, *The Journal of Geology*, volume 113, p. 571-587, J.A. Hurowitz and S.M. McLennan, 2005.

Hutchinson, 1985. New York Bight fault, *Geological Society of America Bulletin*, Volume 96, p 975-989, D. R. Hutchinson and J. A. Crow, 1985.

Inners, 1978. Geology and Mineral Resources of the Berwick Quadrangle, Luzerne and Columbia Counties, Pennsylvania, Pennsylvania Geological Survey, Fourth Series, p 1-34, J.D. Inners, 1978.

Inners, 1988. Bedrock and Glacial Geology of the North Branch Susquehanna Lowland and the Eastern Middle Anthracite Field, 53rd Annual Field Conference of Pennsylvania Geologists, J.D. Inners Ed., p 120-123, J.D. Inners, October 1988.

Jacob, 2004. Earthquakes and the Ramapo fault system in southeastern New York State, Lamont-Doherty Earth Observatory, K. Jacob, W. Kim, A. Lerner-Lam, L. Seeber, Web Site: http://www.ldeo.columbia.edu/news/2004/04_30_04.htm, Date accessed: April 29, 2008.

Jacobeen, 1974. Structure of Broadtop Synclinorium and Its Implications for Appalachian Structural Style, *AAPG Bulletin*, Volume 58, Number 3, p 362-375, Frank Jacobeen, Jr. and William H. Kanes, March 1974.

Jenden, 1993. Mixing of Thermogenic Natural Gases in Northern Appalachian Basin, *AAPG Bulletin*, Volume 77, Number 6, p 980-998, P. D. Jenden, D. J. Drazan, and I. R. Kaplan, June 1993.

Johnston, 1985a. Seismotectonics of the Southern Appalachians, Bulletin of the Seismological Society of America, Volume 75, Number 1, p 291-312, A.C. Johnston, D.J. Reinbold, and S.I. Brewer, February 1985.

Johnston, 1985b. A basement block model for Southern Appalachian Seismicity, Geological Society of America-Abstracts with Programs, Volume 17, Number 2, p 97, A. Johnston and D Reinbold, 1985.

Jordan, 1982. Stratigraphy Of The Sedimentary Rocks Of Delaware, Bulletin No.9, Delaware Geological Survey, Newark, Delaware, Robert R. Jordan, 1982.

Kafka, 1985. Earthquake Activity in the Greater New York City Area: Magnitudes, Seismicity and Geologic Structures, Bulletin of the Seismological Society of America, Volume 75, Number 5, p 1285-1300, A. Kafka, E. Schlesinger-Miller and N. Barstow, 1985.

Kauffman, 1999. Part II, Stratigraphy and Sedimentary Tectonics, Chapter 4: Eocambrian, Cambrian, and Transition to Ordovician, in C.H. Shultz ed., The Geology of Pennsylvania: Pennsylvania Bureau of Topographic and Geologic Survey Special Publication 1, p 59-73, M.E. Kauffman, 1999.

Kim, 2009. The 2008-2009 Earthquake Swarm Near Dillsburg, Pennsylvania, Commonwealth Of Pennsylvania Bureau Of Topographic and Geologic Survey, Open-File Report OFMI 09-01.0 2009. W.Y. Kim, M. Gold, C. Scharnberger, J. Jones, and H. Delano, 2009.

King, 1978. The New York-Alabama lineament: Geophysical Evidence for a Major Crustal Break in the Basement Beneath the Appalachian Basin, Geology, Volume 6, p 312-318, E. King and I. Zietz, 1978.

King, 1999. Part IV. Regional Geophysics, Chapter 24 Aeromagnetism, in C.H. Shultz ed., The Geology of Pennsylvania: Pennsylvania Bureau of Topographic and Geologic Survey Special Publication 1, p 323-327, E. King, 1999.

Klawon, 1995. Light Street Fault Reconsidered in Light of the Structural History of the Berwick Anticlinorium, Abstracts with Programs - Geological Society of America, Vol. 27, Issue 1, p. 61, Jeanne E. Klawon, 1995.

Kline, 1991. Provenance of Arkosic Metasediments in the Virginia Blue Ridge: Constraints on Appalachian Suspect Terrane Models, American Journal of Science, Vol. 291, February, 1991.

Klitgord, 1988. U. S. Atlantic Continental Margin: Structural and Tectonic Framework, R. Sheridan and J. Grow, eds., The Atlantic Continental Margin, U.S., Geological Society of America, The Geology of North America, Volume 1-2, p 19-55, K. Klitgord, D. Hutchinson and H. Schouten, 1988.

Klitgord, 1995. Mid-Atlantic Continental Margin: The Mesozoic-Cenozoic Continent-Ocean Boundary, in L. Glover III and K. Klitgord, Chief Compilers, E-3 Southwestern Pennsylvania to Baltimore Canyon Trough, Geological Society of America Continent/Ocean Transect #19, Explanatory Pamphlet, K. Klitgord, C. Poag, L. Glover, R. Sheridan, D. Hutchinson, R. Mixon and R. Benson, 1995.

Koch, 1978. Geology and geophysics of the Moodus seismic area, Connecticut, Geological Society of America Abstracts with Programs, Volume 10, Number 2, p 71, B. F. Koch, R. J. Fahey, S. S. Quarrier, and J. F. Kick, 1978.

Komor, 1998. Sources of Geospatial Data for Central and Western New York - 1998, U.S. Geological Survey, Open-File Report 99-191, 42 p, S.C. Komor, 1998

Kucks, 1999. Bouguer Gravity Anomaly Data Grid for the Conterminous US, <http://tin.er.usgs.gov/metadata/usgravboug.faq.html> Kucks, 1999.

Kulander, 2005. Regional Seismic Lines Across the Rome Trough and Allegheny Plateau of Northern West Virginia, Western Maryland, and Southwestern Pennsylvania, US Geological Survey, pamphlet to accompany Map I-2791, C.S. Kulander, and R. Ryder, 2005.

Kunk, 2004. Multiple Paleozoic Metamorphic Histories, Fabrics, and Faulting in the Westminster and Potomac Terranes, Central Appalachian Piedmont, Northern Virginia and Southern Maryland, U.S. Geological Survey, 9 p, M. Kunk, R. Wintsch, C. Southworth, B. Mulvey, C. Naeser and N. Naeser, 2004.

Lang, 1996. Pressure-temperature-reaction history of metapelitic rocks from the Maryland Piedmont on the basis of correlated garnet zoning and plagioclase-inclusion composition, Helen M. Lang, American Mineralogist, Volume 81.

Lash, 2009. Tracking the burial and Tectonic History of Devonian Shale of the Appalachian Basin by Analysis of Joint Intersection Style, Geological Society of America Bulletin, vol. 121, p. 265-277. Gary G. Lash and Terry Engelder, 2009.

Laughrey, 1999. Part II, Stratigraphy and Sedimentary Tectonics, Chapter 6: Silurian and Transition to Devonian, in C.H. Shultz ed., The Geology of Pennsylvania: Pennsylvania Bureau of Topographic and Geologic Survey Special Publication 1, p 91-107, C.D. Laughrey, 1999.

Lavin, 1982. Major lineaments and the Lake Erie-Maryland crustal block, Tectonics, Volume 1, p 431-440, P. M. Lavin, D. L. Chaffin, and W. F. Davis, 1982.

Lavin, 1999. Gravity, The Geology of Pennsylvania, Part IV. Regional Geophysics, Chapter 23, p 317-321, P. Lavin, 1999.

Lotto, 1997. Seismic stratigraphy of the New York bight, NY/NJ continental shelf, Geological Society of America Abstracts with Programs, Volume 29, Number 1, p 62, L. Lotto, M. A. Allison, W. C. Schwab, B. Butman, D. Foster, J. Denny, and W. Corso, 1997.

Low, 2002. Geohydrology of Southeastern Pennsylvania, Water-Resources Investigations Report 00-4166, U.S. Geological Survey, U.S. Department of the Interior, In cooperation with the Pennsylvania Department of Conservation and Natural Resources, Bureau of Topographic and Geologic Survey, Dennis J. Low, Daniel J. Hippe, and Dawna Yannacci.

Lyons, 1982. Gravity Anomaly Map of the United States, Society of Exploration Geophysicists, Scale 1: 2,500,000, P. Lyons and N. O'hare, 1982.

MacLachlan, 1999. Part VI, Geologic History, Chapter 34: Mesozoic, in C.H. Shultz ed., The Geology of Pennsylvania: Pennsylvania Bureau of Topographic and Geologic Survey Special Publication 1, p 435-449, D.B. MacLachlan, 1999.

Marple, 2000. Evidence for a Buried Fault System in the Coastal Plain of the Carolinas and Virginia-Implications for Neotectonics in the Southeastern United States, Geological Society of America Bulletin, Volume 112, Number 2, p 200-220, R. Marple and P. Talwani, February 2000.

Marple, 2004. Relationship of the Stafford Fault Zone to the Right-Stepping Bends of the Potomac, Susquehanna and Delaware Rivers and Related Upstream Along the U.S. Mid-Atlantic Fall Line: In Southeastern Geology, Volume 42, Number 3, p 123-144, R. Marple, 2004.

Matmon, 2003. Temporally and Spatially Uniform Rates of Erosion in the Southern Appalachian Great Smoky Mountains, Geology, v. 31, no. 2, p. 155-158, A. Matmon, P.R. Bierman, J. Larsen, S. Southworth, M. Pavich, M. Caffee, 2003.

McDonnell, 2008. Physical Geography of New York, T. McDonnell, Website: http://www.nygeo.org/ny_geo.html, Date accessed: April 9, 2008.

McElroy, 2007. Bedrock Geologic Map of the Allensville Quadrangle, Huntingdon and Mifflin Counties, Pennsylvania, Pennsylvania Geological Survey, 4th ser., OpenFile Report OFBM 07-02.0, T.A. McElroy and D.M. Hoskins, 2007.

McLaughlin, 2002. Results of Trenching Investigations Along the New Castle Railroad Survey-1 Seismic Line, New Castle, Delaware, Delaware Geological Survey, Open-File Report 43, 19 p, P. McLaughlin, S. Baxter, K. Ramsey, T. McKenna and S. Strohmeier, 2002.

McGuire, 2001. Technical Basis for Revision of Regulatory Guidance on Design Ground Motions: Hazard- and Risk-consistent Ground Motion Spectra Guidelines, NUREG/CR-6728, R.K. McGuire, W.J. Silva, and C.J. Costantino, 2001.

Merguerian, 1996. Stratigraphy, Structural Geology, and Ductile- and Brittle Faults of New York City, Website: <http://www.dukelabs.com/Abstracts%20and%20Papers/CM1996c.htm>, 26 p, Date accessed: March 25, 2008.

Merguerian, 1997. Bronx River diversion- Neotectonic implications, International Journal of Rock Mechanics and Mining Sciences, Volume 34, Number 3-4, Paper Number 298, C. Merguerian and J. E. Sanders, 1997.

Milici, 2006. Assessment of Appalachian Basin Oil and Gas Resources: Devonian Shale- Middle and Upper Paleozoic Total Petroleum System, US Geological Survey, Open-File Report Series 2006-1237, p 1-70, R.C. Milici and C.S. Swezey, 2006.

Milici, 2009. The Blue Ridge Thrust Belt Province (068), Piedmont Province (069), Atlantic Coastal Plain Province (070), Adirondack Uplift Province (071), and New England Province (072), U.S. Geological Survey Digital Data Series DDS-30, Release 2, one CD-ROM, Milici, R.C. Online Linkage: <http://certmapper.cr.usgs.gov/data/noga95/prov68/text/prov68.pdf>.

Millot, 2001. Proterozoic Eon: Mesoproterozoic Era-Greenville Orogeny, L. Sniatkowski ed., J. Millot, 2001.

Mixon, 1977. Stafford Fault System: Structure Documenting Cretaceous and Tertiary Deformation Along the Fall Line in Northeastern Virginia, Geology, Vol. 5, p. 437-440, R. Mixon and W. Newell, 1977.

- Mixon, 2000.** Geologic Map of the Fredricksburg 30' x 60' Quadrangle, Virginia and Maryland, Report 2607, IMAP, R. Nixon, L. Pavlides, D. Powars, A. Froelich, R. Weems, J. Schindler, W. Newell, L. Edwards, and L. Ward, 2000.
- Mitra, 1988.** Effects of Deformation Mechanisms on Reservoir Potential in Central Appalachian Overthrust Belt, AAPG Bulletin, Volume 72, Number 5, p 536-554, Shankar Mitra, May 1988.
- Moecher, 2004.** Precise Time and Conditions of Peak Taconian Granulite Facies Metamorphism in the Southern Appalachian Orogen, U.S.A., with Implications for Zircon Behavior during Crustal Melting Events, The Journal of Geology, Volume 112, p 289-304, David P. Moecher, Scott D. Samson, and Calvin F. Miller, 2004.
- Mueller, 2008.** Crustal Evolution in the Southern Appalachian Orogen: Evidence from Hf Isotopes in Detrital Zircons, The Journal of Geology, Volume 116, p 414-422, Paul A. Mueller, George D. Kamenov, Ann L. Heatherington, and Joshua Richards, 2008.
- Murphy, 2000.** Proto-Avalonia: A 1.2-1.0 Ga tectonothermal event and constraints for the evolution of Rodinia, Geology, Volume 28, Number 12, p 1071-1074, J.B. Murphy, R.A. Strachan, R.D. Nance, K.D. Parker, M. B. Fowler, December 2000.
- National Atlas, 2008.** Shaded Relief (200 Meter) 2008.downloaded from www.nationalatlas.gov/mld/srld48i.html, U.S. National Atlas, 2008.
- Nelson, 1983.** The Clingman Lineament: Aeromagnetic Evidence for a Major Discontinuity in the North American Basement, Geological Society of America, Southeastern Section, Abstracts with Programs, Volume 13, Number 1, p 31, A. Nelson and I. Zietz, January 1983.
- NGS, 2010.** USA Topographic Maps, National Geographic Society, i-cubed. ESRI Server: http://services.arcgisonline.com/ArcGIS/rest/services/USA_Topo_Maps/MapServer Date accessed: July 29, 2010.
- NJGS, 2003.** Generalized Glacial Sediments of New Jersey, New Jersey Geological Survey, Website: <http://www.state.nj.us/dep/njgs/geodata/dgs96-1.gif>, Date accessed: December 14, 2007.
- NRC, 1978.** Regulatory Guide 1.70, Standard Format and Content of Safety Analysis Reports for Nuclear Power Plants, LWR Edition, Revision 3, Nuclear Regulatory Commission, 1978.
- NRC, 1997.** Regulatory Guide 1.165, Identification and Characterization of Seismic Sources and Determination of Safe Shutdown Earthquake Ground Motion, Nuclear Regulatory Commission, March 1997.
- NRC, 2003a.** Site Investigations for Foundations of Nuclear Power Plants, Regulatory Guide 1.132, Revision 2, Nuclear Regulatory Commission, 2003.
- NRC, 2003b.** Laboratory Investigations of Soils for Engineering Analysis and Design of Nuclear Power Plants, Regulatory Guide 1.138, Revision 2, Nuclear Regulatory Commission, 2003.
- NRC, 2007a.** Basis Geologic and Seismic Information, Regulatory Guide 1.206, Section 2.5.1, Nuclear Regulatory Commission, June 2007.

- NRC, 2007b.** A Performance-based Approach to Define the Site-specific Earthquake Ground Motion, Regulatory Guide 1.208, U.S. Nuclear Regulatory Commission, March, 2007.
- NRC, 2012.** Practical Implementation Guidelines for SSHAC Level 3 and 4 Hazard Studies, NUREG-2117, U.S. Nuclear Regulatory Commission, February, 2012.
- Obermeier, 2009.** Using Paleoliquifaction-Induced and Other Soft-Sediment Features for Paleoseismic Analysis, in McCalpin, J.P., ed., *Paleoseismology: Volume 95, Second Edition* (International Geophysics), San Diego, Academic Press, p. 497-564, Obermeier, S.F., 2009.
- Oliver, 1970.** Postglacial faulting and seismicity in New York and Quebec: *Canadian Journal of Earth Sciences*, v. 7, p. 579-590, J. Oliver, T. Johnson, and J. Dorman, 1970.
- Olsen, 1990.** Transtensional Arm of the Early Mesozoic Fundy Rift Basin: Penecontemporaneous Faulting and Sedimentation, *Geology*, v. 18, p. 695-698, P.E. Olsen. R.W. Schlische, 1990.
- Ong, 2007.** Early rotation and late folding in the Pennsylvania salient (U.S. Appalachians): Evidence from calcite-twinning analysis of Paleozoic carbonates, *GSA Bulletin*, Volume 119, Number 7/8, p 796-804, Philip F. Ong, Ben A. van der Pluijm and Rob Van der Voo, July/August 2007.
- Owens, 1995.** Geologic map of New Jersey: Central Sheet, U.S. geological Survey Open-File Report 95-0253, 60 p, 3 pls., scale 1:100,000, J. P. Owens, P. J. Sugarman, N. F. Sohl, R. A. Parker, H. F. Houghton, R. A. Volkert, A. A. Drake, R. C. Orndroff, 1995.
- PADEP, 2010.** Pennsylvania Department of Environmental Protection, Bureau of Oil and Gas Management Home Page, <http://www.dep.state.pa.us/dep/deputate/minres/oilgas/2010PermitDrilledmaps.htm>, Date accessed: August 19, 2010.
- PAMAP, 2008.** PAMAP Program Topographic Contours (2 ft interval) of Pennsylvania, PA Department of Conservation and Natural Resources, Bureau of Topographic and Geologic Survey.
- Parker, 1990.** Bedrock geologic map of Monmouth junction quadrangle, New Jersey, U.S. Geological Survey Open-File Report 90-219, 1 pl., scale 1:24000, R. A. parker and H. F. Houghton, 1990.
- Pavlidis, 1986.** Mountain Run fault zone of Virginia, in M. L. Jacobsen and T. R. Rodriguez, comp., *National Earthquake Hazard reduction Program, Summaries of Technical Reports*, Volume XXIII, U.S. Geological Survey Open-File Report 87-63, p 93-93, L. Pavlidis, 1986.
- Pavlidis, 1994.** Early Paleozoic Alkalic and Calc-Alkalic Plutonism and Associated Contact Metamorphism, Central Virginia Piedmont, U.S. Geological Survey Professional Paper 1529, L. Pavlidis, J. Arth, J. Sutter, T. Stern and H. Cortesini Jr., 1994.
- Pazzaglia, 1993.** Stratigraphy, Petrography, and Correlation of Late Cenozoic Middle Atlantic Coastal Plain Deposits: Implications for Late-Stage Passive-Margin Geologic Evolution, *Geological Society of American Bulletin*, Volume 105, p 1617-1634, F.J. Pazzaglia, 1993.

Pazzaglia, 1994. Late Cenozoic Flexural Deformation of the Middle U.S. Atlantic Passive Margin, *Journal of Geophysical Research*, Volume 99, Number B6, p 12143-12157, F. J. Pazzaglia and T.W. Gardner, 1994.

Pazzaglia, 2006. Rivers, glaciers, landscape evolution, and active tectonics of the central Appalachians, Pennsylvania and Maryland, *in* Pazzaglia, F.J., ed., *Excursions in Geology and History: Field Trips in the Middle Atlantic States: Geological Society of America Field Guide 8*, p. 169-197, F.J. Pazzaglia, D.D. Braun, M. Pavich, P. Bierman, N. Potter Jr., D. Merritts, R. Walter, and D. Germanoski, 2006.

Pelletier, 2004. Estimate of three-dimensional flexural-isostatic response to unloading: Rock uplift due to Late Cenozoic glacial erosion in the western United States, *Geology*, Volume 32, Number 2, p 161-164, Jon D. Pelletier, February 2004.

Philpotts, 1985. Differentiation of Mesozoic basalts of the Hartford Basin, Connecticut. *Geological Society of America Bulletin*. v. 96: p. 1131 -1139, A.R. Philpotts and I. Reichenbach, 1985.

Plank, 2000. Bedrock Geology of the Piedmont of Delaware and Adjacent Pennsylvania, Delaware Geological Survey, Report of Investigations No. 59, State of Delaware, Margaret O. Plank, William S. Schenck, LeeAnn Srogi, 2000.

Pohn, 2000. Lateral Ramps in the Folded Appalachians and in Overthrust Belts Worldwide- a Fundamental Element of Thrust-Belt Architecture, *U.S. Geological Survey Bulletin 2163*, p 1-63, H.A. Pohn, 2000.

Ratcliffe, 1971. The Ramapo Fault System in New York and Adjacent Northern New Jersey-A Case of Tectonic Heredity, *Geological Society of America Bulletin*, Volume 82, p 125-142, N. Ratcliffe, 1971.

Ratcliffe, 1982. Tectonic Versus Frost-Wedging Origin of Faulted Glacially Polished Surfaces in the Lower Hudson River Valley, *Geological Society of America Abstracts with Programs*, V. 14, no. 1-2, February 1982, p. 76, N.M. Ratcliffe.

Ratcliffe, 1984. Brittle fault fabrics, mineralogy, and geometry of border faults of the Newark basin, NY-NJ, from drill-core information, *Geological Society of America Abstracts with Programs*, Volume 16, Number 1, p 57, N. M. Ratcliffe and W. C. Burton, 1984.

Ratcliffe, 1985. Fault Reactivation Models For Origin of the Newark Basin And Studies Related To Eastern U.S. Seismicity, *in* *Proceedings of the Second U.S. Geological Survey Workshop on the Early Mesozoic Basins of the Eastern United States*, U.S. Geological Circular 946, G.R. Robinson, Jr., and A.J. Froelich eds., U.S. Geological Survey, N.M. Ratcliffe and W.C. Burton, 1985.

Ratcliffe, 1988. Structural analysis of Furlong fault and the relation of mineralization to faulting and diabase intrusion, Newark basin, Pennsylvania, *in* A. J. Frolich and G. R. Robinson Jr., eds., *Studies of Early Mesozoic basins of the eastern United States*, U.S. Geological Survey Bulletin 1776, p 176-193, N. M. Ratcliffe and W. C. Burton, 1988.

Reese, 2004. Kinematic Constraints on Rodinia Reconstructions from the Core of the Texas Grenville Orogen, *The Journal of Geology*, Volume 112, p 185-205, Joseph F. Reese and Sharon Mosher, 2004.

Resor, 2005. Hartford Basin Cross Section - Southington to Portland, CT, Guidebook for Field Trips in Connecticut, Guidebook no. 8. Ed. McHone, N.W. and Peterson, M.J. Hartford, CT: Department of Environmental Protection, p. 177-189, Phillip G. Resor and J.Z. De Boer, 2005.

Rodgers, 1984. Tyrone-Mt.Union Cross-Strike Lineament of Pennsylvania: A Major Paleozoic Basement Fracture and Uplift Boundary, *AAPG Bulletin*, Volume 68, Number 1, p 92-105, Michael R. Rodgers and Thomas H. Anderson, January 1984.

Rodgers, 1985. Bedrock Geological Map of Connecticut: Connecticut Geological and Natural History Survey, scale 1:125,000, <http://www.tmsc.org/geology/bedrock>, J. Rodgers, 1985.

Root, 1977a. North 40° latitude fault zone, Pennsylvania; a new interpretation, *Geology*, Volume 5, p 719-723, S. I. Root and D. M. Hoskins, 1977.

Root, 1977b. Geology and Mineral Resources Of The Harrisburg West Area, Cumberland and York Counties, Pennsylvania, Atlas 148ab, Pennsylvania Geological Survey, Fourth Series, Harrisburg. Samuel I. Root, 1977.

Root, 1999. Part III, Structural Geology and Tectonics, Chapter 21: Gettysburg-Newark Lowland, in C.H. Shultz ed., *The Geology of Pennsylvania: Pennsylvania Bureau of Topographic and Geologic Survey Special Publication 1*, p 298-305, S.I. Root and D.B. MacLachlan, 1999.

Ryder, 1992. Stratigraphic Framework of Cambrian and Ordovician Rocks in the Central Appalachian Basin from Medina County, Ohio, through Southwestern and South-Central Pennsylvania to Hampshire County, West Virginia, *US Geological Survey Bulletin 1839*, p 1-40, R.T. Ryder, A.G. Harris, and J.E. Repetski, 1992.

Ryder, 1995. Appalachian basin province, in Gautier, D.L., Dolton, G.L., Takahashi, K.I., and Varnes, K.L., eds., 1995 national assessment of United States oil and gas resources--Results, methodology, and supporting data: U.S. Geological Survey Digital Data Series DDS-30, 144 p., R.T. Ryder, 1995.

Saad, 1990. Large Springs in the Valley and Ridge Physiographic Province of Pennsylvania; A Contribution to the Appalachian Valleys - Piedmont Regional Aquifer-System Analysis Study, U.S. Geological Survey Open-File Report 90-164, D.A. Saad and D.J. Hippe, 1990.

Sanders, 1963. Late Triassic Tectonic History of the Northeastern United States, *American Journal of Science*, Vol. 261, p 501-524, J. Sanders, 1963.

Saylor, 1999. Part II, Stratigraphy and Sedimentary Tectonics, Chapter 3C: Precambrian and Lower Paleozoic Metamorphic and Igneous Rocks- in the Subsurface, in C.H. Shultz ed., *The Geology of Pennsylvania: Pennsylvania Bureau of Topographic and Geologic Survey Special Publication 1*, p 51-57, T.E. Saylor, 1999.

Scharnberger, 2006. The Lancaster Seismic Zone of the Southeast Pennsylvania in relation to the Gettysburg-Newark Basin, *Geological Society of America, Abstracts with Programs*, Volume 38, Number 2, p 83, C. Scharnberger, 2006.

Schlische, 2002. Relative Timing of CAMP, Rifting, Continental Breakup, and Basin Inversion: Tectonic Significance, in Hames, W.E., McHone, G.C., Renne, P.R., and Ruppel, C., eds., The Central Atlantic Magmatic Province, American Geophysical Union Monograph 136, Roy W. Schlische, Martha Oliver Withjack, and Paul E. Olsen.

Schlische, 2003. Progress in Understanding the Structural Geology, Basin Evolution, and Tectonic History of the Eastern North American Rift System, P. Letourneau and P. Olsen, eds., The Great Rift Valleys of Pangaea in Eastern North America, Volume 1, p 21-64, R. Schlische, 2003.

Schruben, 1998. Geology of the Conterminous United States at 1:2,500,000 scale - a Digital Representation of the 1974 P.B. King and H.M. Beikman Map: U.S. Department of the Interior, U.S. Geological Survey Digital Data Series DDS-11 CD-ROM, release 2; display software by Russell A. Ambroziak. P.G. Schruben, R.E. Arndt, and W.J. Bawiec, 1998.

Schwab, 1997. Seafloor Characterization Offshore of the New York-New Jersey Metropolitan Area Using Sidescan-Sonar, U.S. Geological Survey, Open-File Report 00-295, 16 p, Schwab, 1997.

Seborowski, 1982. Tectonic implications of recent earthquakes near Ansville, New York, Bulletin of the Seismological Society of America, Volume 72, p 1601-1609, D. D. Seborowski, G. Williams, J. A. Kelleher, and C. T. Statton, 1982.

Seeber, 1998. The 1994 Cacoosing Valley Earthquakes Near Reading, Pennsylvania: A Shallow Rupture Triggered By Quarry Unloading, Journal of Geophysical Research, Volume 103, Number B10, p 24,505-24,521, L. Seeber, J. Armbruster, W. Kim, N. Barstow and C. Scharnberger, 1998.

Senior, 2006. Arsenic, Boron, and Fluoride Concentrations in Ground Water in and Near Diabase Intrusions, Newark Basin, Southeastern Pennsylvania, Lisa A. Senior, Ronald A. Sloto, United States Geological Survey, Scientific Investigations Report 2006-5261, 105 p.

Sevon, 1999a. Pennsylvania and the Ice Age (2nd ed.): Pennsylvania Geological Survey, 4th series, Educational Series 6, 30 p. W.D. Sevon and G.M. Fleeger, 1999.

Sevon, 1999b. Part VI, Geologic History, Chapter 35: Cenozoic, in C.H. Shultz ed., The Geology of Pennsylvania: Pennsylvania Bureau of Topographic and Geologic Survey Special Publication 1, p 451-455, W.D. Sevon and G.M. Fleeger, 1999.

Sevon, 2000a. Regolith in the Piedmont Upland Section, Piedmont Province, York, Lancaster and Chester Counties, Southeastern Pennsylvania, Southeastern Geology, Volume 39, Number 3 and 4, p 223-241, W. Sevon, October 2000.

Sevon, 2000b. Physiographic Provinces of Pennsylvania, Pennsylvania Department of Conservation and Natural Resources, Website: <http://www.dcnr.state.pa.us/topogeo/maps/map13.pdf>, Date accessed: December 14, 2007.

Sevon, 2000c. Glacial Deposits of Pennsylvania, Pennsylvania Department of Conservation and Natural Resources, Website: <http://www.dcnr.state.pa.us/topogeo/maps/map59.pdf>, Date accessed: December 14, 2007.

Sheridan, 1988. The Atlantic Continental Margin, U.S. Geological Society of America, The Geology of North America, Volume 1-2, p 610, R. Sheridan and J. Grow, 1988.

Sheridan, 1993. Deep seismic reflection data of EDGE U.S. mid-Atlantic continental-margin experiment: Implications for Appalachian sutures and Mesozoic rifting and magmatic underplating, *Geology*, Volume 21, p 563-567, Robert E. Sheridan, Douglas L. Musser, Lynn Glover, III, Manik Talwani, John I. Ewing, W. Steven Holbrook, G. Michael Purdy, Robert Hawman, and Scott Smithson, June 1993.

Shumaker, 2002. Reinterpreted Oriskany structure at the North Summit field, Chestnut Ridge anticline, Pennsylvania, *AAPG Bulletin*, Volume 86, Number 4, p 653-670, Robert C. Shumaker, April 2002.

Southworth, 2002. Digital Geologic Map and Database of the Frederick 30' x 60' Quadrangle, Maryland, Virginia, and West Virginia, Version 1.0, Compiled by Scott Southworth, Aeromagnetic map and digital topographic map by D. Daniels, Digital compilation by J.E. Reddy and D. Denenny, Pamphlet to accompany Open-File Report 02-437, U.S. Geological Survey, Reston, Virginia, S. Southworth, D. Brezinski, A.A. Drake, W.C. Burton, R.C. Orndorff, and A.J. Froelich, 2002

Southworth, 2006. Central Appalachian Piedmont and Blue Ridge tectonic transect, Potomac River corridor, in Pazzaglia, F.J., ed., *Excursions in Geology and History: Field Trips in the Middle Atlantic States: Geological Society of America Field Guide 8*, Southworth, S., Drake, A.A., Jr., Brezinski, D.K., Wintsch, R.P., Kunk, M.J., Aleinikoff, J.N., Naeser, C.W., and Naeser, N.D.

Spoljaric, 1972. Geology of the Fall Zone in Delaware, Delaware Geological Survey, p 30, N. Spoljaric, March 1972.

Spoljaric, 1973. Normal Faults in Basement Rocks of the Northern Coastal Plain, Delaware, *Geological Society of America Bulletin*, Volume 84, p 2781-2783, N. Spoljaric, 1973.

SSES FSAR, 2003. Susquehanna Steam Electric Station Units 1 and 2 Final Safety Analysis Report, Section 2.5, Geology, Seismology, and Geotechnical Engineering, Rev. 58, Pennsylvania Power and Light, 2003.

Stanford, 1995. Possible Pliocene-Pleistocene Movement on a Reactivated Mesozoic Fault In Central New Jersey, *Geological Society of America Abstracts with Programs*, Volume 27, Number 1, p 83, S. Stanford, D. Jagel, and D. Hall, 1995.

Steltenpohl, 1988. Kinematics of the Towaliga, Bartletts Ferry, and Goat Rock fault zones, Alabama: The Late Paleozoic dextral shear system in the southernmost Appalachians, *Geology*, Volume 16, p 852-855, Mark. G. Steltenpohl, September 1988.

Stern, 2005. Isostatic rebound due to glacial erosion within the Transantarctic Mountains, *Geology*, Volume 33, Number 3, p 221-224, T.A. Stern, A.K. Baxter, P.J. Barrett, March 2005.

Streepey, 2001. Early History of the Carthage-Colton Shear Zone, Grenville Province, Northwestern Adirondacks, New York (U.S.A), *The Journal of Geology*, Volume 109, p 479-492, M. M. Streepey, E. L. Johnson, K. Mezger, and B. A. van der Pluijm, 2001.

Street, 1977. A study of northeastern North American spectral moments, magnitudes, and intensities, *Bulletin of the Seismological Society of America*, Volume 67, p 599-614, R. L. Street and F. T. Turcotte, 1977.

Sumi, 2008. *Shale Gas: Focus on the Marcellus Shale*, Oil and Gas Accountability Project/Earthworks, Washington, D.C., L. Sumi, 2008.

Swanson, 1982. Preliminary model for early transform history in central Atlantic rifting, *Geology*, 10:317-320, M. Swanson, 1982.

Sykes, 2008. Observations and Tectonic Setting of Historic and Instrumentally Located Earthquakes in the Greater New York City - Philadelphia Area, Lynn R. Sykes, John G. Armbruster, Won-Young Kim, and Leonardo Seeber, *Bulletin of the Seismological Society of America*, Volume 98, Number 4, p. 1696-1719, 2008.

Tanner, 1987. Gravity Anomaly Map of North America, *Decade of North American Geology (DNAG)*, Geological Society of America, J. Tanner, 1987.

Thomas, 2004. Detrital Zircon Evidence of a Recycled Orogenic Foreland Provenance for Alleghanian Clastic-Wedge Sandstones, *The Journal of Geology*, Volume 112, p 23-37, William A. Thomas, Thomas P. Becker, Scott D. Samson, and Michael A. Hamilton, 2004.

Thompson, 1999. Part II, Stratigraphy and Sedimentary Tectonics, Chapter 5: Ordovician, in C.H. Shultz ed., *The Geology of Pennsylvania: Pennsylvania Bureau of Topographic and Geologic Survey Special Publication 1*, p 74-89.

Thompson, 2000. Neotectonics in Coastal Connecticut-Evidence from the Farm River marsh, Branford [abs.]: *Eos, Transactions of the American Geophysical Union*, v. 80, No 17 (Supplement), p. S86, W.G. Thompson, J.C. Varekamp, E. Thomas, and J.Z. de Boer, 2000.

Thompson, 2001. Fault motions along the east border fault, Hartford basin, CT, over the last 2800 years [abs.]: *Eos, Transactions of the American Geophysical Union*, v. 81, No 19 (Supplement), p. S311, W.G. Thompson, J.C. Varekamp, and E. Thomas, 2001. A.M. Thompson, 1999.

Thurber, 1985. Crustal structure along the Ramapo fault zone, New York State, *Earthquake Notes*, Volume 56, p 145-152, C. Thurber and T. Caruso, 1985.

Tremblay, 1997. Taconian Obduction and Silurian Exhumation of the Betts Cove Ophiolite, Canadian Appalachians, *The Journal of Geology*, volume 105, p. 701-716, A. Tremblay, J.H. Bedard, and Kathleen Lauziere, 1997.

Tremblay, 2003. Supracrustal faults of the St. Laurence rift system, Quebec: kinematics and geometry as revealed by field mapping and marine seismic reflection data, *Tectonophysics* 369, p 231-252, Alain Tremblay, Bernard Long and Manon Masse, 2003.

Tuttle, 1991. Historic and prehistoric earthquake-induced liquefaction in Newbury, Massachusetts, *Geology*, Volume 19, p 594-597, M. Tuttle and L. Seeber, 1991.

Tuttle, 2002. Paleoliquefaction study of the Clarendon-Linden fault system, western New York State, *Tectonophysics*, Volume 353, p 263-286, M. Tuttle, K. Dyer-Williams and N. L. Barstow, 2002.

USGS, 1989. 1:24,000 Topographic Maps: Berwick, Pennsylvania, USGS, 1989.

USGS, 2002a. Documentation for the 2002 Update of the National Seismic Hazard Maps, U.S. Geological Survey Open-File Report 02-420, A.D. Frankel, M.D. Petersen, C.S. Mueller, K.M. Haller, R.L. Wheeler, E.V. Leyendecker, R.L. Wesson, S.C. Harmsen, C.H. Cramer, D.M. Perkins, and K.S. Rukstales, 2002.

USGS, 2002b. Physiographic Divisions of the US, Polygon coverage of Physiographic Divisions in the conterminous United States automated from Fenneman and Johnson 1946, 1:7,000,000scale map "Physical Divisions of the United States". <http://water.usgs.gov/GIS/metadata/usgswrd/XML/physio.xml>, USGS, 2002.

USGS, 2008. Documentation for the 2008 update of the United States National Seismic Hazard Maps: U.S. Geological Survey Open-File Report 2008-1128, M.D. Peterson, A.D. Frankel, S.C. Harmsen, C.S. Mueller, K.M. Haller, R.L. Wheeler, R.L. Wesson, Y. Zeng, O.S. Boyd, D.M. Perkins, N. Luco, E.H. Field, C.J. Wills, and K.S. Rukstales, 2008.

VADOT, 2008. Aggregate Plant Certification Study Guide, The Virginia Dept. of Transportation, 32nd Ed., Appendix F, P. F-1~F-26, VADOT, 2008

Valentino, 1995. Paleozoic transcurrent conjugate shear zones in the central Appalachian piedmont of southeastern Pennsylvania, *Journal of Geodynamics*, Volume 19, Issues 3-4, May-July 1995, D. Valentino, and M. Hill.

Valentino, 1999. Interaction between Paleozoic strike-slip and thrust shear zones in the Philadelphia Structural Block, Central Appalachian Piedmont, *Geological Society of America, Special Paper 330*, D.W. Valentino, R.W. Valentino, and B.J. Lamport.

Van Diver, 1993. Plate Tectonics, Roadside Geology of Pennsylvania, Roadside Geology Series, 352 p, Van Diver, 1993.

Varnes, 1978. Slope Movement Types and Processes, in Schuster, R.L., and Krizek, R.J., eds., *Landslides-Analysis and control: National Research Council, Washington, D.C., Transportation Research Board, Special Report 176*, p 11-33, R.L. Schuster and R.J. Krizek, 1978.

VDEQ, 2008. Virginia's Mineral and Energy Resources, Virginia Resource-Use Education Council, Virginia's Natural Resources Education Guide, 17 p., VDEQ, 2008.

Ver Straeten, 2000. Bulge Migration and Pinnacle Reef Development, Devonian Appalachian Foreland Basin, *The Journal of Geology*, Volume 108, p 339-352, Charles A. Ver Straeten and Carlton E. Brett, 2000.

Vlahoic, 1998. Joint hypocenter-velocity inversion for the eastern Tennessee seismic zone, *Journal of Geophysical Research*, Volume 103, p 4,879-4,896, G. Vlahoic, C. A. Powell, M. C. Chapman, and S. Sibol, 1998.

Way, 1999. Part IV. Physiography, Chapter 29: Appalachian Mountain Section of the Ridge and Valley Province, in C.H. Shultz ed., *The Geology of Pennsylvania: Pennsylvania Bureau of Topographic and Geologic Survey Special Publication 1*, p 353-361, J.H. Way, 1999.

Weems, 1998. New recognized en echelon fall lines in the Piedmont and Blue Ridge provinces of North Carolina and Virginia, with a discussion of their possible ages and origins, U.S. Geological Survey Open-File Report 98-374, 52 p, R. E. Weems, 1998.

Wentworth, 1983. Regenerate Faults of Small Cenozoic Offset - Probable Earthquake Sources in the Southeastern United States, U.S. Geological Survey, Professional Paper 1313-S, C. Wentworth and M. Mergner-Keefer, 1983.

Wheeler, 1996. Earthquakes and the Southeastern Boundary of the Intact Iapetan margin in Eastern North America, *Seismological Research Letters*, Volume 67, Number 5, p 77-83, R. Wheeler, 1996.

Wheeler, 2005. Known or suggested Quaternary tectonic faulting, central and eastern United States-New and updated assessments for 2005, U.S. Geological Survey Open-File Report 20051336, p 37, R. L. Wheeler, 2005.

Wheeler, 2006. Quaternary tectonic faulting in the Eastern United States, *Engineering Geology*, Volume 82 (2006), p 165-186, R.L. Wheeler, 2006.

Williams, 1987. Groundwater Resources of the Berwick-Bloomsburg-Danville Area, East-Central Pennsylvania, Pennsylvania Bureau of Topographic and Geologic Survey, Water Resources Report 61, J.H. Williams and D.A. Eckhardt, 1987.

Wise, 1998. Lancaster County seismic zone (Penna)- Reactivation of a tectonic structural feature. *Geological Society of America Abstracts with Programs*, Volume 30, Number 7, p A-320, D. U. Wise and T. R. Fail, 1998.

Withjack, 1998. Diachronous Rifting, Drifting, and Inversion on the Passive Margin of Central Eastern North America: An Analog for Other Passive Margins, *AAPG Bulletin*, Volume 82, Number 5A, p 817-835, M.O. Withjack, R.W. Schlische, and P.E. Olsen, 1998.

Withjack, 2005. A Review of Tectonic Events on the Passive Margin of Eastern North America, 25th Annual Bob F. Perkins Research Center: Petroleum Systems of Divergent Continental Margin Basins, Martha Oliver Withjack and Roy W. Schlische, Martha Oliver Withjack, and Paul E. Olsen.

Wolf, 2003. Ferroaxinite from Lime Crest Quarry Sparta, New Jersey, Adam Wolf, John Rakovan, Christopher Cahill, *Rocks and Minerals*, Volume 78, pp. 252-256.

Wood, 1961. Sweet Arrow Fault, East-Central Pennsylvania, *AAPG Bulletin*, Volume 45, Number 2, p 256-263, Gordon H. Wood, Jr. and Thomas M. Kehn, February 1961.

Yang, 1981. Seismotectonics of Northern United States and Adjacent Canada, *Journal of Geophysical Research*, Volume 86, p 4,981-4,998, J. P. Yang and Y. P. Aggarwal, 1981.

Zietz, 1982. Composite magnetic anomaly map of the United States, Part A: Conterminous United States, U.S. Geological Survey Map GP-54923, Scale 1:2,500,000, I. Zietz, 1982.

Zoback, 1991. Stress magnitudes in the crust: constraints from stress orientation and relative magnitude data, *Philosophical Transactions of the Royal Society of London*, p 181-194, Mary Lou Zoback and Marian Magee, 1991.

Zoback, 2002. Steady-State Failure Equilibrium and Deformation of Intraplate Lithosphere, International Geology Review, Volume 44, p 383-401, Mark D. Zoback, John Townend, and Balz Grollimund, 2002.

2.5.2 Vibratory Ground Motion

The U.S. EPR FSAR includes the following COL Item for Section 2.5.2:

A COL applicant that references the U.S. EPR design certification will review and investigate site-specific details of the seismic, geophysical, geological, and geotechnical information to determine the safe shutdown earthquake (SSE) ground motion for the site and compare site-specific ground motion to the Certified Seismic Design Response Spectra (CSDRS) for the U.S. EPR.

This COL Item is addressed as follows:

{This section provides a detailed description of the vibratory ground motion assessment that was carried out for the BBNPP site, supporting the development of the BBNPP site Safe Shutdown Earthquake (SSE) ground motion response spectra. The assessment follows recommendations provided in NRC Regulatory Guide 1.208, "A Performance-Based Approach to Define Site-Specific Earthquake Ground Motion," March 2007, (NRC, 2007a). The assessment includes:

- ◆ Characterization of seismic sources based on geological, geophysical, and seismological investigations
- ◆ Probabilistic seismic hazard analysis (PSHA) based on the characterized seismic sources and a characterization of ground motion
- ◆ Deaggregation of the mean seismic hazard to identify controlling earthquakes
- ◆ Analysis of seismic wave transmission at the BBNPP site based on results of the PSHA and geotechnical investigations
- ◆ Development of performance-based ground motion response spectra to support the development of the Safe Shutdown Earthquake (SSE)

Nuclear Regulatory Commission (NRC) Regulatory Guide 1.208, "A Performance-Based Approach to Define Site-Specific Earthquake Ground Motion," March, 2007, (NRC, 2007a) states in Section B, Discussion:

"The CEUS is considered to be that part of the United States east of the Rocky Mountain front or east of Longitude 105 West (Refs. 13,14). A Probabilistic Seismic Hazard Analysis (PSHA) in the Central Eastern United States (CEUS) must account for credible alternative seismic sources through the use of a decision tree with appropriate weighting factors that are based on the most up-to-date information and relative confidence in alternative characterizations for each seismic source. Seismic sources identified and characterized by Lawrence Livermore National Laboratory (LLNL) (Refs. 13-15) and the Electric Power Research Institute (EPRI) (Ref. 16, 17) were used for CEUS studies in the past. In addition to the LLNL and EPRI resources, the United States Geological Survey maintains a large database of seismic sources for both the CEUS and the WUS. The characterization of specific seismic sources found in these databases may still represent the latest information

available at the time that a PSHA is to be undertaken. However, if more up-to-date information is available, it should be incorporated."

Currently, the most up-to-date information on seismic sources in the CEUS is the seismic source characterization (SSC) documented in EPRI/DOE/NRC (2012). This model was developed explicitly to replace the EPRI model (EPRI, 1986) and the LLNL model (LLNL, 1989) cited in RG 1.208. The EPRI/DOE/NRC (2012) model was developed following a Level 3 process in the context of NUREG/CR-6372 (SSHAC, 1997) and NUREG-2117 (NRC, 2012). Following this process, a Technical Integration (TI) team evaluated available data and models and then integrated the information to develop a model that represents the center, body, and range of technically defensible interpretations. This model forms the basis for the PSHA carried out for the BBNPP site.

The following subsections describe the vibratory ground motion studies that were carried out for the BBNPP site.

1. Based on the EPRI/DOE/NRC (2012) CEUS SSC model and other information, Section 2.5.2.1 through Section 2.5.2.3 summarize the seismicity, geologic and tectonic characteristics of the site and region, and the correlation of earthquakes with seismic sources..
2. Section 2.5.2.4 develops PSHA parameters at the BBNPP site assuming the very hard rock conditions implied by currently accepted ground motion attenuation models.
3. Section 2.5.2.5 presents information about the seismic wave transmission characteristics of the BBNPP site with reference to more detailed discussion of all engineering aspects of the subsurface in Section 2.5.4.
4. Section 2.5.2.6 describes the development of the horizontal and vertical GMRS ground motion for the BBNPP site, which supports development of the SSE.

2.5.2.1 Seismicity

The record of past earthquakes supports identification of expected areas of future seismicity and characterization of its rate and magnitude distribution. Thus, development of an earthquake catalog was a key component of the EPRI/DOE/NRC (2012) CEUS SSC project. This section summarizes the development of the EPRI/DOE/NRC (2012) earthquake catalog and discusses the spatial distribution of earthquakes in the region surrounding the site.

2.5.2.1.1 Regional Earthquake Catalog

As part of the development of the EPRI/DOE/NRC (2012) CEUS SSC model, an updated regional earthquake catalog was developed. Three specific goals were pursued in developing the CEUS SSC earthquake catalog: (1) inclusion of all known earthquakes in the magnitude range important for assessing future earthquake hazard; (2) use of a uniform earthquake size measure (moment magnitude, **M**) that is consistent with the ground motion model to be used in the PSHA; and, (3) verification of the catalog through extensive review by experienced seismologists. The CEUS SSC report (EPRI/DOE/NRC, 2012) provides a detailed description of each major step in the development of the catalog. A short summary is presented here.

The CEUS SSC earthquake catalog is developed in four steps: catalog compilation; assessment of a uniform magnitude for each event; removal of dependent events; and assessment of completeness as a function of location, time, and earthquake magnitude.

Two earthquake catalogs along with their original sources form the primary basis for the updated CEUS SSC earthquake catalog (EPRI/DOE/NRC, 2012): (1) The earthquake catalog used by the USGS for seismic hazard mapping in the U.S. (USGS, 2008); and, (2) The Geological Survey of Canada (GSC) earthquake catalog for seismic hazard analysis (Adams, 2003). The GSC catalog forms an important source of seismicity data for the northern portion of the CEUS SSC study region. Additionally, special studies of individual earthquakes and earthquake sequences were reviewed and used in compiling the CEUS SSC earthquake catalog. Non-tectonic events were identified and removed from the CEUS SSC earthquake catalog (EPRI/DOE/NRC, 2012).

Moment magnitude (**M**) is used as the uniform size measure for earthquakes in the CEUS SSC earthquake catalog (EPRI/DOE/NRC, 2012). To provide an **M** value for each earthquake in the catalog, conversion relations between different earthquake size measures and **M** were developed. Because compiled catalogs by the USGS and GSC contain converted magnitudes for many earthquakes, the original data from which the magnitude was determined (e.g., epicentral intensity [I_0]) was obtained from the source catalogs. This process required extensive review of the compiled and source catalogs, including the details of magnitude determination. The review also included documentation of the process used in each source catalog to calculate magnitude. Even for the same magnitude scale, the details of calculation used in different catalogs can vary (EPRI/DOE/NRC, 2012).

Once the data and process used to determine each magnitude value was determined, **M** was then estimated from the original size data using the developed conversion relations (EPRI/DOE/NRC, 2012). Conversion to **M** based on the original data, which has an associated uncertainty, ensures that additional uncertainty from multiple conversions is avoided and not propagated through the PSHA. **M** estimates take into account uncertainty in the conversion such that they can be used to obtain unbiased estimates of earthquake recurrence as a function of magnitude. The uncertainty is also used in assigning an equivalent count (N^*) for each earthquake. When determining the number of earthquakes in a magnitude interval and time period, the N^* values are summed rather than the number of earthquakes (EPRI/DOE/NRC, 2012).

Dependent earthquakes (i.e., foreshocks and aftershocks) were identified using the EPRI (EPRI, 1988) declustering approach and removed from the catalog used for recurrence calculations (EPRI/DOE/NRC, 2012). This approach uses statistical testing to identify clusters of earthquakes and determine which need to be removed to obtain a catalog of independent earthquakes. The approach assumes that earthquake occurrence is a stationary Poisson process. A comparison of the results using the EPRI (EPRI, 1988) approach to those for the approach of Gardner and Knopoff (Gardner, 1974) showed only small differences (EPRI/DOE/NRC, 2012).

As part of the development of the EPRI/DOE/NRC (2012) CEUS earthquake catalog, completeness of the catalog was assessed as a function of magnitude and geographic area. The completeness analysis used the approach described in EPRI (EPRI, 1988). In this approach, earthquake occurrence is assumed to be a stationary Poisson process. Based on the earthquake catalog, the approach estimates not just the period of completeness, but the probability of detection for period of partial completeness. The advantage of this approach is that data from periods of partial completeness contribute to assessing rates of occurrence. The approach was applied to geographic areas ("completeness regions") with similar histories of population growth and earthquake recording (EPRI/DOE/NRC, 2012).

The final catalog of the CEUS SSC project contains 3,298 earthquakes of estimated moment magnitude $E[M]$ 2.9 and larger (EPRI/DOE/NRC, 2012) (Figure 2.5-173). It covers the entire study region of the CEUS SSC and adjacent areas and includes earthquakes for the time period of 1568 through the end of 2008. Information on earthquakes occurring after 2008 was unavailable at the time the CEUS SSC earthquake catalog was compiled. A qualitative examination of earthquakes occurring since 2008 indicates that they are consistent with the historically and instrumentally recorded earthquakes included in the catalog. One significant earthquake that occurred since 2008--the Mineral, VA earthquake of August 2011--is addressed in more detail in Section 2.5.2.1.2.

2.5.2.1.2 Updated Seismicity Data

Since the EPRI/DOE/NRC (2012) earthquake catalog was developed, one significant earthquake occurred within 300 mi of the BBNPP site: The August 23, 2011 Mineral, VA earthquake with M 5.8. Its focal depth was 6 km and it was caused by reverse faulting on a plane striking N28E and dipping 50° to the east-southeast (Horton and Williams, 2012). The earthquake was felt widely in the east-central and northeastern United States.

The earthquake was located in the Central Virginia Seismic Zone (CVSZ), an area with an elevated rate of seismicity during historical time compared to most of the CEUS. In the EPRI-SOG seismic source characterization (EPRI, 1986), the CVSZ was characterized as a seismic source, either explicitly or implicitly, by the Earth Science Teams. In most cases, the key factor in defining a source zone based on the CVSZ was the persistent low-level seismicity.

Prior to 2011, the largest earthquake documented in the zone was the 1875 Goochland County event that caused intensity of MMI VII and has an $E[M]$ of 4.77 (EPRI/DOE/NRC, 2012). Recorded seismicity also includes an M_w 4.3 earthquake in 2003 (Kim and Chapman, 2005). Seismicity within the CVSZ is shallow (< 11 km) and interpreted to occur on faults above the detachment that separates Precambrian basement from overlying Paleozoic and Mesozoic deposits.

Although the 2011 Mineral, VA earthquake occurred after the EPRI/DOE/NRC (2012) CEUS SSC model was developed and was in the final stages of review, the earthquake is consistent with that model. Within the framework of the EPRI/DOE/NRC (2012) CEUS SSC model the earthquake is located in three source zones representing alternative interpretations of distributed seismicity. Using the CEUS SSC M_{max} seismic zonation approach, the earthquake is located in the Study Region source zone and the Mesozoic-and-Younger Extension Region (MESE) source zone (both narrow and wide interpretations). For the Seismotectonic zonation approach, the earthquake falls in the Extended Continental Crust-Atlantic Margin (ECC-AM) source zone.

For all these source zones, the M of the 2011 Mineral, VA earthquake is less than the entire M_{max} distribution assessed by EPRI/DOE/NRC (2012). For the Study Region source zone, the M_{max} distribution ranges from 6.5 to 8.1 with the largest weight on M 7.2. For the MESE-Wide source zone, the M_{max} distribution ranges from 6.5 to 8.1 with the largest weight on M 7.3. For the MESE-Narrow source zone, the M_{max} distribution ranges from 6.4 to 8.1 with the largest weight on M 7.2. For the ECC-AM source zone, the M_{max} distribution ranges from 6.0 to 8.1 with the largest weight on M 7.2. The magnitude of the Mineral, VA earthquake (M 5.8) is consistent with all these distributions.

Two approaches for assessing the M_{max} distribution were used in EPRI/DOE/NRC (2012): a Bayesian approach and the approach developed by Kijko (Kijko, 2004). For the Bayesian

approach, the maximum observed earthquake in a source zone is used in developing a likelihood function. For the Kijko approach, it is an input parameter. Thus, while the Mineral, VA earthquake is smaller than the existing M_{max} distributions, it potentially could impact the assessment of the M_{max} distribution for each source zone in which it is located. For the Kijko approach the earthquake would also affect the observed seismicity from the catalog that is used to estimate M_{max} .

For the Study Region, MESE-Wide, and MESE-Narrow source zones, the maximum observed earthquake in the existing catalog is in each case larger than the Mineral, VA earthquake. Furthermore, for these source zones, a larger maximum observed earthquake for the Bayesian approach is taken from the paleoearthquake record. Thus there is no impact from the Mineral, VA earthquake on the M_{max} distribution using the Bayesian approach. There is also no impact for the Kijko approach because the Kijko approach is not used when the maximum observed earthquake is a paleoearthquake.

For the ECC-AM source zone, the Mineral, VA earthquake impacts the assessment of M_{max} , but the impact is small. There is uncertainty in the maximum observed earthquake for the ECC-AM source zone. An earthquake in 1755 (M 6.1) is nominally the maximum observed, but there is uncertainty in its location and it may not be located in the ECC-AM source zone. If it is not located in the ECC-AM source zone, then an earthquake in 1638 ($E[M]=5.32$) is the maximum observed. The Mineral, VA earthquake is larger than the 1638 earthquake and would become the maximum observed if the 1755 earthquake is located in a different source zone. For the Bayesian approach, this would shift some weight in the M_{max} distribution to higher magnitudes, but there is only a small amount of weight in the existing assessment for magnitudes less than 5.8 (EPRI/DOE/NRC, 2012, Figure 7.4.2-2). Thus, the impact on the distribution determined using the Bayesian approach is likely to be small.

For the ECC-AM source zone, the Kijko approach receives a weight of only 0.05 in determining the current M_{max} distribution. While addition of the Mineral, VA earthquake would potentially impact that weight, any increase in the weight would tend to shift the overall M_{max} distribution to lower values. Given these observations, the M_{max} distribution for the ECC-AM source zone is not updated to take into account the Mineral, VA earthquake because the impact on hazard would be insignificant.

The Mineral, VA earthquake also potentially affects the seismicity recurrence rates for the source zones in which it is located. For the overall source zone (Study Region, MESE, or ECC-AM), inclusion of one earthquake of M 5.8 is within the uncertainty in rate from the existing EPRI/DOE/NRC (2012) characterization. However, because the recurrence parameters are spatially smoothed, the impact in the vicinity of the earthquake may be more significant. The Mineral, VA earthquake, however, is located about 240 mi (380 km) from the BBNPP site. At this distance, the impact on recurrence rate may produce some effect on the hazard at the site, but any impact would be small and within the uncertainty of mean hazard calculations (EPRI/DOE/NRC, 2012, Chapter 9.4).

The Mineral, VA earthquake is also consistent with the future earthquake characteristics (EPRI/DOE/NRC, 2012) assessed for the Study Region, MESE, and ECC-AM source zones.

In summary, the nature of the Mineral, VA earthquake is adequately characterized by the existing EPRI/DOE/NRC (2012) CEUS SSC model. This is not unexpected because the EPRI/DOE/NRC (2012) model was developed using a Senior Seismic Hazard Analysis Committee (SSHAC) Level 3 process to ensure the model captures the center, body, and range of technically

defensible interpretations. As such, it is expected to provide a stable regional basis for PSHA in the CEUS. While, if the Mineral, VA earthquake were to be incorporated into an update of the EPRI/DOE/NRC (2012) CEUS SSC model, the computed hazard for the BBNPP site might be affected to a minor degree, any impact is expected to be less than the precision of seismic hazard calculations. Thus, the PSHA for the BBNPP site is adequately estimated using the published version of the EPRI/DOE/NRC (2012) CEUS SSC model without any changes based on the Mineral, VA earthquake.

2.5.2.2 Geologic and Tectonic Characteristics of the Site and Region

As described in Section 2.5.1, a comprehensive review of available geological, seismological, and geophysical data has been performed for the BBNPP site region and adjoining areas. Geological, seismological, and geophysical data for the CEUS, including the BBNPP site region, constitute the basis for defining and characterizing the seismic sources in the EPRI/DOE/NRC (2012) SSC model. Seismic source zones that affect the BBNPP site are taken from that model.

This section summarizes the seismotectonic basis for seismic sources developed in EPRI/DOE/NRC (2012) that are relevant to assessing seismic hazard for the BBNPP site. The summary addresses Regulatory Positions 1 and 2 of Regulatory Guide 1.208 (NRC, 2007a), which recommends that investigation be performed of seismic sources within a 200 mi (322 km) radius. The following sections summarize the EPRI/DOE/NRC (2012) seismic sources that lie at least partially within this radius, along with more distant Repeated Large Magnitude Earthquake (RLME) sources that potentially contribute to hazard, especially at lower response oscillator frequencies.

No geological, seismological, or geophysical information was identified (Section 2.5.1) that requires an update to the EPRI/DOE/NRC (2012) model or that indicates a local seismic source exists that is not represented by the EPRI/DOE/NRC (2012) model. As discussed in Section 2.5.1.2.6, excavation mapping is required during construction; deformational zones, if any are noted, will be evaluated and the NRC notified when excavations are open for inspection.

Section 2.5.2.2.1 and Section 2.5.2.2.1 are added as a supplement to the U.S. EPR FSAR.

2.5.2.2.1 Summary of EPRI/DOE/NRC (2012) Seismic Sources that are Relevant to PSHA for the BBNPP Site

The CEUS SSC model contains two general types of seismic sources (EPRI/DOE/NRC, 2012):

1. Distributed seismicity sources, and
2. Repeated Large Magnitude Earthquake (RLME) sources

Distributed seismicity sources are used to represent future seismicity that is broadly distributed in the study region and not related to specific features that rupture repeatedly in large earthquakes. Two approaches are used for characterization of distributed seismicity source zones (EPRI/DOE/NRC, 2012). One approach, termed the Mmax Zones approach, is based on the interpretation that the only discriminating feature for future seismicity is the maximum magnitude that can occur. Some evidence suggests that maximum earthquake size is related to tectonic characteristics that separate the CEUS into two broad regions.

The second approach for defining distributed seismicity sources, termed the Seismotectonic Zones approach, is based on the interpretation that rupture characteristics of future seismicity is related to seismotectonic characteristics that vary regionally in the CEUS. Following this approach, the CEUS is represented by twelve source zones with varying maximum magnitude,

rupture characteristics (i.e., style of faulting, rupture strike and dip), and seismogenic thickness.

RLME sources are the locations of repeated (more than one) large-magnitude ($M \geq 6.5$) earthquakes (EPRI/DOE/NRC, 2012). RLME sources represent the interpretation that at some locations there are features that will generate repeated large earthquakes in the future. In some cases, a fault is inferred and forms the basis for the RLME source. In other cases, a specific feature cannot be identified, but the history of repeated large earthquakes indicates that a feature exists within a localized area. For this case, the RLME source is defined as an area.

Uncertainty in the conceptual approach to characterizing seismic sources for the CEUS is represented by a logic tree (Figure 2.5-174). Seismic sources characterized following the Mmax Zones approach are given 0.4 weight and those characterized following the Seismotectonic Zones approach are given 0.6 weight. The RLME sources represent additional sources of seismic hazard that are added to the hazard from the distributed seismicity sources.

For the Mmax Zones, Seismotectonic Zones, and RLME approaches to defining seismic sources, only those relevant to the assessment of seismic hazard at the BBNPP site are discussed here. Relevant sources are taken as those distributed seismicity sources located entirely or partially within the 200 mi (322 km) region surrounding the BBNPP site, as well as more distant RLME sources that may contribute to the hazard primarily at lower response oscillator frequencies. Some distributed seismicity sources that extend to just outside the 200 mi (322 km) site region are also included. In the calculation of seismic hazard at the BBNPP site, for distributed seismicity source zones that are included and extend beyond the 200 mile (322-km) site region, integration is carried out to a distance of 435 mi (700 km).

2.5.2.2.1.1 Distributed Seismicity Source Zones

This section describes the distributed seismicity source zones from the EPRI/DOE/NRC (2012) CEUS SSC model that are included in the PSHA for the BBNPP site. Both Mmax and Seismotectonic source zones are addressed. The configuration of the zones, recurrence rates, maximum magnitudes, and rupture characteristics are summarized.

2.5.2.2.1.1.1 Mmax Zones Configuration and Basis

EPRI/DOE/NRC (2012) describes alternative configurations for Mmax source zones. In one configuration the entire study region is considered as a single source zone with a single maximum magnitude (M_{max}) distribution. In an alternative configuration, the study region is divided into two source zones with different M_{max} distributions depending on whether an area was subject to Mesozoic-and-Younger Extension (MESE source) or not (NMESE source). Additional configurations depend on alternative interpretations of the extent of the MESE and NMESE sources. Taking into account the alternative interpretations, three configurations of the Mmax Zones are included in the PSHA for the BBNPP site. For each configuration, the RLME sources are also active.

Mmax Configuration M-I

Mmax Configuration M-I treats the entire CEUS study region as a single source zone (Figure 2.5-175). For this interpretation, the M_{max} distribution, rupture characteristics of future earthquakes, and seismogenic thickness of the crust are uniform for the entire study region. Recurrence varies spatially based on the history of past seismicity. This configuration has an overall weight of 0.16, resulting from the weight of 0.4 assigned to the Mmax Zones approach times the weight of 0.4 for the interpretation that the study region has a single M_{max} distribution (EPRI/DOE/NRC, 2012).

For Mmax Configuration M-I, the Study Region source zone hosts the BBNPP site and contains the entire site region. Hazard at the site for this configuration is controlled by the spatially smoothed earthquake recurrence parameters and the M_{\max} distribution.

Mmax Configuration M-II

Mmax Configuration M-II represents the case for which the study region is divided into two source zones depending on whether an area was subject to Mesozoic-and-Younger Extension (MESE) or not (NMESE), and in which a "wide" interpretation of the extent of the Mesozoic-and-Younger Extension is used (EPRI/DOE/NRC, 2012) (Figure 2.5-176). In an analysis of which geologic and tectonic characteristics of stable continental regions correlate with maximum observed magnitude, Mesozoic-and-Younger Extension was the only characteristic that showed a statistically significant correlation, although the correlation was weak. The interpretation that M_{\max} differs depending on whether a region has experienced Mesozoic-and-Younger Extension is given a slightly higher weight (0.6) than the interpretation that a single M_{\max} applies to the entire CEUS study region.

There is uncertainty in the boundary separating regions that were subject to Mesozoic-and-Younger Extension and those that were not. This uncertainty is represented by two alternative interpretations of the boundary location, a "wide" interpretation and a "narrow" interpretation. The narrow interpretation for the MESE source zone includes the portion of the crust for which there is higher confidence of Mesozoic-and-Younger Extension. This interpretation is given a weight of 0.8. The wide interpretation includes in the MESE source zone additional crust that may have experienced Mesozoic-and-Younger Extension, but for which the evidence is weaker. This interpretation is given a weight of 0.2.

From Mmax Configuration M-II, both Source Zones MESE-W and NMESE-W are considered for the PSHA analysis for the BBNPP site. Source Zone NMESE-W is outside the 200 mi (322 km) site region, but extends very close to the site region boundary.

Mmax Configuration M-II has an overall weight of 0.048, resulting from the weight of 0.4 assigned to the Mmax Zones approach, the weight of 0.6 for the interpretation that the study region is separated into the regions of Mesozoic-and-Younger and Non-Mesozoic-and-Younger Extension, and the weight of 0.2 for the wide interpretation of the extent of the Mesozoic extension (EPRI/DOE/NRC, 2012).

For Mmax Configuration M-II, the MESE-W source zone hosts the BBNPP site and contains the site region. Hazard at the site from the MESE-W source zone is controlled by the spatially smoothed earthquake recurrence parameters and the associated M_{\max} distribution.

Mmax Configuration M-III

Mmax Configuration M-III represents the model for which the study region is divided into MESE and NMESE regions, with a "narrow" interpretation of the extent of the Mesozoic-and-Younger Extension (EPRI/DOE/NRC, 2012) (Figure 2.5-177). The BBNPP site is located near the eastern boundary of Source Zone NMESE-N. The 200 mi (322 km) site region includes portions of both the NMESE-N and MESE-N source zones. Therefore, for Mmax Configuration M-III, both these source zones are included in the PSHA for the BBNPP site.

Mmax Configuration M-III has a weight of 0.192, resulting from the weight of 0.4 assigned to Mmax Zones approach, 0.6 assigned to the interpretation that the study region is separated into the regions of Mesozoic-and-Younger and Non-Mesozoic-and-Younger Extension, and 0.8

for the "narrow" interpretation of the extent of the Mesozoic-and-Younger Extension (EPRI/DOE/NRC, 2012).

Hazard at the BBNPP site from the MESE-N and NMESE-N Mmax source zones is controlled by the spatially smoothed earthquake recurrence parameters and the associated maximum magnitude distributions.

2.5.2.2.1.1.2 Seismotectonic Zones

For the seismotectonic approach to source zonation, the following source zones comprise the CEUS SSC model (EPRI/DOE/NRC, 2012):

- ◆ Atlantic Highly Extended Crust (AHEx)
- ◆ Extended Continental Crust-Atlantic Margin (ECC-AM)
- ◆ Extended Continental Crust-Gulf Coast (ECC-GC)
- ◆ Great Meteor Hotspot (GMH)
- ◆ Illinois Basin Extended Basement (IBEB)
- ◆ Gulf Coast Highly Extended Crust (GHEX)
- ◆ Midcontinent-Craton (MidC-A, MidC-B, MidC-C, and MidC-D)
- ◆ Northern Appalachians (NAP)
- ◆ Oklahoma Aulacogen (OKA)
- ◆ Paleozoic Extended Crust (PEZ-N and PEZ-W)
- ◆ Reelfoot Rift (RR and RR-RCG)
- ◆ St. Lawrence Rift, including the Ottawa and Saguenay grabens (SLR)

Uncertainty in the western boundary of the Paleozoic Extended Crust seismotectonic zone (PEZ) is represented by two alternatives (EPRI/DOE/NRC, 2012): the "narrow" interpretation and the "wide" interpretation. Two alternative interpretations are also provided for the Reelfoot Rift zone: in one the Reelfoot Rift includes the Rough Creek Graben (RR-RGG); in the other it does not (RR). The uncertainties in the western boundary of the PEZ zone and whether or not the Rough Creek Graben is included in the Reelfoot Rift zone together result in four alternative seismotectonic source configurations shown in Figure 2.5-178 through Figure 2.5-181. These configurations are referred to herein as Seismotectonic Configurations S-I, S-II, S-III, and S-IV. The alternative zonation configurations produce alternative versions of the Mid-Continent source zone designated MidC-A, MidC-B, MidC-C, and MidC-D. Inclusion of Seismotectonic source zones in the PSHA for the BBNPP site depends on whether the source zones associated with each model extend to within 200 mi (322 km) of the site. Seismotectonic zones whose closest approach to the site is just beyond the 200 mi (322 km) site region are also included.

Seismotectonic Configuration S-I

Seismotectonic Configuration S-I represents the case for which the PEZ source zone is interpreted as being narrow (PEZ-N) and the RCG is not part of the RR source zone, leading to

the configuration shown in Figure 2.5-178. The version of the Mid-Continent source zone associated with this configuration is designated MidC-A. For this configuration, the following source zones are included in the PSHA for the BBNPP site: AHEX, ECC-AM, PEZ-N, NAP, SLR, and MidC-A. The PEZ-N zone hosts the BBNPP site.

Seismotectonic Configuration S-I has a weight of 0.32, resulting from the assessed weights of 0.6 for the Seismotectonic Zones approach, 0.8 for the “Narrow” interpretation of the PEZ source zone, and 0.667 for the interpretation that the RCG is not part of the RR source zone (EPRI/DOE/NRC, 2012).

Seismotectonic Configuration S-II

Seismotectonic Configuration S-II represents the case for which the PEZ source zone is interpreted as being narrow and the RCG is part of the RR source zone, leading to the configuration shown in Figure 2.5-179. The version of the Mid-Continent source zone associated with this configuration is designated MidC-B. For this configuration, the following source zones are included in the PSHA for the BBNPP site: AHEX, ECC-AM, PEZ-N, NAP, SLR, and MidC-B. As for Configuration S-I, the PEZ-N zone also hosts the BBNPP site for this source zone configuration.

Seismotectonic Configuration S-II has a weight of 0.16, resulting from the weights of 0.6 assigned to the Seismotectonic Zones approach, 0.8 for the “narrow” interpretation of the PEZ source zone, and 0.333 for the interpretation that the RCG is part of the RR source zone (EPRI/DOE/NRC, 2012).

Seismotectonic Configuration S-III

Seismotectonic Configuration S-III represents the case for which the PEZ source zone is interpreted as being wide (PEZ-W) and the RCG is not part of the RR source zone, leading to the configuration shown in Figure 2.5-180. The version of the Mid-Continent source zone associated with this configuration is designated MidC-C. For this model, the following source zones are included in the PSHA for the BBNPP site: AHEX, ECC-AM, PEZ-W, NAP, SLR, and MidC-C. The PEZ-W zone hosts the BBNPP site for this configuration.

Model S-III has a weight of 0.08, resulting from the weights of 0.6 for the Seismotectonic Zones approach, 0.2 for the “wide” interpretation of the PEZ source zone, and 0.667 for the interpretation that the RCG is not part of the RR source zone (EPRI/DOE/NRC, 2012).

Seismotectonic Configuration S-IV

Seismotectonic Configuration S-IV represents the case for which the PEZ source zone is interpreted as being wide (PEZ-W) and the RCG is part of the RR source zone, leading to the configuration shown in Figure 2.5-181. The version of the Mid-Continent source zone associated with this configuration is designated MidC-D. For this configuration, the following source zones are included in the PSHA for the BBNPP site: AHEX, ECC-AM, PEZ-W, NAP, SLR, and MidC-D. As for Configuration S-III, the PEZ-W zone hosts the BBNPP site for this configuration.

Model S-IV has a weight of 0.04, resulting from the weights of 0.6 for the Seismotectonic Zones approach, the 0.2 for the “wide” interpretation of the PEZ source zone, and the 0.333 for the interpretation that the RCG is part of the RR source zone (EPRI/DOE/NRC, 2012).

The source zone configurations from the EPRI/DOE/NRC CEUS SSC model that are used in the PSHA for the BBNPP site are summarized in Table 2.5-46 along with their weights.

Brief summaries of the basis for the Seismotectonic source zones included in the BBNPP PSHA are provided below based on EPRI/DOE/NRC (2012):

Atlantic Highly Extended Crust Zone (AHEx)

The AHEx zone is based on the extent of highly extended continental crust that forms a transition between the extended continental crust of the ECC-AM source zone and oceanic crust further offshore (EPRI/DOE/NRC, 2012). The highly extended crust in this zone is thinner than in the ECC-AM source zone, which is interpreted to affect future earthquake characteristics. The highly extended crust also has a more mafic composition resulting from the introduction of significant igneous material during Triassic and Jurassic rifting to create the Atlantic Ocean basin. The East Coast Magnetic Anomaly marks the transition from highly extended crust to oceanic crust and forms the eastern boundary to the AHEx source zone.

The AHEx zone comes to about 200 mi (322 km) from the BBNPP site for all the seismotectonic configurations. No uncertainty is included in the CEUS SSC model for the boundary between the AHEx and ECC-AM model (EPRI/DOE/NRC, 2012). Thus, the position of the AHEx zone relative to the BBNPP site is identical for seismotectonic Configuration S-I through S-IV. Given the low level of seismicity recorded in this source zone (EPRI/DOE/NRC, 2012), which controls the modeled rate of future earthquakes, its contribution to hazard at the site is small.

Extended Continental Crust-Atlantic Margin Zone (ECC-AM)

The ECC-AM zone is based on the extent of extended continental crust associated with the Mesozoic break-up of Pangea to form the Atlantic Ocean basin (EPRI/DOE/NRC, 2012). The terrane is characterized by rift basins and an underlying detachment surface separating Paleozoic and Mesozoic deposits from the Precambrian basement. The extended nature of the crust is the key characteristic defining the zone. It is distinguished from the AHEx zone by a lesser degree of extension and a related thicker crust.

For the Seismotectonic Zones approach to defining distributed seismicity source zones, the ECC-AM zone lies within the BBNPP site region for all configurations. No uncertainty is included in the CEUS SSC model for the zone boundary (EPRI/DOE/NRC, 2012). Thus, the contribution from the source zone to the total hazard is identical for seismotectonic Configurations S-I through S-IV.

Concentrations of seismicity in southeastern Pennsylvania and New Jersey lead to relatively elevated activity levels for these areas in modeling future earthquake occurrence (EPRI/DOE/NRC, 2012). The maximum magnitude distribution for the ECC-AM zone is the same as for the AHEx zone to the east and slightly higher than for the PEZ zone to the west (EPRI/DOE/NRC, 2012). Hazard from the ECC-AM zone is a contributor to total hazard at the site.

Paleozoic Extended Crust Zone (PEZ)

The PEZ zone is based on the extent of Paleozoic rift-related structures (EPRI/DOE/NRC, 2012). A number of investigators postulate that reactivation of such structures is a cause of contemporary seismicity in portions of the CEUS (EPRI/DOE/NRC, 2012). The western extent of Paleozoic extension is uncertain. Thus, two alternative configurations of the zone are defined (EPRI/DOE/NRC, 2012): a narrow interpretation (PEZ-N) and a wide interpretation (PEZ-W) with weights of 0.8 and 0.2, respectively. While some Paleozoic rift-related structures may have been reactivated during Mesozoic rifting, the zone is distinguished from the ECC-AM zone because evidence for such reactivation is equivocal.

For seismotectonic configurations S-I through S-IV, the PEZ zone hosts the BBNPP site. For the narrow interpretation, within the site region seismicity tends to follow the border between the PEZ zone and the ECC-AM zone to the southeast of the site. In the wide interpretation, there is also a concentration of seismicity to the northwest about 200 mi (322 km) from the site. The maximum magnitude distribution of the PEZ zone is slightly less than for the ECC-AM zone (EPRI/DOE/NRC, 2012). Hazard from the PEZ zone is an important contributor to the total hazard at the site.

Saint Lawrence Rift Zone (SLR)

The SLR Zone is defined on the basis of crust that was initially rifted during the opening of the Iapetus Ocean and reactivated during Mesozoic rifting to form the Atlantic Ocean (EPRI/DOE/NRC, 2012). It has been the location of several moderate-to-large earthquakes documented in the historical record.

The southwestern portion of the zone extends within the 200 mi (322 km) BBNPP site region. At its closest approach it is about 150 mi (240 km) from the site. The overall M_{\max} distribution for the SLR Zone is higher than for other distributed seismicity source zones included in the PSHA. Its distance to the site and recurrence rate results in it providing only a minor relative contribution to hazard.

North Appalachian Zone (NAP)

The NAP Zone is made up of terranes that were accreted to the passive margin of Laurentia during the Taconic and Salinic orogenies. These terranes post-date the rifting that formed the Iapetus Ocean (EPRI/DOE/NRC, 2012). This tectonic history results in normal-faulted basement separated from accreted terranes and continental sediments by a decollement surface. The zone was subject to extension during the Mesozoic, but is not characterized by rift basins as developed in the ECC-AM Zone. The crust comprising the Zone is discriminated from the PEZ and SLR Zones by its younger age. No uncertainty in the zone boundary is included in the CEUS SSC model (EPRI/DOE/NRC, 2012).

The NAP Zone at its closest approach does not extend to within 200 mi (322 km) of the BBNPP site, but because it extends close to the boundary of the site region it is included in the PSHA. The M_{\max} distribution for the zone is slightly higher than for the PEZ Zone and about the same as for the ECC-AM Zone. However, as expected from its distance to the site, it is not an important relative contributor to total hazard.

Midcontinent-Craton Zone (MidC)

The MidC zone encompasses the regions of the continental interior that were not involved in the Phanerozoic orogens along continental margins (EPRI/DOE/NRC, 2012). The crust has not been subject to Mesozoic-and-Younger Extension. Because of uncertainty in the configuration of the PEZ zone (narrow or wide) and the Reelfoot Rift zone (includes the Rough Creek Graben or not), there are four configurations of the MidC zone, designated MidC-A, MidC-B, MidC-C, and MidC-D. These configurations correspond to seismotectonic configurations S-I through S-IV, respectively.

The MidC-A and MidC-B zones lie partially within the 200 mi (322 km) site region and are included in the BBNPP site PSHA. The MidC-C and MidC-D zones lie entirely outside of the site region. They are included in the PSHA, however, because, at their closest approach, they are just outside the 200 mi (322 km) site region boundary. The M_{\max} distribution for the MidC Zone is lower than for other zones included in the BBNPP site PSHA.

Contributions from the MidC zones to the total hazard at the site are small because of their distance from the site and their relatively low rates of earthquake recurrence. The small contribution derives from their distance from the site, a rate of activity that is similar or less than that for zones that are closer to the site, and a maximum magnitude distribution that is lower than for other distributed seismicity zones included in the PSHA.

2.5.2.2.1.1.3 Earthquake Recurrence Parameters for Distributed Seismicity Zones

Future earthquakes in the distributed seismicity source zones are modeled using a doubly truncated exponential model with model parameters fit on the basis of past observed seismicity. Recurrence parameters are determined following an interpretation that the location of past seismicity, in a general sense, indicates where future seismicity will occur. A penalized-likelihood approach is used to determine the recurrence parameters (EPRI/DOE/NRC, 2012). Sensitivity analysis shows that the recurrence parameters that are determined depend on the magnitude range used to fit the parameters and this observation is taken into account in representing the uncertainty in recurrence parameters. Key aspects of the EPRI/DOE/NRC (2012) methodology are summarized below.

Magnitude Interval Weighting

In assessment of recurrence parameters, earthquakes with magnitudes as low as $E[M]$ 2.9 are used (EPRI/DOE/NRC, 2012). Because for lower magnitudes the magnitude-recurrence law may deviate from exponential, or the magnitude conversion models or completeness model may be less reliable, lower magnitude bins are assigned lower weights in the estimation of seismicity parameters. In EPRI/DOE/NRC (2012), uncertainty in the magnitude range that should be used for determining recurrence parameters is represented by three alternative cases of magnitude-dependent weights (Table 2.5-47): Case A, Case B and Case E, with weights of 0.3, 0.3 and 0.4, respectively (EPRI/DOE/NRC, 2012).

Spatial Variability of Recurrence Parameters

In EPRI/DOE/NRC (2012), seismicity rates for distributed seismicity source zones are determined allowing both the a -value and the b -value of the doubly truncated exponential model to vary spatially (Table 2.5-48). Recurrence parameter values are determined for a grid of cells using the penalized-likelihood approach. To resolve any steep gradients that may occur in the more active regions, seismicity parameters are estimated for 1/4 degree longitude by 1/4 degree latitude cells or partial cells for all the distributed seismicity sources, except the Mmax sources and the MidC source in the seismotectonic models. For these source zones, a cell size 1/2 degree longitude by 1/2 degree latitude is used (EPRI/DOE/NRC, 2012). Parameter values are based on the observed data for each cell, but large variations between adjacent cells are penalized to mitigate unrealistic changes.

Degree of Smoothing of Seismicity Rates

EPRI/DOE/NRC (2012) use a single approach to select the degree of spatial smoothing used to determine recurrence parameters for each source. For all sources the "Objective" approach is used (Table 2.5-48). The approach is objective in the sense that it determines the optimal degree of smoothing for each source zone based on the data.

Representation of Uncertainty in Earthquake Recurrence Rates

EPRI/DOE/NRC (2012) represents the uncertainty in recurrence parameters by eight alternative spatial distributions developed from the fitted parameter distributions. The eight maps "jointly represent the central tendency and statistical uncertainty in recurrence parameters, including correlations between cells in the same geographic region" (EPRI/DOE/NRC, 2012). A set of

eight equally weighted recurrence parameter maps is determined for each distributed seismicity source zone (Table 2.5-48). The spatially distributed recurrence parameters for the eight realizations are obtained from the electronic files provided with EPRI/DOE/NRC (2012) and are not duplicated in this FSAR.

Two sets of earthquake recurrence parameters are developed for the distributed seismicity zones: (1) recurrence parameters for PSHA calculations that integrate over magnitude starting from a minimum magnitude of **M** 4.0, which would typically be used for PSHA calculations incorporating the Cumulative Absolute Velocity (CAV) filter, and (2) recurrence parameters for integration from a minimum magnitude of **M** 5.0. This latter set of parameters is used in the PSHA for the BBNPP site.

2.5.2.2.1.1.4 Maximum Magnitude for Distributed Seismicity Sources

The EPRI/DOE/NRC (2012) CEUS SSC model provides M_{\max} distributions in terms of **M** for all seismic sources. For distributed seismicity source zones, two approaches are used to evaluate M_{\max} (EPRI/DOE/NRC, 2012). One is a Bayesian approach with a prior distribution based on worldwide observations of the largest earthquakes occurring in stable continental regions believed to be tectonically similar to CEUS. A second approach, developed by Kijko (Kijko, 2004), is based on the seismicity occurring in each zone. The approaches nominally receive equal weight, but the weight for the Kijko approach is adjusted depending on an assessment of confidence in the determined M_{\max} . Because seismicity data in some parts of the CEUS are sparse, the Kijko approach often receives low or no weight. M_{\max} distributions for Mmax and Seismotectonic Zones are given in Table 2.5-49.

2.5.2.2.1.1.5 Seismogenic Crustal Thickness for Distributed Seismicity Sources

Seismogenic crustal thickness is one characteristic used to define distributed seismicity source zones following the Seismotectonic Zones approach. Thickness is evaluated based on the observed distribution of well-located earthquakes (EPRI/DOE/NRC, 2012). Even for well-located earthquakes, however, the focal depth is somewhat uncertain. Thus, uncertainty in seismogenic thickness is represented by a distribution (Table 2.5-50).

2.5.2.2.1.1.6 Rupture Characteristics for Distributed Seismicity Sources

Hazard from distributed seismicity source zones is calculated using virtual ruptures for future earthquakes. That is, the distance metric for use with a ground motion prediction equation is calculated using a virtual rupture plane consistent with the earthquake epicenter. The CEUS SSC model characterizes the aleatory variability for the rupture characteristics of future earthquakes for each seismic source (EPRI/DOE/NRC, 2012). The characterization includes style of faulting; rupture strike and dip may vary for different styles. The rupture characteristics for the Mmax and Seismotectonic Zones considered in the PSHA for the BBNPP site are summarized in Table 2.5-51.

The assessment of rupture characteristics for future earthquakes in EPRI/DOE/NRC (2012) was carried out in anticipation that new ground motion prediction equations that are developed will include such information in their formulation. Note, however, that the EPRI (EPRI, 2004) ground motion model used in the BBNPP site PSHA does not differentiate ground motion for different styles of faulting. Thus, the variability in virtual rupture planes used in the BBNPP site PSHA is based on combining the characterizations in EPRI/DOE/NRC (2012) for different styles of faulting.

In generating the virtual ruptures used in calculating distance for evaluation of ground motion in the PSHA, a rupture size needs to be determined as a function of **M**. For each source zone,

the area A (in km^2) of each modeled earthquake rupture is determined using equation (2.5-1) (EPRI/DOE/NRC, 2012):

$$\log_{10} A = M - 4.366 \quad (2.5-1)$$

The rupture aspect ratio is taken 1:1 until the rupture reaches the maximum rupture width (EPRI/DOE/NRC, 2012). The maximum rupture width is defined by the seismogenic crustal thickness and the dip angle of the rupture plane. For ruptures that exceed the available rupture width using a 1:1 aspect ratio, the width is fixed at the maximum value and length is increased to obtain the area given by equation 2.5-1. This model is also used for RLME sources (EPRI/DOE/NRC, 2012).

The boundaries of all the distributed seismicity sources are considered to be leaky, allowing rupture to extend beyond the source boundary (EPRI/DOE/NRC, 2012) (Table 2.5-51).

2.5.2.2.1.1.7 RLME Sources

For RLME sources, earthquakes in the historical or paleoearthquake record are used to model the frequency and spatial distribution of RLMEs at specific locations.

RLME sources are defined on the basis of features or areas that have experienced repeated (more than one) large-magnitude ($M \geq 6.5$) earthquakes in the historical or paleoearthquake record (EPRI/DOE/NRC, 2012). Because of the rarity of RLMEs relative to the period of historical observation, evidence for these earthquakes comes largely from the paleoearthquake record, especially from paleo-liquefaction data. As illustrated in Figure 2.5-174, the RLME sources are considered to be additional sources superimposed on the distributed seismicity sources on the seismotectonic branch or on the Mmax branch of the master logic tree for the CEUS SSC model (EPRI/DOE/NRC, 2012).

The RLME sources in the CEUS SSC model are (EPRI/DOE/NRC, 2012):

- ◆ Charlevoix
- ◆ Charleston
- ◆ Cheraw Fault
- ◆ Meers Fault
- ◆ Reelfoot Rift - New Madrid Fault System (NMFS)
- ◆ Reelfoot Rift - Eastern Rift Margin Fault (ERM), consisting of a southern segment (ERM-S) and northern segment (ERM-N)
- ◆ Reelfoot Rift - Marianna
- ◆ Reelfoot Rift - Commerce Fault Zone
- ◆ Wabash Valley.

The RLMEs associated with the NMFS are modeled as occurring on three fault sources: (a) the New Madrid South (NMS) fault; (b) the New Madrid North (NMN) fault; and (c) the Reelfoot Thrust (RFT).

Of the RLME sources, the Charlevoix, Charleston, Reelfoot Rift (NMFS, ERM, Commerce Fault Zone, and Marianna), and Wabash Valley are included in the PSHA for the BBNPP site to assess their contribution to hazard. The Cheraw Fault and Meers Fault RLME sources were judged to have combinations of distance from the BBNPP site, RLME magnitude, and recurrence rate that would result in negligible contribution to total hazard at the site. The total hazard results show that only the NMFS RLME sources make a significant contribution to hazard, especially at lower response frequencies. The RLME sources considered in the PSHA for the BBNPP site are shown in Figure 2.5-182.

2.5.2.2.1.1.7.1 Source Geometry and Style of Faulting for RLME Sources

Charlevoix RLME Source

The Charlevoix RLME source is defined on the basis of repeated large magnitude earthquakes in the historical record (EPRI/DOE/NRC, 2012). Although a specific feature has not been associated with past earthquakes, they occurred in an area of lapetan rift-related faults and impact-related structures. Based on the orientations of mapped faults and results from earthquake fault plane solutions, future earthquakes are characterized with a reverse style of faulting on randomly striking planes with dips between 45 and 60 degrees in either direction (EPRI/DOE/NRC, 2012). The boundary of the source is assessed as leaky, with ruptures allowed to extend 50 percent beyond the boundary. Future rupture characteristics are summarized in Table 2.5-52.

The Charlevoix source is located about 500 to 550 mi (800 to 875 km) from the BBNPP site (Figure 2.5-182). Given its distance from the site, the RLME magnitude ranging from 6.75 to 7.5, and the assessed recurrence rate, the source contributes negligibly to the BBNPP site total hazard.

Charleston RLME Source

Three alternative source zone configurations are considered for the Charleston RLME source in the CEUS SSC model (EPRI/DOE/NRC, 2012) (Figure 2.5-182). The configurations and style of faulting for the three cases are specified as follows (Table 2.5-52):

- ◆ **Charleston Local Source Configuration:** The "local" configuration includes the 1886 meizoseismal area, the majority of the 1886 liquefaction features, and numerous postulated faults. Future ruptures are oriented northeast, parallel to the long axis of the zone. Ruptures are modeled as occurring on vertical strike-slip faults. All boundaries of the Charleston Local source are strict, such that ruptures are not allowed to extend beyond the zone boundaries.
- ◆ **Charleston Narrow Source Configuration:** The "narrow" configuration contains postulated north-northeast-striking structures, including the postulated Woodstock fault and the southern segment of the postulated East Coast Fault System. Future ruptures are oriented north-northeast, parallel to the long axis of the zone. Ruptures are modeled as occurring on vertical strike-slip faults. The northeast and southwest boundaries of the Charleston "narrow" source are leaky, whereas the northwest and southeast boundaries are strict.
- ◆ **Charleston Regional Source Configuration:** The "regional" configuration envelops most of coastal South Carolina, including the majority of pre-1886 paleo-liquefaction features and postulated faults. It extends offshore to include the Helena Banks fault zone. Future rupture orientations are represented by two alternatives: (1) future ruptures oriented parallel to the long axis of the source (northeast) with 0.8 weight,

and (2) future ruptures oriented parallel to the short axis of the source (northwest) with 0.2 weight. In both cases, future ruptures are modeled as occurring on vertical strike-slip faults. All boundaries of the Charleston "regional" source are strict.

The Charleston RLME source lies between about 500 and 700 mi (800 and 1,100 km) from the BBNPP site, depending on which alternative configuration is considered (Figure 2.5-182). The "Local" configuration is given the largest probability (0.5) of representing the Charleston source; the "Regional" configuration, which extends closest to the BBNPP site, is given the lowest probability (0.2). The distance of the source from the site and the combination of the RLME magnitude distribution and the rate of recurrence for the RLME earthquake, result in the source making only a small contribution to total hazard at lower oscillator response frequencies (Section 2.5.2.4.5).

New Madrid Fault System RLME Source

The New Madrid region is the source of the 1811-1812 New Madrid earthquake sequence (EPRI/DOE/NRC, 2012). The earthquake sequence included the three largest earthquakes to have occurred in historical time in the CEUS. The region has also experienced multiple sequences of paleoearthquakes.

The NMFS RLME source consists of three faults (EPRI/DOE/NRC, 2012). Each fault has two alternative geometries (Table 2.5-52). For the NMS fault, the two alternative geometries are the Blytheville Arch-Bootheel Lineament (BA-BL) and the Blytheville Arch-Blytheville fault zone (BA-BFZ) (Figure 2.5-182). Alternative geometries for the NMN fault are New Madrid North (short) (NMN-S) and New Madrid North plus extension (long) (NMN-L) (Figure 2.5-182). For the RFT fault, alternative geometries are Reelfoot thrust (short) (RFT-S) and Reelfoot thrust plus extensions (long) (RFT-L) (Figure 2.5-182). Future NMFS earthquakes are modeled to occur on these faults.

The style of faulting for each of the faults (Table 2.5-52) is based on geologic and seismologic observations (EPRI/DOE/NRC, 2012). The NMS fault is modeled as a vertical right-lateral strike-slip fault. The RFT fault is modeled as a reverse fault dipping an average of 40 degrees southwest. The NMN fault is modeled as a vertical right-lateral strike-slip fault.

The NMFS RLME source lies about 725 to 850 mi (1,150 to 1,350 km) from the BBNPP site (Faults NMN-S, NMN-L, RFT-S, RFT-L, BA-BL, and BA-BFZ on the insert in Figure 2.5-182). Because of its great distance, alternative configurations have negligible impact on total hazard at the site. While very distant from the site, the RLME magnitude distribution and recurrence rate result in a significant total hazard, primarily for lower oscillator response frequencies (Section 2.5.2.4.5).

Eastern Rift Margin RLME Source

The ERM RLME source consists of a northern (ERM-N) and southern (ERM-S) component (EPRI/DOE/NRC, 2012). There are two alternative geometries for the ERM-S RLME source (EPRI/DOE/NRC, 2012): Eastern Rift Margin South/Crittenden County (ERM-SCC) and the Eastern Rift Margin South/River Picks (ERM-SRP). These are shown on Figure 2.5-182 and listed in Table 2.5-52. A single geometry is specified for the ERM-N RLME source (Figure 2.5-182).

Future ruptures are modeled as vertical strike-slip ruptures aligned parallel with the long axis to the RLME source zones (EPRI/DOE/NRC, 2012). Both the northeastern and southwestern ends of the zones are modeled as leaky to allow for uncertainty in the extent of possible reactivated faults along the rift margin.

The ERM RLME source lies about 750 to 875 mi (1,200 to 1,400 km) from the BBNPP site (Figure 2.5-182). Because of its great distance from the site, the alternative configurations produce essentially the same contribution to total hazard at the site. Although included in the PSHA, its RLME magnitude distribution and recurrence rate result in it contributing negligibly to total hazard (Section 2.5.2.4.5).

Marianna RLME Source

The Marianna RLME source is based primarily on paleoliquefaction evidence (EPRI/DOE/NRC, 2012). It is defined as an area source with a single geometry (Figure 2.5-182). Two equally weighted alternatives for future rupture characteristics are modeled: either vertical strike-slip rupture oriented northeasterly, parallel to the sides of the Marianna zone or vertical strike-slip rupture oriented northwesterly parallel to the sides of Marianna zone. All boundaries of the Marianna zone are modeled as leaky (Table 2.5-52).

The Marianna RLME source lies about 900 mi (1,450 km) from the BBNPP site. Although included in the PSHA, its RLME magnitude distribution and recurrence rate result in it contributing negligibly to total hazard at the site.

Commerce Fault Zone RLME Source

The Commerce Fault Zone RLME Source is defined on the basis of geophysical and geological evidence supporting movement during the Quaternary. A single geometry is used (EPRI/DOE/NRC, 2012) (Figure 2.5-182). The Commerce RLME source is characterized as a zone of vertical strike-slip faulting. Ruptures are oriented N47E, subparallel to the Commerce zone boundary. The northeast and southwest boundaries of the zone are modeled as leaky boundaries (Table 2.5-52).

The Commerce Fault Zone RLME source lies about 750 to 800 mi (1,200 to 1,275 km) from the BBNPP site. Although included in the PSHA, its RLME magnitude distribution and recurrence rate result in it contributing negligibly to total hazard at the site.

Wabash Valley RLME Source

The Wabash Valley RLME source is based on paleoliquefaction evidence of repeated large magnitude earthquakes. The source is represented by an area zone with a single geometry (EPRI/DOE/NRC, 2012) (Figure 2.5-182). The boundaries of the Wabash source are modeled as leaky (Table 2.5-52). Future earthquake ruptures are characterized with a random strike (uniform 0 to 360 degree azimuth). The earthquakes are considered to have vertical strike-slip (weight of 2/3) or reverse (weight of 1/3) mechanisms with random dip angles in the range of 40 to 60 degrees.

The Wabash Valley RLME source lies about 600 to 700 mi (975 to 1,125 km) from the BBNPP site. Although included in the PSHA, its RLME magnitude distribution and recurrence rate result in it contributing negligibly to total hazard at the site.

As in the case for distributed seismicity zones (section 2.5.2.2.1.1.6), the rupture area for earthquakes originating from each RLME source is determined using Equation 2.5-1 (EPRI/DOE/NRC, 2012). The rupture aspect ratio is 1:1 until the rupture reaches the maximum rupture width, which is defined by the seismogenic crustal thickness (Table 2.5-50) and the dip angle of the rupture plane. For larger ruptures the width is fixed at the maximum value and length is increased to obtain the area given by Equation 2.5-1.

2.5.2.2.1.1.7.2 Temporal Clustering and Tectonic Features for RLME Sources

Some studies of large earthquakes within stable continental regions (SCRs), including the CEUS, have concluded that large earthquakes occur in "clusters" that are separated from other clusters by long periods of quiescence. In the CEUS SSC model (EPRI/DOE/NRC, 2012), available data for RLMEs were evaluated to assess whether, (1) temporally clustered behavior has been observed, and (2) if this behavior is observed, whether the source is currently within or outside a temporal cluster. In both cases temporal behavior is modeled as a Poisson process.

In addition, available data were evaluated to assess the applicability of the renewal recurrence model to RLME sources (EPRI/DOE/NRC, 2012). Results of the assessments indicate that a renewal model can be applied to the Charleston and New Madrid RLME sources. Available data for other RLME sources were insufficient to allow application of renewal models with confidence (EPRI/DOE/NRC, 2012).

Charlevoix RLME Source

Sufficient data are not available to assess temporal clustering of earthquakes for the Charlevoix RLME source. Spatially, earthquakes are modeled as occurring uniformly throughout the zone (EPRI/DOE/NRC, 2012) (Table 2.5-53).

Charleston RLME Source

The Charleston RLME source is modeled as "in" a temporal cluster with a weight of 0.9 and "out" of a temporal cluster with a weight of 0.1 (EPRI/DOE/NRC, 2012) (Table 2.5-53). For the "out" branch, the Charleston RLME source is not included in the determination of total seismic hazard; rather the area covered by the zone defaults to the background distributed seismicity zone.

With respect to the existence of localizing features for future earthquakes from the Charleston RLME source, the approach is to model future ruptures as occurring randomly within the source (Table 2.5-53).

New Madrid Fault System RLME Source

For the NMFS RLME source, the issue of temporal clustering is modeled by three alternatives (EPRI/DOE/NRC, 2012) (Table 2.5-53):

- ◆ In-cluster (weight of 0.9)
- ◆ Out-of-cluster, with no earthquake activity occurring from the source (weight of 0.05)
- ◆ Out-of-cluster with a long-term rate assigned only to the RFT (weight of 0.05)

With respect to localizing features, earthquakes associated with the NMFS are modeled as occurring on the three faults comprising the source: (1) the NMS fault, (2) the NMN fault, and the RFT fault (EPRI/DOE/NRC, 2012) (Table 2.5-53).

Eastern Rift Margin Fault RLME Source

Sufficient data are not available to assess temporal clustering of earthquakes for the ERM-S and ERM-N RLME sources. Earthquakes from each of these sources are spatially modeled as occurring uniformly throughout the zone (EPRI/DOE/NRC, 2012) (Table 2.5-53).

Marianna Zone RLME Source

For the Marianna Zone RLME source, the alternative that the source is currently in-cluster is assessed a weight of 0.5. The alternative that the source is out-of-cluster is given a weight of 0.5 (EPRI/DOE/NRC, 2012) (Table 2.5-53). On the "out" branch, the Marianna RLME source is not included in calculation of total seismic hazard. Spatially, RLMEs are modeled as occurring randomly in the Marianna Zone (Table 2.5-53).

Commerce Fault RLME Source

Sufficient data are not available to assess temporal clustering of earthquakes for the Commerce Fault RLME source. Spatially, earthquakes are modeled as occurring uniformly throughout the zone (EPRI/DOE/NRC, 2012) (Table 2.5-53).

Wabash Valley RLME Source

Sufficient data are not available to assess temporal clustering of earthquakes for the Wabash Valley RLME source. Spatially, earthquakes are modeled as occurring uniformly throughout the zone (EPRI/DOE/NRC, 2012) (Table 2.5-53).

2.5.2.2.1.1.7.3 RLME Recurrence Models

The recurrence interval for RLME sources is determined based on the available data. Two approaches are considered. In one approach ("Earthquake Recurrence Intervals") recurrence intervals are determined from the ages of past earthquakes. In the other approach ("Earthquake Count in a Time Interval"), the number of earthquakes that occurred in a time period forms the basis for the estimate. For most RLME sources a Poisson model is employed for recurrence. However, for some RLME sources sufficient data exist to support consideration of a renewal model. The approaches and models used for estimating recurrence rate for each RLME source included in the PSHA for the BBNPP site are summarized below.

Charlevoix RLME Source

Both the "Earthquake Recurrence Intervals" and "Earthquake Count in a Time Interval" approaches are used to characterize the recurrence of the Charlevoix RLME (EPRI/DOE/NRC, 2012). The first approach uses one open and one closed interval based on the historical record. The second approach employs two alternative interpretations of the geologic record. The Earthquake Recurrence Intervals approach is assessed a weight of 0.2. The Earthquake Count in a Time Interval approach is given a weight of 0.8. For the latter approach, the two data sets are weighted 0.75 for the shorter time period and 0.25 for the longer time period (Table 2.5-54). The Poisson model is used for recurrence.

Charleston RLME Source

The recurrence data for the Charleston RLME source consists of ages of past RLMEs estimated from the paleo-liquifaction record (EPRI/DOE/NRC, 2012). Therefore, recurrence for the Charleston RLME source is based solely on the "Earthquake Recurrence Intervals" approach (Table 2.5-55). Two alternatives are considered for the length and completeness of the paleo-liquefaction record: the approximately 2,000-year record of Charleston earthquakes with 0.8 weight and the approximately 5,500-year record with weight of 0.2 (EPRI/DOE/NRC, 2012).

Another node of the Charleston logic tree addresses the uncertainty in number of RLMEs that have occurred in the Charleston RLME source (EPRI/DOE/NRC, 2012). For the 2,000-year record, a single model is used. For the 5,500-year, four alternatives are used (Table 2.5-55).

For the regional and local source zones of the Charleston RLME source, only the Poisson model is used as a recurrence model. For the more "fault-like" narrow configuration, the Poisson model is assigned 0.90 weight and the Brownian Passage Time (BPT) renewal model is assigned 0.1 weight (EPRI/DOE/NRC, 2012). Use of the BPT renewal model requires specification of the coefficient of variation of the repeat time, parameter α , for RLMEs. The uncertainty distribution for α is also reported (EPRI/DOE/NRC, 2012) (Table 2.5-55). The coefficient of variation is not applicable to the Poisson model. In total there are 24 uncertainty distributions for the annual frequency of RLMEs from the Charleston source.

New Madrid Fault System RLME Source

For the NMFS RLME source, the "Earthquake Recurrence Intervals" approach is used with weight 1.0 (EPRI/DOE/NRC, 2012) (Table 2.5-56). In-cluster recurrence rates are based on the 1811-1812, 1450 AD, and 900 AD sequences. Out-of cluster recurrence rates for the NMFS are based on timing between clusters (EPRI/DOE/NRC, 2012).

In terms of recurrence model, the Poissonian and renewal recurrence models are assigned weights of 0.75 and 0.25, respectively, for the in-cluster case (EPRI/DOE/NRC, 2012). Distribution of parameter α for the renewal model is given in Table 2.5-56.

ERM Fault RLME Source

The "Earthquake Count in a Time Interval" approach is used to assess RLME recurrence frequency for both the ERM-S and ERM-N sources (EPRI/DOE/NRC, 2012) (Table 2.5-57 and Table 2.5-58). For the ERM-S source, three alternative data sets are used to assess RLME recurrence rates (EPRI/DOE/NRC, 2012): two, three, or four earthquakes in a 17.7 to 21.7 k.y. period. The three alternatives have equal weight. For the ERM-N source, two alternative data sets are used (EPRI/DOE/NRC, 2012): one (weight 0.9) or two (weight 0.1) earthquakes in a 12 to 35 k.y. period. The Poisson model is used as the default earthquake recurrence model with weight 1.0 for both the ERM-S and ERM-N sources (EPRI/DOE/NRC, 2012).

Marianna Zone RLME Source

For the Marianna Zone RLME source, the "Earthquake Recurrence Intervals" approach is used with a weight of 1.0 (EPRI/DOE/NRC, 2012) (Table 2.5-59). The two equally weighted data sets consist of either three or four earthquakes with the oldest occurring approximately 9.9 ka. The Poisson model is used as the default earthquake recurrence model with weight 1.0 for the Marianna Zone RLME source (EPRI/DOE/NRC, 2012).

Commerce Fault RLME Source

For the Commerce Fault RLME source, the "Earthquake Recurrence Intervals" approach is used with weight 1.0 (EPRI/DOE/NRC, 2012) (Table 2.5-60). The preferred interpretation (weight 0.75) is that two earthquakes have occurred in the past 23 k.y. with the alternative possibility that the count is three earthquakes. The Poisson model is used as the earthquake recurrence model with weight 1.0 for the Commerce Fault RLME source (EPRI/DOE/NRC, 2012).

Wabash Valley RLME Source

For the Wabash Valley RLME source, the "Earthquake Recurrence Intervals" approach is used with weight 1.0 (EPRI/DOE/NRC, 2012) (Table 2.5-61). The available data for characterizing the recurrence rate of Wabash Valley RLMEs are the estimated ages for the Vincennes-Bridgeport and Skelton paleoearthquakes. The Poisson model is used as the earthquake recurrence model with weight 1.0 for the Wabash Valley RLME source (EPRI/DOE/NRC, 2012).

2.5.2.2.1.1.7.4 RLME Magnitudes

The RLME sources model the repeated occurrence of large earthquakes of similar size. The magnitude of the RLME is estimated from available sources of information— typically geological data or historical data on past earthquakes—and its uncertainty is expressed by a probability distribution (EPRI/DOE/NRC, 2012). EPRI/DOE/NRC (2012) describes the technical basis for the RLME magnitude distribution for each RLME source. The distributions of RLME magnitudes are given in Table 2.5-62.

2.5.2.2.1.1.7.5 RLME Rupture Characteristics

Alternative geometries and rupture characteristics of the RLME sources are discussed in Section 2.5.2.2.1.2.1. The relevant information is summarized in Table 2.5-52.

2.5.2.2.1.1.7.6 Seismogenic Crustal Thickness for RLME Sources

In developing the CEUS SSC model (EPRI/DOE/NRC, 2012), crustal thickness, including its uncertainty, was characterized for each seismic source based on the available data. The uncertainty distributions for seismogenic crustal thickness for RLME sources are reported in Table 2.5-50.

2.5.2.3 Correlation of Earthquake Activity with Seismic Sources

The Technical Integration (TI) team that developed the EPRI/DOE/NRC (2012) CEUS SSC model considered the correlation of earthquake activity with seismic sources. In the M_{max} Zones approach to SSC, seismicity does not play a role in defining the source zones. For this approach source zones are based on differences in the assessed M_{max} distribution related to whether a region experienced Mesozoic-and-Younger Extension. In the Seismotectonic Zones approach, differences in seismicity play a role in defining source zones based on tectonic properties. Seismotectonic source zones exhibit differences in rate of seismicity, style of faulting, rupture characteristics, and seismogenic crustal thickness based on the observed seismicity.

The CEUS SSC TI team concluded that available data support an interpretation that future activity will occur spatially and temporally following patterns consistent with the paleoseismic, historical, and instrumental record of past earthquakes (EPRI/DOE/NRC, 2012). A penalized-likelihood approach was used to smooth the recurrence parameters based on the observed seismicity.

Seismicity within the 200 mi (322 km) BBNPP site region (Figure 2.5-183) is closest to the site to the southeast. This seismicity is part of a northeasterly-southwesterly trending band that follows the Atlantic coast, extending inland as far as southeastern Pennsylvania. This seismicity is associated with the MESE M_{max} source zone and the ECC-AM and PEZ Seismotectonic source zones (e.g., Figure 2.5-176 and Figure 2.5-178). Farther from the site, seismicity is located within the site region to the northwest in western New York and southern Ontario and to the northeast in central and northern New York.

Within 50 mi (80 km) of the BBNPP site, only five small earthquakes have been recorded (Figure 2.5-184). These earthquakes are all less than **M** 4. Note that the event located about 20 km south of the site is classified by Faill (Faill, 2004) as a quarry blast or mine collapse. None of these earthquakes are related to a capable tectonic source.

2.5.2.4 Probabilistic Seismic Hazard Analysis and Controlling Earthquake

Following Regulatory Guide 1.208 (NRC, 2007a) and 10 CFR 100.23 (CFR, 2007), a PSHA was conducted to support determination of the GMRS and SSE and to account for uncertainties in the seismological and geological evaluations for the BBNPP site.

Section 2.5.2.4.1 through Section 2.5.2.4.5 are added as a supplement to the U.S. EPR FSAR.

2.5.2.4.1 Probabilistic Seismic Hazard Analysis

The seismic hazard for the BBNPP was calculated using seismic source zones from the EPRI/DOE/NRC (2012) CEUS SSC model and with the EPRI ground motion model (EPRI, 2004) and aleatory variability model (EPRI 2006a). This calculation was first made for hard rock conditions, and those results were then modified to account for local site conditions.

The analysis of seismic hazard consists of calculating annual frequencies of exceeding different amplitudes of ground motion, for all combinations of seismic sources, seismicity parameters, maximum magnitudes, ground motion equations, and ground motion aleatory uncertainties. This calculation is made for appropriate combinations of the EPRI/DOE/NRC (EPRI/DOE/NRC, 2012) distributed seismicity and RLME sources, and results in a family of seismic hazard curves. The alternative interpretations of seismic sources, seismicity parameters, maximum magnitudes, and ground motion equations making up each branch of the logic tree are weighted, resulting in a combined weight associated with each hazard curve. From the family of hazard curves and their weights, the mean hazard and the factiles of the hazard distribution are calculated.

The quantification of the Probabilistic Seismic Hazard at hard rock utilized Rizzo's in-house software, RIZZO-HAZARD. This code uses the characterization of seismic sources and ground motion models to estimate the annual exceedance probabilities for various levels of spectral accelerations at different spectral frequencies.

The technical methodology generally follows the formulation by Cornell (Cornell, 1968) (Cornell, 1971) and integrates the product of the conditional probability that a ground motion measure will be exceeded given the earthquake magnitude and distance, and the probability distribution of magnitude and distance over all sources that can significantly contribute to the site seismic ground motion. This is expressed as:

$$v(z) = \sum \alpha_n(m_o) \int f(m) \left[\int f(r|m) P(Z > z | m, r) dr \right] dm$$

in which:

Z is ground motion level (e.g., peak ground acceleration or pseudo-spectral acceleration at prescribed natural frequencies),

$P(Z > z | m, r)$ is the conditional probability that Z will exceed a value z, given an earthquake of magnitude, m, and distance, r,

$f(m)$ and $f(r)$ are the probability density functions for magnitude and distance, and

$\alpha_n(m_0)$ is the number of earthquakes per year above a prescribed minimum magnitude m_0 , in the n -th seismic source.

The integration over magnitude is performed from m_0 to an upper bound magnitude m^u , and the integration over distance is performed usually over a prescribed radius from the site, typically larger than 200 mi (322 km). The probability density function for distance typically assumes that earthquakes occur randomly over the source areas or faults. The functions $f(m)$ and $\alpha(m_0)$ define the recurrence relationships for the respective source zones.

The PSHA incorporates uncertainties and random variability interpreted to characterize inputs to the hazard calculation. Epistemic uncertainty in seismic sources and ground motion models is described through the use of a logic tree formalism. Alternative interpretations are defined to represent the range of uncertainty consistent with the available data. Then weights are assigned to the alternatives reflecting the degree that they are supported by data. For the EPRI/DOE/NRC (2012) CEUS SSC model, interpretations by the TI team are incorporated in the seismic source model for the BBNPP site, and the weights that the team assessed are used. Similarly, weights assigned to alternative ground motion models in EPRI (EPRI, 2004) are used. Aleatory variability in input parameters is represented by probability distributions within the PSHA integral. Thus, uncertainties and variabilities are appropriately taken into account as required by 10 CFR 100.23.

2.5.2.4.2 Seismic Source Characterization Model

Seismic sources included in the PSHA for the BBNPP site are taken from the EPRI/DOE/NRC (2012) CEUS SSC model and are described in Section 2.5.2.2. Distributed seismicity sources that extend within 200 mi (322 km) of the site are included. Some distributed seismicity source zones that extend near to, but not within the site region, are also included. In addition, RLME sources, which represent locations that have generated repeated M 6.5 or greater earthquakes, are included depending on whether an assessment of their magnitude, recurrence rate, and distance indicate they have an ability to contribute to seismic hazard at the site.

2.5.2.4.3 Ground Motion Characterization Model

Ground motion prediction equations (GMPEs) (also referred to as attenuation relations) relate the characteristics of the earthquake source and propagation path to the ground motion at a site. Predicted ground motions are typically quantified in terms of a median value as a function of magnitude, distance, site condition, and other factors, and a probability density function representing variability.

The estimation of strong ground motion for specified magnitude, distance, and site conditions in the CEUS is difficult due to the paucity of strong motion data. Most of the available data correspond to $M < 5.8$ and distances exceeding about 31 mi (50 km). Considerable effort has been directed to developing appropriate GMPEs for the CEUS conditions. In general, the GMPEs utilize standard forms to regress on recorded data in the region, augmented by data from other similar tectonic regimes and stochastic time histories tied to source types and styles of faulting.

For the BBNPP site PSHA, the ground motion model of EPRI (EPRI, 2004) (EPRI, 2006a) is used. In 2004, EPRI (EPRI, 2004) completed a study on strong ground motion prediction in the CEUS following the SSHAC (SSHAC, 1997) guidelines for a Level 3 Analysis. A panel of six ground motion experts was convened during several workshops to provide advice to a Technical Integration (TI) team on the adequacy of available CEUS ground motion relationships. On this

basis, the TI developed a representation of the current scientific understanding on the subject, consisting of "clusters" of ground motion relationships with associated weights to represent the uncertainty in predicting the median ground motion, in terms of moment magnitude (M). Each cluster corresponds to relationships based on a similar approach for ground motion modeling. The uncertainty in the median model for each ground motion cluster is defined by two additional models: one representing the 5th percentile of the median uncertainty distribution and the other corresponding to the 95th percentile.

Epistemic uncertainty is modeled using multiple ground motion equations and multiple estimates of aleatory uncertainty (σ), all with associated weights. Different sets of equations are recommended for sources that represent rifted versus non-rifted parts of the earth's crust. Equations are available for spectral frequencies of 100 Hz (equivalent to peak ground acceleration (PGA)), 25 Hz, 10 Hz, 5 Hz, 2.5 Hz, 1 Hz, and 0.5 Hz, and these equations apply to hard rock conditions, i.e., rock with a shear wave velocity of 9,200 ft/sec (2,800 m/sec).

EPRI published an updated assessment of aleatory variability in 2006 (EPRI, 2006b). This update reflects the observation that sources of aleatory variability in the original EPRI study (EPRI, 2004) were probably too large, resulting in over-estimates of seismic hazard. The 2006 EPRI study (EPRI, 2006b) recommends a revised model of aleatory variability (σ s) with weights that can be used to replace the original aleatory variabilities published in the 2004 EPRI study (EPRI, 2004).

The EPRI (EPRI, 2004) GMPEs are adopted for median ground motion estimates, and the EPRI log-sigma model (EPRI, 2006b) is used to incorporate aleatory variability. Within this context, Figure 2.5-45 shows the logic tree for general area sources and Figure 2.5-44 shows the logic tree for non-general sources. The GMPEs for general area sources are used for the EPRI/DOE/NRC (2012) distributed seismicity source zones and the GMPEs for non-general sources are used for the RLME sources. Adopting the EPRI (EPRI, 2004) ground motion model implies that the seismic hazard is calculated for a hard rock condition characterized by a V_{530} of 9,200 ft/sec (2,800 m/sec).

The EPRI 2004 model (EPRI, 2004) defines four clusters of median ground motion models to represent alternative modeling approaches. Three clusters are used in the ground motion model for general area sources and all four clusters are used for the ground motion model for non-general sources (RLME sources). The rift option was selected for the fourth cluster, instead of the non-rift option that is used for area sources. The three branches of the second level (Ground motion model) of the logic tree on Figure 2.5-44 and Figure 2.5-45 represent the epistemic uncertainty in the median GMPE for each cluster. The branches incorporate a three-point discrete distribution with weights of 0.63, 0.185 and 0.185 for the median, the 5th, and the 95th percentiles, respectively. The third branching level (Aleatory model 1) addresses the uncertainty in the model for the aleatory variability in ground motions about the median attenuation relationship. Models 1A and 1B, as well as their weights, are those proposed by Abrahamson (EPRI, 2006a) (EPRI, 2006b) to account for inter-event and intra-event variability. The EPRI (EPRI, 2004) GMPE relationships use either the closest distance to the rupture plane or closest distance to the surface projection of the rupture plane (Joyner-Boore distance). For implementation using point sources, the EPRI (EPRI, 2004) document presents adjustments. In the current PSHA these adjustments are not used; variability in the rupture characteristics of future earthquakes is incorporated directly in the calculation of the distance metric for the ground motion model. The characteristics specified by the EPRI/DOE/NRC (2012) CEUS SSC model for each source are used.

In assessing aleatory variability in ground motion, EPRI TR-1014381 (EPRI, 2006b) was used in lieu of the Regulatory Guide 1.208 cited document, i.e. EPRI Report 1013105 (EPRI, 2006c). EPRI Report 1013105 (EPRI, 2006c) was an Update Report while EPRI TR-1014381 (EPRI, 2006b) is the final report. For the purposes of revised estimates of aleatory variability in the CEUS, there is no technical difference between the documents. The "Recommended CEUS Sigma" values and "Conclusions" of both reports are identical.

2.5.2.4.4 Deaggregation of Probabilistic Seismic Hazard Analysis Results and Identification of Controlling Earthquakes

Figure 2.5-37 through Figure 2.5-43 and Table 2.5-6 through Table 2.5-12 present the hazard curves resulting from the BBNPP PSHA. The hazard curves show ground motion exceedance for seven response spectral frequencies (100 Hz (equivalent to PGA), 25 Hz, 10 Hz, 5.0 Hz, 2.5 Hz, 1.0 Hz, and 0.5 Hz). The mean and fractile (5%, 16%, 50% (median), 84% and 95%) hazard curves are indicated.

Figure 2.5-15 shows mean uniform hazard spectra for 10^{-4} , 10^{-5} , and 10^{-6} annual probabilities of exceedance from these calculations at seven structural frequencies. Numerical values of these spectra are documented in Table 2.5-4.

The mean rock hazard has been de-aggregated for 10^{-4} , 10^{-5} and 10^{-6} mean annual probabilities of exceedance. The magnitude and distance bins for the de-aggregation table were taken from Regulatory Guide 1.208 (NRC, 2007a). The results are plotted in Figure 2.5-16 through Figure 2.5-19, Figure 2.5-49 and Figure 2.5-50, for the 10^{-4} , 10^{-5} , and 10^{-6} annual probabilities of exceedance, respectively. At each annual probability of exceedance, deaggregation results are shown for a low response spectral frequency range (average of 1 and 2.5 Hz), and a high frequency range (average of 5 and 10 Hz). These figures depict the percent contribution of each magnitude-distance bin to the total hazard.

The deaggregation of the PSHA results was used to identify controlling reference and deaggregation earthquakes for the BBNPP site (Table 2.5-1). Each controlling earthquake is defined by a magnitude and distance. The controlling deaggregation earthquakes also have an associated weight based on the percent contribution to hazard they represent. Controlling earthquakes are determined for both the low response spectral frequency range and the high range for 10^{-4} and 10^{-5} mean annual probabilities of exceedance. The controlling reference earthquakes (REF) are defined by the mean magnitude and distance from the deaggregation. Because there is a significant contribution to hazard at low response spectral frequencies from distant earthquakes, the mean magnitude and distance for the low frequency controlling reference earthquake is determined from deaggregation results for distances greater than 100 km.

In accordance with NUREG/CR-6728 (McGuire, 2001) Approach 2B, controlling deaggregation earthquakes are used to incorporate the effect of magnitude on site response. Earthquakes with a range of magnitude contribute to seismic hazard at the site for a given mean annual probability of exceedance. Because the response spectral shape varies as a function of magnitude, the site response potentially varies depending on the magnitude of the earthquakes contributing to a given ground motion level. To incorporate this potential effect in the site response analysis, for each response spectral frequency range three controlling deaggregation earthquakes are identified to represent a low (DEL), middle (DEM), and high (DEH) magnitude.

Response spectral shapes for the REF, DEL, DEM, and DEH are determined following recommendations in NUREG/CR-6728 (McGuire, 2001) for CEUS earthquakes. Final response spectra are determined by scaling the spectral shapes to the UHRS at the appropriate response spectral frequency (i.e., 1.75 Hz or 7.5 Hz). Figure 2.5-46 and Figure 2.5-47 show the controlling earthquake response spectra for low and high response spectral frequency ranges for ground motion with a 10^{-4} and 10^{-5} mean annual probability of exceedance, respectively.

The deaggregation results show that at high response spectral frequency the hazard is dominated by earthquakes within the 200 mi (322 km) site region. For a 10^{-4} mean annual probability of exceedance, earthquakes with **M** from 5 to 7 contribute with the larger earthquakes contributing from greater distances. At lower mean annual probabilities of exceedance, dominant contributions come from closer distances. For a 10^{-6} mean annual probability of exceedance, the hazard is dominated by **M** 5 to 6.5 earthquakes within 9.3 mi (15 km) of the site.

At low response spectral frequencies, distant sources dominate the hazard for a 10^{-4} mean annual probability of exceedance. Hazard is dominated by earthquakes of **M** greater than 7 at a distance of more than 625 mi (1,000 km). As lower mean annual probabilities of exceedance are considered, the influence of large nearby earthquakes is seen. For a 10^{-6} mean annual probability of exceedance, low response frequency range ground motion is dominated by nearby earthquakes with **M** of 5 to 6.5.

Each of the controlling deaggregation earthquakes, for both the low and high response spectral frequency ranges, was taken as input for the seismic site amplification analyses as described in Section 2.5.2.5.1.5.

2.5.2.4.5 Contribution by Seismic Source

In addition to deaggregation by magnitude and distance bins, the hazard was also decomposed by the contribution to total hazard for each source zone. Representative results are presented for 10-Hz pseudo-spectral acceleration (SA) hazard and 1-Hz SA hazard (Figure 2.5-185 and Figure 2.5-186, respectively).

For 10-Hz SA hazard, ground motion with a 10^{-4} to 10^{-6} mean annual probability of exceedance is dominated by contributions from the PEZ-N Seismotectonic zone with secondary contributions from the NMSE-N and Study Region Mmax zones and the PEZ-W Seismotectonic zone (Figure 2.5-185).

For 1-Hz SA hazard, the NMFS RLME source dominates hazard with 10^{-4} mean annual probability of exceedance (Figure 2.5-186). Secondary contributors include the Charleston RLME source, the Study Region Mmax zone, and the ECC-AM, SLR, and PEZ-N Seismotectonic zones. For 1-Hz SA ground motion with a 10^{-5} mean annual probability of exceedance, the NMFS continues to dominate with stronger contribution from the PEZ-N zone. The Charleston source, the Study Region zone and the ECC-AM zone continue to be secondary contributors. At a 10^{-6} mean annual probability of exceedance, the PEZ-N zone dominates with the NMFS and Charleston sources providing secondary contributions to hazard.

2.5.2.5 Seismic Wave Transmission Characteristics of the Site

The uniform hazard response spectra (UHRS) presented in Section 2.5.2.4.6 and displayed on Figure 2.5-15 are defined for a hard rock site condition with shear-wave velocity of 9,200 ft/sec (2,800 m/sec). At the BBNPP site, rock with this shear-wave velocity is located at depths of about 414 ft (126 m) below the foundation level. To determine the GMRS at the ground

surface, it is necessary to adjust the UHRS for amplification or de-amplification as the vibratory ground motion propagates through the site materials.

The adjustment is made by conducting Site Response Analyses and following Approach 2B described in NUREG/CR-6728 (McGuire, 2001) to combine the site response with the rock UHRS. These analyses consist of defining the shear wave velocity and material damping characteristics of the site material profile between the ground surface and the depth of hard rock. Then one-dimensional site analyses are conducted using an equivalent linear procedure (Schnabel, 1972). The results are used to derive site amplification functions for modifying the response spectra at rock to the corresponding response spectra at the ground surface, taking into account the seismic wave transmission characteristics of the site geotechnical layers. This section describes the steps involved in the calculation and application of the site amplification functions and the seismic wave transmission characteristics and effects of the BBNPP site material column on hard rock ground motions.

Section 2.5.2.5.1 is added as a supplement to the U.S. EPR FSAR.

2.5.2.5.1 Development of Site Amplification Functions

This section describes the methodology, inputs, and results of the site response analysis for the BBNPP site.

2.5.2.5.1.1 Methodology

The calculation of site amplification functions is performed in the following 4 steps:

1. Based on the results of geotechnical and geological investigations at the BBNPP site, develop a best estimate soil and rock column, extending from the surface to the hard rock horizon at depth, consisting of layers defined by their mean low-strain shear wave velocities and by material damping properties, including strain-dependencies. At the BBNPP site, hard rock ($V_s = 9,200$ ft/sec (2,800 m/sec)) is found at 414 ft (126 m);
2. Develop a probabilistic model that describes the random variability in the above properties, locations of layer boundaries, and correlation between the velocities in adjacent layers, and generate a set of 60 artificial "randomized" profiles;
3. For each of the controlling deaggregation earthquakes (DEL, DEM, and DEH) representing ground motions having 10^{-4} and 10^{-5} mean annual probabilities of exceedance, for both low frequency (LF) and high frequency (HF) spectral frequencies, develop and use corresponding time histories for input into dynamic response analysis as the outcrop motion at the hard rock elevation;
4. Use an equivalent-linear time-history site-response formulation to calculate the dynamic response of the site for each of the 60 random profiles, and then calculate the mean site response. This step is repeated for each of the three controlling deaggregation earthquakes.

These steps are described in the following subsections. The calculation of site effects was performed with an in-house version of the computer program SHAKE (Schnabel, 1972). This program computes the response in a system of viscous-elastic, horizontally layered, soil units, overlying a uniform half-space, subjected to transient, vertically travelling shear waves.

The analytical method implemented in SHAKE is based on the solution of the wave equation and the Fast Fourier Transform algorithm. The nonlinearity of the shear modulus and damping

is accounted for by the use of equivalent linear soil properties within an iterative procedure to obtain values for modulus and damping compatible with the effective strains in each layer. Therefore, for any set of layer properties, SHAKE performs a linear analysis.

2.5.2.5.1.2 Investigations to Determine the Base Case Soil/Rock Column for the BBNPP Site

Development of a best estimate soil/rock column is described in detail in Section 2.5.4. This section provides an overview of the soil/rock column and the geotechnical and geological investigations carried out to characterize it.

The BBNPP site was investigated using test borings and geophysical methods. The geotechnical investigation is described in detail in Section 2.5.4.

The layers underlying the BBNPP site consist of the following stratigraphic units:

- ◆ Overburden Soils:
 - ◆ Glacial Overburdens
- ◆ Rock Formations:
 - ◆ Mahantango Shale

The Mahantango Shale consists of three horizons: weathered rock, a transition zone, and sound rock. At the BBNPP site, the overburden soils, weathered rock, and transition zone rock will be excavated and replaced with concrete or engineered fill. The engineered fill and concrete are taken into account in defining the soil/rock column for the BBNPP site response analyses. Section 2.5.4 provides detailed contour information related to the position of the bedrock below the power block's footprint.

The compressional and shear-wave velocities of the in situ materials are taken from geophysical field tests using two different techniques:

1. Three sets of downhole tests,
2. Three sets of suspension logging tests

Of the six geophysical measurements, those from boring G-401 provide the deeper site-specific geophysical information collected during the geotechnical investigation. In this boring, P-S Suspension and downhole tests were performed to a depth of approximately 400 ft (122 m). This boring is at the center of the projected containment footprint.

The downhole profiles consist of average compressional and shear-wave velocities for layers with thickness varying from about 13 ft (4 m) to 140 ft (42.7 m). The suspension logging profiles provide measurements of compressional and shear-wave velocities at approximately 1.5 ft (0.5 m) spacing. Shear-wave velocities of 9200 ft/sec (2800 m/sec), representing the reference rock condition for which seismic hazard was calculated, were not reached in the geophysical surveys. Thus, the deeper portion of the best estimate profile was developed considering the stratigraphy of the rocks underlying the BBNPP site and the best estimate profile from the previous BBNPP site.

The geologic column at the BBNPP site is an extension of the Mahantango Formation, which is a dark gray to black shale with few to no fractures. Some distinctive features are the presence

of calcareous zones, the presence of thin pyrite lenses that increase in abundance with depth, and the presence of calcite veins perpendicular to the bedding plane that are micro-faulted. The upper surface of the Mahantango Formation shows the effects of solution and weathering in a few areas, but is predominately very competent and indurated.

In addition to the in-situ geophysical testing, laboratory measurements of velocity were carried out on samples obtained from BBNPP site borings. Free-free direct arrival tests were performed on undisturbed rock samples by the University of Texas. The free-free direct arrival test results are provided in Table 2.5-31. The tests provided material velocity and damping values associated with shear waves and compressional waves.

A best-estimate velocity profile was determined taking into account the geophysical borehole measurements, the laboratory measurements, and the geology of the BBNPP site. Figure 2.5-21 shows the best-estimate shear-wave velocity profile along with in-situ velocity data from boring G-401 and laboratory velocity measurements on samples from boring B-401. Also shown is the best-estimate coefficient of variation (COV) profile. Figure 2.5-22 shows the best-estimate profiles without the data.

Resonant Column and Torsional Shear Laboratory Tests were performed on soil and backfill samples. The complete set of results from these tests is reported in Section 2.5.4.2.3. Generic cohesionless soil curves (EPRI, 1993) were adopted to describe the strain dependencies of shear modulus and damping for the backfill based on available results from the BBNPP site investigation. As recommended by Regulatory Guide 1.208 (NRC, 2007a) the damping curves for soils were truncated at 15 percent for the BBNPP site response analysis.

The average of the laboratory test results for damping for the Mahantango Shale is 0.86 percent. Lower values, 0.8 and 0.7 percent, are conservatively used for the analysis. The Mahantango Shale has a very high Rock Quality Designation (RQD) and as a rock mass is capable of transmitting shear waves very efficiently with small amounts of damping. Therefore, the lower reported laboratory values are selected for the analysis. The RQD of the Mahantango Shale is reported in the field boring logs.

For the BBNPP site response analyses, the Mahantango Shale and the concrete underlying the power block basemat are assumed to behave linearly during earthquake shaking.

2.5.2.5.1.3 Representation of Variability and Correlations in Soil/Rock Column Properties

To account for variations in shear-wave velocity across the BBNPP site in the site response analysis, 60 randomized profiles were generated for use in determining site amplification functions. In generating the randomized profiles, the coefficient of variation of V_S is used as an approximation to the standard deviation of $\ln(V_S)$ (Ang and Tang, 1975). These artificial profiles represent the soil column from the top of the ground surface to bedrock with a shear-wave velocity of 9,200 ft/s (2,800 m/sec). The model uses as inputs the following quantities:

- ◆ The best estimate of the shear-wave velocity profile and other soil properties described above;
- ◆ The coefficient of variation of the shear wave velocity as a function of depth, developed using available BBNPP site data (refer to Section 2.5.4);
- ◆ The probabilistic characterization of layer thickness as a function of depth, computed assuming a normal distribution;

- ◆ The depth to bedrock with a shear-wave velocity of 9,200 ft/s (2,800 m/s), which is randomized assuming a normal distribution to account for variation in the bedrock-depth data described in Section 2.5.4.

Figure 2.5-22 shows the best estimate V_s and COV profiles for the nuclear island that were used to generate the 60 randomized profiles.

The randomly generated layer thicknesses were computed assuming a normal distribution using a coefficient of variation of 0.15 for each layer. For consistency with the site-specific data, the generated $\ln(-\text{velocities})$ and the generated thicknesses were truncated at ± 2 standard deviations according to the recommendations of Toro (Toro, 1996).

Figure 2.5-23 illustrates the 60 randomized V_s profiles. These profiles include uncertainty in depth to bedrock with a shear-wave velocity of 9,200 ft/s (2,804 m/s). Figure 2.5-24 compares the mean of these 60 V_s profiles to the best estimate V_s profile, indicating very good agreement. This figure also shows the ± 1 standard deviation values of the 60 profiles, reflecting the coefficients of variation indicated on Figure 2.5-22.

Mean values of shear stiffness (G/G_{\max}) and damping for each geologic unit are described in Section 2.5.4. Variation in the properties for each soil/rock column unit is characterized through the use of randomized material property curves. For engineered fill, which is considered a nonlinear material, 60 randomized G/G_{\max} and damping curves are developed. For concrete and sound rock, which are considered linear materials, 60 randomized damping curves are developed. For the linear material, G/G_{\max} is taken as 1. Figure 2.5-25 and Figure 2.5-26 illustrate the randomized shear stiffness and damping curves for engineered fill at less than 30 ft.

These randomized velocity profiles and material property curves are used to take into account variation in site properties when calculating site response, as described in the following sections.

2.5.2.5.1.4 Development of Smooth Uniform Hazard, Controlling, and Reference Response Spectra

In addition to the characterization of site material properties described in Sections 2.5.2.5.1.2 and 2.5.2.5.1.3, the site response analysis also requires time histories representing earthquakes that control the seismic hazard at various response spectral frequencies. To develop the time histories, first the response spectra associated with controlling earthquakes are developed. Then the time histories are developed to be consistent with the controlling earthquake response spectra. The controlling earthquake response spectra are also used to smooth the UHRS originally defined at the limited number of spectral frequencies for which the PSHA was carried out. Development of controlling earthquake response spectra and their use to smooth the UHRS are described in this section.

The identification of controlling earthquakes on the basis of the PSHA deaggregation is described in Section 2.5.2.4.6. Controlling reference earthquakes are determined for ground motion with mean annual frequencies of exceedance of 10^{-4} , 10^{-5} , and 10^{-6} . At each hazard level, a controlling reference earthquake (REF) is determined for a low response spectral frequency range (average of 1 and 2.5 Hz, or 1.75 Hz) and a high range (average of 5 and 10 Hz, or 7.5 Hz) (Table 2.5-1). In addition, for 10^{-4} and 10^{-5} mean annual probabilities of exceedance, controlling deaggregation earthquakes are determined (Table 2.5-1).

The controlling deaggregation earthquakes represent (for each combination of mean annual frequency of exceedance and spectral frequency range) a low, middle, and high magnitude earthquake contributing to the hazard (DEL, DEM, and DEH, respectively). These earthquakes are used to generate input for the site response analysis such that the site response analysis takes into account the effects of the range of earthquake magnitude (i.e., differing spectral shapes) contributing to the hazard at the BBNPP Site. For both the controlling reference earthquakes and the controlling deaggregation earthquakes, response spectral shapes are determined following the recommendations in NUREG/CR-6728 (McGuire, 2001). The response spectral shapes are scaled to the UHRS at the appropriate spectral frequency to give the final controlling response spectra. Figure 2.5-46 and Figure 2.5-47 show the reference earthquake response spectra for the low and high spectral frequency range for 10^{-4} and 10^{-5} mean annual frequencies of exceedance, respectively. These figures also show the deaggregation earthquake response spectra.

To smooth and extrapolate the UHRS defined from the PSHA results, the spectral shapes of the controlling reference earthquakes are used. In addition to the controlling reference earthquakes for the spectral frequency ranges of 1 to 2.5 Hz and 5 to 10 Hz, to smooth the UHRS, controlling reference earthquake response spectra are also determined for response spectral frequencies of 0.5 Hz and 25 Hz, respectively. For spectral frequencies less than 0.5 Hz, the spectral shape of the controlling reference earthquake for 0.5 Hz is used. For spectral frequencies from 0.5 Hz to 2.5 Hz, 2.5 Hz to 10 Hz, and 10 Hz to 100 Hz, the spectral shapes of the 1 to 2.5 Hz, 5 to 10 Hz, and 25 Hz controlling reference earthquakes are used, respectively, to guide the smoothing. The smoothed UHRS are shown in Figure 2.5-20 for ground motion with mean annual frequencies of exceedance of 10^{-4} , 10^{-5} , and 10^{-6} . For mean annual frequencies of exceedance of 10^{-4} and 10^{-5} , the smoothed UHRS are presented on Figure 2.5-46 and Figure 2.5-47 along with the scaled controlling earthquake response spectra.

2.5.2.5.1.5 Controlling Time Histories

Time histories representing the controlling deaggregation earthquakes are developed by adjusting a seed time history such that its response spectrum matches the associated controlling deaggregation earthquake response spectrum. As an example, a comparison of the time history response spectra to the target response spectrum is shown in Figure 2.5-48 for DEL and DEM controlling earthquakes for the low response spectral frequency range and a 10^{-4} mean annual frequency of exceedance.

The spectral matching is carried out to meet the criteria recommended in Appendix F of Regulatory guide 1.208 (NRC, 2007a). The seed time histories are selected taking into account the magnitude and distance associated with each controlling deaggregation earthquake. For each controlling deaggregation earthquake, two sets of two horizontal time histories are developed, leading to a total of 24 sets (i.e., two sets of time histories x three controlling deaggregation earthquakes x two spectral frequency ranges x two annual frequencies of exceedance). As documented in NUREG/CR-6728 (McGuire, 2001), the seed time histories are strong motion accelerograms recorded during past earthquakes that have been modified to represent CEUS conditions. The seed time histories used to develop the time histories for the controlling deaggregation earthquakes are listed in Table 2.5-5.

2.5.2.5.1.6 Site Response Analysis

The site response analysis performed for the BBNPP site used a time history-based procedure in conjunction with the following assumptions:

- ◆ Vertically-propagating shear waves are the dominant contributor to site response.

- ◆ An equivalent-linear formulation of soil nonlinearity is adequate for the characterization of site response.

The site response analysis is carried out to determine the surface response for an outcrop of competent Mahantango Formation, which is the site for which the GMRS is determined. The 60 randomized V_s profiles (Figure 2.5-23), which are developed to also support site response analyses for determination of the Foundation Input Response Spectrum (FIRS), are truncated at the top of the Mahantango Formation 1 layer to carry out site response analyses for the GMRS. To determine the GMRS, the engineered fill and concrete layers are not included.

Sixty response analyses were performed using the RIZZO in-house version of the program SHAKE (Schnabel, 1972) to calculate the site amplification function for each controlling deaggregation earthquake. The 60 randomized velocity profiles were paired with the 60 randomized damping curves (one profile with damping curves) to define 60 soil columns. When site response is carried out for the FIRS level, randomized sets of modulus reduction curve and damping curves are included for the engineered fill layers and randomized damping curves are included for the concrete layer. These inputs are not required for the site response analysis supporting development of the GMRS.

Each of the four spectrally matched time histories corresponding to each controlling deaggregation earthquake was used to compute the response of the sixty soil/rock columns.

For each analysis, the response spectrum computed at the Mahantango Formation 1 outcrop (top of competent material) was divided, frequency by frequency, by the response spectrum for the hard rock input motion to obtain a site amplification function. The arithmetic mean of these 60 individual response spectral ratios was taken as the mean site amplification function for each controlling deaggregation earthquake.

For each combination of spectral frequency range (LF, HF) and mean annual frequency of exceedance (10^{-4} , 10^{-5}), a weighted average is determined of the mean amplification factors for the DEL, DEM, and DEH controlling earthquakes. The results for the three controlling deaggregation earthquakes are weighted according to their relative contribution to seismic hazard at the BBNPP site.

The following figures and table show results of the site response analysis:

- ◆ Figure 2.5-27: individual and mean hard-rock-to-ground-surface amplification functions (factors) for the 60 randomized rock columns for the high spectral frequency range (HF) DEM earthquake representing ground motion with a 10^{-4} mean annual frequency of exceedance
- ◆ Figure 2.5-28: maximum strains versus depth for the 60 randomized rock columns for the HF DEM earthquake representing ground motion with a 10^{-4} mean annual frequency of exceedance (left side- 0 to 50 ft, right side- 50 to 450 ft)
- ◆ Figure 2.5-29: individual and mean hard-rock-to-ground-surface amplification factors for the 60 randomized rock columns for the low spectral frequency range (LF) DEM earthquake representing ground motion with a 10^{-4} mean annual frequency of exceedance
- ◆ Figure 2.5-30: maximum strains versus depth for the for the 60 randomized rock columns for the LF DEM earthquake representing ground motion with a 10^{-4} mean annual frequency of exceedance (left side- 0 to 50 ft, right side- 50 to 450 ft)

- ◆ Figure 2.5-31: individual and mean hard-rock-to-ground-surface amplification factors for the 60 randomized rock columns for the HF DEM earthquake representing ground motion with a 10^{-5} mean annual frequency of exceedance
- ◆ Figure 2.5-32: maximum strains versus depth for the 60 randomized rock columns for the HF DEM earthquake representing ground motion with a 10^{-5} mean annual frequency of exceedance (left side- 0 to 50 ft, right side- 50 to 450 ft)
- ◆ Figure 2.5-33: individual and mean hard-rock-to-ground-surface amplification factors for the 60 randomized rock columns for the LF DEM earthquake representing ground motion with a 10^{-5} mean annual frequency of exceedance
- ◆ Figure 2.5-34: maximum strains versus depth for the 60 randomized rock columns for the LF DEM earthquake representing ground motion with a 10^{-5} mean annual frequency of exceedance (left side- 0 to 50 ft, right side- 50 to 450 ft)
- ◆ Table 2.5-3: hard-rock-to-ground-surface amplification factors for controlling deaggregation earthquakes, and their weighted average, for HF and LF ranges and ground motion with mean annual frequencies of exceedance of 10^{-4} and 10^{-5}

2.5.2.6 Ground Motion Response Spectra

The U.S. EPR FSAR includes the following COL Item in Section 2.5.2.6:

A COL applicant that references the U.S. EPR design certification will compare the final strain-dependent soil profile with the U.S. EPR design soil parameters and verify that the site-specific seismic response is enveloped by the CSDRS and the soil profiles discussed in Sections 2.5.2, 2.5.4.7 and 3.7.1 and summarized in Table 3.7.1-6, Table 3.7.1-8 and Table 3.7.1-9.

This COL Item is addressed as follows:

{As described in Section 2.5.2.5.1.6, the results of the site response analysis are a suite of mean site amplification factors. This section describes the use of the site amplification factors to determine the site-specific response spectra at the ground surface for the top of competent rock (Mahantango Formation 1). First, the mean amplification factors for the three controlling deaggregation earthquakes for each combination of spectral frequency range (HF, LF) and mean annual frequency of exceedance (10^{-4} , 10^{-5}) are averaged. In computing the average, the amplification factor for each controlling deaggregation earthquake (i.e., DEL, DEM, DEH) is weighted according to the contribution to the seismic hazard that it represents. This calculation results in weighted average amplification factors for high and low spectral frequency ranges for both 10^{-4} and 10^{-5} mean frequencies of exceedance. Table 2.5-3 summarizes the controlling deaggregation amplification factors, weights, and final average amplification factors.

Next the weighted average amplification factors are used to modify the smooth UHRS for hard rock to give the UHRS at the ground surface. The spectral amplitude for each frequency of the hard-rock UHRS is multiplied by the value of the amplification factor at that frequency. For high frequencies, the weighted average amplification function for the high spectral frequency range is used; for low frequencies, the amplification function for the low range is used. For intermediate frequencies, use of the low or high frequency range amplification function is based on whether the reference earthquake response spectrum for the low or high frequency

range lies closest to the UHRS. The resulting surface UHRS for 10^{-4} and 10^{-5} mean annual frequencies of exceedance are shown on Figure 2.5-35.

The ASCE (ASCE, 2005) performance-based approach was used to derive a ground motion response spectrum (GMRS) from the 10^{-4} and 10^{-5} surface UHRS. The GMRS is derived at each structural frequency as follows:

$$\text{GMRS} = 10^{-4} \text{ UHRS} \times \text{DF}$$

in which

$$\text{DF} = \max \{1.0, 0.6(A_R)^{0.8}\}$$

and

$$A_R = (10^{-5} \text{ UHRS}) / (10^{-4} \text{ UHRS})$$

unless A_R is greater than 4.2. In that case,

$$\text{GMRS} = 0.45 (10^{-5} \text{ UHRS})$$

The resulting horizontal GMRS is a performance-based surface response spectrum (PBSRS) and is plotted in Figure 2.5-36 and listed in Table 2.5-2.

A vertical GMRS was constructed from the horizontal GMRS following the approach described in NUREG/CR-6728 (McGuire, 2001).

The vertical GMRS is determined from the horizontal GMRS using a frequency- and PGA-dependent vertical-to-horizontal response spectral ratio (V/H ratio). The V/H ratio is based on ratios given in NUREG/CR-6728 (McGuire, 2001) for CEUS. These ratios depend on PGA and are for a rock site. Because the horizontal GMRS PGA is less than 0.2 g, values for the low PGA range are used. The shear-wave velocities at the site are in the range 2,000 m/s to 2,500 m/s, which are deemed similar to the 2800 m/s conditions for which the NUREG/CR-6728 values are determined.

The vertical GMRS is shown on Figure 2.5-36 and listed in Table 2.5-2 along with the V/H ratios used.

Refer to Section 3.7.1 and Section 3.7.2 for a description of the FIRS, SSE, and soil-structure interaction analyses performed for the U.S. EPR design certification.

2.5.2.7 Conclusions

This section is added as a supplement to the U.S. EPR FSAR.

An updated evaluation of the vibratory ground motion has been conducted for the BBNPP site. A PSHA was selected as the appropriate basis for evaluating the vibratory ground motion accounting for all credible alternative seismic sources. The seismic source characterization provided in the EPRI/DOE/NRC (2012) CEUS SSC model constitutes the best current representation of seismic source inputs for PSHA in the CEUS. The model was developed using a SSHAC Level 3 process to ensure confidence that the center, body, and range of technically defensible interpretations were captured and represented. The PSHA for the BBNPP site makes

use of the logic tree approach with appropriate weighting factors used in the EPRI/DOE/NRC CEUS SSC model.

On the basis of the PSHA results, mean Uniform Hazard Response Spectra were determined for a hard-rock outcrop. Following Approach 2B of NUREG/CR-6728 (McGuire, 2001) the hard-rock outcrop UHRS were modified to corresponding UHRS for the free-field ground surface. First, controlling earthquake response spectra, based on deaggregation of the PSHA results, and information on the dynamic properties of the soil and rock material at the BBNPP site, were used to conduct a site response analysis. Site amplification functions determined from the site response analysis were then used to modify the hard-rock outcrop UHRS to produce UHRS for the free-field ground surface.

The horizontal GMRS was determined from the UHRS for the free-field ground surface following the guidance of Regulatory Guide 1.208, "A Performance -Based Approach to Define the Site-Specific Earthquake Ground Motion," (NRC, 2007a). The vertical GMRS was developed from the horizontal GMRS using appropriate V/H spectral ratios. These performance-based spectra adequately represent the regional and local seismic hazards and appropriately include the effects of the local rock and soils at the BBNPP site.

The performance-based approach uses not only the seismic hazard characterization of the site from the PSHA but also basic seismic fragility SSC modeling to define a ground motion that directly targets a structural performance frequency value. It is concluded that the application for the BBNPP site is acceptable from a geologic and seismologic standpoint and meets the requirements of 10 CFR 100.23(d) (CFR, 2007). Deviations from the NRC guidance Regulatory Guide 1.208 (NRC, 2007a), or review criteria in Standard Review Plan 2.5.2 (NRC, 2007b) have been identified and acceptable alternatives, including technical justification, have been provided.

2.5.2.8 References

This section is added as a supplement to the U.S. EPR FSAR.

Adams, 2003. Fourth Generation Seismic Hazard Maps of Canada: Values for over 650 Canadian Localities Intended for the 2005 National Building Code of Canada: Geological Survey of Canada, Open File 4459, Adams, J., and Halchuck, S., 2003.

Ang and Tang, 1975. Probabilistic Concepts in Engineering Planning and Design, Volume 1, A.H. Ang and W.H. Tang, John Wiley and Sons, New York, 1975.

ASCE, 2005. Seismic Design Criteria for Structures, Systems, and Components in Nuclear Facilities, ASCE/SEI 43-05, American Society for Civil Engineers/Structural Engineering Institute, 2005.

Code of Federal Regulations (CFR, 2007). Title 10, Code of Federal Regulations, Part 100.23(d), Geologic and Seismic Siting Factors, 2007.

Cornell, 1968. Engineering Seismic Risk Analysis, C.A. Cornell, Bulletin of Seismological Society of America, Volume 58, pp, 1583-1606, 1968.

Cornell, 1971. Probabilistic Analysis of Damage to Structure Under Seismic Loads, C.A. Cornell, Dynamic Waves in Civil Engineering, Chapter 27, edited by D.A. Howells, I.P Haigh, and C. Taylor, 1971.

- EPRI, 1986.** Seismic Hazard Methodology for the Central and Eastern United States, NP-4726, Volumes 1-10, Electric Power Research Institute, July 1986.
- EPRI, 1988.** Seismic Hazard Methodology for the Central and Eastern United States, NP-4726-A, Revision 1, Volume 1, Part 2, Electric Power Research Institute, 1988.
- EPRI, 1993.** Guidelines for Determining Design Basic Ground Motions, TR-102293, Volume 1, Electric Power Research Institute, 1993.
- EPRI, 2004.** CEUS Ground Motion Project Final Report, TR-1009684 2004, Electric Power Research Institute, December 2004.
- EPRI, 2006a.** Program on Technology Innovation: Use of Cumulative Absolute Velocity (CAV) in Determining Effects of Small Magnitude Earthquakes on Seismic Hazard Analyses, Report 1014099, Electric Power Research Institute, Palo Alto, CA, and U.S. Department of Energy, Germantown, MD, 2006.
- EPRI, 2006b.** Program on Technology Innovation: Truncation of the Lognormal Distribution and Value of the Standard Deviation for Ground Motion Models in the Central and Eastern United States, TR-1014381, Electric Power Research Institute, August 2006.
- EPRI, 2006c.** Program on Technology Innovation: Truncation of the Lognormal Distribution and Value of the Standard Deviation for Ground Motion Models in the Central and Eastern United States, Technical Update 1013105, Electric Power Research Institute, February 2006.
- EPRI/DOE/NRC, 2012.** Technical Report: Central and Eastern United States Seismic Source Characterization for Nuclear Facilities, EPRI Report # 1021097, U.S. DOE Report # DOE/NE-0140, U.S. NRC NUREG-2115, Electric Power Research Institute, Palo Alto, CA, U.S. DOE, U.S. NRC, 2012.
- Fail, 2004.** Earthquake Catalog and Epicenter Map of Pennsylvania: Pennsylvania Department of Conservation and Natural Resources, Fail, R.T. (compiler), 2004.
- Gardner, 1974.** Is the sequence of earthquakes in Southern California, with aftershocks removed, Poissonian?, Bulletin of the Seismological Society of America, Volume 64, Gardner, J.K., and Knopoff, L., 1974.
- Horton and Williams, 2012.** The 2011 Virginia Earthquake: What are Scientists Learning?, EOS, Transactions of the American Geophysical Union, Vol. 98, No. 33, pp. 317-318, American Geophysical Union, Washington, D.C, Horton, J.W. and Williams, R.A., 2012.
- Kijko, 2004.** Estimation of the maximum earthquake magnitude, m_{max} : Pure and Applied Geophysics, v. 161, pp. 1-27, Kijko, A., 2004.
- Kim and Chapman, 2005.** The 9 December 2003 central Virginia earthquake sequence: A compound earthquake in the Central Virginia seismic zone: Bulletin of the Seismological Society of America, v. 95, no. 6, pp. 2428-2445, Kim, W.Y., and Chapman, M., 2005.
- McGuire, 2001.** Technical Basis for Revision of Regulatory Guidance on Design Ground Motions: Hazard- and Risk-consistent Ground Motion Spectra Guidelines, McGuire, R.K., W.J. Silva, and C.J. Constantino, NUREG/CR-6728, U.S. Nuclear Regulatory Commission, 2001.

NRC, 2007a. A Performance-Based Approach to Define the Site-Specific Earthquake Ground Motion, Regulatory Guide 1.208, U. S. Nuclear Regulatory Commission, March 2007.

NRC, 2007b. Vibratory Ground Motion, Standard Review Plan, NUREG-0800, Section 2.5.2, Revision 4, U.S. Nuclear Regulatory Commission, March 2007.

NRC, 2012. Practical Implementation Guidelines for SSHAC Level 3 and 4 Hazard Studies, U.S. Nuclear Regulatory Commission, April 2012.

Schnabel, 1972. SHAKE - A Computer Program for Earthquake Response Analysis of Horizontally Layered Sites, P.B. Schnabel, J. Lysmer and H.B. Seed, Report No. EERC 72-12, University of California, Berkeley, 1972.

Senior Seismic Hazard Analysis Committee (SSHAC), 1997. Recommendations for Probabilistic Seismic Hazard Analysis: Guidance on Uncertainty and Use of Experts, Prepared by Senior Seismic Hazard Analysis Committee (SSHAC), NUREG/CR-6372, U. S. Nuclear Regulatory Commission, 1997.

Toro, 1996. Probabilistic Models of Site Velocity Profiles for Generic and Site-Specific Ground Motion Amplification Studies, G. R. Toro, Published as an appendix in W. J. Silva, N. Abrahamson, G. Toro and C. Costantino, 1997, Description and validation of the stochastic ground motion model, Report Submitted to Brookhaven National Laboratory, Associated Universities, Inc. Upton, New York 11973, Contract No. 770573, 1996.

USGS, 2008, USGS web database: http://neic.usgs.gov/neis/epic/epic_circ.html, last accessed November 2008.

2.5.3 Surface Faulting

The U.S. EPR FSAR includes the following COL Item in Section 2.5.3:

A COL applicant that references the U.S. EPR design certification will investigate site-specific surface and subsurface geologic, seismic, geophysical, and geotechnical aspects within 25 miles around the site and evaluate any impact to the design. The COL applicant will demonstrate that no capable faults exist at the site in accordance with the requirements of 10 CFR 100.23 and 10 CFR 50, Appendix S. If non-capable surface faulting is present under foundations for safety-related structures, the COL applicant will demonstrate that the faults have no significant impact on the structural integrity of safety-related structures, systems or components.

This COL Item is addressed as follows:

{There is no potential for tectonic fault rupture and there are no capable tectonic sources within a 25 mi (40 km) radius of the BBNPP site. A capable tectonic source is a tectonic structure that can generate both vibratory ground motion and tectonic surface deformation, such as faulting or folding at or near the earth's surface in the present seismotectonic regime (NRC, 1997). The following Sections provide the data, observations, and references to support this conclusion. Information contained in these Sections was developed in accordance with RG 1.208 (NRC, 2007), and is intended to satisfy 10 CFR 100.23, "Geologic and Seismic Siting Criteria" (CFR, 2007a) and 10 CFR 50, Appendix S, "Earthquake Engineering Criteria for Nuclear Power Plants" (CFR, 2007b).

Section 2.5.3.1 through Section 2.5.3.9 are added as a supplement to the U.S. EPR FSAR.

2.5.3.1 Geological, Seismological, and Geophysical Investigations

The following investigations were performed to assess the potential for surface fault rupture out to a 25 mile (40 km) radius of the BBNPP site:

- ◆ Site subsurface investigations including geotechnical borings and seismic refraction surveys. (Section 2.5.3.1.1)
- ◆ Interpretation of aerial photography and satellite imagery. (Section 2.5.3.1.2)
- ◆ Field reconnaissance. (Section 2.5.3.1.3)
- ◆ Compilation and review of existing geologic and seismologic data and literature, including a review of seismic data. (Section 2.5.3.1.4)

2.5.3.1.1 Subsurface Investigations at the BBNPP Site

Geologic sections developed from geotechnical data collected from 44 boreholes as part of the BBNPP study (as discussed in Section 2.5.4) provide detailed information in the upper 420 ft (128 m) (Based on deepest boring B-401) of strata for the presence of structures directly beneath the site. The interpretations developed from the previous investigation at the SSES site confirm the interpretation of the new borehole data at the BBNPP site:

Unfaulted Middle Devonian shale shallowly dipping to the north-northwest with a strong south-southeast dipping cleavage, and covered by a layer of undeformed residual soil that formed from weathering of the underlying shale bedrock (Figure 2.5-141, Figure 2.5-142, Figure 2.5-143, Figure 2.5-144, and Figure 2.5-145). However, the location of the Essential Service Water Emergency Makeup System (ESWEMS) is below the break in slope of the hill and is located on glacial outwash and till (Figure 2.5-146).

Although the bedrock formations underlying the BBNPP site have experienced folding during the Alleghanian Orogeny (Williams, 1987; Fail, 1999), residual soils and surficial sediments within and near the site (Figure 2.5-144 and Figure 2.5-145) display no signs of faulting or folding during the Quaternary time period, and rest unconformably on the eroded surface of the tilted beds of the local shale bedrock.

Geotechnical boreholes provide additional evidence of the lateral continuity between the residual overburden and the Devonian Mahantango Formation. Figure 2.5-141, Figure 2.5-142, and Figure 2.5-145 display a general thickening of the weathered rock and transition zone sequence that form an east-west to southeast-northwest depression in the solid rock surface in the central portion of the site (Figures Figure 2.5-54 and Figure 2.5-146). This consistency in strata across the site support detailed published reports of the site area local geology, and confirm that recent surficial faulting and folding are absent in the interpreted sections within the BBNPP site.

Seismic refraction surveys were performed to support site characterization studies for the BBNPP (Section 2.5.4.2.2.2.3). Because earth materials exhibit characteristic wave propagation velocities, they can be classified simply in terms of their seismic velocity. Seismic refraction data were interpreted for this study to assist in characterizing the local subsurface geologic materials regarding the thickness of the soil overburden, depths to weathered or fractured bedrock, and competent bedrock. Seismic refraction surveys were performed along 9 profile

lines totaling 7440 linear feet (2267 m) of coverage. The data for the surveys were collected from May 26 to June 5, 2010 using approved quality assurance procedures. The complete report of this survey (GeoVision, 2010) is included in COLA Part 11G.

Figure 2.5-53 is a map depicting the layout of the 9 lines used during the survey (Lines A1 through A5, oriented west; and Lines B1 through B4, oriented north-south). Seismic refraction velocity profiles are presented on Figure 2.5-57 through Figure 2.5-65 with the vertical scale measuring elevation in feet. Tomographic inversion routines are the most appropriate data modeling technique for this site because velocity gradients are assumed to be present within weathered bedrock at this site, and refraction tomography techniques are often able to resolve complex velocity structure (e.g. velocity gradients) that can be observed in bedrock weathering profiles. Layer based modeling techniques such as the Generalized Reciprocal Method (GRM) are not able to accurately model the velocity gradients that can be observed in weathered bedrock such as at the BBNPP site. However, the GRM method was used to confirm velocity ranges in the tomographic models.

These interpreted velocity profiles indicate that the elevation of the competent rock is highest in the northern portion of the site, and forms an east-west to southeast-northwest trending depression in the central portion of the site with elevation increasing again to the south. Figure 2.5-54 is a representation of the surface of the competent bedrock. The top of this surface is based on an interpreted compressional-wave velocity in the 11,000 to 13,000 feet per second (ft/s) range (3400 to 4000 meters per second (mps)). The approximate locations of the top of the decomposed, weathered and competent shale identified in boreholes within 50 ft (15.2 m) of the seismic lines is included on the seismic models to aid with interpretation (Figure 2.5-57 through Figure 2.5-65).

Two possible weathered shale units are identified within the tomographic profiles; one based on geologic description (WS1) and the other based on the depth at which RQD exceeds 0% (WS2) (GeoVision, 2010). The locations of the 4,000, 6,000 and 12,000 ft/s (1200, 1800 and 3700 mps) contours from intersecting lines are also shown on the seismic models for discussion. There is a distinct possibility at this site that velocity structure may be slightly different at intersecting lines because of the complex velocity structure of the weathered shale (GeoVision, 2010). Additionally, bedding and fracture attitudes relative to the seismic line orientation may have a significant impact on modeled seismic velocity structure. A review of the data in the figures shows no offsets or abrupt changes in the tops of the bedrock that could indicate recent deformation. See section 2.5.4 for a more detailed discussion of the geophysical analysis.

The map of the top of the competent Mahantango Shale (sound rock) from the boring log data (Figure 2.5-66) shows a surface similar to that shown in Figure 2.5-54 that was developed for the top of competent rock from the geophysical data. Both maps show that the interpreted elevation of the top of the competent rock, as mentioned above, is highest in the northern and southern portions of the site, with an east-west to southeast-northwest trending depression in the center of the site.

Because the interpreted upper surfaces of the decomposed shale and weathered shale (Figure 2.5-55 and Figure 2.5-56) generally parallel surface topography at the site, the depression in the top of the competent rock in the center of the site is related to a thickened weathered shale layer, as can be seen in the reflection profiles (Figure 2.5-57 through Figure 2.5-65) and cross-sections (Figure 2.5-141 through Figure 2.5-145). The reason for over-thickened weathered and fractured rock zone in the center of the site is presumably

because this zone is located under a gully in the hill, which is oriented parallel to major structural orientations within the site area. Within this gully, precipitation is channeled off of the hill and leads to greater subsurface penetration of water within this zone, leading to deeper weathering and fracture propagation in the Mahantango Formation. However, because the top surfaces of the decomposed shale and weathered shale are parallel to the ground surface, with no obvious offset, it is clear that no Quaternary faulting has affected the site.

The close correlation between the seismic data and the boring log data, both in locating the top of rock elevation and in the lack of observed faulting in the rock mass, further confirms the interpretation by earlier researchers in the area (Inners, 1978, Williams, 1987) that there is no evidence of faulting in the Quaternary deposits underlying the site.

2.5.3.1.2 Interpretation of Aerial Photography and LIDAR Imagery

Aerial reconnaissance within a 25 mi (40 km) radius of the site was conducted by various personnel using aerial photographs from numerous publications. Figure 2.5-76 is a sample of the aerial imagery used, and it contains selected way points from the field reconnaissance. LIDAR imagery of the BBNPP site vicinity was also acquired for review and interpretation (Figure 2.5-160 through Figure 2.5-166). The LIDAR image contains elevation data with a 2 ft (0.6 m) contour interval. The aerial reconnaissance investigated geomorphology and targeted numerous previously mapped geologic features and potential seismic sources (e.g., Berwick fault, Light Street fault, and Berwick Anticlinorium).

Figure 2.5-147 and Figure 2.5-151 contain four topographic cross-sections (A, B, C on Figure 2.5-147, and D on Figure 2.5-151) based on the new LiDAR data set from Luzerne County. The intent of these figures is to review the LiDAR data set in both plan and section view to evaluate the detailed surface of the land as captured by the LiDAR process.

Figure 2.5-150 shows the BBNPP site geology on the LiDAR data base map. Figure 2.5-160 depicts the surficial sediment description including glacial derived features and deposit contacts overlaid on the LiDAR data base map. The same LiDAR data base map without the surficial sediment description is shown in Figure 2.5-161.

The site area geology is presented on the LiDAR data base map in Figure 2.5-162 and Figure 2.5-163 shows the same image without the site area geology coloration and patterns for better clarity. Figure 2.5-164 is similar to Figure 2.5-163 but has the higher altitudes eliminated to better show the detail for the lower elevations where the BBNPP site is located.

The site vicinity geology along with the LiDAR base map is presented in Figure 2.5-165. Figure 2.5-166 shows the LIDAR base map without the site vicinity geology coloration and patterns for better clarity. Figure 2.5-165 and Figure 2.5-166 include not only the trace for the Lightstreet and Berwick faults, but also all of the described geologic features at this scale.

The interpretation of the plan-view LiDAR maps incorporates an evaluation of the fracture traces and lineaments visible on the images as linear valleys and swales and straight segments of streams. The features are especially visible for the site on Figure 2.5-161. The orientations of the fractures observed in the outcrop of the Mahantango Shale are within the reported envelope of orientations reported by Inners (1978, Figure 3). There is a single dominant set striking just west of north, with a subordinate set at nearly right angles to the first. These appear to be nearly vertical. The right-angle bend in Walker Run to the southwest of the BBNPP center point, illustrates those trends, as the Run has eroded through the glacial cover

to expose the underlying bedrock structures. Other fracture orientations are present in the outcrop areas of formations to the north and south of the mapped Mahantango Shale, as is also reported by Inners (1978, Figures 4 and 5).

The topographic cross sections presented in Figure 2.5-147 and Figure 2.5-151 display no offsets that are attributable to the actions of the Berwick or Light Street Faults. The current work confirms the work by Inners (Inners, 1978) who reports the faults to be locally buried beneath the glacial terrace gravels. In the excavations for the Susquehanna Units, Inners found several slickensided surfaces at low-angles to the bedding planes located less than 1 mile (1.6 km) to the east of the site (Figure 2.5-150). He interpreted these surfaces as wedge faults that developed along small-scale drag folds during the deformation of the units in the Alleghanian Orogeny (Inners, 1978), approximately 340 to 250 Ma. The displacement on these faults was generally less than 3 ft (1 m) (Inners, 1978). The current investigation found similar slickensided surfaces, the closest at a distance of 0.45 miles (0.7 km) to the southwest of the site (Figure 2.5-150). The field team observed no offset of the glacial materials overlying these features.

As shown in the following section, field reconnaissance coupled with interpretation of remote imagery (review and inspection of features preserved on the images) shows that there are no geomorphic features indicative of potential Quaternary activity along trends of the postulated folds and faults interpreted by Inners and Williams (Inners, 1978; Williams, 1987). No features suggestive of tectonic deformation were observed in the Quaternary glaciofluvial deposits, and no potential liquefaction features were observed along the Susquehanna River.

2.5.3.1.3 Field Reconnaissance

Information developed from the literature and the imagery interpretation was supplemented by field reconnaissance within a 25 mi (40 km) radius of the site. These field-based studies were performed to verify, where possible, the existence of mapped bedrock faults in the BBNPP site area and to assess the presence or absence of geomorphic features suggestive of potential Quaternary fault activity along the mapped faults, or previously undetected faults. Features reviewed during the field reconnaissance and office-based analysis of aerial photography and LIDAR imagery were based on a compilation of existing regional geologic information in the vicinity of the BBNPP site, as referred to in Section 2.5.3.1.2.

Field reconnaissance was conducted by geologists in teams of two or more. Field reconnaissance visits in 2007, 2008, 2009, and 2010 focused on exposed portions of the Mahantango Formation, other formation exposures along the faces of Lee, Huntington and Nescopeck Mountains, and roads traversing the site vicinity. Key observations and discussion items were documented in field notebooks and photographs. Field locations were logged by hand on detailed topographic base maps and with hand-held Global Positioning System (GPS) receivers (Figure 2.5-148). There were no faults or other forms of deformation noted in the field. No surface expression of either the Berwick or Light Street faults was noted, consistent with the conclusions of Inners (Inners, 1978). Figure 2.5-67 and Figure 2.5-68 (Waypoint 12 on Figure 2.5-148) show that there is no offset in the Quaternary deposits along Syber Creek, where the trace of Light Street Fault crosses it. Photos of the shale bedrock on the site show the steeply dipping nature of the strong persistent cleavage. Bedding dipping to the north-northwest is visible, but highly obscured by this cleavage (Figure 2.5-73 and Waypoint WF3 on Figure 2.5-76). Outcrops in a nearby borrow area show an undeformed contact between the glacial overburden and the shale bedrock (Figure 2.5-74, and Figure 2.5-75 and Waypoint WF5 on Figure 2.5-76).

A supplemental reconnaissance was conducted during the fall of 2008, to investigate the occurrence of potential liquefaction features along the Susquehanna River. The field reconnaissance was carried out by a team of geologists and engineers from Paul C. Rizzo Associates, Inc, and John Sims & Associates from both the land and water approaches to the river banks. The investigation was conducted for the course of the river for a reach of 25 miles (40 km) upstream and downstream of the site (Figure 2.5-148). Because of the prevalent bedrock exposures in both the river banks and the river bottoms, few locations were encountered where liquefaction conditions were possible and no locations were encountered where liquefaction had occurred. Figure 2.5-69 through Figure 2.5-72 show the rocky nature of the riverbed and its banks and some of the typical exposures found during the investigation (for Waypoints WP1, WP10, WP20, and WP22 respectively).

A third reconnaissance was conducted during the Spring of 2009 to further investigate the occurrence of potential liquefaction features along the Susquehanna River. The study was conducted along approximately 10 miles of the Susquehanna River along the south and east bank in areas accessible by auto and on foot. The investigated areas lie south and east of the BBNPP site within the Berwick 7.5-minute topographic quadrangle.

Two tributaries of the Susquehanna River, the Wapwallopen and Little Wapwallopen creeks, were found to run on bedrock and are relatively small, but similar to other tributaries of the Susquehanna and this region. These two tributaries, like many other streams in the original study, have been disturbed by coal mining activities.

Following the additional reconnaissance, the conclusions about the low potential for liquefaction in the area remain unchanged. The rugged terrain of the Allegheny Mountains, narrow floodplains, and intense modification of the topography through anthracite coal mining confirm those conclusions. The Susquehanna River is a gently meandering river with numerous rock-core islands and boulder-cobble gravel bars. At nearly all sites that were visited, bedrock was present or nearby. The ubiquitous presence of bedrock at or near the surface militates against liquefaction and the presence of paleoliquefaction structures. The tributaries of the Susquehanna have narrow floodplains. Coal mining debris from mine waste dumps, carried by the tributary streams of the Susquehanna, form the visible floodplain deposits of the tributaries.

Fine-grained sediments, when present, are thin and lack the usual prerequisites for liquefiable deposits, which are a fine to medium sand overlain by 1-2 meters of fine upward silt with a clay cap. However, the banks are commonly vegetated, which significantly reduces accessibility to exposures in the river banks. Further modification of the banks by manmade stone walls, built to prevent erosion of the railroad right-of-way and sections of an early canal, exist through the studied section of the Susquehanna River.

In the spring of 2010, another reconnaissance was undertaken to investigate the new portion of the site area (5 mile radius (8 km)) that was made available by relocation of the site approximately 1000 feet (305 m) to the north-northwest. The area studied forms a crescent shaped zone on the north-northwest edge of the new site area that is 1000 feet (305 m) wide at its widest, by approximately 15 miles (24 km) long. As is typical with most of Pennsylvania and the site area, outcrop is limited. For this reason, targets for investigation and ground truthing were areas of known or suspected outcrop within and around the crescent zone. The main areas of investigation were therefore locations on Lee Mountain, Huntington Mountain, Shickshinny Mountain, Penobscot Mountain, and the Mocanaqua, Pond Hill and Berwick

Heights areas, as well as a few locations outside of the site area where the Light Street Fault has been mapped.

In all outcrops investigated, the orientations of bedding, joint surfaces and lineations were measured and rock lithologies recorded. Due to prior detailed mapping in the area (Inners, 1978) all rock units had previously been identified. The other main objective of the reconnaissance was to look for any evidence of Quaternary faulting.

The observations and measurements made as part of this investigation did not reveal anything inconsistent with the findings of the previous BBNPP reconnaissance efforts or with prior geologic mapping in the area (e.g., Inners, 1978). All measurements were consistent with the mapped structures, all rock lithologies were consistent with unit descriptions and no evidence of recent faulting was observed, including in the area of the mapped Light Street Fault.

2.5.3.1.4 Compilation and Review of Existing Data and Literature

The existing body of geologic and geotechnical data regarding faulting in the vicinity of the proposed BBNPP site is contained in the following principal sources, as discussed in the three sections below:

1. Work performed for the existing Susquehanna Steam Electric Station (SSES) Units 1 and 2 and complementary structures (SSES FSAR, 2003).
2. Published geologic mapping performed primarily by the USGS and Pennsylvania Department of Conservation and Natural Resources (DCNR, 2007).
3. Seismicity data compiled and analyzed in published journal articles.

2.5.3.1.4.1 Work at the SSES Units 1 and 2

The most detailed previous subsurface exploration near the BBNPP site was performed as part of the original SSES FSAR (SSES FSAR, 2003) for the SSES Units 1 and 2 foundation and supporting structures. That exploration covered an area that is located adjacent to the east side of the BBNPP site and was completed to address the same issues as the current BBNPP FSAR investigation. The high level of detail in that earlier study, and the close proximity to the BBNPP site make that study especially relevant to the current effort. The level of effort for that earlier FSAR study included drilling 250 geotechnical boreholes, collecting down-hole geophysical data, and acquiring seismic refraction data from across the site. Previous site investigations performed for the existing units are summarized in the SSES Final Safety Analysis Report (FSAR) (SSES FSAR, 2003). As cited in the SSES FSAR, these previous investigations provide the following results documenting the absence of Quaternary faults:

- ◆ Interpretation of satellite photos and topographic maps. This interpretation revealed no evidence of surface rupture, surface warping, or offset of geomorphic features indicative of active faulting.
- ◆ Interviews with personnel from government agencies and private organizations. These interviews concluded that no known faults are present beneath the existing SSES Units 1 and 2 site area.
- ◆ Seismicity Analysis -This analysis showed that no microseismic activity has occurred in the site area; the site is located in a region that has experienced only infrequent minor earthquake activity approximately 35 mi (56 km) northeast of the BBNPP site, between

Lackawanna and Wyoming Counties; the closest fault-related epicentral location (the Anthracite Zone) is greater than 25 mi (40 km) away. No earthquake within 50 mi (80 km) of the SSES site has been large enough to cause significant damage in the time the region has been populated, approximately 270 years.

- ◆ Approximately 250 exploratory boreholes were drilled at the SSES Units 1 and 2 site area. Borehole data have provided evidence for the lateral continuity of strata across the existing SSES site area (SSES FSAR, 2003). The inspection of soil samples has revealed no adverse effects indicative of geologically recent or active faulting.
- ◆ Field reconnaissance of many surface outcrops at the site and within the 25 mi (40 km) radius of the site, coupled with geophysical surveys, provided no evidence for faulting at the SSES site.
- ◆ At the time of the original studies for the SSES FSAR (SSES FSAR, 2003), published maps showing bedrock faults within a 5 mi (8 km) radius of the SSES site identified only the Light Street fault. The closest significant bedrock faults mapped prior to 1975 were faults located about 80 mi (129 km) southwest of the SSES site near Lewistown, PA (SSES FSAR, 2003).

2.5.3.1.4.2 Published Geologic Mapping

Since the late 1960s, extensive mapping of the BBNPP site region within the Ridge and Valley Province has been performed by the Pennsylvania Geological Survey (PGS) and other governmental agencies to improve knowledge of the Ridge and Valley stratigraphy and other geologic structures within the region (Inners, 1978; Wheeler, 2006). Local mapping includes geologic mapping across the BBNPP site area (Inners, 1978) (Figure 2.5-134), a developed geologic section through the central Appalachian Basin (Ryder, 1992) (Figure 2.5-128) and associated stratigraphic column (Figure 2.5-52), and a Precambrian Basement Map (Gold, 2005) based on borehole and seismic reflection data (Figure 2.5-130). This compilation of previous mapping and exploration studies provides the principal basis for the few bedrock faults recognized within the site area.

A local geologic section, oriented approximately north-south within the site area (5 mi (8 km) radius), depicts slightly faulted anticlinal Silurian-Mississippian bedrock that is unconformably overlain by unconsolidated Pliocene-Holocene deposits, as shown in Figure 2.5-135 (Inners, 1978). A review of the SSES FSAR reported the presence of the Light Street Fault but failed to uncover evidence, through either published reports or field investigations, to support the existence of the inferred Berwick fault (SSES FSAR, 2003). Folds, as reported by Inners (Inners, 1978), are prevalent structures throughout the bedrock of the BBNPP site, mainly in second- and third-order. The major structure of the area is the Berwick Anticlinorium, a moderately complex, first order fold that passes through the center of Figure 2.5-134 and 2.5-135 (Inners, 1978).

However, the most detailed section of the site area was created by Inners (Inners, 1978) as part of a study conducted on behalf of the Commonwealth of Pennsylvania Department of Environmental Resources-Bureau of Topographic and Geologic Survey. This geologic cross-section, Figure 2.5-135 (see Figure 2.5-134 for location of cross-section), was developed extending from just north of Lee Mountain, northwest of the BBNPP site, to near Black Creek, just south of Nescopeck Mountain, south of the BBNPP site. This section depicts moderately dipping, un-deformed geologic contacts between the Middle Devonian Mahantango Formation, the overlying Middle Devonian Harrell Formation, and underlying Marcellus Formation.

As shown on Figure 2.5-134 and Figure 2.5-140, the Light Street Fault (DCNR, 2007) and the Berwick Anticlinorium (Inners, 1978) have been mapped within the 5 mi (8 km) radius of the BBNPP site. In addition, two other structures have been proposed within the 5 mi (8 km) radius of the site, the Lackawanna Synclinorium (Inners, 1978), approximately 4 mi (6.4 km) northwest of the BBNPP site, and the inferred Berwick fault (Inners, 1978) (DCNR, 2007), approximately 3 mi (4.8 km) southwest of the BBNPP site. All of these structural features are consistent with published evidence of the intense folding and faulting that occurred to the bedrock formations during the Alleghanian Orogeny, as discussed in Section 2.5.1 (Faill, 1999; Harper, 1999; Way, 1999). The Light Street fault, inferred Berwick fault (Inners, 1978) (DCNR, 2007) and inferred folds (Inners, 1978) are described previously in Section 2.5.1. None of these features are considered capable tectonic sources, as defined in Appendix A of Regulatory Guide 1.165 (NRC, 1997).

Considering the evidence provided above, as well as the previous site investigations (SSES FSAR, 2003) discussed in Section 2.5.3.1.1, and the field reconnaissance interpretation undertaken for the BBNPP study, no evidence of Quaternary deformation has been reported in the literature or observed on the site for the Light Street or Berwick faults, or the Berwick Anticlinorium.

In summary, numerous investigations of the BBNPP site vicinity have found that the Alleghanian aged folding is not associated with any active deep seated basement faulting beneath the BBNPP site area, and no signs of tectonic deformation exist within the exposed Quaternary deposits near the BBNPP site. Collectively, the published geologic information for the BBNPP site area, combined with regional geologic sections (Inners, 1978; Williams, 1987) and site and aerial reconnaissance, indicate the absence of Pleistocene and younger faulting and folding. A review of local geologic sections (Figure 2.5-135 and Figure 2.5-141) suggest that the features, if present, are not prominent structures and are not developed within the Quaternary age units. In conclusion, there are no known tectonically active faults within the site area, and the Light Street fault and Berwick fault (if present) have been last active in the Late Permian (Inners, 1978).

2.5.3.1.4.3 Recent Seismicity Compilations

The USGS completed a compilation of all Quaternary faults, liquefaction features, and possible tectonic features in the eastern U.S. (Crone, 2000) (Wheeler, 2005) (Wheeler, 2006). These compilations do not show any Quaternary faults or features within a 25 mi (40 km) radius of the site, as shown in Figure 2.5-140. The nearest reported capable Quaternary feature (Crone, 2000) is the Cacoosing Valley earthquake (Number 7 on Figure 2.5-131), part of the Lancaster seismic zone (Number 8), approximately 52 mi (84 km) south of the BBNPP site. The closest documented paleo-liquefaction site is known as the Clinton-Newbury liquefaction features (Number 21), and is located over 260 mi (418 km) from the BBNPP site, in northeastern Massachusetts (Crone, 2000).

As was reported in Section 2.5.2, the locations of earthquakes were accounted for by an updated CEUS SSC catalog (EPRI/DOE/NRC, 2012). Figure 2.5-51 shows two earthquakes lying within the 25 mi (40 km) radius of the BBNPP site. Faill (Faill, 2004) identifies the event to the south of the site as a quarry blast or mine collapse. The event to the east-northeast is a microearthquake with $E[M]$ 2.49. Neither of these events was related to a capable tectonic source. Based on this information, there are no significant hazard potential faults within a 25 mi (40 km) radius of the BBNPP site.

2.5.3.2 Geological Evidence, or Absence of Evidence, for Surface Deformation

Based on the discussions in the preceding sections, no evidence for surface deformation has been found for this site vicinity. The evidence against that deformation is as follows:

- ◆ No subsurface offsets within the BBNPP Property Boundary, on the adjacent property for the SSES, or in the site vicinity where literature sources infer faults to exist.
- ◆ No capable faults mapped within 25 miles (40 km) of the site (at the local or regional scale).
- ◆ Only very minor tectonically related seismic activity recorded within 25 miles (40 km) of the site.
- ◆ No evidence of prehistoric ground motion (liquefaction features) within the site area.

2.5.3.3 Correlation of Earthquakes with Capable Tectonic Sources

As presented in Figure 2.5-51, two seismic event epicenters are located within the 25 mi (40 km) radius of the BBNPP site. Faill (Faill, 2004) places the event to the south in the category of quarry blast or mine collapse. No reported historical earthquake epicenters have been associated with either of the bedrock faults (Light Street or Berwick faults) located within the 25 mi (40 km) radius of the BBNPP site vicinity. The distribution of earthquakes from the catalog supports the following conclusions:

- ◆ There are no earthquakes within the site vicinity that are associated with a known geologic or tectonic structure.
- ◆ The updated catalog of earthquake events does not indicate a unique cluster of seismicity in the area that would suggest a local seismic source outside of the EPRI/DOE/NRC CEUS SSC model (EPRI/DOE/NRC, 2012).
- ◆ The catalog does not show a pattern of seismicity that would require significant revision to the EPRI/DOE/NRC (2012) seismic source geometry.

2.5.3.4 Ages of Most Recent Deformations

As presented in Section 2.5.1.2.4, the local tectonic features located within 5 mi (8 km) of the BBNPP site (the Light Street fault, the inferred Berwick fault, the Berwick Anticlinorium, and the Lackawanna Synclinorium) do not exhibit evidence of Quaternary activity. They are interpreted to have formed during the Paleozoic Era as part of the regional Alleghanian Orogeny and have been inactive since that time (Inners, 1978). This interpretation is based on detailed field mapping that showed that these faults are covered by undisturbed terrace gravels and that the faults and folds are observed to affect only Mississippian and older units (Inners, 1978). Other than highly folded and cleaved Mahantango Shale in the vicinity of the mapped Light Street fault and thickened or missing Devonian units in a limited number of well logs (Inners, 1978), there is no other evidence of these faults. Because of the undeformed surficial cover over the faulted areas, no conclusive evidence that would indicate the nature or orientation of the faults can be observed (Inners, 1978), further supporting that there has been no Quaternary movement on these faults.

Lack of Quaternary deformation is further confirmed for the site by the seismic refraction survey performed during all field investigation efforts. All refraction profiles (Figure 2.5-57 through Figure 2.5-65) indicate consistent layering of soils and rock units below the site with no offset of contacts. The profiles indicate that erosion and weathering have been the

dominant geologic activities affecting the Mahantango Shale since the Alleghanian Orogeny ended in the Late Permian Period.

Through all of the field efforts undertaken during this investigation, no evidence of Quaternary deformation of any kind was observed in any surficial sediments or at the Quaternary deposits-bedrock interface, confirming the earlier detailed field studies. Based on a review of available published geologic literature, field reconnaissance, and interpretation of aerial photography, tectonic deformation associated with the local structures is constrained to the Late Permian Period at the latest, and does not affect Quaternary aged deposits (Inners, 1978) (Williams, 1987) (DCNR, 2007).

2.5.3.5 Relationship of Tectonic Structures in the Site Area to Regional Tectonic Structures

All four of the features evaluated within the 5 mi (8 km) radius of the BBNPP site (Light Street fault, Berwick fault, Berwick Anticlinorium, and Lackawanna Synclinorium) have been linked with regional tectonic events, mainly the Alleghanian Orogeny, and have been inactive since Late Permian time. Tectonic models hypothesize that the crystalline basement underlying the BBNPP site was accreted to a pre-Taconic North American margin during the Precambrian (Eriksson, 2003). Episodes of continental collisions have produced a series of accreted terrains that are separated, in part, by low-angle detachment faults (Pohn, 2000), as discussed in detail in Section 2.5.1.1.2. In association with these continental collisions, the Paleozoic bedrocks of eastern North America, including the Ridge and Valley Province, contain a number of generally northeast striking thrust faults (Schlische, 2003) such as the Light Street fault and the inferred Berwick fault. The Berwick Anticlinorium and Lackawanna Synclinorium are both results of regional extension and compression due to the orogenic events discussed in detail in Section 2.5.1.1.2.

2.5.3.6 Characterization of Capable Tectonic Sources

None of the mapped bedrock structures located within the site vicinity is considered to be a capable tectonic source as defined by Regulatory Guide 1.208 (NRC, 2007). This conclusion is based on the following observations:

- ◆ The Light Street and the inferred Berwick faults are inactive, and were most recently active in the Late Permian, approximately 250 Ma.
- ◆ There is no deformation of Quaternary age deposits identified in either the literature review or during the site investigations for this study.
- ◆ There is no association of historical earthquakes with any local fault or any cluster of seismicity within the site area that would indicate the presence of a capable source.

2.5.3.7 Designation of Zones of Quaternary Deformation Requiring Detailed Fault Investigation

There are no zones of Quaternary deformation requiring detailed investigation within the BBNPP site area. A review and interpretation of digital elevation models coupled with aerial reconnaissance identified few discontinuous north to northeast-striking lineaments. None of these lineaments are interpreted as fault-related, or are coincident with the Light Street fault or the inferred Berwick fault.

2.5.3.8 Potential for Tectonic or Non-Tectonic Deformation at the Site

The potential for tectonic deformation at the BBNPP site is negligible. This conclusion is based on the following:

1. No evidence for faulting in the subsurface investigation of the BBNPP site.
2. No evidence of faulting in either the detailed subsurface investigation at the adjacent SSES site, or in outcrops within the site area.
3. No evidence of paleoliquefaction found at the site or surrounding site area.
4. No historical seismic activity or mapped capable faults within the site vicinity.

Collectively, these data support the interpretation for the absence of any Quaternary surface faults or capable tectonic sources within the BBNPP site area. In addition, there is no evidence of non-tectonic deformation at the site, such as glacially induced faulting, collapse structures, growth faults, salt migration, or volcanic intrusion.

2.5.3.9 References

CFR, 2007a. Title 10, Code of Federal Regulations, Part 100, Reactor Site Criteria, 2007.

CFR, 2007b. Title 10, Code of Federal Regulations, Part 50, Appendix S, Earthquake Engineering Criteria for Nuclear Power Plants, 2007.

Crone, 2000. Data for Quaternary Faults, Liquefaction Features, and Possible Tectonic Features in the Central and Eastern United States, East of the Rocky Mountain Front, U.S. Geological Survey, Open-File Report 00-260, p 1-332, A.J. Crone and R.L. Wheeler, 2000.

DCNR, 2007. Geologic Map of Pennsylvania, Pennsylvania Department of Conservation and Natural Resources, Website: <http://www.dcnr.state.pa.us/topogeo/maps/map7.pdf>, Date accessed: December 14, 2007.

Eriksson, 2003. Predominance of Grenvillian Magmatism Recorded in Detrital Zircons from Modern Appalachian Rivers, *The Journal of Geology*, Volume 111, p 707-717, Kenneth A. Eriksson, Ian H. Campbell, J. Michael Palin, and Charlotte M. Allen, 2003.

EPRI/DOE/NRC, 2012. Technical Report: Central and Eastern United States Seismic Source Characterization for Nuclear Facilities, EPRI Report # 1021097, U.S. DOE Report # DOE/NE-0140, U.S. NRC NUREG-2115, Electric Power Research Institute, Palo Alto, CA, U.S. DOE, U.S. NRC, 2012.

Fail, 1999. Appalachian Mountain Section of the Ridge and Valley Province, *The Geology of Pennsylvania*, Part III. Structural Geology and Tectonics, Chap. 19, p. 268-285, R. Fail and R. Nickelsen, 1999.

Fail, 2004. The Birdsboro Basin, *Pennsylvania Geology*, Volume 34, Number 4, p 2-11, R. T. Fail, 2004.

GeoVision, 2010. Final Report - Seismic Refraction Investigation Bell Bend Nuclear Power Plant, Luzerne County, Pennsylvania Report 10171-03 Rev. 0, Report Prepared for RIZZO by GeoVision Geophysical Services, Corona, CA, August 2010.

Gold, 2005. Basement depth and related geospatial database for Pennsylvania, Pennsylvania Geological Survey, 4th ser., Open-File General Geology Report 05-01.0, Pennsylvania Department of Conservation and Natural Resources, downloaded from www.dcnr.state.pa.us/topogeo/openfile/basementmap.aspx, D. Gold, 2005.

Harper, 1999. Part II, Stratigraphy and Sedimentary Tectonics, Chapter 7: Devonian, in C.H. Shultz ed., *The Geology of Pennsylvania: Pennsylvania Bureau of Topographic and Geologic Survey Special Publication 1*, p 108-127, J.A. Harper, 1999.

Inners, 1978. Geology and Mineral Resources of the Berwick Quadrangle, Luzerne and Columbia Counties, Pennsylvania, Pennsylvania Geological Survey, Fourth Series, p 1-34, J.D. Inners, 1978.

NRC, 1997. Identification and Characterization of Seismic Sources and Determination of Safe Shutdown Earthquake Ground Motion, Regulatory Guide 1.165, U.S. Nuclear Regulatory Commission, March 1997.

NRC, 2007. A Performance-Based Approach to Define the Site-Specific Earthquake Ground Motion, Regulatory Guide 1.208, U. S. Nuclear Regulatory Commission, March 2007.

Pohn, 2000. Lateral Ramps in the Folded Appalachians and in Overthrust Belts Worldwide- a Fundamental Element of Thrust-Belt Architecture, U.S. Geological Survey Bulletin 2163, p 1-63, H.A. Pohn, 2000.

Ryder, 1992 Stratigraphic Framework of Cambrian and Ordovician Rocks in the Central Appalachian Basin from Medina County, Ohio, through Southwestern and South-Central Pennsylvania to Hampshire County, West Virginia, US Geological Survey Bulletin 1839, p 1-40, R.T. Ryder, A.G. Harris, and J. E. Repetski, 1992

Schlische, 2003. Progress in Understanding the Structural Geology, Basin Evolution, and Tectonic History of the Eastern North American Rift System, P. leTourneau and P. Olsen, eds., *The Great Rift Valleys of Pangea in Eastern North America*, Vol. 1, p 21-64, R. Schlische, 2003.

SSES FSAR, 2003. Susquehanna Steam Electric Station Final Safety Analysis Report, Section 2.5, Geology, Seismology, and Geotechnical Engineering, Rev. 58, PPL Susquehanna, LLC, 2003.

Way, 1999. Part IV, Physiography, Chapter 29: Appalachian Mountain Section of the Ridge and Valley Province, in C.H. Shultz ed., *The Geology of Pennsylvania: Pennsylvania Bureau of Topographic and Geologic Survey Special Publication 1*, p 353-361, J.H. Way, 1999.

Wheeler, 2005. Known or Suggested Quaternary Tectonic Faulting, Central and Eastern United States-New and Updated Assessments for 2005, U.S. Geological Survey, Open-File Report 2005-1336, R.L. Wheeler, 2005.

Wheeler, 2006. Quaternary tectonic faulting in the Eastern United States, *Engineering Geology*, Volume 82 (2006), p 165-186, R.L. Wheeler, 2006.

Williams, 1987. Groundwater Resources of the Berwick-Bloomsburg-Danville Area, East-Central Pennsylvania, Pennsylvania Dept of Environmental Resources, Topographic and Geologic Survey, Water Resource Report 61, 76 p., J. Williams and D. Eckhardt, 1987.

2.5.4 Stability of Subsurface Materials and Foundations

The U.S. EPR FSAR includes the following COL Item for Section 2.5.4:

A COL applicant that references the U.S. EPR design certification will present site-specific information about the properties and stability of soils and rocks that may affect the nuclear power plant facilities, under both static and dynamic conditions including the vibratory ground motions associated with the CSDRS and the site-specific SSE.

This COL Item is addressed as follows:

{This section addresses site-specific subsurface materials and foundation conditions. It was prepared based on the guidance in relevant sections of NRC Regulatory Guide 1.206, Combined License Applications for Nuclear Power Plants (LWR Edition) (NRC, 2007a).

The Susquehanna Steam Electric Station (SSES) Units 1 and 2 Final Safety Analysis Report (FSAR) (PPL, 2011) contains a summary of the geotechnical information collected previously for the construction of SSES Units 1 and 2. The planned Bell Bend NPP is to be located approximately 0.5 mi (0.8 km) west of SSES Units 1 and 2. The geologic and geotechnical work performed for the BBNPP is a "stand-alone" investigation. The outcome and conclusions do not rely on the existing SSES Units 1 and 2 FSAR.

During the period from August 2007 through November 2007, an initial geotechnical and geophysical site investigation program was implemented at the BBNPP site. In 2010, the BBNPP Power Block location was moved approximately 1,000 ft (304.8 m) north-northwest (NNW) of the original location, and a second site-specific investigation was performed for the new location. Data from the 2007 field investigation were used to a great extent in the development of the 2010 field investigation program. The information presented in this section is based on results of the 2010 site-specific subsurface investigation program implemented at the BBNPP site, and evaluation of the collected data, unless stated otherwise.

For the establishment of the horizontal datum, Pennsylvania State Plane Coordinate System (North Zone), North American Datum of 1983 (NAD 1983) is utilized. For the establishment of the vertical datum, North American Vertical Datum of 1988 (NAVD 88) is utilized, unless stated otherwise.

2.5.4.1 Geologic Features

Section 2.5.1.1 addresses the regional geologic settings, including regional physiography and geomorphology, regional geologic history, regional stratigraphy, regional tectonic and non-tectonic conditions, and geologic hazards, as well as maps, cross-sections, and references. Section 2.5.1.2 addresses the geologic conditions specific to the site, including site structural geology, site physiography and geomorphology, site geologic history, site stratigraphy and lithology, site structural geology, seismic conditions, and site geologic hazard evaluation, accompanied by figures, maps, and references. Pre-loading influences on soil deposits, including estimates of consolidation, pre-consolidation pressures, and methods used for their estimation are addressed in Section 2.5.4.2. Related maps and stratigraphic profiles are also addressed in Section 2.5.4.2.

The BBNPP site is located in the Ridge and Valley Physiographic Province (Inners, 1978). The overburden soil at the site is composed of residual soils that formed from weathering of the underlying Devonian Shale bedrock, with only isolated patches of glacial till present in some places. The thickness of what could be associated with till deposits, is no more than 3 ft (0.9 m). The hill within the BBNPP Power Block was likely completely covered by some thickness of till after the glaciers retreated, but has been largely eroded away at this time. However, at lower elevations, below the break in slope of this upland region, such as the location of the Essential Service Water Emergency Makeup System (ESWEMS), the overburden transitions into glaciofluvial sediments. Below the soil is a zone of soft weathered rock typically followed by harder, competent shale. The result of glacial erosion above the break in the slope, is found to have only partially removed the top of the weathered bedrock, which is thicker at the site location, and is thinner downhill. Underneath the residual soil and the weathered and fractured rock lies the middle Devonian bedrock denominated the Mahantango Formation, part of the Hamilton Group. This formation is characterized by dark gray, slightly fossiliferous, hard shale and was found to be at least 420 ft (128 m) thick based upon the BBNPP site geotechnical investigation. Harper (Harper, 1999) describes the Mahantango Formation as "a complex series of interbedded shales, siltstones, and sandstones ranging from 1,200 ft (366 m) to 2,200 ft (671 m)" although Inners (Inners, 1978) reports a site specific thickness of approximately 1,500 ft (457 m). The shales and siltstones encountered during the BBNPP site investigation were typically dark gray, ranged in hardness from soft to moderately hard, increased progressively in the level of calcareous content with depth, and were slightly pyritic and fossiliferous throughout. Harper (Harper, 1999) suggests that the Mahantango Formation was deposited as a prograding marine shoreline during the early stages of the Catskill delta.

The glacial overburden soils and the Mahantango Formation were the subject of a detailed subsurface exploration for the COL investigation, as described below.}

2.5.4.2 Properties of Subsurface Materials

The U.S. EPR FSAR includes the following COL Item in Section 2.5.4.2:

A COL applicant that references the U.S. EPR design certification will reconcile the site-specific soil and backfill properties with those used for design of U.S. EPR Seismic Category I structures and foundations described in Section 3.8.

This COL Item is addressed as follows:

{A comprehensive field investigation and associated laboratory testing has been performed for the BBNPP site. This subsection presents the properties of underlying materials encountered. It is divided into five subsections, as follows.

- ◆ Section 2.5.4.2.1 provides an introduction to the soil profile and subsurface conditions,
- ◆ Section 2.5.4.2.2 provides a description of the field investigation program, including borings, sampling, and in-situ tests,
- ◆ Section 2.5.4.2.3 provides a description of the laboratory testing program,
- ◆ Section 2.5.4.2.4 provides a narrative on the origin and characteristics of the engineered fill soils, and
- ◆ Section 2.5.4.2.5 provides the BBNPP recommended soil properties for analysis and design of foundations.

2.5.4.2.1 BBNPP Soil Profile

The natural topography at the BBNPP site, at the time of the subsurface exploration, was a downward gentle slope towards the west and south of the Power Block, and gently sloping within the vicinity of the ESWEMS Pond. The maximum variation in relief was about 135 ft (41 m) across the site. Ground surface elevations at the time of field exploration ranged from approximately 667 to 802 ft (203 to 244 m), with an average elevation of about 739 ft (225 m). The ground surface elevations in the Power Block area ranged from about 694 to 802 ft (211 to 244 m), with the centerline of the BBNPP through the Reactor Building at an elevation of 748 ft (228 m). The Power Block includes the Reactor Building, Fuel Pool Building, Reactor Auxiliary Building, Safeguard Buildings, Radioactive Waste Processing Building, Emergency Power Generator Buildings, Essential Service Water Buildings, and Turbine Building. The ESWEMS Pump House is the only building located in the ESWEMS Pond area.

The upper 420 ft (128 m) of the subsurface structure were the subject of the BBNPP subsurface investigation. The site geology is comprised of an overburden soil deposit underlain by bedrock. In general, the subsurface structure is divided into the following stratigraphic units:

- ◆ **Overburden Soil** - Glacial Till
- ◆ **Mahantango Formation** - this unit was further divided into three horizons for the BBNPP site as follows:
 - ◆ **Weathered Rock** - intensely weathered yellowish gray shale
 - ◆ **Transition Zone** - moderately weathered, moderately fractured, medium to dark gray shale
 - ◆ **Sound (Competent) Rock** - massive medium to dark gray shale.

Identification of soil and rock layers was based on their physical and engineering characteristics. The characterization of the soils and rocks was based on a suite of tests performed on these soils and rocks, consisting of standard penetration tests (SPT) in soil borings including auto-hammer energy measurements, rock coring, geophysical testing, pressuremeter tests (PMTs) and laboratory testing.

Figure 2.5-122 and Figure 2.5-123 provide the generic subsurface profiles for the Power Block and ESWEMS Pond area, respectively. Within the Power Block, the overburden soils were derived from intensely weathered shale, and there are two generic subsurface profiles (Subsurface Profiles 1 and 2) as shown in Figure 2.5-122. In Subsurface Profile 1, there is a clear distinction between the Weathered Rock and Transition Zone. However, in Subsurface Profile 2 there is no clear distinction between the Weathered Rock and Transition Zone. Within the ESWEMS Pond area, the overburden soils were derived from fluvial and glacial deposits, and there were no Weathered Rock and/or Transition Zone present as shown in Figure 2.5-123 (Subsurface Profile 3).

The thickness of the overburden soil varies from 7.5 to 60 ft (2.3 to 18.3 m) within the Power Block, and from 12.2 to 54.5 ft (3.7 to 16.6 m) within the ESWEMS Pond area. The thicknesses of the Weathered Rock and Transition Zone vary from 0 to 46.3 ft (0 to 14.1 m) and from 0 to 84 ft (0 to 25.6 m), respectively. The overburden soil, weathered rock and transition zone are not adequate foundation strata for safety-related structures or facilities that will impose high contact pressures, even though these subsurface horizons have shear wave velocities in excess of 1000 ft/sec (305 m/s).

The Sound (Competent) Rock of the Mahantango Formation is dark gray to black, thin-bedded to massive-bedded shale, with few to no fractures. There are also calcareous zones, thin pyrite lenses that increase in abundance with depth, and calcite veins perpendicular to the bedding plane that show 0 to 0.25 in (0 to 0.64 cm) displacement. During field investigation, Sound Rock was defined as having a Rock Quality Designation (RQD) greater than 75 percent. For SSES Units 1 and 2, this layer supports safety-related structures (PPL, 2011).

The thicknesses and termination elevations of stratigraphic units are summarized in Table 2.5-13. The table provides the minimums, maximums, and averages of forty-four (44) geotechnical and nine (9) hydrogeological boring logs, for the entire site, Power Block and ESWEMS Pond Area. The positions of the soil and rock strata are best visualized using cross section drawings and contour elevation plots that are developed at locations of the safety related facilities. The following figures are presented for visualization purposes:

- ◆ Figure 2.5-77, Boring Location Plan
- ◆ Figure 2.5-78, Location of Geotechnical Subsurface Sections
- ◆ Figure 2.5-141, Geotechnical Subsurface Section A-A
- ◆ Figure 2.5-142, Geotechnical Subsurface Section B-B
- ◆ Figure 2.5-143, Geotechnical Subsurface Section C-C
- ◆ Figure 2.5-144, Geotechnical Subsurface Section D-D
- ◆ Figure 2.5-145, Geotechnical Subsurface Section E-E
- ◆ Figure 2.5-146, Geotechnical Subsurface Section F-F
- ◆ Figure 2.5-79, Surface Elevation Contours for Powerblock
- ◆ Figure 2.5-80, Overburden Soil Thickness for Powerblock
- ◆ Figure 2.5-81, Thickness of Weathered Rock for Powerblock
- ◆ Figure 2.5-84, Thickness of Transition Zone for Powerblock
- ◆ Figure 2.5-82, Elevation Sound (Competent) Rock for Powerblock
- ◆ Figure 2.5-83, Overburden Soil Thickness and Elevation of Sound Rock (Area near Essential Service Water Emergency Makeup System - ESWEMS)

2.5.4.2.2 Field Investigation Program

A thorough field investigation program was designed and implemented at the BBNPP site. The program included:

- ◆ Boring Program,
- ◆ Wash Rotary Drilling/NQ Wireline Coring,
- ◆ In-Situ Pressuremeter Testing,
- ◆ Geophysical Exploration,

- ◆ Downhole Tests,
- ◆ PS Suspension Logging Tests,
- ◆ Deviation Surveys,
- ◆ Refraction Surveys.

The field investigation was performed under the guidance provided in NRC Regulatory Guide 1.132, "Site Investigations for Foundations of Nuclear Power Plant" (NRC, 2003a). The work was performed in accordance with work procedures developed specifically for the BBNPP subsurface exploration, including a subsurface exploration plan developed under the Rizzo Quality Assurance Program. Subsection 2.5.4.2.2.1 provides a brief summary of the field investigation conducted for SSES Units 1 and 2, and the field investigation performed during 2007 for the initial BBNPP Power Block location, and subsection 2.5.4.2.2.2 details the field investigation program for the current (2010) BBNPP Power Block location.

2.5.4.2.2.1 Previous Subsurface Investigations

Based on information available from the SSES FSAR (PPL, 2011), it was determined that approximately 250 exploratory borings were made in the soil and rock at the SSES site. The subsurface investigations for SSES Units 1 and 2 began in late 1970 (100 and 200 series borings) to establish general geologic relationships over the site area and to determine the general soil and rock conditions at the site. A more intensive program (300 series borings) was conducted in the Spring of 1971 to define foundation conditions in the principal plant structures area. Two 45-degree angle holes were drilled in the reactor area. Additional exploration drilling was necessary to locate the site for the Susquehanna River intake and discharge structures (700-800 series borings), to define soil and rock conditions at the spray pond and ESSW pumphouse (1100 series and some 400 series borings), and to investigate foundation conditions for the cooling towers (borings B1 to B10) and the railroad spur and bridge over State Highway 11 (borings 417 to 455 and 929 to 940). An investigation program (borings 1 through 7) was conducted in 1983 to determine soil and rock conditions in the area of the diesel generator 'E' building. Because of the safety-related (Category 1) function of the spray pond and ESSW pumphouse, the exploration program for these facilities was comprehensive and included split spoon and undisturbed samples, laboratory testing, hydrologic surveys, permeability tests, and seismic cross-hole and up-hole surveys. Split spoon sample laboratory testing, hydrologic surveys, and permeability tests were also performed in the area of the diesel generator 'E' fuel tank. After completion of geologic borings, static water levels were measured in some of the borings drilled on the site.

Geological descriptions in the SSES FSAR (PPL, 2011) indicate that two primary layers existed at the site, the glacial overburden soils and the bedrock. The site is blanketed by till and glacial outwash which grades upward from a gravelly boulder zone to a surface layer of silty fine sands and sandy silt. The surface layer is believed to be reworked loess. The maximum thickness of overburden is around 40 ft (12 m) in the southern half of the site, with bedrock occasionally cropping out at the surface. North of the east-west bedrock ridge situated just north of the reactors, the glacial deposits fill a valley eroded into bedrock to a depth exceeding 100 ft (30.5 m). The upper bedrock at the site area includes the Middle Devonian Mahantango Formation. The upper part of the Mahantango is a dark gray siltstone, with bedding generally delineated by thin, consistent, light gray, fine-grained sandstone stringers. Beneath the upper member, the Mahantango is comprised of 120 to 150 ft (37 to 46 m) of dark gray, hard calcareous siltstone, typically having bedding obscure to absent and displaying cleavage. This member, which supports the SSES power block structures, is harder, more

massive, and more resistant to erosion than the upper member. Minor faulting in the form of small bedding-plane slips and intraformational shear zones occur, but they are of no significance to the site. They apparently developed during the Paleozoic (more than 200 million years ago) during the Appalachian Orogeny. The zones are typically healed with calcite and quartz.

During the period from August 2007 through November 2007, 45 exploratory boreholes were made in soil and rock at the initial BBNPP Power Block location, for sampling and standard penetration test (SPT) purposes. These boreholes were designated as B-300 Series boreholes. In addition, three G-300 Series boreholes were performed for geophysical testing purposes. Twenty-seven of the B-300 Series boreholes were located in the vicinity of the proposed Category I structures, and the remainder were located in other plant locations. One boring (B-301) was extended to a depth of 400 ft (122m) for detailed core logging and geophysical testing at the proposed location of the Nuclear Island structure. Three G-300 Series destructive drilling boreholes were extended for geophysical testing purposes in the proposed location of the Reactor Building and two Essential Service Water Buildings.

Forty-five (45) B-300 Series borings were advanced with SPT sampling, and 12 undisturbed samples (using Shelby push tubes) collected from the overburden soils. Due to the extremely rocky nature of the overburden, the majority of the borings were advanced using a three inch casing advancer system. All boreholes advanced during the field investigation program, penetrated the rock layer.

The site geology was comprised of glacial soil deposits (glacial till) with an average thickness of 38.7 ft (11.8 m) underlain by bedrock. The Mahantango Formation (bedrock) encountered was thin bedded to massive bedded, with few or no fractures. The upper surface of the Mahantango Formation shows the effects of solution and weathering in a few areas, but it is predominantly very competent and indurated. Previous analysis found the overburden soil to be liquefiable, therefore it was proposed that no in-situ soils in their natural state would be used for foundation or lateral support purposes.

Comparable observations were made on these soil and rock layers from the current (2010) BBNPP investigation borings. Given the reasonably parallel geologic conditions between SSES Units 1 and 2, and BBNPP sites, exploration and testing at BBNPP resulted in enhanced characterization of the subsurface conditions. Findings from previous investigations are not discussed further, unless a differing condition is encountered.

2.5.4.2.2.2 BBNPP Subsurface Exploration

The BBNPP subsurface exploration was performed in accordance with the guidance outlined in Regulatory Guide 1.132 (NRC, 2003a). Deviations are identified at point of use and alternatives and/or basis for deviations are provided.

Regulatory Guide 1.132 (NRC, 2003a) provides guidance on spacing and depth of borings, sampling procedures, in-situ testing, geophysical investigations, etc. This guidance was used in preparing a technical specification, addressing the basis for the BBNPP subsurface exploration. Per Regulation Guide 1.132 (NRC, 2003a), "the minimum required depth of borings in competent bedrock should extend to the greatest depth where discontinuities or zones of weakness or alteration can affect foundations or at least 20 ft (6 m) into sound rock. For safety-related structures, one boring per 10,000 ft² (929 m²) and at least one-fourth of those borings should penetrate into sound rock." In accordance with this guideline, a subsurface exploration program was developed.

In total, 44 boreholes were completed for sampling and standard penetration test (SPT) purposes. These boreholes were designated as the B-400 Series boreholes. In addition, 3 boreholes were advanced for geophysical testing purposes. These boreholes were designated as the G-400 series boreholes.

B-400 Series boreholes were completed for the BBNPP site, of which 27 boreholes were located in the vicinity of the proposed Category I structures and the remainder were located in other plant locations. It was determined that 1 boring (B-401) should be extended to a depth of 420 ft (128 m) for detailed core logging at the location of the proposed Nuclear Island structure. Three G-400 Series destructive drilling boreholes were extended for geophysical testing purposes in the proposed location of the Reactor Building, and two were extended for the Essential Service Water Buildings (ESWBs).

A team consisting of a geologist, a geotechnical engineer, and a member of the project management performed a site reconnaissance prior to start of the field investigation. The focus of this task was to observe the site and assess conditions, locations of borings and wells, and identify potential test relocation areas.

According to Regulatory Guide 1.132 (NRC, 2003a), boreholes with depths greater than 100 ft (30.5 m) should be surveyed for deviation. At the BBNPP site, rock was penetrated at an average depth of 24 ft (7.3 m) and deviation surveys were limited to boreholes with geophysical testing.

Regulatory Guide 1.132 (NRC, 2003a) provides guidance for color photographs of all cores to be taken immediately upon removal from the borehole to document the condition of the soils and rocks at the time of drilling. Undisturbed samples were sealed in steel tubes, and could not be photographed. Sample photography was taken of SPT and rock core samples.

The BBNPP subsurface geotechnical field exploration was conducted from April 2010 through June 2010. This work consisted of an extensive investigation to define the subsurface conditions at the BBNPP site. Locations of the geotechnical field investigation field tests are shown in Figure 2.5-77 (Boring Location Plan), and information relating to the field tests is summarized in Table 2.5-14. Surveying was conducted in order to establish the horizontal and vertical locations of exploration points as shown in Table 2.5-15. Each boring location was investigated for the presence of underground utilities prior to drilling boreholes.

Subsurface explorations were performed using geotechnical drill rigs mounted on trucks or tracked vehicles. Field borings logs and other field records were maintained by a rig geologist (geologist or geotechnical engineer). A rig geologist was assigned to each rig and was responsible for maintaining the field records associated with activities conducted at a specific exploration point.

Forty-four (44) B-Series borings were advanced with SPT sampling, and 11 undisturbed samples (using Shelby push tubes) collected from the overburden soils. Soils were sampled using the SPT sampler in accordance with ASTM D1586 (ASTM, 2008a). Disturbed soil samples were obtained using 1.5-in (3.8-cm) inside diameter split-spoon samplers in conjunction with the SPT, as described by ASTM D1586 (ASTM, 2008a). The split spoon sampler was driven a minimum of 18 in (46 cm) or to refusal. The sampling interval was continuous or 2.5 ft (0.76 m) for borings in the vicinity of Category I structures, and 5 ft (1.5 m) in the vicinity of the proposed non-safety-related structures. At least one boring below each proposed safety-related structure was performed with continuous sampling. The recovered soil samples

were visually described and classified by the rig geologist in accordance with ASTM D2488 (ASTM, 2009b). Two representative samples of the soil recovered from each SPT were placed in glass jars with moisture-preserving lids. The sample jars were labeled, placed in boxes, and transported to the on-site storage facility.

Undisturbed samples were obtained in accordance with ASTM D1587 (ASTM, 2008b) using the push Shelby tubes. Immediately upon sample retrieval, the disturbed portions at both ends of the tube were removed and both ends were trimmed square to establish an effective seal. Both ends of the sample were then sealed with hot wax, filled with sand to the top, covered with plastic caps, and sealed once again using electrician tape and wax to preserve their natural moisture content and prevent soil movement. The tubes were labeled and transported in a vertical orientation to the on-site storage area. Undisturbed samples were stored in an upright position with the top side of the sample up.

All boreholes advanced during the field investigation program, penetrated the rock layer. Rock coring was initiated once the presence of rock was confirmed, that is, 50 blows/6" or 10 hammer refusals. The top of the rock layer was identified by the refusal of the split-spoon sampler and/or by the presence of shale rock fragments in the sampler. Rock coring was performed using wire line core barrels and NQWL dual tube (1.875 in (47.6 mm) core diameter), diamond-tipped rock core tools. Dual tube core barrels, 5 ft or 10 ft (1.5 m or 3 m) in length were used to collect continuous rock samples in accordance with ASTM D2113 (ASTM, 2008c). The recovered rock samples were visually described and classified by the geologist or engineer in accordance with ASTM D5434 (ASTM, 2009a). "Routine care" and "special care" rock core samples were collected during this exploration. Routine care samples were placed directly into wooden rock core boxes with a locking lid and photographed. Wood spacers were placed in the core box when needed to stabilize the core laterally. Special care samples were wrapped tightly in a plastic film and aluminum foil, coated with wax, wrapped in a bubble wrap and stored in a polyvinyl chloride (PVC) tube to preserve the in-situ characteristics.

The rig geologist visually described the core and noted the presence of joints and fractures, distinguishing mechanical breaks from natural breaks where possible. The rig geologist also calculated percent recovery and Rock Quality Designation (RQD) prior to moving the core from the drill site. Field boring logs and photographs were used to document the drilling operations and recovered materials. In borings to be geophysically logged, PVC casing was grouted in place in lieu of the temporary casing.

An on-site storage facility for soil and rock samples was established prior to initiating the boring exploration program. The site facility had to provide adequate temperature control conditions in accordance with Regulatory Guide 1.132 (NRC, 2003a). The soil and rock samples obtained were logged into an inventory system. Samples removed from the facility were noted in the logbook. A chain-of-custody form was completed for all samples removed from the facility. Material storage and handling were in accordance with ASTM D4220 (ASTM, 2007a) and ASTM D5079 (ASTM, 2008d) for soil and rock samples, respectively.

2.5.4.2.2.1 Hammer Calibration and SPT Measurements

The depth of soil and rock penetrated by each borehole is shown in Table 2.5-15. Soil and rock samples retrieved are identified on the boring logs included with the COLA.

Energy measurements were made on the hammer-rod system on the 4 drilling rigs used during the subsurface investigation.

A Pile Driving Analyzer (PDA) was used to acquire and process hammer energy data. A summary of measured energies is provided in Table 2.5-16. Five energy measurements were made for each of the 4 drilling rigs. Energy transfer to the gage locations was estimated using the Case Method, in accordance with ASTM D4633 (ASTM, 2010a). The average energy transfer efficiency measurements ranged from 87 to 91 percent, with an average of 89 percent. As shown in Figure 2.5-141 through Figure 2.5-146, the soil on site is relatively consistent.

Soil samples were collected from the borings by means of Standard Penetration Test (SPT) and tube samples. Samples were collected more frequently in the borings located in the vicinity of the proposed Category I (safety-related) structures for BBNPP. SPT N-values were measured during the sampling and recorded on the boring logs included with the COLA. SPT N-values ranged from 2 blows/ft to 100 blows/ft (2 blows/0.3 m to 100 blows/0.3 m), with an average measured N-value of 43 blows/ft (43 blows/0.3 m). Most of the recordings were done in the overburden soils. It was possible to take a limited amount of readings in the weathered part of the Mahantango Shale. These were typically above 50 counts. SPT information on the overburden soil layer is presented in Table 2.5-17. The variability of measured SPT N-values is presented in Figure 2.5-85. The figure indicates that there is not a consistent relationship between the SPT values and depth. There were some instances for which the behavior of the hammer allowed for the continuation of the test beyond 50 blow counts. The selected subsurface profiles, Figure 2.5-141 through Figure 2.5-146 show the samples collected with their corresponding SPT N-values and classification symbols.

The SPT N-value used in correlations with engineering properties is the value corresponding to 60 percent hammer efficiency, the measured SPT N-values were adjusted based on the energy measurements, in accordance with American Society for Testing and Materials (ASTM) D6066 (ASTM, 2004b). The average energy transfer ratio (ETR) obtained from hammer energy measurements for each drilling rig was applied to the measured SPT N-values. A summary of the measured ETR values for each drill rig is shown in Table 2.5-16. The measured SPT N-values from each boring were adjusted using the ETR value shown in Table 2.5-16 for the drill rig utilized. The adjusted average field-measured N-values are shown in Table 2.5-18.

Figure 2.5-85 indicates the scatter of the SPT blow counts versus the depth. There is no clear pattern and the plot is a reflection of the natural composition of the overburden soil.

2.5.4.2.2.2 Pressuremeter Tests

Pressuremeter tests were conducted in two boreholes on the BBNPP site, PMT-401 and PMT-402 in accordance with ASTM D4719 (ASTM, 2007b) at four depth intervals to measure the volumetric change of a pressurized cell surrounded by in-situ rock, specifically by the weathered Mahantango Formation. The Pressuremeter test is an in situ stress-strain test performed on the wall of a borehole using a cylindrical probe that is expanded in the radial stress direction. The Pressuremeter was field-calibrated using a steel pipe as the surrounding media of the pressure cell. The pressure and displacement gages were properly calibrated and the field geologists matched the serial numbers with the calibration records documentation. Table 2.5-19 presents the results of the borehole pressuremeter tests. These results are later discussed in Section 2.5.4.2.4 within the context of soil and rock properties.

2.5.4.2.2.3 Geophysical Tests

Geophysical tests were conducted in the three G-400 Series boreholes, and one B-Series borehole. Geophysical logging consisted of surface seismic refraction surveys, P-S suspension logging surveys, and downhole velocity measurements.

This section provides a summary of the geophysical surveys undertaken for the BBNPP site. Information obtained from these surveys was utilized in the analysis of and discussions pertaining to the site geology and characterization of geologic features as presented in Subsection 2.5.1.2, and surface faulting potential presented in Subsection 2.5.3.

The location of each test is shown in Figure 2.5-77. Figure 2.5-86, Figure 2.5-87, and Figure 2.5-88, present the plots for compressional and shear wave velocities at the three geophysical borings. The plots provide the results from the two different surveys performed: downhole test, and P-S Suspension Logging.

A surface seismic refraction survey was performed for the 9 profile lines indicated by Figure 2.5-77. The results of the survey are provided by Figure 2.5-54 through Figure 2.5-65. The findings of the refraction survey are consistent with the boring program in the sense that the rock horizon was defined at the position indicated by the boreholes. The measured compressional shear wave velocities are consistent with those obtained from downhole and PS-suspension logging.

Downhole Seismic Velocity Surveys

Downhole seismic velocity surveys were conducted in borings G-401, G-423 and G-426, no less than 10 ft (3 m) and no more than 15 ft (4.6 m) from their corresponding B-400 Series borings. In the three borings, installation of PVC casing was critical for acquiring good downhole data. The space between the outside of the casing was filled with low-strength grout to ensure that the casing follows the motions of the adjacent soil exactly. The boreholes were purged of water to a depth of 40 ft (12.2 m) to reduce the effect of tube waves, traveling down the borehole.

Downhole seismic velocity surveys are conducted by measuring the time for seismic waves (generated by an impulsive source at the surface) to travel to a sensor located at a sequence of depths in the borehole. A typical sensor consists of three orthogonal geophones. The two horizontal geophones are used to detect shear-wave (S-wave) arrivals and a vertical geophone is used to detect compression-wave (P-wave) arrivals. Various methods are used to align one of the horizontal geophones with the source polarization. At each measurement level, the sensor assembly is locked to the borehole wall using a clamping mechanism so that the geophones will couple with the seismic signals propagating in the earth.

Seismic waveforms for each depth interval are analyzed and the travel time picked from those waveforms. Interval velocities are calculated and reported as seismic velocity versus depth. This procedure is typically repeated every 2.5 ft (0.76 m) through overburden soil, and every 5 ft (1.5 m) through bedrock. The shear wave source was a wooden plank approximately 6 in x 6 in x 8 ft (15 cm x 15 cm x 2.4 m) with steel end caps and cleats attached to the bottom to better couple with the ground. The compressional wave (P-wave) source was sledge hammer blows on a steel or aluminum plate adjacent to the borehole.

P-S Suspension Logging

P-S suspension logging was performed in three boreholes. P-S suspension velocity logging was performed in borings G-401, G-423, and G-426 shown in Figure 2.5-77. The objective of the suspension and downhole logging tests was to obtain shear wave (V_s) and compressional wave (V_p) velocity measurements as a function of depth within each borehole.

In the absence of an accepted ASTM standard, the following procedure was used to perform P-S suspension velocity logging. P-S suspension velocity logging uses a 21 ft (6.4 m) probe

containing a source near the bottom, and two geophone receivers spaced 3.3 ft (1 m) apart, suspended by a cable. The probe is lowered into the borehole to a specified depth where the source generates a pressure wave in the borehole fluid. The pressure wave is converted to seismic waves (P-wave and S-wave) at the borehole wall. At each receiver location, P- and S-waves are converted to pressure waves in the fluid and received by the geophones mounted in the probe, which in turn send the data to a recorder on the surface. At each measurement depth, two opposite horizontal records and one vertical record are obtained. This procedure is typically repeated every 1.6 ft (0.5 m) or 3.3 ft (1 m) as the probe is moved from the bottom of the borehole toward the ground surface. The elapsed time between arrivals of the waves at the geophone receivers is used to determine the average velocity of a 3.3 ft (1 m) high column of soil around the borehole.

Surface Seismic Refraction Surveys

Surface seismic refraction surveys are used to generate a cross sectional acoustic image of the subsurface strata. This method identifies mapping depth to bedrock, identifying voids, determining strength and quality of bedrock, and locating faults or steeply dipping contacts. The geophysical refraction seismic survey was performed in 9 selected lines as shown by Figure 2.5-77. The seismic data acquisition system consisted of two 24-channel Geometrics Geode signal enhancement seismographs, combined to form a 48-channel system. Other equipment for the P-wave refraction survey consisted of 10 Hz vertical geophones, 15 to 25-foot takeouts, a truck-mounted accelerated weight drop (AWD), a downhole percussion firing rod (DPFR) with 500 grain loads, a 20 lb (9.1 kg) sledgehammer, and an aluminum plate. Each seismic line consisted of two or three spreads of 48 geophones, spaced 10 ft (3m) apart, aligned in a linear array. Up to 24 shot point locations were occupied on each spread. The AWD was used in all shots accessible to AWD truck and the DPFR or the 20 lb (9.1 kg) sledgehammer was used for the remaining shots. The final seismic record at each shot point was the result of stacking 3 to 15 shots to increase the signal to noise ratio.

For a seismic survey, acoustic energy is input to the subsurface by an energy source. The acoustic waves propagate into the subsurface at a velocity dependent upon the elastic properties of the material through which they travel. When the waves reach an interface where the density or velocity changes significantly, a portion of the energy is reflected back to the surface and the remainder is transmitted into the lower layer. Where the velocity of the lower layer is higher than that of the upper layer, a portion of the energy is also critically refracted along the interface. Critically refracted waves travel along the interface at the velocity of the lower layer and continually refract energy back to the surface. Receivers (geophones) laid out in linear array on the surface, record the incoming refracted and reflected waves. The seismic refraction method involves analysis of the travel times of the first energy to arrive at the geophones. These first arrivals are from either the direct wave (at geophones close to the source), or critically refracted waves (at geophones further from the source).

The results of the survey are provided by Figure 2.5-54 through Figure 2.5-65. Interpreted subsurface geologic conditions at the site consists of a thin layer of sediments overlying shale bedrock of the Mahantango Formation. The shale unit grades from a decomposed shale (Weathered Rock) near the surface to a weathered shale (Transition Zone) and then to a competent shale (Sound Rock) with depth. The top of the decomposed shale (Weathered Rock) was typically interpreted as having compressional (P-wave) velocities in the range of 3,500 to 4,500 ft/s (1067 to 1372 m/s). The seismic velocity of this unit is often similar to that of the overlying sediments. The top of the weathered shale (Transition Zone) was typically interpreted in the 5,000 to 6,000 ft/s (1524 to 1829 m/s) P-wave velocity range. While, the top

of competent shale (Sound Rock) was typically interpreted in the 11,000 to 13,500 ft/s (3353 to 4115 m/s) velocity range.

The subsurface strata presented in Figure 2.5-57 through Figure 2.5-65 show that the interpreted elevations of the top of Weathered Rock and Transition Zone generally parallels the surface topography at the BBNPP site. However, the top of Sound Rock forms an east-west to southeast-northwest trending depression in the central portion of the site with elevation increasing to the north and south. The interpreted contour map of the top of Sound Rock is shown in Figure 2.5-54.

The results and interpretation of the geophysical tests are further discussed in the following Sections:

- ◆ Section 2.5.3, in the context of surface faulting
- ◆ Section 2.5.4.2.5, in the context of recommended soil properties for engineering design purposes,
- ◆ Section 2.5.4.4, in the context of the approach to select the best estimate soil column profile for dynamic analysis at the BBNPP site.

2.5.4.2.2.2.4 Hydrogeologic Investigation

The hydrogeologic field investigation included a site specific data collection to support a comprehensive hydrogeological evaluation of the BBNPP site and surrounding areas as required for Section 2.4.

The objective of the hydrogeological field investigation was to collect the necessary data and information to characterize the existing surface water and groundwater flow conditions at the site, including subsurface borings for geological stratigraphy, monitoring of groundwater potential and quality, slug and pumping tests for analysis of aquifer parameters, and gauging of surface water flow in creeks.

The data collected in the field and from other sources (i.e., SSES FSAR, USACE, USGS) were utilized to support the surface hydrology analysis, hydrogeological characterization, and the development of a groundwater flow model. The model has the capability to evaluate the impact of successive rain events on groundwater elevations across the facility as well as the hypothetical discharge of water from facility operations and storage structures to the ground and the resulting impact to groundwater flow and transport of radionuclides from the facility, including the release of radionuclides and other potential contaminants into these flow systems.

Section 2.4 presents the detailed information related to the hydrogeological field investigation.

2.5.4.2.3 Laboratory Testing Program

The laboratory investigation of soils and rocks was performed in accordance with the guidance of the NRC Regulatory Guide 1.138, "Laboratory Investigations of Soils and Rocks for Engineering Analysis and Design of Nuclear Power Plants" (NRC, 2003b). Soil and rock samples were shipped under chain-of-custody from the on-site storage to the testing laboratories. ASTM Standards ASTM D4220 (ASTM, 2007a) and ASTM D5079 (ASTM, 2008d) provide guidance on standard practices for preserving and transporting soil and rock core samples, respectively. These guidelines were referenced in preparing technical specifications for the

BBNPP subsurface investigation, addressing sample storage and transportation, as well as other subsurface investigation and geotechnical requirements.

Laboratory testing consisted of testing soils and rocks samples obtained from the subsurface investigation program. Laboratory testing of soil samples consisted of static/index, dynamic, and chemical properties tests on selected SPT disturbed samples, rock cores recovered from borings, and samples gathered from potential borrow areas of fill. Laboratory tests included the following: engineering classification, moisture (water) content, unit weight, specific gravity, Atterberg limits, grain size (sieve and hydrometer), permeability, consolidated-undrained triaxial compression (C \bar{U}), unconfined compression (UC), compaction, resonant column torsional shear (RCTS), free-free resonant column (FF), pH, resistivity, chloride ion content, and sulphate ion content.

The number and types of tests selected were consistent with the field investigation findings, and the uniform conditions encountered at the site. Overall, the SPT blow counts were very consistent both in depth and spatial distribution. The soil strata at the site were distinguishable and there was a good correlation between the in-situ soil classification and the SPT results. At the BBNPP, the comprehensive index testing program along with refined testing at strategically selected locations has provided the required information to adequately characterize the soil properties.

A summary of laboratory tests and specifications used for the laboratory testing program is shown in Table 2.5-20. The soil and rock laboratory tests listed in Regulatory Guide 1.138 (NRC, 2003b) are common tests performed in most well-equipped soil and rock testing laboratories. Additional tests that are not covered in regulatory guides were also performed for the BBNPP field exploration (i.e. RCTS, FF, and chemical tests).

Resonant Column Torsional Shear (RCTS) and Free-Free Resonant Column (FF) tests were performed at the University of Texas under the RIZZO Quality Assurance Program.

The following sections provide a summary of each test, showing the most important and relevant results.

2.5.4.2.3.1 Laboratory Index Tests

Soil samples were classified in the laboratory using the Unified Soil Classification System (USCS) in accordance with ASTM D2487 (ASTM, 2010b). Rock samples were classified in the laboratory using the Unified Rock Classification System (URCS) in accordance with ASTM D5878 (ASTM, 2008e).

2.5.4.2.3.1.1 Grain Size Analyses

Grain size analyses were performed on selected SPT samples of overburden soils and bulk samples (fill material). The grain size tests were done in accordance with ASTM D422-63 (ASTM, 2007c). The results of these tests were used for classification and correlation purposes. The fines content and USCS symbols for overburden soil samples are provided in Table 2.5-21.

2.5.4.2.3.1.2 Moisture Content and Atterberg Limits

Moisture content was determined from samples in accordance with ASTM D2216 (ASTM, 2005b). Moisture content was also obtained during unconfined compressive strength tests of rock core samples. Consistently throughout the site, and down through the depth of the borings, the laboratory results showed natural moisture content in the overburden soils ranging between 4 and 17 percent and an average of 11.3 percent. Moisture content

laboratory results are provided by Table 2.5-22 The moisture content of Sound Rock samples is extremely low, sometimes not even recorded. This condition is due to the extremely high density of the shales at the site.

SPT samples of soil were tested to evaluate their plasticity characteristics, in accordance with ASTM D4318 (ASTM, 2010d). The results of these tests were used for classification and correlation purposes. The Atterberg Limits of overburden soil and fill material are provided by Table 2.5-23.

The moisture content and Atterberg Limits are plotted versus depth in Figure 2.5-96. Consistently throughout the site, and down through the depth of the borings, the natural moisture content is close to the plastic limit. The Casagrande plasticity chart for the overburden soil is shown in Figure 2.5-95, using the following equation for the A-line and U-line:

$$\text{A-line: PI} = 0.73 (\text{LL}-20) \quad \text{Eq. 2.5.4-1}$$

$$\text{U-line: PI} = 0.90 (\text{LL}-8) \quad \text{Eq. 2.5.4-1}$$

2.5.4.2.3.1.3 Unit Weight Determinations

Unit weight determinations were made based on a weight-volume relationship on Mahantango Formation rock core samples and bulk samples. Table 2.5-24 lists the samples with the corresponding dry and wet unit weights. Unit weight measurements on rock samples were performed during "Free-Free" tests and during unconfined compressive strength tests.

2.5.4.2.3.1.4 Specific Gravity

Specific gravity tests were performed on overburden soil samples in accordance with ASTM D854 (ASTM, 2010c). Typical values of specific gravity of most soils lie within the narrow range of 2.7 ± 0.1 . For rocks samples, ASTM D6473 (ASTM, 2005a) was used to determine the specific gravity. Specific Gravity results are listed in Table 2.5-25.

2.5.4.2.3.1.5 Chemical Classification Tests

Chemical tests were conducted on bulk samples and the Mahantango Formation in accordance with AASHTO T289 (AASHTO,2004), AASHTO T290 (AASHTO, 2007a), and AASHTO T291 (AASHTO, 2008) and ASTM G187 (ASTM, 2005c). These tests provide quantitative information related to the aggressiveness of the soil conditions, and the potential for deterioration of a foundation material. The following chemical tests were conducted on samples from the BBNPP site: pH; resistivity; chloride ion content; and sulphate ion content . The results of the tests are provided in Table 2.5-26.

2.5.4.2.3.2 Laboratory Performance Test

2.5.4.2.3.2.1 Unconfined Compression

Unconfined Compression tests were conducted on representative rock core samples to determine their compressive strength, in accordance ASTM D7012-04 (ASTM, 2010e). Table 2.5-27 presents a summary of the Unconfined Compression test results. The core samples of the Mahantango formation are typically a medium to dark gray shale rock with a recovery ratio of 90 percent and a RQD of 75 percent or higher. Therefore, most of the samples did not present problems during the specimen preparation. Section 2.5.4.2.4 provides the recommended geotechnical performance parameters which in part are based on the results of the unconfined compressive strength. The unconfined compressive strength of the specimens

from the Mahantango formation is medium high to high with an average slightly above 7000 psi (48 MPa).

2.5.4.2.3.2.2 Rock Sample URCS Engineering Classification

Table 2.5-28 provides the URCS engineering classification of the rock core samples tested for unconfined compression. The Sound Rock of the Mahantango Formation was the main target of the investigation, and the specimens showed: minimum to no weathering (Grade A); unconfined compressive strength between 3000 and 8000 psi (21 to 55 MPa) (Grade C); no discontinuities (Grade C); and a unit weight around 170 pcf (27 kN/m³) (Grade A). The URCS classification of the Mahantango formation is ACCA.

2.5.4.2.3.2.3 Hydraulic Conductivity

Laboratory tests were performed to determine the permeability of bulk samples, according to ASTM D2434 (ASTM, 2006). Results of the tests are presented in Table 2.5-29. The tests were performed on bulk samples obtained from borrow areas of fill. Section 2.4 presents detailed information related to the hydrogeological field investigation and additional information regarding permeability and hydraulic conductivity.

2.5.4.2.3.2.4 Resonant Column Torsional Shear

Resonant Column Torsional Shear (RCTS) tests were conducted according to the procedure developed by the University of Texas at Austin (UTA) entitled, PBRCTS-1, Rev. 4, Technical Procedures for RCTS Tests, (UTA, 2004a). The tests targeted the Glacial Overburden soils and four remolded samples recovered from borrow area sites. For the fill samples, laboratory staff had to scalp the specimens so that the largest particles had a diameter less than 1/6th of the specimen diameter. The focus of the RCTS testing program was to evaluate the material that will likely form the foundation fills for the plant facilities. These materials will originate from either excavation soils or from borrow areas and will be screened and compacted according to specifications. The RCTS on borrow area material was performed on remolded samples.

The RCTS test is performed in a series of steps that incorporate different confining pressures and loading frequencies. The Torsional Shear portion of the test is able to capture physical properties at large strains under lower frequency loading that best resembles the seismic demand. The details of the testing methodology are documented by the procedure, PBRCTS-1, Revision 4, Technical Procedures for RCTS Tests, (UTA, 2004a).

Resonant Column (RC) and/or Resonant Column Torsional Shear (RCTS) testing are performed to measure two critical parameters in laboratory soil (and sometimes rock) specimens:

1. Shear modulus, which is directly related to shear wave velocity of the soil (Equation 2.5.4-1)

$$G = \rho V_s^2 \quad \text{Eq. 2.5.4-1}$$

2. Damping, which allows for the dissipation of the energy released during an earthquake or any given vibratory process.

Both the shear modulus and damping depend on:

- ◆ The amount of strain (or unit deformation),
- ◆ The confining pressure,

- ◆ The frequency of the motion, in this context, the frequency of the cyclic load applied during testing.

Table 2.5-30 presents the results for shear modulus and damping at low strains. The table highlights the medium range confining pressure applied during testing. The values of the shear stress in the samples range between the 2500 and 6500 ksf and damping ranged between 1.4 and 4.8 percent. A discussion of the recommended values for engineering purposes is included in Section 2.5.4.2.4. The recommended properties take into account the effect that confining pressure has on the low strain shear modulus. The strain dependency variation of the shear modulus and damping is shown in the form of normalized plots by Figure 2.5-89, Figure 2.5-90, Figure 2.5-91, and Figure 2.5-92 respectively for each of the samples tested. A discussion for recommended values is presented in Section 2.5.4.2.4 and Section 2.5.4.7.

2.5.4.2.3.2.5 Unconfined Resonant Column "Free-Free" Testing

The Free-Free Resonant Column Tests (FF) was conducted according to the procedure, also developed by UTA, entitled, Free-Free (Fr-Fr) Testing of Soil and Rock Samples, Internal Procedure Fr-Fr-1, Revision 0 (UTA, 2009). The Free-Free resonant column device allows for a simpler approach compared to the RCTS that can measure small-strain shear modulus (G_{max}) and small-strain material damping (D_{min}). The term "Free-Free" is used to differentiate from the "Fixed-Free" condition of the typical RC test, meaning that one end of the sample is fixed while the other is free to rotate or displace. No confining pressure is used in this test. A total of four "Free-Free" tests were performed on special care rock samples retrieved from various boring locations. Table 2.5-31 lists the samples and presents the results. A discussion of how the "Free-Free" testing results are used for the analysis is presented in Section 2.5.4.2.4 and Section 2.5.4.7.

2.5.4.2.3.2.6 Consolidated-Undrained Triaxial Compression with Pore Pressure Measurements

Consolidated-undrained triaxial compression tests with pore water pressure measurements were performed on bulk samples (fill material) under three effective all around confining pressures of 1000 psf, 2000 psf, and 3500 psf for each sample tested. The tests were conducted in accordance with ASTM D4767 (ASTM, 2004a) in order to determine strength parameters. Table 2.5-32 provides a summary of the results.

2.5.4.2.4 Engineered Soils

Category 1 Granular Structural Fills will be created from screened granular soils from either the excavated in-situ soils or borrow areas in the proximity of the project. Cohesive fill (permeability lowered to less than $1.0E-08$ m/s) will be required for the construction of the ESWEMS Retention Pond. The term "Category 1 Structural Fill" or "fill" is used for engineered soil that will be placed around and above the foundation level of safety-related facilities. The foundation of all the safety-related facilities at the BBNPP site will rest directly on top of concrete fill and/or Sound Rock of the Mahantango Formation.

2.5.4.2.4.1 Category 1 Granular Structural Fill

Bowers Construction (Bowers) of Berwick, PA provided excavation of test pits to collect subsurface soil and perform screening of soil samples for the purpose of composite soil sampling soil collection for geotechnical analysis. The borrow site is approximately 2.3 mi (3.7 km) northeast of the site close to the intersection of Mingle Inn Road (State Route 4002) and Salem Boulevard (Route 11), Berwick, PA.

Soil samples were collected from two identified test pits (Test Pit B-01 and Test Pit B-02) using a CAT325BL track excavator. Samples collected from Test Pit B-01 (N 41°06'48.4"; W 76°08'33.6"; El. 640 ft (195.1 m)) were loaded on a TEREX scraper and transported to the screening area located just West of Salem Boulevard (Route 11), 0.65 mi (1.05 km), North of its intersection with Mingle Inn Road (State Route 4002). Samples collected from Test Pit B-02 (N 41°07'11.9"; W 76°08'23.6"; El. 617 ft (18.1 m)) were transported to the same screening area using a CAT 966E front end loader.

Upon collection of soil, a FINTEC 540 screening machine was utilized in order to prepare the composite soil sample. Each of the collected samples was screened, and the material passing the 2 in (5 cm) sieve was then stockpiled in two different locations. These two stockpiles (6.5 ft (1.98 m) tall and 12 ft (3.66 m) in diameter) were then sampled using the ASTM D75 (ASTM, 2003), and eight representative 5 gallon (0.005 cubic meters) buckets were filled from each of the stockpiles and shipped to the representative laboratories. The description of the collected soil consisted of well-graded gravel with sand (GW) (Test Pit B-01) and poorly graded sand with silt and gravel (SP-SM) (Test Pit B-02), no plasticity, no diltancy, no toughness, and low strength.

For RCTS testing, the results of two test pit samples (Test Pit Face and Test Pit #5) collected during the 2007 BBNPP field investigation are also presented. These soil samples were collected from the same borrow site as Test Pit B-01 and Test Pit B-02.

A Laboratory Testing Program has been implemented to fully characterize the properties of the proposed material. The tests included:

- ◆ Modified Proctor tests,
- ◆ Grain size,
- ◆ Consolidated-Undrained Triaxial Compression Test with Pore Pressure Measurement
- ◆ Resonant Column Torsional Shear,
- ◆ Chemical Tests

The Modified Proctor Test results, showing optimum moisture content and maximum unit weight are provided by Table 2.5-33. The optimum water content is about 6 percent and the material proved to be quite dense with maximum moist unit weights above about 145 pcf (22.8 kN/m³). The grain size analysis results are compared against the required specification. Table 2.5-33 provides the properties for structural fill. Structural fill should be compacted to 95 percent of the optimum dry unit weight Modified Proctor. The fill moist, saturated, and dry unit weights exceed the U.S. EPR specified values of 128 pcf (20.1 kN/m³), 134 pcf (21.1 kN/m³), and 110 pcf (17.3 kN/m³), respectively. The unit weight for the structural fills at the BBNPP site will be exceeded. This represents a departure from the U.S. EPR FSAR and is further discussed in Section 2.5.4.2.5.1.

2.5.4.2.5 Recommended Soil, Fill, and Rock Properties

The following sections provide recommendations of soil properties for engineering analysis and design purposes. The properties are based on a combination of field measurements, laboratory testing, engineering analysis, engineering judgment, and available reference material. For a cohesionless structural fills at the site, the soil below and adjacent to the safety-related foundation basemat will have a friction angle in excess of 30 degrees. This

strength meets the requirements of the U.S. EPR FSAR. The requirement is also met and exceeded by the high strength parameters of the foundation bedrock. Details are provided in the following subsections.

The properties are given for each of the geologic units found during the investigation as described by Section 2.5.4.2.1. Those units are listed below:

- ◆ Overburden Soil
- ◆ Mahantango Formation
 - ◆ Weathered Rock
 - ◆ Transition Zone
 - ◆ Sound (Competent) Rock.

In addition to the existing soils, it is necessary to provide properties for engineered fills that will likely be placed around and above the foundation for safety-related structures. Therefore, soil properties are also given for:

- ◆ Category I Granular Structural Fill

This Section is divided into:

- ◆ Classification and Index Properties,
- ◆ Strength Properties,
- ◆ Performance Properties,
- ◆ Static Elastic Properties,
- ◆ Dynamic Elastic Properties, and
- ◆ Chemical Properties.

The overburden soils consist of one soil layer characterized as silty sand and gravel with varying amounts of clay and silt. The existing soil matter is not suitable for the support of large or safety-related structures due to the potential for liquefaction and will be removed in order for the foundation mats to bear directly on either of the Sound Rock of the Mahantango Formation, or concrete fill. Additional discussion related to this matter is presented in Section 2.5.4.8. The thickness of the overburden soils varies from about 7.5 to 60 ft (2.3 to 18.3 m), with an average thickness of 24 ft (7.3 m). The depth from surface boring elevation to the Mahantango Formation is shown by Figure 2.5-80. The thickness of the soil layers is based on estimating the termination elevations encountered for the layer at the boring locations from the boring logs included with the COLA.

2.5.4.2.5.1 Index Properties

Index properties are:

- ◆ USCS Classification (or URCS Classification for Rocks),
- ◆ Water Content,

- ◆ Atterberg Limits
- ◆ Unit Weight,
- ◆ Specific Gravity,
- ◆ Grain Size (or Fines Content),

Index properties determined for rocks are:

- ◆ Classification,
- ◆ Unit Weight,
- ◆ Specific Gravity.

Selected samples were submitted for laboratory index tests and testing for determination of engineering properties. Section 2.5.4.2.3 presents the detail of the laboratory testing program. Table 2.5-34 provides the recommended index properties.

Of the index properties, only the dry, moist, and saturated unit weights are discussed in the U. S. EPR Tier 2 FSAR documentation. The site-specific unit weights found at the BBNPP site exceed the U. S. EPR FSAR values of:

- Saturated soil = 134 lb/ft³.
- Moist soil = 128 lb/ft³.
- Dry soil = 110 lb/ft³.

At BBNPP:

- Saturated soil = 145 lb/ft³.
- Moist soil = 142lb/ft³.
- Dry soil = 135 lb/ft³.

This is not necessarily a geotechnical problem. The U. S. EPR FSAR values were established according to one previous site-specific experience.

2.5.4.2.5.2 Strength Properties

Strength properties are obtained directly from laboratory tests or from field measurements and supplemental calculations. The overburden soils, Weathered Rock, and Transition Zone will be removed and replaced by concrete fill or engineered fill. Strength properties include the Mohr-Coulomb parameters commonly used for many geotechnical analysis issues such as bearing capacity, slope stability, retaining walls, and foundation design.

An equivalent friction and cohesion was estimated for the Sound Rock of the Mahantango Formation. The parameters were determined according to the classification system proposed by Hoek et al. (Hoek, 2002) using the Geological Strength Index (GSI) and unconfined

compressive strength test results. Table 2.5-35 provides a summary of the Rock Mass Rating (RMR) and GSI for the Mahantango Formation.

The following recommended strength properties for soil and rock at the site are provided by Table 2.5-36:

- ◆ Penetration Resistance (SPT)
- ◆ Rock Mass Rating (RMR)
- ◆ Cohesion
- ◆ Friction Angle
- ◆ Unconfined Compression.

Strength properties were determined by either correlation with SPT blow counts or by statistical averaging of the laboratory tests. Strength properties of the foundation formation (Mahantango Formation) exceed the requirements established in the U.S. EPR FSAR.

2.5.4.2.5.3 Performance Properties

Two performance properties are discussed: (1) hydraulic conductivity, and (2) consolidation.

Hydraulic Conductivity

Section 2.4 presents detailed information related to the hydrogeological field investigation, and additional information regarding permeability and hydraulic conductivity is available. The Laboratory Testing Program of Section 2.5 focused on specific values at the site and tests were performed on samples extracted from the geotechnical boring program. Table 2.5-37 provides the recommended values for hydraulic conductivity. The recommendation is based on the results from field tests performed on the wells installed as part of the Hydrogeologic investigation.

Consolidation

The soils encountered at the site are granular in nature and long term settlement due to consolidation would not occur if these were used as foundation support.

2.5.4.2.5.4 Static Elastic Properties

The static elastic properties of interest are the elastic modulus, the shear modulus, and the Poisson's ratio. The shear modulus is derived directly from the elastic modulus and the Poisson's ratio.

Elastic Modulus

The static elastic modulus of soils and rocks is determined from data retrieved during the field investigation and laboratory testing. Several criteria are used, depending on the soil or fill analyzed:

1. Geophysical Testing,
2. SPT N-Value,
3. Pressuremeter,

4. Rock Mass Rating,
5. American Concrete Institute (ACI).

Each of the criteria is applied and an average or a conservative approach is used for the recommended parameter. Table 2.5-38 presents the values according to each criterion and the recommended elastic modulus value. It is anticipated that static loading in excess of the current in-situ overburden pressure will not occur below the Mahantango Formation, and, therefore, the static elastic modulus is not a critical parameter.

Poisson's Ratio

Poisson's ratio is obtained directly from the shear wave and compressional wave velocity measurements. Equation 2.5.4-2 is used to establish the Poisson's ratio.

$$\frac{V_p}{V_s} = \sqrt{\frac{2-2\nu}{1-2\nu}} \quad \text{Eq. 2.5.4-2}$$

Static Shear Modulus

The static shear modulus is directly determined from the Elastic Modulus and the Poisson's Ratio with the use of Eq. 2.5.4-3.

$$G = \frac{E}{2(1+\nu)} \quad \text{Eq. 2.5.4-3}$$

where G is the static shear modulus, E is the Elastic Modulus and ν is Poisson's Ratio.

Table 2.5-39 provides the recommendation for the static elastic properties.

2.5.4.2.5.5 Dynamic Elastic Properties

A comprehensive field geophysical investigation program and laboratory testing program were undertaken to establish the dynamic properties for the BBNPP. The properties are required for site amplification analysis, Soil Structure Interaction (SSI) analysis, and foundation design. The dynamic properties established are:

- ◆ Shear Wave Velocity (V_s),
- ◆ Compressional Wave Velocity (V_p),
- ◆ Density (ρ),
- ◆ Poisson's Ratio (ν),
- ◆ Maximum Dynamic Shear Modulus (G_{max}),
- ◆ Maximum Dynamic Elastic Modulus (E_{max}),
- ◆ Damping at small strain or initial damping (DS_o),

◆ Strain dependent shear modulus and damping (for borrow area soils).

The shear wave velocity profile was determined by means of a data interpretation analysis that incorporated the results from downhole, P-S Suspension Logging tests. The details of the analysis are described in Section 2.5.4.4. The recommended values for dynamic properties are presented in Table 2.5-40. More descriptions of the procedures followed to provide the recommendation are included in Section 2.5.4.7. The recommended shear wave velocity profile under the Nuclear Island is plotted by Figure 2.5-93.

The two strain dependent properties of interest are Shear Modulus and Damping. Figure 2.5-94 presents the recommended curves for the engineered fill.

2.5.4.2.5.6 Chemical Properties of Soils

The chemical properties of the soils are given by Table 2.5-26.

2.5.4.3 Foundation Interfaces

This section discusses the interfaces between the planned structures and other components and the subsurface characteristics. A plot plan showing the location of the borings, seismic lines, and downhole surveys is provided by Figure 2.5-77. Based on the information obtained during the subsurface investigation and laboratory testing program for the BBNPP, it was determined that exploratory trenches were not necessary in order to characterize the soils at the BBNPP. Cross sections showing the main geologic units are presented by Figure 2.5-141 through Figure 2.5-146. Contour plans of geologic unit elevations are given by Figure 2.5-80 through Figure 2.5-84.

2.5.4.3.1 U.S. EPR FSAR

The U.S. EPR FSAR provides criteria related to various siting issues, which must be satisfied by the particular features of the BBNPP site. The U.S. EPR FSAR identifies the type of information that should be developed to demonstrate that the site is in compliance with the design. Generic soil profiles are listed by the U.S. EPR FSAR and these represent a broad range of foundation media characterized by shear wave velocities ranging from 700 ft/sec (213 m/sec) to those typical of hard rock conditions. It is expected that this range captures the static and dynamic response of plant Structures, Systems and Components which will, in general, envelop the actual response at sites exhibiting foundation soils with shear wave velocity at foundation level greater than 1,000 ft/sec (305 m/sec). At BBNPP, the shear wave velocity of foundation media (Mahantango Formation) for the Nuclear Island (NI), Emergency Power Generation Buildings, and Essential Service Water Buildings facilities is higher than 6500 fps (1981 m/s). The NI basemat is a monolith that includes the Reactor Building (RB), Safeguards Buildings (SGBs mechanical and electrical) and Fuel Building. No departures or deviations from the soil conditions evaluated in the U.S. EPR FSAR were identified.

The seismic ground motion reported in Section 2.5.2 was defined as a hypothetical free-field outcrop motion at the ground surface. On the other hand, the design of adjacent safety-related structures founded near the ground surface (Plant Grade) use the free-field soil surface ground motion for design. Section 2.5.2 presents ground motion response spectra (GMRS) at the ground surface for the NI. Both the GMRS as well as the seismic response of the soil structure system depends on the subsurface soil stratigraphy including the soil layering, layer thickness, layer shear wave velocities and damping and impedance mismatch.

The foundation interface analysis relates to how the foundation medium and its variability affect the bearing pressure distribution and the settlement of the NI Basemat, and other

safety-related structures (Emergency Power Generation Buildings and Essential Service Water Buildings) in the vicinity, particularly for soil sites. The foundation interface analysis also determines how these same items affect the seismic response of the structures and the foundation medium. The structural design of the NI Basemat is governed by the bearing pressure and its distribution due to dead and live load and seismic forces, as well as the foundation settlements. On the other hand, the seismic loads on the plant structures and foundations are determined by the vertical and the coupled horizontal and rocking response analysis as estimated with Soil-Structure Interaction (SSI) analysis or Rock-Structure Interaction (RSI) analysis, as the case may be.

Dynamic aspects of the foundation interface are discussed in BBNPP FSAR Sections 3.7 and 3.8. Static aspects such as bearing capacities, settlement and horizontal variability of stiffness and subgrade reaction under the base mats are discussed in Section 2.5.4.10. The subsurface soils beneath the NI base mat should have the capacity to support the bearing pressures with a factor of safety of 3.0 under static conditions and 2.0 under Safe Shutdown Earthquake conditions.

2.5.4.3.2 Site Characteristics

Based on the review of the subsurface conditions at existing nuclear power plant sites, the potential sites for the U.S. EPR can be broadly categorized into four primary groups:

- ◆ Rock sites,
- ◆ Thin soil sites,
- ◆ Shallow soil sites, and
- ◆ Deep soil sites.

This categorization provides a framework for reporting site-specific conditions in a COLA referencing the U.S. EPR FSAR relative to the Plant Parameter Envelope (PPE) considered in the U.S. EPR design. Based on several combinations of site groups and their respective parameters, as specified by the U.S. EPR FSAR, the BBNPP site is classified as a Thin Soil Site over Hard or Firm Rock. As such, the Ground Motion Response Spectra (GMRS) is defined at the ground surface. For the NI, this level corresponds to the top of rock or top of Mahantango Formation. The static and dynamic bearing capacity is verified without the need of time dependant settlement computations. Details related to shear wave velocity are included in Sections 2.5.4.2.5.5 and 2.5.4.2.2.2.3.

2.5.4.3.3 Horizontal Layering

Most geotechnical analyses, including SSI analysis, settlement analysis and bearing capacity analysis, assume that the soil layers are horizontal and effects of non-horizontal layering are practically ignored. This assumption will hold if there is no significant inclination in the soil profiles such as the top of rock horizon.

Figure 2.5-82 shows the inclination of the top surface of the Mahantango Formation. In the direction of maximum gradient, the top of rock surface drops about 45 ft (14 m) in a distance of 980 ft (299 m), which corresponds to a 4.6 degree sloping angle. It is still applicable to assume a horizontal layered model for both Site Amplification and Soil Structure Interaction Analyses. Additional discussion is provided in Section 2.5.4.10.3.

2.5.4.3.4 Uniform Site Conditions

The variation of the dynamic properties between distant points of the NI facilities may be represented by a Lower Bound, Best Estimate and Upper Bound for the Vs value at the center point of the facility. The site uniformity is also discussed in Section 2.5.4.10.3.

The thickness of the Sound Rock of the Mahantango Formation was not determined since the BBNPP geotechnical investigation did not reach the bottom of the formation. The maximum exploration depth was 420 ft (128 m), and the average depth to reach the top of this formation is 67.4 ft (20.5 m) with respect to the ground level. Based on contour maps, the Mahantango Formation extends across the entire footprint of the power block. As such, the site may be considered as uniform.

2.5.4.3.5 Interface Figures

The Interface Figures present cross sections of the site subsurface conditions with the location of the main components of the Project. Safety-related structures are shown at their planned foundation elevation and on top of the corresponding foundation material. Table 2.5-41 provides the depth, elevation, and foundation footprint of the BBNPP safety-related structures. Figure 2.5-97 provides a plan view of an excavation and fill plan with the location of four cross-sections. Two east-west excavation profiles (Excavation Sections A and D) are shown in Figure 2.5-98 and Figure 2.5-107 respectively, and two north-south excavation profiles (Excavation Sections B and C) are shown in Figure 2.5-101 and Figure 2.5-104 respectively. The Nuclear Island (NI), Essential Service Water Buildings (ESWBs) and Emergency Power Generation Buildings (EPGBs) will sit on top of a concrete fill between its mat and the top of bedrock. On the north side, only ESWB1 will bear directly on the Sound Rock.

Section 2.5.4.5 provides the excavation details and Section 2.5.4.10 presents bearing capacities and estimated settlements.

2.5.4.4 Geophysical Surveys

Section 2.5.4.2.2.3 presents the results of the geophysical investigation surveys .
Section 2.5.4.2.5.5 provides the recommended dynamic soil properties, based on the results from the field investigation and on the post-processing analysis of the retrieved data.

2.5.4.5 Excavation and Backfill

Sections 2.5.4.5.1 through Section 2.5.4.5.5 are added as a supplement to the U.S. EPR FSAR.

BBNPP will utilize a combination of excavation slopes and temporary retaining structures to facilitate construction of below grade portions of the nuclear facility. The planned finish grade is at an elevation of approximately 719 ft (219.2 m).

The materials excavated as part of the site grading are overburden soils (sand and gravel units), weathered rock and transition zone. However, in-situ soils from the excavation may be used for fills and backfills if adequate screening and compaction techniques are implemented. These soils are predominantly of low plasticity or non plastic and their composition consists of sand and gravels. No rebound (heave) in the ground due to the removal of the soils is expected at the Mahantango Formation.

The U.S. EPR minimum shear wave velocity is 1000 fps.

- Category I (safety-related) Structures, such as the Nuclear Island, EPGBs, ESWBs, and ESWEMS Pump House will bear on concrete or the Mahantango Formation, which have shear wave velocities higher than 1000 fps.

- Category II SSE structures, such as the Fire Protection Building will bear on either bedrock, concrete or engineered fill, which will be constructed to achieve a shear wave velocity of higher than 1000 fps.

2.5.4.5.1 Source and Quantity of Backfill and Borrow

As previously mentioned in Section 2.5.4.2.4.1, Bowers Construction (Bowers) of Berwick, PA provided excavation of test pits to collect subsurface soil and perform screening of soil samples for the purpose of composite soil sampling soil collection for geotechnical analysis. The borrow site is approximately 2.3 mi (3.7 km) northeast of the site close to the intersection of Mingle Inn Road (State Route 4002) and Salem Boulevard (Route 11), Berwick, PA and has sufficient material to support site construction needs. Earthwork operations will be performed to achieve the planned site grades. Excavations for foundations of the proposed Category I structures within the Power Block area will result in removing the overburden soils in their entirety, and will extend to top of the Sound Rock of the Mahantango Formation. The maximum depth of cut in the weathered rock and transition zone is estimated to be about 95 ft (29 m) below the final grade of 719 ft (219.2 m). The estimated upper bound of the excavation and backfill volume is approximately 1400 thousand cubic yards (1070 thousand cubic meters).

2.5.4.5.2 Extent of Excavations

Permanent excavation and fill slopes, created due to site grading, are addressed in Section 2.5.5. Temporary excavation slopes, such as those for foundation excavation, would be graded on an inclination of at least 1.5:1.0 horizontal to vertical (H:V) for the material above the sound (competent) rock, and at least 0.25:1.0 in the sound rock, offset by 20 ft (6.0 m) at the base of the excavation with a bench of 20 ft. The ESWEMS Retention Pond will be constructed by placing cohesive fill from the bottom of the excavation to the bottom of the pond at elevation 677.5 ft (207 m). The dike of the pond will consist of cohesive and granular fill materials. The inner side slope of the pond is 3:1 H:V, and outer side slope is 2:1 H:V. For the Power Block area, an excavation plan is provided by Figure 2.5-97, and concrete fill will be required beneath all safety-related structures. The approach for excavation, confirmed by the slope stability analysis (Section 2.5.5), will implement 1.5:1.0 H:V slopes. Figure 2.5-98 through Figure 2.5-104 and Figure 2.5-107 show an excavation scheme for the Nuclear Island structures (NI), the Emergency Power Generation Building (EPGB), the Essential Service Water Building (ESWB), and the Turbine Building (TB).

2.5.4.5.3 Compaction Specifications

Structural fill sources were identified, as discussed in Section 2.5.4.5.1. Several samples of the materials were obtained and tested for index and engineering properties, including moisture-density relationships. For foundation support, fill against walls is compacted to 95 percent Modified Proctor optimum dry density, as determined based on the Modified Proctor compaction test procedure. The fill is compacted to within 3 percent of its optimum moisture content, which is about 6 percent. Fill placement and compaction control procedures are addressed in a technical specification prepared during the detailed design stage of the project. It includes requirements for suitable fill, sufficient testing to address potential material variations, and in-place density and moisture content testing frequency, e.g., a minimum of one test per 10,000 ft² (900 m²) of fill placed. The technical specification also includes requirements for an on-site testing laboratory for quality control, especially material gradation

and plasticity characteristics, the achievement of specified moisture-density criteria, fill placement/compaction, and other requirements to ensure that the fill operations conform to the earthwork specification for BBNPP. The soil testing company is required to be independent of the earthwork contractor and to have an approved quality program. A sufficient number of laboratory tests are required to be performed to ensure that variations in the fill material are accounted for. A trial fill program is normally conducted for the purposes of determining an optimum number of compactor coverages (passes), the maximum loose lift thickness, and other relevant data for optimum achievement of the specified moisture-density (compaction) criteria.

2.5.4.5.4 Dewatering and Excavation Methods

During construction activities, three different site areas will be excavated down to competent bedrock and the excavations will then be partially backfilled with concrete in preparation for construction of structures and buildings. These three areas include:

- ◆ the Power Block,
- ◆ the ESWEMS Pond area, and
- ◆ the area beneath the cooling towers.

Each of these three areas will encounter variable amounts of groundwater during excavation. Because the excavation, backfilling, and construction activities need to be performed in dry excavations, temporary groundwater controls will be required during construction. Groundwater conditions and dewatering are discussed in greater detail in Section 2.4.12.5 and 2.5.4.6.

Once the Overburden materials are dewatered, excavations are expected to be performed using conventional earth-moving equipment. Excavations will not present any major difficulties. Excavations in the top of the Mahantango Formation will not require greater excavating effort, such as ripping tools and possibly explosives. Upon reaching the final excavation levels, all excavations will be cleaned of any loose materials, by either removal or compaction in place. All final subgrades will be inspected and approved prior to being covered by backfill or concrete. The inspection and approval procedure(s) will be addressed in the foundation and earthwork specifications that will be developed during the detailed design stage of the project. These specifications will include measures, such as proof-rolling, excavation and replacement of unsuitable soils, and protection of surfaces from deterioration.

2.5.4.5.5 Monitoring and Quality Control

Groundwater monitoring program specifications will be developed during the detailed design stage of the project. The specification document will address issues, such as the installation of a sufficient quantity of instruments in the excavation zone, monitoring and recording frequency, and evaluation of the magnitude of settlement during excavations and foundation construction.

2.5.4.6 Groundwater Conditions

Details of available ground water conditions at the site are given in Section 2.4.12.

Groundwater elevations in the bedrock beneath the Power Block range from an elevation of approximately 662 to 712 ft (201.8 to 217 m), with an average of about 690 ft (210 m). Groundwater flow in the shallow bedrock beneath the Power Block area is to the south and southwest. Some of the overburden soil above the rock is saturated, but the overburden will

be dewatered and will be stripped off the rock surface before the Power Block excavation proceeds downward into the weathered shale.

Groundwater flow in the low topographic areas occurs primarily in the Glacial Outwash (sand and gravel) aquifer. The aquifer is 34 to 54 ft thick beneath the EWSEMS Pond and Pump House. The groundwater elevation in the Glacial Outwash aquifer is at an elevation of approximately 656 to 664 ft (199.9 to 202.4 m). Groundwater in this aquifer is generally flowing south and southwest toward Walker Run and Tributary No. 1 (See Section 2.4.12). The groundwater in this aquifer will provide the majority of seepage into the excavation during construction of the ESWEMS Pond area.

Groundwater flow in the area underlying the Cooling Towers also occurs primarily in the overburden soil. However, in this area, the overburden material is thinner (24 to 35 ft (7.3 to 10.7 m) thick) and the saturated thickness is also less than the Glacial Outwash in the EWSEMS Pond area. Groundwater in the Cooling Tower area ranges from an elevation of approximately 713 to 717 ft (217.3 to 218.5 m) in the overburden soil aquifer. The Cooling Towers lie in an area that is at or very near a groundwater divide. As a result, shallow groundwater is flowing both to the east toward Tributary No. 1 and to the west toward Walker Run. The Cooling Tower area will be excavated down to the competent bedrock surface during construction. The excavation will therefore intersect saturated sand and gravel and the excavation will need to be dewatered.

Sections 2.5.4.6.1 through 2.5.4.6.4 are added as a supplement to U.S. EPR FSAR.

2.5.4.6.1 Dewatering During Construction

Active construction dewatering systems will be implemented prior to construction to maintain the site conditions dry in the three excavation areas. The systems will continue to operate until the subgrade portions for the structures are completed and the excavations are backfilled. The dewatering systems will be decommissioned as the structures are completed and the backfill is placed to establish the final grade in each area. Detailed descriptions of the hydrogeologic conditions are presented in Section 2.4.12.

Prior to initiating dewatering activities, preparations must be made to receive the water discharged from the excavations. Effluent from the dewatering systems will be routed through a temporary groundwater storage pond which will be used during construction. Thus, it would be beneficial to construct this pond prior to excavation activities in order to use it as a collection area for the dewatering systems.

On the hill where the Power Block will be built, the overburden soil will first be removed from the hill. The excavation will then proceed down through weathered and/or fractured shale. Dewatering wells will be installed around the excavation area and dewatering of the hilltop will start prior to and extend during excavation to keep the excavation dry at all times. The dewatering wells may be augmented by or entirely replaced with sumps and sump pumps in the bottom of the excavation. Groundwater elevation in the excavation area will be kept below the floor of the excavation. The required pumping rate will be partially dependent on when the dewatering system is implemented and how fast the excavation proceeds downward.

The greatest amount of groundwater flow could potentially be encountered while excavating the ESWEMS Pond area. Approximately 20 ft (6.1 m) of saturated, highly permeable, sand and gravel (i.e., the Glacial Outwash aquifer) overlies the Mahantango Shale at this location. The

excavation needs to extend down to competent bedrock. Groundwater will need to be pumped continuously from the area to keep the excavation dry. Besides groundwater pumping, there is a wetland immediately northwest of the ESWEMS Pond area that would likely be temporarily affected by the dewatering. In order to reduce the amount of groundwater extraction during construction of the ESWEMS Pond and Pump House, and minimize impacts to the wetland, a groundwater flow barrier (e.g., soil-bentonite slurry wall) will be installed to reduce dewatering during construction. The flow barrier would be installed around the entire ESWEMS Pond area (including the pumphouse) and would greatly reduce the dewatering rate and the number of dewatering wells needed to keep the excavation dry. The slurry wall will be rendered non-functional after completion of construction.

The saturated thickness of the overburden soil aquifer and the depth to competent bedrock is much less in the Cooling Tower area. As a result, a groundwater flow barrier is probably not necessary for dewatering purposes; however, groundwater pumping will be required to keep the Cooling Towers excavation dry during construction.

In summary, groundwater pumping will be required to keep the three excavations dry. The majority of dewatering will be achieved with shallow dewatering wells, in the ESWEMS Pond area, where the Glacial Outwash aquifer is being dewatered. The majority or all of the groundwater extraction from the Power Block area may be achievable with simple sumps and sump pumps in the floor of the excavation.

To facilitate quality construction methods in the Power Block, and ESWEMS Pond and Cooling Tower areas, the excavations should be performed in a dry condition with conventional construction equipment. Given the layout of these areas, a common dewatering system consisting of deep wells surrounding the excavations is designed to facilitate both excavation areas. These excavations can proceed as the dewatering takes place provided the dewatering system maintains the groundwater level below that of the excavations. As the excavation advances, a series of groundwater monitoring wells will be observed to verify the effectiveness of the dewatering system in reducing the groundwater level.

The existing monitoring wells should be utilized to monitor the effectiveness of the flow barrier. Additional monitoring wells will be installed to provide adequate monitoring on all four sides of the excavations. The monitoring program should include recording water levels on both the inside and outside of the flow barrier.

2.5.4.6.2 Analysis and Interpretation of Seepage

Analysis of the groundwater conditions at the site is described in Section 2.4.12. A groundwater model, based on information currently available, has been prepared for the overall groundwater conditions at the site and is addressed in detail in Section 2.4.12.

2.5.4.6.3 Permeability Testing

Evaluation of permeability of the fill materials was performed with lab testing of soil samples obtained from borrow sites. Slug, packer, and pumping tests were performed on monitoring wells screened in the overburden soil and shale bedrock aquifers. A detailed description of the tests and results are provided in Section 2.4.12.

2.5.4.6.4 History of Groundwater Fluctuations

A detailed discussion of the groundwater conditions is provided in Section 2.4.12.

2.5.4.7 Response of Soil and Rock to Dynamic Loading

The Safe Shutdown Earthquake (SSE) spectra and its specific location at a free ground surface reflect the seismic hazard in terms of Probabilistic Seismic Hazard Analysis (PSHA) and geologic characteristics of the site and represent the site-specific ground motion response spectrum. These spectra would be expected to be modified as appropriate to develop ground motion for design considerations. Detailed descriptions on response of site soils and rocks to dynamic loading are addressed in Section 2.5.2.

Sections 2.5.4.7.1 through 2.5.4.7.6 are added as a supplement to the U.S. EPR FSAR.

2.5.4.7.1 Seismic History

The seismic history of the area and the site, including any prior history of seismicity, evidence of liquefaction or boils, is addressed in Section 2.5.1.1 and Section 2.5.1.2.

2.5.4.7.2 Field Dynamic Measurements

The following techniques were used to measure field dynamic properties:

- ◆ P-S suspension logging surveys in 3 borings ranging in depth from about 250 to 420 ft (76 to 128 m) below ground surface, including overburden soil and rock.
- ◆ Downhole seismic velocity surveys in 3 borings ranging in depth from about 240 to 410 ft (73 to 125 m) below ground surface, including overburden soil and rock.
- ◆ Seismic refraction surveys were performed along 9 profile lines.
- ◆ Geophysical testing borehole locations are shown on Figure 2.5-77. The results for each of the tests are shown in Figure 2.5-86 through Figure 2.5-88.

Data obtained from borehole survey techniques were integrated for development of the site velocity profiles. Each borehole velocity profile was evaluated and compared against the stratigraphic logging and laboratory test data of borehole samples to correlate velocities with soil and rock types by elevation and corresponding depth below ground surface. After each individual borehole velocity data set was evaluated, borehole profiles were grouped based on site-specific location and were compiled using a common reference point (elevation or depth below ground surface).

2.5.4.7.3 Dynamic Laboratory Testing

Dynamic testing, consisting of FF tests, to obtain data on shear modulus and damping characteristics of rocks, is described by Section 2.5.4.2.3.2.5.

2.5.4.7.4 Recommended Soil Profile

The Uniform Hazard Spectra (UHS) described in Section 2.5.2 are defined on hard rock, which is located 350 to 400 ft (107 to 122 m) below the ground surface at the BBNPP site. This location was confirmed with shear wave velocity measurements above the 9200 ft/sec (2800 m/sec) threshold. To determine the dynamic motion at the ground surface, it was necessary to adjust the UHS for amplification or de-amplification as the vibratory ground motion propagated through the rock and soil media. The adjustment was made by conducting Site Response Analyses following Approach 2B described in NUREG-6728 (NRC, 2001). These analyses consist of defining the shear wave velocity and material damping characteristics in the soil and rock profile between the ground surface and the depth of hard rock, and then

conducting site response studies using a one-dimensional, equivalent linear computer code: SHAKE (Schnabel, 1972).

The NI foundation material is the concrete fill which has a shear-wave velocity of approximately 8510 fps (2594 m/s). The site amplification to define the GMRS for the BBNPP site is computed at the ground surface.

The Subsurface Investigation at the BBNPP site included extensive Boring and Geophysical Exploration Programs. The field data available are divided into three sets:

1. Shear-wave velocities,
2. Compressional wave velocities, and
3. Layer thickness.

Nine seismic refraction lines were concentrated near the center of the NI Reactor Building. The spatial variability of geotechnical properties along the site was investigated through the boring program, the point geophysical measurements (P-S Suspension and Downhole), and the surface measurements (Refraction). The stratigraphy, layer notation and layer thickness are taken from the geotechnical boring logs. The results from the geophysical investigations are provided in Section 2.5.4.2.2.2.3.

The following steps have been used to develop the best estimate of the compression and shear-wave velocity profiles for the BBNPP site:

- ◆ The P-S suspension logging, downhole data and Free-Free test results from G-401 and B-401 are consistent, as shown in Figure 2.5-86. The P-S suspension logging and downhole data from G-426 are consistent, as shown in Figure 2.5-88. The shear wave velocity is taken as the average of survey results and laboratory tests.
- ◆ For G-423, P-S suspension logging data was less reliable than downhole data, as shown by the data scatter in Figure 2.5-87. Thus, a higher weight (65%) is given to downhole data in this boring.
- ◆ For the Overburden Soil, Weathered Rock and Transition Zone, the best estimate shear wave velocity is obtained by averaging the data from the three geophysical borings. However, for Sound Rock, the geophysical results from G-401 and G-426 were averaged, and G-423 is treated separately.
- ◆ Data for G-423 show a lower shear wave velocity for Sound Rock southeast of the Nuclear Island. This lower velocity agrees with a lower unconfined compressive strength of rock samples (See Table 2.5-27) obtained from that section of the BBNPP site, in slightly more weathered shale. Closer fracture spacing, as observed at the site, has limited vertical and lateral extension, and increases the weathering on the commonly massive moderately fresh shales of the Mahantango Formation. The presence of an artesian well in that section of the site further supports the observed closer spaced fractures and the subsequent, slightly more weathered shale, with lower shear wave velocities.
- ◆ G-401 is the deepest geophysical boring at the BBNPP site, but the geophysical measurements do not reach 9,200 ft/s (hard rock), which is required for site response

studies. To extend the current profile at G-401 to hard rock, the geology of the BBNPP site vicinity and best estimate shear wave velocity profile for the NI for the initial (2007) BBNPP site was considered. Note that, the geophysical measurements at the initial BBNPP site provided measurements in excess of 9,200 ft/s (2800 m/s) at depths of about 300 ft (91 m). The bedding planes of the Sound Rock of the Mahantango Formation dips 10 degrees to the north-northwest (NNW) in the vicinity of the 2007 and 2010 BBNPP sites. Also, the center of the NI at the 2007 BBNPP Power Block location is approximately 1010 ft (308 m) NNW of the center of the NI at the 2010 BBNPP Power Block location.

- ◆ Lower bound and upper bound estimates are determined by analyzing the spread in the data through a standard deviation. The standard deviation is obtained by grouping readings from similar formations.
- ◆ The best estimate is built using the results from the field tests along with engineering judgment and general knowledge gathered from the field conditions and the borehole conditions.
- ◆ The overburden soils, weathered rock and transition zone will be replaced by either engineered fill or concrete fills.
- ◆ The Coefficient of Variation (COV) is determined by analyzing the spread in data from the mean and the standard deviation.

Dynamic Parameters of Concrete Fill

A concrete fill is placed between the foundation mat of the NI and the top of rock. The dynamic properties of the fill are determined as follows:

- ◆ Match the shear modulus of the concrete to the best estimate of the underlying rock;
- ◆ Back calculate the shear modulus and elastic modulus with the use of equations from elasticity;

The shear wave velocity assigned to the concrete fill is 8510 fps (2594 m/s), the unit weight is 150 pcf (23.6 kN/m³), and the Poisson's Ratio is 0.2. These parameters are indicated by Table 2.5-40.

Fill Dynamic Parameters

Table 2.5-40 provides the dynamic properties assigned to the fill materials. These properties are not used for the calculation of the GMRS for the NI. The GMRS are determined as free-field outcrop motions at the ground surface.

Compliant base

Regulatory Guide 1.208 (NRC, 2007b) defines "Hard Rock" as materials with a shear-wave velocity of 9,200 ft/sec (2,800 m/sec) or higher. Site amplification models need to include the soil and soft rock materials down to a rock formation with a minimum shear-wave velocity of 9,200 ft/sec (2,800 m/sec). The BBNPP Subsurface Exploration Program (Figure 2.5-77) included deep borings with depths of 420 ft (128 m). As mentioned in Section 2.5.4.7.4, the BBNPP site geology and initial (2007) BBNPP investigation results are used to extend the soil profile to 9200 ft/s (2800 m/s). Geophysical measurements in excess of 9200 ft/s (2800 m/s) are expected

at depths of about 530 ft (161 m) below the existing ground surface for G-401. For the NI amplification model, the base of the foundation is placed 36 ft (11 ft) below grade. The grade elevation is raised 8 ft (2.4 m) due to flooding levels and the compliant base is placed at a distance of 240 ft (73 m) below the position of the foundation mat.

Strain-Dependent and Linear Properties

Resonant Column, Torsional Shear, Combined Resonant Column Torsional Shear, and Unconfined Resonant Column ("Free-Free") Laboratory Tests were performed on soil and rock samples. The complete set of results from these tests is reported in Section 2.5.4.2. To account for variations in shear-wave velocity across the site, 60 artificial profiles were generated. The procedures and methodologies to incorporate uncertainties of strain-dependent properties are described in Section 2.5.2.5.1.3.

2.5.4.7.5 Acceleration Time Histories for Soil-Structure Interaction

For reconciliation of site-specific design parameters affecting the SSE analysis results, refer to Sections 3.7.1 and 3.7.2.

2.5.4.8 Liquefaction Potential

The potential for soil liquefaction at the Bell Bend Nuclear Power Plant site was evaluated following NRC Regulatory Guide 1.198 (NRC, 2003c). The soil properties and profiles utilized are those described in Section 2.5.4.2.

Section 2.5.4.8.1 and Section 2.5.4.8.2 are added as a supplement to the U.S. EPR FSAR.

2.5.4.8.1 Regulatory Guide 1.198

Regulatory Guide 1.198, Procedures and Criteria for Assessing Seismic Soil Liquefaction at Nuclear Power Plant Sites, (NRC, 2003c) was used for the evaluation of the potential for soil liquefaction at the BBNPP site.

Under "Screening Techniques for Evaluation of Liquefaction Potential," NRC Regulatory Guide 1.198 (NRC, 2003c) lists the most commonly observed liquefiable soils as fluvial-alluvial deposits, eolian sands and silts, beach sands, reclaimed land, and uncompacted hydraulic fills. The liquefaction evaluation included all soils at the BBNPP site. NRC Regulatory Guide 1.198 (NRC, 2003c) indicates that clay to silt, silty clay to clayey sand, or silty gravel to clayey gravel soils can be considered potentially liquefiable. The geology at the BBNPP site includes glacial overburden soils that consist of wind deposited and glacial transported sands and boulders. These soils will not be used for foundation purposes and are classified as liquefiable due to the presence of loose sand pockets that returned extremely low blow counts. NRC Regulatory Guide 1.198 (NRC, 2003c) indicates that if the geologic site evaluation indicates the presence of potentially liquefiable soils, the resistance of these soils to liquefaction or significant strength loss to cyclic pore pressure generation should be evaluated. The liquefaction evaluation (Section 2.5.4.8.2) indicates that some zones at the BBNPP site are susceptible to liquefaction. Residual shear strength is not evaluated since these soils will be removed from the site and will not be used for the foundation of the facilities.

2.5.4.8.2 Liquefaction Analysis

The in-situ, overburden soils will not be directly used for the foundation of safety-related facilities. Even though recorded shear wave velocities were in the excess of 1000 fps (305 m/s),

the liquefaction potential evaluation identified "pockets" or zones of loose sand with extremely low blow counts.

Assessments of liquefaction for the BBNPP site were based on observations and conclusions from the filed investigation. The NI structures will be built on top of concrete. Shallow foundations for other Category I and non-Category I Power Block structures are to be founded on concrete or the Mahantango Formation.

Based on the information obtained during the investigations of the underlying soil encountered at the BBNPP site, an evaluation of the soil liquefaction potential was performed using the screening techniques proposed in the Regulatory Guide 1.198 (NRC, 2003c).

More than 500 samples at different depths, from 0 ft to 53 ft (0 m to 16.2 m), were used in the evaluation.

The guidelines proposed by Youd (Youd, 2001) were followed in the evaluation. The factor of safety against liquefaction is determined by Equation 2.5.4-9

$$FS = \left(\frac{CRR_{7.5}}{CSR} \right) MSF \cdot K_{\sigma} \cdot K_{\alpha} \quad \text{Eq. 2.5.4-9}$$

- $CRR_{7.5}$ → Cyclic Resistance Ratio for a 7.5 Magnitude Earthquake,
- CSR → Cyclic Stress Ratio,
- MSF → Magnitude Scaling Factor for a different magnitude earthquake,
- K_{σ} → Confining Stress Correction Factor,
- K_{α} → Sloping Ground Correction Factor,

The CSR is provided by Equation 2.5.4-10

$$CSR = 0.65(a_{max}) \left(\frac{\sigma_{vo}}{\sigma'_{vo}} \right) r_d \quad \text{Eq. 2.5.4-10}$$

- p_{AS} → Peak horizontal ground acceleration (0.30 g)
- σ_{vo} → Total vertical stress
- σ'_{vo} → Effective vertical stress
- r_d → Stress reduction coefficient (flexibility of soil profile)

The estimation of the Peak Ground Acceleration (PGA) should correspond to the maximum amplified acceleration at the point of the liquefaction assessment. For the purpose of the liquefaction evaluation, a PGA equal to 0.30 g is used. This value envelops the maximum Ground Motion Response Spectra for the BBNPP site. Refer to Section 2.5.2 for GMRS parameters.

Two criteria are applicable to evaluate the Cyclic Resistance Ratio (CRR):

1. Shear Wave Velocity Criterion
2. Standard Penetration Resistance

2.5.4.8.2.1 Shear Wave Velocity Criterion for Liquefaction Analysis

The Shear Wave Velocity criterion uses the shear wave velocity of the soils to provide a reasonable estimate of the CRR. Disadvantages of the shear wave velocity method are that no samples are extracted and that thin liquefiable layers may be undetected. Another disadvantage is that there is usually limited number of measurements at a site and a specific location with liquefaction potential might be left undetected.

The CRR is determined from Equation 2.5.4-11

$$\text{CRR} = a \left(\frac{V_{s1}}{100} \right)^2 + b \left(\frac{1}{V_{s1}^* - V_{s1}} - \frac{1}{V_{s1}^*} \right); V_{s1} = V_s \left(\frac{P_a}{\sigma'_{vo}} \right)^{0.25}; V_{s1} \leq V_{s1}^* \quad \text{Eq. 2.5.4-11}$$

- CRR → Cyclic Resistance Ratio,
 a → Curve fitting parameter (0.022),
 b → Curve fitting parameter (2.8),
 V_{s1} → Shear wave velocity with correction for overburden stress,
 V_{s1}^* → Limiting shear wave velocity,
 P_a → Atmospheric Pressure,
 σ'_{vo} → Effective vertical stress.

The limiting shear wave velocity varies between 656 fps (200 m/s) for soils with 35 percent fine content and 705 fps (215 m/s) for soils with fines content of 5 percent or less. A value of 676 fps (206 m/s) was used for the evaluation. The potential for liquefaction is analyzed by plotting the CRR against the corrected shear wave velocity and comparing against a curve that represents the onset of liquefaction (Youd, 2001). The plot is provided by Figure 2.5-119. The BBNPP data points are clearly away from the liquefaction zone. According to the shear wave velocity method, there is no potential for liquefaction at the site. However, as previously stated, one of the disadvantages of this methodology is the limited number of measurements and this is the case at the BBNPP site. Therefore, an SPT analysis approach is required.

2.5.4.8.2.2 SPT Criteria for Liquefaction Analysis

The SPT data was used to estimate liquefaction potential. The abundant amount of gravels and boulders encountered during the investigation may reduce the effectiveness of the SPT method. However, it is the best means to detect liquefiable sand pockets. With this method, the CRR is calculated as follows:

$$\text{CRR}_{7.5} = \frac{1}{32 - (N_1)_{60}} + \frac{(N_1)_{60}}{135} + \frac{50}{(10 \cdot (N_1)_{60} + 45)^2} - \frac{1}{200} ; (N_1)_{60} < 30 \quad \text{Eq. 2.5.4-12}$$

where $(N_1)_{60}$ is the drill rod energy ratio divided by 60.

If $(N_1)_{60}$ is greater than 30, the soil is considered to be non-liquefiable. $(N_1)_{60}$ is calculated by dividing the drill rod energy ratio by 60. The lowest energy ratio recorded at the field from hammer calibration was 78 percent. This value is used to determine $(N_1)_{60}$ from the raw blow counts.

Figure 2.5-120 provides the results of the SPT liquefaction analysis. Each sample data point is categorized as liquefiable, non-liquefiable, or borderline liquefiable. It is worth noting that some instances registered zero blow counts, meaning that the weight of the hammer and the drilling rod was enough to penetrate the soil. These zones correspond to areas of wind deposited sands placed during the coldest period of the glacial event. Figure 2.5-120 provides a diagram of the location of the liquefiable zones. The depth of these zones is variable, ranging in depth from 10 ft (3 m) to 45 ft (14 m).

Based on the SPT analysis, it is concluded that the "In-Situ" overburden soils at the BBNPP site are prone to liquefaction. Since the overburden soil was determined to be liquefiable using SPT data, the lack of CPT data is not an issue.

2.5.4.8.2.3 Liquefaction Analysis - Conclusion

Regardless of the high shear wave velocity of the Glacial Overburden, these soils will be removed from the site and will not be used in their natural condition for foundation or lateral support. The soils from this formation are candidates for engineered fill or backfill through enforcement of appropriate screening and compaction techniques.

Section 2.5.4.5 describes material specifications and compaction for structural fill and backfill..

Liquefaction in engineered fill is not an issue if the recommended compaction practices are followed. Liquefaction occurs in loose sands and/or silts with poor gradation. An engineered fill is a compacted and well graded soil structure. Compaction practices need to be monitored during construction.

Liquefaction of granular engineered fills will be prevented by assuring that the fill and backfill specifications are met during the implementation stages. Particular attention will be placed on the grain size and compaction requirements to ensure the specifications are fully met. Section 2.5.4.2.3 provides information related to the specifications for engineered soils. It is emphasized that the specification will include requirements for an on-site testing laboratory for quality control, especially material gradation and plasticity characteristics, the achievement of specified moisture-density criteria, fill placement/compaction, and other requirements to ensure that the fill operations conform to the earthwork specification for BBNPP.

2.5.4.9 Earthquake Site Characteristics

Section 2.5.2.6 describes the development of the Safe Shutdown Earthquake ground motion for the BBNPP site. The selected ground motion is based on the risk-consistent/performance-based approach of NRC Regulatory Guide 1.208, "A Performance-Based

Approach to Define the Site-Specific Earthquake Ground Motion" (NRC, 2007b) with reference to NUREG/CR-6728 (NRC, 2001) and ASCE/SEI 43-05 (ASCE, 2005). Any deviation from the guidance provided in Regulatory Guide 1.208 is discussed in Section 2.5.2. Horizontal ground motion amplification factors are developed in Section 2.5.2.5 using site-specific data and estimates of near-surface soil and rock properties presented in Sections 2.5.4.2, 2.5.4.4 and 2.5.4.7. These amplification factors are then used to scale the hard rock spectra, presented in Section 2.5.4.2, to develop Uniform Hazard Response Spectra (UHRS), accounting for site-specific conditions using Approach 2B of NUREG/CR-6769 (NRC, 2002). Horizontal SSE spectra are developed from these soil UHS, using the performance-based approach of ASCE/SEI 43-05, accepted by Regulatory Guide 1.208. The Ground Motion Response Spectra (GMRS) is defined at the ground surface. Section 2.5.2.6 also describes vertical ground motion, which was developed by scaling the horizontal spectrum by a frequency-dependent vertical-to-horizontal (V:H) factor.

2.5.4.10 Static Stability

The area of planned BBNPP is graded to establish the final plant elevation, which is to be at elevation 719 ft (219 m) at the center of the Reactor Building. The Reactor, Safeguard, and Fuel Buildings are seismic Category I structures and are supported on a common basemat. The common basemat has an irregular shape, estimated to be approximately 80,170 ft², (7450 m²) in plan. All Category I structures' size and depth ranges are summarized in Table 2.5-41.

Structure locations and designations are shown in Figure 2.5-77. Other major structures in the Power Block area are the Nuclear Auxiliary Building, RadWaste Building, and the Turbine Building, which are non-Category I structures.

Construction of the Nuclear Island basemat requires an excavation of about 39 ft (12 m) from the existing elevation of approximate elevation 667 ft (203 m) msl. No rebound (heave) in the ground due to the removal of the soils is expected at the Mahantango Formation. The Mahantango rock is extremely dense and was heavily consolidated by marine deposition. The removal of overburden soils will have no effect since the elastic modulus of the rock is very high.}

2.5.4.10.1 Bearing Capacity

The U.S. EPR FSAR includes the following COL Item in Section 2.5.4.10.1:

A COL applicant that references the U.S. EPR design certification will verify that site-specific foundation soils beneath the foundation basemats of Seismic Category I structures have the capacity to support the bearing pressure with a factor of safety of 3.0 under static conditions, or 2.0 under dynamic conditions, whichever is greater.

This COL Item is addressed as follows:

{The bearing capacity of the subsurface materials depends (1) on the properties of the foundation soils or rocks, including dimensions of bearing strata and geotechnical strength parameters, (2) on the geometry of the building foundations, (3) on the foundation depth, and (4) on the position of the water table. Geotechnical properties and soil profiles are detailed in Section 2.5.4.2. The foundation depth, building geometry and contact pressure are provided in Section 2.5.4.3, and particularly in Table 2.5-41. The Seismic Category I NI and the other facilities are founded on either sound rock of the Mahantango Formation or the concrete fill. The bearing capacity estimates for the Mahantango Formation are determined with the use of

Rock Mass Rating (RMR), cohesion, internal friction angle, and the unconfined compressive strength. The upper bound of the ultimate bearing capacity of structures placed on top of concrete is set at the compressive strength of concrete. If the bearing capacity of rock is higher than this threshold, then the concrete compressive strength is used as the recommended value. The bearing capacities from either concrete or bedrock are very high and they exceed the minimum requirements established by the U.S. EPR FSAR. Section 2.5.4.10 details the methodologies used to obtain bearing capacity and settlement according to the reference documents. Table 5.0-1 of the U.S. EPR Tier 1, and U.S. EPR FSAR Table 2.1-1 identify identifies the soil bearing capacity as a required parameter to be enveloped. It is defined as "Maximum static bearing demand is 24,000 lbs/ft² at the bottom of the Seismic Category I structure basemats." Accordingly, the Seismic Category I NI foundation is sized and reinforced to accommodate these bearing pressure values.

The ultimate bearing capacity of rock underlying the concrete fill or foundations is estimated by two different methods: the traditional Buisman-Terzaghi (Terzaghi, 1943) and Hoek and Brown (1997). Conservatively, the minimum of the results from the two approaches is selected as a recommended bearing capacity.

The bearing capacity per Buisman-Terzaghi (Terzaghi, 1943) is determined by Eq. 2.5.4-13.

$$q_{ult} = cN_c + 0.5 \gamma B N_\gamma + \gamma_D D N_q \quad \text{Eq. 2.5.4-13}$$

q_{ult}	→	Ultimate bearing capacity
c	→	Cohesion intercept for rock mass
γ	→	Effective unit weight of rock mass
γ_D	→	Effective unit weight of material(s) above foundation depth
B	→	Width of foundation
D	→	Foundation depth

The terms N_c , N_γ , and N_q are bearing capacity factors defined by Eqs. 2.5.4-14 through 2.5.4-17, respectively.

$$N_c = 2N_\phi^{0.5}(N_\phi + 1) \quad \text{Eq. 2.5.4-14}$$

$$N_\gamma = N_\phi^{0.5}(N_\phi^2 - 1) \quad \text{Eq. 2.5.4-15}$$

$$N_q = N_\phi^2 \quad \text{Eq. 2.5.4-16}$$

Eq. 2.5.4-17

$$\text{where } N_{\phi} = \tan^2\left(45 + \frac{\phi}{2}\right)$$

ϕ → Internal friction angle of rock mass

The surcharge pressure (i.e., $Y_D DN_q$ in Eq. 2.5.4-13) is neglected conservatively herein.

Assuming a failure mode approximated by active and passive wedge, Hoek and Brown (1997) propose a conservative, lower bound estimate of bearing capacity determined via Hoek-Brown strength parameters (m and s). Considering equilibrium of failure wedges, the vertical stress (i.e., ultimate bearing capacity) applied on a strip footing is expressed by Eq. 2.5.4-18.

$$q_{ult} = q_u(s^{0.5} + m) \quad \text{Eq. 2.5.4-18}$$

q_u → Unconfined compressive strength of rock mass

The Hoek-Brown strength parameters (m and s) are listed in Table 10.4.6.4-4 of the AASHTO LRFD Design Specification (AASHTO, 2007b) in terms of Rock Mass Rating (RMR) value and rock types. For the sound rock of the Mahantango Formation, the average of the measured RMR of 63 and the rock type of B (i.e., Shale) are used for the Hoek-Brown strength parameters.

The subsurface conditions and properties were described in Section 2.5.4.2. The rock properties of the Mahantango Formation, conservatively designated for the rock strata, were used for the bearing capacity estimation, as shown by the recommended RMR and strength parameters presented on Table 2.5-35 and Table 2.5-36, respectively.

The ultimate bearing capacity per the two methods is for a strip footing, which is hence modified for a desired foundation shape via shape correction factor according to the length-width ratio of foundation (Sowers, 1979). Then, the allowable static and dynamic bearing capacities are determined using the corresponding factors of safety of 3 and 2, respectively. Of the resulting allowable bearing capacities of rock and the factored bearing strength of concrete per ACI 318-05 (ACI, 2005), the minimum values are conservatively recommended and shown on Table 2.5-43.

For the BBNPP site-specific conditions, the calculated allowable bearing pressures for the NI meet the maximum static bearing demand of 24 ksf identified in the U.S. EPR FSAR. The site-specific foundation soils beneath the NI basemat and other safety class facilities have been verified to have the capacity to support the required bearing pressures with a Factor of Safety of 3.0 under static conditions and a Factor of Safety of 2.0 under dynamic conditions.}

2.5.4.10.2 Settlement

The U.S. EPR FSAR includes the following COL Items in Section 2.5.4.10.2:

A COL applicant that references the U.S. EPR design certification will provide an assessment of predicted settlement values across the basemat of Seismic Category I structures during and post construction. The assessment will address both short term (elastic) and long term (heave and consolidation) settlement effects with the site specific soil parameters, including the soil loading effects from adjacent structures.

A COL applicant that references the U.S. EPR design certification will verify that the predicted tilt settlement value of ½ inch per 50 ft in any direction across the foundation basemat of a Seismic Category I structure is not exceeded. Settlement values larger than this may be demonstrated acceptable by performing additional site specific evaluations.

These COL Items are addressed as follows:

{This COL Item is addressed in the following section and in Section 3.8.5.

The safety-related Category I facilities at the BBNPP site will bear either on top of the Mahantango Formation or concrete or a combination of both materials. The overburden deposits will not be used as foundation material due to their inherent risk of liquefaction.

ELASTIC SETTLEMENT EVALUATION

Elastic settlement for the rigid foundation case is evaluated using the solution for the homogenous isotropic rock case and based on a closed-form solution given in Rock Foundations, Technical Engineering and Design Guides as adapted from the US Army Corps of Engineers, No. 16, American Society of Civil Engineers (ASCE, 1996).

Homogeneous, Isotropic Rock

Vertical settlement, δ_v , for foundations bearing on homogeneous isotropic rock can be estimated with Eq. 2.5.4-20 (Wyllie, 1992)

$$\delta_v = \frac{C_d q B (1 - \mu^2)}{E}$$

Eq. 2.5.4-20

C_d	=	factor accounting for the foundation shape and location where settlement is calculated;
q	=	uniformly distributed bearing pressure or contact pressures;
B	=	smaller dimension of a rectangular foundation, or diameter of a circular foundation;
μ	=	Poisson's ratio;
E	=	Young's modulus.

Closed-form Solution

The equation for the closed-form solution is shown in Eq. 2.5.4-21.

$$\delta_a = \frac{1.12qB(1 - \mu^2) \left(\frac{L}{B}\right)^{0.5}}{E_d} \quad \text{Eq. 2.5.4-21}$$

δ_a	=	maximum deformation at center of foundation;
q	=	uniformly distributed bearing pressure or contact pressures;
B	=	smaller dimension of a rectangular foundation, or diameter of a circular foundation;
L	=	foundation length;
μ	=	Poisson's ratio;
E_d	=	modulus of deformation of the foundation rock.

Although Eq. 2.5.4-21 is suitable for rectangular foundation, the circular foundation of the Reactor Building with Diameter ~ 183 ft within the Nuclear Island is considered as a square foundation with each side of the foundation $B \sim 183$ ft for the purpose of this simplified elastic settlement analysis.

For rigid foundations where rigid uniformly loaded foundations settle uniformly, the estimated elastic settlement is obtained by multiplying the maximum estimated settlement for a flexible foundation of the same dimensions using Eq. 2.5.4-21 by a reduction factor.

Additionally, the elastic modulus of the foundation bearing material is derived from the best estimate shear modulus based on the in-situ seismic velocity tests. The seismic elastic modulus at low strains is usually reduced for the static elastic modulus at high strains. The modulus reduction factor, β , varies with the rock quality. Based on the boring logs, the rock quality designation (RQD) of the Mahantango Formation averages about 86%. The reduction factor, β , ranges between 0.3 to 1 for RQD at 86%. A β value of 0.5 is applied to the Elastic modulus used in this analysis.

Elastic settlement considering the flexible foundation option is evaluated using the Boussinesq's Solution and the closed-form solution (Eq. 2.5.4-21) adapted from the US Army Corps of Engineers. Eq. 2.5.4-21 provides the maximum settlement at the center of a flexible foundation; therefore, depending on the location of the rectangular foundation where settlement is desired, a "location" reduction factor is applied to the resulting settlement according.

Boussinesq's Solution

For circular foundation at depth $z=0$, displacement at the center of the circular loaded area can be estimated by using Eq. 2.5.4-22

$$w = \frac{q_b B (1 - \nu^2)}{E} \quad \text{Eq. 2.5.4-22}$$

At the edge of the circular loaded area, vertical displacement can be estimated using Eq. 2.5.4-23

Eq. 2.5.4-23

$$w = \frac{2q_b B(1 - \nu^2)}{\pi E}$$

- q_b = uniformly distributed bearing pressure or contact pressures;
 B = smaller dimension of a rectangular foundation, or diameter of a circular foundation;
 ν = Poisson's ratio;
 E = Young's modulus.

The settlement under the corner of a rectangular foundation is given by Eq. 2.5.4-24 (Salgado 2008)

Eq. 2.5.4-24

$$w = I \frac{q_b B(1 - \nu^2)}{E}$$

I = influence factor

$$I = \frac{1}{2\pi} \left\{ m \left[\ln \left(\frac{\sqrt{1 + m^2} + 1}{\sqrt{1 - m^2} - 1} \right) \right] + \ln \left(\frac{\sqrt{1 + m^2} + m}{\sqrt{1 - m^2} - m} \right) \right\}$$

$m = L/B$; and B, L = dimensions of rectangular load.

Closed-form Solution

The same closed-form solution described earlier for the rigid foundation is used to estimate settlement for the flexible foundation. Eq. 2.5.4-21 is used to estimate the maximum elastic settlement at the center of the flexible foundation. To obtain the elastic settlement at the corner of the flexible foundation, the settlement at the center is multiplied by a "location" reduction factor based on the length and width ratio of the foundation.

SETTLEMENT ANALYSIS CONCLUSION

Elastic settlement analyses for both the rigid and flexible foundations for all the Category 1 structures of BBNPP are presented in Table 2.5-44.

Settlement at the BBNPP Site is considered negligible since the foundations are founded on competent rock and/or concrete. Differential settlement within each foundation is also well within the tolerable limit set forth in the U. S. EPR FSAR, 0.5 in/50 ft.

The BBNPP Site generally consists of favorable competent surficial materials on which foundations can be placed without significant settlement, and differential settlement concerns.}

2.5.4.10.3 Uniformity and Variability of Foundation Support Media

The U.S. EPR FSAR includes the following COL Item in Section 2.5.4.10.3:

A COL applicant that references the U.S. EPR design certification will investigate and determine the uniformity of the soil layer(s) underlying the foundation basemats of Seismic Category I structures.

This COL Item is addressed as follows:

{Foundations of all Seismic Category I structures at the BBNPP site are supported on either bedrock or concrete fill which is in turn supported on bedrock. Regardless of the variable depth to bedrock, as depicted by Figure 2.5-82, non-uniform foundation conditions resulting from combined soil-rock support are not applicable to foundations at the BBNPP site. Each of the Seismic Category 1 structures will be founded either on top of rock or concrete fill.

The Mahantango formation extends across the Power Block Area with similar properties. Using a large volume of concrete as the foundation bearing layer also promotes the uniformity around the site. Combined rock/concrete layers underneath the Power Block area constitute competent and laterally uniform layers underneath the foundations.

The V_s values were evaluated to a depth of approximately 500 ft (152 m) below the Nuclear Island (NI) foundation basemat. The 500 ft (152 m) value was selected based on the three U.S. EPR FSAR criteria of: 1) 1.5 times an equivalent radius of foundation basemat, 2) 1.0 times the maximum foundation basemat dimension, or 3) no less than 200 ft below the bottom of the foundation basemat; with criterion (2) selected as the governing condition for the BBNPP NI basemat for its greater dimension. It is noted that minor appendages and protrusions in the irregularly-shaped U.S. EPR NI foundation were ignored in selecting this depth.

Detailed V_s data are presented in Section 2.5.4.2.2, along with an evaluation of the shear wave velocity conditions. Figure 2.5-86 through Figure 2.5-88 present the plots for compressional and shear wave velocities. The plots provide the results from the two different surveys performed: downhole test, and PS-Suspension Logging. Overburden soils will not be used for foundation purposes and therefore an analysis of the variation of the shear wave velocity is only applicable for the Mahantango Formation.

The recommended shear wave velocity profile under the Nuclear Island is plotted by Figure 2.5-93. The shear wave velocity shows an increasing trend, directly related to depth or confining pressure. Therefore, as shown by the figure, the Mahantango Formation was subdivided in sub-layers to depict the vertical variation of the shear wave velocity. In a distance of about 350 ft (107 m) the shear wave velocity increases up to 9600 fps (2930 m/s). At each sub-layer the Coefficient of Variation (COV) originated from different readings at different locations and with different methodologies is close to 10% and not exceeding 15%. Variation in the vertical direction was accounted for in the site amplification analysis by the layer subdivision of this formation. Therefore, it has been accounted for in developing the site-specific horizontal and vertical ground motion response spectra (GMRS) shown in Figure 2.5-36.

Evaluation of Horizontal Layer Assumption

The dipping angle of the competent Mahantango rock is less than 8%. This angle is well within the U.S. EPR Final Safety Analysis Report which reads: "If the dip is less than or equal to 20 degrees, the layer is defined as horizontal and analyses using horizontal layers are applicable." In addition, the concrete above the Mahantango formation will have a close shear wave velocity and therefore, the sloping effects will be mitigated.

The rock/concrete interface is horizontal beneath the totality of the foundation of each particular building. As described in Section 2.5.2, the site response analysis accounts for the variability in thickness of the subsurface layers through randomization of the soil profiles and properties. Furthermore, the proposed concrete fill configuration will promote a uniform and coherent seismic response throughout the foundations at the site. On this basis, the soil layers at the BBNPP site are considered horizontal.

It is therefore concluded that the non-horizontal nature of rock/concrete interface does not impact the results obtained with the use of one-dimensional seismic wave propagation analysis as recommended in the current regulatory guidance (RG. 1.208).}

2.5.4.10.4 Site Investigation for Uniform Sites

No departures or supplements.

2.5.4.10.5 Site Investigations for Non-uniform Sites

No departures or supplements.

{Section 2.5.4.10.6 is added as a supplement to the U.S. EPR FSAR.

2.5.4.10.6 Earth Pressure

Static and seismic lateral earth pressures are addressed for plant below-grade walls. Seismic earth pressure diagrams are structure-specific. They are only addressed generically herein. Specific earth pressure diagrams are developed for specific structures based upon each structure's final configuration. Fill and backfill will be granular, compacted soils formed by sand/gravel mixtures. Typical values of the friction angle for these types of fills are in excess of 38 degrees (Carter, 1991). A friction angle is conservatively selected. Structural backfill material is verified to meet the design requirements prior to use during construction.

2.5.4.10.6.1 Static Lateral Earth Pressures

$$p_{AS} = K_{AS}\gamma z$$

The static active earth pressure, p_{AS} , is estimated using the following expression:

$$p = K \gamma z \quad \text{Eq. 2.5.4-16}$$

p_{AS}	→ Active (p_a), Passive (p_p), or At Rest (p_o) Pressure,
K_{AS}	→ Active (K_a), Passive (K_p), or At Rest (K_o) Pressure Coefficient as defined by Section 2.5.4.10.6.5,
γ	→ Unit weight of backfill (140 pcf),
z	→ Depth below ground surface.

2.5.4.10.6.2 Dynamic Earth Pressures

The following symbols apply:

P_{ae}	→	Dynamic active earth force,
P_{pe}	→	Dynamic passive earth force,
K_{ae}	→	Dynamic active earth pressure coefficient,
K_{pe}	→	Dynamic passive earth pressure coefficient,
k_h	→	Horizontal earthquake acceleration
k_v	→	Vertical earthquake acceleration
γ_{sat}	→	Saturated Unit Weight,
γ'	→	Effective Unit Weight,
F_r	→	Resultant force associated with dynamic soil pressure distribution,
M_r	→	Resultant overturning moment about base of retaining structure,
H	→	Embedment Height,
α_h	→	Horizontal earthquake acceleration (g),
ν	→	Poisson's ratio,
$C_v D_v$	→	Empirical Coefficients as a function of Poisson's ratio.

The active/passive earth force on a wall (cohesionless and dry backfill) is estimated as follows:

$$P_{ae} = \frac{1}{2} \gamma K_{ae} H^2 K_{AE} \quad ; \quad P_{pe} = \frac{1}{2} \gamma K_{pe} H^2 K_{PE} \quad \text{Eq. 2.5.4-17}$$

The total active/passive thrust, P_{ae} , can be divided into a static component, P_a , and a dynamic component, ΔP_{ae} :

$$P_{ae} = P_a + \Delta P_{ae} \quad ; \quad P_{pe} = P_a + \Delta P_{pe} \quad \text{Eq. 2.5.4-18}$$

2.5.4.10.6.3 Sample Earth Pressure Diagrams

Using the relationship outlined above and assumed backfill properties, sample earth pressures are estimated. Sample earth pressure diagrams are provided in Figure 2.5-121 for a wall height of 36 ft (11 m), level ground surface, and, for conservative purposes, with groundwater level at 13.14 ft (4.00 m) below the surface. The backfill is a granular soil, with an angle of friction of 35 degrees and a unit weight of 140 pcf (22.4 kN/m³). The horizontal ground acceleration is taken as 0.17g. The validity of assumptions regarding surcharge loads, backfill properties, and structural configurations is confirmed during the detailed design stage. Actual earth pressure evaluations are performed at that time for the design of below-grade walls, based on actual project conditions. The results of these earth pressure evaluations shall be included in an update to this FSAR at that time.

2.5.4.10.6.4 Selected Design Parameters

The field and laboratory test results are discussed in Section 2.5.4.2. The parameters employed for the bearing capacity, settlement, and earth pressure evaluations are based on the material characterization addressed in Section 2.5.4.2. Normal Groundwater Elevation is approximately 15 ft (4.6 m) below grade. A value of 3.0 is commonly used as the factor of safety when determining the bearing capacity of soils. An angle of shearing resistance of 35 degrees is used for characterization of a structural backfill for earth pressure evaluations, which is considered conservative for granular fill compacted to 90 percent Modified Proctor compaction.

2.5.4.10.6.5 Earth Pressure Coefficients

Active, passive, and at-rest lateral earth pressure coefficients, K_A , K_P , and K_O , respectively, are estimated assuming frictionless vertical walls and horizontal backfill by the following relationships:

Active Earth Pressure Coefficient:

$$K_a = \tan^2 \left(45 - \frac{\phi'}{2} \right) \quad \text{Eq. 2.5.4-4}$$

Passive Earth Pressure Coefficient:

$$K_p = \tan^2 \left(45 + \frac{\phi'}{2} \right) \quad \text{Eq. 2.5.4-5}$$

At-Rest Earth Pressure Coefficient:

The At-Rest Earth pressure coefficient depends mainly on the deposition process of the formation, and the stress history. Its value is between the active and passive earth pressure coefficients and there are documented relationships to estimate its value, for example:

$$\text{General Application (Bowles, 1996), } K_o = 1 - \sin \phi \quad \text{Eq. 2.5.4-6}$$

In order to account for compaction effects on engineered fills, the Passive Earth Pressure Coefficient is modified with Equation 2.5.4-10 (Bowles, 1996).

$$K_{oc} = K_o (5.8 \sin(\phi') - 2.1)$$

Eq. 2.5.4-7

Dynamic Active and Passive Earth Pressure Coefficient:

The Dynamic Active and Passive Earth Pressure Coefficients are determined according to the Mononobe-Okabe theory. For a vertical wall and a horizontal grade the theory provides Equations 2.5.4-8(a) through 2.5.4-8(c).

$$K_{PE} = \frac{\sin^2(\alpha - \theta + \phi)}{\cos \theta * \sin^2 \alpha * \sin(\alpha - \theta - \delta) \left[1 - \sqrt{\frac{\sin(\phi + \delta) * \sin(\phi + \beta - \theta)}{\sin(\alpha - \theta - \delta) * \sin(\alpha - \beta)}} \right]} \quad \text{Eq. 2.5.4-8 (a)}$$

$$K_{AE} = \frac{\sin^2(\alpha + \theta - \phi)}{\cos \theta * \sin^2 \alpha * \sin(\alpha + \theta + \delta) \left[1 - \sqrt{\frac{\sin(\phi + \delta) * \sin(\phi - \beta - \theta)}{\sin(\alpha + \theta + \delta) * \sin(\alpha - \beta)}} \right]} \quad \text{Eq. 2.5.4-8 (b)}$$

$$\theta = \text{atan} \left(\frac{F_h}{F_v} \right) = \frac{k_h}{1 \pm k_v} \quad \text{Eq. 2.5.4-8 (c)}$$

Where:

- K_{AE} → Dynamic active earth pressure coefficient,
- K_{PE} → Dynamic passive earth pressure coefficient,
- θ → Angle of resultant of seismic load,
- ϕ → Friction angle (Drained conditions),
- δ → Friction between wall and soil ($\delta=2\phi/3$ (Das, 1993)),
- F_h → Horizontal earthquake force,
- F_v → Vertical earthquake force,
- k_h → Horizontal earthquake acceleration (0.25 g),
- k_v → Vertical earthquake acceleration (0.25 g).

Based on the previous equations, Table 2.5-42 provides the recommended earth pressure coefficients .}

2.5.4.11 Design Criteria

No departures or supplements.

2.5.4.12 Techniques to Improve Subsurface Conditions

{Major structures will derive support from the Mahantango Formation or concrete or engineered structural fills. Ground improvement will be limited to excavation of unsuitable

soils, such as liquefiable sands. No in-situ soils in their natural state will be used for foundation or lateral support purposes. Foundation soils will include proof-rolling of foundation subgrade for the purpose of identifying any unsuitable soils for further excavation and replacement, which further densifies the upper portions of the subgrade. In absence of subsurface conditions at the site that require ground improvement, ground control, that is, maintaining the integrity of existing dense or stiff foundation soils, will be the primary focus of earthworks during foundation preparation. These measures will include such steps as groundwater control, use of appropriate measures and equipment for excavation and compaction, subgrade protection, and other similar measures.

2.5.4.13 References

This section is added as a supplement to the U.S. EPR FSAR.

AASHTO, 2004. Standard Method of Test for Determining pH of Soil for Use in Corrosion Testing. AASHTO T289-91, American Association of State Highway and Transportation Officials, 2004.

AASHTO, 2007a. Water Soluble Sulfate Content in Soil. AASHTO T290-95, American Association of State Highway and Transportation Officials, 2007.

AASHTO, 2007b. AASHTO LRFD Bridge Design Specification, 4th ed., American Association of State Highway and Transportation Officials, 2007.

AASHTO, 2008. Standard Method of Test for Determining Water-Soluble Chloride Ion Content in Soil. AASHTO T291-94, American Association of State Highway and Transportation Officials, 2008.

ACI, 2005. Manual of Concrete Practices, ACI-318, American Concrete Institute, 2005.

ASCE, 1996. Rock Foundations, Technical Engineering and Design Guides as adapted from the US Army Corps of Engineers, No. 16, American Society of Civil Engineers, 1996

ASCE, 2005. Seismic Design Criteria for Structures, Systems, and Components in Nuclear Facilities, ASCE/SEI 43-05, American Society for Civil Engineers/Structural Engineering Institute, 2005.

ASTM, 2003. Standard Practice for Sampling Aggregates, ASTM D75-03, American Society for Testing and Materials, 2003.

ASTM, 2004a. Standard Test Method for Consolidated Undrained Triaxial Compression Test for Cohesive Soils, ASTM D4767-04, American Society for Testing and Materials, 2004.

ASTM, 2004b. Standard Practice for Determining the Normalized Penetration Resistance of Sands for Evaluation of Liquefaction Potential, ASTM D6066-96(2004), American Society for Testing and Materials, 2004.

ASTM, 2005a. Standard Test Method for Specific Gravity and Absorption of Rock for Erosion Control, ASTM D6473-99(2005), American Society for Testing and Materials, 2005.

- ASTM, 2005b.** Standard Test Method for Laboratory Determination of Water (Moisture) Content of Soil and Rock by Mass, ASTM D2216-05, American Society for Testing and Materials, 2005.
- ASTM, 2005c.** Standard Test Method for Measurement of Soil Resistivity Using the Two Electrode Soil Box Method, ASTM G187-05, American Society for Testing and Material, 2005.
- ASTM, 2006.** Standard Test Method for Permeability of Granular Soils (Constant Head), ASTM D2434-68(2006), American Society for Testing and Materials, 2006.
- ASTM, 2007a.** Standard Practices for Preserving and Transporting Soil Samples, ASTM D4220-95(2007), American Society for Testing and Materials, 2007.
- ASTM, 2007b.** Standard Test Method Prebored Pressuremeter Testing in Soils, ASTM D4719-07, American Society for Testing and Materials, 2007.
- ASTM, 2007c.** Standard Test Method for Particle Size Analysis of Soils, ASTM D422-63(2007), American Society for Testing and Materials, 2007.
- ASTM, 2008a.** Standard Test Method for Penetration Test and Split-Barrel Sampling of Soils, ASTM D1586-08, American Society for Testing and Materials, 2008.
- ASTM, 2008b.** Standard Practice for Thin-Walled Tube Sampling of Soils for Geotechnical Purposes, ASTM D1587-08, American Society for Testing and Materials, 2008.
- ASTM, 2008c.** Standard Practice for Rock Core Drilling and Sampling of Rock for Site Investigation, ASTM D2113-08, American Society for Testing and Materials, 2008.
- ASTM, 2008d.** Standard Practices for Preserving and Transporting Rock Core Samples, ASTM D5079-08, American Society for Testing and Materials, 2008.
- ASTM, 2008e.** Standard Test Method for Standard Guide for Using Rock Mass Classification Systems for Engineering Purposes, ASTM D5878-05, American Society for Testing and Materials, 2005.
- ASTM, 2009a.** Standard Guide for Field Logging of Subsurface Explorations of Soil and Rock, ASTM D5434-09, American Society for Testing and Materials, 2009.
- ASTM, 2009b.** Standard Practice for Description and Identification of Soils (Visual-Manual Procedure), ASTM D2488-09a, American Society for Testing and Materials, 2009.
- ASTM, 2010a.** Standard Test Method for Energy Measurement for Dynamic Penetrometers, ASTM D4633-10, American Society for Testing and Materials, 2010.
- ASTM, 2010b.** Standard Test Method for Classification of Soils for Engineering Purposes (Unified Soil Classification System), ASTM D2487-10, American Society for Testing and Materials, 2010.
- ASTM, 2010c.** Test Method for Specific Gravity of Soil Solids by Water Pycnometer, ASTM D854-10, American Society for Testing and Materials, 2010.

- ASTM, 2010d.** Standard Test Methods for Liquid Limit, Plastic Limit, and Plasticity Index of Soils, ASTM D4318, American Society for Testing and Materials, 2010.
- ASTM, 2010e.** Standard Test Method for Compressive Strength and Elastic Moduli of Intact Rock Core Specimens under Varying States of Stress and Temperatures, ASTM D7012-10, American Society for Testing and Materials, 2010.
- Bowles, 1996.** Foundation Analysis and Design, 5th Edition, McGraw-Hill Book Company, J. Bowles, 1966.
- Carter, 1991.** Correlations of Soil Properties, Pentech Press Limited, M. Carter and S.P Bentley, 1991.
- Harper, 1999.** Part II. Stratigraphy and Sedimentary Tectonics, Chapter 7: Devonian, in C.H. Shultz ed., The Geology of Pennsylvania: Pennsylvania Bureau of Topographic and Geologic Survey Special Publication 1, J.A. Harper, 1999 .
- Hoek, 1997.** "Practical estimates of rock mass strength", International Journal of Rock Mechanics and Mining Sciences, Vol. 34, No. 8, pp. 1165-1186., E. Hoek and E.T. Brown, 1997.
- Hoek, 2002.** Hoek-Brown Failure Criterion - 2002 Edition, Proceedings of North American Rock Mechanics Symposium and Tunnelling Association of Canada Conference, 2002 E. Hoek, C. Carranza-Torres, and B Corkum, 2002.
- Inners, 1978.** Geology and Mineral Resources of the Berwick Quadrangle, Luzerne and Columbia Counties, Pennsylvania, Pennsylvania Geological Survey, Fourth Series, J.D. Inners, 1978.
- NRC, 2001.** Technical Basis for Revision of Regulatory Guidance on Design Ground Motion: Hazard- and Risk- Consistent Ground Motion Spectra Guidelines, NUREG/CR 6728, Nuclear Regulatory Commission, 2001.
- NRC, 2002.** Technical Basis for Revision of Regulatory Guidance on Design Ground Motion: Development of Hazard- and Risk- Consistent Seismic Spectra for Two Sites, NUREG/CR 6769, Nuclear Regulatory Commission, 2002.
- NRC, 2003a.** Site Investigations for Foundations of Nuclear Power Plants, Regulatory Guide 1.132, Revision 2, Nuclear Regulatory Commission, 2003
- NRC, 2003b.** Laboratory Investigations of Soils for Engineering Analysis and Design of Nuclear Power Plants, Regulatory Guide 1.138, Revision 2, Nuclear Regulatory Commission, 2003.
- NRC, 2003c.** Procedures and Criteria for Assessing Seismic Soil Liquefaction at Nuclear Power Plant Sites, Regulatory Guide 1.198, Nuclear Regulatory Commission, 2003.
- NRC, 2007a.** Combined License Applications for Nuclear Power Plants (LWR Edition), Regulatory Guide 1.206, Nuclear Regulatory Commission, 2006.
- NRC, 2007b.** A performance-Based Approach to Define the Site-Specific Earthquake Ground Motion, Regulatory Guide 1.208, Nuclear Regulatory Commission, 2007.

PPL, 2011. Susquehanna Steam Electric Station, Units 1 and 2, Final Safety Analysis Report, PPL, 2011.

Salgado, 2008. The Engineering of Foundations, 2nd edition McGraw-Hill, R. Salgado, 2008.

Schnabel, 1972. SHAKE, A Computer Program for Earthquake Response Analysis Of Horizontally Layered Site, B. Schnabel, J. Lysmer and H.B. Seed, 1972.

Seed, 1970. Design of Earth Retaining Structures for Dynamic Loads, ASCE Specialty Conference on Lateral Stresses and Earth Retaining Structures, H.B. Seed and R.V. Whitman, June 1970.

Sowers, 1979. Introductory Soil Mechanics and Foundations: Geotechnical Engineering, 4th ed., McMillan, G. Sowers, 1979.

Terzaghi, 1943. Theoretical Soil Mechanics, John Wiley, Terzaghi K., 1943.

UTA, 2009. Free-Free (Fr-Fr) Testing of Soil and Rock Samples, Internal Procedure Fr-Fr-1, Revision 0 Department of Civil Engineering, University of Texas, Austin, Texas, May 2009.

UTA, 2004b. URC-1, Revision 4, Technical Procedures for URC Tests, Department of Civil Engineering, University of Texas, Austin, Texas, August 2004.

Wyllie, 1992. Foundations on Rock, 2nd Edition, E&FN SPON, D. Wyllie, 1992

Youd, 2001. Liquefaction Resistance of Soils: Summary Report from the 1996 NCEER and 1998 NCEER/NSF Workshops on Evaluation of Liquefaction Resistance of Soils, Journal of Geotechnical and Geoenvironmental Engineering, T.L. Youd, M. Idriss, R.D. Andrus, I. Arango, G. Castro, J.T. Christian, R. Dobry, W.D. Finn, L.F. Harder Jr., M.E. Hynes, K. Ishihara, J.P. Koester, S.S. Liao, W.F. Marcuson III, G.R. Martin, J.K. Mitchell, Y. Moriwaki, M.S. Power, P.K. Robertson, R.B. See, and K.H. Stokoe II, October 2001.}

2.5.5 Stability of Slopes

The U.S. EPR FSAR includes the following COL Item for Section 2.5.5:

A COL applicant that references the U.S. EPR design certification will evaluate site-specific information concerning the stability of earth and rock slopes, both natural and manmade (e.g., cuts, fill, embankments, dams, etc.), of which failure could adversely affect the safety of the plant.

This COL Item is addressed as follows:

{References to elevations values in this section are based on the North American Vertical Datum of 1988 (NAVD 88), unless stated otherwise. This section addresses the stability of constructed and natural slopes. It is based on the relevant guidance in NRC Regulatory Guide 1.206, "Combined License Applications for Nuclear Power Plants (LWR Edition)," (NRC, 2007). Constructed slopes evolve as part of the overall site development.

The natural topography at the Bell Bend Nuclear Power Plant (BBNPP) site, at the time of subsurface exploration, is a downward gentle slope towards the west and south of the Power Block, and gently sloping within the vicinity of the Essential Service Water Emergency Makeup

System (ESWEMS) Retention Pond. The site is graded in order to establish the final grade for the project, resulting in minor cuts and fills, as well as slopes. The stability of these slopes and their potential impact on safety related structures are evaluated in this section. In the vicinity of the primary structures and components, there are no significant natural slopes at the site or any steep slopes, undergoing continuous erosion. There is a nine degree slope on the North side of the Power Block, stability of which is assessed in this section.

2.5.5.1 Slope Characteristics

The characteristics of constructed and natural slopes are described below.

2.5.5.1.1 Characteristics of Constructed Slopes

Site grading areas for the BBNPP include the structures in the Power Block, switchyard, cooling towers, Essential Service Water Emergency Makeup System (ESWEMS) Pump House Building, and ESWEMS Retention Pond. The Power Block includes the Reactor Building, Fuel Building, Safeguards Building, Emergency Power Generation Building, Nuclear Auxiliary Building, Access Building, Radioactive Waste Building, and Turbine Building. The centerline of the BBNPP Power Block is graded to elevation 719 ft (219.2 m). The finished grade in the area of each major structure is:

- ◆ Power Block: Elevation 719 ft (219.2 m)
- ◆ Switchyard: Elevation 710 ft (216.4 m)
- ◆ Cooling Tower: Elevation 700 ft (213.4 m)
- ◆ ESWEMS Retention Pond Top of Dike: Elevation 700 ft (213.4 m)

Within the Power Block, site grading requires the excavation of the overburden soil, weathered rock and/or transition zone to an estimated maximum depth of 115.5 ft (35.2 m) and an average depth of 67.4 ft (20.5 m). However, for the ESWEMS Retention Pond, site grading requires excavation of the overburden soils to an estimated maximum depth of 54.5 ft (16.6 m) and an average depth of 40.3 ft (12.3 m). For the BBNPP site, the overburden soil, weathered rock and transition zone are inadequate for the foundation of large safety-related facilities. These materials are replaced with engineered (granular) fill and/or concrete for the Power Block. Inadequate materials are replaced with engineered (granular fill), and cohesive fill for the ESWEMS Retention Pond construction. The ESWEMS Pump House foundation area is excavated to the Mahantango bedrock and replaced with concrete fill. The cut/fill operations result in permanent slopes mainly north of the Power Block, and around the ESWEMS Retention Pond area. Figure 2.5-97 and Figure 2.5-117 present the site grading plan for the Power Block and ESWEMS Retention Pond area, respectively.

2.5.5.1.1.1 Temporary Slopes

Temporary construction slopes are cuts with the steepest slope being 1.5:1 (horizontal-to-vertical). Within the Power Block and the ESWEMS Retention Pond, two typical cross-sections that represent the typical excavation configuration are selected for evaluation based on location (e.g., proximity to Category 1 structures), slope geometry (e.g., height), and soil conditions. Figure 2.5-97, Figure 2.5-98, Figure 2.5-101, Figure 2.5-104, and Figure 2.5-107 show the locations and cross-sections of the slopes within the Power Block, and Figure 2.5-117, Figure 2.5-118 and Figure 2.5-113 show the locations and cross-sections of the slopes within the ESWEMS Retention Pond area. The slope cross sections show final constructed conditions. Temporary slopes are shown by removing fill and concrete and only considering overburden

and rock formations. Figure 2.5-97 and Figure 2.5-117 are excavation plans for the Power Block and ESWEMS Retention Pond area, respectively.

2.5.5.1.1.2 Permanent Slopes

The cut and fill operations at the BBNPP site result in permanent slopes around the Power Block and within the ESWEMS Retention Pond area. Permanent slopes, requiring retaining structures, are constructed with a minimum 1.5:1 (minimum horizontal-to-vertical ratio) slope around the Power Block and north of the ESWEMS Retention Pond area. The dike of the ESWEMS Retention Pond has a 3:1 (horizontal to vertical) upstream slope. The bottom of the ESWEMS Retention Pond is at an elevation of 677.5 ft (206.5 m). The ESWEMS Pump House is supported on concrete fill on top of the Mahantango bedrock. The stability of the ESWEMS Pump House is not affected by the adjacent slopes and its presence does not affect the stability of adjacent slopes. The design of the retention pond is addressed in Section 2.4 and Section 9.2.5 of the BBNPP FSAR.

The location of cross-sections that represent the typical site grading configuration are selected for evaluation based on location, slope geometry and soil conditions as shown in Figure 2.5-97 for the Power Block and in Figure 2.5-117 for ESWEMS Retention Pond area. The cross-sections of the permanent slopes are shown in Figure 2.5-98, Figure 2.5-101, Figure 2.5-104, and Figure 2.5-107 (Power Block) and Figure 2.5-113 and Figure 2.5-118 (ESWEMS Retention Pond area).

2.5.5.1.2 Characteristics of Natural Slopes

The BBNPP Site is located on top of a hill, having its highest point in the northeast area of the Power Block. The finish grade elevation along the center line of the Power Block is 719 ft (219.2 m). Within the Power Block, the natural grade elevation varies from 693.8 to 802.0 ft (211.5 to 244.5 m), with an average elevation of 750.6 ft (228.8 m). Within the ESWEMS Retention Pond area, the natural grade elevation varies from 666.9 to 687.3 ft (203.3 to 209.5 m), with an average elevation of 677.9 ft (206.6 m). There are no natural slope instability concerns in the plant vicinity. Section 2.5.5.2 provides the slope stability analysis results.

2.5.5.1.3 Exploration Program and Geotechnical Conditions

The geotechnical exploration program, groundwater conditions, sampling, materials and properties, liquefaction potential, and other geotechnical parameters are addressed in Section 2.5.4. A summary relevant to the slope stability evaluation is presented below.

A geotechnical subsurface investigation was performed to characterize the upper 420 ft (128 m) of soil and rock materials. The site geology is comprised of an overburden soil deposit underlain by the Mahantango formation.

As explained in Section 2.5.4, the subsurface is divided into the following stratigraphic units:

Overburden Soil: silty sand and gravel with varying amount of clay and silt.

Mahantango Formation: this unit is further divided into three horizons as follows:

- ◆ Weathered Rock: intensively weathered yellowish gray shale
- ◆ Transition Zone: moderately weathered, moderately fractured, medium to dark gray shale

◆ Sound (Competent) Rock: massive medium to dark gray shale

Within the Power Block, the overburden soil is derived from intensely weathered shale, and varies in thickness from 7.5 to 60.0 ft (2.3 to 18.3 m). The thicknesses of the weathered rock and transition zone vary from 0 to 46.3 ft (0 to 14.1 m) and from 0 to 84.0 ft (0 to 25.6 m), respectively. The sound rock of the Mahantango formation is encountered at an average elevation of 682.8 ft (208.1 m).

The overburden soil of the ESWEMS Retention Pond area consists of fluvial and glacial deposits, and varies in thickness from 12.2 to 54.5 ft (3.7 to 16.6 m). There is no Weathered Rock and/or Transition Zone present in the ESWEMS Retention Pond area. The sound rock of the Mahantango formation is encountered at an average elevation of 640.7 ft (195.3 m).

The overburden soil, weathered rock and transition zone are not adequate foundation strata for safety related structures or facilities, which can impose high contact pressures. In addition, the overburden soils are susceptible to liquefaction as discussed in Section 2.5.4.8.

The overburden soils, the weathered rock, and the transition zone are excavated in the Power Block area. At the Power Block area, permanent slopes result from the excavation and placement of granular fill and concrete. At the ESWEMS Retention Pond, the lack of cohesion of the in-situ soils could result in sloughing failures of the ESWEMS Retention Pond slopes with a high probability of erosion. These soils are replaced with a cohesive fill. In such a case, the slopes of the ESWEMS Retention Pond are protected from erosion through the use of the cohesive fill to avoid soil debris falling into the pond and reducing the design retention capacity.

The elevation of the groundwater tables varies from 665.61 to 712.03 ft (202.9 to 217.03 m), with an average elevation of 689.58 ft (210.18 m) within the Power Block. Within the ESWEMS Retention Pond area the groundwater elevation varies from 655.66 to 665.07 ft (199.85 to 202.71 m) with an average elevation of 659.69 ft (201.07 m). Since the plant grade at the bottom of the ESWEMS Retention Pond is placed at elevation of 677.5 ft (206.5 m), the slope stability is governed by the forces imposed by the pond normal water level of 695 ft (211.8 m).

Temporary slopes are developed under dry conditions within a dewatered zone. Fill material placed on any slope for added stability is assumed to be free-draining.

2.5.5.2 Design Criteria and Analysis

The stability of constructed slopes is assessed using limit equilibrium methods, which generally consider moment or force equilibrium of a potential sliding mass by discretizing the mass into vertical slices. This approach results in a Factor-of-Safety (FOS) that can be defined as (Gregory, 2003):

$$\text{FOS} = \frac{\text{Shear Strength of Soil}}{\text{Mobilized Shear Stress in Soil}}$$

Factor-of-Safety is defined as the ratio of the available strength of the cross section to the driving forces, such as water or seismic force. A Factor-of-Safety greater than one indicates that the available strength is greater than driving forces and implies that there is no measureable damage or permanent displacements of the cross section.

Various limit equilibrium methods are available for slope stability evaluation, including Bishop's simplified method (Bishop, 1955), and Janbu's simplified method (Janbu, 1968), among others. These methods are routinely used for the evaluation of the slopes and their limitations, and advantages, are well documented. The main difference between the two methods is the equilibrium equations that are included and satisfied.

Bishop's (Bishop, 1955) and Janbu's (Janbu, 1968) simplified methods satisfy moment of equilibrium and horizontal force equilibrium, respectively. Both Bishop's (Bishop, 1955) simplified method and Janbu's (Janbu, 1968) simplified method include the interslice normal force, but ignore the interslice shear force. The Bishop's (Bishop, 1955) and Janbu's (Janbu, 1968) simplified methods are used to calculate the factors-of-safety for temporary and permanent constructed slopes at the BBNPP Site.

The slope stability analysis is performed using version 2.004 of Computer Program GSTABL7 with STEDwin (Gregory, 2003). This program was originally developed by Purdue University for the Indiana State Highway Commission in 1986 and later revised and marketed by Geotechnical Engineering Software Company. The program calculates the factor-of-safety against slope failure utilizing a two-dimensional limit equilibrium method. The calculation of the factor-of-safety against slope instability is performed using the Simplified Bishop method of slices, which is applicable to circular shaped failure surfaces, and the Simplified Janbu method of slices, which is applicable to failure surfaces of a general shape. GSTABL7 may incorporate up to 20 soil options with nonlinear undrained effective shear strength parameters, isotropic or anisotropic soils, and fiber reinforcement. Stabilizing structures such as piles, tiebacks, or nails may also be considered. None of these stabilizing options are required at the BBNPP site and isotropic soils are used in the analysis.

Dynamic analysis of the slopes is performed using a pseudostatic (dynamic) approach, which represents the effects of seismic shaking that create inertial forces. These forces act in the horizontal and vertical directions at the centroid of each slice, and are defined as:

$$F_h = (a_h / g)W = k_h W \quad (\text{Eq. 2.5.5-2})$$

$$F_v = (a_v / g)W = k_v W \quad (\text{Eq. 2.5.5-3})$$

Where a_h and a_v are the equivalent horizontal and vertical ground accelerations, respectively, W is the slice weight, and g is the gravitational acceleration constant. The inertial effect is specified by k_h and k_v coefficients, based on the site seismic considerations.

Typical minimum acceptable values of FOS are 1.5 for normal long-term loading conditions and 1.0 to 1.2 for infrequent loading conditions (Duncan, 2005), e.g., during earthquakes.

2.5.5.2.1 Stability of Constructed Slopes

The permanent slopes of the Power Block are constructed by either excavation of the overburden soil, weathered rock and transition zone, and replacement of excavated material with concrete and/or engineering (granular) fill or through construction of retaining walls. Category I structures with their foundation base above the sound rock of the Mahantango Formation rest directly on top of concrete fill. In all other areas, engineering fill is used as the replacement material up to final grade. Figure 2.5-100, Figure 2.5-103, Figure 2.5-106 and Figure 2.5-109 present the critical results of static and pseudostatic (dynamic) evaluations for each cross-section presented in the Power Block, shown in Figure 2.5-98, Figure 2.5-101, Figure 2.5-104, and Figure 2.5-107. For each section, the phreatic surface is assumed to be the

maximum groundwater elevation within the Power Block, which is 712.03 ft (217.03 m). Using the maximum groundwater elevation is considered a conservative assumption as the phreatic surface lowers resisting forces in the soil below it by reducing the effective stress in the soil. The phreatic surface also increases the driving forces in the slope by increasing water weight. Therefore, at maximum groundwater elevation, the maximum reduction in resisting forces in the soil due to groundwater is occurring. GSTABL7 models the effects of the phreatic surface by using effective stress analysis to calculate resisting forces in the soil and saturated unit weights for soil below the phreatic surface to calculate driving forces.

The ESWEMS Retention Pond is constructed primarily via excavation of overburden soils and replacement of soils with cohesive fill, concrete, and engineering (granular) fill. The granular fill is placed on the north side of the ESWEMS Retention Pond area. The ESWEMS Pump House is founded on top of concrete, and all other areas of the ESWEMS Retention Pond constructed using cohesive fill. Figure 2.5-111, Figure 2.5-112, Figure 2.5-115, and Figure 2.5-116 present the results of static and pseudostatic (dynamic) evaluations based on the East-West Section A and North-South Section B shown in Figure 2.5-118 and Figure 2.5-113, respectively. The four separate sections are analyzed to represent the various design differences of the slopes for the ESWEMS Retention Pond, and represent the elevations on each side of the rectangular ESWEMS Retention Pond. The embankment sides are built up to the ESWEMS Pump House building grade at 700 ft (213.4 m).

The slope stability evaluation is conducted on the upstream and downstream slopes of the east, west and south sides of the retention pond (See Figure 2.5-111, Figure 2.5-112, Figure 2.5-116). For the slope section on the north side of the retention pond, the analysis is conducted on the upstream slope and on the hill north of the embankment (See Figure 2.5-115).

Separate analysis is performed on the retaining wall structures west of the Power Block and south of the ESWEMS Retention Pond.

For the ESWEMS Retention Pond, the phreatic surface is defined as the boundary between the saturated and unsaturated zones in the cross-sectional profiles. Casagrande's solution for seepage through an earthen dam is used to calculate the expected phreatic surface (Das, 2002) within the embankment on the east, west and south sides of the retention pond.

For the north side slope of the ESWEMS Retention Pond, the groundwater elevation is considered as the pond water level.

The analysis is performed for steady state loading conditions as well as earthquake loading conditions. The total stress strength parameters of the soils provided in Section 2.5.4 are utilized in the analyses.

Both circular and wedge analyses are performed on the cross sections. The circular failure analysis uses the Simplified Bishop Method. Wedge analysis utilizes the Simplified Janbu method.

For the Power Block and ESWEMS Retention Pond slopes not held by retaining structures, Safe Shutdown Earthquake (SSE) time histories are used to determine the horizontal and vertical seismic accelerations used in the pseudostatic (dynamic) slope stability analyses. For the slope stability analysis, the SSE PGA is considered to be 0.2g. The horizontal (k_h) and vertical (k_v)

seismic coefficients are calculated to be 0.1g by applying a 0.5 amplification factor to the SSE PGA (Hynes-Griffin, 1984).

For the slopes west of the Power Block and south of the ESWEMS Retention Pond, which are held by retaining structures, the 100% + 40% + 40% method is used to apply seismic loading for a rigid structure (NRC, 1978). SSE horizontal and vertical PGA values are considered to be 0.21g and 0.18g respectively. Calculation revisions have been approved lowering both the horizontal and vertical SSE PGA values; however the original values are still used as conservative inputs into the retaining structure slope stability analysis.

Total stress parameters for the soil properties are used for the earthquake loading analysis.

In order to find the worst case slope failure, the program GSTABL7 allows the calculation of numerous iterations and provides the corresponding location and Factor-of-Safety of the worst case scenario. The worst case is the location exhibiting the lowest Factor-of-Safety.

The factors-of-safety (FOS) for the permanent slopes evaluated at the BBNPP site are summarized in Table 2.5-45. In the Power Block, FOS ranging from 1.554 to 67.708 is obtained under static conditions, and 1.079 to 51.063 is obtained under pseudostatic (dynamic) conditions. The critical failure surfaces of the permanent slopes within the Power Block for static and dynamic conditions are presented in Figure 2.5-100, Figure 2.5-103, Figure 2.5-106 and Figure 2.5-109. For ESWEMS Retention Pond, the FOS values obtained under static conditions vary from 1.804 to 5.575, and 1.354 to 2.574 under dynamic conditions. The critical failure surfaces for static and dynamic conditions of slopes in the Power Block and ESWEMS Retention Pond are presented in Figure 2.5-111, Figure 2.5-112, Figure 2.5-115, and Figure 2.5-116.

For slopes held by retaining wall structures, the FOS values obtained under static conditions vary from 1.345 to 10.80 and vary under dynamic conditions from 0.996 to 12.62. For both static and dynamic conditions there exists one retaining wall slope with a FOS under the required minimum. However, neither of these slopes are in close enough proximity to safety related structures to have any effect 290 ft (88.4 m) for the slope with $FOS = 1.345 < 1.5$ under static conditions and 1250 ft (381 m) for the slope with $FOS = 0.996 < 1.0$ under dynamic conditions).

As stated previously, typical minimum acceptable values of FOS are 1.5 for normal long-term loading conditions and 1.0 to 1.2 for infrequent loading conditions. The calculated FOS for all non-retained slopes in the Power Block and ESWEMS Retention Pond exceed the minimum acceptable values. Therefore, the slopes in the Power Block and ESWEMS Retention Pond area have sufficient static and dynamic stability against slope failure.

At the BBNPP site, there are no dams or embankments, for which adverse conditions such as high water levels attributable to the Probable Maximum Flood (PMF), sudden drawdown, or steady seepage at various levels may occur.

The static slope stability analysis at the ESWEMS Retention Pond site is performed with the normal water elevation of 695 ft (211.8 m) for upstream slopes and the PMF water elevation of 698.4 ft (212.9 m) on the downstream slopes. The use of normal water elevation on upstream slopes is a conservative approach as an increase in pool water elevation would add resisting surcharge load to the slope, raising the FOS. The pseudostatic (dynamic) slope stability analysis at the ESWEMS Retention Pond site is performed with the normal water elevation of

695 ft (211.8 m), since the probability of simultaneous occurrence of an earthquake and PMF conditions is very low.

2.5.5.2.2 Stability of Temporary Fill Slopes

Temporary cut and fill slopes are expected to exist in dry condition during construction. The analysis for temporary construction slopes is performed only under static conditions, using circular and wedge failure analysis. The factors-of-safety (FOS) for the temporary slopes evaluated at the BBNPP site are summarized in Table 2.5-45, and their critical slip surfaces are presented in Figure 2.5-99, Figure 2.5-102, Figure 2.5-105, Figure 2.5-108, Figure 2.5-110, and Figure 2.5-114. Under static conditions, FOS varied from 1.499 to 3.041 and 1.746 to 1.897 for the Power Block and ESWEMS Retention Pond area, respectively.

2.5.5.2.3 Concluding Remarks

Based on analyses provided in this Section, it is concluded that the constructed and natural slopes at the site are sufficiently stable and present no failure potential under the conditions to which they could be exposed during the life of the plant that would adversely affect the safety of the proposed BBNPP.

2.5.5.3 Logs of Borings

Logs of borings, and associated references, are provided in Part 11F of the COLA.

2.5.5.4 Compacted Fill

Compacted fill, and associated references, are addressed in Section 2.5.4.5.

2.5.5.5 References

Bishop, 1955. The Use of Slip Surface Circle in Stability Analysis of Slopes, Geotechnique Volume 5, Number 1, pp. 7-17, A.W. Bishop, 1955.

Das, 2002. Principles of Geotechnical Engineering, Fifth Edition, Brooks/Cole, B. Das, 2002.

Duncan, 2005. Soil Strength and Slope Stability, Wiley and Sons, J.M. Duncan and S.G. Wright, 2005.

Gregory, 2003. GSTABL7 with STEDwin: Slope Stability Analysis System Program Manual, G.H. Gregory, 2003.

Hynes-Griffin, 1984. Rationalizing the Seismic Coefficient Method, Prepared for Department of the Army US Army Corps of Engineers, CWIS Work Unit 31145.

Janbu, 1968. Slope Stability Computations, Soil Mechanics and Foundation Engineering, The Technical University of Norway, N. Janbu, 1968.

NRC, 1978. Development of Criteria for Seismic Review of Selected Nuclear Power Plants, NUREG-CR-0098, N.M. Newmark and W.J. Hall, May 1978.

NRC, 2007. Combined License Applications For Nuclear Power Plants (LWR Edition), Regulatory Guide 1.206, U.S. Nuclear Regulatory Commission, 2007.}

2.5.6 References

No departures or supplements.

|

Table 2.5-1— {Controlling Earthquakes for BBNPP}

Mean Annual Probability of Exceedance	Response Spectral Frequency Range (Hz)	Identification	Distance Range (km [mi])	Magnitude (M)	Distance (km [mi])	Weight
10 ⁻⁴	1 to 2.5	REF	> 100 [62]	7.3	545 [337]	N/A
		DEL	0 to 200 [124 to 435]	6.2	53 [33]	0.446
		DEM	200 to 700 [124 to 435]	7.1	364 [226]	0.199
		DEH	> 700 [435]	7.7	1245 [774]	0.354
	5 to 10	REF	> 0 [0]	6.1	68 [42]	N/A
		DEL	0 to 50 [0 to 31]	5.6	21 [13]	0.427
		DEM	50 to 200 [31 to 124]	6.2	115 [71]	0.416
		DEH	> 200 [124]	7.1	445 [277]	0.157
10 ⁻⁵	1 to 2.5	REF	> 100 [62]	7.5	537 [334]	N/A
		DEL	0 to 200 [0 to 124]	6.3	28 [17]	0.671
		DEM	200 to 700 [124 to 435]	7.3	353 [219]	0.100
		DEH	> 700 [435]	7.8	1264 [785]	0.228
	5 to 10	REF	> 0 [0]	6.0	20 [12]	N/A
		DEL	0 to 50 [0 to 31]	5.8	14 [8.7]	0.847
		DEM	50 to 200 [31 to 124]	6.8	107 [65]	0.131
		DEH	> 200 [124]	7.4	368 [227]	0.022
10 ⁻⁶	1 to 2.5	REF	> 100 [62]	7.7	461 [286]	N/A
	5 to 10	REF	> 0 [0]	6.1	12 [7.5]	N/A

Notes:

N/A = not applicable

For some cases, weights do not add to 1.0 because of round-off error.

Table Acronyms and Abbreviations:

REF = Controlling Reference Earthquake

DEL = Controlling Deaggregation Earthquake, Low Magnitude

DEM = Controlling Deaggregation Earthquake, Medium Magnitude

DEH = Controlling Deaggregation Earthquake, High Magnitude

Table 2.5-2— {Horizontal and Vertical GMRS Amplitudes and V/H Ratio}

Frequency (Hz)	Horizontal GMRS (g)	Vertical GMRS (g)	V/H Ratio
0.1000	0.0216	0.0145	0.670
0.1269	0.0248	0.0166	0.670
0.1610	0.0284	0.0190	0.670
0.2043	0.0326	0.0218	0.670
0.2593	0.0373	0.0250	0.670
0.3290	0.0429	0.0288	0.670
0.4175	0.0493	0.0330	0.670
0.5000	0.0546	0.0366	0.670
0.5298	0.0553	0.0371	0.670
0.6723	0.0583	0.0390	0.670
0.8532	0.0614	0.0411	0.670
1.0000	0.0636	0.0426	0.670
1.0826	0.0676	0.0453	0.670
1.3738	0.0799	0.0535	0.670
1.7434	0.0956	0.0640	0.670
1.7500	0.0959	0.0642	0.670
2.2124	0.1149	0.0770	0.670
2.5000	0.1263	0.0846	0.670
2.8074	0.1419	0.0951	0.670
3.5625	0.1765	0.1183	0.670
4.5208	0.2140	0.1434	0.670
5.0000	0.2300	0.1541	0.670
5.7372	0.2487	0.1666	0.670
7.2780	0.2728	0.1827	0.670
7.5000	0.2728	0.1828	0.670
9.2336	0.2865	0.1919	0.670
10.0000	0.2921	0.1957	0.670
11.7233	0.3244	0.2196	0.677
14.8810	0.3792	0.2613	0.689
18.8679	0.4287	0.3005	0.701
23.9234	0.4559	0.3388	0.743
25.0000	0.4564	0.3423	0.750
30.3951	0.4252	0.3261	0.767
38.6100	0.4049	0.3312	0.818
49.0196	0.3550	0.3046	0.858
50.0000	0.3465	0.2983	0.861
62.1118	0.2795	0.2512	0.899
78.7402	0.1993	0.1738	0.872
100.0000	0.1590	0.1240	0.780

Table 2.5-3— {Amplification Factors for 10⁻⁴ and 10⁻⁵ Input Motions and HF and LF Rock Spectra}

Page 1 of 2

Frequency (Hz)	10 ⁻⁴ LF				10 ⁻⁴ HF			
	DEL	DEM	DEH	Weighted Average	DEL	DEM	DEH	Weighted Average
	0.4460*	0.1990*	0.3540*		0.4270*	0.4160*	0.1570*	
0.1000	1.0051	0.9981	0.9999	1.0009	1.0081	1.0597	1.0024	1.0287
0.1269	1.0027	1.0008	1.0000	1.0003	1.0121	1.0200	1.0033	1.0140
0.1610	1.0018	1.0008	1.0000	1.0000	1.0053	1.0042	1.0007	1.0041
0.2043	1.0029	1.0029	1.0002	1.0010	1.0060	1.0136	1.0018	1.0085
0.2593	1.0021	1.0014	1.0005	1.0004	1.0057	1.0027	1.0032	1.0041
0.3290	1.0040	1.0032	1.0007	1.0017	1.0062	1.0047	1.0029	1.0051
0.4175	1.0043	1.0038	1.0016	1.0022	1.0043	1.0047	1.0030	1.0043
0.5000	1.0049	1.0028	1.0022	1.0025	1.0068	1.0059	1.0020	1.0057
0.5298	1.0071	1.0034	1.0025	1.0038	1.0097	1.0059	1.0044	1.0073
0.6723	1.0064	1.0065	1.0049	1.0049	1.0074	1.0095	1.0057	1.0080
0.8532	1.0127	1.0093	1.0079	1.0093	1.0136	1.0069	1.0108	1.0104
1.0000	1.0156	1.0135	1.0090	1.0119	1.0189	1.0146	1.0114	1.0159
1.0826	1.0183	1.0166	1.0099	1.0139	1.0194	1.0175	1.0156	1.0180
1.3738	1.0247	1.0261	1.0167	1.0211	1.0253	1.0215	1.0220	1.0232
1.7434	1.0341	1.0300	1.0261	1.0294	1.0414	1.0358	1.0313	1.0375
1.7501	1.0390	1.0298	1.0271	1.0319	1.0411	1.0364	1.0324	1.0378
2.2124	1.0536	1.0544	1.0465	1.0502	1.0575	1.0571	1.0540	1.0568
2.5000	1.0705	1.0643	1.0611	1.0649	1.0574	1.0655	1.0680	1.0624
2.8074	1.0819	1.0810	1.0703	1.0766	1.0853	1.0776	1.0800	1.0812
3.5625	1.1079	1.1137	1.1000	1.1052	1.1103	1.1012	1.1103	1.1065
4.5208	1.1333	1.1349	1.1319	1.1320	1.1180	1.1399	1.1298	1.1290
5.0000	1.1374	1.1418	1.1351	1.1363	1.1199	1.1347	1.1303	1.1277
5.7372	1.1316	1.1286	1.1217	1.1263	1.1319	1.1251	1.1191	1.1271
7.2780	1.0711	1.0791	1.0977	1.0810	1.0738	1.0800	1.0726	1.0762
7.5019	1.0641	1.0652	1.0968	1.0748	1.0686	1.0754	1.0704	1.0717
9.2336	1.0131	1.0302	1.0550	1.0303	1.0073	1.0101	1.0086	1.0087
10.0000	0.9965	1.0142	1.0408	1.0147	0.9817	1.0030	1.0001	0.9935
11.7233	0.9874	0.9764	1.0280	0.9986	0.9864	0.9778	0.9877	0.9830
14.8810	1.0173	1.0132	1.0376	1.0227	1.0132	1.0075	1.0107	1.0104
18.8679	1.0442	1.0301	1.0651	1.0478	1.0420	1.0524	1.0312	1.0446
23.9234	1.0607	1.0597	1.0529	1.0567	1.0529	1.0394	1.0452	1.0461
25.0000	1.0436	1.0540	1.0598	1.0503	1.0406	1.0458	1.0408	1.0428
30.3951	0.9946	0.9863	1.0541	1.0130	0.9798	0.9846	0.9763	0.9812
38.6100	0.9914	0.9997	1.0463	1.0115	0.9736	0.9917	0.9815	0.9824
49.0196	0.9693	0.9689	1.0430	0.9943	0.9673	0.9892	0.9795	0.9783
50.0000	0.9768	0.9636	1.0436	0.9969	0.9625	0.9812	0.9717	0.9717
62.1118	0.9580	0.9606	1.0447	0.9883	0.9518	0.9482	0.9729	0.9536
78.7402	0.9699	0.9874	1.0403	0.9973	0.9471	0.9844	1.0037	0.9715
100.0000	1.0474	1.0671	1.0471	1.0502	1.0042	1.0756	1.0925	1.0478

* weight of controlling earthquake
 Note: Distance range of each event
 DEL: Low distance range
 DEM: Medium distance range
 DEH: High distance range

Table 2.5-3— {Amplification Factors for 10⁻⁴ and 10⁻⁵ Input Motions and HF and LF Rock Spectra}

Page 2 of 2

Frequency (Hz)	10 ⁻⁵ LF				10 ⁻⁵ HF			
	DEL	DEM	DEH	Weighted Average	DEL	DEM	DEH	Weighted Average
	0.6710*	0.1000*	0.2280*		0.8470*	0.1310*	0.0218*	
0.1000	1.0000	1.0034	0.9999	0.9993	1.0086	1.0023	1.0010	1.0074
0.1269	1.0014	1.0006	1.0000	1.0000	1.0071	1.0012	1.0004	1.0060
0.1610	1.0005	1.0007	1.0001	0.9994	1.0069	1.0013	1.0019	1.0059
0.2043	1.0008	1.0019	1.0002	0.9997	1.0033	1.0020	1.0011	1.0029
0.2593	1.0007	1.0011	1.0004	0.9996	1.0061	1.0028	1.0015	1.0053
0.3290	1.0038	1.0023	1.0007	1.0019	1.0061	1.0014	1.0017	1.0052
0.4175	1.0049	1.0039	1.0014	1.0030	1.0055	1.0026	1.0043	1.0049
0.5000	1.0039	1.0031	1.0024	1.0025	1.0077	1.0044	1.0032	1.0070
0.5298	1.0046	1.0044	1.0026	1.0031	1.0064	1.0039	1.0039	1.0059
0.6723	1.0074	1.0069	1.0041	1.0056	1.0110	1.0062	1.0069	1.0101
0.8532	1.0083	1.0101	1.0071	1.0072	1.0129	1.0082	1.0083	1.0120
1.0000	1.0123	1.0097	1.0100	1.0105	1.0179	1.0173	1.0135	1.0175
1.0826	1.0228	1.0108	1.0115	1.0180	1.0178	1.0186	1.0153	1.0177
1.3738	1.0202	1.0242	1.0150	1.0184	1.0256	1.0220	1.0201	1.0248
1.7434	1.0360	1.0351	1.0328	1.0341	1.0295	1.0340	1.0346	1.0300
1.7501	1.0356	1.0356	1.0337	1.0341	1.0298	1.0337	1.0346	1.0302
2.2124	1.0586	1.0527	1.0479	1.0545	1.0543	1.0550	1.0490	1.0541
2.5000	1.0666	1.0673	1.0552	1.0630	1.0611	1.0655	1.0599	1.0615
2.8074	1.0806	1.0772	1.0705	1.0769	1.0816	1.0805	1.0756	1.0811
3.5625	1.1098	1.1079	1.1046	1.1073	1.1108	1.1069	1.1014	1.1099
4.5208	1.1390	1.1294	1.1166	1.1318	1.1316	1.1289	1.1298	1.1310
5.0000	1.1348	1.1424	1.1285	1.1330	1.1333	1.1471	1.1310	1.1349
5.7372	1.1328	1.1368	1.1306	1.1316	1.1295	1.1360	1.1179	1.1299
7.2780	1.0745	1.0606	1.0893	1.0754	1.0820	1.0805	1.0725	1.0814
7.5019	1.0687	1.0588	1.0936	1.0723	1.0621	1.0608	1.0615	1.0617
9.2336	1.0095	1.0013	1.0333	1.0131	0.9992	1.0136	1.0021	1.0010
10.0000	0.9949	1.0081	1.0387	1.0052	0.9797	0.9956	1.0023	0.9821
11.7233	0.9775	0.9797	1.0232	0.9871	0.9911	1.0058	0.9915	0.9928
14.8810	1.0198	1.0098	1.0417	1.0227	1.0266	1.0124	1.0102	1.0242
18.8679	1.0381	1.0422	1.0469	1.0395	1.0530	1.0426	1.0425	1.0512
23.9234	1.0581	1.0483	1.0749	1.0599	1.0462	1.0603	1.0441	1.0478
25.0000	1.0527	1.0505	1.0762	1.0568	1.0375	1.0489	1.0294	1.0386
30.3951	0.9764	0.9808	1.0524	0.9932	0.9851	0.9985	0.9828	0.9866
38.6100	0.9806	0.9911	1.0482	0.9961	0.9973	0.9781	0.9909	0.9945
49.0196	0.9569	0.9681	1.0427	0.9766	0.9795	0.9833	0.9614	0.9794
50.0000	0.9657	0.9706	1.0416	0.9825	0.9756	0.9733	0.9630	0.9749
62.1118	0.9645	0.9684	1.0432	0.9818	0.9772	0.9566	0.9715	0.9742
78.7402	0.9529	0.9817	1.0449	0.9758	0.9617	0.9690	0.9925	0.9631
100.0000	1.0123	1.0628	1.0588	1.0269	0.9904	1.0522	1.1186	1.0011

* weight of controlling earthquake
 Note: Distance range of each event
 DEL: Low distance range
 DEM: Medium distance range
 DEH: High distance range

Table 2.5-4— {Uniform Hazard Response Spectra (Hard Rock Conditions)}

Frequency (Hz)	Pseudo-spectral Acceleration (g)		
	10 ⁻⁴ Mean Annual Probability of Exceedance	10 ⁻⁵ Mean Annual Probability of Exceedance	10 ⁻⁶ Mean Annual Probability of Exceedance
0.5	3.96E-02	1.12E-01	2.46E-01
1.0	4.95E-02	1.27E-01	2.97E-01
2.5	8.63E-02	2.44E-01	6.81E-01
5.0	1.32E-01	4.28E-01	1.26E+00
10.0	1.77E-01	6.39E-01	2.00E+00
25.0	2.57E-01	9.50E-01	3.16E+00
100.0 (PGA)	8.95E-02	3.43E-01	1.13E+00

Notes:
 PGA = peak ground acceleration
 Hard rock condition is that condition consistent with the EPRI (2004) ground motion model ($V_{S30} = 2800$ m/s)

Table 2.5-5— {Seed Time Histories Selected for Controlling Deaggregation Earthquakes}
 Page 1 of 4

1E-4 Annual Frequency of Exceedance, Response Spectral Frequency Range: 5 to 10 Hz									
Controlling Deaggregation Earthquake					Seed Time History				
Identification	Magnitude (M)	Distance (km)	Distance (mi)	Earthquake	Station	Magnitude (M)	Distance (km)	Distance (mi)	
DEL	5.3	12	7	Coalinga	Anticline Ridge Free-Field	5.2	11	6.8	
				North Palm Springs	Hurkey Creek Park	6.0	34.9	21.7	
DEM	5.9	78	49	San Fernando	San Onofre – So Cal Edison	6.6	122	76	
				San Fernando	Maricopa Array #1	6.6	115	71	
DEH	7.5	1007	626	Landers	Calabasas – N Las Virg #	7.3	194.1	120.6	
				San Fernando	San Onofre – So Cal Edison	6.6	122	76	

Table 2.5-5— {Seed Time Histories Selected for Controlling Deaggregation Earthquakes}
 Page 2 of 4

1E-4 Annual Frequency of Exceedance, Response Spectral Frequency Range: 1 to 2.5 Hz									
Controlling Deaggregation Earthquake					Seed Time History				
Identification	Magnitude (M)	Distance (km)	Distance (mi)	Earthquake	Station	Magnitude (M)	Distance (km)	Distance (mi)	
DEL	6.0	53	33	Whittier Narrows	Riverside Airport	6.0	56.8	35.3	
				Northridge	Duarte Mel Canyon Rd.	6.7	51.6	32.1	
DEM	7.5	864	537	Landers	Calabasas – N Las Virg	7.3	194.1	120.6	
				San Fernando	San Onofre – So Cal Edison	6.6	122	76	
DEH	7.5	1236	768	Whittier Narrows	Castaic- Hasley Canyon	6.0	70.9	44.1	
				San Fernando	Maricopa Array #1	6.6	115	71	

Table 2.5-5— {Seed Time Histories Selected for Controlling Deaggregation Earthquakes}
 Page 3 of 4

1E-5 Annual Frequency of Exceedance, Response Spectral Frequency Range: 5 to 10 Hz									
Controlling Deaggregation Earthquake					Seed Time History				
Identification	Magnitude (M)	Distance (km)	Distance (mi)	Earthquake	Station	Magnitude (M)	Distance (km)	Distance (mi)	
DEL	5.4	10	6	Whittier Narrows	Garvey Res.- Control Bldg.	6.0	12.1	7.5	
				Lytle Creek	Wrightwood – 6074 Park Dr	5.4	15.4	9.6	
DEM	6.3	62	39	San Fernando	Cedar Springs, Allen Ranch	6.6	86.6	53.8	
				Northridge	Riverside Airport #	6.7	101.3	62.9	
DEH	7.7	973	605	Landers	Calabasas - N Las Virg	7.3	194.1	120.6	
				San Fernando	San Onofre – So Cal Edison	6.6	122'	76	

Table 2.5-5— {Seed Time Histories Selected for Controlling Deaggregation Earthquakes}
 Page 4 of 4

1E-5 Annual Frequency of Exceedance, Response Spectral Frequency Range: 1 to 2.5 Hz									
Controlling Deaggregation Earthquake					Seed Time History				
Identification	Magnitude (M)	Distance (km)	Distance (mi)	Earthquake	Station	Magnitude (M)	Distance (km)	Distance (mi)	
DEL	6.1	28	17	Morgan Hill	Corralitos	6.2	22.7	14.1	
				San Fernando	Lake Hughes #4	6.6	24.2	15.0	
DEM	7.7	858	533	Landers	Calabasas – N Las Virg	7.3	194.1	120.6	
				San Fernando	San Onofre – So Cal Edison	6.6	122	76	
DEH	7.5	1236	768	Whittier Narrows	Castaic-Hasley Canyon	6.0	70.9	44.1	
				San Fernando	Maricopa Array #1	6.6	115	71	

Table 2.5-6— {Mean and Fractile Rock Hazard Curves for PGA}

Acceleration (g)	Annual Probability of Exceedance					
	Mean	5 th	16 th	50 th	84 th	95 th
0.01	3.71E-03	1.91E-03	2.31E-03	3.28E-03	4.89E-03	6.41E-03
0.02	1.39E-03	6.63E-04	8.27E-04	1.19E-03	1.86E-03	2.59E-03
0.03	7.17E-04	3.32E-04	4.16E-04	6.14E-04	9.88E-04	1.37E-03
0.04	4.34E-04	2.02E-04	2.52E-04	3.70E-04	5.90E-04	8.42E-04
0.05	2.90E-04	1.36E-04	1.70E-04	2.48E-04	3.90E-04	5.51E-04
0.06	2.08E-04	9.99E-05	1.23E-04	1.78E-04	2.76E-04	3.86E-04
0.07	1.56E-04	7.62E-05	9.60E-05	1.35E-04	2.05E-04	2.85E-04
0.08	1.23E-04	6.00E-05	7.58E-05	1.07E-04	1.60E-04	2.18E-04
0.09	9.90E-05	4.86E-05	6.16E-05	8.92E-05	1.29E-04	1.74E-04
0.10	8.19E-05	4.02E-05	5.11E-05	7.41E-05	1.07E-04	1.42E-04
0.20	2.48E-05	1.14E-05	1.50E-05	2.25E-05	3.35E-05	4.26E-05
0.25	1.71E-05	7.81E-06	1.02E-05	1.51E-05	2.31E-05	2.96E-05
0.30	1.26E-05	5.51E-06	7.44E-06	1.11E-05	1.71E-05	2.22E-05
0.40	7.69E-06	3.11E-06	4.29E-06	6.90E-06	1.05E-05	1.40E-05
0.50	5.18E-06	1.94E-06	2.72E-06	4.54E-06	7.52E-06	9.99E-06
0.60	3.70E-06	1.29E-06	1.85E-06	3.15E-06	5.44E-06	7.62E-06
0.70	2.76E-06	9.42E-07	1.30E-06	2.31E-06	4.09E-06	5.88E-06
0.80	2.12E-06	6.85E-07	9.97E-07	1.72E-06	3.17E-06	4.65E-06
0.90	1.67E-06	5.10E-07	7.54E-07	1.32E-06	2.49E-06	3.75E-06
1.00	1.34E-06	3.90E-07	5.83E-07	1.05E-06	2.01E-06	3.08E-06
2.00	2.54E-07	5.14E-08	8.37E-08	1.74E-07	3.94E-07	7.18E-07
3.00	7.72E-08	1.19E-08	2.04E-08	4.82E-08	1.15E-07	2.40E-07
5.00	1.27E-08	1.36E-09	2.54E-09	6.79E-09	1.92E-08	4.49E-08

Table 2.5-7— {Mean and Fractile Rock Hazard Curves for 25-Hz PSA}

Pseudo- Spectral Acceleration (g)	Annual Probability of Exceedance					
	Mean	5 th	16 th	50 th	84 th	95 th
0.01	8.08E-03	4.38E-03	5.26E-03	7.20E-03	1.05E-02	1.37E-02
0.02	4.08E-03	1.97E-03	2.40E-03	3.44E-03	5.61E-03	7.87E-03
0.03	2.60E-03	1.18E-03	1.47E-03	2.13E-03	3.61E-03	5.24E-03
0.04	1.82E-03	8.08E-04	9.99E-04	1.50E-03	2.56E-03	3.79E-03
0.05	1.36E-03	5.82E-04	7.35E-04	1.10E-03	1.90E-03	2.88E-03
0.06	1.06E-03	4.40E-04	5.58E-04	8.60E-04	1.48E-03	2.25E-03
0.07	8.46E-04	3.47E-04	4.41E-04	6.82E-04	1.20E-03	1.83E-03
0.08	6.94E-04	2.81E-04	3.57E-04	5.55E-04	9.98E-04	1.50E-03
0.09	5.79E-04	2.32E-04	2.96E-04	4.60E-04	8.38E-04	1.26E-03
0.10	4.91E-04	1.96E-04	2.50E-04	3.88E-04	7.12E-04	1.08E-03
0.20	1.55E-04	6.28E-05	8.11E-05	1.22E-04	2.17E-04	3.41E-04
0.25	1.05E-04	4.28E-05	5.55E-05	8.51E-05	1.44E-04	2.25E-04
0.30	7.64E-05	3.12E-05	4.06E-05	6.24E-05	1.05E-04	1.61E-04
0.40	4.61E-05	1.86E-05	2.48E-05	3.84E-05	6.47E-05	9.74E-05
0.50	3.11E-05	1.25E-05	1.67E-05	2.63E-05	4.35E-05	6.32E-05
0.60	2.26E-05	9.31E-06	1.20E-05	1.92E-05	3.16E-05	4.47E-05
0.70	1.72E-05	6.99E-06	9.50E-06	1.46E-05	2.40E-05	3.36E-05
0.80	1.36E-05	5.39E-06	7.41E-06	1.14E-05	1.91E-05	2.64E-05
0.90	1.10E-05	4.28E-06	5.92E-06	9.70E-06	1.55E-05	2.13E-05
1.00	9.15E-06	3.46E-06	4.83E-06	8.03E-06	1.29E-05	1.77E-05
2.00	2.54E-06	7.85E-07	1.11E-06	2.04E-06	3.84E-06	5.73E-06
3.00	1.12E-06	2.79E-07	4.30E-07	8.55E-07	1.71E-06	2.79E-06
5.00	3.60E-07	6.61E-08	1.05E-07	2.35E-07	5.61E-07	1.00E-06

Table 2.5-8— {Mean and Fractile Rock Hazard Curves for 10 Hz PSA}

Pseudo-Spectral Acceleration (g)	Annual Probability of Exceedance					
	Mean	5 th	16 th	50 th	84 th	95 th
0.01	8.34E-03	5.13E-03	6.00E-03	7.76E-03	1.03E-02	1.25E-02
0.02	3.66E-03	2.07E-03	2.44E-03	3.27E-03	4.65E-03	6.05E-03
0.03	2.10E-03	1.14E-03	1.38E-03	1.86E-03	2.68E-03	3.60E-03
0.04	1.37E-03	7.43E-04	8.94E-04	1.21E-03	1.76E-03	2.39E-03
0.05	9.61E-04	5.13E-04	6.20E-04	8.56E-04	1.24E-03	1.68E-03
0.06	7.10E-04	3.76E-04	4.55E-04	6.28E-04	9.29E-04	1.24E-03
0.07	5.44E-04	2.89E-04	3.48E-04	4.82E-04	7.08E-04	9.70E-04
0.08	4.30E-04	2.29E-04	2.76E-04	3.80E-04	5.57E-04	7.61E-04
0.09	3.48E-04	1.86E-04	2.24E-04	3.07E-04	4.47E-04	6.05E-04
0.10	2.87E-04	1.54E-04	1.86E-04	2.55E-04	3.67E-04	4.95E-04
0.20	8.00E-05	4.37E-05	5.40E-05	7.46E-05	1.02E-04	1.27E-04
0.25	5.33E-05	2.86E-05	3.57E-05	4.98E-05	6.90E-05	8.52E-05
0.30	3.84E-05	2.02E-05	2.55E-05	3.59E-05	5.01E-05	6.16E-05
0.40	2.31E-05	1.15E-05	1.47E-05	2.13E-05	3.03E-05	3.74E-05
0.50	1.55E-05	7.69E-06	9.98E-06	1.41E-05	2.05E-05	2.56E-05
0.60	1.12E-05	5.32E-06	7.03E-06	1.02E-05	1.48E-05	1.86E-05
0.70	8.50E-06	3.88E-06	5.19E-06	7.89E-06	1.11E-05	1.42E-05
0.80	6.64E-06	2.94E-06	3.96E-06	6.12E-06	9.20E-06	1.13E-05
0.90	5.32E-06	2.27E-06	3.10E-06	4.85E-06	7.42E-06	9.62E-06
1.00	4.34E-06	1.80E-06	2.48E-06	3.93E-06	6.10E-06	7.99E-06
2.00	1.00E-06	3.58E-07	5.15E-07	8.78E-07	1.42E-06	2.01E-06
3.00	3.70E-07	1.16E-07	1.72E-07	3.08E-07	5.51E-07	8.06E-07
5.00	8.74E-08	2.37E-08	3.66E-08	6.98E-08	1.27E-07	2.02E-07

Table 2.5-9— {Mean and Fractile Rock Hazard Curves for 5 Hz PSA}

Pseudo-Spectral Acceleration (g)	Annual Probability of Exceedance					
	Mean	5 th	16 th	50 th	84 th	95 th
0.01	7.50E-03	4.57E-03	5.41E-03	7.08E-03	9.29E-03	1.10E-02
0.02	2.91E-03	1.65E-03	1.96E-03	2.63E-03	3.65E-03	4.65E-03
0.03	1.55E-03	8.46E-04	1.01E-03	1.38E-03	1.95E-03	2.59E-03
0.04	9.51E-04	5.05E-04	6.13E-04	8.45E-04	1.21E-03	1.65E-03
0.05	6.41E-04	3.34E-04	4.06E-04	5.60E-04	8.19E-04	1.13E-03
0.06	4.58E-04	2.38E-04	2.89E-04	3.97E-04	5.82E-04	8.20E-04
0.07	3.43E-04	1.77E-04	2.15E-04	2.96E-04	4.31E-04	6.08E-04
0.08	2.65E-04	1.38E-04	1.68E-04	2.30E-04	3.33E-04	4.67E-04
0.09	2.11E-04	1.10E-04	1.34E-04	1.84E-04	2.64E-04	3.66E-04
0.10	1.72E-04	9.12E-05	1.10E-04	1.50E-04	2.15E-04	2.95E-04
0.20	4.37E-05	2.28E-05	2.85E-05	4.02E-05	5.67E-05	7.18E-05
0.25	2.83E-05	1.44E-05	1.83E-05	2.60E-05	3.68E-05	4.59E-05
0.30	1.99E-05	1.00E-05	1.26E-05	1.81E-05	2.59E-05	3.23E-05
0.40	1.14E-05	5.57E-06	7.25E-06	1.04E-05	1.48E-05	1.86E-05
0.50	7.34E-06	3.46E-06	4.56E-06	6.83E-06	9.98E-06	1.20E-05
0.60	5.10E-06	2.31E-06	3.08E-06	4.69E-06	7.00E-06	8.93E-06
0.70	3.73E-06	1.62E-06	2.19E-06	3.39E-06	5.15E-06	6.64E-06
0.80	2.82E-06	1.19E-06	1.62E-06	2.54E-06	3.92E-06	5.13E-06
0.90	2.20E-06	9.33E-07	1.23E-06	1.94E-06	3.04E-06	4.02E-06
1.00	1.75E-06	7.25E-07	9.97E-07	1.53E-06	2.43E-06	3.24E-06
2.00	3.35E-07	1.14E-07	1.65E-07	2.84E-07	4.86E-07	6.94E-07
3.00	1.10E-07	3.39E-08	5.06E-08	9.12E-08	1.59E-07	2.43E-07
5.00	2.28E-08	5.69E-09	8.97E-09	1.69E-08	3.43E-08	5.73E-08

Table 2.5-10— {Mean and Fractile Rock Hazard Curves for 2.5-Hz PSA}

Pseudo- Spectral Acceleration (g)	Annual Probability of Exceedance					
	Mean	5 th	16 th	50 th	84 th	95 th
0.01	4.88E-03	2.72E-03	3.29E-03	4.48E-03	6.22E-03	7.72E-03
0.02	1.67E-03	8.41E-04	1.02E-03	1.45E-03	2.19E-03	3.06E-03
0.03	8.22E-04	3.84E-04	4.75E-04	6.85E-04	1.06E-03	1.61E-03
0.04	4.81E-04	2.16E-04	2.67E-04	3.84E-04	6.09E-04	9.94E-04
0.05	3.11E-04	1.38E-04	1.71E-04	2.43E-04	3.83E-04	6.50E-04
0.06	2.15E-04	9.66E-05	1.18E-04	1.68E-04	2.58E-04	4.46E-04
0.07	1.56E-04	6.97E-05	8.70E-05	1.22E-04	1.86E-04	3.18E-04
0.08	1.18E-04	5.23E-05	6.55E-05	9.37E-05	1.40E-04	2.37E-04
0.09	9.13E-05	4.05E-05	5.09E-05	7.28E-05	1.09E-04	1.82E-04
0.10	7.27E-05	3.22E-05	4.05E-05	5.82E-05	8.86E-05	1.42E-04
0.20	1.55E-05	7.14E-06	9.23E-06	1.32E-05	2.00E-05	2.78E-05
0.25	9.43E-06	4.29E-06	5.61E-06	8.42E-06	1.23E-05	1.67E-05
0.30	6.29E-06	2.81E-06	3.71E-06	5.64E-06	8.61E-06	1.11E-05
0.40	3.33E-06	1.41E-06	1.90E-06	2.96E-06	4.60E-06	6.09E-06
0.50	2.02E-06	8.50E-07	1.12E-06	1.77E-06	2.82E-06	3.77E-06
0.60	1.34E-06	5.36E-07	7.40E-07	1.15E-06	1.85E-06	2.53E-06
0.70	9.38E-07	3.61E-07	5.04E-07	8.28E-07	1.30E-06	1.81E-06
0.80	6.85E-07	2.52E-07	3.57E-07	5.98E-07	9.92E-07	1.33E-06
0.90	5.17E-07	1.84E-07	2.62E-07	4.46E-07	7.53E-07	1.02E-06
1.00	3.99E-07	1.36E-07	1.96E-07	3.39E-07	5.81E-07	8.37E-07
2.00	6.34E-08	1.65E-08	2.59E-08	5.01E-08	9.64E-08	1.45E-07
3.00	1.85E-08	4.00E-09	6.64E-09	1.34E-08	2.83E-08	4.73E-08
5.00	3.22E-09	4.95E-10	9.04E-10	2.11E-09	5.10E-09	9.20E-09

Table 2.5-11— {Mean and Fractile Rock Hazard Curves for 1 Hz PSA}

Pseudo-Spectral Acceleration (g)	Annual Probability of Exceedance					
	Mean	5 th	16 th	50 th	84 th	95 th
0.01	1.87E-03	7.58E-04	9.92E-04	1.55E-03	2.67E-03	3.93E-03
0.02	5.97E-04	1.84E-04	2.44E-04	4.10E-04	8.72E-04	1.59E-03
0.03	2.81E-04	7.58E-05	1.01E-04	1.72E-04	3.84E-04	8.28E-04
0.04	1.57E-04	3.85E-05	5.28E-05	9.17E-05	2.00E-04	4.73E-04
0.05	9.78E-05	2.26E-05	3.12E-05	5.41E-05	1.16E-04	2.89E-04
0.06	6.49E-05	1.46E-05	2.03E-05	3.51E-05	7.45E-05	1.93E-04
0.07	4.54E-05	1.01E-05	1.41E-05	2.42E-05	5.01E-05	1.31E-04
0.08	3.29E-05	7.39E-06	1.03E-05	1.76E-05	3.55E-05	9.55E-05
0.09	2.45E-05	5.48E-06	7.79E-06	1.32E-05	2.61E-05	6.98E-05
0.10	1.88E-05	4.19E-06	5.99E-06	1.03E-05	1.97E-05	5.22E-05
0.20	2.93E-06	7.19E-07	1.05E-06	1.89E-06	3.66E-06	6.85E-06
0.25	1.59E-06	3.93E-07	5.99E-07	1.10E-06	2.13E-06	3.68E-06
0.30	9.74E-07	2.39E-07	3.72E-07	7.19E-07	1.35E-06	2.27E-06
0.40	4.57E-07	1.08E-07	1.72E-07	3.49E-07	6.99E-07	1.08E-06
0.50	2.57E-07	5.77E-08	9.61E-08	1.95E-07	4.00E-07	6.36E-07
0.60	1.61E-07	3.33E-08	5.73E-08	1.20E-07	2.51E-07	4.04E-07
0.70	1.08E-07	2.05E-08	3.63E-08	8.16E-08	1.68E-07	2.75E-07
0.80	7.64E-08	1.34E-08	2.41E-08	5.63E-08	1.17E-07	1.95E-07
0.90	5.59E-08	9.42E-09	1.68E-08	4.01E-08	8.95E-08	1.43E-07
1.00	4.22E-08	6.58E-09	1.20E-08	2.94E-08	6.79E-08	1.11E-07
2.00	5.59E-09	4.95E-10	1.07E-09	3.27E-09	9.17E-09	1.68E-08
3.00	1.45E-09	8.62E-11	2.08E-10	7.51E-10	2.31E-09	4.87E-09
5.00	2.13E-10	6.90E-12	1.95E-11	8.70E-11	3.30E-10	7.73E-10

Table 2.5-12— {Mean and Fractile Rock Hazard Curves for 0.5 Hz PSA}

Pseudo-Spectral Acceleration (g)	Annual Probability of Exceedance					
	Mean	5 th	16 th	50 th	84 th	95 th
0.01	9.72E-04	2.26E-04	3.29E-04	6.53E-04	1.55E-03	2.69E-03
0.02	3.30E-04	4.86E-05	7.44E-05	1.57E-04	4.76E-04	1.17E-03
0.03	1.65E-04	1.81E-05	2.82E-05	6.23E-05	1.94E-04	6.48E-04
0.04	9.82E-05	8.97E-06	1.40E-05	3.05E-05	9.70E-05	4.02E-04
0.05	6.39E-05	4.99E-06	8.14E-06	1.73E-05	5.38E-05	2.57E-04
0.06	4.40E-05	3.08E-06	5.09E-06	1.09E-05	3.28E-05	1.71E-04
0.07	3.17E-05	2.04E-06	3.39E-06	7.43E-06	2.12E-05	1.21E-04
0.08	2.34E-05	1.42E-06	2.39E-06	5.22E-06	1.44E-05	8.68E-05
0.09	1.77E-05	1.04E-06	1.75E-06	3.83E-06	1.05E-05	6.33E-05
0.10	1.37E-05	7.90E-07	1.32E-06	2.89E-06	7.98E-06	4.94E-05
0.20	1.94E-06	1.05E-07	1.96E-07	4.74E-07	1.22E-06	5.38E-06
0.25	9.47E-07	5.46E-08	1.05E-07	2.64E-07	7.05E-07	2.35E-06
0.30	5.16E-07	3.05E-08	6.27E-08	1.61E-07	4.39E-07	1.23E-06
0.40	1.95E-07	1.19E-08	2.61E-08	7.71E-08	2.07E-07	5.16E-07
0.50	9.22E-08	5.67E-09	1.29E-08	4.12E-08	1.14E-07	2.63E-07
0.60	5.08E-08	2.92E-09	7.37E-09	2.40E-08	7.26E-08	1.51E-07
0.70	3.12E-08	1.61E-09	4.36E-09	1.51E-08	4.78E-08	9.98E-08
0.80	2.07E-08	9.99E-10	2.74E-09	1.02E-08	3.34E-08	7.00E-08
0.90	1.45E-08	6.26E-10	1.77E-09	7.31E-09	2.40E-08	5.05E-08
1.00	1.06E-08	4.09E-10	1.20E-09	5.25E-09	1.76E-08	3.74E-08
2.00	1.32E-09	1.68E-11	7.09E-11	4.43E-10	2.10E-09	5.10E-09
3.00	3.44E-10	1.92E-12	9.99E-12	8.53E-11	5.33E-10	1.36E-09
5.00	5.09E-11	9.36E-14	6.36E-13	8.16E-12	7.21E-11	2.17E-10

Table 2.5-13— {Summary Of Thicknesses And Termination Elevations For Various Strata}
English Units

Entire Site		Thickness			Termination Elevation		
		(ft)			(ft msl)		
		Min	Max	Avg	Min	Max	Avg
OVERBURDEN SOIL		7.5	60.0	24.0	612.4	768.5	714.6
MAHANTANGO FORMATION	Weathered Rock	0.0	46.3	13.7	612.4	764.4	697.8
	Transition Zone	0.0	84.0	23.3	612.4	754.2	677.2
	Sound Rock	>1000			---		
Powerblock Area		Thickness			Termination Elevation		
		(ft)			(ft msl)		
		Min	Max	Avg	Min	Max	Avg
OVERBURDEN SOIL		7.5	60.0	21.0	653.8	768.5	729.6
MAHANTANGO FORMATION	Weathered Rock	0.0	46.3	17.2	653.8	764.4	710.1
	Transition Zone	0.0	84.0	28.9	624.1	754.2	682.8
	Sound Rock	>1000			---		
ESWEMS Pond Area		Thickness			Termination Elevation		
		(ft)			(ft msl)		
		Min	Max	Avg	Min	Max	Avg
OVERBURDEN SOIL		12.2	54.5	37.2	612.4	675.1	640.7
MAHANTANGO FORMATION	Weathered Rock ⁽¹⁾	NA			NA		
	Transition Zone ⁽²⁾	NA			NA		
	Sound Rock	>1000			---		
The Sound Rock of the Mahantango Formation was not penetrated in its entirety. ⁽¹⁾ - Weathered Rock not encountered in any borings. ⁽²⁾ - Only Boring B-435 had the Transition Zone present, thus statistical distribution not considered. NA - Not Applicable							

Table 2.5-13— {Summary Of Thicknesses And Termination Elevations For Various Strata}
SI Units

Entire Site		Thickness			Termination Elevation		
		(m)			(m msl)		
		Min	Max	Avg	Min	Max	Avg
OVERBURDEN SOIL		2.3	18.3	7.3	186.7	234.2	217.8
MAHANTANGO FORMATION	Weathered Rock	0.0	14.1	4.2	186.7	233.0	212.7
	Transformation Zone	0.0	25.6	7.1	186.7	229.9	206.4
	Sound Rock	>304.8			---		
Powerblock Area		Thickness			Termination Elevation		
		(m)			(m msl)		
		Min	Max	Avg	Min	Max	Avg
OVERBURDEN SOIL		2.3	18.3	6.4	199.3	234.2	222.4
MAHANTANGO FORMATION	Weathered Rock	0.0	14.1	5.2	199.3	233.0	216.4
	Transformation Zone	0.0	25.6	8.8	190.2	229.9	208.1
	Sound Rock	>304.8			---		
ESWEMS Pond Area		Thickness			Termination Elevation		
		(ft)			(ft msl)		
		Min	Max	Avg	Min	Max	Avg
OVERBURDEN SOIL		3.7	16.6	11.3	186.7	205.8	195.3
MAHANTANGO FORMATION	Weathered Rock ⁽¹⁾	NA			NA		
	Transformation Zone ⁽²⁾	NA			NA		
	Sound Rock	>304.8			---		
The Sound Rock of the Mahantango Formation was not penetrated in its entirety. ⁽¹⁾ - Weathered Rock not encountered in any borings. ⁽²⁾ - Only Boring B-435 had the Transition Zone present, thus statistical distribution not considered. NA - Not Applicable							

Table 2.5-14— {Summary Of Geotechnical Field Tests}

Test	Specification	Quantity
Standard Penetration Test (SPT)	ASTM D 1586-08	44 Boreholes
Rock Coring	ASTM D 2113-08	44 Boreholes
Pressuremeter Test (PMT)	ASTM D4719-07/OYO Manual	2 Boreholes
P-S Suspension Logging	GeoVision Procedure for OYO P-S Suspension Seismic Velocity Logging Rev. 1.4, 5/20/09.	3 Boreholes
Downhole Seismic Survey	NGA Procedure: "Downhole Seismic Velocity Surveys Data and Acquisition and Analysis Guideline and Procedures by Rowland French and Brue Redpath Rev. 4 March 2007".	3 Boreholes
Deviation Survey	GeoVision Procedure for the Robertson Geologging Hi-Resolution Acoustic Televiewer (HiRAT).	3 Boreholes
Seismic Refraction Survey	GeoVision Procedure for Seismic Refraction Method Rev. 1.1, 6/23/08.	9 Refraction Lines

Table 2.5-15— {Summary of As-Conducted Boring Information}
(Page 1 of 3)

Structure (Foundation)	Boring	Horizontal Coordinates (ft)		Surface Elevation (ft)	Overburden Soil	Boring Depth (ft)				Type of Test
		State N	State E			Weathered Rock	Mahantango Formation Transition Zone	Sound Rock	Total	
Reactor Building	B-401	340123.51	2405131.34	747.68	19.50	15.50	55.00	330.00	420.00	SPT/Coring
	B-402	340214.84	2405121.84	761.79	15.00	45.00	35.00	255.00	350.00	SPT/Coring
	B-403	340114.59	2405041.43	737.56	19.90	6.10	49.60	124.40	200.00	SPT/Coring
	B-404	340031.69	2405136.97	744.44	17.75	46.25	31.15	105.00	200.15	SPT/Coring
	B-405	340131.91	2405221.36	757.56	11.00	28.00	60.00	105.00	204.00	SPT/Coring
Nuclear Island Facilities: Safeguard Building Mechanical Safeguard Building Electrical Fuel Building Nuclear Auxiliary Building Access Building	B-406	340286.99	2405115.50	771.88	11.00	63.00		146.00	220.00	SPT/Coring
	B-407	340169.21	2404971.67	734.19	25.50	34.50	11.00	4.50	75.50	SPT/Coring
	B-408	340045.08	2404983.01	728.44	25.00	8.00	43.00	128.50	204.50	SPT/Coring
	B-409	339978.74	2405035.71	735.15	17.50	53.50		29.50	100.50	SPT/Coring
	B-410	339957.85	2405145.85	744.85	17.50	43.50	19.00	20.00	100.00	SPT/Coring
	B-411	339979.47	2405273.90	758.15	23.45	16.55	40.00	20.90	100.90	SPT/Coring
	B-412	340068.40	2405294.49	763.35	22.00	19.00	59.00	21.20	121.20	SPT/Coring
	B-413	340208.12	2405283.00	772.20	9.00	101.50		8.50	119.00	SPT/Coring
Radioactive Waste Processing Building	B-414	339887.65	2404983.51	730.32	16.50	17.75	5.00	70.00	109.25	SPT/Coring
	B-415	339896.90	2405085.97	739.64	15.50	16.00	84.00	85.00	200.50	SPT/Coring
	B-416	339788.65	2404992.39	728.86	25.00	5.00	15.00	60.00	105.00	SPT/Coring
	B-417	339799.26	2405095.47	734.74	20.00	10.40	5.10	68.70	104.20	SPT/Coring
Emergency Diesel Generator Building	B-418	339853.39	2405203.43	744.02	20.00	21.50		179.10	220.60	SPT/Coring
	B-419	339860.44	2405278.15	748.14	23.75	30.20		54.65	108.60	SPT/Coring
	B-420	340403.18	2405150.67	778.81	15.60	30.90	23.50	154.60	224.60	SPT/Coring
	B-421	340410.50	2405228.92	783.85	15.40	41.60	13.00	30.70	100.70	SPT/Coring

POWERBLOCK

Table 2.5-15— {Summary of As-Conducted Boring Information}
(Page 2 of 3)

Structure (Foundation)	Boring	Horizontal Coordinates (ft)		Surface Elevation (ft)	Boring Depth (ft)				Type of Test			
		State N	State E		Overburden Soil	Mahantango Formation						
						Weathered Rock	Transition Zone	Sound Rock		Total		
POWERBLOCK	Essential Service Water Building	UQBURB	B-422	339721.35	2405472.52	724.95	16.00	0.00	0.00	104.20	120.20	SPT/Coring
			B-423	339727.11	2405533.75	724.06	13.20	0.00	25.80	184.00	223.00	SPT/Coring
			B-424	339868.96	2405458.50	745.40	23.40	7.80	58.40	113.20	202.80	SPT/Coring
			B-425	339874.33	2405519.37	744.91	23.90	13.10	49.75	13.55	100.30	SPT/Coring
			B-426	340296.20	2404892.65	745.20	20.00	38.00		165.00	223.00	SPT/Coring
			B-427	340301.39	2404954.97	753.97	12.70	41.50	5.10	41.70	101.00	SPT/Coring
			B-428	340444.20	2404878.07	750.57	17.00	8.00	22.00	73.80	120.80	SPT/Coring
			B-429	340449.24	2404939.62	757.19	21.00	7.00	24.00	168.30	220.30	SPT/Coring
			B-430	340146.97	2405389.90	775.32	21.80	61.20		48.20	131.20	SPT/Coring
			B-431	340160.61	2405519.42	783.22	20.30	23.70	55.00	5.20	104.20	SPT/Coring
			B-432	340173.52	2405665.64	789.49	28.00	19.00	50.00	33.10	130.10	SPT/Coring
			B-433	340485.71	2405380.47	792.77	25.00	45.00	7.00	43.00	120.00	SPT/Coring
			B-434	339641.97	2404822.94	709.00	15.70	0.00	14.10	13.50	43.30	SPT/Coring
OTHER STRUCTURES	Essential Service Water Emergency Makeup System	ESWEMS	B-435	339687.56	2406056.31	687.27	12.20	0.00	23.20	24.80	60.20	SPT/Coring
			B-436	339698.74	2406180.69	682.97	33.00	0.00	0.00	27.00	60.00	SPT/Coring
			B-437	339709.67	2406305.29	679.59	40.90	0.00	0.00	19.10	60.00	SPT/Coring
			B-438	339721.41	2406429.61	679.00	39.00	0.00	0.00	22.50	61.50	SPT/Coring
			B-439	339757.11	2406541.81	677.06	44.80	0.00	0.00	15.40	60.20	SPT/Coring
			B-440	339706.74	2406546.24	675.97	34.30	0.00	0.00	66.00	100.30	SPT/Coring
			B-441	339619.81	2407095.21	666.90	54.50	0.00	0.00	9.50	64.00	SPT/Coring
			B-442	339570.73	2406579.03	673.20	40.10	0.00	0.00	20.70	60.80	SPT/Coring
			B-443	341137.47	2405090.24	728.19	35.00	5.00		31.50	71.50	SPT/Coring
			B-444	341108.61	2405751.32	782.61	24.50	5.50	0.00	40.50	70.50	SPT/Coring

Table 2.5-15— {Summary of As-Conducted Boring Information}
(Page 3 of 3)

Structure (Foundation)	Boring	Horizontal Coordinates (ft)		Surface Elevation (ft)	Boring Depth (ft)				Type of Test	
		State N	State E		Overburden Soil	Weathered Rock	Transition Zone	Sound Rock		Total
AUX	G-401	340119.93	2405141.09	759.09	19.00	15.00	55.00	326.00	415.00	Geophysical
	G-423	339738.64	2405527.45	729.82	12.00	0.00	27.00	216.00	255.00	Geophysical
	G-426	340306.23	2404892.64	658.18	20.00	38.00		204.00	262.00	Geophysical
	PMT-401	340151.69	2405219.62	759.09	17.50	17.30	60.00	20.00	114.80	Pressuremeter
	PMT-402	340053.75	2405001.22	729.82	28.00	52.00		6.00	86.00	Pressuremeter

In some borings, there is not a clear distinction between Weathered Rock and Transition Zone, therefore in those borings the Weathered Rock and the Transition Zone are treated as one layer.

Table 2.5-16— {Summary of Hammer-Rod Energy Measurements}

Drill Rig	Measurement in Boring No.	ETR Range (%)	Average ETR (%)	Energy Adjustment (ETR%/60%)
CME 55 (Track)	B-443A/B-443B	87-90	88	1.47
CME 550X	B-438A	90-92	91	1.52
CME 55 (Truck)	B-438B/B-438C	86-92	89	1.48
Deidrich D-120	B-44C	84-91	87	1.46

Note: ETR = Percentage of theoretical hammer energy measured in the field

Table 2.5-17— {Summary Of Field-Measured Standard Penetration Test (SPT) N-Values}

Unit	SPT N-values (blows/ft)		
	Minimum	Maximum	Average
Overburden Soil	2	100	43

Table 2.5-18— {Summary of Adjusted Standard Penetration Test (SPT) N-Values based on Energy Measurements}

Unit	SPT N-values (blows/ft)			Recommended N-Value for Engineering Purposes (blows/ft)
	Minimum	Maximum	Average	
Overburden Soil	3	100	54	30

Table 2.5-19— {Summary Of Pressuremeter Test Results}
English Units

	Unit	Boring	Depth (ft)	E_s (ksf)	G (ksf)	p_l (ksf)	s_u (ksf)
MAHANTANGO FORMATION	Weathered Rock	PMT-401	20	4381	1635	456.97	124.84
	Transition Zone	PMT-401	50	55846	19947	---	---
	Transition Zone	PMT-401	94	53826	19226	---	---
	Sound Rock	PMT-401	114	114571	44301	---	---
	Weathered Rock	PMT-402	30	75927	28339	---	---
	Transition Zone	PMT-402	50	147561	52707	---	---
	Transition Zone	PMT-402	70	3968	1417	716.15	262.52
	Sound Rock	PMT-402	85	60388	23350	---	---
<p>Note: <i>E_s - elastic modulus</i> <i>G - shear modulus</i> <i>p_l - pressuremeter limit pressure</i> <i>s_u - undrained shear strength</i> --- Tests terminated before creep and limit pressures could be established</p>							

Table 2.5-19— {Summary Of Pressuremeter Test Results}
SI Units

Unit		Boring	Depth (m)	E_s (kPa)	G (kPa)	p_l (kPa)	s_u (kPa)
MAHANTANGO FORMATION	Weathered Rock	PMT-401	6.1	209760	78280	21880	5980
	Transition Zone	PMT-401	15.2	2673910	955060	---	---
	Transition Zone	PMT-401	28.7	2577190	920540	---	---
	Sound Rock	PMT-401	34.7	5485660	2121130	---	---
	Weathered Rock	PMT-402	9.1	3635380	1356870	---	---
	Transition Zone	PMT-402	15.2	7065220	2523610	---	---
	Transition Zone	PMT-402	21.3	189990	67850	34290	12570
	Sound Rock	PMT-402	25.9	2891380	1118000	---	---
<p>Note: E_s - elastic modulus G - shear modulus p_l - pressuremeter limit pressure s_u - undrained shear strength --- Tests terminated before creep and limit pressures could be established</p>							

Table 2.5-20— {Summary Of Laboratory Tests}

	Test	Standard/Method	Quantity
Static/Index	Unit Weight	From weight-volume relationship	32
	Sieve Analysis	ASTM D422-63(2007) and D1140-00(2006)	23
	Specific Gravity of Soil Solids	ASTM D 854-10	7
	Compaction Test	ASTM D1557-09	4
	Moisture Content	ASTM D2216-05	68
	Unified Soil Classification System	ASTM D2487-10	23
	Atterberg Limits	ASTM D4318-10	22
	CU Triaxial with Pore Pressure Measurement	ASTM D4767-04	4
	Permeability	ASTM D5084-03 Method A	4
	Unified Rock Classification System	ASTM D5878-08	21
	Specific Gravity and Absorption of Rock	ASTM D6473-99(2005)	9
Dynamic	Unconfined Compression	ASTM D7012-07	21
	Resonant Column Torsional Shear Test	PBRCTS-1 Technical Procedures for RCTS	2
Chemical	"Free-Free" Resonant Column Test	Internal Procedures Fr-Fr-1, Rev. 0, dated May-09	4
	Sulfate Ion Content	AASHTO T290	13
	Chloride Ion Content	AASHTO T291	13
	pH	ASTM D 4972-01 (2007)	13
	Resistivity	ASTM G 187-05	13

Table 2.5-21 — {Summary of Fines Content and USCS for Overburden Soil}

Unit	Boring Number	Sample ID	Depth (ft)	Depth (m)	USCS (1) Symbol	Percent Passing No. 200 Sieve (Fines Content) [%]
OVERBURDEN SOIL	B-401	S-4 + S-5	6.0	1.8	GC-GM	16.0
	B-403	S-4 + S-5	6.0	1.8	GC	27.8
	B-404	S-4 + S-5	7.5	2.3	SC-SM	23.5
	B-405	S-5 + S-6	8.0	2.4	gw	2.0
	B-406	S-3 + S-4	4.5	1.4	gw-gc	6.2
	B-408	S-3 + S-4	4.5	1.4	NM	
	B-412	S-2 + S-3	3.0	0.9	SM	32.5
	B-412	S-9 + S-10	13.5	4.1	GC-GM	17.7
	B-415	S-7 + S-8	11.0	3.4	GP-GC	8.4
	B-422	S-4 + S-5	10.3	3.1	GC-GM	18.6
	B-423	S-6 + S-7 + S-8	9.3	2.8	SC	20.6
	B-426	S-6 + S-7 + S-8	9.8	3.0	SW-SC	9.2
	B-428	S-2 + S-3	3.0	0.9	SC	25.3
	B-428	S-5 + S-6	7.5	2.3	SC	28.8
	B-429	S-2 + S-3 + S-4	5.8	1.8	SC	41.7
	B-429	S-6 + S-7	14.5	4.4	GM	20.3
	B-430	S-3 + S-4	7.0	2.1	SC	19.9
	B-431	S-1 + S-2	2.0	0.6	CL	56.0
B-432	S-5 + S-6	12.0	3.7	GC-GM	13.6	
B-433	S-2 + S-3	8.3	2.5	GC	13.9	
FILL	"Bulk Sample 1(B-01)"	Test 1	NA	NA	GP	4.1
	"Bulk Sample 2(B-02)"	Test 2	NA	NA	GP	3.6
FILL	"Bulk Sample 1(B-01)"	Test 1	NA	NA	SP-SM	8.9
	"Bulk Sample 2(B-02)"	Test 2	NA	NA	SP-SM	9.2

NM - Not Measured
 NA - Not Applicable

(1) Lower case USCS symbols were based on assumptions

Table 2.5-22— {Summary Of Moisture Content}

(Page 1 of 3)

Unit	Boring	Sample ID	Depth		Moisture Content (%)
			(ft)	(m)	
OVERBURDEN SOIL	B-401	S-4 + S-5	6	1.8	12.5
	B-403	S-4 + S-5	6	1.8	14.6
	B-404	S-4 + S-5	7.5	2.3	10.6
	B-405	S-5 + S-6	8	2.4	8.6
	B-406	S-3 + S-4	4.5	1.4	8.7
	B-408	S-3 + S-4	4.5	1.4	13.6
	B-412	S-2 + S-3	3	0.9	12.8
	B-412	S-9 + S-10	13.5	4.1	12.5
	B-415	S-7 + S-8	11	3.4	7.2
	B-422	S-4 + S-5	10.3	3.1	10.1
	B-423	S-6 + S-7 + S-8	9.3	2.8	12.6
	B-426	S-6 + S-7 + S-8	9.8	3	9.4
	B-428	S-2 + S-3	3	0.9	16.1
	B-428	S-5 + S-6	7.5	2.3	17.4
	B-429	S-2 + S-3 + S-4	5.8	1.8	15.6
	B-429	S-6 + S-7	14.5	4.4	11.9
	B-430	S-3 + S-4	7	2.1	10.4
	B-431	S-1 + S-2	2	0.6	12.5
	B-432	S-5 + S-6	12	3.7	3.8
	B-433	S-2 + S-3	8.3	2.5	5.5

11.3

Table 2.5-22— {Summary Of Moisture Content}

(Page 2 of 3)

Unit	Boring	Sample ID	Depth		Moisture Content (%)		
			(ft)	(m)			
MAHANTANGO FORMATION	Weathered Rock/ Transition Zone	B-406	SC-3	70.7	21.5	9.6	9.6
	Transition Zone	B-401	SC-2	64.2	19.6	2.9	3.0
		B-404	SC-2	90.6	27.6	4.4	
		B-431	SC-2	67.9	20.7	2.0	
		B-432	SC-2	68.3	20.8	2.7	
	Sound Rock	B-401	SC-3	91.5	27.9	0.8	
		B-401	SC-4	141.4	43.1	0.6	
		B-401	SC-5	195.8	59.7	0.6	
		B-401	SC-6	248.1	75.6	0.5	
		B-401	SC-7	293.8	89.5	0.6	
		B-401	SC-8	343.4	104.7	0.5	
		B-401	SC-9	400.5	122.1	0.7	
		B-402	SC-3	132.7	40.4	0.4	
		B-403	SC-2	75.9	23.1	0.5	
		B-403	SC-3	153.6	46.8	0.6	
		B-404	SC-3	98.6	30.0	0.7	
		B-404	SC-4	146.9	44.8	0.6	
		B-404	SC-5	193.1	58.9	0.5	
		B-405	SC-4	129.3	39.4	0.9	
		B-408	SC-3	83.7	25.5	0.6	
		B-411	SC-2	82.0	25.0	0.6	
		B-412	SC-2	107.8	32.8	1.8	
		B-421	SC-2	75.3	22.9	0.6	
		B-423	SC-2	118.2	36.0	1.0	
		B-423	SC-3	178.6	54.4	0.8	
		B-423	SC-4	219.4	66.9	0.7	
		B-426	SC-4	152.9	46.6	0.6	
		B-426	SC-5	207.1	63.1	0.6	
		B-429	SC-2	104.2	31.7	0.5	
		B-429	SC-3	148.9	45.4	0.4	
B-429		SC-4	201.2	61.3	0.7		
B-433		SC-3	81.9	24.9	0.5		

Table 2.5-22— {Summary Of Moisture Content}

(Page 3 of 3)

Unit	Boring	Sample ID	Depth		Moisture Content (%)	
			(ft)	(m)		
FILL	Bulk Sample 01 (B-01)	Test 1	NA	NA	4.9	5.4
		Test 2	NA	NA	4.6	
		Test 3	NA	NA	5.5	
		Test 4	NA	NA	4.8	
		Test 5	NA	NA	4.3	
		Test 6	NA	NA	5	
		Test 7	NA	NA	5.1	
		Test 8	NA	NA	4.5	
	Bulk Sample 02 (B-01)	Test 1	NA	NA	6.2	
		Test 2	NA	NA	6.5	
		Test 3	NA	NA	6.4	
		Test 4	NA	NA	5.8	
		Test 5	NA	NA	6.1	
		Test 6	NA	NA	4.9	
		Test 7	NA	NA	5.8	
		Test 8	NA	NA	5.8	

NA - Not Applicable

Table 2.5-23— {Summary of Atterberg Limits}

Unit	Boring Number	Sample ID	Depth		Liquid Limit [%]	Plastic Limit [%]	Plasticity Index [%]
			(ft)	(m)			
OVERBURDEN SOIL	B-401	S-4 + S-5	6.0	1.8	27	20	7
	B-403	S-4 + S-5	6.0	1.8	25	17	8
	B-404	S-4 + S-5	7.5	2.3	24	18	6
	B-405	S-5 + S-6	8.0	2.4	---	---	---
	B-406	S-3 + S-4	4.5	1.4	---	---	---
	B-408	S-3 + S-4	4.5	1.4	25	17	8
	B-412	S-2 + S-3	3.0	0.9	20	17	3
	B-412	S-9 + S-10	13.5	4.1	25	20	5
	B-415	S-7 + S-8	11.0	3.4	28	21	7
	B-422	S-4 + S-5	10.3	3.1	24	18	6
	B-423	S-6 + S-7 + S-8	9.3	2.8	27	16	11
	B-426	S-6 + S-7 + S-8	9.8	3.0	28	16	12
	B-428	S-2 + S-3	3.0	0.9	24	13	11
B-428	S-5 + S-6	7.5	2.3	43	26	17	
B-429	S-2 + S-3 + S-4	5.8	1.8	30	16	14	
B-429	S-6 + S-7	14.5	4.4	29	23	6	
B-430	S-3 + S-4	7.0	2.1	22	13	9	
B-431	S-1 + S-2	2.0	0.6	26	14	12	
B-432	S-5 + S-6	12.0	3.7	19	12	7	
B-433	S-2 + S-3	8.3	2.5	21	12	9	
FILL	"Bulk Sample 1(B-01)"	Test 1	NA	NA	NP	NP	NP
		Test 2	NA	NA	NP	NP	NP
	"Bulk Sample 2(B-02)"	Test 1	NA	NA	NP	NP	NP
		Test 2	NA	NA	NP	NP	NP
--- Not enough material to be measured NA - Not Applicable NP - Non-Plastic							

Table 2.5-24— {Summary Of Unit Weights}
English Units

Unit		Boring	Sample ID	Depth (ft)	Dry Unit Weight [pcf]		Moist Unit Weight [pcf]	
MAHANTANGO FORMATION	Weathered Rock/ Transition Zone	B-406	SC-3	70.7	137	137	150	150
	Transition Zone	B-401	SC-2	64.2	167	162	172	167
		B-404	SC-2	90.6	154		161	
		B-431	SC-2	67.9	165		168	
		B-432	SC-2	68.3	162		167	
	Sound Rock	B-401	SC-3	91.5	171	171	172	172
		B-401	SC-4	141.4	171		172	
		B-401	SC-5	195.8	171		172	
		B-401	SC-6	248.1	171		172	
		B-401	SC-7	293.8	172		173	
		B-401	SC-8	343.4	172		173	
		B-401	SC-9	400.5	172		173	
		B-402	SC-3	132.7	171		172	
		B-403	SC-2	75.9	171		172	
		B-403	SC-3	153.6	172		173	
		B-404	SC-3	98.6	170		171	
		B-404	SC-4	146.9	171		172	
		B-404	SC-5	193.1	172		172	
		B-405	SC-4	129.3	170		171	
		B-408	SC-3	83.7	171		172	
		B-411	SC-2	82	171		172	
		B-412	SC-2	107.8	159		162	
		B-421	SC-2	75.3	171		172	
		B-423	SC-2	118.2	170		172	
		B-423	SC-3	178.6	170		171	
		B-423	SC-4	219.4	170		171	
		B-426	SC-4	152.9	171		172	
		B-426	SC-5	207.1	183		184	
	B-429	SC-2	104.2	171	172			
	B-429	SC-3	148.9	172	173			
	B-429	SC-4	201.2	170	171			
	B-433	SC-3	81.9	171	172			
FILL	Bulk Sample 1 (B-01)	Test 1	NA	142	142	150	150	
		Test 2	NA	141		150		
	Bulk Sample 2 (B-02)	Test 1	NA	142		149		
		Test 2	NA	142		150		
NA - Not Applicable								

Table 2.5-24— {Summary Of Unit Weights}
(SI Units)

Unit		Boring	Sample ID	Depth (m)	Dry Unit Weight (kN/m ³)		Moist Unit Weight (kN/m ³)	
MAHANTANGO FORMATION	Weathered Rock/ Transition Zone	B-406	SC-3	21.5	21.6		23.7	23.7
	Transition Zone	B-401	SC-2	19.6	26.3	25.5	27	26.2
		B-404	SC-2	27.6	24.3		25.3	
		B-431	SC-2	20.7	25.9		26.4	
		B-432	SC-2	20.8	25.5		26.2	
	Sound Rock	B-401	SC-3	27.9	26.8	26.9	27	27.0
		B-401	SC-4	43.1	26.9		27	
		B-401	SC-5	59.7	26.9		27	
		B-401	SC-6	75.6	26.9		27	
		B-401	SC-7	89.6	27		27.2	
		B-401	SC-8	104.7	27		27.1	
		B-401	SC-9	122.1	27		27.2	
		B-402	SC-3	40.4	26.9		27.1	
		B-403	SC-2	23.1	26.8		27	
		B-403	SC-3	46.8	27		27.1	
		B-404	SC-3	30.1	26.7		26.9	
		B-404	SC-4	44.8	26.9		27.1	
		B-404	SC-5	58.9	27		27.1	
		B-405	SC-4	39.4	26.7		26.9	
		B-408	SC-3	25.5	26.9		27.1	
		B-411	SC-2	25	26.9		27	
		B-412	SC-2	32.9	25		25.5	
		B-421	SC-2	23	26.8		27	
		B-423	SC-2	36	26.8		27	
		B-423	SC-3	54.4	26.7		26.9	
		B-423	SC-4	66.9	26.7		26.9	
		B-426	SC-4	46.6	26.9		27	
		B-426	SC-5	63.1	28.7		28.9	
		B-429	SC-2	31.8	26.9		27	
	B-429	SC-3	45.4	27	27.1			
	B-429	SC-4	61.3	26.7	26.9			
	B-433	SC-3	25	26.9	27.1			
	FILL	Bulk Sample 1 (B-01)	Test 1	NA	22.3	22.3	23.6	23.6
Test 2			NA	22.2	23.5			
Bulk Sample 2 (B-02)		Test 1	NA	22.3	23.5			
		Test 2	NA	22.3	23.6			

NA - Not Applicable

Table 2.5-25— {Summary Of Specific Gravity}

Unit		Boring	Sample ID	Depth		Specific Gravity
				(ft)	(m)	
OVERBURDEN SOIL		B-401	S-4 + S-5	6.0	1.8	2.65
		B-405	S-5 + S-6	8.0	2.4	2.62
		B-408	S-3 + S-4	4.5	1.4	2.6
		B-412	S-2 + S-3	3.0	0.9	2.61
		B-415	S-7 + S-8	11.0	3.4	2.67
		B-429	S-2 + S-3 + S-4	5.8	1.8	2.64
		B-429	S-6 + S-7	14.5	4.4	2.70
MAHANTANGO FORMATION	Transition Zone	B-404	SC-2	90.6	27.6	2.50
	Sound Rock	B-401	SC-5	195.8	59.7	2.76
		B-401	SC-6	248.1	75.6	2.74
		B-401	SC-8	343.4	104.7	2.78
		B-404	SC-5	193.1	58.9	2.76
		B-412	SC-2	107.8	32.8	2.62
		B-423	SC-2	118.2	36.0	2.74
		B-426	SC-5	207.1	63.1	2.75
	B-429	SC-4	201.2	61.3	2.74	
FILL		Bulk Sample 1 (B-01)	Test 1	NA	NA	2.61
			Test 2	NA	NA	2.58
		Bulk Sample 2 (B-02)	Test 1	NA	NA	2.58
			Test 2	NA	NA	2.60
<i>NA - Not Applicable</i>						

Table 2.5-26— {Summary of Chemical Tests Results}

Unit	Boring	Sample ID	Depth		pH	Resistivity (W-cm)	Sulfate Ion Concentration (ppm)	Chloride Concentration (ppm)
			(ft)	(m)				
MAHANTANGO FORMATION	B-408	SC-3	83.7	25.5	8.7	10050	14.50	4.71
	B-411	SC-2	82.0	25.0	9.0	12395	10.96	3.82
	B-421	SC-2	75.3	22.9	8.9	13065	12.21	4.34
	B-423	SC-2	118.2	36.0	8.3	5193	49.08	3.62
	B-429	SC-2	103.9	31.7	8.7	7370	18.04	4.44
	B-433	SC-3	81.9	24.9	8.9	12395	12.42	3.79
FILL	Bulk Sample 1 (B-01)	Test 1	NA	NA	5.4	15578	14.92	9.47
		Test 2	NA	NA	5.3	15075	11.17	14.53
	Bulk Sample 2 (B-02)	Test 1	NA	NA	6.1	16080	< 9.71	10.61
		Test 2	NA	NA	6.2	12730	< 9.71	10.16

*Test data from Boring B-412 (Sample SC-2), B-431 (Sample SC-2), and B-433 (Sample SC-2) are excluded due to inconsistency of results.
NA - Not Applicable*

Table 2.5-27— {Summary of Unconfined Compressive Strength Test Results}

English Units
Page 1 of 2

Unit		Boring	Sample ID	Depth (ft)	UCS (psi)		UCS (ksf)	
MAHANTANGO FORMATION	Weathered Rock/ Transition Zone	B-406	SC-3	70.7	1660	1660	239	239
	Sound Rock	B-401	SC-3	91.5	8170	7096	1176	1022
		B-401	SC-5	195.8	8770		1263	
		B-401	SC-6	248.1	8670		1248	
		B-401	SC-8	343.4	2800		403	
		B-402	SC-3	132.7	9210		1326	
		B-403	SC-2	75.9	9670		1392	
		B-403	SC-3	153.6	6190		891	
		B-404	SC-3	98.6	8780		1264	
		B-404	SC-4	146.9	7160		1031	
		B-404	SC-5	193.1	8400		1210	
		B-405	SC-4	129.3	6490		935	
		B-408	SC-3	83.7	9380		1351	
		B-423	SC-2	118.2	3130		451	
		B-423	SC-3	178.6	2980		429	
		B-423	SC-4	219.4	3130		451	
		B-426	SC-4	152.9	8200		1181	
		B-426	SC-5	207.1	7690		1107	
		B-429	SC-2	104.2	9020		1299	
		B-429	SC-3	148.9	6900		994	
B-429	SC-4	201.2	7170	1032				

Table 2.5-27— {Summary of Unconfined Compressive Strength Test Results}

SI Units
Page 2 of 2

	Unit	Boring	Sample ID	Depth (m)	UCS (kPa)	
MAHANTANGO FORMATION	Weathered Rock/ Transition Zone	B-406	SC-3	21.5	11445	11445
	Sound Rock	B-401	SC-3	27.9	56330	48922
		B-401	SC-5	59.7	60467	
		B-401	SC-6	75.6	59778	
		B-401	SC-8	104.7	19305	
		B-402	SC-3	40.4	63501	
		B-403	SC-2	23.1	66672	
		B-403	SC-3	46.8	42679	
		B-404	SC-3	30.0	60536	
		B-404	SC-4	44.8	49366	
		B-404	SC-5	58.9	57916	
		B-405	SC-4	39.4	44747	
		B-408	SC-3	25.5	64673	
		B-423	SC-2	36.0	21581	
		B-423	SC-3	54.4	20546	
		B-423	SC-4	66.9	21581	
		B-426	SC-4	46.6	56537	
		B-426	SC-5	63.1	53021	
		B-429	SC-2	31.7	62191	
		B-429	SC-3	45.4	47574	
B-429	SC-4	61.3	49435			

Table 2.5-28— {Unified Rock Classification System (URCS) of Rock Samples}

Unit	"SampleID"	Depth		Weathering	Strength	Discontinuity	Unit Weight	
		(ft)	(m)					
MAHANTANGO FORMATION	Weathered Rock/ Transition Zone	SC-3	70.7	21.5	C	D	C	D
	Sound Rock	SC-3	91.5	27.9	A	C	C	A
		SC-5	195.8	59.7	A	C	C	A
		SC-6	248.1	75.6	A	C	C	A
		SC-8	343.4	104.7	A	C	C	A
		SC-3	132.7	40.4	A	C	C	A
		SC-2	75.9	23.1	A	C	C	A
		SC-3	153.6	46.8	A	C	C	A
		SC-3	98.6	30.0	A	C	C	A
		SC-4	146.9	44.8	A	C	C	A
		SC-5	193.1	58.9	A	C	C	A
		SC-4	129.3	39.4	A	C	C	A
		SC-3	83.7	25.5	A	C	C	A
		SC-2	118.2	36.0	A	C	C	A
		SC-3	178.6	54.4	B	C	C	A
		SC-4	219.4	66.9	A	C	C	A
SC-4	152.9	46.6	A	C	C	A		
SC-5	207.1	63.1	A	C	C	A		
SC-2	104.2	31.7	A	B	C	A		
SC-3	148.9	45.4	A	C	C	A		
SC-4	201.2	61.3	A	C	C	A		

Table 2.5-29— {Summary of Permeability Test Results}

Unit	Material	Sample ID	Permeability	
			ft/s	cm/s
FILL	Bulk Sample 1 (B-01)	Test 1	1.71E-03	5.20E-02
			1.74E-03	5.30E-02
			1.77E-03	5.40E-02
		Test 2	7.87E-04	2.40E-02
			7.55E-04	2.30E-02
			7.87E-04	2.40E-02
	Bulk Sample 2 (B-02)	Test 1	2.13E-04	6.50E-03
			2.23E-04	6.80E-03
			2.43E-04	7.40E-03
		Test 2	3.94E-04	1.20E-02
			3.61E-04	1.10E-02
			3.61E-04	1.10E-02

NA - Not Applicable

Table 2.5-30— {Resonant Column Low Strain Properties}

English Units
Page 1 of 2

Unit	Sample	Laboratory	Moist Unit Weight (pcf)	Confining Pressures (psf)	Low Amplitude		
					Shear Modulus, G _{max} (ksf)	Shear Wave Velocity, V _s (fps)	Damping Ratio, D (%)
FILL	Test Pit Face	FUGRO	136	---	---	---	---
				---	---	---	---
				---	---	---	---
	Test Pit #5	FUGRO	132.9	576	1307	562	1.64
				2448	2839	828	1.47
				9936	5877	1189	1.34
	Bulk Sample 1 (B-01)	UTexas	139.3	720	2193	712	4.41
				2880	4576	1027	3.38
				11520	9524	1479	2.82
	Bulk Sample 2 (B-02)	UTexas	139.8	720	3582	908	5.72
				2880	6242	1198	4.75
				11520	1146	1619	3.72

RCTS specimens only consist of materials passing the 1/2" sieve.

RCTS specimens were compacted to at least 95% of its maximum dry density prior to testing.

--- Data unavailable.

Table 2.5-30— {Resonant Column Low Strain Properties}

SI Units
Page 2 of 2

Unit	Sample	Laboratory	Moist Unit Weight (kN/m ³)	Confining Pressures (kPa)	Low Amplitude		
					Shear Modulus, G _{max} (MPa)	Shear Wave Velocity, V _s (m/a)	Damping Ratio, D (%)
FILL	Test Pit Face	FUGRO	21.4	---	---	---	---
				---	---	---	---
				---	---	---	---
	Test Pit #5	FUGRO	20.9	28	63	171	1.64
				117	136	252	1.47
				475	282	362	1.34
	Bulk Sample 1 (B-01)	UTexas	21.9	34	105	217	4.41
				138	219	313	3.38
				552	457	451	2.82
	Bulk Sample 2 (B-02)	UTexas	22.0	34	172	277	5.72
				138	299	365	4.75
				552	549	493	3.72

RCTS specimens only consist of materials passing the 1/2" sieve.
 RCTS specimens were compacted to at least 95% of its maximum dry density prior to testing.
 --- Data unavailable.

Table 2.5-31— {"Free-Free" Test Results}
English Units

Layer	Boring	Sample ID	Depth (ft)	γ (pcf)	V_s (fps)	D_s (%)	V_c (fps)	D_c (%)	V_p (fps)
Transition Zone	B-401	SC-2	64.2	167	2621	7.8	4391	5.9	9910
Sound Rock	B-401	SC-4	141.3	171	8317	1.54	12565	1.42	14193
	B-401	SC-7	293.7	172	6931	2.37	11005	2.21	13822
	B-401	SC-9	400.7	172	7463	1.86	12064	1.86	13940

γ -- Unit Weight
 V_s - Shear Wave Velocity
 D_s - Shear Wave Damping
 V_c - Compression Wave Velocity (Unconstrained Test)
 D_c - Compression Wave Damping
 V_p - Compression Wave Velocity (Constrained Test)

Table 2.5-31— {"Free-Free" Test Results}
SI Units

Layer	Boring	Sample ID	Depth (m)	γ (kN/m ³)	V_s (m/s)	D_s (%)	V_c (m/s)	D_c (%)	V_p (m/s)
Transition Zone	B-401	SC-2	19.6	26.3	799	7.8	1338	5.9	3021
Sound Rock	B-401	SC-4	43.1	26.9	2535	1.54	3830	1.42	4326
	B-401	SC-7	89.5	27.0	2113	2.37	3354	2.21	4213
	B-401	SC-9	122.1	27.0	2275	1.86	3677	1.86	4249

γ -- Unit Weight
 V_s - Shear Wave Velocity
 D_s - Shear Wave Damping
 V_c - Compression Wave Velocity (Unconstrained Test)
 D_c - Compression Wave Damping
 V_p - Compression Wave Velocity (Constrained Test)

Table 2.5-32— {Consolidated-Undrained Triaxial Compression Test Results with Pore Pressure Measurements}

Unit	Material	Sample ID	Depth	c' (psf)	φ' (degrees)
FILL	Bulk Sample 1 (B-01)	Test 1	NA	0.00	44.5
		Test 2	NA	0.00	38.4
	Bulk Sample 2 (B-02)	Test 1	NA	0.00	34.5
		Test 2	NA	0.00	36.9
<i>c' - effective cohesion</i> <i>φ' - effective angle of internal friction</i> <i>NA - Not Applicable</i>					

Table 2.5-33—{Category 1 Structural Fill Properties}
English Units

Parameters		Category 1 Structural Fill ¹
Grain Size Analysis	Gravel [%]	52
	Sand [%]	44
	Fines [%]	4
Volume	Total V_t [ft ³]	1.000
	Solids V_s [ft ³]	0.831
	Water V_w [ft ³]	0.126
	Air V_a [ft ³]	0.043
	Voids V_v [ft ³]	0.169
Porosity	n	0.17
	Void Ratio e	0.20
Mass	Solids m_s [lbm]	135
	Water m_w [lbm]	7.9
	Total m_t [lbm]	142
Moisture Content	w [%]	6.0
	Saturation S [%]	7.5
Specific Gravity	G_s [—]	2.60
	Dry g_{dry} [pcf]	135
Unit Weight	Wet g_{moist} [pcf]	142
	Saturated g_{sat} [pcf]	145

¹ 95% Modified Proctor

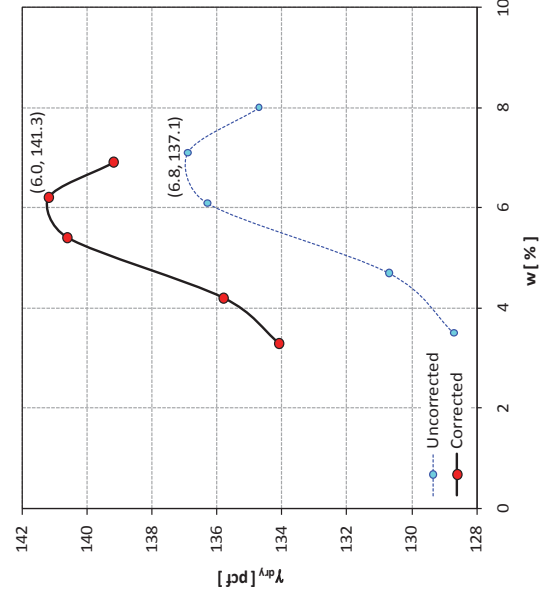
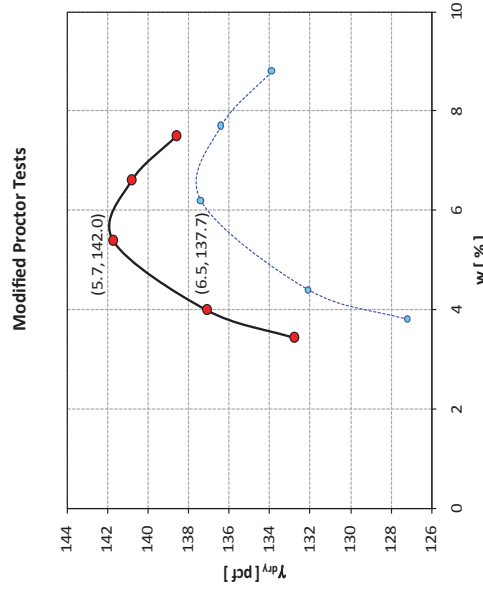
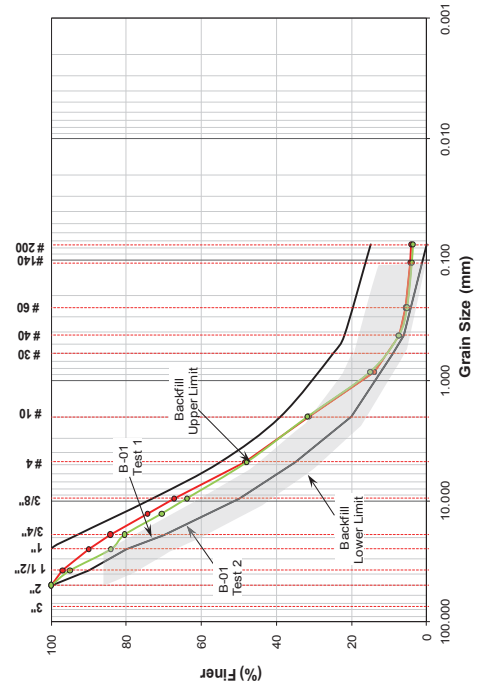


Table 2.5-33—{Category 1 Structural Fill Properties}
SI Units

Parameters		Category 1 Structural Fill ¹
Grain Size Analysis	Gravel	52
	Sand	44
Volume	Fines	4
	Total	V_t [m ³]
	Solids	V_s [m ³]
	Water	V_w [m ³]
	Air	V_a [m ³]
	Void Ratio	V_v [m ³]
Porosity	n	0.17
	e	0.20
Mass	Solids	m_s [kg]
	Water	m_w [kg]
	Total	m_t [kg]
Moisture Content	w [%]	6.0
	Saturation	S [%]
Specific Gravity	G_s	2.60
	Dry	g_{dry} [kN/m ³]
Unit Weight	Wet	g_{moist} [kN/m ³]
	Saturated	g_{sat} [kN/m ³]

¹ 95% Modified Proctor

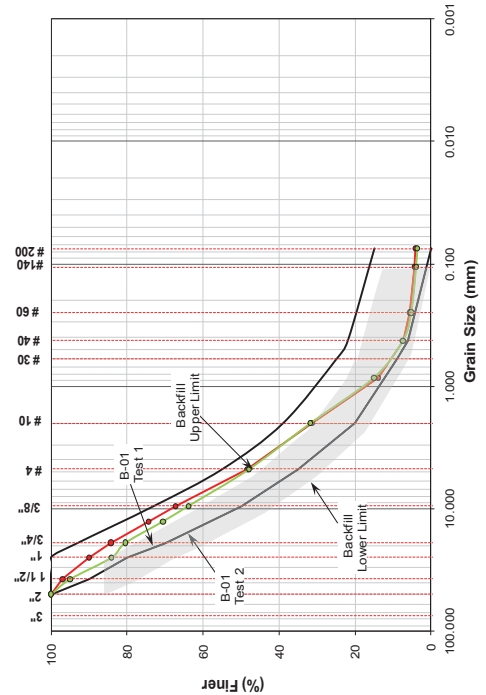
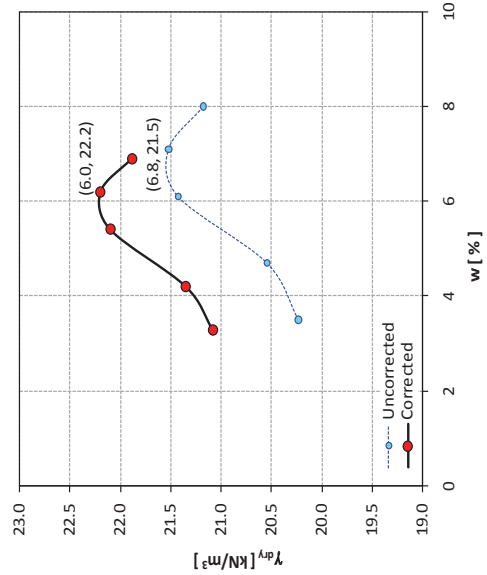
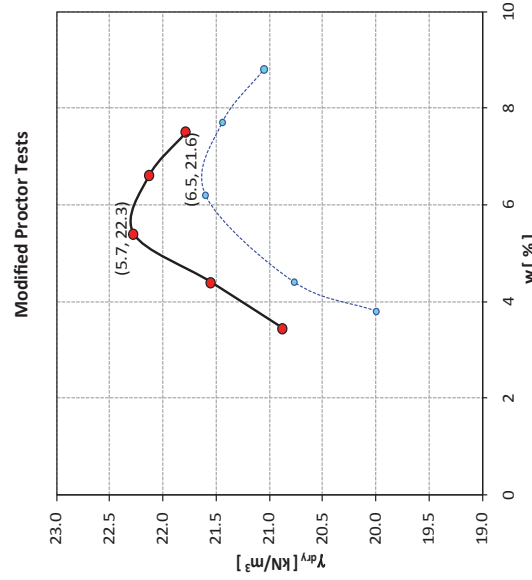


Table 2.5-34— {Recommended Values Of Index Properties}
English Units

Unit	USCS or URCS	Fines Content (%)	Moistur e Content (%)	Atterberg Limits (%)			Unit Weight (pcf)			Specific Gravity	
				Liquid Limit	Plastic Limit	Plastic Index	Dry	Moist	Sat		
OVERBURDEN SOIL	GC-GM SC	20	10.0	26	17	9	NA	NA	NA	2.64	
MAHANTANGO FORMATION	Weathered Rock	NA	NA	NA	NP	NP	NP	NA	NA	NA	NA
	Transition Zone	NA	NA	3.0	NP	NP	NP	160	165	160	2.50
	Sound Rock	ACCA	NA	0.7	NP	NP	NP	170	170	170	2.74
FILLS	Bulk Sample 1	GP	4	6.0	NP	NP	NP	130	140	140	2.60
	Bulk Sample 2	SP-SM	9	6.0	NP	NP	NP	130	140	140	2.60
	Concrete	NA	NA	NA	NA	NA	NA	NA	150	NA	NA

- Values are determined from observation and statistical analysis of field and laboratory tests.
 - URCS Classification: (Weathering, Strength, Discontinuity, Unit Weight)
 - NP: Non-Plastic
 - NA: None Available

Table 2.5-34— {Recommended Values Of Index Properties}

SI Units

Unit	USCS or URCS	Fines Content (%)	Moistur e Content (%)	Atterberg Limits (%)			Unit Weight (kN/m ³)			Specific Gravity	
				Liquid Limit	Plastic Limit	Plastic Index	Dry	Moist	Sat		
OVERBURDEN SOIL	GC-GM SC	20	10.0	26	17	9	NA	NA	NA	2.64	
MAHANTANGO FORMATION	Weathered Rock	NA	NA	NA	NP	NP	NP	NA	NA	NA	NA
	Transition Zone	NA	NA	3.0	NP	NP	NP	25.2	25.9	25.2	2.50
	Sound Rock	ACCA	NA	0.7	NP	NP	NP	26.7	26.7	26.7	2.74
FILLS	Bulk Sample 1	GP	4	6.0	NP	NP	NP	20.4	22.0	22.0	2.60
	Bulk Sample 2	SP-SM	9	6.0	NP	NP	NP	20.4	22.0	22.0	2.60
	Concrete	NA	NA	NA	NA	NA	NA	NA	23.6	NA	NA
<p>- Values are determined from observation and statistical analysis of field and laboratory tests. - URCS Classification: (Weathering, Strength, Discontinuity, Unit Weight) - NP: Non-Plastic - NA: None Available</p>											

Table 2.5-35— {Rock Mass Rating (RMR) and Geological Strength Index (GSI) for Mahantango Formation}

Unit		RMR			GSI		
		Minimum	Maximum	Average	Minimum	Maximum	Average
MAHANTANGO FORMATION	Weathered Rock	15	76	43	23	84	50
	Transition Zone	27	87	52	35	84	60
	Sound Rock	20	87	63	28	87	71

Table 2.5-36— {Recommended Values For Strength Properties}
English Units

Unit		SPT	RMR	c (ksf)	Φ' (degrees)	q _u (ksf)
MAH ANTA NGO FOR MATI ON	OVERBURDEN SOIL	30	NA	0	36	NA
	Weathered Rock	NA	43	NA	NA	NA
	Transition Zone	NA	52	NA	NA	NA
	Sound Rock	NA	63	60	30	1020
FILLS	Granular	NM	NA	0	35	NA
	Concrete	f'c = 3000 psi				

- Friction obtained from SPT Correlation for dense sands and gravels (Peck, Hanson, and Thornburn, 1974)

- q_u determined based on Unconfined Compressive Test (UCS)

- For the Sound Rock, cohesion and friction are obtained correlation with Geological Strength Index and unconfined compressive strength (Hoek, 2002)

- NA - Not Applicable/None Available

- NM - Not Measured

Table 2.5-36— {Recommended Values For Strength Properties}

SI Units

Unit		SPT	RMR	c (kPa)	Φ' (degrees)	q _u (kPa)
MAH ANTA NGO FOR MATI ON	OVERBURDEN SOIL	30	NA	0	36	NA
	Weathered Rock	NA	43	NA	NA	NA
	Transition Zone	NA	52	NA	NA	NA
	Sound Rock	NA	63	2870	30	48438
FILLS	Granular	NM	NA	0	35	NA
	Concrete	f _c = 20680				

- Friction obtained from SPT Correlation for dense sands and gravels (Peck, Hanson, and Thornburn, 1974)

- q_u determined based on Unconfined Compressive Test (UCS)

- For the Sound Rock, cohesion and friction are obtained correlation with Geological Strength Index and unconfined compressive strength (Hoek, 2002)

- NA - Not Applicable/None Available

- NM - Not Measured

Table 2.5-37— {Recommended Values for Hydraulic Conductivity}
English Units

Unit		Hydraulic Conductivity, K (fps)		
		Laboratory	Field ⁽⁴⁾	Recommended
OVERBURDEN SOIL ⁽¹⁾		NM	2.35E-03 ⁽⁴⁾	2.35E-03
MAHANTANGO FORMATION	Shallow ⁽²⁾	NM	2.15E-03 ⁽⁴⁾	2.15E-03
	Deep ⁽³⁾	NM	3.87E-06 ⁽⁵⁾	3.87E-06
FILLS	Granular	7.78E-04	NM	7.78E-04
	Concrete	NM	NM	3.30E-12

Notes:

- (1) Glacial deposits in the low-lying areas*
- (2) Shallow bedrock is above 175 ft below ground surface*
- (3) Deep bedrock is greater than 175 ft below ground surface*
- (4) Geometric mean value of pumping test results (see Table 2.4-57)*
- (5) Geometric mean value of slug test results (see Table 2.4-56)*

Table 2.5-37— {Recommended Values For Hydraulic Conductivity}
SI Units

Unit		Hydraulic Conductivity, K (cm/s)		
		Laboratory	Field ⁽⁴⁾	Recommended
OVERBURDEN SOIL ⁽¹⁾		NM	7.26E-02 ⁽⁴⁾	7.16E-02
MAHANT ANGO FORMATION	Shallow ⁽²⁾	NM	6.55E-02 ⁽⁴⁾	6.55E-02
	Deep ⁽³⁾	NM	1.18E-04 ⁽⁵⁾	1.18E-04
FILLS	Granular	2.37E-02	NM	2.37E-02
	Concrete	NM	NM	1.01E-10

Notes:

- (1) Glacial deposits in the low-lying areas*
- (2) Shallow bedrock is above 53.34 m below ground surface*
- (3) Deep bedrock is greater than 53.34 m below ground surface*
- (4) Geometric mean value of pumping test results (see Table 2.4-57)*
- (5) Geometric mean value of slug test results (see Table 2.4-56)*

Table 2.5-38— {Recommended Values For Static Elastic Modulus}
English Units

Unit		Elastic Modulus, E (ksf)					Recommended
		Method 1	Method 2	Method 3	Method 4	Method 5	
OVERBURDEN SOIL		2501	1215	---	---	---	1860
MAHANTANGO FORMATION	Weathered Rock	11780	---	40154	139587	---	11780
	Transition Zone	23770	---	65300	83542	---	23770
	Sound Rock	400000	---	87480	543021	---	400000
FILLS	Granular	1000	---	---	---	---	1000
	Concrete	369600	---	---	---	---	369600

Method 1 based on geophysical test results

Method 2 based on SPT N-Value correlation

Method 3 based on pressuremeter test results

Method 4 based on Rock Mass Rating (RMR) correlation

Method 5 based on ACI318

Table 2.5-38— {Recommended Values For Static Elastic Modulus}

SI Units

Unit		Elastic Modulus, E (MPa)					Recommended
		Method 1	Method 2	Method 3	Method 4	Method 5	
OVERBURDEN SOIL		120	58	---	---	---	89
MAHANTANGO FORMATION	Weathered Rock	564	---	1923	6683	---	564
	Transition Zone	1138	---	3127	4000	---	1138
	Sound Rock	19152	---	4189	26000	---	19152
FILLS	Granular	48	---	---	---	---	48
	Concrete	17697	---	---	---	---	17697

Method 1 based on geophysical test results

Method 2 based on SPT N-Value correlation

Method 3 based on pressuremeter test results

Method 4 based on Rock Mass Rating (RMR) correlation

Method 5 based on ACI318

Table 2.5-39— {Recommended Values For Static Elastic Properties}
English Units

Unit		Poisson's Ratio, ν	Static Elastic Modulus, E [ksf]	Static Shear Modulus, G [ksf]	Observation
OVERBURDEN SOIL		0.33	1860	700	Recommended values are based on the following: - Overburden Soil: SPT correlation and geophysical testing - Weathered Rock, Transition Zone and Sound Rock: Geophysical Testing - Concrete: Shear modulus matched to that of Sound Rock
MAHANTANGO FORMATION	Weathered Rock	0.36	11780	4330	
	Transition Zone	0.39	23770	8520	
	Sound Rock	0.30	400000	154000	
FILLS	Granular	0.20	369600	154000	- Engineered Fill: Geophysical Testing
	Concrete	0.35	1000	370	

Table 2.5-39— {Recommended Values For Static Elastic Properties}
SI Units

Unit		Poisson's Ratio, ν	Static Elastic Modulus, E [MPa]	Static Shear Modulus, G [MPa]	Observation
OVERBURDEN SOIL		0.33	89	34	Recommended values are based on the following: - Overburden Soil: SPT correlation and geophysical testing - Weathered Rock, Transition Zone and Sound Rock: Geophysical Testing - Concrete: Shear modulus matched to that of Sound Rock
MAHANTANGO FORMATION	Weathered Rock	0.36	564	207	
	Transition Zone	0.39	1138	408	
	Sound Rock	0.30	19152	7374	
FILLS	Granular	0.20	17697	7374	- Engineered Fill: Geophysical Testing
	Concrete	0.35	48	18	

Table 2.5-40—{Recommended Values For Low Strain Dynamic Elastic Properties at Center Of Nuclear Island Footprint}

English Units
(Page 1 of 2)

Unit	D ^{top} [ft]	γ [pcf]	V _s [fps]	V _p [fps]	v	G _{max} [ksf]	E _{max} [ksf]	DS _o [%]
FILLS	Engineered Fill Layer 1	0	800	1670	0.35	2780	7510	1.26
	Engineered Fill Layer 2	10	900	1880	0.35	3520	9510	1.26
	Engineered Fill Layer 3	20	1000	2100	0.35	4350	11770	1.26
ROCK FORMATIONS	Concrete	36	8510	13900	0.20	337360	809810	0.80
	Mahantango Formation Layer 1	61	8000	14900	0.30	337890	876810	0.80
	Mahantango Formation Layer 2	182	8210	15100	0.29	355860	918230	0.80
	Mahantango Formation Layer 3	262	7200	14000	0.32	273690	722650	0.80
	Mahantango Formation Layer 4	311	7880	14660	0.30	327830	850290	0.70
	Mahantango Formation Layer 5	386	8500	16100	0.31	381440	996910	0.70
	Mahantango Formation Layer 6	450	8950	16750	0.30	422900	1099710	0.70
Mahantango Formation Layer 7	500	9600	16850	0.26	486560	1225840	0.70	

Table 2.5-40— {Recommended Values For Low Strain Dynamic Elastic Properties at Center Of Nuclear Island Footprint}

English Units
(Page 2 of 2)

Unit	D _{top} [ft]	γ [pcf]	V _s [fps]	V _p [fps]	v	G _{max} [ksf]	E _{max} [ksf]	DS _o [%]
D _{top} : Depth of top of layer $G_{max} = \rho V_p^2$ $E_{max} = 2(1 + \nu)G_{max}$ Velocities are determined from best estimate soil profile Poisson's ratio determined from velocity ratio squared Initial shear damping (DS _o) determined from "Free-Free" Testing for Rocks, and RCTS Testing for Fill								

Table 2.5-40—{Recommended Values For Low Strain Dynamic Elastic Properties at Center Of Nuclear Island Footprint}

SI Units
(Page 1 of 2)

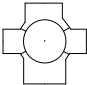









Unit	D _{top} [m]	γ [kN/m ³]	V _s [m/s]	V _p [m/s]	v	G _{max} [MPa]	E _{max} [MPa]	DS _o [%]
FILLS	Engineered Fill Layer 1	22.0	244	509	0.35	133	360	1.26
	Engineered Fill Layer 2	22.0	274	573	0.35	169	455	1.26
	Engineered Fill Layer 3	22.0	305	640	0.35	208	564	1.26
ROCK FORMATIONS	Concrete	23.6	2594	4237	0.20	16153	38774	0.80
	Mahantango Formation Layer 1	26.7	2438	4542	0.30	16178	41982	0.80
	Mahantango Formation Layer 2	26.7	2502	4602	0.29	17039	43965	0.80
	Mahantango Formation Layer 3	26.7	2195	4267	0.32	13104	34601	0.80
	Mahantango Formation Layer 4	26.7	2402	4468	0.30	15697	40712	0.70
	Mahantango Formation Layer 5	26.7	2591	4907	0.31	18263	47732	0.70
	Mahantango Formation Layer 6	26.7	2728	5105	0.30	20249	52654	0.70
Mahantango Formation Layer 7	26.7	2926	5136	0.26	23297	58694	0.70	

Table 2.5-40— {Recommended Values For Low Strain Dynamic Elastic Properties at Center Of Nuclear Island Footprint}

SI Units
(Page 2 of 2)

Unit	D _{top} [m]	γ [kN/m ³]	V _s [m/s]	V _p [m/s]	v	G _{max} [MPa]	E _{max} [MPa]	DS _o [%]
<p>D_{top} : Depth of top of layer $G_{max} = \rho V_s^2$ $E_{max} = 2(1 + \nu)G_{max}$ Velocities are determined from best estimate soil profile Poisson's ratio determined from velocity ratio squared Initial shear damping (DS_o) determined from "Free-Free" Testing for Rocks, and RCTS Testing for Fill</p>								

Table 2.5-41 — {Foundation Elevations}
English Units

STRUCTURE	FOUNDATION		FOOTPRINT SHAPE	CONTACT MATERIAL ⁽²⁾	Area (ft ²)	Contact Pressure (ksf) ⁽³⁾		
	DEPTH (ft)	EI. ⁽¹⁾ (ft msl)				Average Static	Maximum Static	Maximum Dynamic
Nuclear Island	35.4	683.6		C	80,170	16.6 ⁽⁴⁾	24	35
Nuclear Auxiliary Building	48.3	670.7		C	12,510	9.7	24	35
Radioactive Waste Building	36.0	683.0		C	16,880	6.5	24	35
Essential Service	33.0	686.0		M	26,061	5.5	24	35
	33.0	686.0		C	26,061	5.5	24	35
Water Building	33.0	686.0		C	26,061	5.5	24	35
	33.0	686.0		C	26,061	5.5	24	35
Emergency Power	11.0	708.0		C	12,650	3.4	24	35
Generation Building	11.0	708.0		C	12,650	3.4	24	35
	33.0	686.0		M	100,000	4.4	10	12

(1) Plant Grade El. (ft msl) 719

(2) Concrete (C), Mahantango Formation (M)

(3) As prescribed by the U.S. EPR FSAR

(4) The contact pressure for the RB is selected, as this is the highest contact pressure of the buildings on the NI mat.

Table 2.5-41 — {Foundation Elevations}
SI Units

STRUCTURE	FOUNDATION		FOOTPRINT SHAPE	CONTACT MATERIAL ⁽²⁾	Area (m ²)	Contact Pressure (kPa) ⁽³⁾		
	DEPTH (m)	EI. ⁽¹⁾ (m msl)				Average Static ⁽⁴⁾	Maximum Static	Maximum Dynamic
Nuclear Island	10.8	208.4		C	7,448	794.8 ⁽⁴⁾	1149.1	1675.8
Nuclear Auxiliary Building	14.7	204.4		C	1,162	469.2	1149.1	1675.8
Radioactive Waste Building	11.0	208.2		C	1,568	311.2	1149.1	1675.8
Essential Service	10.1	209.1		M	2,421	263.3	1149.1	1675.8
	10.1	209.1		C	2,421	263.3	1149.1	1675.8
Water Building	10.1	209.1		C	2,421	263.3	1149.1	1675.8
	10.1	209.1		C	2,421	263.3	1149.1	1675.8
Emergency Power	3.4	215.8		C	1,175	162.8	1149.1	1675.8
Generation Building	3.4	215.8		C	1,175	162.8	1149.1	1675.8
Turbine Building	10.1	209.1		M	9,290	210.7	478.8	574.6

(1) Plant Grade El. (m msl) 219.2

(2) Concrete (C), Mahantango Formation (M)

(3) As prescribed by the U.S. EPR FSAR

(4) The contact pressure for the RB is selected, as this is the highest contact pressure of the buildings on the NI mat.

Table 2.5-42— {Earth Pressure Coefficients}

Formation	ϕ [°]	k_a	k_p	$k_{ae}^{(1)}$	$k_{pe}^{(1)}$	Observations
Glacial Overburden	36.00	0.26	3.85	0.38	9.77	NA - Not Applicable
Weathered Rock	NA	NA	NA	NA	NA	k_a - Active Earth Pressure Coefficient
Transition Zone	NA	NA	NA	NA	NA	
Mahantango Formation (Sound Rock)	NA	NA	NA	NA	NA	k_p - Passive Earth Pressure Coefficient
Structural Fill	35.00	0.27	3.69	0.39	8.71	k_{ae} - Active Seismic Earth Pressure Coefficient k_{pe} - Passive Seismic Earth Pressure Coefficient
Granular Fill/ Backfill	35.00	0.27	3.69	0.39	8.71	
Concrete Fill	NA	NA	NA	NA	NA	

(1) The coefficients reported provide the maximum lateral earth pressure distribution.

Table 2.5-43— {Allowable Bearing Capacity}
English Units

Structure		Foundation		Contact Soil ⁽¹⁾	Simplified Foundation Dimension			Allowable Bearing Capacity (ksf)	
		Depth, D (ft)	EI. (ft msl)		B (ft)	L (ft)	L/B	Static	Dynamic
Nuclear Island	NI	35.4	683.6	C	274	312	1.1	122	184
Reactor Auxiliary Building	NAB	48.3	670.7	C	106	122	1.2	122	184
Radioactive Waste Processing Building	RWB	36.0	683	C	130	130	1.0	122	184
Essential Service Water Building (ESWB)	1ESWB	33.0	686	M	140	196.5	1.4	122	184
	2ESWB	33.0	686	C	140	196.5	1.4	122	184
	3ESWB	33.0	686	C	140	196.5	1.4	122	184
	4ESWB	33.0	686	C	140	196.5	1.4	122	184
Emergency Power Generator Building (EPGB)	1-2EPGB	11.0	708	C	84	150	1.8	122	184
	3-4EPGB	11.0	708	C	84	150	1.8	122	184
Essential Service Water Emergency Makeup System (ESWEMS)	ESWEMS	5.0	714	C	51	80	1.6	122	184
Turbine Building	TB	33.0	686	C	188	385	2.0	122	184

⁽¹⁾ Concrete (C), Mahantango Formation (M)

Table 2.5-43— {Allowable Bearing Capacity}

SI Units

Structure		Foundation		Contact	Simplified Foundation Dimension			Allowable Bearing Capacity (kPa)	
		Depth, D (m)	El. (m msl)		B (m)	L (m)	L/B	Static	Dynamic
Nuclear Island	NI	10.8	208.4	C	83.5	95.1	1.1	5541	8810
Reactor Auxiliary Building	NAB	14.7	204.4	C	32.3	37.2	1.2	5541	8810
Radioactive Waste Processing Building	RWB	11.0	208.2	C	39.6	39.6	1.0	5541	8810
Essential Service Water Building (ESWB)	1ESWB	10.1	209.1	M	42.7	59.9	1.4	5541	8810
	2ESWB	10.1	209.1	C	42.7	59.9	1.4	5541	8810
	3ESWB	10.1	209.1	C	42.7	59.9	1.4	5541	8810
	4ESWB	10.1	209.1	C	42.7	59.9	1.4	5541	8810
Emergency Power Generator Building (EPGB)	1-2EPGB	3.4	215.8	C	25.6	45.7	1.8	5541	8810
	3-4EPGB	3.4	215.8	C	25.6	45.7	1.8	5541	8810
Essential Service Water Emergency Makeup System (ESWEMS)	ESWEMS	1.5	211.8	C	15.5	24.4	1.6	5541	8810
Turbine Building	TB	10.1	209.1	C	57.3	117.3	2.0	5541	8810

⁽¹⁾ Concrete (C), Mahantango Formation (M)

Table 2.5-44 — {Elastic Settlement Results}
English Units
(Page 1 of 2)

STRUCTURE	Simplified Foundation Dimensions		Foundation	Contact Surface(2)	Contact Pressure(3) [ksf]	E ⁽⁴⁾ [ksf]	Reduced E [ksf]	ν ⁽⁴⁾	Estimated Settlement on Rigid Foundation [in]			Estimated Settlement on Flexible Foundation [in]							
	B [ft]	L [ft]							Depth [ft]	Homogeneous Rock (Wyllie)	US Army Corps of Engineers		Tilt Limit	Boussinesq (Salgado)		US Army Corps of Engineers		Tilt Limit	
	Center=Edge=Corner		Center=Corner	Center	Max. Differential	Center	Max. Differential	Center			Max. Differential								
Nuclear Island ⁽¹⁾	RB ⁽⁴⁾	Diameter = 183	35.4	C	16.61	8.10E+05	8.10E+05	0.2	0.034	0.034	0.034	<0.5in/50ft	0.043	0.028	0.016	0.048	0.025	0.024	0.000
	SGB1	88	99	C	11.9	8.10E+05	8.10E+05	0.2	0.015	0.014	0.014	<0.5in/50ft	0.035	0.009	0.027	0.018	0.009	0.009	0.001
	FB	67	163	C	13.4	8.10E+05	8.10E+05	0.2	0.021	0.018	0.018	0.0007	0.042	0.011	0.032	0.022	0.011	0.011	0.001
	SGB4	88	101	C	11.3	8.10E+05	8.10E+05	0.2	0.014	0.013	0.013	<0.5in/50ft	0.034	0.009	0.026	0.017	0.009	0.008	0.001
	SGB23	91	184	C	10.4	8.10E+05	8.10E+05	0.2	0.02	0.017	0.017	<0.5in/50ft	0.041	0.01	0.031	0.021	0.011	0.011	0.001
Nuclear Auxiliary Building	NAB	106	122	48.3	9.7	8.10E+05	8.10E+05	0.2	0.014	0.014	0.014	0.0000	0.035	0.009	0.026	0.018	0.009	0.009	0.000
Radioactive Waste Building	RWB	130	130	36	6.5	8.10E+05	8.10E+05	0.2	0.012	0.012	0.012	0.0000	0.027	0.007	0.02	0.013	0.007	0.007	0.000
ESWS Cooling	1ESWB	140	196.5	33	5.47	8.77E+05	4.38E+05	0.3	0.026	0.018	0.018	0.0000	0.05	0.013	0.038	0.023	0.011	0.011	0.001
	2ESWB	140	196.5	33	5.47	8.10E+05	8.10E+05	0.2	0.015	0.011	0.011	0.0000	0.029	0.007	0.022	0.014	0.007	0.007	0.000
	3ESWB	140	196.5	33	5.47	8.10E+05	8.10E+05	0.2	0.015	0.011	0.011	0.0000	0.029	0.007	0.022	0.014	0.007	0.007	0.000
Towers	4ESWB	140	196.5	33	5.47	8.10E+05	8.10E+05	0.2	0.015	0.011	0.011	0.0000	0.029	0.007	0.022	0.014	0.007	0.007	0.000
	2EPGB	84	150	11	3.4	8.10E+05	8.10E+05	0.2	0.006	0.005	0.005	0.0000	0.012	0.003	0.009	0.006	0.003	0.003	0.000

Table 2.5-44 — {Elastic Settlement Results}
English Units
(Page 2 of 2)

STRUCTURE	Simplified Foundation Dimensions		Foundation	Contact Surface(2)	Contact Pressure(3) [ksf]	Contact Pressure E (4) [ksf]	Reduced E [ksf]	ν (4)	Estimated Settlement on Rigid Foundation [in]			Estimated Settlement on Flexible Foundation [in]			
	B [ft]	L [ft]							Depth [ft]	Homogeneous Rock (Wyllie)	US Army Corps of Engineers	Tilt Limit	Boussinesq (Salgado)	US Army Corps of Engineers	Tilt Limit
	Center=Core	Max. Differential	Center=Core	Max. Differential	Center=Core	Max. Differential	Center=Core	Max. Differential	Center=Core	Max. Differential	Center=Core	Max. Differential			
Generation Building	84	150	11	C	3.4	8.10E +05	8.10E +05	0.2	0.006	0.005	0.000	0.000	0.006	0.003	0.000
Pumphouse	51	80	5	C	2.5	8.10E +05	8.10E +05	0.2	0.003	0.002	0.000	0.000	0.003	0.001	0.000
Turbine Building	188	385	33	M	4.4	7.50E +05	3.75E +05	0.3	0.037	0.031	0.000	0.000	0.039	0.019	0.001

(1) Individual building dimensions at the Nuclear Island (NI) are simplified

(2) C - Concrete, M - Mahantango formation

(3) As prescribed by the U.S. EPR FSAR

(4) Instead of a circular foundation, a square foundation is considered for the Reactor Building (RB).

Table 2.5-44 — {Elastic Settlement Results}

SI Units
(Page 1 of 2)

STRUCTURE	Simplified Foundation Dimensions		Foundation	Contact Surface(2)	Contact Pressure(3) [kPa]	E(4) [MPa]	Reduced E [MPa]	ν(4)	Estimated Settlement on Rigid Foundation [cm]				Estimated Settlement on Flexible Foundation [cm]														
	B [m]	L [m]							Homogeneous Rock (Wyllie)	US Army Corps of Engineers	Tilt Limit	Center	Corner	Max. Differential	Center	Corner	Max. Differential	Center	Corner	Max. Differential	Tilt Limit						
	Depth [m]		Center=Edge	Center=Corner	Center=Corner	Center	Corner	Max. Differential														Center	Corner	Max. Differential	Center	Corner	Max. Differential
Nuclear Island (1)	RB(4)	Diameter = 55.8	10.8	C	795	388E+04	388E+04	0.2	0.087	0.09(6)	0.03	0.05	0.076	0.09	0.07	0.04	0.11	0.07	0.04	0.12	0.06	0.06	0.06	0.06	0.06	0.04	0.004
	SGB1	26.8	30.2	10.8	C	569	388E+04	388E+04	0.2	0.037	0.03	0.05	0.076	0.09	0.02	0.07	0.09	0.02	0.07	0.04	0.02	0.02	0.02	0.02	0.02	0.02	0.004
	FB	20.4	49.7	10.8	C	642	388E+04	388E+04	0.2	0.053	0.087	0.05	0.076	0.09	0.03	0.08	0.11	0.03	0.08	0.06	0.06	0.03	0.03	0.03	0.03	0.03	0.005
	SGB4	26.8	30.8	10.8	C	543	388E+04	388E+04	0.2	0.036	0.03	0.03	0.076	0.09	0.02	0.06	0.09	0.02	0.06	0.04	0.04	0.02	0.02	0.02	0.02	0.02	0.004
	SGB23	27.7	56.1	10.8	C	497	388E+04	388E+04	0.2	0.052	0.04	0.04	0.076	0.09	0.03	0.08	0.11	0.03	0.08	0.06	0.05	0.03	0.03	0.03	0.03	0.03	0.005
Nuclear Auxiliary Building	NAB	32.3	37.2	14.7	C	464	388E+04	388E+04	0.2	0.037	0	0.03	0	0.03	0	0.03	0.03	0.02	0.07	0.04	0.04	0.02	0.02	0.02	0.02	0.02	0.004
Radioactive Waste Building	RWB	39.6	39.6	11	C	311	388E+04	388E+04	0.2	0.03	0	0.03	0	0.03	0	0.03	0.03	0.02	0.05	0.03	0.03	0.02	0.02	0.02	0.02	0.003	
ESWS Cooling	1ESW B	42.7	59.9	10.1	M	262	420E+04	210E+04	0.3	0.066	0	0.04	0	0.04	0	0.13	0.03	0.03	0.1	0.06	0.03	0.03	0.03	0.03	0.03	0.006	
	2ESW B	42.7	59.9	10.1	C	262	388E+04	388E+04	0.2	0.038	0	0.03	0	0.03	0	0.07	0.02	0.02	0.05	0.04	0.02	0.02	0.02	0.02	0.02	0.004	
Towers	3ESW B	42.7	59.9	10.1	C	262	388E+04	388E+04	0.2	0.038	0	0.03	0	0.03	0	0.07	0.02	0.02	0.05	0.04	0.02	0.02	0.02	0.02	0.02	0.004	
	4ESW B	42.7	59.9	10.1	C	262	388E+04	388E+04	0.2	0.038	0	0.03	0	0.03	0	0.07	0.02	0.02	0.05	0.04	0.02	0.02	0.02	0.02	0.02	0.004	

Table 2.5-44 — {Elastic Settlement Results}
 SI Units
 (Page 2 of 2)

STRUCTURE	Simplified Foundation Dimensions		Foundation	Contact Surface ⁽²⁾	Contact Pressure ⁽³⁾ [kPa]	E ⁽⁴⁾ [MPa]	Reduced E [MPa]	ν ⁽⁴⁾	Estimated Settlement on Rigid Foundation [cm]				Estimated Settlement on Flexible Foundation [cm]								
	B [m]	L [m]							Depth [m]	Homogeneous, Isotropic Rock (Wyllie)	US Army Corps of Engineers	Tilt Limit	Boussinesq (Salgado)		US Army Corps of Engineers		Tilt Limit				
				Center	Max. Differential	Center	Max. Differential	Center	Max. Differential	Center	Max. Differential	Center	Max. Differential	Center	Max. Differential						
Emergency Power	25.6	45.7	3.4	C	163	3.88E+04	3.88E+04	0.2	0.015	0	0.01	0	0.03	0.01	0.02	0.02	0.01	0.01	0.01	0.01	0.001
Generation Building	25.6	45.7	3.4	C	163	3.88E+04	3.88E+04	0.2	0.015	0	0.01	0	0.03	0.01	0.02	0.02	0.01	0.01	0.01	0.01	0.001
Pumphouse	15.5	24.4	1.5	C	120	3.88E+04	3.88E+04	0.2	0.006	0	0.01	0	0.01	0	0.01	0.01	0	0	0	0	0.001
Turbine Building	57.3	117.3	10.1	M	211	3.59E+04	1.80E+04	0.3	0.093	0	0.08	0	0.19	0.05	0.14	0.14	0.05	0.05	0.05	0.05	0.009

(1) Individual building dimensions at the Nuclear Island (NI) are simplified
 (2) C - Concrete, M - Mahantango formation
 (3) As prescribed by the U.S. EPR FSAR
 (4) Instead of a circular foundation, a square foundation is considered for the Reactor Building (RB).

Table 2.5-45— {Computed Factors of Safety for Critical Slip Surfaces}

Type of Slope	Affected Area	Slope Section	Circular Failure		Wedge Failure	
			Static	Pseudostatic (Dynamic)	Static	Pseudostatic (Dynamic)
Temporary	Power Block	AA West	1.655	NA ⁽¹⁾	1.687	NA ⁽¹⁾
Temporary	Power Block	AA East	2.777	NA ⁽¹⁾	3.041	NA ⁽¹⁾
Temporary	Power Block	BB North	1.879	NA ⁽¹⁾	2.001	NA ⁽¹⁾
Temporary	Power Block	BB South	1.499	NA ⁽¹⁾	1.888	NA ⁽¹⁾
Temporary	Power Block	CC North	1.629	NA ⁽¹⁾	1.818	NA ⁽¹⁾
Temporary	Power Block	DD East	1.828	NA ⁽¹⁾	1.742	NA ⁽¹⁾
Temporary	ESWEMS Retention Pond	AA West	1.825	NA ⁽¹⁾	1.746	NA ⁽¹⁾
Temporary	ESWEMS Retention Pond	AA East	1.897	NA ⁽¹⁾	1.836	NA ⁽¹⁾
Temporary	ESWEMS Retention Pond	BB North	1.845	NA ⁽¹⁾	1.791	NA ⁽¹⁾
Temporary	ESWEMS Retention Pond	BB South	1.787	NA ⁽¹⁾	1.878	NA ⁽¹⁾
Permanent	Power Block	AA West	1.963	1.341	1.84	1.272
Permanent	Power Block	AA East	1.833	1.373	1.844	1.102
Permanent	Power Block	BB North	1.882	1.403	1.914	1.439
Permanent	Power Block	BB South	1.663	1.079	1.554	1.317
Permanent	Power Block	CC North	1.919	1.424	1.847	1.562
Permanent	Power Block	CC South	67.708	51.063	66.803	50.698
Permanent	Power Block	DD West	6.692	3.325	6.570	3.630
Permanent	Power Block	DD East	2.243	1.611	2.345	1.734
Permanent	ESWEMS Retention Pond	AA West, Upstream	4.143	2.531	4.146	2.361
Permanent	ESWEMS Retention Pond	AA West, Downstream	2.337 (2.278) ⁽²⁾	1.673	2.312 (2.025) ⁽²⁾	1.655
Permanent	ESWEMS Retention Pond	AA East, Upstream	4.173	2.574	3.938	2.511
Permanent	ESWEMS Retention Pond	AA East, Downstream	1.874 (1.790) ⁽²⁾	1.354	2.024 (1.774) ⁽²⁾	1.390
Permanent	ESWEMS Retention Pond	BB North, Case I	1.822 (1.804) ⁽²⁾	1.381	2.064 (1.695) ⁽²⁾	1.358
Permanent	ESWEMS Retention Pond	BB North, Case II	4.069	2.138	3.784	2.142
Permanent	ESWEMS Retention Pond	BB South, Upstream	4.876	2.179	5.575	2.220
Permanent	ESWEMS Retention Pond	BB South, Downstream	3.938 (2.469) ⁽²⁾	2.505	NA ⁽³⁾	NA ⁽³⁾

(1) Pseudostatic (dynamic) analysis was not considered for temporary slopes

(2) PMF condition

(3) Wedge failure analysis creates unreasonably high Factor of Safety results due to access road berm surcharge

Table 2.5-46— {EPRI/DOE/NRC (2012) Sources used in the PSHA for the BBNPP Site}

Source Configuration	Configuration Weight	Distributed Seismicity Source Zones	Repeated Large Magnitude Earthquake Sources
M-I	0.160	Study Region	NMFS, Commerce, ERM-N, ERM-S, Marianna, Wabash, Charleston, Charlevoix
M-II	0.048	MESE-W, NMESE-W	NMFS, Commerce, ERM-N, ERM-S, Marianna, Wabash, Charleston, Charlevoix
M-III	0.192	MESE-N, NMESE-N	NMFS, Commerce, ERM-N, ERM-S, Marianna, Wabash, Charleston, Charlevoix
S-I	0.320	AHEX, ECC-AM, PEZ-N, NAP, SLR, MidC-A	NMFS, Commerce, ERM-N, ERM-S, Marianna, Wabash, Charleston, Charlevoix
S-II	0.160	AHEX, ECC-AM, PEZ-N, NAP, SLR, MidC-B	NMFS, Commerce, ERM-N, ERM-S, Marianna, Wabash, Charleston, Charlevoix
S-III	0.080	AHEX, ECC-AM, PEZ-W, NAP, SLR, MidC-C	NMFS, Commerce, ERM-N, ERM-S, Marianna, Wabash, Charleston, Charlevoix
S-IV	0.040	AHEX, ECC-AM, PEZ-W, NAP, SLR, MidC-D	NMFS, Commerce, ERM-N, ERM-S, Marianna, Wabash, Charleston, Charlevoix

Notes:

The weights represent the relative support in the data for the various alternatives and sum to 1.0.

Table Acronyms and Abbreviations:

AHEX = Atlantic Highly Extended Crust Seismotectonic Source Zone

ECC-AM = Extended Continental Crust-Atlantic Margin Seismotectonic Source Zone

ERM-N = Eastern Rift Margin-North RLME Source

ERM-S = Eastern Rift Margin-South RLME Source

MESE-N = Mesozoic-and-Younger Extension Mmax Source Zone (Narrow interpretation)

MESE-W = Mesozoic-and-Younger Extension Mmax Source Zone (Wide interpretation)

MidC-A, MidC-B, MidC-C, MidC-D = Midcontinent-Craton Seismotectonic Source Zone (Configurations A, B, C, and D)

NAP = North Appalachian Seismotectonic Source Zone

NMESE-N = Non-Mesozoic-and-Younger Extension Mmax Source Zone (Narrow interpretation)

NMESE-W = Non-Mesozoic-and-Younger Extension Mmax Source Zone (Wide interpretation)

NMFS - New Madrid Fault System RLME Source

PEZ-N = Paleozoic Extended Crust Seismotectonic Source Zone (Narrow Interpretation)

PEZ-W = Paleozoic Extended Crust Seismotectonic Source Zone (Wide Interpretation)

SLR = St. Lawrence Rift Seismotectonic Source Zone

STUDY-R = Study Region Mmax Source Zone

Table 2.5-47— {Alternative Magnitude Weighting Schemes Used for Recurrence Parameter Estimation}

Weighting Schemes		Magnitude (M) Bin and Weight in Recurrence Parameter Estimation					
Case	Weight	2.9-3.6	3.6-4.3	4.3-5.0	5.0-5.7	5.7-6.4	>6.4
A	0.3	1.0	1.0	1.0	1.0	1.0	1.0
B	0.3	0.1	1.0	1.0	1.0	1.0	1.0
E	0.4	0.0	0.3	1.0	1.0	1.0	1.0

Note: The weights for the three weighting schemes (A, B, and E) are relative weights and sum to 1.0.
 Source: EPRI/DOE/NRC (2012, Table 5.3.2-1)

Table 2.5-48— {Uncertainty Representation of Recurrence Parameters for Distributed Seismicity Source Zones}

Source Zones	Magnitude Range Weighting		Spatial Variability Approach		Smoothing Approach		Seismicity Parameters	
	Case	Weight	Approach	Weight	Approach	Weight	Realization	Weight
STUDY-R MESE-N MESE-W NMESE-N NMESE-W	Case A	0.3	Variable <i>a</i> - and <i>b</i> -value	1.0	Objective	1.0	01	0.125
							02	0.125
							03	0.125
							04	0.125
							05	0.125
							06	0.125
							07	0.125
							08	0.125
AHEX EEC-AM MidC-A MidC-B MidC-C MidC-D NAP	Case B	0.3	Variable <i>a</i> - and <i>b</i> -value	1.0	Objective	1.0	01	0.125
							02	0.125
							03	0.125
							04	0.125
							05	0.125
							06	0.125
							07	0.125
							08	0.125
PEZ-N PEZ-W SLR	Case E	0.4	Variable <i>a</i> - and <i>b</i> -value	1.0	Objective	1.0	01	0.125
							02	0.125
							03	0.125
							04	0.125
							05	0.125
							06	0.125
							07	0.125
							08	0.125

Notes:

The weights represent the relative support in the data for the various alternatives and sum to 1.0.

Table Acronyms and Abbreviations:

- AHEX = Atlantic Highly Extended Crust Seismotectonic Source Zone
- ECC-AM = Extended Continental Crust-Atlantic Margin Seismotectonic Source Zone
- ERM-N = Eastern Rift Margin-North RLME Source
- ERM-S = Eastern Rift Margin-South RLME Source
- MESE-N = Mesozoic-and-Younger Extension Mmax Source Zone (Narrow interpretation)
- MESE-W = Mesozoic-and-Younger Extension Mmax Source Zone (Wide interpretation)
- MidC-A, MidC-B, MidC-C, MidC-D = Midcontinent-Craton Seismotectonic Source Zone (Configurations A, B, C, and D)
- NAP = North Appalachian Seismotectonic Source Zone
- NMESE-N = Non-Mesozoic-and-Younger Extension Mmax Source Zone (Narrow interpretation)
- NMESE-W = Non-Mesozoic-and-Younger Extension Mmax Source Zone (Wide interpretation)
- NMFS - New Madrid Fault System RLME Source
- PEZ-N = Paleozoic Extended Crust Seismotectonic Source Zone (Narrow Interpretation)
- PEZ-W = Paleozoic Extended Crust Seismotectonic Source Zone (Wide Interpretation)
- SLR = St. Lawrence Rift Seismotectonic Source Zone
- STUDY-R = Study Region Mmax Source Zone

Source: EPRI/DOE/NRC (2012, Appendix H)

Table 2.5-49— {M_{max} Distribution Representing Uncertainty in Maximum Magnitude for Distributed Source Zones}
 (Page 1 of 2)

Weight	Mmax Zones				
	STUDY-R	MESE-N	MESE-W	NMESE-N	NMESE-W
0.101	6.5	6.4	6.5	6.4	5.7
0.244	6.9	6.8	6.9	6.8	6.1
0.310	7.2	7.2	7.3	7.1	6.6
0.244	7.7	7.7	7.7	7.5	7.2
0.101	8.1	8.1	8.1	8.0	7.9

Table 2.5-49— {M_{max} Distribution Representing Uncertainty in Maximum Magnitude for Distributed Source Zones}

(Page 2 of 2)

Weight	Seismotectonic Zones					
	AHEX	ECC-AM	MidC-A MidC-B MidC-C MidC-D	NAP	PEZ-N PEZ-W	SLR
0.101	6.0	6.0	5.6	6.1	5.9	6.2
0.244	6.7	6.7	6.1	6.7	6.4	6.8
0.310	7.2	7.2	6.6	7.2	6.8	7.3
0.244	7.7	7.7	7.2	7.7	7.2	7.7
0.101	8.1	8.1	8.0	8.1	7.9	8.1

Note: The weights represent the relative support in the data for the various alternatives and sum to 1.0.

Table Acronyms and Abbreviations:

AHEX = Atlantic Highly Extended Crust Seismotectonic Source Zone

ECC-AM = Extended Continental Crust-Atlantic Margin Seismotectonic Source Zone

ERM-N = Eastern Rift Margin-North RLME Source

ERM-S = Eastern Rift Margin-South RLME Source

MESE-N = Mesozoic-and-Younger Extension Mmax Source Zone (Narrow interpretation)

MESE-W = Mesozoic-and-Younger Extension Mmax Source Zone (Wide interpretation)

MidC-A, MidC-B, MidC-C, MidC-D = Midcontinent-Craton Seismotectonic Source Zone (Configurations A, B, C, and D)

NAP = North Appalachian Seismotectonic Source Zone

NMESE-N = Non-Mesozoic-and-Younger Extension Mmax Source Zone (Narrow interpretation)

NMESE-W = Non-Mesozoic-and-Younger Extension Mmax Source Zone (Wide interpretation)

NMFS - New Madrid Fault System RLME Source

PEZ-N = Paleozoic Extended Crust Seismotectonic Source Zone (Narrow Interpretation)

PEZ-W = Paleozoic Extended Crust Seismotectonic Source Zone (Wide Interpretation)

SLR = St. Lawrence Rift Seismotectonic Source Zone

STUDY-R = Study Region Mmax Source Zone

Source: EPRI/DOE/NRC (2012, Table H-3-3 and Table H-4-4)

Table 2.5-50— {Distributions Representing Uncertainty in Seismogenic Thickness for Seismic Sources}

Source Zones	Distribution of Seismogenic Crustal Thickness	Weight
Mmax Distributed Seismicity Source Zones		
Study Region	13	0.4
MESE-N	17	0.4
MESE-W	22	0.2
NMESE-N		
NMESE-W		
Seismotectonic Distributed Seismicity Source Zones		
AHEX	8	0.5
	15	0.5
ECC-AM	13	0.4
MidC-A	17	0.4
MidC-B	22	0.2
MidC-C		
MidC-D		
NAP		
PEZ-N		
PEZ-W		
SLR	25	0.5
	30	0.5
RLME Sources		
Charlevoix	25	0.8
	30	0.2
Charleston	13	0.4
	17	0.4
	22	0.2
Commerce	13	0.4
ERM-N	15	0.4
ERM-S	17	0.2
Marianna		
NMFS		

Note: The weights represent the relative support in the data for the various alternatives and sum to 1.0

Source: EPRI/DOE/NRC (2012, Table H-3-1 and Table H-4-2)

Table Acronyms and Abbreviations:

- AHEX = Atlantic Highly Extended Crust Seismotectonic Source Zone
- ECC-AM = Extended Continental Crust-Atlantic Margin Seismotectonic Source Zone
- ERM-N = Eastern Rift Margin-North RLME Source
- ERM-S = Eastern Rift Margin-South RLME Source
- MESE-N = Mesozoic-and-Younger Extension Mmax Source Zone (Narrow interpretation)
- MESE-W = Mesozoic-and-Younger Extension Mmax Source Zone (Wide interpretation)
- MidC-A, MidC-B, MidC-C, MidC-D = Midcontinent-Craton Seismotectonic Source Zone (Configurations A, B, C, and D)
- NAP = North Appalachian Seismotonic Source Zone
- NMESE-N = Non-Mesozoic-and-Younger Extension Mmax Source Zone (Narrow interpretation)
- NMESE-W = Non-Mesozoic-and-Younger Extension Mmax Source Zone (Wide interpretation)
- NMFS - New Madrid Fault System RLME Source
- PEZ-N = Paleozoic Extended Crust Seismotectonic Source Zone (Narrow Interpretation)
- PEZ-W = Paleozoic Extended Crust Seismotectonic Source Zone (Wide Interpretation)
- SLR = St. Lawrence Rift Seismotonic Source Zone
- STUDY-R = Study Region Mmax Source Zone

Table 2.5-51 — {Representation of Aleatory Variability in the Characteristics of Future Earthquake Ruptures for Distributed Seismicity Source Zones}
(Page 1 of 2)

Source Zones	Source Boundary Characteristic	Style of Faulting	Relative Frequency	Rupture Strike (deg)	Relative Frequency	Rupture Dip (deg)	Relative Frequency
Study Region MESE-N MESE-W NMESE-N NMESE-W	Leaky	Strike-slip	0.67	310	0.20	Uniformly distributed from 60 to 90	0.20
				0	0.20		0.20
				35	0.40		0.40
				60	0.10		0.10
				90	0.10		0.10
AHX ECC-AM MidC-A MidC-B MidC-C MidC-D PEZ-N PEZ-W	Leaky	Strike-slip	0.67	310	0.20	Uniformly distributed from 60 to 90	0.20
				0	0.20		0.20
				35	0.40		0.40
				60	0.10		0.10
				90	0.10		0.10
NAP	Leaky	Strike-slip	0.33	310	0.20	Uniformly distributed from 60 to 90	0.20
				0	0.20		0.20
				35	0.40		0.40
				60	0.10		0.10
				90	0.10		0.10
		Reverse	0.67	310	0.20	Uniformly distributed from 30 to 60	0.20
				0	0.20		0.20
				35	0.40		0.40
				60	0.10		0.10
				90	0.10		0.10

Table 2.5-51 — {Representation of Aleatory Variability in the Characteristics of Future Earthquake Ruptures for Distributed Seismicity Source Zones}
(Page 2 of 2)

Source Zones	Source Boundary Characteristic	Style of Faulting	Relative Frequency	Rupture Strike (deg)	Relative Frequency	Rupture Dip (deg)	Relative Frequency
SLR	Leaky	Strike-slip	0.33	25	0.20	Uniformly distributed from 60 to 90	Equally likely
				40	0.20		
				70	0.20		
				310	0.15		
				290	0.15		
				0	0.05		
				90	0.05		
		Reverse	0.67	25	0.20	Uniformly distributed from 30 to 60	Equally likely
				40	0.20		
				70	0.20		
				310	0.15		
				290	0.15		
				0	0.05		
				90	0.05		

Notes "Leaky" boundary denotes the case in which a virtual earthquake rupture is centered on an epicenter that lies within a source zone, but the rupture is allowed to extend beyond the source zone boundary.

Source: EPRI/DOE/NRC (2012, Table H-3-2 and Table H-4-3)

Table Acronyms and Abbreviations:

- AHEX = Atlantic Highly Extended Crust Seismotectonic Source Zone
- ECC-AM = Extended Continental Crust-Atlantic Margin Seismotectonic Source Zone
- ERM-N = Eastern Rift Margin-North RLME Source
- ERM-S = Eastern Rift Margin-South RLME Source
- MESE-N = Mesozoic-and-Younger Extension Mmax Source Zone (Narrow interpretation)
- MESE-W = Mesozoic-and-Younger Extension Mmax Source Zone (Wide interpretation)
- MidC-A, MidC-B, MidC-C, MidC-D = Midcontinent-Craton Seismotectonic Source Zone (Configurations A, B, C, and D)
- NAP = North Appalachian Seismotonic Source Zone
- NMESE-N = Non-Mesozoic-and-Younger Extension Mmax Source Zone (Narrow interpretation)
- NMESE-W = Non-Mesozoic-and-Younger Extension Mmax Source Zone (Wide interpretation)
- NMFS = New Madrid Fault System RLME Source
- PEZ-N = Paleozoic Extended Crust Seismotectonic Source Zone (Narrow Interpretation)
- PEZ-W = Paleozoic Extended Crust Seismotectonic Source Zone (Wide Interpretation)
- SLR = St. Lawrence Rift Seismotonic Source Zone
- STUDY-R = Study Region Mmax Source Zone

Table 2.5-52— {Representation of Aleatory Variability in the Characteristics of Future Earthquake Ruptures for RLME Sources}
(Page 1 of 2)

RLME Source	Configuration	Weight	Source Boundary Characteristic	Style of Faulting	Relative Frequency	Rupture Strike (deg)	Relative Frequency	Rupture Dip (deg)	Relative Frequency
Charlevoix	N/A	N/A	Leaky, ruptures can extend beyond border by 50 percent	Reverse	1.0	Uniformly distributed 0 to 360	1.0	Uniformly distributed between 45 and 60	1.0
	Local	0.5	Strict	Strike-slip	1.0	NE (parallel to long axis)	1.0	90	1.0
Charleston	Narrow	0.3	Leaky NE and SW Strict NW and SE boundaries	Strike-slip	1.0	NNE (parallel to long axis)	1.0	90	1.0
	Regional	0.2	Strict	Strike-slip	1.0	NE (parallel to long axis)	0.8	90	1.0
				Strike-slip	1.0	NW (parallel to long axis)	0.2	90	1.0
NMF5	BA-BL	0.6	N/A	Strike-slip	1.0	Parallel to fault trace	1.0	90	1.0
	BA-BFZ	0.4	N/A	Strike-slip	1.0	Parallel to fault trace	1.0	90	1.0
ERM-S	NMN-S	0.7	N/A	Strike-slip	1.0	Parallel to fault trace	1.0	90	1.0
	NMN-L	0.3	N/A	Strike-slip	1.0	Parallel to fault trace	1.0	90	1.0
ERM-N	RFT-S	0.7	N/A	Reverse	1.0	Parallel to fault trace	1.0	40	1.0
	RFT-L	0.3	N/A	Reverse	1.0	Parallel to fault trace	1.0	40	1.0
ERM-S	ERM SCC	0.6	Leaky NE and SW	Strike-slip	1.0	NE (parallel to long axis)	1.0	90	1.0
	ERM SRP	0.4	Leaky NE and SW	Strike-slip	1.0	NE (parallel to long axis)	1.0	90	1.0
ERM-N	N/A	N/A	Leaky NE and SW	Strike-slip	1.0	NE (parallel to long axis)	1.0	90	1.0

Table 2.5-52— {Representation of Aleatory Variability in the Characteristics of Future Earthquake Ruptures for RLME Sources}
(Page 2 of 2)

RLME Source	Configuration	Weight	Source Boundary Characteristic	Style of Faulting	Relative Frequency	Rupture Strike (deg)	Relative Frequency	Rupture Dip (deg)	Relative Frequency
Marianna	N/A	N/A	Leaky	Strike-slip	1.0	NE (parallel to Zone sides)	0.5	90	1.0
Commerce	N/A	N/A	Leaky NE and SW	Strike-slip	1.0	NW (parallel to Zone sides)	0.5	90	1.0
					0.666	Uniformly distributed 0 to 360	1.0	90	1.0
Wabash Valley	N/A	N/A	Leaky	Strike-slip	0.334	Uniformly distributed 0 to 360	1.0	Uniformly distributed between 40 and 60	1.0

Notes

"Leaky" boundary denotes the case in which a virtual earthquake rupture is centered on an epicenter that lies within a source zone, but the rupture is allowed to extend beyond the source boundary. For a "strict" boundary the virtual rupture is constrained to remain within the source.

- Table Acronyms and Abbreviations:

- BA-BL = Blytheville Arch-Bootheel Lineament
 - BA-BFZ = Blytheville-Arch-Blytheville fault zone
 - ERM-N = Eastern Rift Margin-North
 - ERM-S = Eastern Rift Margin-South
 - ERM-SCC = Eastern Rift Margin South/Crittenden County
 - ERM-SRP = Eastern Rift Margin South/River Picks
 - NMFS = New Madrid Fault System
 - NMN = New Madrid North
 - NMN-L = New Madrid North plus extension (long)
 - NMN-S = New Madrid North (short)
 - NMS = New Madrid South
 - RFT = Reelfoot Thrust
 - RFT-L = Reelfoot thrust plus extensions (long)
 - RFT-S = Reelfoot thrust (short)
 - RLME = Repeated Large Magnitude Earthquake
 - N/A = not applicable
- Source: EPRI/DOE/NRC (2012, Appendix H)

Table 2.5-53— {Characterization of Temporal Clustering and Localizing Features for RLME Sources}

RLME Source	Temporal Clustering Assessment		Localizing Tectonic Feature	
	In/Out	Weight	Description	Weight
Charlevoix	N/A	N/A	Random in zone	1.0
Charleston	In	0.9	Random in zone	1.0
	Out	0.1	Default to background	N/A
NMFS	In	0.9	NMS, RFT, NMN	1.0
	Out	0.05	Default to background	N/A
	Out, except RFT	0.05	Only RFT	1.0
ERM-S	N/A	N/A	Random in zone	1.0
ERM-N	N/A	N/A	Random in zone	1.0
Marianna	In	0.5	Random in zone	1.0
	Out	0.5	Default to background	N/A
Commerce Fault Zone	N/A	N/A	Random in zone	1.0
Wabash Valley	N/A	N/A	Random in zone	1.0

Note: The weights represent the relative support in the data for the various alternatives and sum to 1.0

Table Acronyms and Abbreviations:
 ERM-N = Eastern Rift Margin-North
 ERM-S = Eastern Rift Margin-South
 NMFS = New Madrid Fault System
 NMN = New Madrid North
 NMS = New Madrid South
 RFT = Reelfoot Thrust
 RLME = Repeated Large Magnitude Earthquake

Source: EPRI/DOE/NRC (2012, Appendix H)

Table 2.5-54— {Representation of Uncertainty in Recurrence of Charlevoix RLMEs}

RLME Source	Recurrence Method		Recurrence Data		Earthquake Recurrence Model		RLME Annual Frequency	
	Method	Weight	Data	Weight	Model	Weight	Frequency	Weight
Charlevoix	Earthquake Recurrence Intervals	0.2	Set 1	1.0	Poisson	1.0	9.3E-03	0.101
							6.7E-03	0.244
							4.2E-03	0.310
							2.2E-03	0.244
							7.7E-04	0.101
	Earthquake Count in a Time interval	0.8	Set 2	0.75	Poisson	1.0	1.3E-03	0.101
							8.4E-04	0.244
							5.7E-04	0.310
							3.7E-04	0.244
			Set 3	0.25	Poisson	1.0	1.9E-04	0.101
							9.8E-04	0.101
							6.7E-04	0.244
							4.7E-04	0.310
							3.2E-04	0.244
1.8E-04	0.101							

Table Acronyms and Abbreviations: RLME = Repeated Large Magnitude Earthquake
 Source: EPRI/DOE/NRC (2012, Appendix H)

Table 2.5-55 — {Representation of Uncertainty in Recurrence of Charleston RLMEs}
(Page 1 of 6)

RLME Source	Source Geometry	Recurrence Method		Time Period		Earthquake Count		Earthquake Recurrence Model		Coefficient of Variation (a)		RLME Annual Frequency	
		Method	Wt.	Period (Yrs)	Wt.	Count	Model	Wt.	Value	Wt.	Freq.	Wt.	
Charleston	Regional	Earthquake Recurrence Intervals	1.0	2,000	0.8	1886,A,B,C	1.0	Poisson	1.0	N/A	N/A	4.7E-03	0.101
												3.1E-03	0.244
												2.1E-03	0.310
												1.3E-03	0.244
												6.8E-04	0.101
												4.7E-03	0.101
				3.1E-03	0.244								
				2.1E-03	0.310								
				1.3E-03	0.244								
				6.8E-04	0.101								
				2.7E-03	0.101								
				1.9E-03	0.244								
1.3E-03	0.310												
8.8E-04	0.244												
5.0E-04	0.101												
1.9E-03	0.101												
1.3E-03	0.244												
9.2E-04	0.310												
6.4E-04	0.244												
3.4E-04	0.101												
2.2E-03	0.101												
1.5E-03	0.244												
1.1E-03	0.310												
7.8E-04	0.244												
4.6E-04	0.101												
4.7E-03	0.101												
3.1E-03	0.244												
2.1E-03	0.310												
1.3E-03	0.244												
6.8E-04	0.101												
2,000	0.8	1886,A,B,C	1.0	Poisson	1.0	N/A	N/A	N/A	N/A	N/A	N/A	N/A	
				5,500	0.2	1886,A,B,C,D	0.3	Poisson	1.0	N/A	N/A	N/A	N/A
						1886,A,B,C,E	0.2	Poisson	1.0	N/A	N/A	N/A	N/A
						1886,A,B,C,D,E	0.3	Poisson	1.0	N/A	N/A	N/A	N/A
				2,000	0.8	1886,A,B,C	1.0	Poisson	1.0	N/A	N/A	N/A	N/A

Table 2.5-55—{Representation of Uncertainty in Recurrence of Charleston RLMEs}
(Page 2 of 6)

RLME Source	Source Geometry	Recurrence Method		Time Period		Earthquake Count		Earthquake Recurrence Model		Coefficient of Variation (a)		RLME Annual Frequency					
		Method	Wt.	Period (Yrs)	Wt.	Count	Wt.	Model	Value	Wt.	Freq.	Wt.					
Charleston	Local	Earthquake Recurrence Intervals	1.0	5,500	0.2	1886,A,B,C	0.2	Poisson	1.0	N/A	N/A	4.7E-03	0.101				
												3.1E-03	0.244				
												2.1E-03	0.310				
												1.3E-03	0.244				
												6.8E-04	0.101				
												2.7E-03	0.101				
												1.9E-03	0.244				
												1.3E-03	0.310				
												8.8E-04	0.244				
												5.0E-04	0.101				
												1.9E-03	0.101				
												1.3E-03	0.244				
						9.2E-04	0.310										
						6.4E-04	0.244										
						3.4E-04	0.101										
						2.2E-03	0.101										
						1.5E-03	0.244										
						1.1E-03	0.310										
						7.8E-04	0.244										
						4.6E-04	0.101										
						4.7E-03	0.101										
						3.1E-03	0.244										
						2.1E-03	0.310										
						1.3E-03	0.244										
						6.8E-04	0.101										
						6.4E-05	0.101										
						7.6E-06	0.244										
						9.5E-07	0.310										
						8.5E-08	0.244										
						2.3E-09	0.101										
						1886,A,B,C	1.0	0.2	0.1	0.3	0.2						
						2,000	0.8	0.1	0.1	0.3	0.2						

Table 2.5-55—{Representation of Uncertainty in Recurrence of Charleston RLMEs}
(Page 3 of 6)

RLME Source	Source Geometry	Recurrence Method		Time Period		Earthquake Count		Earthquake Recurrence Model		Coefficient of Variation (a)		RLME Annual Frequency	
		Method	Wt.	Period (Yrs)	Wt.	Count	Wt.	Model	Value	Wt.	Freq.	Wt.	
Charleston	Narrow	Earthquake Recurrence Intervals	1.0	2,000	0.8	1886,A,B,C	1.0	Renewal	0.1	0.5	0.5	1.4E-03	0.101
												3.8E-04	0.244
												9.5E-05	0.310
												1.7E-05	0.244
												1.0E-06	0.101
												2.6E-03	0.101
								9.8E-04	0.244				
								3.2E-04	0.310				
								7.1E-05	0.244				
								5.6E-06	0.101				
								4.7E-03	0.101				
								3.1E-03	0.244				
				2.1E-03	0.310								
				1.3E-03	0.244								
				6.8E-04	0.101								
				6.8E-05	0.101								
				8.0E-06	0.244								
				1.0E-06	0.310								
				9.2E-08	0.244								
				2.5E-09	0.101								
				1.4E-03	0.101								
				3.9E-04	0.244								
				9.8E-05	0.310								
				1.7E-05	0.244								
1.1E-06	0.101												
2.7E-03	0.101												
9.9E-04	0.244												
3.3E-04	0.310												
7.3E-05	0.244												
5.8E-06	0.101												

Table 2.5-55—{Representation of Uncertainty in Recurrence of Charleston RLMEs}
(Page 4 of 6)

RLME Source	Source Geometry	Recurrence Method		Time Period		Earthquake Count		Earthquake Recurrence Model		Coefficient of Variation (a)		RLME Annual Frequency	
		Method	Wt.	Period (Yrs)	Wt.	Count	Wt.	Model	Value	Wt.	Freq.	Wt.	
								Poisson	0.9	N/A	N/A	2.7E-03	0.101
												1.9E-03	0.244
												1.3E-03	0.310
												8.8E-04	0.244
												5.0E-04	0.101
												3.5E-07	0.101
										0.3	0.2	2.5E-08	0.244
				5,500	0.2	1886,A,B,C,D	0.3					2.2E-09	0.310
												1.4E-10	0.244
												2.7E-12	0.101
												2.2E-04	0.101
												4.5E-05	0.244
								Renewal	0.1	0.5	0.5	9.3E-06	0.310
												1.4E-06	0.244
												7.6E-08	0.101
												1.0E-03	0.101
												3.3E-04	0.244
												9.5E-05	0.310
												2.0E-05	0.244
												1.5E-06	0.101
												1.9E-03	0.101
												1.3E-03	0.244
								Poisson	0.9	N/A	N/A	9.2E-04	0.310
												6.4E-04	0.244
												3.4E-04	0.101
												4.5E-09	0.101
												2.0E-10	0.244
												1.2E-11	0.310
												5.4E-13	0.244
						1886,A,B,C,E	0.2					6.4E-15	0.101

Table 2.5-55—{Representation of Uncertainty in Recurrence of Charleston RLMEs}
(Page 5 of 6)

RLME Source	Source Geometry	Recurrence Method		Time Period		Earthquake Count		Earthquake Recurrence Model		Coefficient of Variation (a)		RLME Annual Frequency	
		Method	Wt.	Period (Yrs)	Wt.	Count	Wt.	Model	Value	Wt.	Freq.	Wt.	
								Renewal	0.1	0.5	0.5	5.2E-05	0.101
												8.2E-06	0.244
												1.4E-06	0.310
												1.7E-07	0.244
												7.0E-09	0.101
												5.2E-04	0.101
												1.4E-04	0.244
										0.7	0.3	3.4E-05	0.310
												6.1E-06	0.244
												3.9E-07	0.101
												2.2E-03	0.101
												1.5E-03	0.244
								Poisson	0.9	N/A	N/A	1.1E-03	0.310
				5,500		1886,A,B,C,D,E	0.3					7.8E-04	0.244
												4.6E-04	0.101
												1.5E-08	0.101
												8.7E-10	0.244
												7.0E-11	0.310
												4.4E-12	0.244
												8.2E-14	0.101
												7.0E-05	0.101
												1.3E-05	0.244
												2.5E-06	0.310
												3.7E-07	0.244
												2.1E-08	0.101
												5.7E-04	0.101
												1.6E-04	0.244
												4.5E-05	0.310
												9.2E-06	0.244
												7.6E-07	0.101

Table 2.5-55—{Representation of Uncertainty in Recurrence of Charleston RLMEs}
(Page 6 of 6)

RLME Source	Source Geometry	Recurrence Method		Time Period		Earthquake Count		Earthquake Recurrence Model		Coefficient of Variation (α)		RLME Annual Frequency	
		Method	Wt.	Period (Yrs)	Wt.	Count	Wt.	Model	Wt.	Value	Wt.	Freq.	Wt.
<p>Note: N/A = not applicable - <u>Table Acronyms and Abbreviations:</u> RLME = Repeated Large Magnitude Earthquake Source: EPRI/DOE/NRC (2012, Appendix H)</p>													

Table 2.5-56—{Representation of Uncertainty in Recurrence of NMFS RLMEs}

RLME Source	In or Out of Cluster	Recurrence Method		Recurrence Data		Earthquake Recurrence Model		Coefficient of Variation (a)		RLME Annual Frequency	
		Method	Wt.	Sequences/ Clusters	Wt.	Model	Wt.	Value	Wt.	Freq.	Wt.
NMFS	In-Cluster	Earthquake Recurrence Intervals	1.0	1811-1812, 1450, and 900 AD	1.0	Poisson	0.75	N/A	-	6.0E-03	0.101
										3.7E-03	0.244
										2.4E-03	0.310
										1.4E-03	0.244
										6.2E-04	0.101
										3.5E-03	0.101
										1.1E-03	0.244
										3.2E-04	0.310
										6.4E-05	0.244
										4.7E-06	0.101
										4.8E-03	0.101
										2.2E-03	0.244
										8.9E-04	0.310
										2.6E-04	0.244
3.1E-05	0.101										
4.4E-03	0.101										
2.2E-03	0.244										
1.0E-03	0.310										
3.4E-04	0.244										
4.7E-05	0.101										
1.3E-03	0.101										
7.2E-04	0.244										
4.2E-04	0.310										
2.2E-04	0.244										
8.0E-05	0.101										
	Out-of-Cluster Except RFT	Earthquake Recurrence Intervals	1.0	2000 BC and 1000 AD Clusters	1.0	Poisson	1.0	N/A	-		

Note: - Table Acronyms and Abbreviations:

NMFS = New Madrid Fault System

RLME = Repeated Large Magnitude Earthquake

N/A = not applicable

Source: EPRI/DOE/NRC (2012, Appendix H)

Table 2.5-57 — {Representation of Uncertainty in Recurrence of Eastern Rift Margin-South RLMES}

RLME Source	Recurrence Method		Recurrence Data		Earthquake Recurrence Model		RLME Annual Frequency	
	Method	Wt.	Sequences/Clusters	Wt.	Model	Wt.	Freq.	Wt.
ERM-S	Earthquake Count in a Time Interval	1.0	2 Earthquakes in 17.7-21.7 ky.	0.333	Poisson	1.0	3.5E-04	0.101
							2.1E-04	0.244
							1.4E-04	0.310
							8.0E-05	0.244
							3.6E-05	0.101
							4.3E-04	0.101
			3 Earthquakes in 17.7-21.7 ky.	0.334	Poisson	1.0	2.8E-04	0.244
							1.9E-04	0.310
							1.2E-04	0.244
							6.2E-05	0.101
							5.0E-04	0.101
							3.4E-04	0.244
4 Earthquakes in 17.7-21.7 ky.	0.333	Poisson	1.0	2.4E-04	0.310			
				1.6E-04	0.244			
				9.0E-05	0.101			

Table Acronyms and Abbreviations:
 ERM-S = Eastern Rift Margin-South
 RLME = Repeated Large Magnitude Earthquake
 Source: EPRI/DOE/NRC (2012, Appendix H)

Table 2.5-58—{Representation of Uncertainty in Recurrence of Eastern Rift Margin-North RLMEs}

RLME Source	Recurrence Method		Recurrence Data		Earthquake Recurrence Model		RLME Annual Frequency	
	Method	Wt.	Sequences/Clusters	Wt.	Model	Wt.	Freq.	Wt.
ERM-N	Earthquake Count in a Time Interval	1.0	1 Earthquake in 12-35 k.y.	0.9	Poisson	1.0	2.9E-04	0.101
							1.5E-04	0.244
							8.0E-05	0.310
							4.0E-05	0.244
			1.4E-05	0.101				
			3.9E-04	0.101				
			2.2E-04	0.244				
			1.3E-04	0.310				
7.2E-05	0.244							
3.2E-05	0.101							

Table Acronyms and Abbreviations:

RLME = Repeated Large Magnitude Earthquake

Source: EPRI/DOE/NRC (2012, Appendix H)

Table 2.5-59— {Representation of Uncertainty in Recurrence of Marianna Zone RLMs}

RLME Source	Recurrence Method		Recurrence Data		Earthquake Recurrence Model		RLME Annual Frequency	
	Method	Wt.	Sequences/Clusters	Wt.	Model	Wt.	Freq.	Wt.
Marianna	Earthquake Recurrence Intervals	1.0	3 Earthquakes in 9.6-10.2 k.y.	0.5	Poisson	1.0	6.9E-04	0.101
							4.2E-04	0.244
							2.7E-04	0.310
							1.6E-04	0.244
							7.2E-05	0.101
			8.4E-04	0.101				
			5.5E-04	0.244				
			3.7E-04	0.310				
			2.4E-04	0.244				
			1.2E-04	0.101				

Table Acronyms and Abbreviations:

RLME = Repeated Large Magnitude Earthquake

Source: EPRI/DOE/NRC (2012, Appendix H)

Table 2.5-60—{Representation of Uncertainty in Recurrence of Commerce RLMEs}

RLME Source	Recurrence Method		Recurrence Data		Earthquake Recurrence Model		RLME Annual Frequency	
	Method	Wt.	Sequences/ Clusters	Wt.	Model	Wt.	Freq.	Wt.
Commerce	Earthquake Recurrence Intervals	1.0	2 Earthquakes in 18.9-23.6 k.y.	0.75	Poisson	1.0	2.5E-04	0.101
							1.4E-04	0.244
							8.0E-05	0.310
							4.0E-05	0.244
							1.4E-05	0.101
			3 Earthquakes in 18.9-23.6 k.y.	0.25	Poisson	1.0	3.3E-04	0.101
							2.0E-04	0.244
							1.3E-04	0.310
							7.6E-05	0.244
							3.4E-05	0.101

Table Acronyms and Abbreviations:
 RLME = Repeated Large Magnitude Earthquake
 Source: EPRI/DOE/NRC (2012, Appendix H)

Table 2.5-61 — {Representation of Uncertainty in Recurrence of Wabash Valley RLMs}

RLME Source	Recurrence Method		Recurrence Data		Earthquake Recurrence Model		RLME Annual Frequency	
	Method	Wt.	Sequences/Clusters	Wt.	Model	Wt.	Freq.	Wt.
Wabash Valley	Earthquake Recurrence Intervals	1.0	2 Earthquakes in 11-13 k.y.	1.0	Poisson	1.0	4.4E-04 2.5E-04 1.4E-04 7.2E-05 2.4E-05	0.101 0.244 0.310 0.244 0.101

Table Acronyms and Abbreviations:
 RLME = Repeated Large Magnitude Earthquake
 Source: EPRI/DOE/NRC (2012, Appendix H)

Table 2.5-62— {Representation of Uncertainty in RLME Magnitude}

(Page 1 of 2)

RLME Sources	Maximum Magnitude	
	Value	Weight
NMS	7.9	0.167
	7.8	0.167
	7.6	0.250
	7.2	0.083
	6.9	0.250
	6.7	0.083
RFT	7.8	0.167
	7.7	0.167
	7.8	0.250
	7.4	0.083
	7.3	0.250
	7.1	0.083
NMN	7.6	0.167
	7.5	0.167
	7.5	0.250
	7.2	0.083
	7.0	0.250
	6.8	0.083
Commerce	6.7	0.15
	6.9	0.35
	7.1	0.35
	7.3	0.10
	7.7	0.05
ERM-S	6.7	0.15
	6.9	0.20
	7.1	0.20
	7.3	0.20
	7.5	0.20
	7.7	0.05
ERM-N	6.7	0.30
	6.9	0.30
	7.1	0.30
	7.4	0.10
Mariana	6.7	0.15
	6.9	0.20
	7.1	0.20
	7.3	0.20
	7.5	0.20
	7.7	0.05
Wabash Valley	6.75	0.05
	7.0	0.25
	7.25	0.35
	7.5	0.35

Table 2.5-62— {Representation of Uncertainty in RLME Magnitude}

(Page 2 of 2)

Charleston	6.7	0.10
	6.9	0.25
	7.1	0.30
	7.3	0.25
	7.5	0.10
Charlevoix	6.75	0.20
	7.0	0.50
	7.25	0.20
	7.5	0.10

- Table Acronyms and Abbreviations:

ERM-N = Eastern Rift Margin-North

ERM-S = Eastern Rift Margin-South

NMN = New Madrid North

NMS = New Madrid South

RFT = Reelfoot Thrust

RLME = Repeated Large Magnitude Earthquake

Source: EPRI/DOE/NRC (2012, Appendix H, Tables H-5.1-1, H-5.2-1, H-5.5-1, H-5.6-1, H-5.6-2, H-5.7-1, H-5.8-1, and H-5.9-1)